Chiral-at-metal Iridium(III) Complexes Containing Dithienylethene-Based Photoswitchable Ligands

PhD Student: FRANCISCO BORJA URQUIOLA ZABALLA

Supervisors: DRA. ZORAIDA FREIXA FERNÁNDEZ

DR. NATHAN D. MCCLENAGHAN

Euskal Herriko Unibertsitatea UPV-EHU

Donostia (Gipuzkoa), 2022

THÈSE PRÉSENTÉE

POUR OBTENIR LE GRADE DE

DOCTEUR DE

L'UNIVERSITÉ DE BORDEAUX

ÉCOLE DOCTORALE DES SCIENCES CHIMIQUES
SPÉCIALITÉ
CHIMIE ORGANIQUE

Par Francisco Borja URQUIOLA ZABALLA

Chiral-at-metal Iridium(III) Complexes Containing Dithienylethene-Based Photoswitchable Ligands

Sous la direction de : Nathan D. MCCLENAGHAN et Zoraida FREIXA

Soutenue le 18 mars 2022

Membres du jury :

Mme. RODRIGUEZ, Laura	Professeur, Université du Barcelona	Président/Rapporteur
M. ANDRÉASSON, Joakim	Professeur, Université de Technologie Chalmers	Rapporteur
Mme. LÓPEZ, Rosa Maria	Professeur, Université du Pays Basque	Examinateur
M. JONUSAUSKAS, Gediminas	Directeur de Recherche, Université de Bordeaux	Examinateur
M. CANO, Israel	Assistant Professeur, Université Complutense Madrid	Examinateur
Mme. FREIXA, Zoraida	Directeur de Recherche, Université du Pays Basque	Co-directeur
M. MCCLENAGHAN, Nathan D.	Directeur de Recherche, Université de Bordeaux	Directeur

SCIENTIFIC ACKNOWLEDGEMENTS

Table of Contents

Glossary of Terms and Abbreviations

GLOSSARY OF TERMS AND ABBREVIATIONS

Acac	Acetylacetone
ATP	Adenosine Triphosphate
CD	Circular Dichroism Spectroscopy
CF	Closed-form
CI	Conical Intersection
COSY	Correlation Spectroscopy
CPL	Circulary Polarized Luminescence
DAE	Diarylethene
DFT	Discrete Fourier Transform
DNBS	Dinitrobenzenesulfonyl
DTE	Dithienylethene
EA	Elemental Analysis
fac	facial
FD	Field Desorption Mass Spectroscopy
HPLC	High Performance Liquid Chromatography
HSQC	Heteronuclear Single Quantum Correlation
ICT	Intramolecular Electron Transfer
ISC	Intersystem Crossing
LC	Ligand-Centered
LD	Linear Dichroism Spectroscopy
LEC	Light-Emitting Electrochemical Cell
LLCT	Ligand-to-Ligand Charge Transfer
mer	meridional
MLCT	Metal-to-Ligand Charge Transfer
MO	Molecular Orbitals
NBS	N-Bromosuccinimide
n-BuLi	n-Butyl Lithium
NCH	Heterocyclic Carbene
NF	Naphtalene
NIR	Near-Infrared Spectroscopy
NMR	Nuclear Magnetic Resonance

OF	Open-form
OLED	Organic Light-Emitting Diode
PDT	Photodynamic Therapy
ppm	Parts per million
ppy	phenylpyridine
PS	Photosensitizer
PSS	Photostationary State
SDS	Sodium Docecyl Sulfate Micelles
TE	Thienylethene
TFA	Trifluoroacetic Acid
UV	Ultraviolet
UV-Vis	Ultraviolet-Visible
Δ	Delta Isomer
Φ_{EM}	Emission Quantum Yield
Λ	Lambda Isomer
$\Phi_{O \to C}$	Photocyclization Quantum Yield
$\Phi_{C \to O}$	Photocycloreversion Quantum Yield
τ	Emission Half-Life Time

CHAPTER 1

MOLECULAR SWITCHES AND IR(III) COMPLEXES: BACKGROUND AND STATE OF THE ART
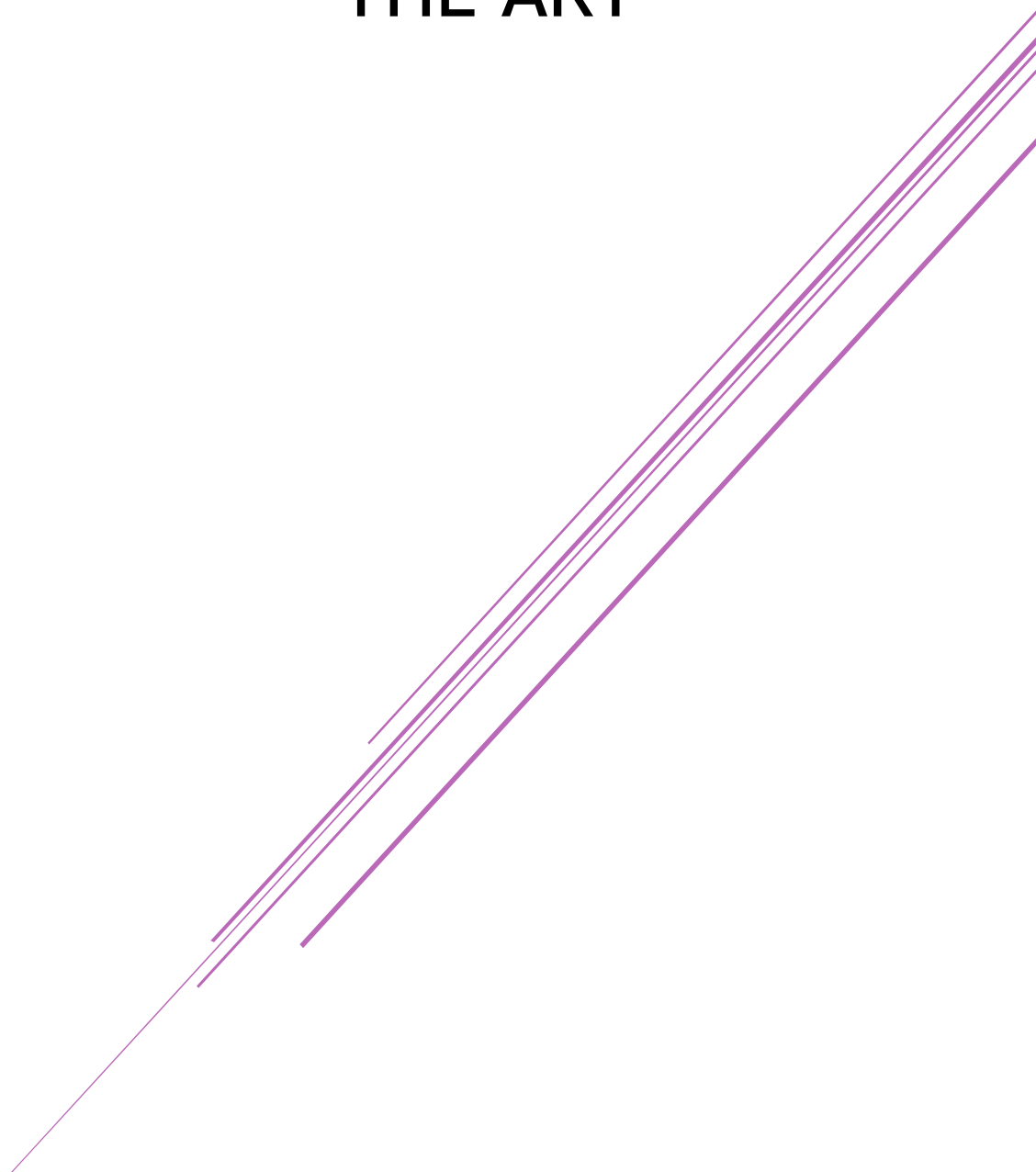
1.1 MOLECULAR SWITCH: GENERAL BEHAVIOR

Molecular switches are chemical species capable of transforming reversibly between two or more different states due to the application of external stimuli (light, temperature, pressure, pH, amongst others). The different states observed in a switchable compound can present different physical and chemical properties such as the color/absorption spectra, geometrical structure, magnetic properties, or oxidation/reduction potential.[1-4] Light-induced reversible transformation of a chemical compound between two isomers with different absorption spectra is referred to as photochromism.
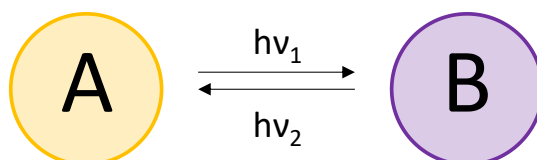
Figure 1.1. Principle of photochromic molecular devices.

Many photochromic systems can be found in nature. At the end of the 90s and the beginning of this century, different natural biological systems containing photochromic units in their photoreceptors such as phytochrome[5], chlamydomonas[6], or bacteriorhodopsin[7] were studied in detail. There are also many photochromic compounds of synthetic origin. These compounds have been studied widely during the last 30 years due to their potential application in different technological fields, such as molecular motors[8], coordination cages[9] or optical memory devices.[10] Scheme 1.1. shows the best-known families of photochromic systems applied for the construction of artificial molecular photo-switches. Each one has a different isomerization mechanism, granting different properties and nature. The isomerization comprises two processes (forward and reverse) where both can occur due to the incidence of light of specific wavelengths. However, in some cases, returning to the original form can also occur due to a thermal contribution. Accordingly, photochromic systems can be categorized into two large families, T- or P-type. This classification is based on the thermal stability of the metastable state. If the process of returning to the original state of the compound can be achieved through a thermal transformation, it is designated a T-type photochrome. On the contrary, if the metastable state is sufficiently stable to be irreversible employing thermal energy (hence, light radiation is needed to produce the change), they are classified as P-type photochromes. The best-known T-type photochromic compounds are azobenzenes and spiropyrans, also known as thermochromic systems.
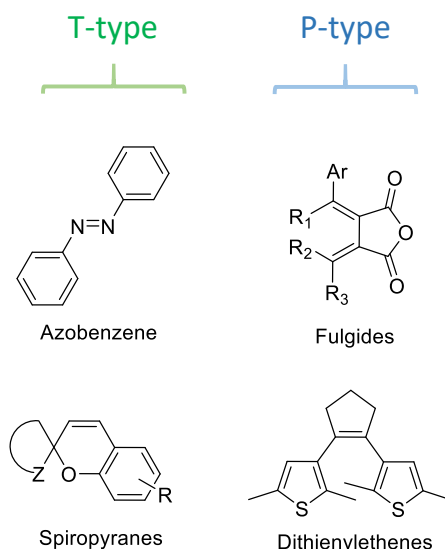
Scheme 1.1. Representative examples of T- and P-type molecular switches.

T-type photochromic compounds generally are not considered ideal photoswitchable systems for possible applications due to their inherently poor thermal stability. Rather, P-type systems are preferred since they do not show thermal deterioration of their properties in their metastable states. Fulgides and derivatives of diarylethenes fall into this class of compounds. The latter will be the object of study during this project and will be described in more detail below.

1.2 DITHIENYLETHENE (DTE)

1.2.1 BACKGROUND AND HISTORY

Diarylethene derivatives (DAE) were discovered in the 1980s during a study on photosensitive polymers in which azobenzene and stilbene were used as the photochromic groups.[11-14] The most straightforward DAE derivative is the stilbene. Like azobenzene, stilbene can also undergo *trans-cis* photoisomerization reactions. Schnabel *et al*. observed that a polymer that contained stilbene groups in its structure after performing the first *E/Z* isomerization due to UV irradiation was not susceptible to photoreversion.[15] Instead, they observed the formation of poly-9,10-dimethylenephenanthrene by elimination of hydrogen in the presence of oxygen (Scheme 1.2).[16]
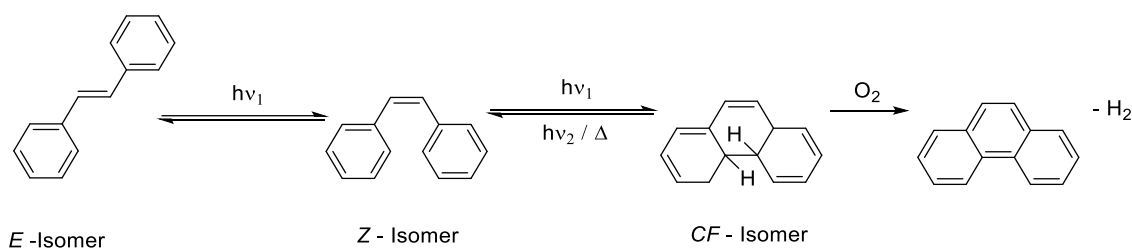
Scheme 1.2 Stilbene *E/Z* isomerization and H_2 elimination yielding phenanthrene.

Intending to inhibit the formation of phenanthrene, they synthesized a new derivative of stilbene, cotaining methyl substituents in the 2- and 6-positions of the phenyl groups. Scheme 1.3 shows how, with this modification, the hydrogen elimination reaction could be avoided, and the material was photochromic. However, the stability of the closed-form (**CF**) was minimal.
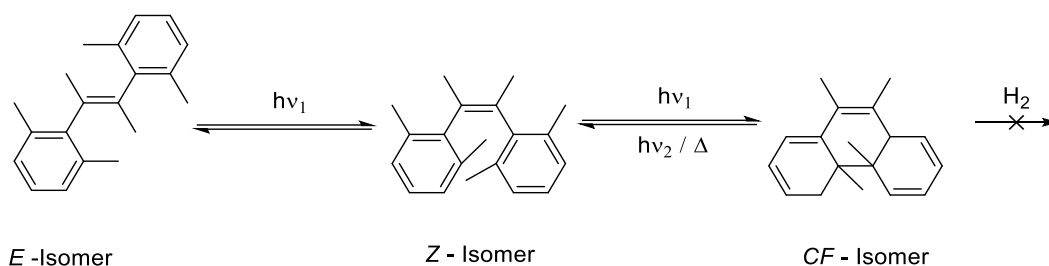
Scheme 1.3. Photochromic stilbene derivative.

To improve the stability of the **CF** isomer, different research groups replaced the phenyl rings of stilbene with aromatic five-membered heterocycles such as furan and thiophene[17,18]. The change of the heterocycle group varies the aromaticity of the system, which results in the axiom that the lower the aromaticity in the open form of DTE, the longer its half-life will be in the **CF** isomer. The stabilization energy values collected in Table 1.1, (calculated by Herradón et al.) show the large difference between the energy of the phenyl group (35.84 kcal/mol) and that of the thiophene group (18.57 kcal/mol).[19] This difference can affect both the effectiveness of the cyclization process (the greater the stability, the more difficult it is to break), and the stability of the **CF-DAE** (the more stable form of the molecule will be preferred).

Table 1.1. Calculated aromatic stabilization energy.

Group	Energy (kcal/mol)
Phenyl	35.84
Pyridine	33.23
Cyclohexadiene	2.15
Pyrrole	20.57
Thiophene	18.57
Furyl	14.77

This behavior was observed by Mohri and coworkers, who synthesized a polymer with 2,5-dimethylthiophene groups. This new polymer in its closed form was thermally stable (P-type compound), without observing any change in the process even when heated to 100 °C. The open isomer was recovered by irradiation with visible light.
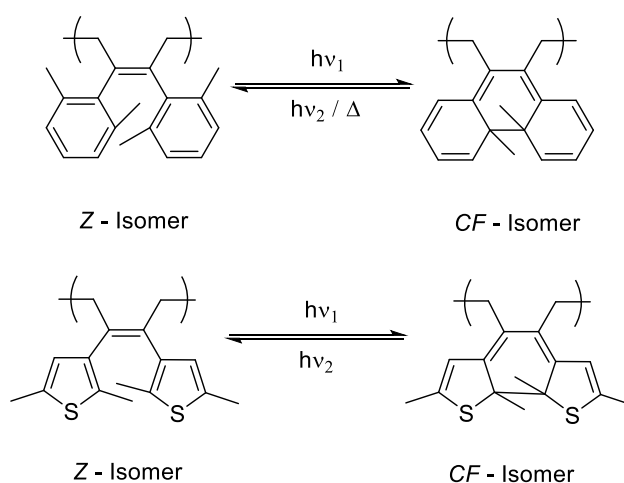
Scheme 1.4. Stability of **CF** isomer of DAE and DTE in a polymer structure.

Therefore, dithienylethenes (DTEs) seemed suitable compounds for the construction of photo-functional materials. Nevertheless, these 1,2-bisthiophene substituted "open alkenes" showed two competitive processes under UV irradiation: the already known *trans/cis* isomerization of the double bond, and the cyclization reaction. Therefore, to improve the quantum yield of the photocyclization reaction, the double bond was introduced as part of a cyclic structure (such as maleic anhydride or maleimide) to avoid *trans/cis* photoisomerization. These new DTEs showed good photocyclization quantum yields in slightly polar solvents, but in more polar solvents such as acetonitrile or methanol, the photochromic behavior was strongly inhibited. Therefore, to improve the photochromic reactivity of the compounds in more polar solvents, perfluorinated cyclic alkenes (four, five, and six-membered rings) were chosen as bridging units.[20,21]
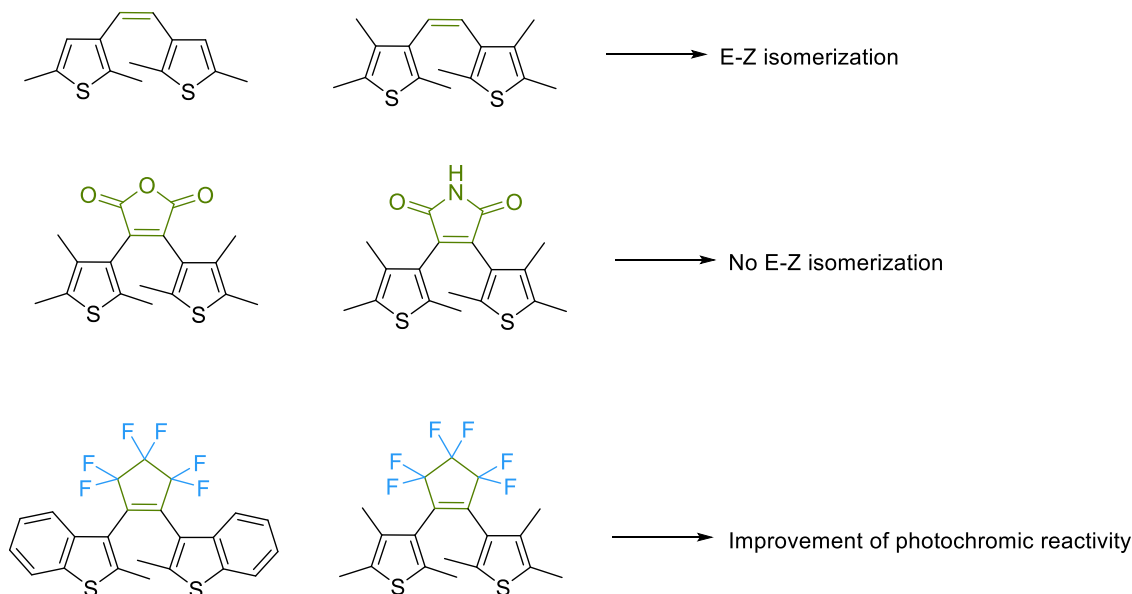
Scheme 1.5. Influence of central ring on *E-Z* isomerization in DTEs.

1.2.2 PROPERTIES: PHOTOCHROMISM, FATIGUE RESISTANCE AND THERMAL STABILITY

DTE molecules are photochromic compounds that perform an isomerization process based on a photocyclization/photocycloreversion reaction. This type of photochromic system has very characteristic properties that other photochromes do not show:

- The color change associated with the difference in light absorption in UV-Vis spectroscopy is one of the key properties of these compounds because the spectra obtained are so different that they can be modulated using specific wavelengths for each of them, this being a factor of vital importance for applications such as readout systems.
- In order to use a photoswitch system properly, its resistance to fatigue (no decomposition after several opening-closing cycles) must be taken into account. DTEs are among the best compounds described against decomposition due to fatigue.
- DTEs have been called P-type chromophores, and this means that they should only be able to activate isomerization processes through light irradiation. Therefore, it is essential to study the thermal stability of DTE compounds to rule out possible thermochromic mechanisms during photoisomerization processes.

1.2.2.1 PHOTOCHROMISM IN SOLUTION AND CRYSTALLINE STATE

DTEs experience isomerization by light irradiation, generating a cycling process (photocyclization) or an opening process (photocycloreversion) depending on the wavelength at which the system is irradiated. As will be explained later, these cycling/opening processes are based on the cyclical movement of the electrons of the π-system present in the molecule. This movement of electrons generates the formation of a new sigma bond. This rearrangement of electrons and the formation/breaking of bonds cause significant changes in the UV-Vis spectrum, as can be seen in Figure 1.2, taking **E-1** as an example. The **OF-E-1** spectrum is shown in black, with absorption bands in the 200-350 nm region. The **CF-E-1** isomer (in red) presents completely different bands with the most characteristic band around 450-600 nm. This low energy band is principally responsible for the color of the **CF-DTE** and it is the most suitable wavelength at which it should be irradiated to return to the **OF** of the DTE.[22]
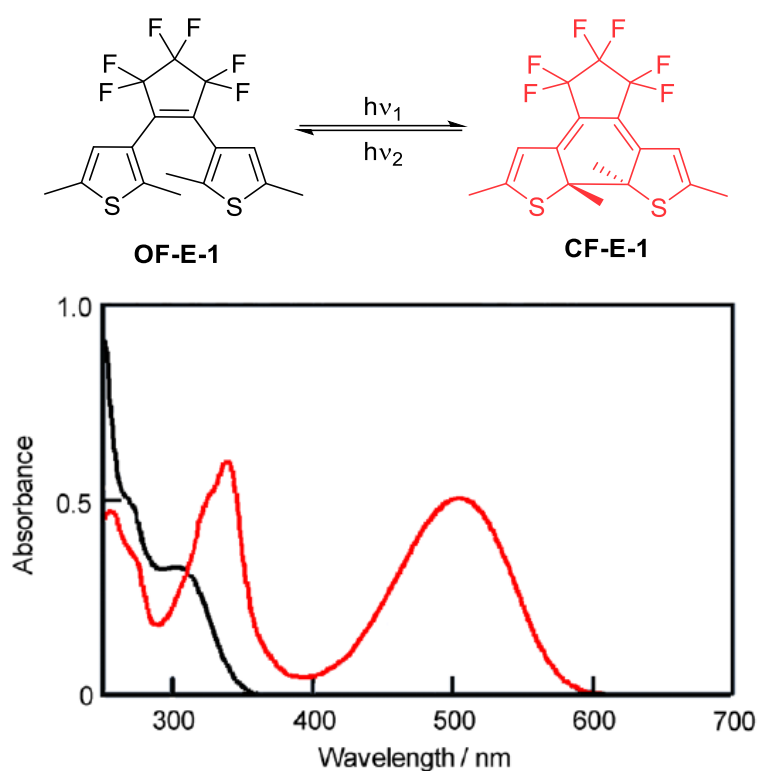
Figure 1.2. Electronic redistribution and resulting color/absorption change for **E-1**.[22]

Therefore, the characteristic band of the **CF-DTE** will give us the color of the compound in its closed form. By modulating the structure of the DTE, incorporating functional groups, expanding the conjugated system, or altering the heterocycles, a wide range of colors can be observed, being able to design DTE systems for each of the colors of the visible spectrum. In the Scheme 1.6 different DTE molecules are shown together with the different values of the absorption maximum, which are related to the color of the **CF-DTE**.[22] This originated that multiple research groups synthesized large families of DTE (symmetric and non-symmetric DTEs) in order to obtain a wide range of colors.[23]

CF-E-1

$\lambda_{máx}$ = 505 nm

CF-E-2

$\lambda_{máx}$ = 534 nm

CF-E-3

$\lambda_{máx}$ = 562 nm

CF-E-4

$\lambda_{máx}$ = 516 nm

CF-E-5

$\lambda_{máx}$ = 458 nm

Scheme 1.6. Different λ_{max} for DTEs.[22]
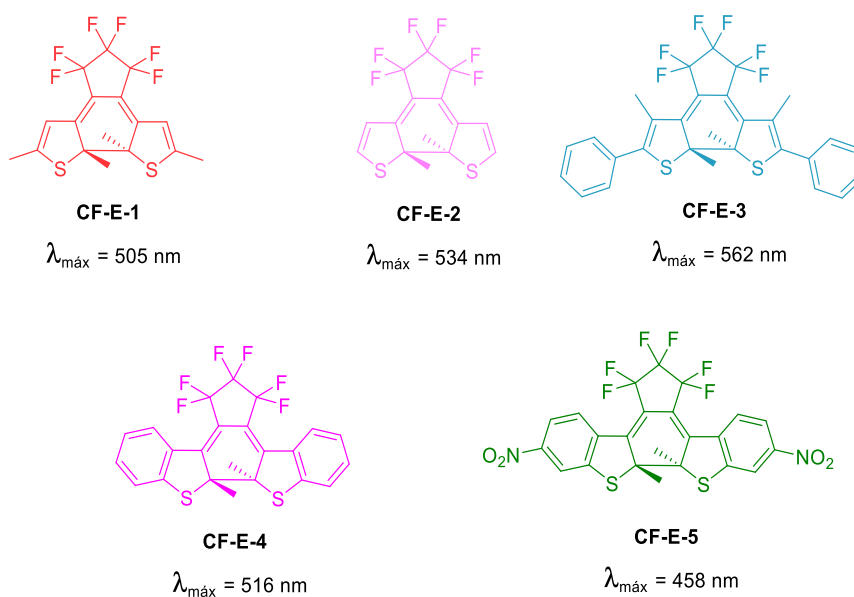
On the other hand, if the photochromism of DTEs in their crystalline state is studied, interesting changes in their structure can be seen during the cyclization and cycloreversion processes. When the photocyclization process is induced, it can be observed how the open form of the DTE "shrinks" in length and "elongates" in height, as shown in the **E-1** example in Figure 1.3. This structural change is due to the formation of the sigma bond between the two reactive carbons, generating a rigid structure free of observable rotational bonds in the **OF-DTE**.
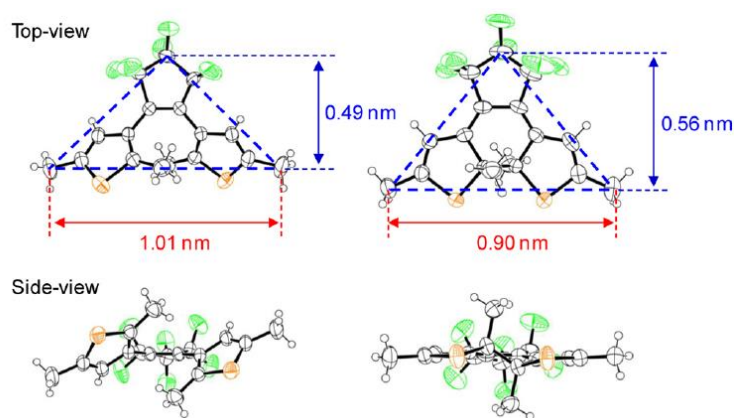
Figure 1.3. Structural change of **E-1** after isomerization.[22]

1.2.2.2 THERMAL STABILITY

The thermal stability of the **CF-DTEs** is one of the fundamental properties of this type of molecular switch. As seen in the section on the origin of DTEs, those systems that have aromatic heterocycles present better thermal stability during the thermochromic cycloreversion process than those derived from stilbene (phenyl ring as π-electron system). Studying DTEs with aromatic heterocycles such as thiophenes, furans or benzothiophenes tend to have good thermal stability at temperatures close to 100 °C. Scheme 1.7 shows compound **E-6**, described by M. Irie et al., which demonstrated high thermal resistance.[24] They reported a DTE that did not show any change in the absorption of the closed isomer heating at 100 °C for 48 h. In order to study how high its stability is, they increased the temperature to 140 °C, observing a minor

6

discoloration of the ligand. It can be observed that even heating the sample for 400 hours at 140 °C, the absorption only decreases by 20%, which increases as the temperature increases during the study. The observed decrease in absorbance at 140 °C followed a first-order kinetics, indicating that the cycloreversion process occurs in a thermochromic way by heating at high temperatures.

48 hours at 100 ºC $\longrightarrow$ no absorption change

400 hours at 140 ºC $\longrightarrow$ decay of 20% of the absorption
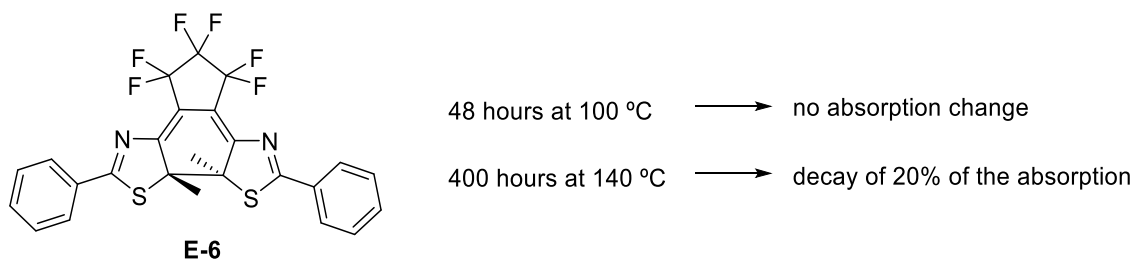
Scheme 1.7. Thermal effects on **E-6**.

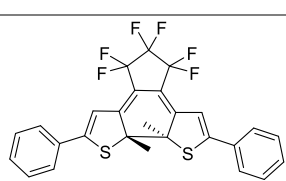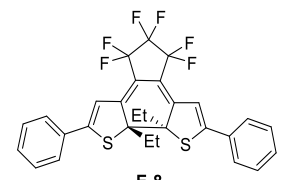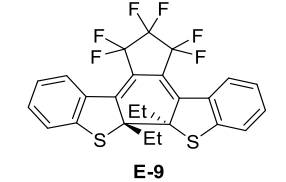The thermal stability of the derivatives of DAEs has been thoroughly studied.[24] Compounds **E-8** and **E-9** were studied by replacing the methyl groups at positions 2-2' for more voluminous groups, such as ethyl groups.[25] The studies carried out by Kobatake and coworkers show how modifying the cycling positions by larger groups causes a decrease in thermal stability. It is observed that **E-7** methyl-containing DTE offers thermal stability, without loss of absorption, at 100 °C for 24 hours, while the **E-8** ethyl-containing DTE presents a loss of absorption close to 10 % after 20 hours at 50-60 °C. This loss increases as the temperature increases; for example, **E-9** loses 70 % of the initial value of its absorbance in less than 50 hours at 90 °C. From these data, the activation energies can be obtained. These values can also be estimated from the transition energy barrier at the ground state surface potential using DFT calculations. Table 1.2 collects some of the data published in the literature.[26]

Table 1.2. Activation energy for **E-7 – E-9** DTEs

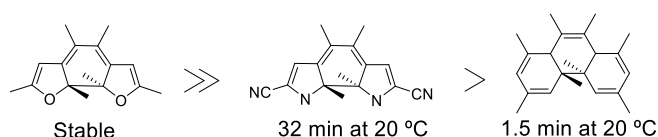| *Compound*	*Process*	*Activation energy (kJ.mol^{-1})*
E-7	**E-7 CF $\longrightarrow$ E-7 OF**	139 (150 °C)
E-8	**E-8 CF $\longrightarrow$ E-8 OF**	132 (60 °C)
E-9	**E-9 CF $\longrightarrow$ E-9 OF**	118 (60 °C)

There are three factors as to how the thermal stability of DTE derivatives depends on the aryl groups present in the structure:
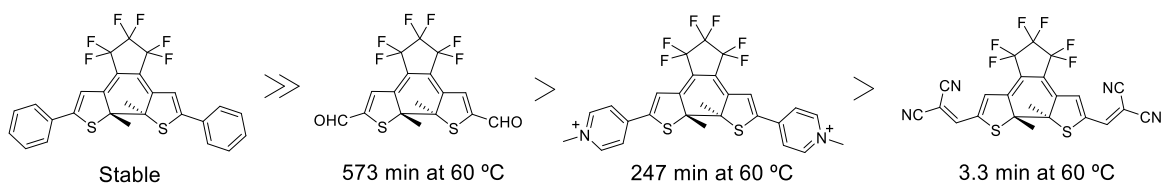
- The aromatic stabilization energy of the aryl groups. This is ascribed to the increased energy level of the closed-ring isomer due to the loss of the aromatic stabilization energy.[27]
- The electronic nature of the substituents. When electron-withdrawing substituents are introduced at the aryl groups, it the central carbon-carbon bond of the **CF** is weakened.[28]
- Finally, steric hindrance of substituents on reactive carbons. The bulky substituents at the reacting position facilitate the thermal cycloreversion process of the closed-ring derivatives.

Scheme 1.8. shows various illustrative examples collected from the literature, where this classification can be seen.[29]

1) Aromatic stabilization energy of the aryl groups

Stable   >>   32 min at 20 ºC   >   1.5 min at 20 ºC

2) Electron-withdrawing substituents

Stable   >>   573 min at 60 ºC   >   247 min at 60 ºC   >   3.3 min at 60 ºC

3) Steric hindrance of the substituents

Stable   >   40 h at 100 ºC   >   0.33 h at 100 ºC
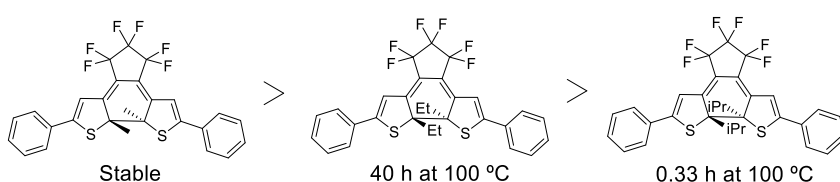
Scheme 1.8. Thermal stability for different DAEs/DTEs.[29]

1.2.2.3 RESISTANCE TO FATIGUE

Resistance to fatigue is a necessary property for practical applications of photochromic molecules. Fatigue resistance (or number of repeatable cycles - RCN) is defined as the number of photochromic cycles that a DAE can repeat under certain conditions until the absorbance of one of the isomers decreases to 80% with respect to the first cycle. Although numerous photochromic compounds have been described, only a few have RCN greater than 1000. Even so, DAEs capable of repeating the process up to 14,000 times in solution, and up to 30,000 in the crystalline phase, have been recorded.[20]
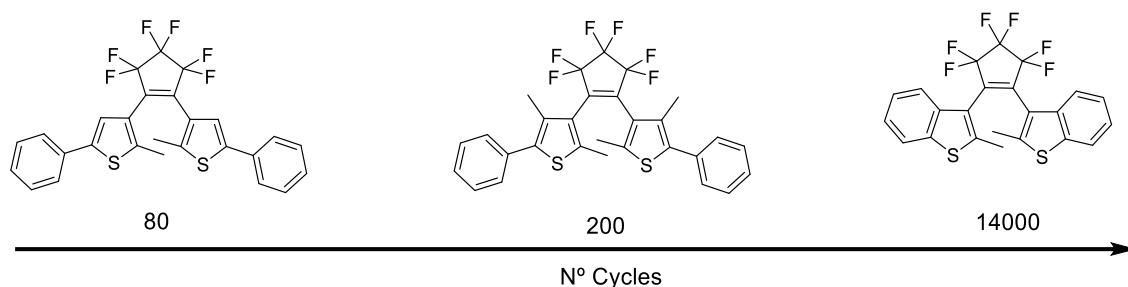
Figure 1.4. Increasing substituent dependent fatigue resistance. [30,31]

Photochromic reactions are considered non-destructive chemical bond rearrangements. However, essentially every process has unwanted secondary reactions that generate side products. In the case of DAE compounds, the best-known secondary reactions are oxidation reactions and photoreactions. Oxidation reactions generate endoperoxides in the presence of air.[32] This decomposition affects the **OF** of DAEs, making the generation of the **CF-isomer** impossible. Instead, photoreaction generates decomposition products due to a long period of irradiation on the closed isomer.[33] This long exposure to UV light causes the formation of two six-membered heterocycles. The formation of this by-product is irreversible since there is no mechanism by which the photoprocess becomes reversible. This process must be considered because the by-product can absorb in a very similar manner than the closed isomer, which can lead to uncertainty when processing data.
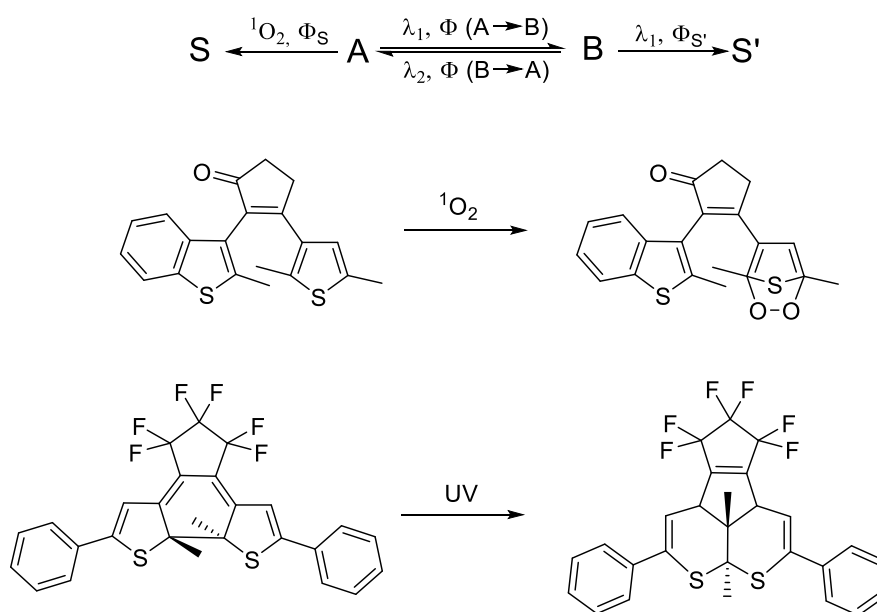
Scheme 1.9. Secondary photochemical reactions.

Two possible mechanisms are known by which the **CF** of DAEs can form the by-product obtained by UV irradiation. Figure 1.5 shows both possible routes.[34] Route 1 shows how photoexcited cyclohexadiene derivatives can produce five-membered rings. This occurs due to the radical migration process, where a bond-formation and cleavage mechanism occurs, producing a condensed-ring by-product. The second option (*Route 2*) is based on the C-S bond length. This bond is much longer in the closed-ring isomer in comparison with the open-isomer one. This length permits the C-S bond cleavage by photoexcitation, which continues with a radical migration forming the five-membered ring as a condensation reaction product. Both routes are valid for the by-product formation, but the second route has more options available.

This is because by-product formation becomes more likely when the sample is irradiated with ultraviolet light and no other process is observed when it is switched to visible light, which would occur through the conical intersection. Additionally, *Route 2* is consistent with theoretical calculations published by Masunov and coworkers.[35]
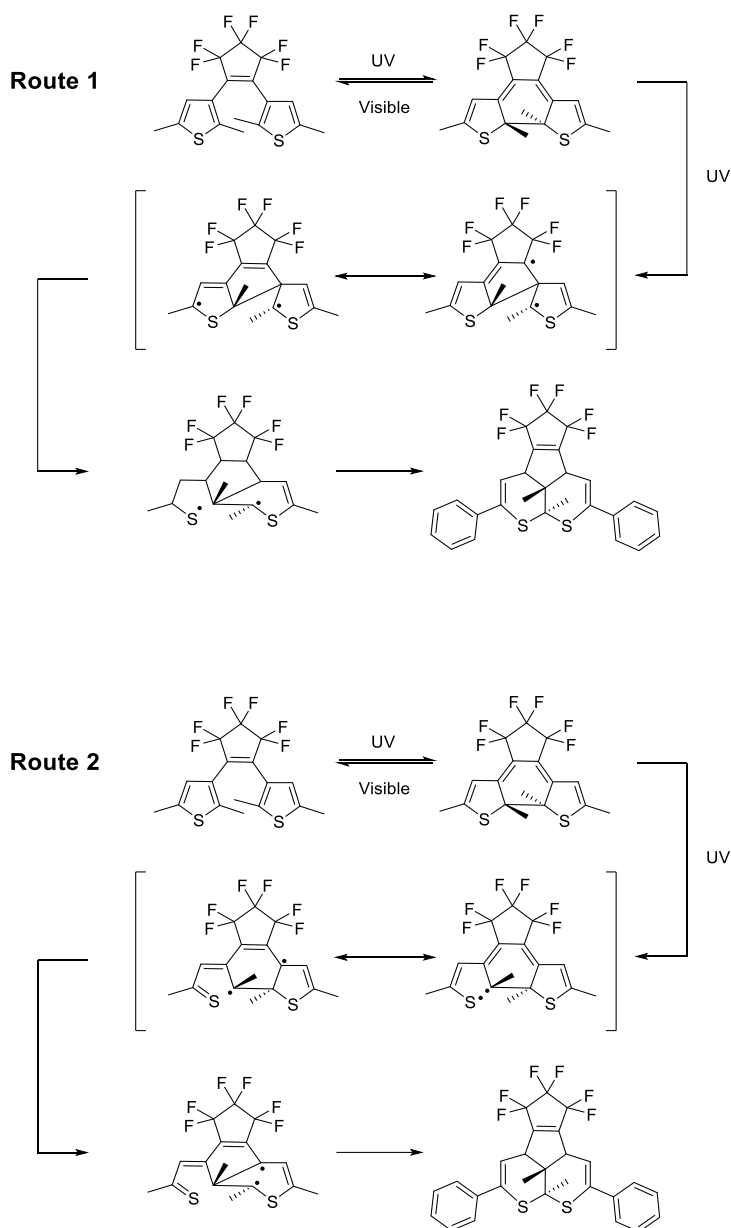
Figure 1.5. Two routes for the by-product formation.[34]

1.2.3 PHOTOISOMERIZATION MECHANISM

The mechanisms upon which the DTEs photocyclization/photocycloreversion processes are based are explained below in detail (Scheme 1.10), using as a model the pericyclic reaction from 1,3,5-hexatriene to cyclohexadiene, since both systems are based on the same 6π-electron system. Both systems have six atoms that show overlapping π orbitals, thus obtaining six molecular orbitals.
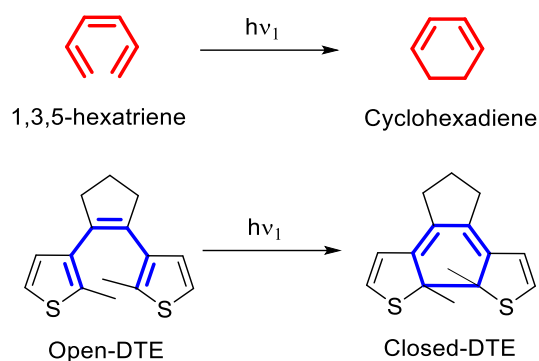
Scheme 1.10. 1,3,5-hexatriene and DTE 6π-electron system
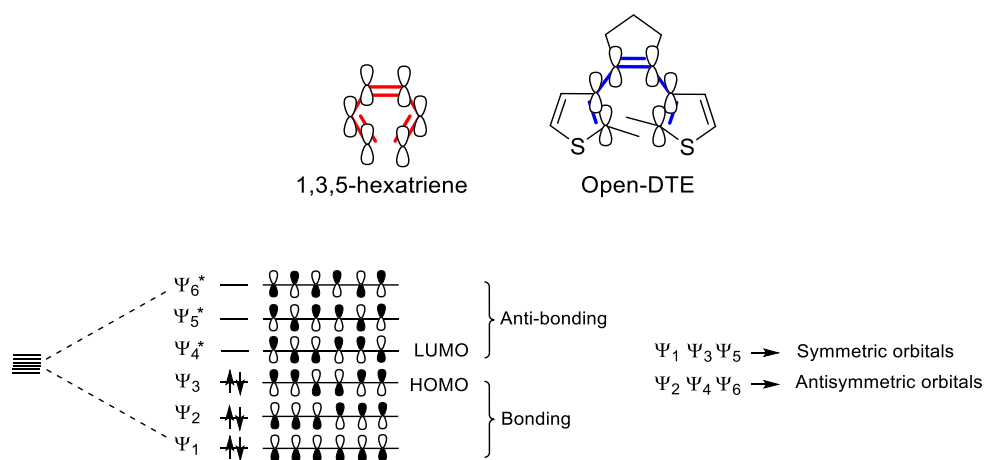
Scheme 1.11. Molecular orbital for 6π-electron system.

In this type of system, the HOMO (Ψ_3) orbital is a symmetric orbital, while the LUMO (Ψ_4^*) is an antisymmetric orbital. The symmetry of these orbitals is essential to understand the mechanism of the pericyclic reaction that occurs in DTEs. A pericyclic reaction is one in which, by cyclical movement of the π-electrons of a system, a sigma bond is formed between the terminations of the system itself. The process by which cyclization occurs can be governed by two possible mechanisms: conrotatory or disrotatory. Scheme 1.12 shows the representation of the mechanisms for the cycling reaction for a DTE depending on the energy state in which it is, following the Woodward-Hoffman rules for pericyclic reactions.[36,37] The first mechanism details the cycling mechanism from Ψ_3, which is through thermal activation of a system of symmetric orbitals. This system causes cyclization through a disrotatory mechanism. As can be seen in the upper part of the diagram, one of the system terminations rotates in a clockwise direction, while the other termination does it counterclockwise, causing the DTE methyls to project towards the plane of the **CF** molecule. Even though this mechanism is described for various cycling processes, it cannot be applied as a valid mechanism for DTEs because they cannot activate the thermocycling process, since they have an enormous activation energy barrier at the ground state, which does not allow the photocyclization process activation

The conrotatory mechanism (bottom part in Scheme 1.12), requires irradiation on the system. Due to this irradiation, a change occurs in the localization of the HOMO orbital ($\Psi_3 \rightarrow \Psi_4$) while changing the symmetry of this molecular orbital. In this case, for the cyclization to be effective,

both terminations must rotate clockwise, projecting each methyl towards one of the faces of the DTE.
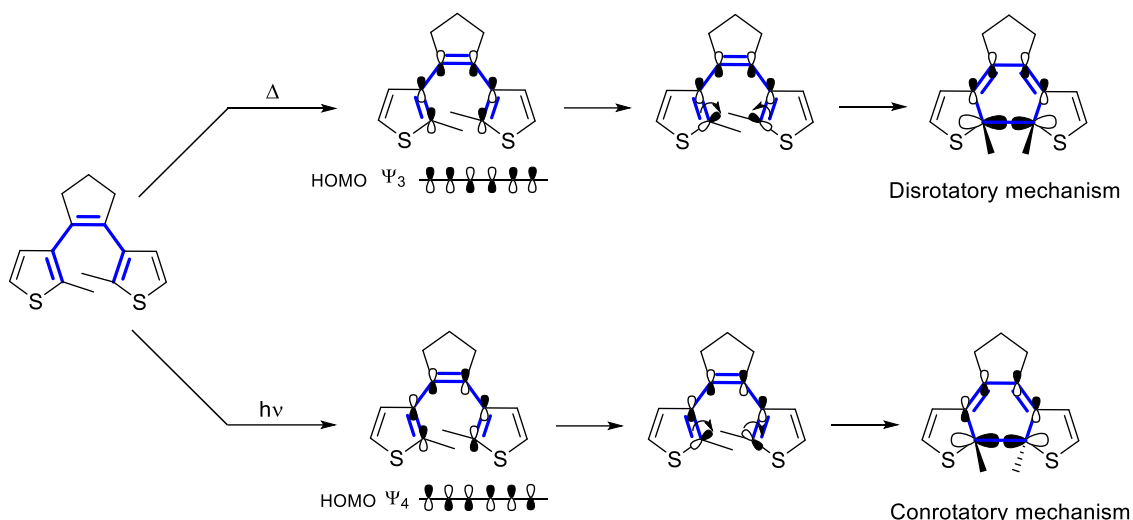
Scheme 1.12. Conrotatory/disrotatory mechanism for a 6π electron system.

The photochemical mechanism for both processes has been theoretically studied in depth by various research groups to understand the isomerization of DTEs.[38] Figure 1.6 shows a graphic scheme obtained from the literature, from which the possible photochemical mechanisms will be explained. As mentioned above, DTEs are photochromic compounds; they activate isomerization processes through light excitation. This is due to a vast activation barrier in the ground state (ΔE_1), which prevents the cycling process and subsequent cycloreversion in S_0, while on the contrary, the energy barrier in S_1 is significantly lower, which allows the photocyclization/photocycloreversion process.
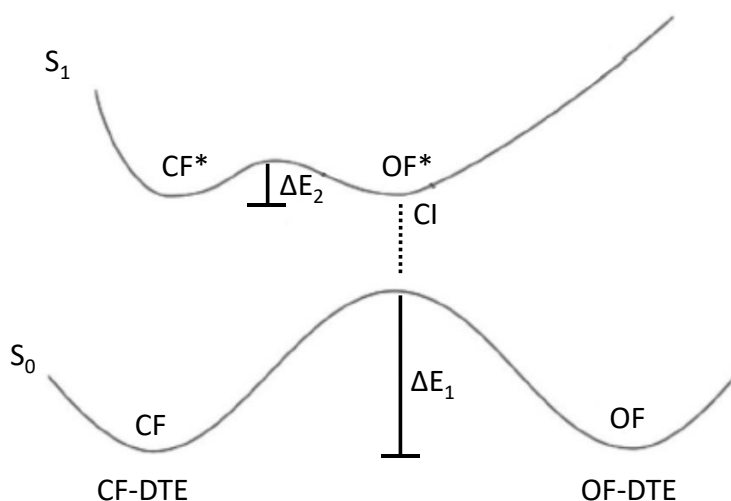
Figure 1.6. Potential energy surface for a model DTE molecule.[39]

Through these theoretical studies (Figure 1.7.) it can be defined that the cyclization mechanism begins after irradiation of the system with UV light, exciting the **OF-DTE** molecules to an excited

state S_1 (solid yellow arrow). Once the molecule is in the excited state, it will seek the greatest stability, moving to the minimum **OF*** energy (dot yellow arrow), coinciding with the conical intersection CI. This coincidence favors the relaxation of the excited state to the ground state, promoting the formation of the closed DTE molecule (purple solid arrow).
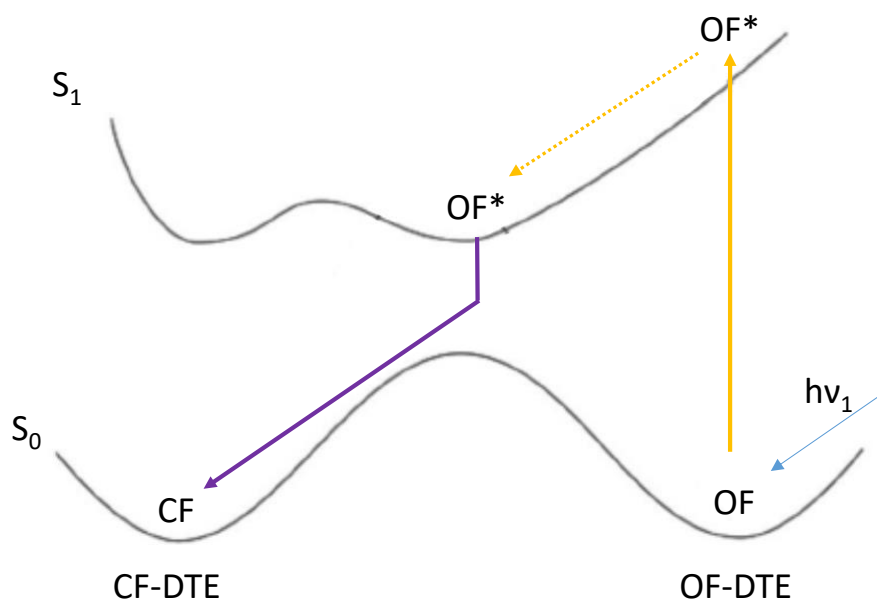
Figure 1.7. Theoretical representation of photocyclization mechanism

The reverse process occurs similarly, where after excitation with visible light, the closed molecule state (**CF**) changes to the S_1 state (**CF***) (solid purple arrow). Once in the excited state, **CF*** can "jump" the activation barrier due to the energy obtained from irradiation, reaching CI (dot purple arrow), where it will decay to the ground state, closing the isomerization process (solid yellow arrow).
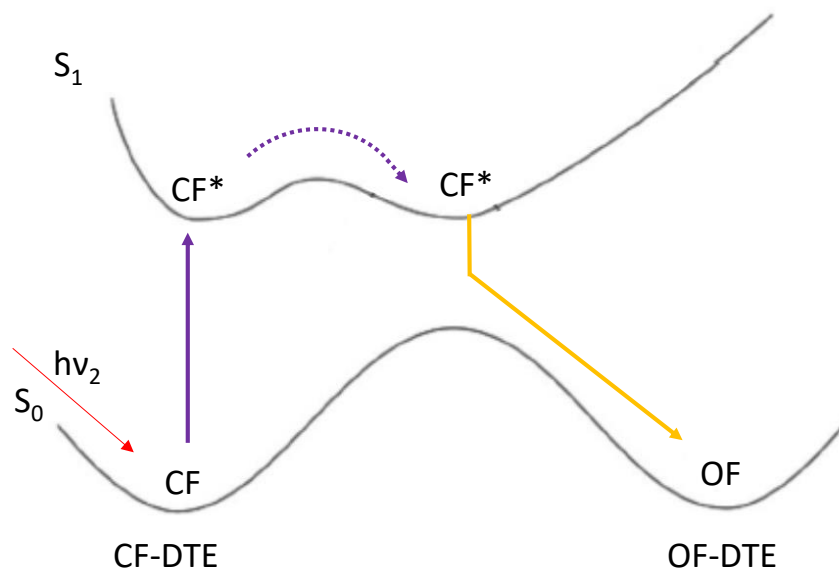
Figure 1.8. Theoretical representation of photocycloreversion mechanism

1.2.4. PHOTOCYCLIZATION AND PHOTOCYCLOREVERSION QUANTUM YIELDS.

In their open form, DTEs can be found in two different configurations, depending on the relative orientation of the thiophene groups, called parallel and antiparallel. Both configurations are in equilibrium, which can interconvert due to the free rotating bonds present in the DTEs open structure. The cyclization process depends on the conformation in which the DTE is found. The antiparallel configuration is the only one that allows the cyclization of the molecule since it is governed by a conrotatory mechanism following the rules described by Woodward and Hoffman.
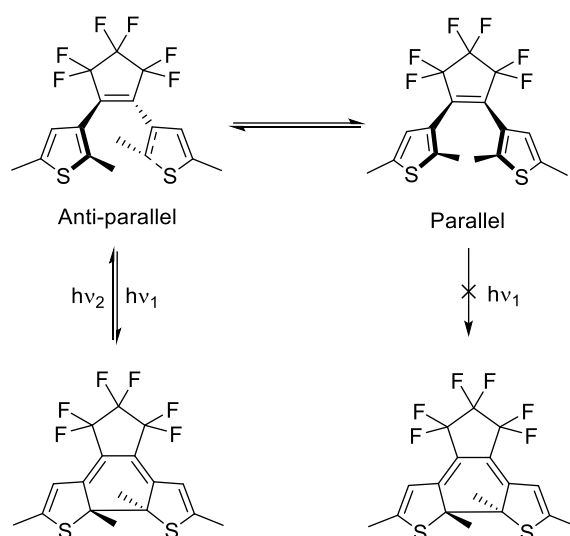
Scheme 1.13. Allowed and forbidden photocyclization process depending on DTEs conformation (anti-parallel or parallel).

Assuming that for each photon absorbed by a DTE, an **OF**-**CF** transformation takes place, the cycling quantum efficiency will be exclusive due to the antiparallel configuration since the parallel configuration of the DTE does not allow cycling. For this reason, during the last decades, different strategies have been studied to increase the efficiency of the process, favoring the antiparallel configuration of the DTE over the parallel configuration in its **OF**. Some of the strategies are shown below:

❖ The introduction of bulky groups or long chains (alkenes) in areas close to the reactive carbons of thiophenes.

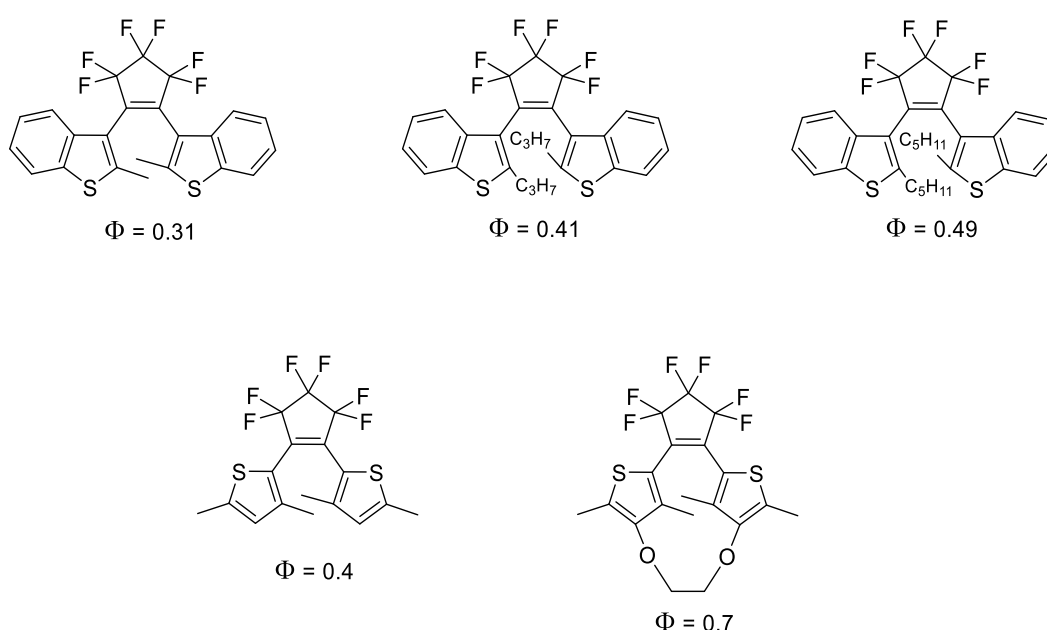❖ The generation of unions that act as bridges between thiophenes, thus reducing their free rotation.

Scheme 1.14 shows different DTEs described in the literature evidencing the differences in the quantum cycling performance depending on the strategy followed, compared to a common DTE.[40,41,42]

Scheme 1.14. Photocyclization yield improvement depending on free-rotation molecules.

Another possible strategy is to generate a larger population of molecules with an antiparallel orientation in the molecule's excited state. The hypothesis is based on an energy transfer from a DTE with a parallel configuration in the excited state to an unexcited DTE molecule in its antiparallel orientation. This hypothesis is only valid when more than one DTE fragment is in the molecule.

Different research groups have tried to confirm this theory. To do this, they designed and synthesized different molecules that contained more than one cyclization point and studied the cyclization process for the individual DTE and the entire molecule.[43] Scheme 1.15 shows some examples published in the literature where they observed that the higher the amount of DTE fragments in the structure, the quantum cycling efficiency increased, although not very significant compared to the individual DTE unit. Despite this, they demonstrated that regardless of the number of DTE fragments in the molecule, only one of the fragments was cyclized, suggesting an energy transfer between the DTEs, allowing an increment in the molecule's photocyclization efficiency.

$\Phi = 0.21$

$\Phi = 0.31$

$\Phi = 0.36$
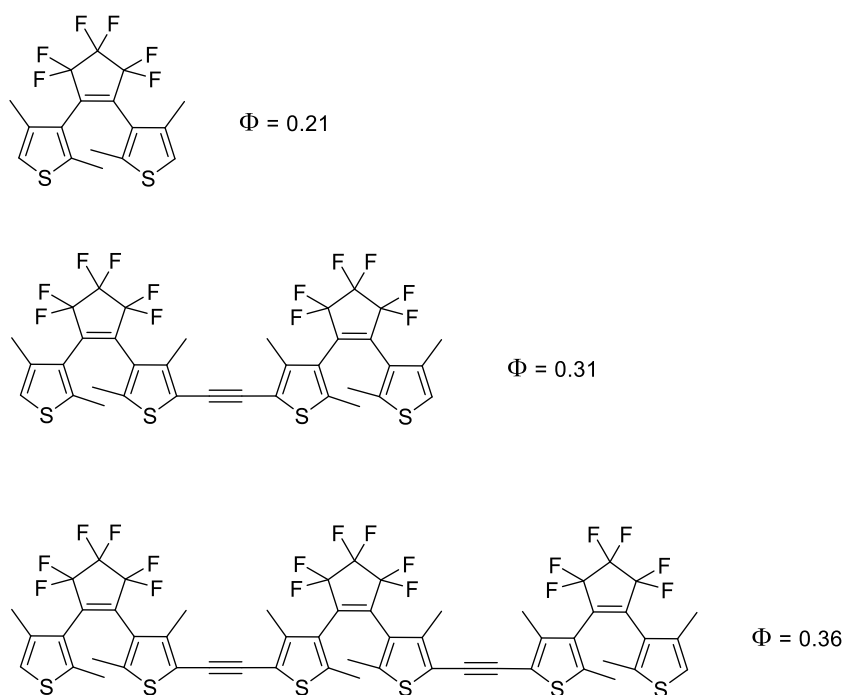
Scheme 1.15. Photocyclization yield depending on number of DTE fragment in the molecule structure.

In addition to the design of the DTE fragment, the reaction conditions in which the pericyclic reaction occurs can also affect the quantum yield, with the polarity of the reaction solvent being the one that generates the most significant changes. Different research works have shown that the use of apolar solvents increases the quantum efficiency of cyclization, while as the polarity of the solvent increases, the quantum yield of cyclization begins to decrease and even be inhibited in some cases.[44] The TICT (Twisted intramolecular charge transfer) effect can explain this trend. This effect influences the orientation of the DTE in the excited state, which can vary between a flat orientation (allows cyclization), using apolar solvents, and a twisted orientation (prevents cyclization), as the polarity of the solvent increases. As can be seen in Figure 1.9, the planar orientation in the excited state is the configuration with the lowest energy (most stable) in apolar solvents. As the polarity increases, the stability of both orientations varies, causing the twisted configuration to become the most stable one. The loss of stability of the planar orientation is due to the generation of a strong dipole between the thiophenes and the hexafluorocyclopentene ring. The appearance of this dipole explains why the cycling process is deactivated, being able to inhibit the process entirely.
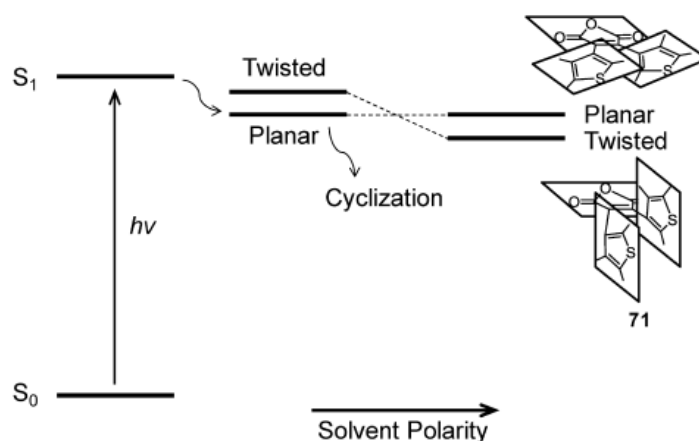
Figure 1.9. Solvent's effect on the DTEs excited state.[44]

On the other hand, a priori, the quantum performance of cycloreversion has a lower efficiency than that of cyclization. This is due, as explained before, to the existence of an energy barrier in the excited state of the molecule, which has to be overcome to reach the minimum energy at which the conical intersection between systems is found. Despite this, the system's effectiveness can be controlled through different strategies:

- ❖ The first factor to take into account is the suppression of the aryl system with long π-conjugation in the system. This is because this type of system generates a red-shift of the absorption maximum of the band corresponding to the **CF**-isomer and, therefore, needs a longer wavelength to excite **CF** to **CF***. The longer the wavelength, the less energetic it is and therefore the more it will cost to overcome the energy barrier of the excited state, reducing the efficiency of the cycloreversion process.
- ❖ Another factor that affects the quantum yield is the introduction of electron attractor groups or electron donor groups near the reactive carbons of the DTE. The introduction of electron attractor groups removes electron density from the system, favoring the cleavage of the bond between the reactive carbons of the DTE, while the donors generate the opposite effect, strengthening the bond created in the cyclization.
- ❖ Finally, the introduction of bulky alkoxy groups causes cycloreversion, but not through the excited state. The insertion of these groups generates that the DTE gains a thermochromic character, decreasing its thermal stability, generating the cycloreversion from the fundamental state **CF** to the ground state **OF**, without the need for light excitation, this effect is observed at 160 °C.

1.2.5 CHIRAL INDUCTION

As previously described, photochromic compounds show two different chemical species that can be interconverted by irradiating with light at a specific wavelength. These transformations generate changes in the compound's properties, such as the color of the material, its structure, or alteration of the magnetic properties, among others. However, one of the most remarkable properties of this isomerization between states is the possibility to generate/modify the chirality of these species through irradiation. There are several examples in the literature where the compounds show chiroptical properties, where changes in the chirality of a compound are observed after photoirradiation, such as fulgides or stilbenes (Scheme 1.16).
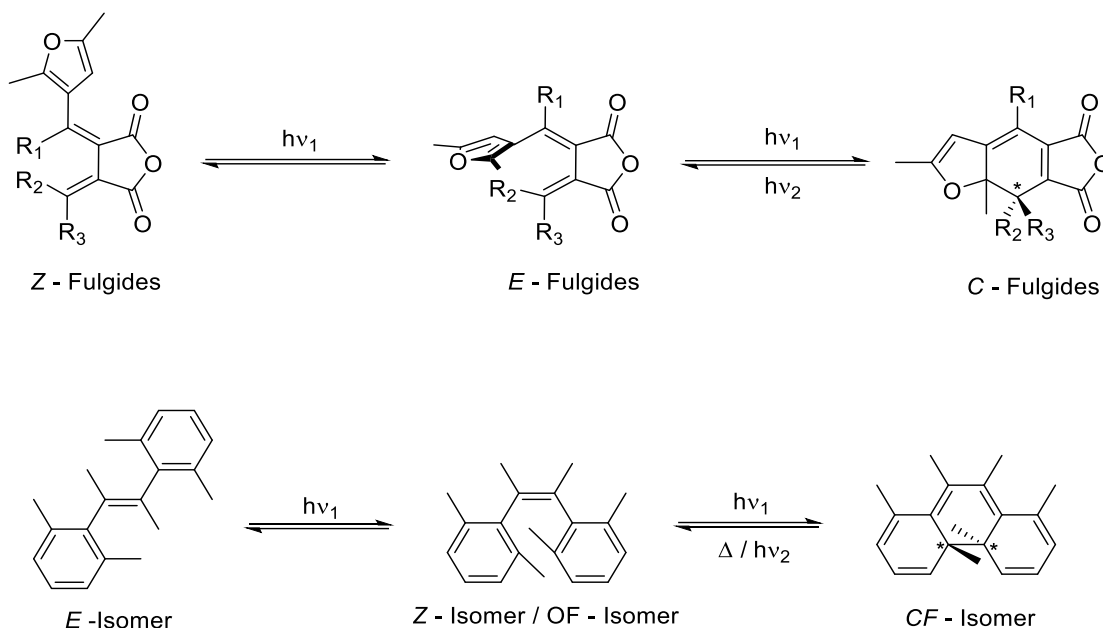
Scheme 1.16. Chiral fulgides/stilbene photoproducts.

This behavior is also observed in DTEs. As indicated above, DTE compounds possess two possible conformations in **OF-DTE**, which rapidly interconvert in equilibrium with the parallel configuration of DTEs.The DTEs structure in their open form contains freely rotating bonds (marked in red in Scheme 1.17), which allows the interconversion of the structure between both conformations, generating an equilibrium between species. Additionally, the antiparallel form of the **OF-DTE**, having C_2 symmetry, is a chiral molecule (formally *P* and *M* isomers). This chirality of the **OF-DTE** is of practical importance only in those examples in which the steric hindrance restricts the rotation of the bonds between the central alkene and the thiophene fragments. Otherwise, they will rapidly interconvert through the parallel isomer.
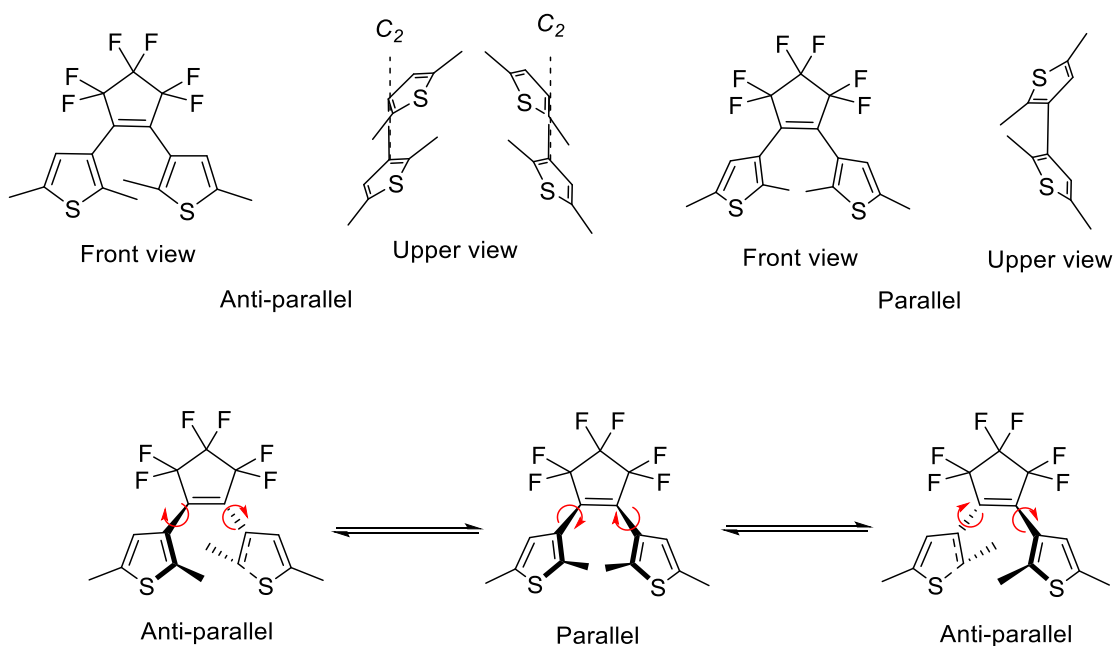
Scheme 1.17. Representative scheme for DTEs anti-parallel and parallel isomers.

A DTE ligand by itself can never induce selective isomerization towards an excess of one of the possible configurations. Therefore, it needs the presence of a factor that introduces chirality in the system (diastereoselective isomerization). The insertion of chiral groups in the structure allows one of the configurations to be favored through steric hindrances, facilitating the generation of a diastereomeric excess after the photocyclization process. Different strategies can be differentiated for the generation of diastereomeric excesses. One strategy tries to obtain a higher percentage of one of the configurations in the **OF-DTE**. The insertion of chiral groups can favor an antiparallel configuration over the other (*M/P* configurations), inhibiting interconversion between isomers. The photocyclization process will also be affected by achieving an excess of antiparallel **OF-DTE**, obtaining an excess of one of the diastereoisomers. The other strategy focuses on the **CF-DTE** isomer. If the insertion of a chiral group favors a configuration after the photocyclization process (*RR* < *SS*), it would be necessary for **OF-DTE** to maintain a rapid equilibrium between the different configurations. Therefore, the use of non-bulky chiral groups would favor a rapid equilibrium between isomers, favoring one of the configurations of the **CF-isomer**. Lastly, a chiral environment could be used as a chiral factor for an enantiomeric isomerization (be it due to the action of a chiral solvent or the presence of, for example, a DNA fragment in the environment), which favors isomerization towards one of the diastereoisomers.

Various research groups studied the concept of generating a diastereoselective cyclization of a DAE. Yamaguchi et al. synthesized two DAEs (**E-10** and **E-11**), which had an *L/D*-menthyl group in position 2 of one of the benzothiophenes, close to the reactive carbon during the pericyclic reaction.[45] The strategy of introducing the chiral group near the reactive carbon aims to favor one of the diastereomers during the photophysical process, generating a diastereomeric excess.
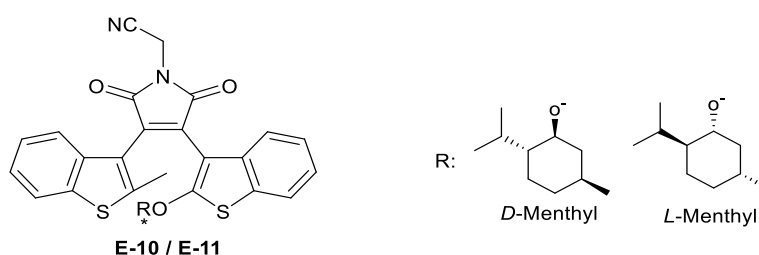

Scheme 1.18. **E-10** DTE by Yamaguchi and coworkers.

The photochromic character of the compound could be confirmed utilizing UV-Vis spectroscopy; despite this, it was found that compound **E-10** did not generate a diastereomeric excess after the photocyclization reaction in solution. They observedthe presence of part of the open isomer **OF-E-10**, and the formation of the two diastereomers *RR*-**CF-E-10** and *SS*-**CF-E-10**, in equal proportions as confirmed by circular dichroism spectroscopy. In order to study asymmetric induction, Yamaguchi et al. decided to proceed with the photocyclization reaction for compound **E-10** by altering the polarity of the solvent where the photophysical process was carried out. From the results obtained, they determined that the solvent and temperature play a fundamental role in the formation of diastereomeric excesses after the cyclization process, obtaining better diastereomeric excesses with more polar solvents at low temperatures (-40 °C). (Figure 1.10)
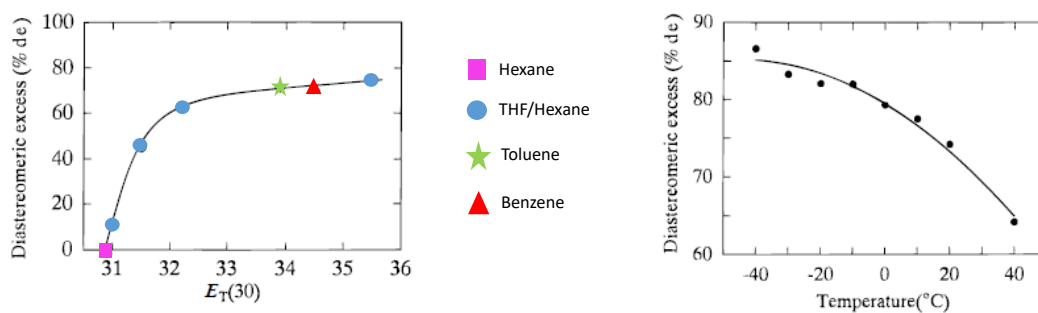
Figure 1.10. Left) Comparison of the effect of solvent polarity with the generation of diastereomers; Right) Comparison of the effect of temperature on the generation of diastereomers in toluene.

Few years later, Feringa *et. al.* synthesized a DTE compound that contained chiral (*R/S*)-1-phenylethylamides appended to the thiophene fragments.[46] These systems were capable of self-aggregation due to the amide bonds present in the structure.
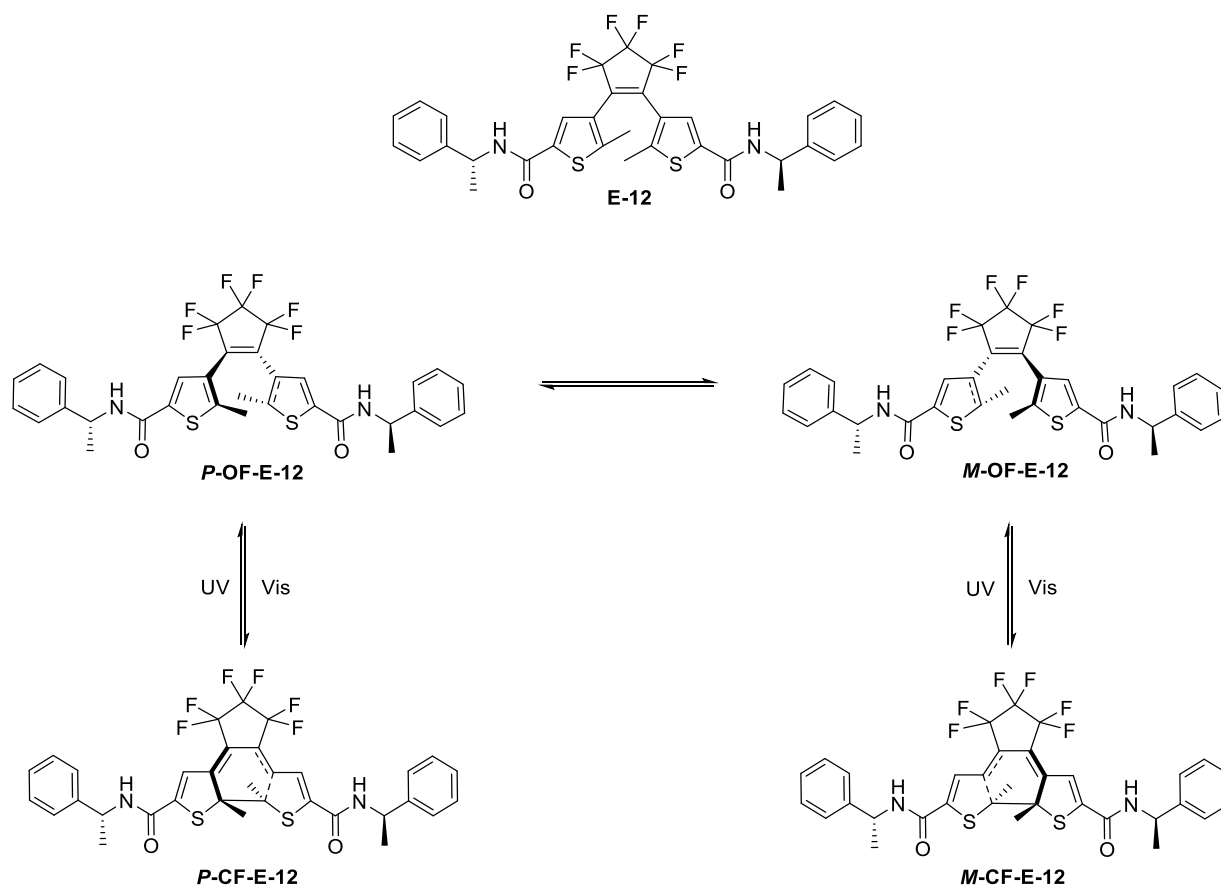
**Scheme 1.19.** Schematic representation of synthetized **E-12** and its possible isomers.

Although the system did not present diastereoselective photocyclization in solution, TEM studies on the aggregated material in gel solutions (toluene at concentration >1.6 mM) showed that it is arranged in the form of a helix in space, resulting in a chiral macrostructure already in the **OF-isomer** (Figure 1.11).
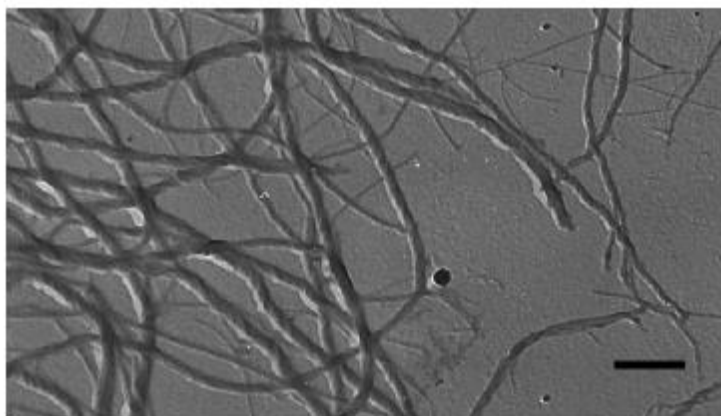
Figure 1.11. TEM image of *P*-**E-12** aggregated system.

The gel or aggregated system is obtained by cooling down a solution of the selected DTE in toluene, which shows photochromic properties under UV-Vis light irradiation. Following the photocyclization process of the aggregated material by circular dichroism spectroscopy they observed the generation of an enantioenriched system due to the appearance of strong band around 320 nm. This band disappears as the sample is heated up due to a decrease in viscosity generated by a liquid environment that, as previously demonstrated, did not offer chiral induction. The 320 nm signal in CD can be recovered by cooling the **E-12** solution when the aggregated is regenerated. The observed chirality was attributed to the preferential formation of *M*- or *P*-supramolecular aggregates of the **OF** isomers. As can be shown in Figure 1.12, by NMR spectroscopy, they observed a clear correlation between the measured diastereomeric excess and the degree of aggregation, confirming the correlation existing between both phenomena. Upon irradiation of this aggregated system at 313 nm, they observed a PSS containing 40% of **CF-DTE** with an excellent diastereomeric ratio (98:2). As expected, the chirality P or M of the gelified supramolecular structure in the open form and the one formed upon its photocyclization depended on the chirality (R or S) of the appended amide. This was the first example described in the literature where an outstanding chiral induction was obtained in an aggregate system since, until this moment, satisfactory chiral induction results had been observed exclusively in crystalline DTE systems[47,48].
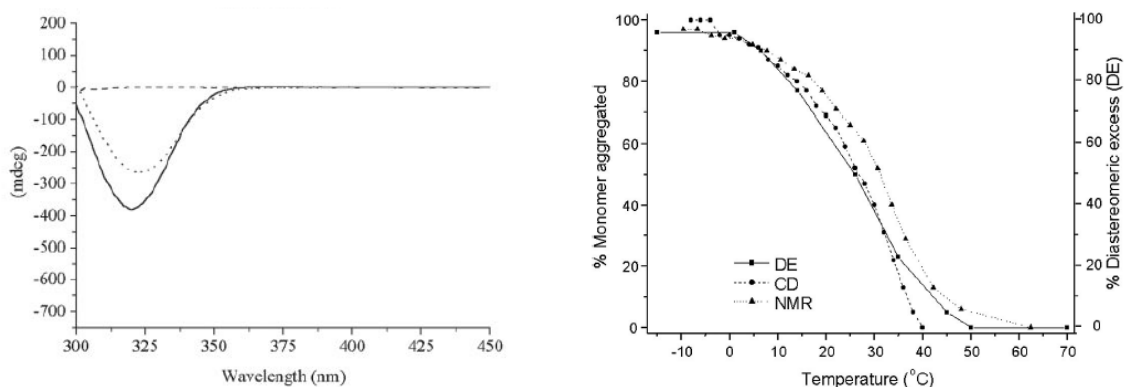

Figure 1.12. Left) CD spectrum for DTE-aggregate confirming chiral induction. Right) Dependency between %monomer aggregates and % diastereomeric excess vs temperature.

Thus, these results confirmed a very effective chiral induction in the supramolecular aggregation of a chiral DTE system, both in the open and closed forms.

Various research groups confirmed that the diastereoselective photocyclization of a chiral DTE could not be achieved when the system is in solution, while, for crystalline systems[49] or gel-like aggregates, it could work with high selectivity.

In a seminal work, Andréasson *et al.* demonstrated that it was possible to induce enantioselectivity in the photocyclization of a a non-chiral DTE system in solution, through its interaction with DNA strands.[50] They synthesized methylpyridinum and methylquinolium-appended DTEs (**E-13** and **E-14** in Scheme 1.20). These compounds showed an effective photochromic behavior under irradiation at λ = 366 nm, obtaining photostationary states (PSS) with 98% **CF-E-13** and 96% by **CF-E-14**. The photocycloreversion process was induced through irradiation (λ > 530 nm).
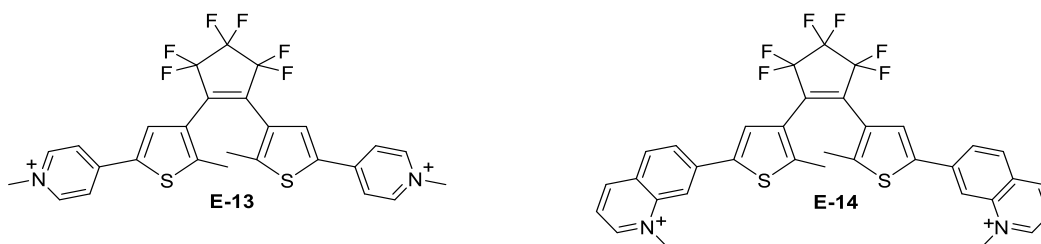

Scheme 1.20. DTE compounds synthetized by Andréasson for chiral induction studies.[50]

Adding DNA to these compounds induced a significant change in the absorption spectrum associated with the interaction between DTE and DNA. Similarly, they studied the behavior of different DTE/DNA ratios through UV-Vis spectroscopy. They observed how at high DTE/DNA ratios, the intensity of the band obtained decreased while the maximum absorption remained constant. On the other hand, when the DTE/DNA ratio decreased, they observed that the band's intensity increased; in addition, the absorption maximum shifted to longer wavelengths. Andréasson associated this displacement of the absorption maximum with different types of binding between DTE compounds and DNA strands.

To observe if there was a chiral induction in the pericyclic reaction, they studied the cyclization process through circular dichroism spectroscopy. By adding the strands of DNA, they observed how these samples did offer a signal by CD. Studying the type of interaction between DTE and DNA, it was established that the intensity of the CD signal depends exclusively on the type of interaction that occurs, and it may be an electrostatic interaction (little contribution to the CD signal), observed for high ratios DTE/DNA or a specific interaction generated at lower DTE/DNA ratios, which offers a high contribution to the CD signal.

Likewise, they studied the DTE-DNA interaction employing linear dichroism spectroscopy (LD), where the signal can be negative or positive depending on the type of interaction with DNA. The signal sign depends exclusively on whether the DTE fragment is bound between base pairs of the DNA (negative signal) or generates an iteration through interaction in the groove of the DNA (negative and positive signal). As shown in Figure 1.13, it can be seen how the **OF-isomers** and **CF-E-14** exclusively offer a negative signal, while only **CF-E-13** have a contribution from both signals, thus indicating that the binding of the DTEs varies depending on the isomer in which they are found.
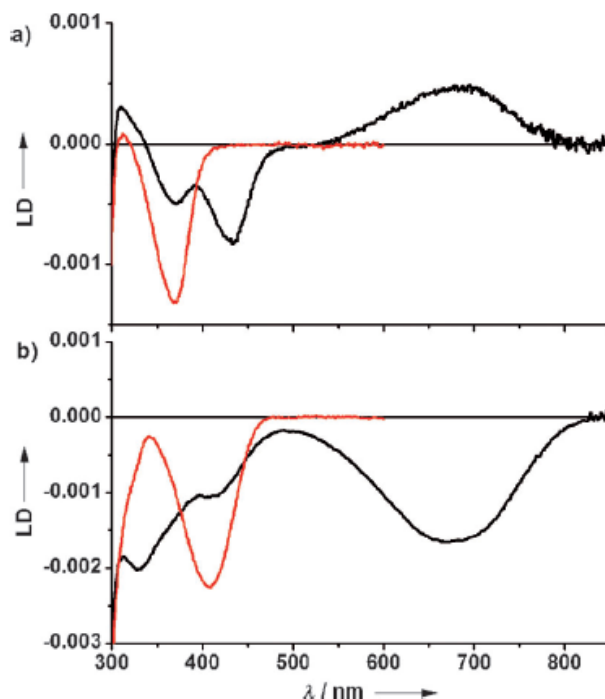
Figure 1.13. a) LD spectra for **OF-E-13** (red) and **CF-E-13** (black). b) LD spectra for **OF-E-14** (red) and **CF-E-14** (black).

Due to the possibility of different interactions between DTE and DNA, depending on the isomer in which they are found, Andréasson studied the the photocycling process in different chiral environments to observe whether these environments generated a stable chiral induction in the DTE. Two **OF-E-14** samples were irradiated: - a sample in the presence of DNA (*sample A*), and an **E-14** sample to which DNA fragments were added after the cyclization process (*sample B*). The induction process was followed in the presence of DNA utilizing CD, observing, a small band at 670 nm indicating a slight enantiomeric excess in the sample. On the contrary, after cyclization of **E-14,** and subsequent addition of DNA, they observed an intense signal at 668 nm, that is generated when DNA is added. The appearance of the signal was associated with the union between DTE-DNA, indicating that even in solution, the closed isomers rearrange after the addition of the DNA, obtaining an enantiomeric excess. Finally, to verify that this induction was stable without DNA, they used SDS (sodium dodecyl sulfate micelles) to remove the DNA from the sample. As Figure 1.14 shows, when extracting the DNA from *sample A*, the shoulder associated with a slight enantiomeric excess disappears, generating a racemic mixture of isomers in 1:1 proportion, while for *sample B* (DNA added after photocyclization), the signal in the CD spectrum is maintained, showing for the first time the chiral induction of a photochromic system in solution.
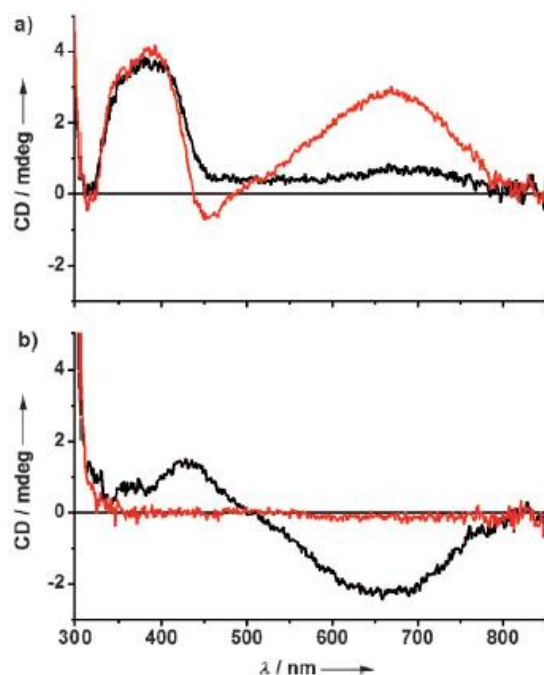
Figure 1.14 a) CD spectra of *sample A* (black) and *sample B* (red) after photocyclization process. b) CD spectra of *sample A* after SDS treatment (red) and *sample B* after SDS treatment (black).

1.2.6 APPLICATIONS BASED ON DITHIENYLETHENES DERIVATIVES

DTEs are the most promising photochromic molecules for in the development of new photo-functional materials. Its high potential is due to their high thermal stability, which inhibits the cycloreversion reaction, a short response time to the photocycling process through a UV stimulus, and high quantum yields of photoisomerization. In addition, DTE offers excellent fatigue resistance, as explained before. Therefore, this type of molecular switch has been used in various applications such as molecular motors, photochromic cages, or memory devices.

Photochromic memory is based on a photochromic recording method that differs from conventional optical memory methods. The photochemical recording has certain advantages in terms of image resolution, writing speed, or multiplex recording. The information reading property provided by the photoswitchable molecules must be non-destructive to be applied as an optical memory device. This is because if the UV-Vis absorption spectral regions are used as the recording and reading wavelengths of the device, it will cause the recorded information to fade during the process.[51] Because of this, one of the most effective reading methods for these materials is the use of IR absorption. The use of IR light is very effective when significant changes in this region of the spectra are detected between the open and closed isomers because it does not affect the isomerization process, so the information recorded on the material can be read indefinitely without any decomposition.[52,53]

To create systems capable of acting as photochromic recorders, Uchida et al. designed two DTE ligands (**E-15** and **E-16**), which presented excellent thermal cycloreversion resistance and fatigue resistance, essential properties for an excellent non-destructive readout system (Scheme 1.21).[54]

24

E-15   **E-16**
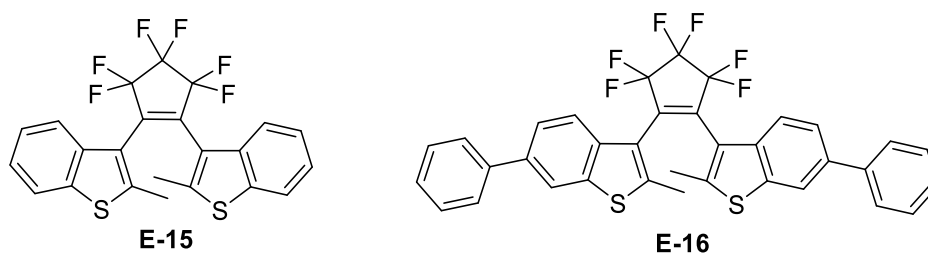
Scheme 1.21. DTE ligands synthetized by Uchida for construction of readout devices.

They studied possible variations in the absorption of these compounds in the IR region depending on whether the DTE was in its open or closed form. For the **OF-E-15** compound, no band was observed in the spectral region between 1500–1700 cm^{-1}, while after the photocyclization process, the **CF-E-15** isomer showed three different bands in this spectrum region (1625 cm^{-1}, 1585 cm^{-1}, and 1549 cm^{-1}). On the other hand, **E-16** did show absorption bands in that region in the open form of the DTE, but these did intensify after the photocyclization process (**CF-E-16**). Uchida's group inserted the **E-16** compound into a polymeric matrix (Zeonex), which does not have any absorption in the IR region, which guarantees that any observable change is dueto the DTE fragment. The readout process is based on irradiating the whole film, causing the photocyclization of the inserted DTE fragments. After that, the system is irradiated with visible light, through a mask that has the information to be transcribed, generating the photocycloreversion process only in the areas where polymer is exposed to light. Later, the image is revealed under IR light at 1590 cm^{-1} (Figure 1.15). It can be seen how the IR absorption difference between **OF-E-16** and **CF-E-16** is such that it allows obtaining the information clearly and without changes during long periods of time.
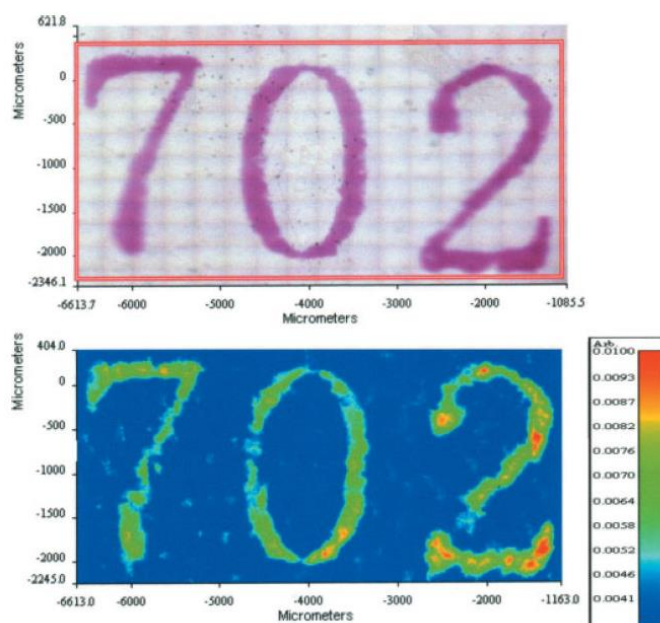

Figure 1.15. IR imaging for readout devices based on **E-16**.

Similarly, the substituents' effect can increase the difference between the absorption of open and closed isomers in the IR region. This effect is produced by the difference of electron donor substituents versus electron attractors at the 5,5' position, since they exhibit a push-pull-push effect.[55,56] On this basis, several examples of non-destructive IR reading were described, using DTE-doped films[57,58], polymers[59] or amorphous films[60].

Another application in which DTEs can take part are photomechanical materials. Organic

photomechanical materials are those that, through a photoisomerization process, can promote a mechanical effect on a macroscopic scale such as bending, twisting or rolling movement.[61,62] These systems can be created by introducing DTE fragments in solid-state materials or polymeric systems, showing excellent advantages in their introduction in nanostructures, such as the high hardness of the material or a high speed of response to the stimulus.

When the photochromic system is in its solid-state and reproduces the cyclization reaction, it undergoes an anisotropic expansion of its crystal structure, as is shown in Figure 1.16. The material expansion can be limited to one phase of the crystal lattice, producing mechanical bending, twisting, or extension movements.[63,64,65] However, using this type of system entails different limitations, such as the proper growth of the crystal or the low resistance to mechanical fatigue, leading to the rupture of the crystalline phase due to stress.
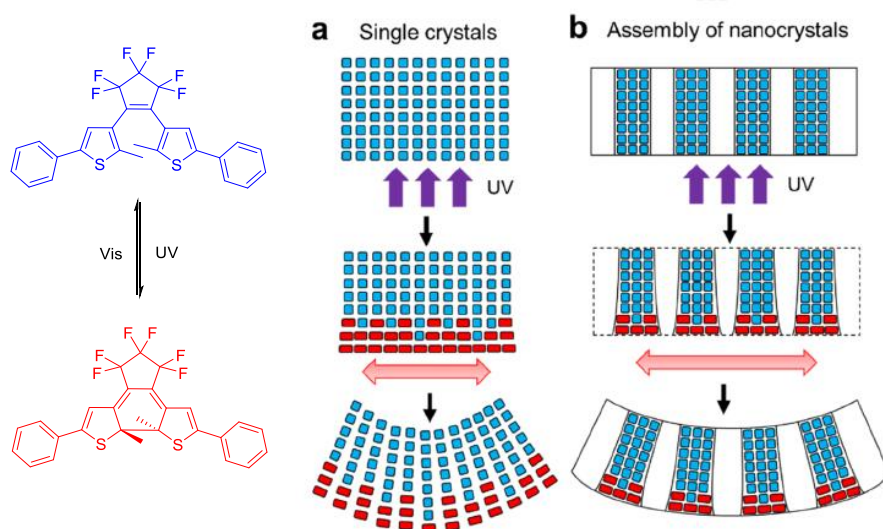
Figure 1.16. Schematic vision of the anisotropic expansion due to the photomechanical process for DTE solid state materials.[66]

Morimoto and Irie described a crystalline system capable of bending under the irradiation of UV light.[67] They designed and synthesized a DTE that exhibited an effective photochromic character (photocycling at λ = 365 nm and photocycloreversion at λ = 440 nm) and used it to create a photomechanical system. They obtained hybrid crystals composed of a mixture of **E-17** and naphthalene (NF), where they were able to observe an effective arrangement of the DTEs in their antiparallel form[68], presenting a distance between the two reactive carbon atoms sufficiently small to be able to carry out the cyclization (3.7 Å). (Scheme 1.22)
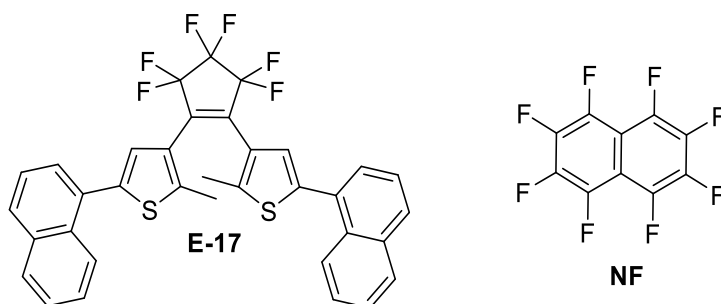
Scheme 1.22. DTE ligand synthetized for photomechanical studies.

They conducted a photomechanical study irradiating the crystal on one of its faces at 365 nm.

As the crystal was irradiated with UV, they observed how it generated a bend in the opposite direction to the light. This bending process increased as the irradiation time increased, stopping when the irradiation was stopped. On the other hand, after irradiating the glass with visible light, they were able to see how it returned to its original shape, verifying that the photochromic effect directly affected the photomechanical effect of the crystal. Morimoto describes that, by studying the photomechanical effect of the crystal, they were able to associate the bending only with a thin layer of the DTEs that made it up. This is due to the high efficiency of the compact glass to absorb UV light, preventing it from reaching the inner layers of the glass, as can be seen in Figure 1.17.
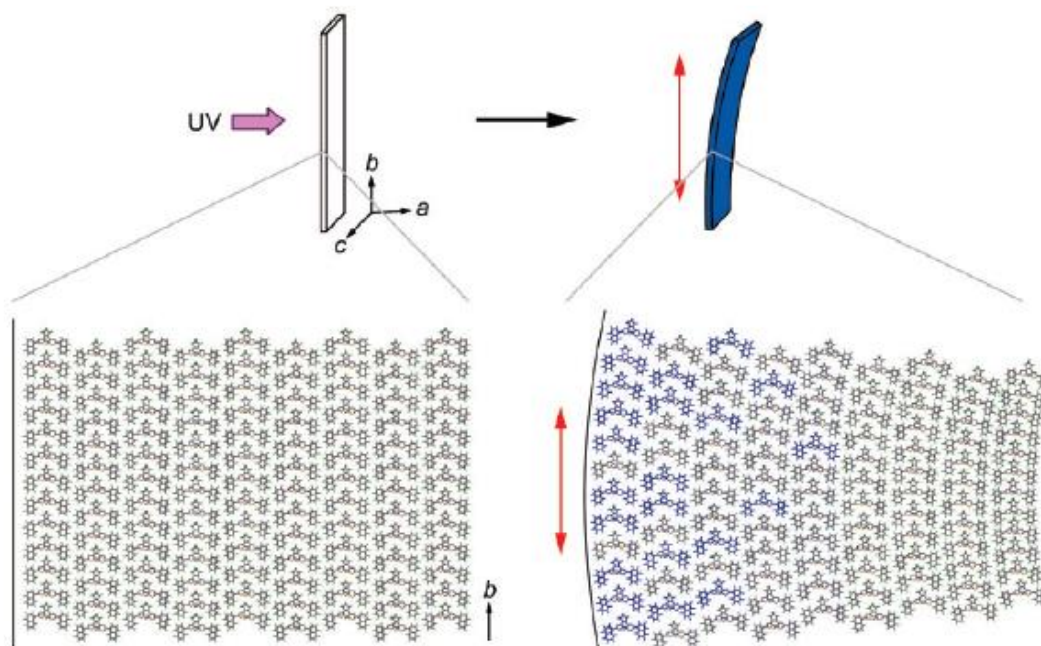

Figure 1.17. DTE-based crystal bending studied by Morimoto et al.[67]

This high absorption efficiency also prevents the rupture of the crystal due to mechanical fatigue that the photocycling process can generate throughout the crystal. In addition, Morimoto highlights two other factors that help the glass not break due to fatigue. On the one hand, the design of the ligand is essential due to the conformational change that it generates after cyclization. The choice of **E-17** was to guarantee that the unit cell of the **OF-E-17** and **CF-E-17** compound was not completely deformed during the process. It reorganizes without significantly affecting the structure of the unit cell. On the other hand, using naphthalene in the crystal structure has a reorganizing effect. This is due to the π-π interactions generated between the NF and the hexafluorocyclopentene of the DTE fragments. When photocycling occurs, the intermolecular distances between these two components are reorganized, generating stability in the crystal despite suffering large deformations.

With this, Morimoto created a photomechanical system that effectively induces the bending of a crystal based on a mixture of DTE and NF fragments, thus generating a photomechanical system that, from molecular processes, is capable of generating a change on a macroscopic scale.

One of the significant challenges of applying molecular switches in the real world is their application in systems that act as molecular machines. Feringa was among the first to investigate this possible application of photochromic systems, inspired by molecular motors that can be observed in nature, such as muscle contraction or the generation of ATP in a living system. Feringa et al. described a new concept that used light irradiation to generate movement of a

highly hindered alkene system (overcrowded alkene), which was capable of carrying out an *E-Z* isomerization of the alkene, generating unidirectional mobility of the system (Scheme 1.23)[69-71]
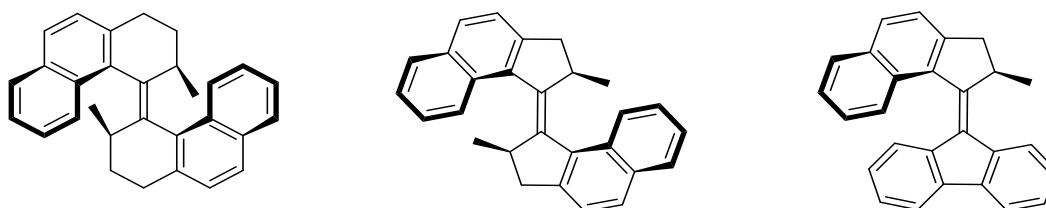
Scheme 1.23. Unidirectional molecular motors examples described by Feringa.

After successfully creating this type of system, Feringa was interested in inserting a second different photochromic fragment that could act as a second motor in the system, controlling the mobility of the molecular machine. For this reason, DTE fragments were coupled to the overcrowded alkene system because their isomerization generates characteristic absorption bands, where usually the rest of the system does not absorb.[72] Based on this idea, compound **E-18** was designed and synthesized, where the insertion of the DTE through an alkyne spacer to the molecular machine can be observed (Scheme 1.24).
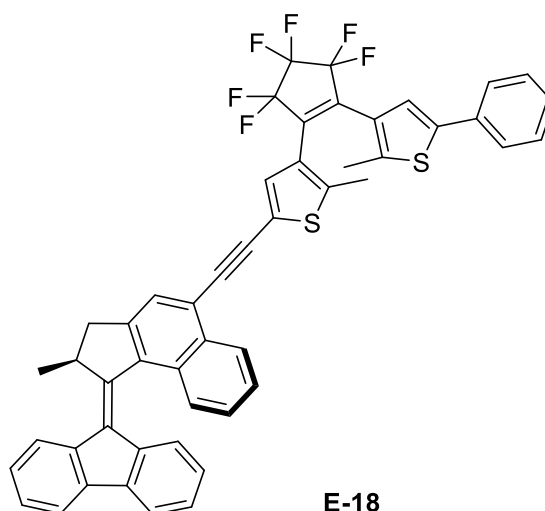
E-18

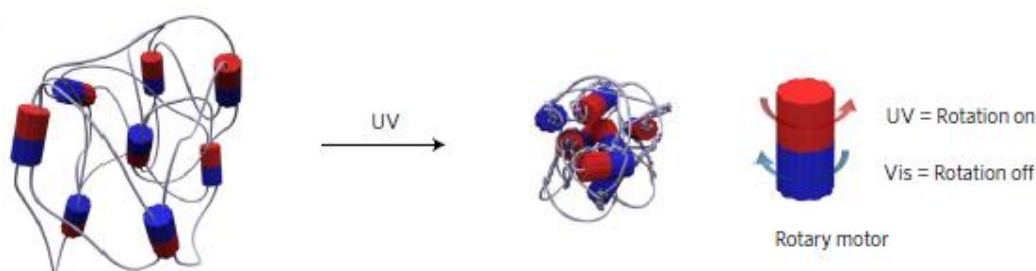**Scheme 1.24**. Molecular motor combaining *E-Z* and phoyocyclization/photocycloreversion processes.

When comparing the free molecular rotor and **E-18** properties, they observed that the addition of the DTE fragment generated a red-shifted absorption, from λ = 395 nm to λ = 425 nm, allowing the use of visible light to activate the molecular motor. This red-shift was associated with the extension of π-conjugated bonds generated by the insertion of the DTE. This aspect is of great importance because, at this wavelength the DTE fragment does not absorb, which allows the use of a specific wavelength only to activate the unidirectional motor. After verifying that the efficiency of the molecular motor with the incorporated DTE did not present significant differences compared to molecular motors previously synthesized by the group they studied the effect of the isomerization of the DTE on the system. The system was irradiated with UV light (λ = 312 nm), quickly observing the photocycling process of the DTE through the appearance of the band associated with the closed DTE (λ = 602 nm), demonstrating the photochromic character of the DTE in the system. Once the PSS of the system had been reached, they irradiated the molecular motor at the specific wavelength for the unidirectional motor (λ = 455 nm), without actually observing significant changes in the ultraviolet-visible spectrum, thus indicating that the photocycling of the DTE prevents the E-Z isomerization from the system under irradiation in the

visible. Finally, after irradiating the closed system at a longer wavelength (λ = 528 nm), they verified the photocycloreversion process of the DTE and the subsequent activation of the unidirectional system, activating the molecular motor movement again (Figure 1.18). In this manner, Feringa introduced a new concept regarding molecular machines were using different wavelengths; the motor can be activated/deactivated, controlling its movement.
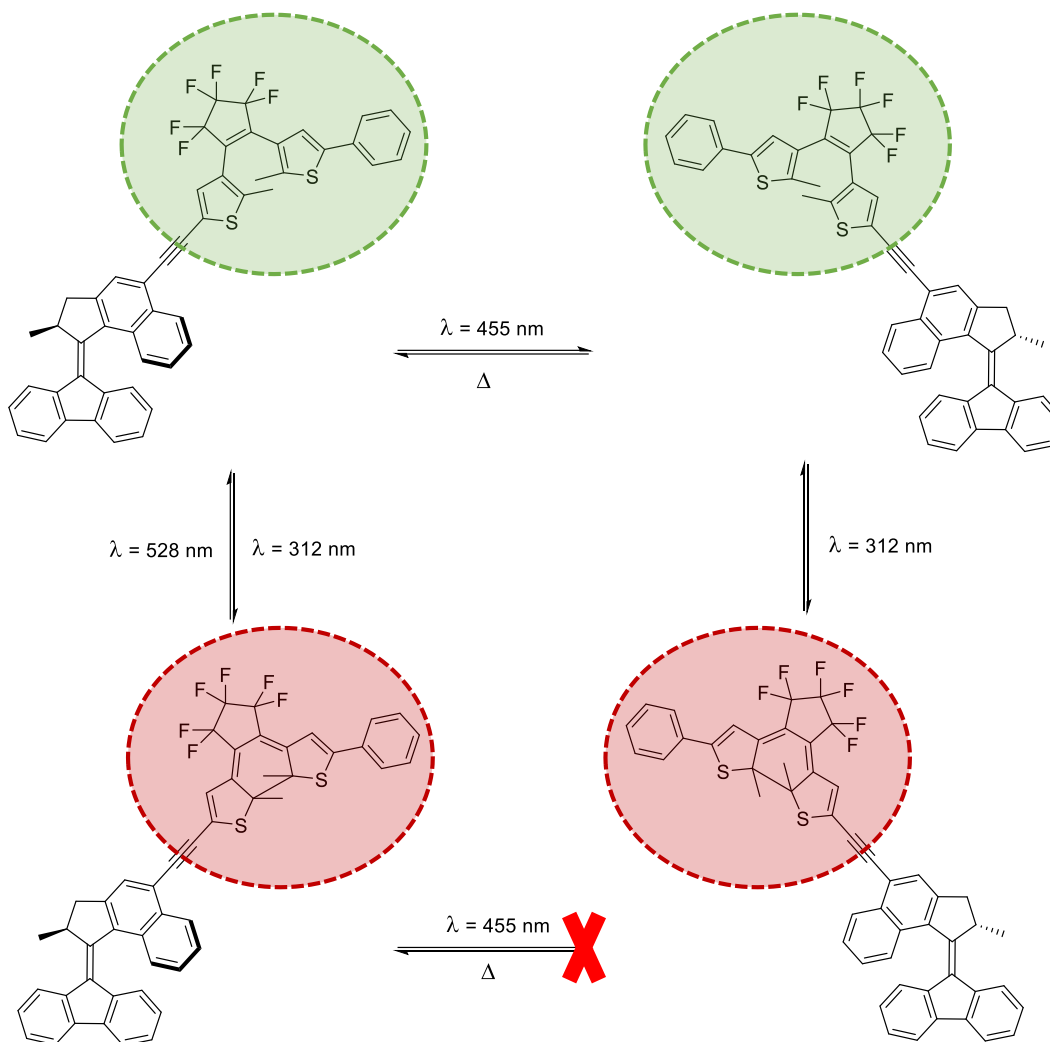

Figure 1.18. Representative scheme for the on/off mechanism for **E-18**.

Inspired by Feringa's molecular machines, Giuseppone et al. focused on obtaining polymer matrices capable of contracting through the incorporation of overcrowded alkenes as nodes. Under UV irradiation, the continuous unidirectional rotational motors cause the progressive folding of the polymer matrix and shrinking of the material, as shown in Figure 1.19.[73]

In their desire to generate a reversible process (controlled folding-unfolding of the polymeric material), they incorporated DTE fragments intending to generate the opposite movement to generated by the molecular rotors.[74] The main idea was to use the overcrowded alkene as a mechanism of polymer contraction through UV irradiation, and the photo-cycloreversion of a closed DTE to expand the polymeric matrix, as represented in Figure 1.20.
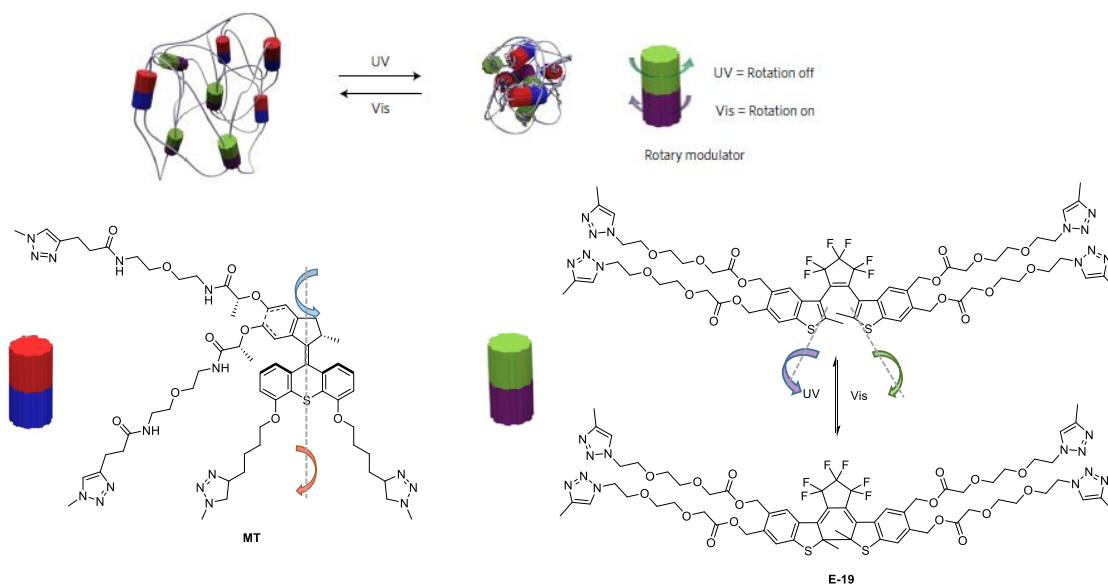
Figure 1.20. Polymeric matrix introducing a motor (MT) and **E-19** as modulator fragment.[74]

They synthesized gels with different percentages of molecular motor (overcrowded alkene) and modulator (DTE fragment), obtaining four different matrices. (Table 1.3).

Table 1.3. Motor-Modulator (**E-19**) ratios for the formation of polymeric motors.

Polymer Gel	Motor (%)	Modulador (%)
G-0	100	0
G-12	88	12
G-25	75	25
G50	50	50

They initially studied the polymer compression process employing UV irradiation and observed that the four systems contracted after irradiation with UV light, also observing that the contraction speed depended to a great extent on the percentage of the modulator, being faster the less modulator the system had, which may be due to a competitive process between both isomerization (E-Z isomerization and photocyclization/photocycloreversion). He also verified that the DTE doped systems had a maximum absorption band around 530 nm, associated with the **CF-E-19** band. This may be due to a competitive process between both isomerizations. On the other hand, he observed that the UV irradiation did not reach the inner layers of the polymer matrix but that it generated only change in the outer layers, as Morimoto observed in his crystalline systems.

Once it was verified that the shrinkage of the polymeric system was effective, they irradiated the different polymers with white light. They verified that, as expected, the system that was formed exclusively by the molecular motor did not show any changes. On the other hand, the gel doped with modulator systems unfolded, returning to the initial shape. They associated this

movement with the DTE photocycloreversion process, from which the DTE fragments cease to exist in their planar and rigid form to give rise to greater mobility of the system. Furthermore, they included two additional factors that can influence the expansion of the system: the polymer's inherent elasticity, which drastically influences the expansion process, and the polymeric matrix's medium (studies in suspension or solid reported different results). For instance, the presence of solvent in the structure facilitates its expansion, while in a solvent-free environment, the system's expansion could not be observed.

The examples described are just selected examples of how there are plenty of opportunities to use DTE ligands in different applications of great utility to society. For this reason, in recent years, the number of new applied systems based on these photochromic fragments has increased significantly, focusing the scientific community's attention on the development of improved systems for existing applications and the search for new applications.

1.2.7 ORGANOMETALLIC DITHIENYLETHENE DERIVATIVES

The use of photoswitchable organic molecules has spread to other areas of chemistry, such as organometallic chemistry. For several decades, there has been an interest in the insertion of molecular switches in organometallic complexes to improve/alter the properties of the compounds through the use of light.

The first example of organometallics containing DTE in their structure was described in 1999 by Lehn and coworkers.[75] Lehn's work used pyridine-functionalized non-symmetric and symmetric DTE ligands (Scheme 1.25), to generate mononuclear complexes of tungsten and rhenium, or dinuclear ruthenium, tungsten or rhenium complexes.
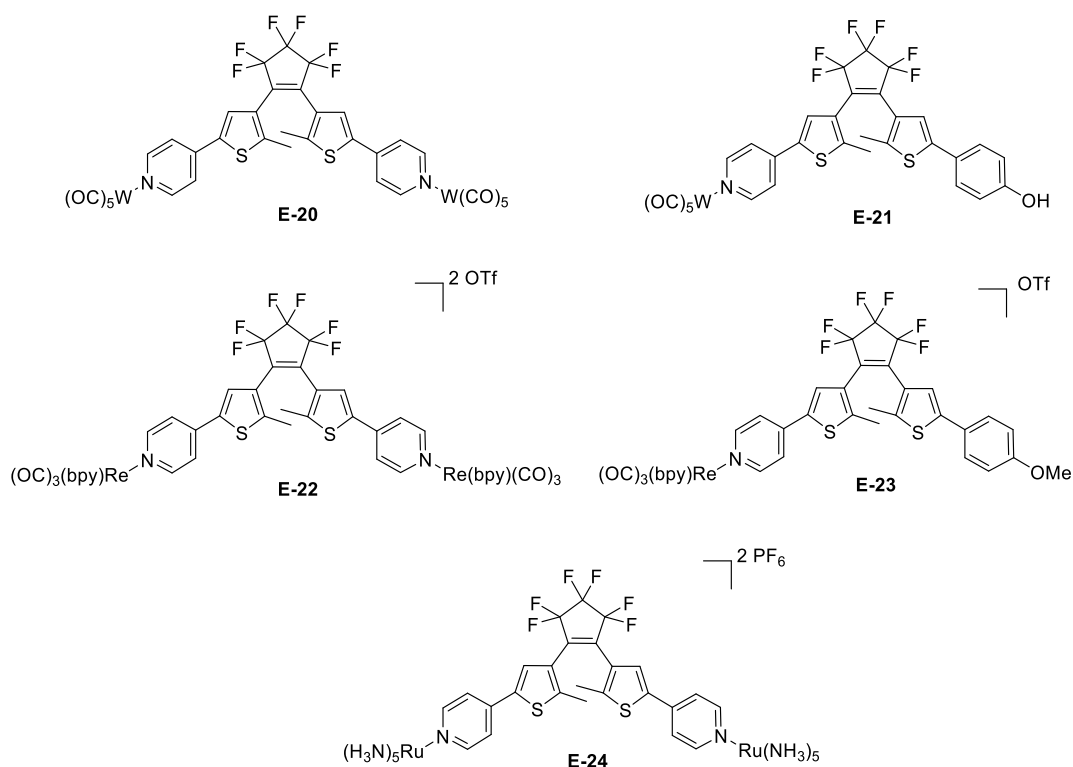
Scheme 1.25. First examples of organometallics containing DTEs described by Lehn et al.

Lehn successfully verified that the **E-20** and **E-21** tungsten compounds and **E-22–E-23** rhenium complexes offered a photochromic character similar to that obtained for the free DTE ligands.

At the same time, the isomerization process was not observed for **E-24** since the ruthenium compound decomposed under UV irradiation. Subsequently, they carried out a study to verify the emitting properties of the compounds, choosing a wavelength in which the photocyclization process had the least possible impact (λ = 240 nm). The results obtained from the rhenium complexes show that the open form of the complexes (both monomer (**E-23**) and dimer (**E-22**)) shows a higher emission intensity and a higher quantum yield (Φ_{EM}) than the closed isomers. Surprisingly, although tungsten carbonyls are not luminescent, adding a pyridyl-coordinative unit in the structure allows MLCT-derived emission for both examples (mononuclear (**E-21**) and binuclear tungsten (**E-20**) complexes), observing better luminescence properties for the **CF** isomers than for the **OF** isomers, as shows Table 1.4.

Table 1.4. Fluorescence values comparison for Lehn's synthesized DTE-based complexes

Compound	Fluorescence wavelength (nm)	Fluorescence Intensity*	Emission Quantum Yield (Φ_{EM})*
E-20-OF	382	$2.4 \cdot 10^6$	0.03
E-20-CF	382	$7.8 \cdot 10^6$	0.08
E-21-OF	400	$5.6 \cdot 10^6$	0.03
E-21-CF	400	$4.1 \cdot 10^7$	0.15
E-22-OF	372	$9.3 \cdot 10^5$	0.01
E-22-CF	372	$3.4 \cdot 10^5$	$4 \cdot 10^{-3}$
E-23-OF	368	$1.1 \cdot 10^6$	0.03
E-23-CF	368	$3.8 \cdot 10^5$	0.01

* Arbitrary Units, Φ_{EM} referenced to naphthalene (Φ_{EM} = 0.27)

These results present a new opportunity for potential devices as responsive readout devices and new wide range of opportunities for the implementation of DTE ligands.

For this reason, De Cola et al. proposed a system in which, incorporating phenylene groups as a spacer, they tried to avoid electronic delocalization by the system after excitation since this group acts as a semiconductor spacer between both units.[76] De Cola and coworkers combined a DTE with a double coordination point with two different metal centers, Ru(II) (**E-26**) and Os(II) (**E-27**) (Scheme 1.26).
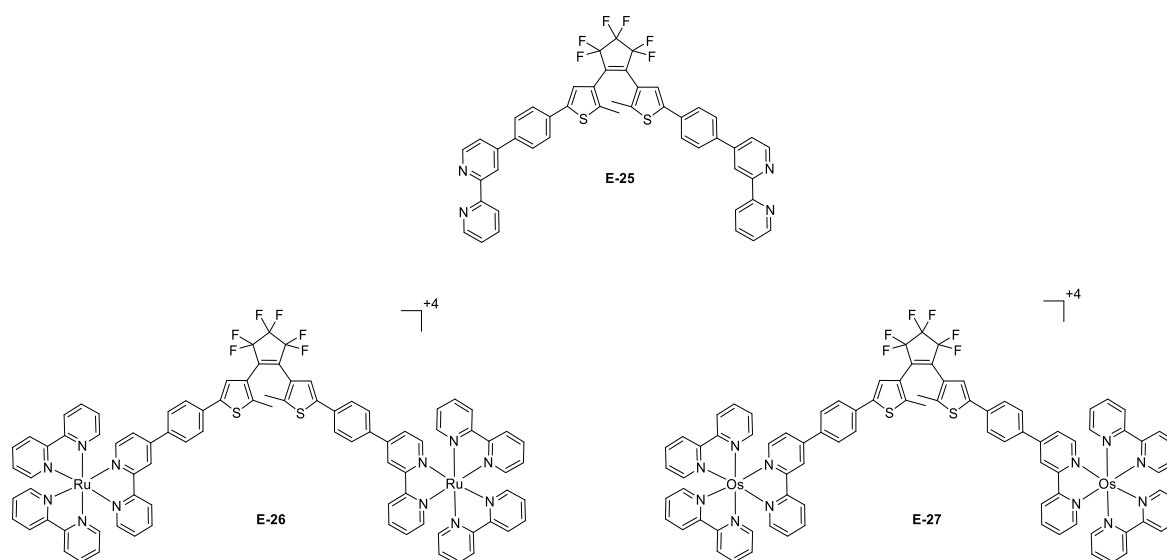
Scheme 1.26. Ru(II) and Os(II) DTE-based dimer described by De Cola.

The coordination of **E-25** to the metallic centers of ruthenium and osmium caused surprising changes in the spectroscopic properties of the compounds when compared to the free form of the ligand. The photocycling process for the synthesized dimers is considerably lower compared to the free ligand ($\Phi_{O \rightarrow C}$ = 0.72), with $\Phi_{O \rightarrow C}$ = 0.37 for **E-26** and $\Phi_{O \rightarrow C}$ = 0.0045 for **E-27**. Surprisingly, using degassed or non-degassed samples directly affects the quantum efficiency of photocycling the ruthenium complex, while the value shows no change for the free ligand and the osmium dimer, as shown in Table 1.5. Table 1.5 also shows the luminescent properties of complexes in their open form. As expected, **E-25** does not have phosphorescent properties while the complexes do. When the cyclization process of the DTE fragment occurs, it can be seen how the luminescence of the synthesized compounds falls drastically, indicating the absence of luminescent properties for the closed isomers.

Table 1.5. Comparison of the different photophysical values obtained for **E-25 - E-27**.

Compound	Photocyclization Quantum Yield ($\Phi_{O \rightarrow C}$)		Emission Wavelenght (λ_{EM})	Emission Lifetime (τ, ns)		Emission Quantum Yield (Φ_{EM})	
	aerated	deaerated		aerated	deaerated	aerated	deaerated
E-25	0.72	0.74	--	--	--	--	--
E-26	0.37	0.88	630	140	310	0.006	0.014
E-27	0.0045	0.0041	759	44	62	0.004	0.005

When the complexes were measured employing UV-vis spectroscopy, they observed an absorption band due to a possible metal to ligand charge transfer (MLCT), observable at lower energy than the $S_0 \rightarrow S_1$ transition of the photochromic free ligand. Because of this, the S_1 state is not populated after irradiating in the MLCT band. However, it has been shown that the Ru(II) and Os(II) complexes show very efficient intercrossing systems from ^{1}MLCT to ^{3}MLCT, thus populating the T_1 of the molecular switch. This research group explains that the use of these transition metals is for comparison purposes, as there is a significant difference in energy between their MLCT states. After studying the complexes in-depth, they observed that this difference caused the properties of the DTE in its excited state to change radically, obtaining photochromic systems that differ in photochemical, electrochemical, and photophysical behavior as an isomer function (**OF** isomer or **CF** isomer).

A few years later, Akita and coworkers described the synthesis of a sandwich ruthenium complex linked to a photoswitchable DTE ligand (**E-7**).[77] This study revealed that the metalated DTE derivatives (**E-28** and **E-29,** Scheme 1.27) showed photochromic behavior through the photochemical, electrocyclic conrotatory ring-closing and ring-opening processes in a manner analogous to the organic free ligand (). However, the photochromic process' efficiency depends on the attached metal fragments. Irradiating the different compounds at 360 nm wavelength, it can be observed how the **CF** isomer population in the PSS varies as a function of the number of metal centers, increasing the number of closed isomers when more ruthenium centers are in the structure, as shown in Table 1.6.
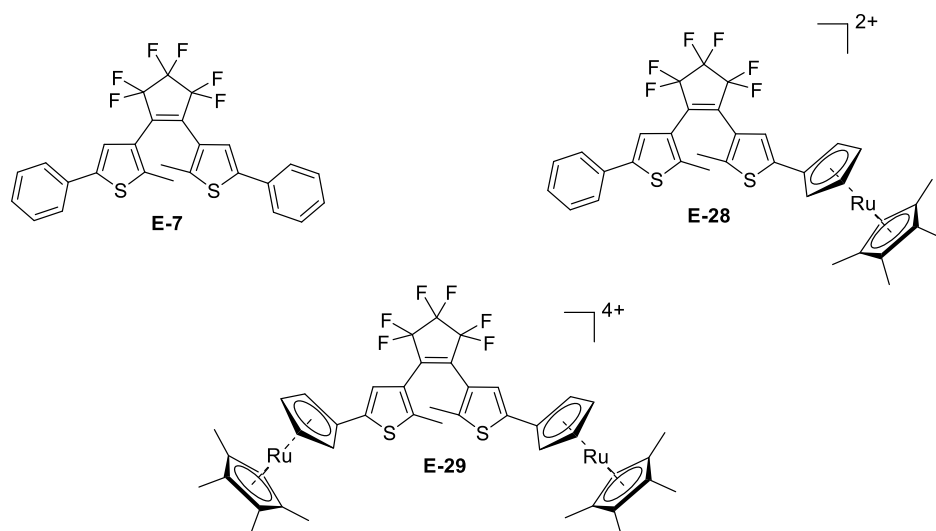
Figure 1.21. Ru(II) complexes described by Akita.

Table 1.6. Comparison of the presence of one/two units of ruthenium in the **CF** isomer population in the PSS.

Compound	CF Isomer $\lambda_{máx.}$	Ratio OP-CF at PSS
E-7	589	43 : 57
E-28	600	16 : 84
E-29	594	12 : 88

A few years later, Raithby research group reported a study describing the photophysical study of a new platinum dimer (**E-31**), using a DTE fragment as a bridge (**E-30**).[78] The complex described showed photochromic properties in solution and crystalline state, showing a more significant population of **CF** isomers in the PSS than the free ligand (80% and 15%, respectively). In addition, Raithby studied the phenomenon whereby under irradiation in the visible spectrum ($\lambda = 420$ nm), the photocycling process for the metal complex was effective when the DTE fragment does not absorb at that wavelength. The conclusion was that platinum atoms' presence and an MLCT electronic transition permits an intersystem crossing facilitating the direct $S_0 \rightarrow T_1$ transition, which involves the platinum centers causing absorption in the visible region. This is the property by which Raithby observed the photocycling process using a less energetic wavelength than commonly used UV irradiation.
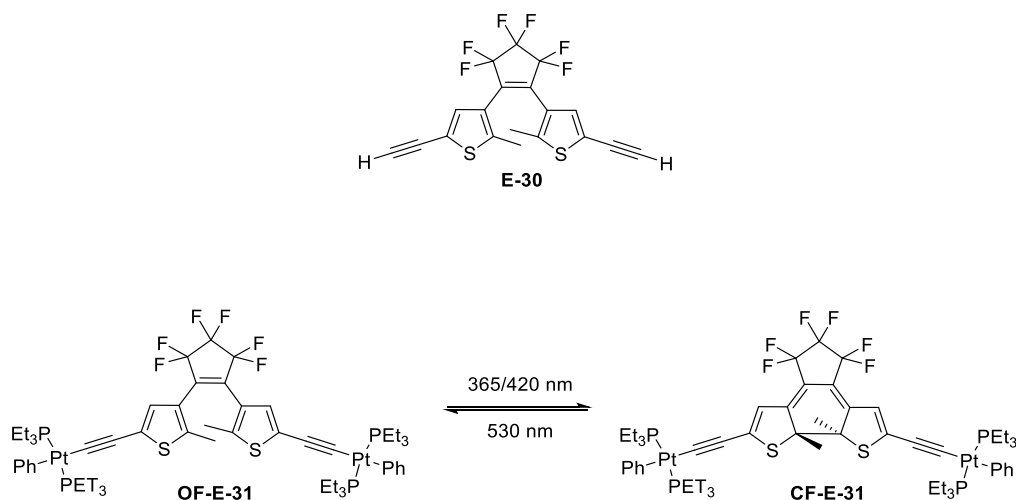
Scheme 1.27. Platinum DTE-appended dimer published by Raithby et al.

More recently, Sun et. al. studied the stereocontrolled self-assembly of europium dinuclear complexes using bridging DTE ligands.[79] The work is based on the use of chiral DTE ligands (***RR/SS*-E-32**) to generate helices through coordination to europium centers. In previous works, they developed the theory that the use of enantiopure chiral ligands induces the chirality of metals through a strong cooperative mechanical effect between the Λ/Δ configuration of europium and the *SS/RR* configurations of the chiral ligand, giving rise to the formation of the *M*-helix and the *P*-helix.[80,81] The helical arrangement obtained by the ligands is of great importance for the photocycling process of the DTE fragments since they predispose an antiparallel spatial orientation of the methyl groups.
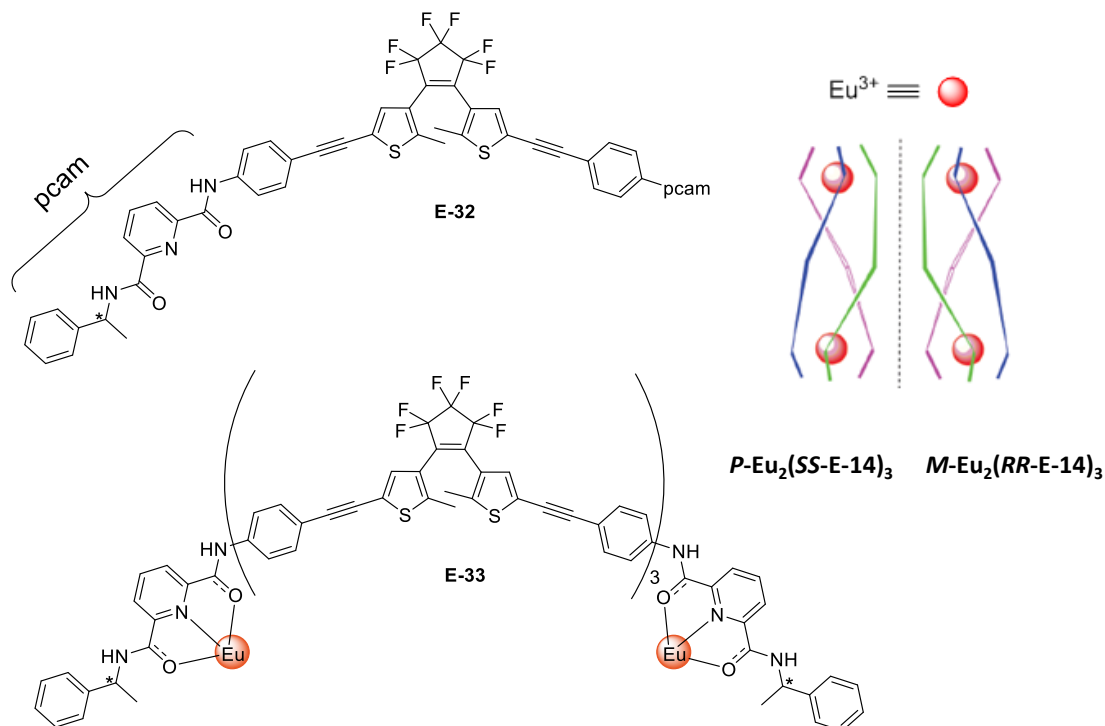
Figure 1.22. Stereocontrolled self-assembly system proposed by Sun and co-workers.

This new and innovative concept is studied by NMR spectroscopy and circular dichroism spectroscopy (CD). Figure 1.23 shows the CD spectra obtained by the Sun group. Four different spectra can be observed. Spectrum A shows the spectrum obtained from the measurement of the free ligand **OF-E-32**, where a change in the spectrum can be appreciated that is attributed to the chiral center existing in the "pcam" fragment of the free ligand. Likewise, spectrum B shows the europium dimer in its open form (**OF-E-33**). In this case, a noticeable dichroic change can be seen in the europium compound (250-450 nm) region. When the photocycling reaction occurs, significant changes are shown in the CD spectra. In the specific case of the **CF-E-32** ligand (C, Figure 1.23), a minimal change can be observed in the region of 550-650 nm, indicating that the orientation of the methyl at the time of cyclization is minimally selective, induced by the chiral centers of the ligand. Finally, in the case of the **CF-E-33** complex, this change is striking. As can be seen in the D spectrum, when the cyclization photoreaction occurs, it causes a significant change in the CD spectrum in the region of the spectrum associated with the closed isomer of the complex. For this reason, Sun demonstrated that chirality could be induced from a DTE ligand, and also, diastereoselective isomerization can be carried out.
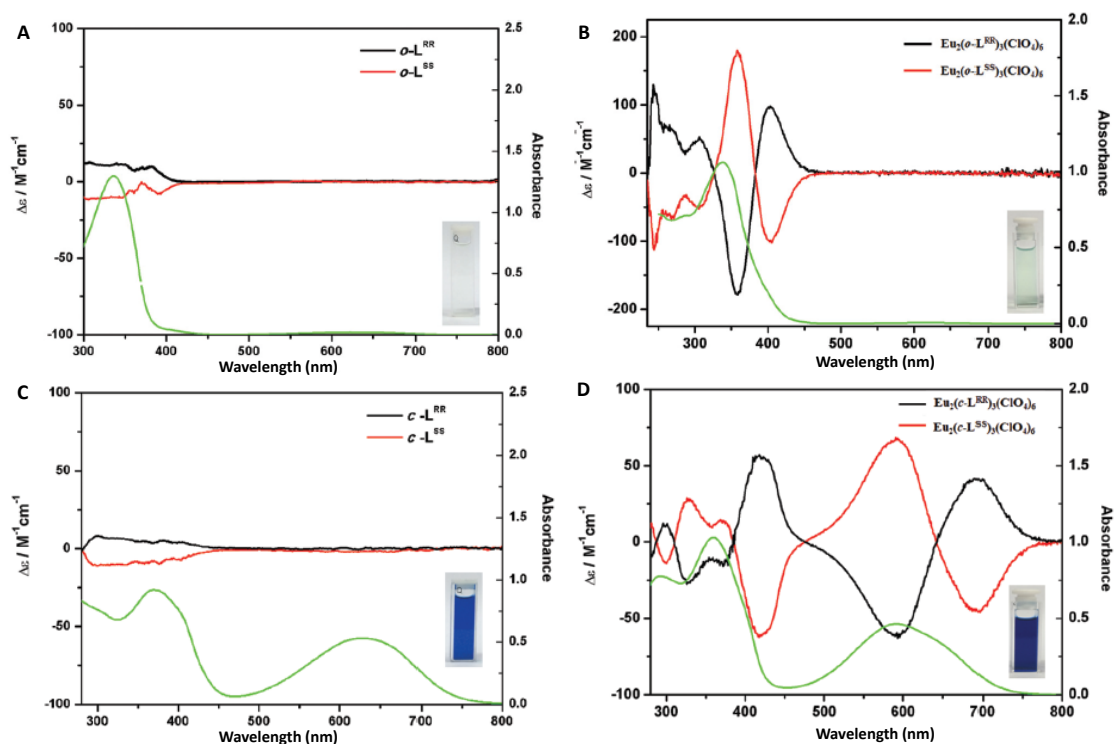
Figure 1.23. CD spectroscopy studies for **E-32** and **E-33** for selective photocyclization studies

Photomodulable organometallic systems have shown novel properties that can potentially be applied as modulators of the photochromic activity since they modify the photochromic properties of DTEs by coordinating with them. Numerous studies describe the effect of DTE ligands' coordination to metal centers, but the examples based on Ir(III) complexes are scarce. In 2009, Tian's group studied the coordination of this type of molecular switches to iridium units.[82] They chose Ir(III) because of the strong spin-orbit coupling of the 5d ion, which causes intense phosphorescence at ambient temperatures. This luminescence is attributed to the combination of electronic metal-to-ligand charge transfer transitions (MLCT) and ($\pi \rightarrow \pi *$) states.[83] This property opens the door for the use of this type of compounds as dopants for organic light-emitting diodes (OLED)[84]. For this, they prepared a new Ir(III) complex where the DTE ligand (**E-34**) was directly coordinated to the central metal. The synthetic strategy followed by Tian was based on the formation of a chloride-bridged dimer, where the DTEs are cyclometalated. The chloride bridges were then cleaved by introducing an acetylacetonate ancillary ligand (Scheme 1.28).
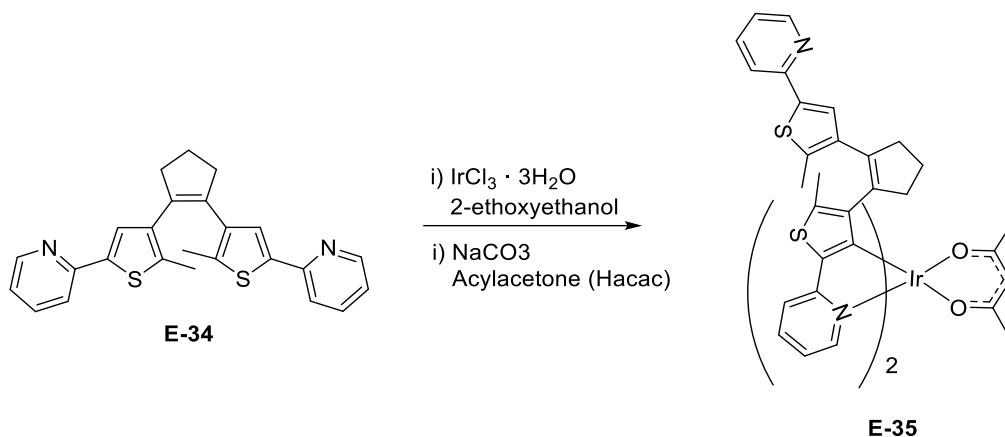
Scheme 1.28. Synthetic methodology proposed by Tian for the formation of DTE-cyclometalated based Ir(III) complex.

Photochromic studies were carried out for the free ligand (**E-34**) and the photochromic metal complex (**E-35**). They observed how the coordination of the DTE to the metal center generated a red-shift effect, shifting the maximum absorption obtained for the free ligand (λ = 320 nm) towards longer wavelengths (λ = 330 nm). Similarly, **E-35** presents a second maximum at 450 nm. This band is associated with MLCT and π-π* transitions of the organometallic complex, previously observed in the literature for other Ir(III) complexes. The photochromic character of the molecules was studied, Tian studied the efficiency of the photocycling/photocycloreversion processes, observing how the **CF-E-35** shows new bands at at λ = 492 nm and λ = 649 nm. The studies provided the photocyclization and photocycloreversion efficiency for **E-34** and **E-35**, showing quantum cyclization yields of $\Phi_{O\rightarrow C}$ = 0.3 and $\Phi_{O\rightarrow C}$ = 0.2, while smaller values for the photocycloreversion process were obtained, being $\Phi_{C\rightarrow O}$ = 0.016 and $\Phi_{C\rightarrow O}$ = 0.01, respectively. Tian concluded that a new iridium complex was described with direct coordination of the moiety DTE, which showed good photochromic behavior in the near-infrared, in addition to high thermal stability and resistance to fatigue.

Recently, Pu *et al*. synthesized a novel cyclometalated Ir(III) compound, which includes two DTE fragments in the cyclometalated ligands (Scheme 1.29)[85]. This compound has a dinitrobenzenesulfonyl group (DNBS) attached to the ancillary ligand, which was intended to act as a probe for detecting thiophenol groups and as quenching moiety of the luminescence due to the strong electron-withdrawing character of the fragment, creating an intramolecular electron transfer (ICT) from the organometallic complex to the DNBS. Upon addition of a thiol group (Ph-SH), the DNBS fragment is released, obtaining the fluorescent compound **E-37**. Both photoswitchable complexes show photochromic behavior Pu et al. showed that, even though both compounds had two DTE fragments in the structure, only one of them carried out the cyclization process, still maintaining irradiation for long periods. When studying the emissive properties of the compounds, it was observed that compound **E-36** did not present fluorescence, inhibited by the presence of the DNBS group, while **E-37**, in its open form, did present an emission band at 450 nm. When studying the emission of **E-37** under UV irradiation, Pu et al. observed that the competitive cyclization process took place, generating **CF** isomer of **E-37**, which significantly quenched the emission of the compound.
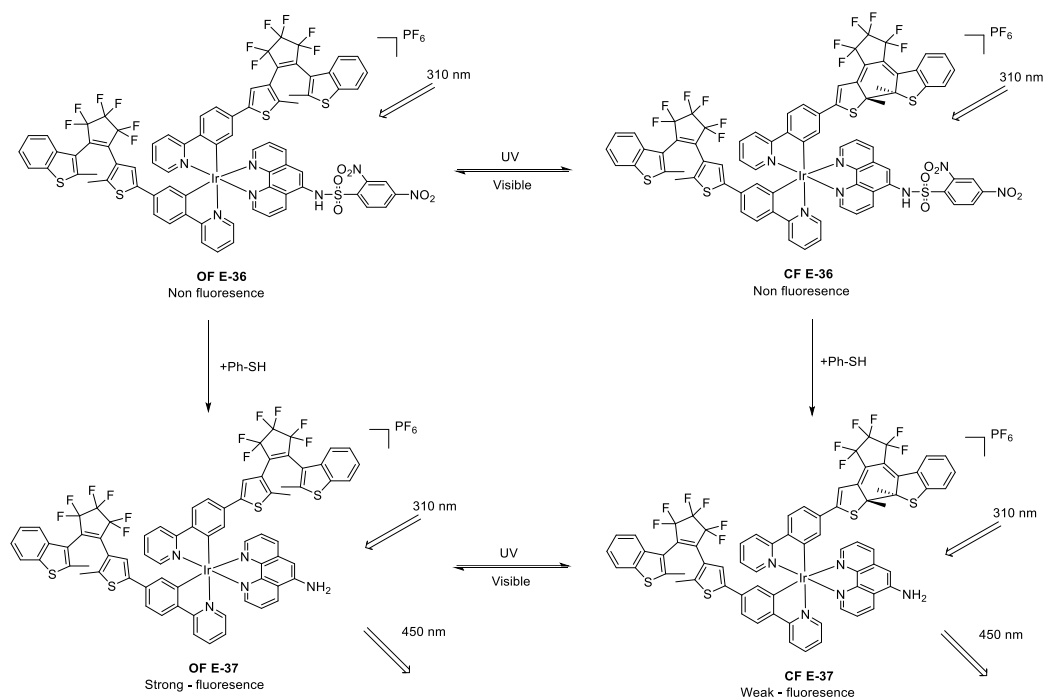
Scheme 1.29. Representative scheme for the photochromic-emissive system published by Pu et al.

As has been observed, there are many studies about DTE incorporated in organometallic complexes for their subsequent application in different fields. Different studies were made in which changes in the emission of the compound or cause an electronic change in the metallic centers after the isomerization process of the molecular switch. Depending on the linker used between the DTE ligand and the metal center, its effect on the isomerization process can be controlled. Many factors must be considered since it has been observed how this combination provides compounds where the isomerization process occurs in the visible region, but in the same way, cases have been observed where the photoswitch-metal combination has led to the inhibition of the photocyclization. Therefore, a balance must be achieved in the interaction in the photoswitchable organometallics.

1.3 BIS- /TRIS-CYCLOMETALATED IR(III) COMPLEXES

1.3.1 PROPERTIES OF IR(III) COMPLEXES

Ir(III) cyclometalated complexes have received significant attention from the scientific community in recent decades due to the exceptional photophysical properties they present in addition to the photochemical and chemical stability of this type of compounds.[86,87] This growing interest arises from the previously studied complexes of Ru(II), Os(II), and Re(I), which also have a d^6 electronic configuration.[88] The difference between these transition metals and iridium lies in the relative ease that Ir(III) has to form bis- and tris-cyclometalated complexes, which provide high chemical and thermal stability, excellent excited lifetimes, and the possibility of altering the color of the emission through modifications in the structure of the cyclometalated ligands[89]. These properties make iridium cyclometalated complexes promising candidates for luminescence applications, such as bioimaging, photoredox catalyst, or as photosensitizers.

The luminescence is produced by the excitation of a molecule in its ground state to higher energy states or excited states. By relaxation back to ground state, energy can be released in two different ways, thermal or light. The latter is called luminescence. In order to understand the luminescence process of cyclometalated Ir(III) complexes, it is necessary to know in more detail the molecular orbital system of this type of compounds.

As it is well known, in octahedral complexes, d orbitals lose degeneration due to the influence of the ligands, splitting into two sets (t_{2g} and e_g). This phenomenon is called ligand-field splitting and is significant in the case of Ir(III) ($5d^6$ configuration). The energy difference increases even further in the case of cyclometalating ligands, making the LUMO orbital of these compounds have a π*-ligand character (see Figure 1.24). Considering this basic molecular orbital (MO) diagram, when considering the excitation of the molecule, the following electronic transitions are possible.

❖ MC: metal-centered
❖ LC: ligand-centered
❖ MLCT: metal-to-ligand charge transfer
❖ LMCT: ligand-to-metal charge transfer
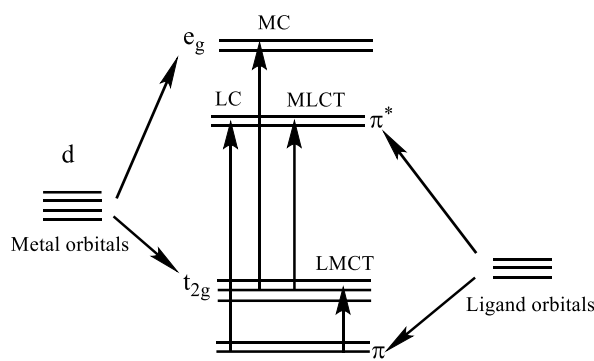
Figure 1.24. Representative of an electronic transitions diagram for a d-metal complex.

Therefore, by exciting the compound, it will generate a transition to an excited state ^{1}MLCT, which will relax to the ground state emitting light which can occur in different emissive forms: fluorescence or phosphorescence. Fluorescence is a phenomenon based on a process between states of the same multiplicity ($S_1 \longrightarrow S_0$). On the contrary, phosphorescence is a process that occurs due to relaxation from a triplet state to the ground state of the molecule ($T_1 \longrightarrow S_0$). Therefore, for a molecule to be phosphorescent, it must before relax from S_1 to T_1. An intersystem crossing (ISC), allows this initial access to state T_1.[90] In the specific case of Ir(III) the ISC process is very effective due to the high spin-orbit coupling that the iridium metal ion possesses, making these molecules phosphorescent.[91]
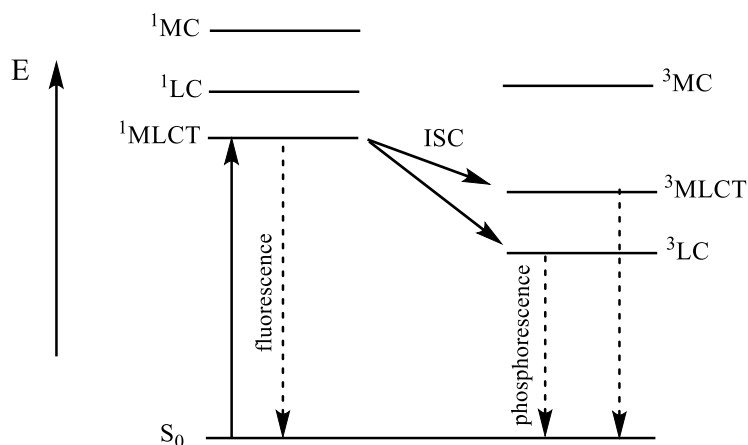
Figure 1.25. Energy level diagram for one/many-electron states in d^6 MLCT-LC complexes.

Ultimately, the color of the emission will depend on the HOMO-LUMO gap. In the case of bis- or tris-cyclometalated complexes (with ligands such as ppy), the HOMO and LUMO are well localized in different parts of the molecule. The HOMO is centered mainly in the phenyl group of cyclometalated ligands and the metal center, while LUMO is located in the pyridyl fragment of the ligand (or in the ancillary ligand in the case of heteroleptic compounds with bipyridyl ligands). For this reason, ligands can be designed in such a way as to control the energetic difference between HOMO and LUMO, thereby controlling the emission color of the compound.[92]

[Ir(ppy)$_2$(bpy)]   [Ir(ppy)$_3$]
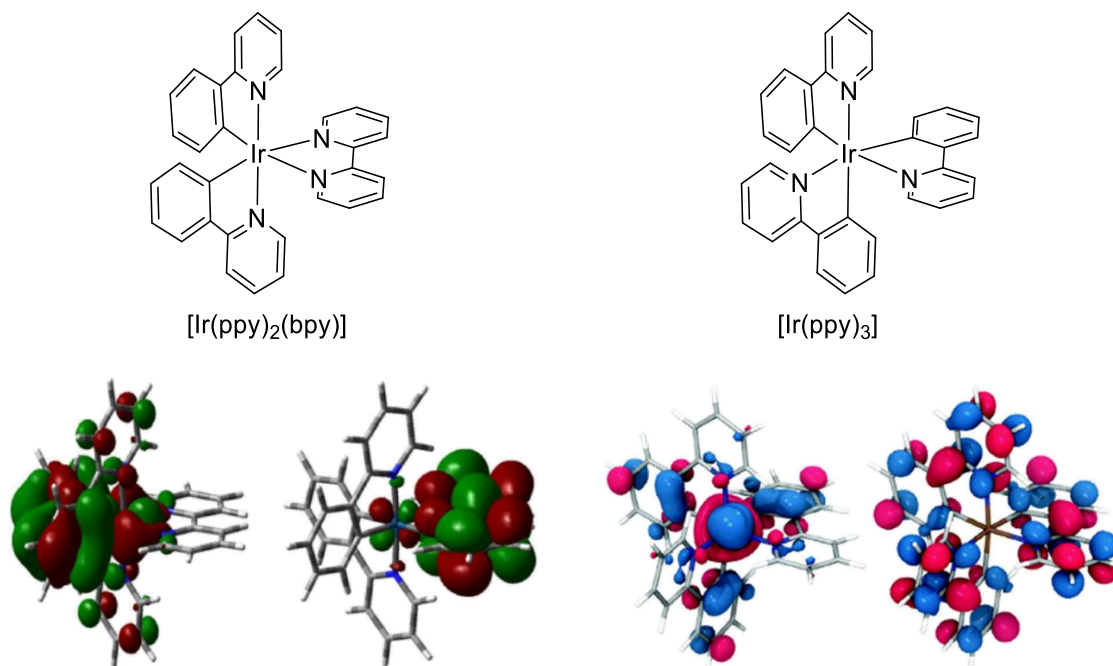
Figure 1.26. HOMO-LUMO distribution in bis- /tris-cyclometalated Ir(III) complexes.

1.3.2 SYNTHESIS OF BIS- AND TRIS-CYCLOMETALATED IR(III) COMPLEXES

Therefore, the choice of the ligands is crucial to generate suitable light-emitting complexes. Over the years, various studies have described that the emissive process of Ir(III) complexes require at least two cyclometalated (CN) ligands.[93] The first example of tris-cyclometalated

complex was described by Watts in 1985, creating the *fac*-[Ir(ppy)$_3$][94]. In addition, Ir(III) complexes have an octahedral structure, generating different optical isomers depending on how the ligands are coordinated. Two optical isomers are known, meridional (*mer*) and facial (*fac*).
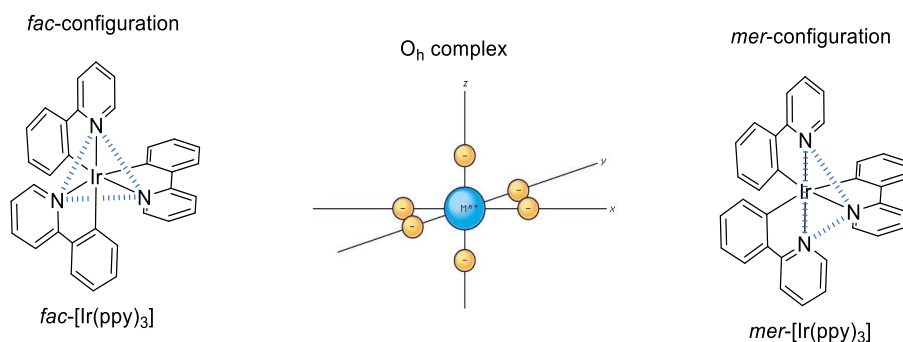
Figure 1.27. Graphical representation of the *fac/mer* configuration for O$_h$ iridium complexes.

The *mer*-isomer is considered the reaction kinetic product, while the *fac*-isomer is the thermodynamic one. For tris-cyclometalated compounds, the *fac*-isomers present all the nitrogen atoms of a CN ligand in *trans* position to a carbon atom of another ligand (trans N–Ir–C), while the *mer*-isomers show two nitrogen atoms in *trans* of each other and the third nitrogen in *trans* to an aromatic carbon. In terms of properties, both isomers have different properties, as they present structural differences between them. The most significant difference resides in the fact that complexes with *mer*-configuration generate an asymmetric environment due to the different bond lengths between Ir–N and Ir–C caused by the trans effect of nitrogen and carbon atoms. This distortion is not found in the case of facial complexes since a symmetrical environment is present; all the Ir–N and Ir–C bonds are identical. Because this reason, the facial isomers show better properties in the photophysical field, for example in emission lifetime or emission quantum yield.[95] Table 1.7 presents different values of the luminescence quantum yield of *mer/fac* complexes, showing better values for the *fac* configured complexes.

Table 1.7. Comparison of half-life and emission quantum yield properties of *fac/mer* isomers.[87,96]

Compound	Φ_{PL}*	$\tau(\mu s)$*	k_r*	k_{nr}*
fac-Ir(ppy)$_3$	0.40	1.9	$2.1 \cdot 10^5$	$3.2 \cdot 10^5$
mer-Ir(ppy)$_3$	0.036	0.15	$2.4 \cdot 10^5$	$6.4 \cdot 10^6$
fac-Ir(tpy)$_3$	0.50	2.0	$2.5 \cdot 10^5$	$2.5 \cdot 10^5$
mer-Ir(tpy)$_3$	0051	0.26	$2.0 \cdot 10^5$	$3.6 \cdot 10^6$
fac-Ir(4,6dfppy)$_3$	0.43	1.6	$2.7 \cdot 10^5$	$3.6 \cdot 10^5$
mer-Ir(4,6dfppy)$_3$	0.053	0.21	$2.5 \cdot 10^5$	$4.5 \cdot 10^6$
fac-Ir(F$_3$ppy)$_3$	0.025	0.128	--	--
mer-Ir(F$_3$ppy)$_3$	0.018	0.054	--	--
fac-Ir(F$_4$ppy)$_3$	0.034	0.14	--	--
mer-Ir(F$_4$ppy)$_3$	0.012	0.068	--	--

* Φ_{PL} (emission quantum yield), τ (emisión half-life), k_r (radiative rate constant), k_{nr} (nonradiative rate constant).

Tris-cyclometalated Ir(III) complexes have generated significant attention and impact in organometallic chemistry due to the excellent photophysical properties they present, due to their possible application as phosphors for OLEDs, as chemosensors, or as catalysts, among other applications. The synthesis of bis- and tris-cyclometalated octahedral Ir(III) complexes has been studied assiduously in recent decades, observing multiple and diverse synthetic routes to obtain this type of compound. This section describes briefly the synthetic routes most frequently used in the literature.

Depending on the spatial arrangement of the C-N ligands in the metal, two optical isomers can be generated, a meridional isomer (it is the kinetic reaction product and has two of the nitrogen atoms of the C-Ns in trans position and a third nitrogen of the third ligand C-N in trans to the carbon atom of the aromatic ring) and a facial isomer (thermodynamic reaction product, has the arrangement of all the nitrogen atoms C-N in trans to aromatic carbons), as shown in the examples of the Scheme 1.30.

fac-Ir(ppy)$_3$ mer-Ir(ppy)$_3$
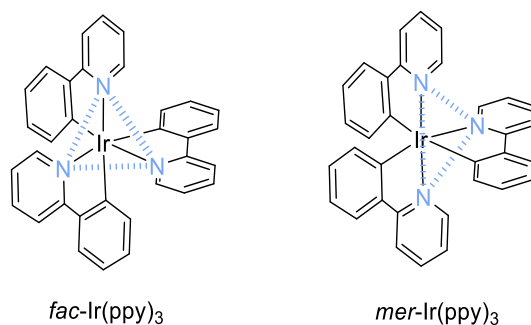
Scheme 1.30. Facial and meridional isomers of [Ir(ppy)$_3$].

Fac/*mer* compounds, being optical isomers, can have different properties. As explained in the introduction section, for example, the use of facial complexes in the construction of OLEDs exceeds the values and results obtained for the same compound in its *mer*-configuration in terms of luminescence efficiency (Φ) or emission lifetime (τ). For a correct implementation of these complexes, their synthesis must be precise to generate the correct isomer. Throughout the last decades, different methodologies have been described for the generation of facial complexes and meridional complexes. The main difference in the synthesis of these iridium complexes resides in the reaction temperature, higher for the generation of the facial isomers (thermodynamic product). Scheme 1.31 presents alternative synthetic routes, pioneered in the generation of *fac*-Ir(III) complexes. Three different synhtetic routes can be observed, proposed by Thompson[97] and Xia[98]. The routes described use different types of metal precursors, depending on the reaction conditions to be used. On the one hand, we have the metallic precursor [Ir(acac)$_3$], used in synthetic *routes 1* and *route 3*. The first route (*route 1*) described reacts this iridium precursor with three equivalents of the required cyclometalated ligand in glycerol, heating the reaction up to 200 °C. On the other hand, *route 3* describes the acid digestion bomb proposed by Xia, a method that does not require the presence of solvent and extremely high temperatures (240 °C). It should be noted that this last route is optimal for the generation of homoleptic compounds, while it generates mixtures of isomers in order to obtain heteroleptic complexes since the coordination selectivity of the ligands in the central metal is not controlled. Finally, *route 2* uses chloride bridged iridium dimers (synthesized with previously chosen C-N ligands). The synthetic strategy consists of breaking the chloride bridges and cyclometallating a third C-N ligand. The conditions of this reaction require the presence of a base (usually K$_2$CO$_3$ or Na$_2$CO$_3$) and temperatures close 200 °C in glycerol. This route allows the synthesis of heteroleptic complexes relatively easily.
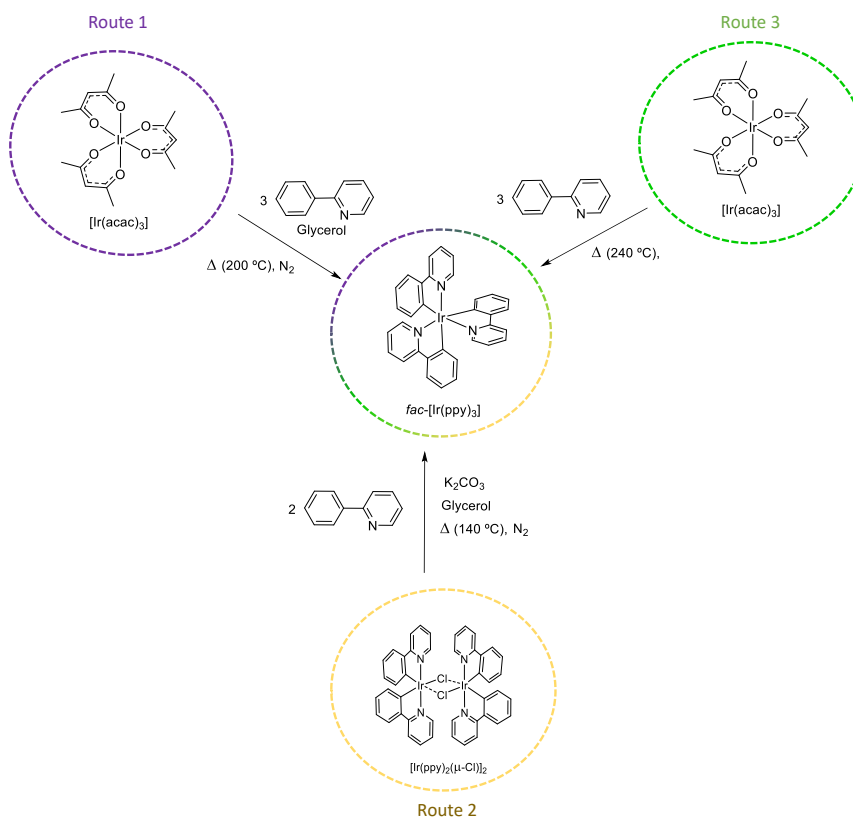
Scheme 1.31. Synthetic procedures described in the literature for the synthesis of *fac*-Ir(III) complexes

On the other hand, for the synthesis of the meriodinal compound few synthetic protocols were described by Thompson[97] and Crutchley[99] at the beginning of the century (Scheme 1.32). Considering that the meridional isomers are the kinetic reaction product, they require lower reaction temperatures than those used to generate the *fac* compounds. For this reason, Thompson described *route 4* as a synthetic route to obtain *mer-* [Ir(ppy)$_3$], which mimics the conditions of route 2 for the *fac* compounds, altering only the reaction temperature, reducing it to 140 °C. On the other hand, in 2004 Crutchley (*route 5*) described a synthetic process in which he substitutes glycerol for acetone and the base (K$_2$CO$_3$ for Et$_3$N), in addition to using a chloride abstractor to cleave the chlorine bridges present in the dimers. These changes directly affect the reaction temperature since it does not require temperatures above 60 °C, providing a synthetic route with milder conditions.
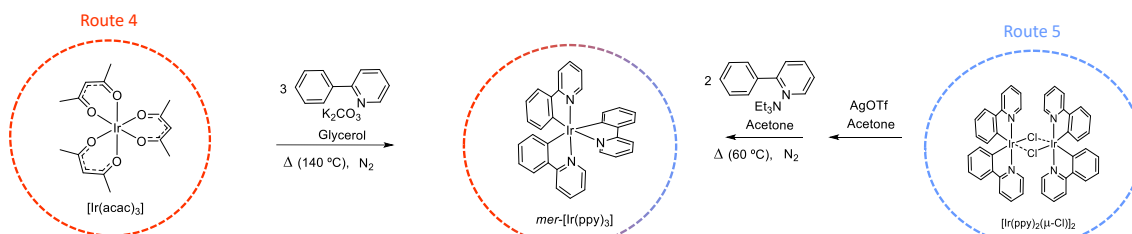
Scheme 1.32. Synthetic procedures described in the literature for the synthesis of *mer*-Ir(III) complexes.

As already mentioned in the introduction, Bis-/ tris-cyclometalated iridium compounds can show different configurations depending on the arrangement in which the ligands coordinate and be classified according to the nature of those ligands. This last classification is based on whether the coordinated ligands are identical or if, on the contrary, the coordinated ligands

have different organic structures. The octahedral compound with three identical cyclometalated ligands is called a homoleptic complex, while if it has different coordinated ligands, they are called heteroleptic complexes. Several examples for both classes of complexes are shown in Scheme 1.33.

Homoleptic:

E-1 E-2 E-3

Heteroleptic:

E-4 E-5 E-6
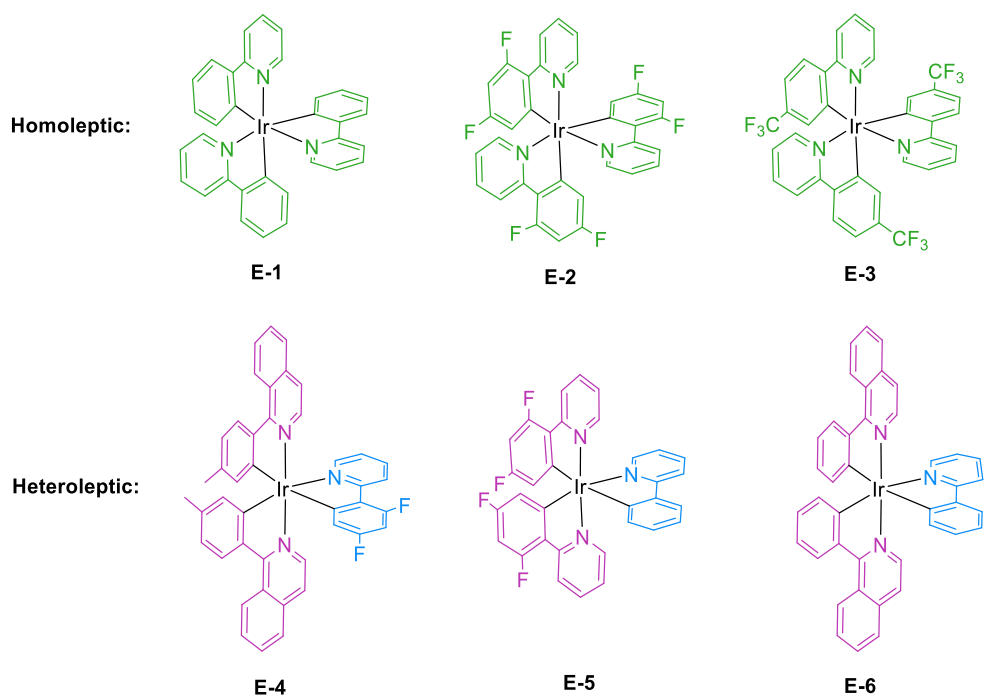
Scheme 1.33. Examples of homoleptic and heteroleptic complexes described in the literature.

These methodologies and the many variations published made it possible to obtain new, vast and promising families of Ir(III) complexes.

1.3.3 APPLICATIONS OF BIS- AND TRIS-CYCLOMETALATED IR(III) COMPLEXES

One of the most significant applications of the octahedral iridium complexes comes from their phosphorescence, which is used to construct light-emitting systems. One of the best known are OLEDs (organic light-emitting devices). The research emphasis is based on obtaining emission colors that cover the entire region of the visible spectrum. Achieving this milestone would provide a breakthrough in OLEDs applications. As mentioned above, the color obtained from the complex emission depends, mostly, on the coordinated ligands. Therefore, the design and structure of the organic ligands add the possibility of tuning the color of the emitted light depending on functional groups present in the organic structure.[100]
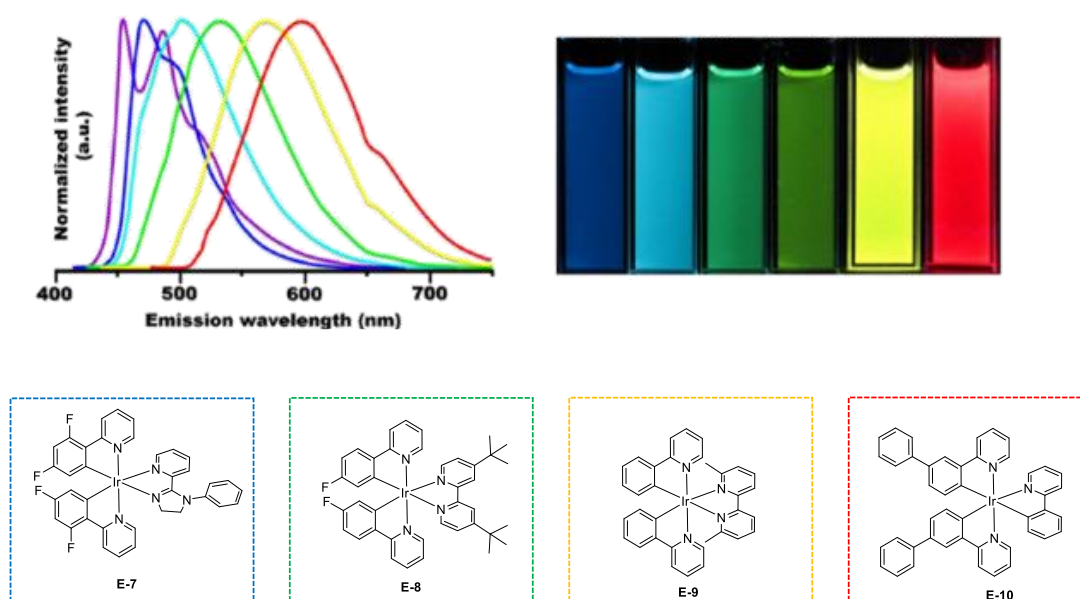
Figure 1.28. Emission colour changes depending on the coordinated ligands in Ir(III) bis-cyclometalated complexes.[100]

The structure of the OLEDs and some interesting examples are reviewed below, where different emission colors are obtained for the formation of OLEDs are presented. Figure 1.29 shows the general structure of OLEDs.[101] Generally, the complexes are attached to host materials, creating an emission layer (EML). In addition to the host layer, other layers are incorporated that facilitate injection (HIL and EIL), transport (HTL and ETL), and charge carriers (HBL). The mechanism consists of applying an electric potential by injecting electrons from the cathode (EIL) and holes (electron vacancies) from the anode (HIL), producing their migration towards the emitter layer through the transport layers, ETL and HTL, respectively. Once they reach the emitting layer, a recombination of the charges takes place, causing the appearance of an excited state, whose energy can be transferred to the iridium molecules. Once the iridium compounds are in their excited state, they release the absorbed energy in the form of light (phosphorescence).

- **ITO**: Anode
- **HIL**: Hole Injection Layer
- **HTL**: Hole Transporting Layer
- **EML**: Emission Layer
- **HBL**: Hole Blocking Layer
- **ETL**: Electron Transporting Layer
- **EIL**: Electron Injection Layer
- **AL**: Cathode
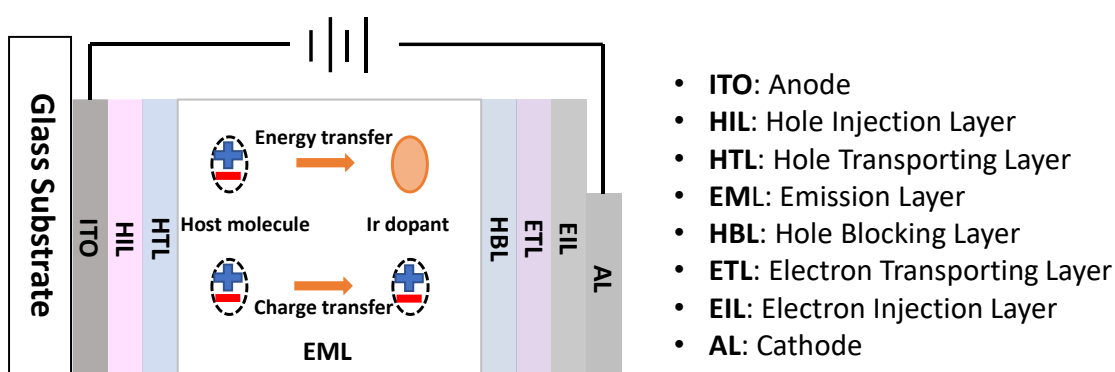
Figure 1.29. OLEDs general structure.

The first Ir(III) complex implemented in an OLED was described in 1999 by Thompson and Forrest, reporting a *fac*-Ir(ppy)₃ (**E-1**), which had a green emission.[102] Based on this complex, developing the ligand field strength and the ligands' energy levels, many complexes with green emission were described. Ma and Wong simultaneously described the behavior of a series of

complexes (**E-11 – E15**) (Scheme 1.34), where the different modifications of the phenylpyridine chelate ligands (ppy) generated complexes capable of emitting colors in the 490-530 nm regions (blueish-green and greenish-yellow).[103]

E-1 λ = 510 nm   **E-11** λ = 497 nm   **E-12** λ = 520 nm

E-13 λ = 525 nm   **E-14** λ = 528 nm   **E-15** λ = 530 nm
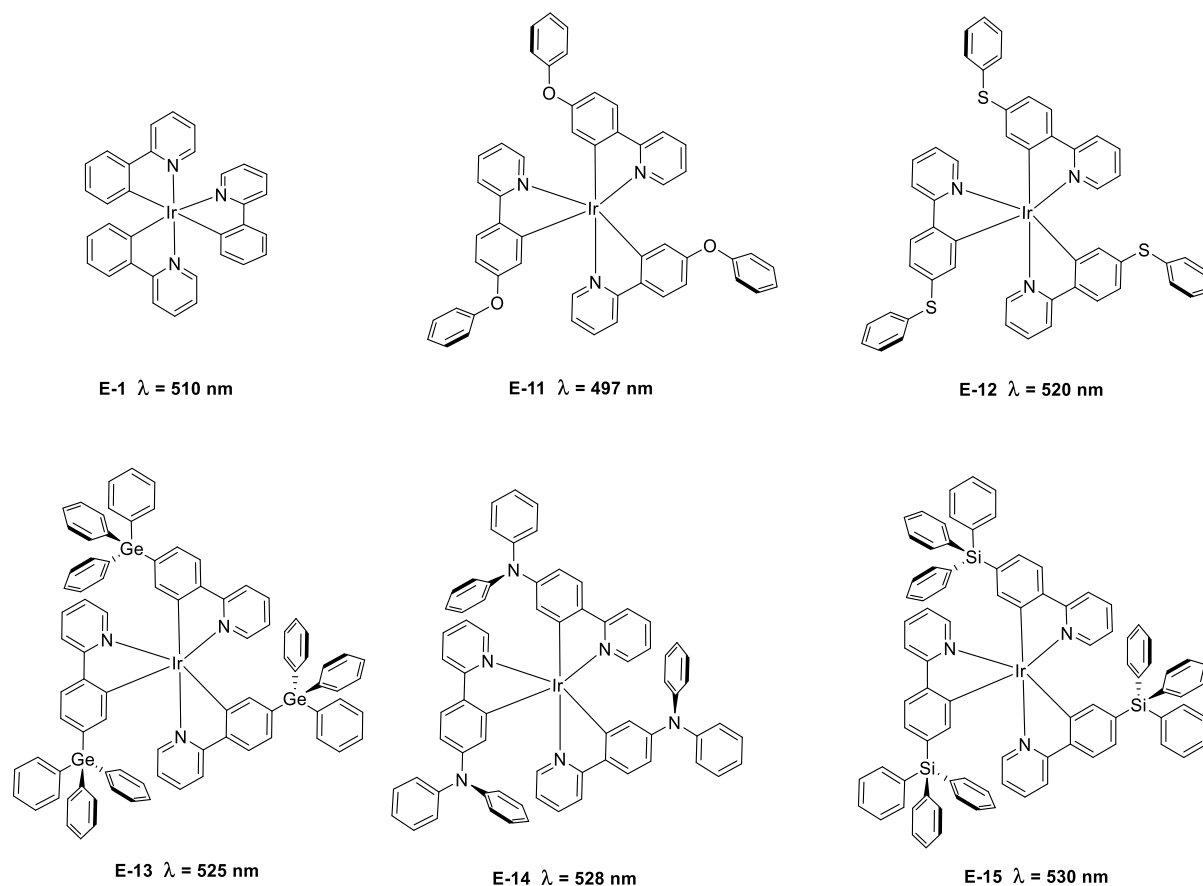
Scheme 1.34. Green emissive examples described in the literature.[102,103]

One of the biggest challenges of forming OLEDs is the creation of compounds that emit in the blue region of the visible spectrum. Thompson and Forrest described in 2005 four complexes, *mer/fac*-**E-16** and *mer/fac*-**E-17** (Scheme 1.35) that contain heterocyclic carbene-type ligands (NCH) that present emissions very close to the UV (400 nm).[104] Many investigations faced this challenge, in which the design of the ligands is critical to find the balance between a strong ligand field that has a large separation between the HOMO-LUMO orbitals and the resultant bluish emission of the complexes.

mer-**E-16**   *fac*-**E-16**   *mer*-**E-17**   *fac*-**E-17**
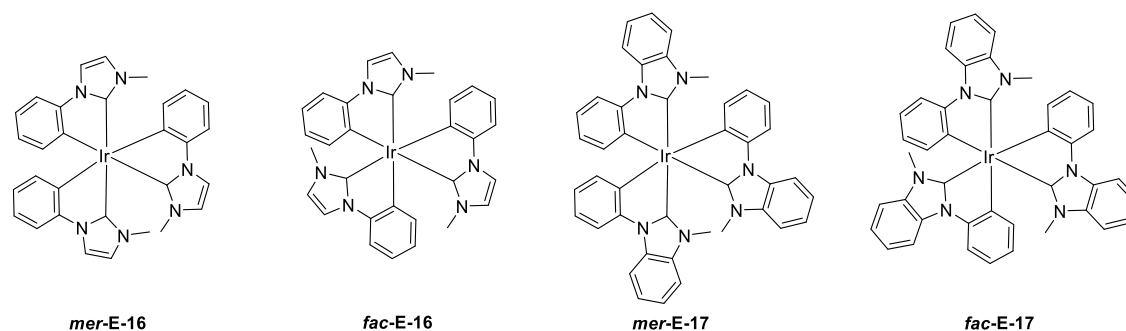
Scheme 1.35. Blue emissive system described by Thompson-Forrest.

On the other hand, to obtain complexes that emit orange/red colors, the structures of the iridium complexes described above must be modified. In the specific case of emitting red, the phosphorescence complexes must have a small energy gap between the HOMO-LUMO orbitals, guaranteeing an emission of low energy light. There are two ways to manipulate structural designs in order to lower the HOMO-LUMO gap: Increase the conjugated structure of the organometallic ligand through the insertion of aromatic rings, or introduce electron-rich aromatic heterocyclic groups such as thiazole or thiophene groups.[105] Quinoline derivatives are usually used for this type of emitting compound design because they have extensive conjugation, making it an optimal ligand for red-shift emissions. Lee et al.[106] in 2014 and Jin et al.[107] in 2017 described the synthesis and study of two new red-wavelength emitting Ir(III) complexes. Lee reported a facial homoleptic iridium complex composed of a thiophene phenylquinoline derivative (**E-18**) presenting an emission band close to 600 nm. Also shown in the Scheme 1.36 is the complex designed and synthesized by Jin, which replaces the thiophene ring with a selenophene ring (**E-19**). This change influences the emission wavelength due to the greater polarity of the selenium atom, thus shifting the emission towards the red, 614 nm.

E-18 λ = 601 nm   **E-19** λ = 614 nm
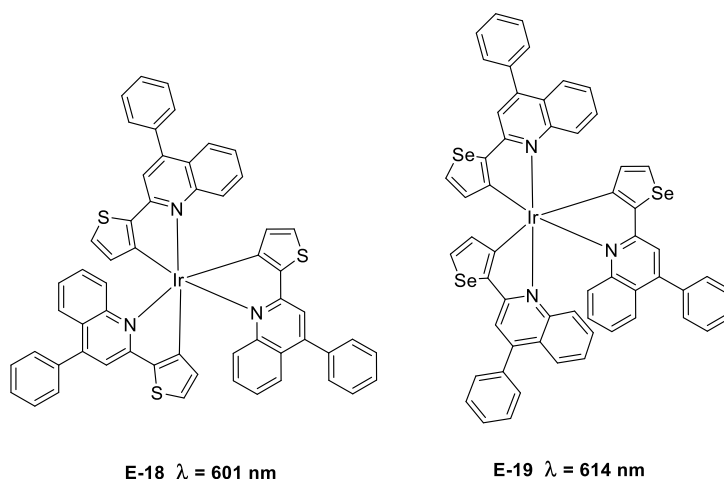
Scheme 1.36. Red emitter iridium complexes described by Lee[106] and Jin.

Iridium complexes have also been used as viable systems for medical applications[108]. Despite the medical advances reached in recent decades, an effective treatment has not yet been found to treat various diseases, such as cancer, and the current existing cancer treatments often cause very harmful side effects to the human body, such as chemotherapy. Cisplatin complex is one of the clinically approved anticancer compounds, showing great results in such treatments.[109] However, cisplatin derivatives show many side effects, such as vomiting, neurotoxicity, kidney problems, and other adverse effects.[110] New research focuses on the study and development of alternative systems based on organometallic structures to treat carcinogenic activity. Ir(III) complexes showed optimal properties to act as an anticancer because they are stable and inert in biosystems, have high water solubility, and they are promising systems in the antiproliferation of carcinogenic activity.[111,112] Therefore, in recent years various studies have developed and studied the efficacy of these complexes. Here two examples of the many published will be described to show the potential of iridium compounds in this area. Recently Liu et al. developed two bis-cyclometalated Ir(III) complexes which were tested as anticancer drugs[113]. Compounds **E-20** and **E-21** did not show anticancer activity by themselves. The researchers designed a biocompatible system, where the iridium complexes are encapsulated in liposomes, which are responsible for delivering them to the corresponding place. These new systems did show

anticancer activity, generating apoptosis of cells due to the increase in reactive intracellular oxygen species and reducing the mitochondrial membrane potential, inducing their dysfunction.
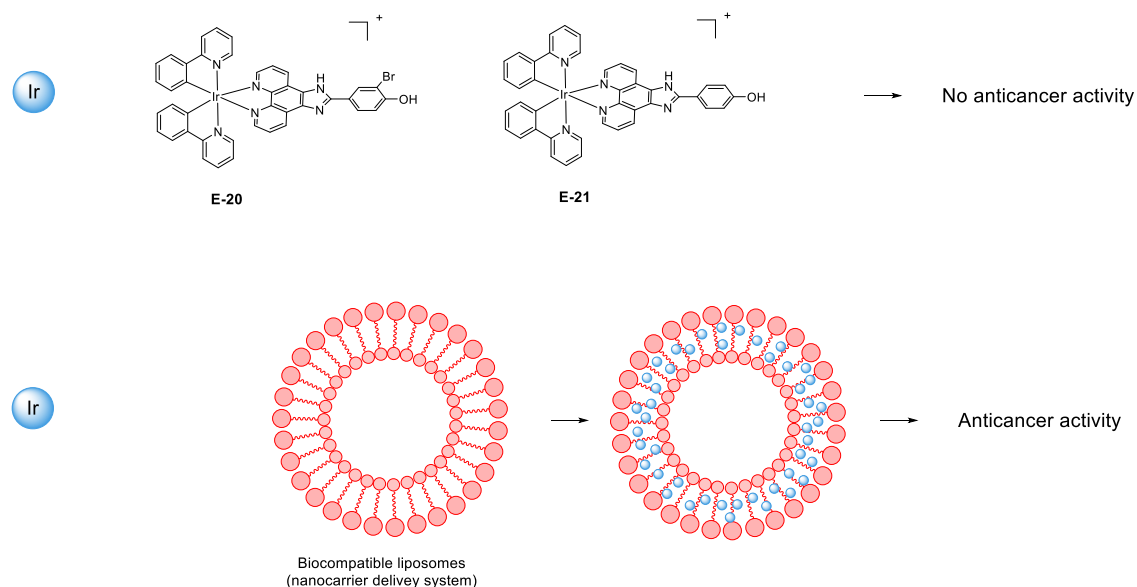
Figure 1.30. Ir(III) anti-cancer systems developed by Liu and coworkers.[113]¡Error! Marcador no definido.

In the same year, Gao's research group reported a new bis-cyclometalated Ir(III) system targeting photodynamic therapy (PDT) (Figure 1.31).[114] PDT is a new, minimally invasive, and highly efficient therapeutic technique applied to cancer treatment. This therapy is based on photosensitizer (PS) and light irradiation to eradicate cancer cells. For effective treatment and the least harmful to the body, it is considered that PS must show high emission quantum yields, as well as have an emission close to NIR, reducing the interference that the body tissues can generate, as reported by Yang in 2017[115]. Gao synthesized a bis-cyclometalated complex (**E-22**) that emits at λ = 600 nm. The system encapsulates the iridium PS in supported nanoparticles, which penetrate the cancer cells via endocytosis. Once inside, the iridium PS handles two possible functions, on the one hand, its function of ablating cancer cells (selective destruction), causing the cellular-death. On the other hand, due to its red emission, it can be used as a target in bioimaging to control the selective transport and selective distribution of drugs delivery inside the body in real-time. This example represents the advances in this area of research over the last decade in the race to implement minimally-invasive anticancer systems for the human body.
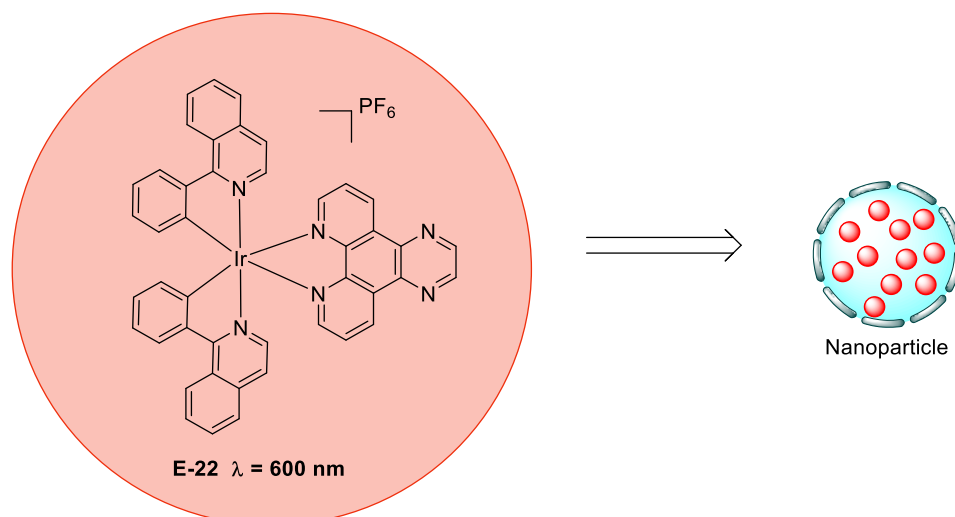
Figure 1.31. Ir(III) system developed by Gao et al. for PDT applications.

1.3.4 ENANTIOPURE BIS- /TRIS-CYCLOMETALATED IR(III) COMPLEXES

As mentioned before, Ir(III) complexes have a wide variety of applications that can be implemented, generating a promising future for this type of chemistry. Even so, the applications of these complexes could be further expanded, taking into account other properties that these complexes possess. Due to the octahedral configuration of Ir(III) complexes, bis- and tris-cyclometalated complexes have two additional optical isomers, the lambda isomer (Λ, right-handed) and delta isomer (Δ, left-handed). The difference between these isomers resides in the arrangement of the cyclometalated ligands around the metal, being enantiomeric. The enantiomers have the same physical and chemical properties except for their response to polarized light irradiation or their interaction with other chiral enantiopure molecules. [116,117,118] Therefore, using the enantiomers separately can be very useful in some of the applications mentioned above. The main problem in implementing these systems in applications is to have an efficient methodology to obtain the compounds in an enantiopure form in large quantities.

rac-[Ir(ppy)₃]

Δ-[Ir(ppy)₃]   Λ-[Ir(ppy)₃]

Left-handed   Right-handed
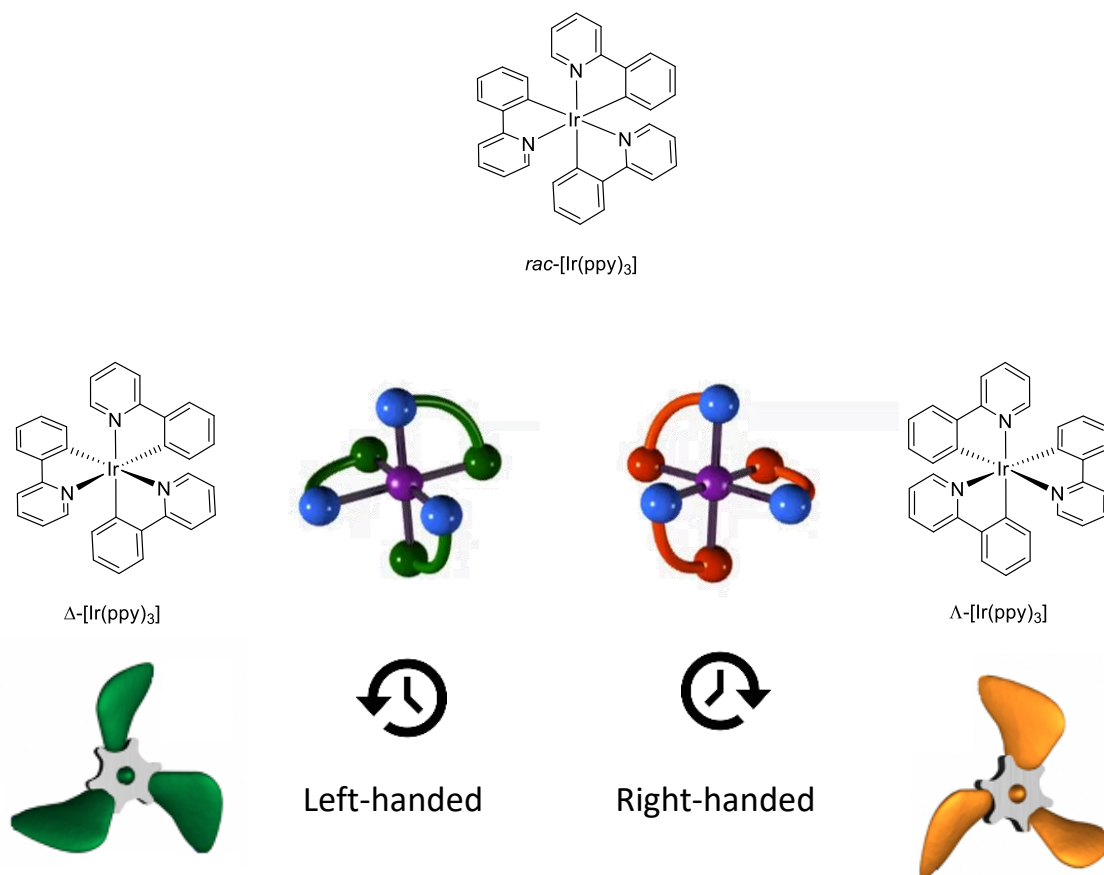
Figure 1.32. Graphic representation of Λ/Δ-isomers for [Ir(ppy)₃].

Therefore, for several decades there has been an effort to discover and implement a methodology that allows the separation of the metal enantiomers present in the octahedral complexes. An early and related example of an enantiopure complex was a Ru(II) complex described by Fontecave in 2003. They described Ru(II) polypyridyl enantiopure complex employing an enantioselective precipitation procedure using chiral counterions.[119] This compound was successfully tested in the enantioselective oxidation catalysis of organic sulfides

to sulfoxides. This breakthrough development introduced the innovative chiral-only-at-metal asymmetric catalysts concept and put it in the spotlight of the scientific community.
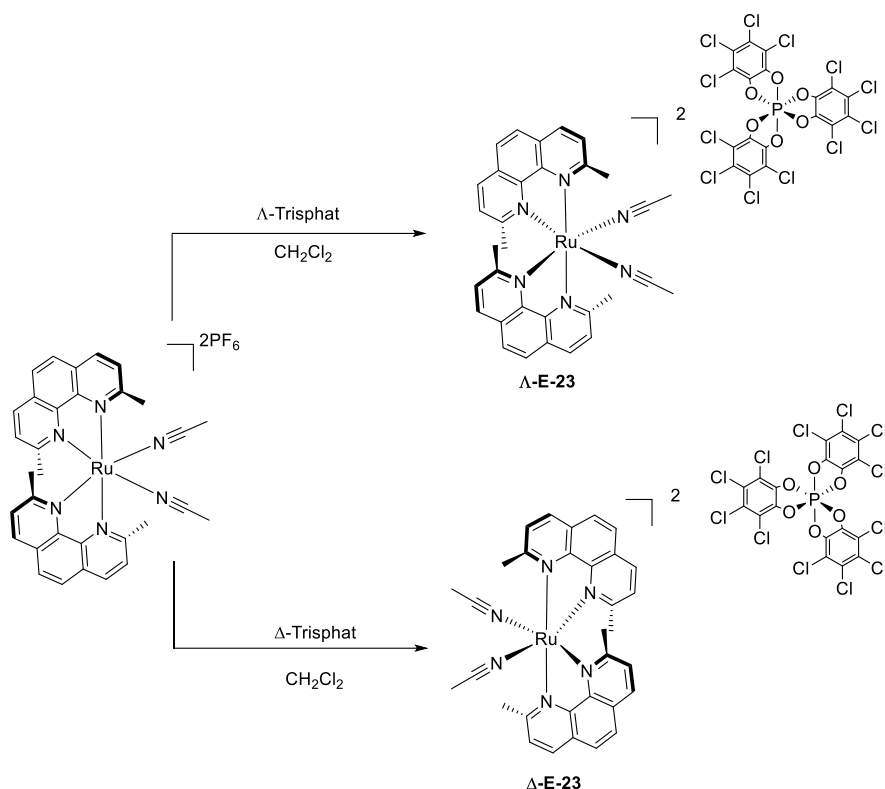
Scheme 1.37. Enantiopure Ru(II) catalyst (Fontecave **E-23**)[119].

For the synthesis of enantiopure Ir(III) complexes, there are some limitations: The lack of feasible synthetic methodologies to obtain the compounds, and the expensive strategies or difficulties in the enantiomeric purification (chiral preparative HPLC). Several synthetic methodologies to obtain enantiopure complexes were described using chiral counterions, solving the enantiomers by diastereoselective precipitation, based on the solubility principle of the diastereomeric salts obtained, as decribed by Fontecave for Ru(II) derivatives.[119,120] More recently, the synthesis of chiral-at-metal complexes using chiral auxiliary ligands was described by Meggers et al.[121,122] The strategy is to separate the enantiomers present in a racemic mixture of a particular complex by creating diastereomers using an enantiopure chiral ligand as chiral resolution agent. The use of chiral ligands causes the generation of diastereomers, which have different chemical/physical properties. Therefore, the purification of these complexes can be done through the classical purification methodologies (precipitation, column chromatography, etc).

Enantiomers:

- Identical chemical/physical properties
- Hard to purify with classic methodologies
- Expensive equipment is needed (chiral HPLC)

Diastereomers

- Different chemical/physical properties
- Easy to purify with classic methodologies
- Expensive equipment not required
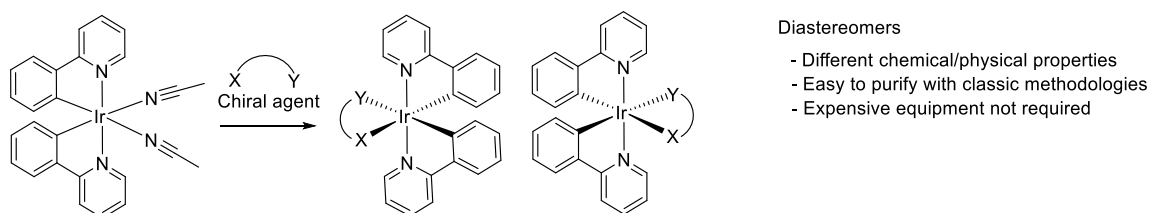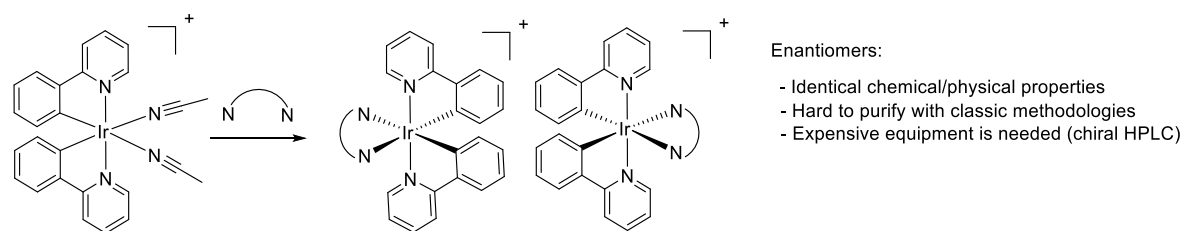
Scheme 1.38. Benefits of using diastereomers forming strategy over the classical enantiomer forming strategy.

In 2018 Meggers published a detailed protocol for the synthesis of some bis-cyclometalated octahedral Ir(III) and Rh(III) enantiopure chiral-at-metal complexes (Scheme 1.39). The process consists of several reaction steps. They are described here for one of them as an example:

- First, it is necessary to synthesize a metallic precursor. In this case, commercially available $IrCl_3·3H_2O$ reacts in a mixture of ethoxyethanol/H_2O with the desired cyclometalated ligand (5-(tert-butyl)-2-phenylbenzothiazole, Hpbt). Once the corresponding $[Ir(pbt)_2(Cl)]_2$ is formed, the cleavage of the chloride bridges takes place using a chloride abstractor ($AgPF_6$) in CH_3CN, obtaining the racemic precursor **rac-E-24**.

- Second, the **rac-E-24** precursor reacts in the presence of a base (Et_3N) with the chiral and enantiopure ligand ((**S**)-2-(4-isopropyl-4,5-dihydrothiazol-2-yl)phenol) in CH_2Cl_2, obtaining a mixture of diastereomers (**Δ-(S)-E-25** and **Λ-(S)-E-25**). The separation and purification of the desired enantiopure compounds are carried out through conventional methodologies (chromatography column in silica using hexane/ethyl acetate solvent mixtures (10:1)).

- Finally, the chiral agent must be removed once the diastereomers are separated. For this purpose, the compounds are dissolved separately in CH_3CN, and TFA (trifluoroacetic acid) is added. TFA will protonate the chiral ligand, thus creating empty coordination vacancies that solvent molecules will occupy (acetonitrile), obtaining the enantiopure precursor **Λ/Δ-E-24**.
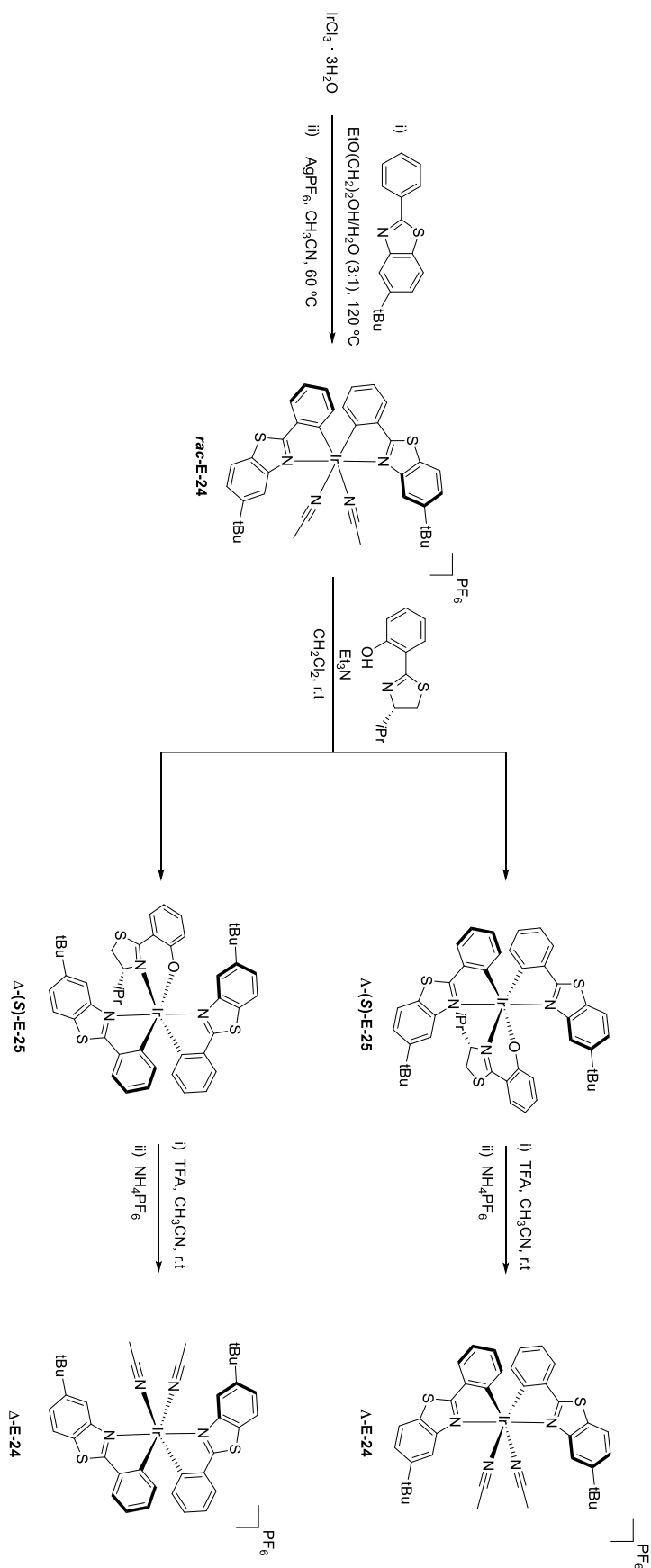
Scheme 1.39. Chiral resolution to obtain enantiopure Ir(III) complexes.

Through this protocol, Meggers et al. present a simple way to generate enantiopure chiral-at-metal octahedral complexes using conventional purification methodologies. This efficient procedure opens the possibility of improving and developing more sophisticated applications. The applications most related to Ir(III) complexes, such as OLEDs, their implementation as catalysts in photoredox reactions, their use in bioimaging applications, or their action in photodynamic therapy (PDT) such as metallodrugs, evolve toward more sophisticated applications as polarized light emitters, or its use in asymmetric catalysis, fundamental for the pharmaceutical industry. Likewise, using enantiopure complexes in bio-imaging or PDT applications can generate highly selective applications to selective interactions with living beings. In the following paragraphs, two applications already described in the literature will be explained, as representative examples of some of the applications improved by using enantiopure complexes.

The photoredox asymmetric catalysis induced by visible light is one of the most prominent applications. Typically, if it was possible to carry out an asymmetric photoredox catalysis, it was necessary to use two catalysts simultaneously, one responsible for the photoredox catalysis and the other as a catalyst for the asymmetric reaction.[123] This changes with bis-cyclometalated enantiopure Ir(III) catalysts as they combine the ability to serve as asymmetric and photoredox catalysts.[124,125] Mechanistic studies were described for the catalysis of 2-acyl imidazoles from **E-26** (Figure 1.33), demonstrating high reaction yield and high enantioselectivity under mild reaction conditions.[126]
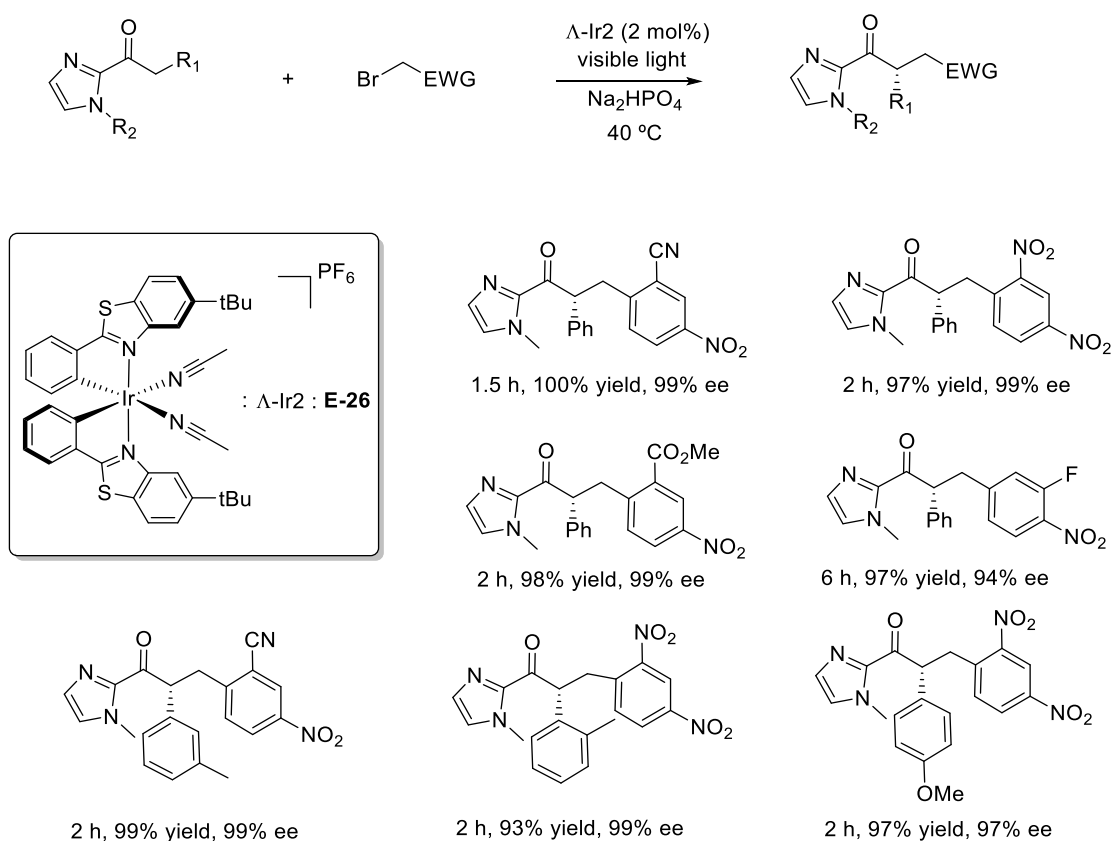
Figure 1.33. Meggers' results using enantiopure **E-26** as catalyst for photoredox asymmetric catalysis.

Besides that, different enantiopure Ir(III) complexes have been tested as polarized light emitters (CPL-OLEDs). Zheng and Zuo published in 2019 a study in which they synthesized four enantiopure iridium complexes (**Λ/Δ-E-27** and **Λ/Δ-E-28**), which were tested as CPL emitters (Scheme 1.40).[127]

[Λ/Δ-(tfpz)₂-Ir-(R-L1)]   **E-27**   [Λ/Δ-(tfpz)₂-Ir-(R-L2)]   **E-28**
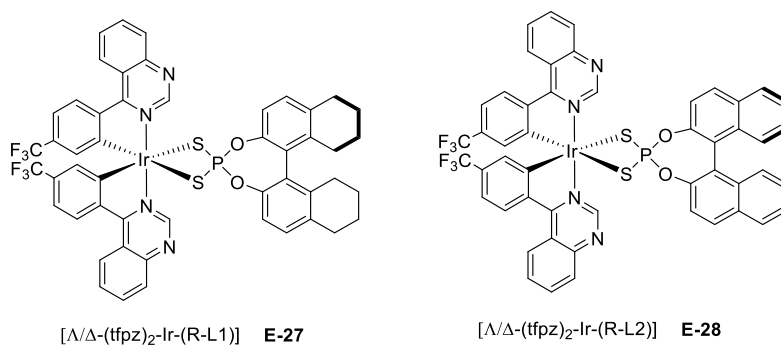
Scheme 1.40. **E-27** and **E-28** enantiopure complexes synthetized by Zuo et al.

The strategy followed by Zuo is to obtain iridium complexes with a dual stereogenic center, coordination of a chiral agent and the enantiopure metal center. Since the compounds were diastereomers, they were purified by simple chromatographic columns. Additionally, these compounds showed suppression of the self-quenching effect due to large sterically-hindered groups.[128] These compounds were tested as light-emitting systems (OLEDs) in their racemate mixture, showing good emitting efficiency. For further development, it was tried to study the efficiency of these diastereomers as CPL- OLEDs. They studied them by circular dichroism (CD) and circularly polarized luminescence (CPL) techniques. Figure 1.34 shows the results obtained by Zuo et al. In graphs a and b, it can be observed how, employing CD, they verify that they were able to obtain the four possible diastereomers, and that they were (as expected) two pairs of enantiomers, both for **E-27** and **E-28**. In the lower graphs (c and d), the results obtained from CPL spectroscopy are presented, showing that using enantiopure complexes as light emitters (OLEDs), a polarized emission can be obtained. Taking as an example graph C (corresponding to the **E-27** complex), the representation obtained for the results of a racemic mixture of *rac*-**E-27** can be seen in light green. As expected, the absence of an enantiopure chiral sample does not generate signal by CPL. While for the diastereomers **Λ-E-27** (red) and **Δ-E-27** (blue), a signal is observed by CPL, confirming the creation of polarized light-emitting OLED systems.
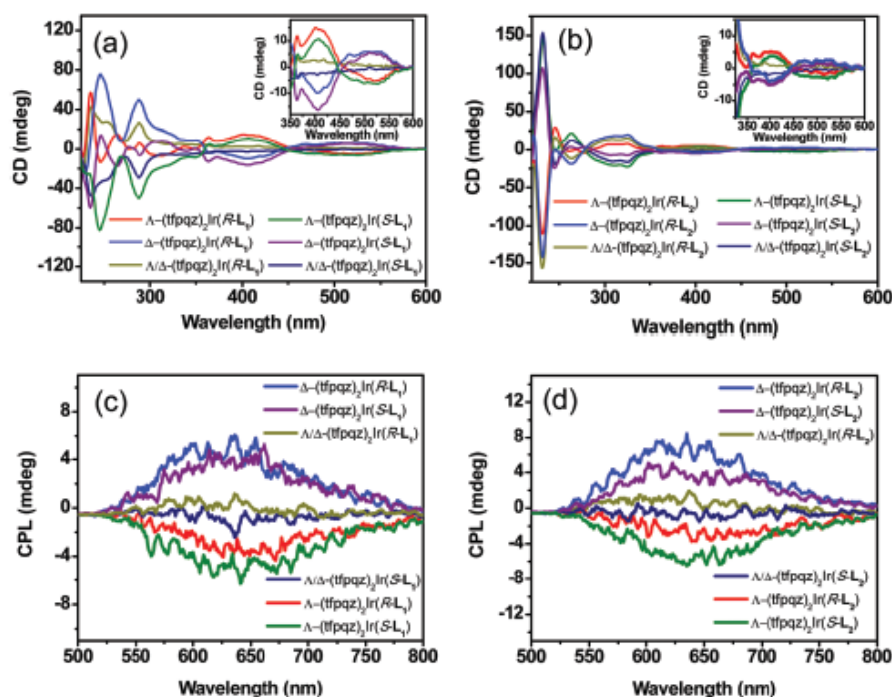
Figure 1.34. CD and CPL spectra for compound **E-27** and **E-28**.[128]

After studying in-depth the state of the art for the concepts of photomodulable molecules, organometallic compounds, and their possible applications, different arguments have been extracted for the study of these compounds in the following work:

❖ DTE compounds are among the best described molecular switch families due to their excellent photochromic properties, high fatigue resistance, and excellent thermal stability.

❖ Its high thermal stability inhibits the possible thermochromic character of the compounds, which means that the isomerization process is only generated employing light irradiation.

❖ Concerning the structure of DTEs, these allow the system to be functionalized, enabling the generation of large families of DTEs. In addition, the modification in the molecules' open form (**OF**) allows the obtaining of a wide range of colors through the entire UV-Vis spectrum, once the photocyclization process (**CF**) occurs.

❖ The modification of the structure also allows the coordination of the photoswitch compounds to metallic centers, rendering organometallic compounds with new properties and advantageous applications.

❖ The use of bis- and tris-cyclometalated iridium compounds has been widely studied due to their high stability and luminescence properties, such as the high half-life of phosphorescence and their high tunability for obtaining different emissive colors.

❖ Due to their excellent qualities, Ir(III) complexes have been used in various applications in OLED systems construction, photoredox catalysis, or drug delivery, demonstrating a high diversity of applicability.

❖ In addition, recent synthetic protocols allow the generation of Ir(III) enantiopure complexes, enabling improvements and greater selectivity in the applications already described.

1.4 GENERAL OBJETIVES

The general objective of this thesis is the synthesis of new DTE-based ligands and their subsequent coordination to iridium metal precursors for the formation of photoswitchable organometallic complexes capable of altering their properties through an external stimulus (light).

On a later stage, these compounds will be synthesized in a chiral-at-metal enantiopure manner, to study the possibility of inducing a diastereoselective isomerization of the coordinated DTE.

Figure 1.32 graphically collects the objectives set for this thesis, synthesis of DTE ligands, their coordination to racemic metal Ir(III) center and subsequent coordination to enantiopure Ir(III) precursors to study for the diastereoselective photocyclization of the DTE.

In short, we pursue a light-induced amplification of the chirality.
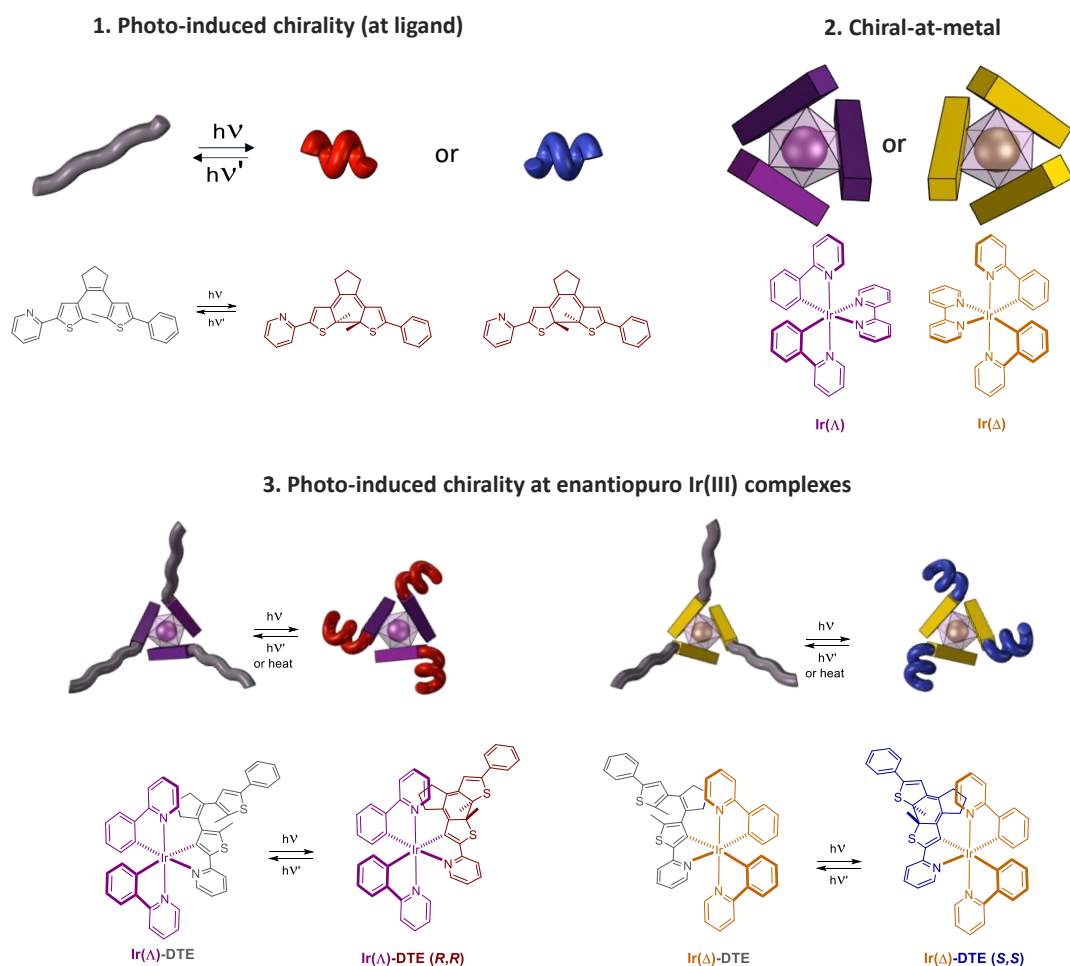
Figure 1.35. Graphic representation of the general objectives proposed for this work.

1.5 REFERENCES

[1] G. H. Brown, *Photochromism*, Wiley-Interscience, New York, **1971**.

[2] H. Dürr, H. Bouas-Laurent, *Photochromism: Molecules and systems*, Elsevier, Amsterdam, **2003**.

[3] H. Dürr, H. Bouas-Laurent, *Pure Appl. Chem*., **2001**, *73*, 639-665.

[4] B. L. Feringa, R. A. van Delden, N. Koumura, E. M. Geertsema, *Chem. Rev*., **2000**, *100*, 1789-1816.

[5] C. Fankhauser, *J. Biol. Chem*., **2001**, *276*, 11453-11456.

[6] P. Hegemann, *Planta*, **1997**, *203*, 265-274.

[7] H. Luecke, B. Schobert, J-P. Cartailler, H-T. Richter, A. Roengarth, R. Needleman, J. K. Laniy, *J. Mol. Biol*., **2000**, *300*, 1237-1255.

[8] D. Kitagawa, S. Kobatake, *Chem. Commun*., **2015**, *51*, 4421-4424.

[9] R-J. Li, J. J. Holstein, W. G. Hiller, J. Andréasson, G. H. Clever, *J. Am. Chem. Soc*., **2019**, *141*, 2097-2103.

[10] K. Uchida, M. Saito, A. Murakami, S. Nakamura, M. Irie, *Adv. Mater*., **2003**, *15*, 121-125

[11] M. Mohri. M. Irie, *J. Org. Chem*., **1988**, *53*, 803-808.

[12] S. Nakamura, M. Irie, *J. Org. Chem*., **1988**, *53*, 6136-6138.

[13] M. Irie, K. Hayashi*., J. Macromol. Sci. Chem*., **1979**, 511.

[14] M. Irie, A. Menju, K. Hayashi., *Macromolecules*, **1979**, *12*, 1176.

[15] M. Irie, W. Schnabel. *Eur. Polymer J*., **1982**, *18*, 15.

[16] W. H. Laarhoven in *Photochromism. Molecules and Systems*. (Ed.: H. Dürr, H. Bouas-Laurent), rev. ed. Elvesier, Amsterdam, **2006**.

[17] M. Irie, M. Mohri, *J. Org. Chem*., **1988**, *53*, 803-808.

[18] M. B. Groen, H. Wynberg, R. M. Kellogg, *J. Org. Chem*., **1967**, *32*, 3093-3100.

[19] M. Alonso, B. Herradón, *Chem. Eur. J*., **2007**, *13*, 3913-3923.

[20] M. Hanazawa, R. Sumiya, Y. Horikawa, M. Irie*, J. Chem. Soc., Chem. Commun*., **1992**, 206-207.

[21] M. Irie, T. Eriguchi, T. Takada, K. Uchida, *Tetrahedron*, **1997**, *53*, 12263-12271.

[22] M. Irie, T. Fukaminato, K. Matsuda, S. Kobatake, *Chem. Rev*., **2014**, *114*, 12174-12277.

[23] G. Szalóki, J-L. Pozzo, *Chem. Eur. J*., **2013**, *19*, 11124-11132.

[24] S. Takami, S. Kobatake, T. Kawai, M. Irie, *Chem. Lett*., **2003**, *32*, 892-893.

[25] S. Kobatak, K. Uchida, E. Tsuchida, M. Irie, *Chem. Let.*, **2000**, 1340-1341.

[26] M. Irie, T. Lifka, S. Kobatake, N. Kato, *J. Am. Chem. Soc*., **2000**, *122*, 4871-4876.

[27] S. Nakamura, M. Irie, *J. Org. Chem*., **1988**, *53*, 6136-6138.

[28] S. L. Gilat, S. H. Kawai, J-M. Lehn, *Chem. Eur. J*., **1995**, *1*, 275-285.

[29] D. Kitagawa, K. Sasaki, S. Kobtake*, Bull. Chem. Soc. Jpn*., **2011**, *84*, 141-147

[30] M. Irie, T. Lifka, K. Uchida, S. Kobatake, Y. Shindo, *Chem. Commun., **1999**, 747-750.

[31] M. Irie, E. Tsuchida, Y. Aoi, S. Nakamura, M. Irie, *Chem. Lett*., **1995**, *60*, 8305-8309.

[32] M. V. Oplachko, A. B. Smolentsev, I. M. Magin, I. P. Pozdnyakov, V. A. Nichiporenko, V. P. Grivin, V. F. Plyusnin, V. V. Vyazovkin, V. V. Yanshole, M. V. Parkhats, A. V. Yadykov, V. Z. Shirinian, E. M. Glebov, *Phys. Chem. Chem. Phys*., **2020**, *22*, 5220-5228.

[33] M. Herder, B. M. Schmidt, L. Grubert, M. Pätzel, J. Schwarz, S. Hecht, *J. Am. Chem. Soc*., **2015**, *137*, 2738-2747.

[34] K. Higashiguchi, K. Matsuda, S. Kobatake, T. Yamada, T. Kawai, M. Irie, *Bull. Chem. Soc. Jpn*., **2000**, *73*, 2389-23994.

[35] P. D. Patel, I. A. Mikhailov, K. D. Belfield, A. E. Masunov, *Int. J. Quantum Chem*., **2009**, *109*, 3711-3722.

[36] R. B. Woodward, R. Hoffmann, *Angew. Chem. Int. Ed*., **1969**, *8*, 781-932.

[37] R. B. Woodward, R. Hoffmann, *J. Am. Chem. Soc*., **1969**, *87*, 395-397.

[38] T. Sumi, Y. Takagi, M. Morimoto, M. Irie, *Chem. Commun*., **2014**, *50*, 3928-3930.

[39] M. Boggio-Pasqua, M. Ravaglia, M. J. Bearpark, M. Garavelli, M. A. Robb*, J. Phys. Chem. A*., **2002**, *107*, 11139.

[40] T. Sumi, Y. Takagi, M. Morimoto, M. Irie, *Chem. Commun*., **2014**, *50*, 3928-3930.

[41] T. Yamaguchi, M. Irie, *Photochem. Photobiol*., **2006**, *178*, 162-169.

[42] M. Takeshita, S. Yamaguchi, *Chem. Lett*., **2011**, *40*, 646-647.

[43] T. Kaide, S. Kobatake, H. Miyasaka, M. Murakami, N. Iwai, Y. Nagata, A. Itaya, M. Irie, *J. Am. Chem. Soc*., **2002**, *124*, 2015-2024.

[44] M. Irie, K. Sayo, *J. Phys. Chem*., **1992**, *96*, 7671-7674.

[45] T. Yamaguchi, K. Uchida, M. Irie, *J. Am. Chem. Soc*., **1997**, *119*, 6066-6071.

[46] J. J. D. de Jong, L. N. Lucas, R. M. Kellogg, J. H. van Esch, B. L. Feringa, *Science*, **2004**, *304*, 278-281.

[47] T. Kodani, K. Matsuda, T. Yamada, S. Kobatake, M. Irie, J. Am. Chem. Soc., 2000, 122, 9631-9637.

[48] K. Uchiad, M. Walko, J. J. D de Jong, S-I. Sukata, S. Kobatake, A. Meetsma, J. van Esch, B. L. Feringa, *Org. Biomol. Chem.,* **2006**, *4*, 1002-1006.

[49] C. Shen, X. He, L. Toupet, L. Norel, S. Rigaut, J. Crassous, *Organometallics*, **2018**, *37*, 697-705.

[50] T. C. S. Pace, V. Müller, S. Li, P. Lincoln, J. Andréasson, *Angew. Chem. Int. Ed.*, **2013**, *52*, 4393-4396.

[51] Z. Chen, Z-Y. Li, Y. Bin, L. Huang, F-S. Zhang, *Sci. China Ser. B-Chem.*, **2008**, *51*, 263-268.

[52] C. Liu, B. Hu, C. Yu, J. Li, *Yingyong Xuaxue*, **2017**, *34*, 527-533.

[53] H. Al Sabea, L. Norel, O. Galangau, H. Hijazi, R. Métivier, T. Roisnel, O. Maury, C. Bucher, F. Riobé, S. Rigaut, *J. Am. Chem. Soc.*, **2019**, *414*, 20026-20030.

[54] K. Uchida, M. Saito, A. Murakami, S. Nakamura, M. Irie, *Adv. Mater.*, **2003**, *15*, 121-125.

[55] A. Takata, S. Yokojima, H. Nakagawa, Y. Matsuzawa, A. Murakami, S. Nakamura, M. Irie, K. Uchida, *J. Phys. Org. Chem.,* **2007**, *20*, 988-1006.

[56] A. Bianco, C. Bertrarelli, J. F. Rabolt, G. Zerbi, *Chem. Mater.*, **2005**, *17*, 869-874.

[57] M. Saito, T. Miyata, A. Murakami, S. Nakamura, M. Irie, K. Uchida, *Chem. Lett.*, **2004**, *33*, 786-787.

[58] K. Uchida, A. Takata, M. Saito, A. Murakami, S. Nakamura, M. Irie, *Adv. Mater.*, **2003**, *15*, 785-788.

[59] K. Uchida, A. Takata, M. Saito, A. Murakami, S. Nalamura, M. Irie, *Adv. Funct. Mater.*, **2003**, *13*, 755-762.

[60] A. Takata, M. Saito, S. Yokojima, A. Murakami, S. Nakamura, M. Irie, K. Uchida, *Jpn. J. App. Phys.*, **2006**, *45*, 7114-7120.

[61] T. Kim, L. Zu, R. O. Al-Kasy, C. J. Bardeen, *ChemPhysChem*, **2014**, *15*, 400-414.

[62] D-D. Han, Y-L. Zhang, J-N. Ma, Y-Q. Liu, B. Han, H-B. Sun, *Adv. Mater.*, **2016**, *28*, 8328-8343.

[63] D. Kitagawa, H. Nishi, S. Kobatake, Angew. Chem. Int. Ed., 2013, 52, 9320-9322.

[64] D. Kitagawa, H. Tsujioka, F. Tong, X. Dong, C. J. Bardeen, S. Kobatake, *J. Am. Chem. Soc.*, **2018**, *140*, 4208-4212.

[65] R. O. Al-Kaysi, A. M. Müller, C. J. Bardeen, *J. Am. Chem. Soc.*, **2006**, *128*, 15938-15939.

[66] X. Dong, F. Tong, K. M. Hanson, R. O. Al-Kaysi. D. Kitagawa, S. Kobatake, C. J. Bardeen, *Chem. Mater.*, **2019**, *31*, 1016-1022.

[67] M. Morimoto, M. Irie, *J. Am. Chem. Soc.*, **2010**, *132*, 14172-14178.

[68] M. Irie, O. Miyatake, K. Uchida, *J. Am. Chem. Soc.*, **1992**, *114*, 8715-8716.

[69] B. L. Feringa, *Nature*, **2000**, *408*, 151-153.

[70] B. L. Feringa, *Acc. Chem. Res.*, **2001**, *34*, 504-513.

[71] J. Vicario, M. Walko, A. Meetsma, B. Feringa, *J. Am. Chem. Soc.*, **2006**, *128*, 5127-5135.

[72] D. Roke, C. Stuckhardt, W. Danowski, S. J. Wezenberg, B. L. Feringa, *Angew. Chem. Int. Ed.*, **2018**, *57*, 10515-10519.

[73] J. T. Foy, Q. Li, A. Goujon, J-R. Colard-Itté, G. Fuks, E. Moulin, O. Schiffmann, D. Dattler, D. P. Funeriu, N. Giuseppone, *Nat. Nanotec.h*, **2017**, *12*, 540-545.

[74] Q. Li, G. Fuks, E. Moulin, M. Maaloum, M. Rawiso, I. Kulic, J. T. Foy, N. Giuseppone, *Nat. Nanotech*, **2015**, *10*, 161-165.

[75] A. Fernández-Acebes, J-M. Lehn, *Chem. Eur. J.*, **1999**, *5*, 3285-3292.

[76] R. T. F. Jukes, V. Adamo, F. Hartl, P. Belser, L. de Cola, *Inorg. Chem.*, **2004**, *43*, 2779-2792.

[77] K. Uchida, A. Inagaki, M. Akita, *Organometallics*, **2007**, *26*, 5030-5041.

[78] S. K. Brayshaw, S. Schiffers, A. J. Stevenson, S. J. Teat, M. R. Warren, R. D. Bennett, I. V. Sazanovich, A. R. Buckley, J. A. Weinstein, P. R. Raithby, *Eur. Chem. J.*, **2011**, *17*, 4385-4395.

[79] L-X. Cai, L-L. Yan, S-C. Li, L-P. Zhou, Q-F. Sun, *Dalton Trans.*, **2018**, *47*, 14204-14210.

[80] C-T. Yeung, W. T. K. Chan, S-C. Yan, K-L. Yu, K-H Yim, W-T. Wong, G-L. Law, *Chem. Commun.*, **2015**, *51*, 592-595

[81] T. Zhang, G-L. Zhang, L-P. Zhou, X-Q. Guo, Q-F. Sun, *Tetrahedron: Asymmetry*, **2017**, *28*, 550-554.

[82] W. Tan, Q. Zhang, J. Zhang, H. Tian, *Org. Lett.*, **2009**, *11*, 161-164.

[83] S. Sprouse, K. A. King, P. J. Spellane, R. J. Watts, *J. Am. Chem. Soc.*, **1984**, *106*, 6647-6653.

[84] X. Wei, J. peng, J. Cheng, M. Xie, Z. Lu, C. Li, Y. Cao, *Adv. Mater.*, **2007**, *17*, 3319-3325.

[85] Y. Guo, D. Zhang, J. Wang, H. Lu, S. Pu, *Dyes & Pigm*ents, **2020**, *175*, 108191.

[86] M. A. Baldo, D. F. O'Brien, Y. You, A. Shoustivto, S. Sibley, M. E. Thompson, S. R. Forrest, *Nature*, **1998**, *395*, 151-154.

[87] A. B. Tamayo, B. D. Alleyne, P. I. Djurovich, S. Lamansky, I. Tsyba, N. N. Ho, R. Bau, M. E. Thompson, *J. Am. Chem. Soc.*, **2003**, *125*, 7377-7397.

[88] R. C. Evans, P. Douglas, C. J. Winscom, *Coord. Chem. Rev.*, **2006**, *250*, 2093-2126.

[89] S. I. Bezzubov, Y. M. Kiselev, A. V. Churakov, S. A. Kozyukhin, A. A. Sadovnikov, V. A. Grinberg, V. V. Emets, V. D. Doljenko, *Eur. J. Inorg. Chem*., **2016**, 347-354

[90] A. R. B. M. Yusoff, A. J. Huckaba, M. K. Nazeeruddin, *Top. Curr. Chem*., **2017**, *375*, 1-30.

[91] H. Yersin and W. J. Finkenzeller, **2008**, *Triplet Emitters for Organic Light-Emitting Diodes: Basic Properties*, 1-97. H. Yersin, *Highly Efficient OLEDs with Phosphorescent Materials*, Wiley-VCH.

[92] J. C. Deaton, F. N. Castellano, Archetypal i*ridium(III) compounds for optoelectronic and photonic applications: photophysical properties and synthetic methods*, **2017**, 1-50. E. Zysman-Colman, *Iridium(III) in Optoelectronic and Photonics Applications.* Wiley-VCH.

[93] Y. Chi, P-T. Chou, *Chem. Soc. Rev*., **2010**, *39*, 638-655.

[94] K. A. King, P. J. Spellane, R. J. Watts, *J. Am. Chem. Soc*., **1985**, *107*, 1431-1432.

[95] A. R. McDonald, M. Lutz, L. S. von Chrzanowski, G. P. M. Klink, A. L. Spek, G. van Koten, *Inorg. Chem*., **2008**, *47*, 6681-6692.

[96] R. Ragni, E. A. Plummer, K. Brunner, J. W. Hofstraar, F. Babudri, G. M. Farinola, F. Naso, L. de Cola, *J. Mater. Chem.,* **2006**, *16*, 1161-1170.

[97] A. B. Tamayo, B. D. Alleyne, P. I. Djurovich, S. Lamansky, I. Tsyba, N. N. Ho, R. Bau, M. E. Thompson, *J. Am. Chem. Soc*., **2003**, *125*, 7377-7397.

[98] C. Xia, B. Alleyne, R. C. Kwong, J. Fiordeliso, J. Brooks, V. Adamovich, M. S. Weaver, *US Patent*, **2011**/0227049.

[99] M. C. De Rosa, D. J. Hodgson, G. D. Enright, B. Dawson, C. E. B. Evans, R. J. Crutchley, *J. Am. Chem. Soc.,* **2004**, *126*, 7619-7626.

[100] A. F. Henwood, E. Zysman-Colman, *Top. Curr. Chem*., **2016**, *374*, 46-87.

[101] T-Y. Li, J. Wu, Z-G. Wu, Y-X. Zheng, J-L. Zuo, Y. Pan, *Coord. Chem. Rev*., **2018**, *374*, 55-92.

[102] M. A. Baldo, S. Lamasky, P. E. Burrows, M. E. Thompson, S. R. Forrest, *Appl. Phys. Lett*., **1999**, *75*, 4-6.

[103] G. Zhou, Q. Wang, C-L. Ho, W-Y. Wong, D. Ma, L. Wang, Z. Lin, *Chem. Asian. J*., **2008**, *3*, 1830-1841.

[104] T. Sajoto, P. I. Djurovich, A. Tamayo, M. Yousufuddin, R. Bau, M. E. Thompson, *Inorg. Chem*., **2005**, *44*, 7992-8003.

[105] X-F. Ren, G-J. Kang, S-F. Zhang, A-M. Ren, W-Y. Wong, G. Zhou, Y-L. Liu, *J. Photochem. Photobiol., A* *2015, 311,* 85-94*.*

[106] T. Giridhar, T-H. Han, W. Cho, C. Saravanan, T-W. Lee, S-H. Jin, *Chem. Eur. J*., **2014**, *20*, 8260-8264.

[107] W. Cho, G. Sarada, H. Lee, M. Song, Y-S. Gal, Y. Lee, S-H. Jin, *Dyes & Pigm*ents, **2017**, *136*, 390-397.

[108] C. C. Konkankit, S. C. Marker, K. M. Knopf, J. J. Wilson, *Dalton Trans.,* **2018**, *47*, 9934-9974.

[109] P. J. O' Dwyer, J. P. Stevenson, S. W. Johnson, *Drugs*, **2000**, *59*, 19-27

[110] R. Oun, Y. E. Moussa, N. J. Wheate, *Dalton Trans*., **2018**, *47*, 6645-6653.

[111] T-S. Kang, W. Wang, H-J. Zhong, Z-Z. Dong, Q. Huang, S. W. F. Mok, C-H. Leung, V. K. W. Wong, D-L. Ma, *Cancer Letters*, **2017**, *396*, 76-84.

[112] K. Xiong, Y. Chen, C. Ouyang, R-L. Guan, L-N. Ji, H. Chao, *Biochimie*, **2016**, *125*, 186-194.

[113] W-Y. Zhang, F. Du, M. He, L. Bai, Y-Y. Gu, L-L. Yang, Y-J. Liu, *European Journal of Medicinal Chemistry*, **2019**, *178*, 390-400.

[114] Y. Zhang, H. Fu, S. Chen, b. liu, W. Sun, H. Gao, *Chem Commun*., **2019**, *199*, 110757.

[115] L. Feng, Y. Dai, B. Liu, G. Yang, S. Gai, N. Niu, R. Lv, C. Li, P. Yang, *ACS Appl. Mater. Interfaces*, **2017**, *9*, 12993-13008.

[116] L. Zhang, E. Meggers, *Chem. Asian. J.,* **2017**, *12*, 2335-2342.

[117] Z-Y. Cao, W. D. G. Brittain, J. S. Fossey, F. Zhou, *Catal. Sci. Technol*., **2015**, *5*, 3441-3451.

[118] L. gong, L-A. Chen, E. Meggers, *Angew. Chem. Int. Ed*., **2014**, *53*, 10868-10874.

[119] M. Chavarot, S. Ménage, O. Hamelin, F. Charnay, J. Pécaut, M. Fontecave, *Inorg. Chem*., **2003**, *42*, 4810-4816.

[120] U. Knof, A. von Zelewsky, *Angew. Chem. Int. Ed*., **1999**, *38*, 302-322.

[121] E. Meggers, *Chem. Eur. J*., **2010**, *16*, 752-758.

[122] J. Ma, X. Zhang, X. Huang, S. Lo, E. Meggers, *Nature Protocols*, **2018**, *13*, 605-632.

[123] K. L. Skubi, T. R. Blum, T. P. Yoon, *Chem. Rev*., **2016**, *116*, 10035-10074.

[124] E. Meggers, *Chem. Commun*., **2015**, *51*, 3290-3301.

[125] R. Brimioulle, D. Lenhart, M. M. Maturi, T. Bach, *Angew. Chem. Int. Ed.,* **2015**, *54*, 3872-3890.

[126] H. Huo, X. Shen, C. Wang, L. Zhang, P. Röse, L-A. Chen, K. Harms, M. Marsch, G. Hilt, E. Megger, *Nature*, **2014**, *515*, 100-103.

[127] Z-P. Yan, K. Liao, H-B. Han, J. Su, Y-X. Zheng, J-L. Zuo, *Chem. Commun*., **2019**, *55*, 8215-8220.

[128] H. Z. Xie, M. W. Liu, O. Y. Wang, X. H. Zhang, C. S. Lee, L. S. Hung, S. T. Lee, P. F. Teng, H. L. Kwong, H. Zheng, C. M. Che, *Adv. Mater*., **2001**, *13*, 1245-1248.

CHAPTER 2

PYRIDYL-CONTAINING DITHIENYLETHENES: SYNTHESIS AND COORDINATION TO IR(III)
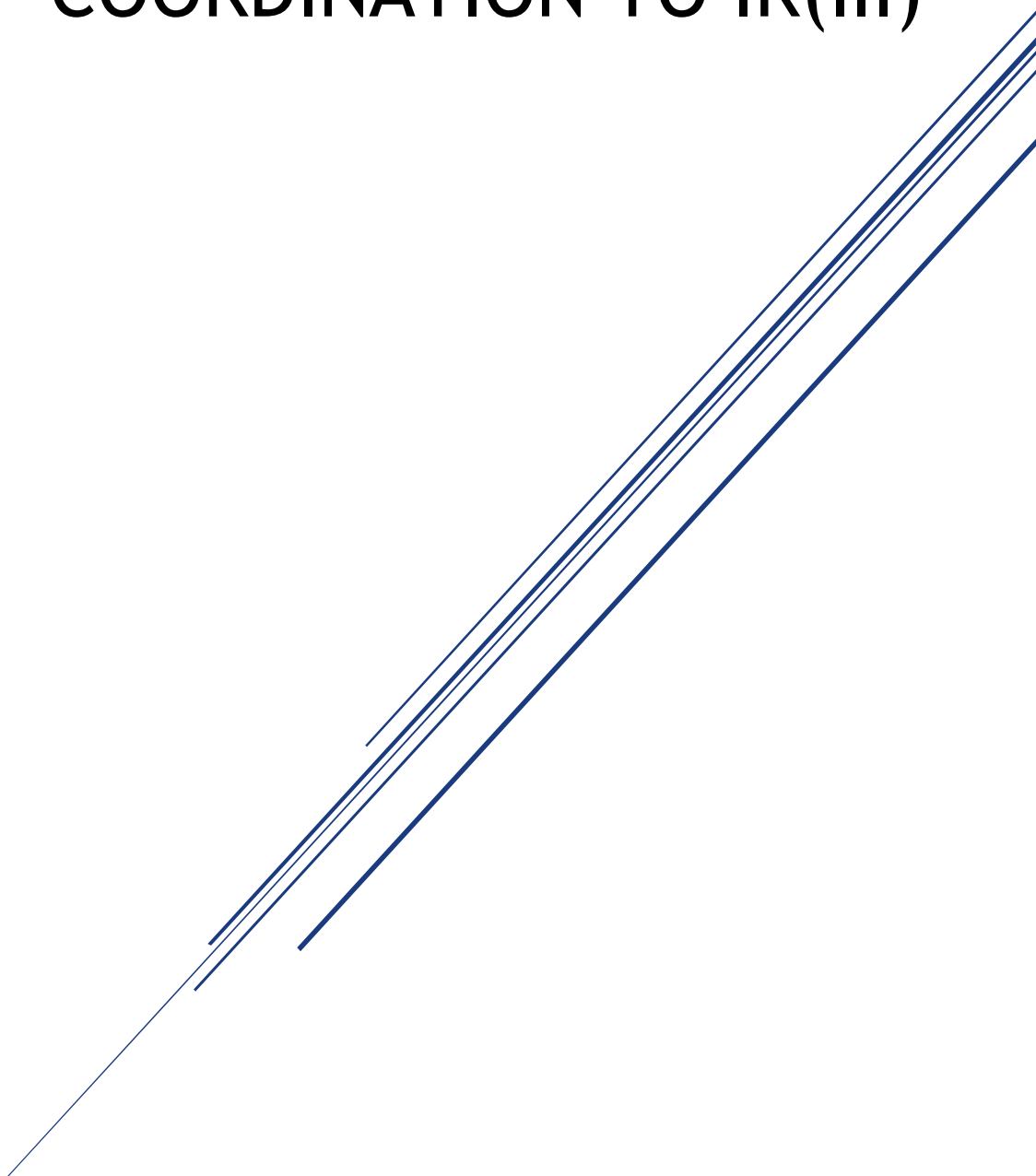
2. SYNTHESIS

The general objectives of the thesis are focused on obtaining enantiopure complexes of Ir(III) that contain cyclometalated DTE ligands in their organic structure. Therefore, this chapter will explore the synthesis of different DTE ligands (symmetric and non-symmetric) for their subsequent coordination via C-N to Ir(III) metal centers.

Once the coordination of photoswitch ligands has been studied, an attempt will be made to demonstrate how, through the use of enantiopure octahedral metal centers, a selective induction of the DTE photocyclization process can be generated.

2.1 LIGANDS

This chapter describes the synthesis of racemic bis-cyclometalated Ir(III) complexes containing a DTE-based auxiliary cyclometalated ligand. For this purpose, the synthesis of four potentially cyclometalating symmetric/non-symmetric DTEs was envisaged (shown in Scheme 2.1). The ligands (**L1-A**, **L1-B**, **L1-C** and **L1-D**) differ in their characteristics such as geometry, electronic conjugation and number or relative position of the coordinative site. They contain a pyridyl-thiophene fragment in their structure, which is intended to act as the cyclometalating fragment to coordinate to iridium. Additionally, they show differences in the non-coordinative thiophene moieties. These differences may be anticipated to lead to changes in the photoswitching behavior.
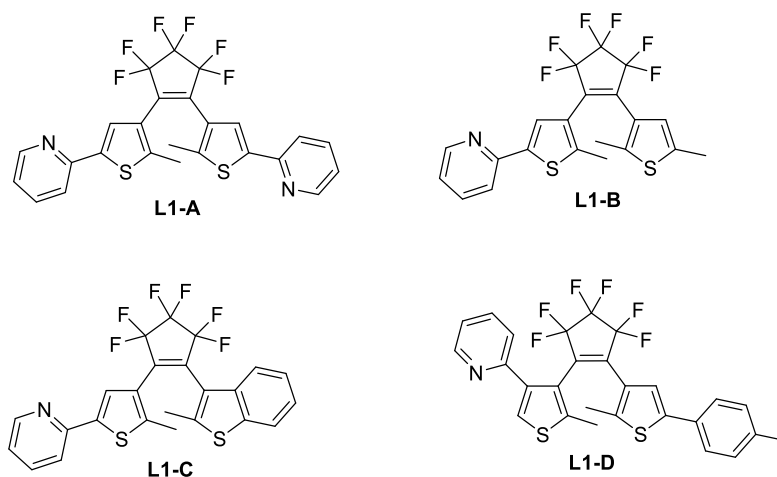
Scheme 2.1. Target symmetric/non-symmetric DTE ligands synthesized.

The DTE ligands can be configured varying the thiophene "arms" and the fluorinated cyclopentene that acts as a bridging unit. Figure 2.1 shows different synthetic routes from which the DTE ligands proposed for this section can be obtained. Each one of these ligands (**L1-A**, **L1-B**, **L1-C** and **L1-D**) can be obtained through alternative synthetic routes. The chosen synthetic path depends on the availability of reactants and/or intermediates and the different results obtained for previously synthesized DTEs. In the following sections, representative examples of each of the individual steps involved in the different routes and the synthesis of the required intermediates will be described.
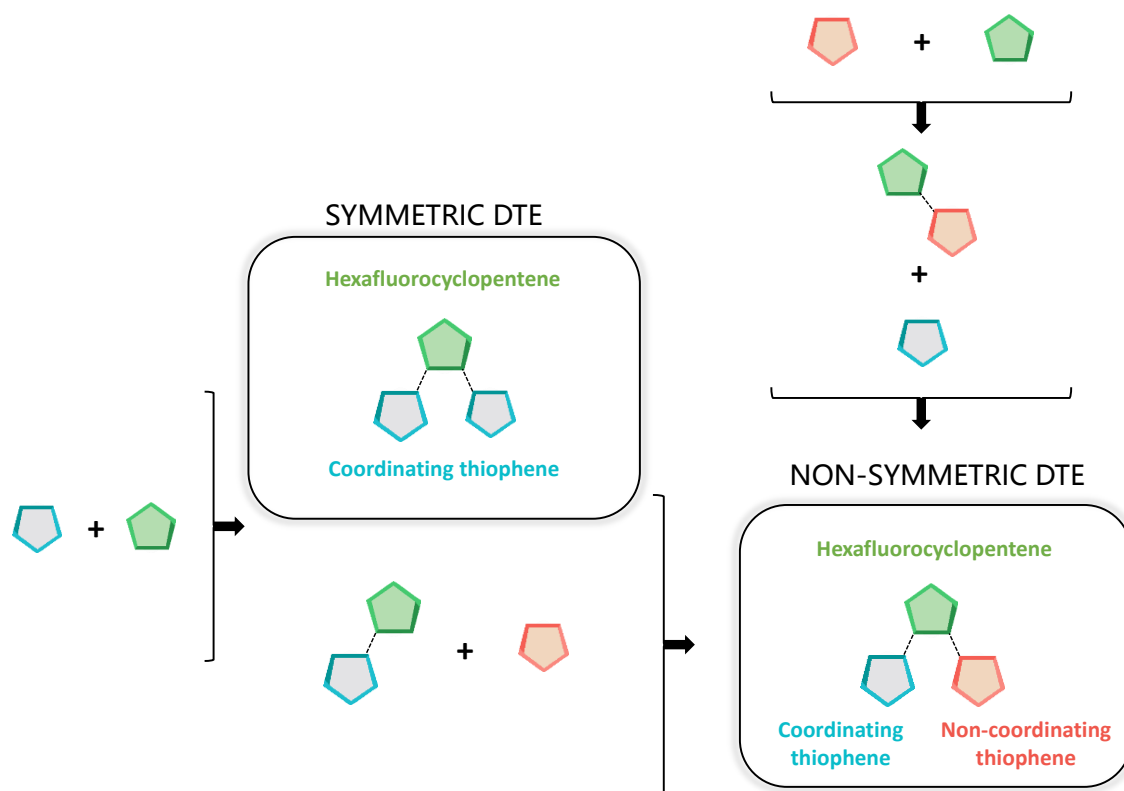
Figure 2.1. Conceptual scheme showing different synthetic routes for the proposed DTE ligands.

2.1.1. NON-COORDINATING THIOPHENE
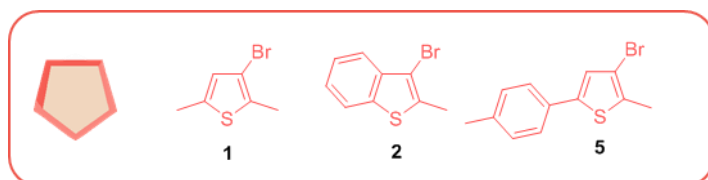
Three widely employed thiophenes were chosen to be used as non-coordinating thiophene modules: 2,5-dimethylthiophene, 2-methylbenzo[*b*]thiophene, 2-methyl-5-tolylthiophene. These commercially available compounds require a selective bromination on position 3 of the thiophene ring to be ready for their incorporation into the final DTE. The syntheses of the resulting 3-bromo derivatives **1**, **2**, and **5** were previously described in the literature.[1,2,3] The synthesis of intermediates **1** and **2** consisted of reacting the starting compound with N-bromosuccinimide (NBS) using acetic acid and/or CH_2Cl_2 as solvent (Scheme 2.2). When required, the reaction residue after workup was purified by column chromatography using silica gel as the stationary phase (see the experimental section for details). In the case of **5**, it was synthesized starting from commercially available 2-methylthiophene, through a double bromination using NBS, obtaining intermediate **3**, following a similar procedure as the one described for compounds **1** and **2**. After that, boronic acid intermediate **4** was obtained by reaction with *n*-BuLi and B(O^{i}Pr)$_3$ at -78 °C in dry Et$_2$O and subsequent workup. Finally, compound **5** was obtained by Suzuki-Miyaura coupling between **4** and 4-iodotoluene, using a mixture of THF/H$_2$O (9:1). All these compounds were obtained with moderate to high yields, and their identity and purity were confirmed by ^{1}H-NMR analysis. The spectra obtained are shown in Figure 2.2.
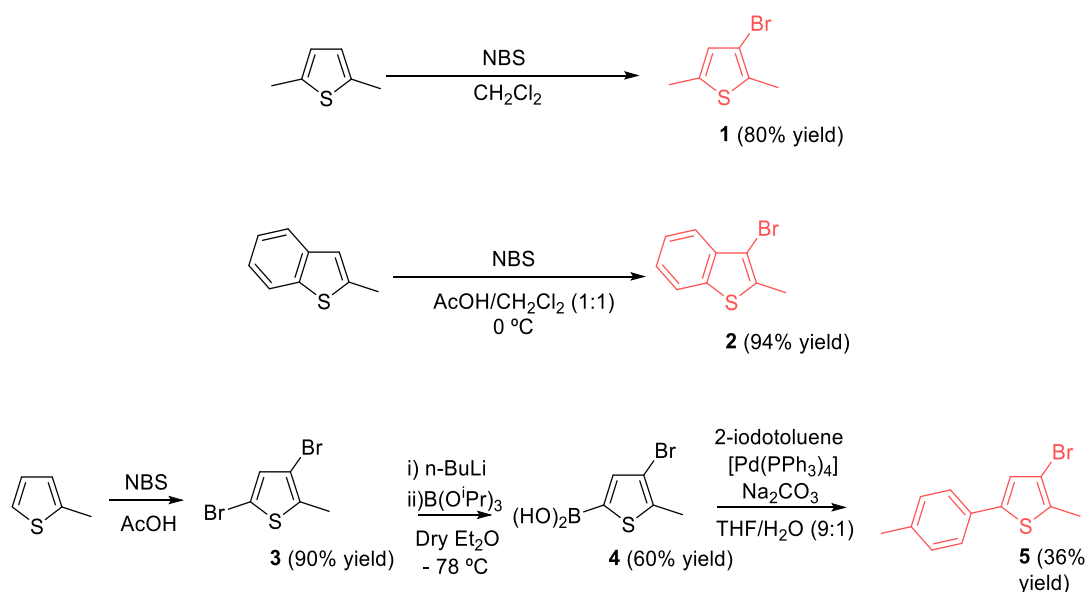
Scheme 2.2. Synthesis of non-coordinating thiophenes **1**, **2** and **5**.

In the case of derivative **1**, the ^{1}H-NMR spectrum shows a broad quadruplet in the aromatic region due to the thiophene proton and two signals in the aliphatic region of the spectra, a pseudo-quadruplet and a singlet, which are attributed to the two non-equivalent methyl groups. The ^{1}H-NMR spectrum of compound **2** shows a more complicated pattern. Two doublets and two doublets of doublets can be distinguished in the aromatic region. This multiplicity is consistent with the expected spin system. Additionally, a singlet due to the methyl group is observed in the aliphatic region of the spectra. Finally, for compound **5**, the two expected doublets are observed in the aromatic region which are assigned to the toluene aromatic protons, in addition to the singlet corresponding to the aromatic proton of the thiophene group. In the aliphatic region of the spectrum, two singlets attributed to the methyl group of the toluene and methyl thiophene are observed. These spectroscopic patterns are in agreement with those described in the literature for the same compounds.[1,2,3]
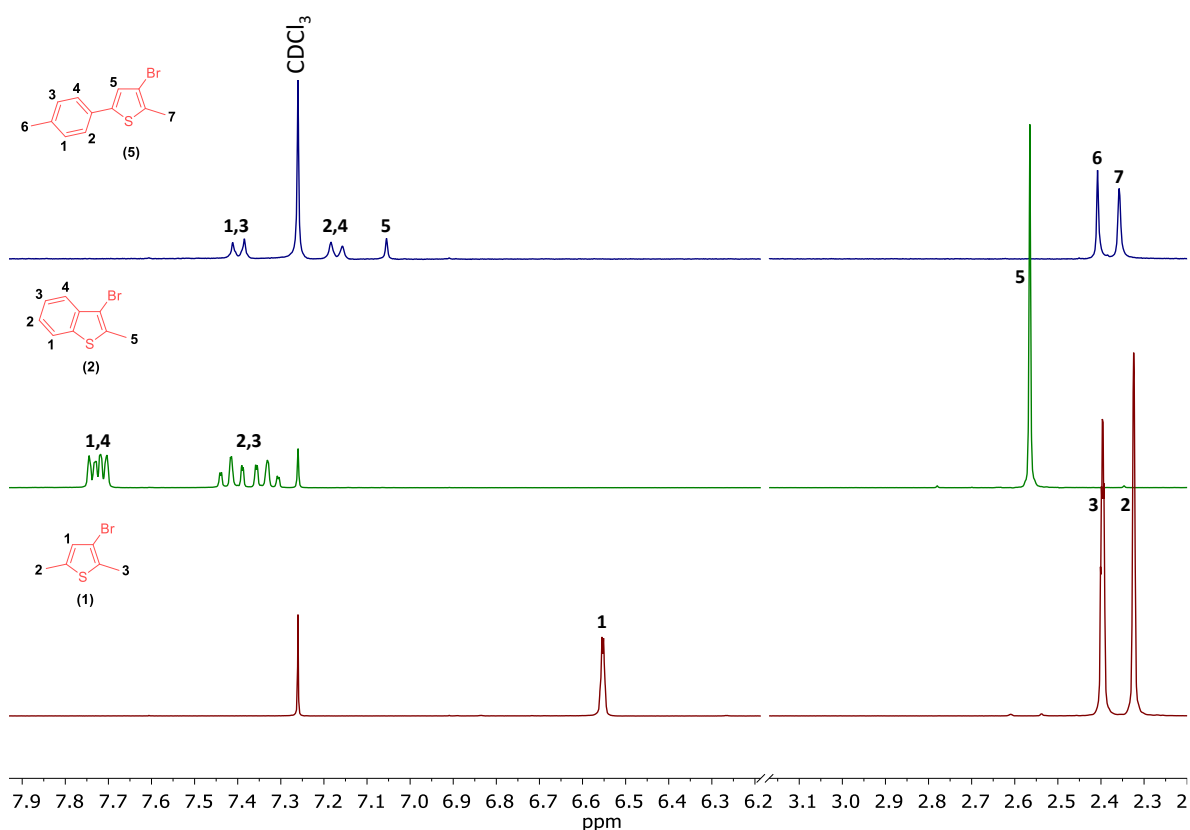
Figure 2.2. ^{1}H-NMR spectra of compounds **1** (red), **2** (green) and **5** (blue). (CDCl$_3$, 300 MHz).

2.1.2. COORDINATING THIOPHENE

  As is shown in Figure 2.1, several synthetic routes can be employed to obtain the required DTE ligands. For the final construction of these DTEs, the presence of a pyridyl functional group attached to the coordinative thiophene is required. The synthesis of these fragments will be described in this section.
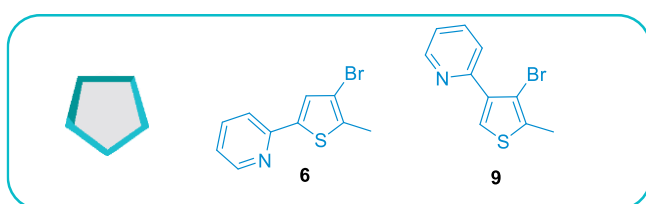
We designed two different coordinating thiophene fragments differing in the anchoring position of the pyridyl unit within the thiophene. The synthesis of these derivatives (shown in Scheme 2.3) was previously described in the literature.[4] The synthesis of compound **6** resembles the one described above for compound **5**. It starts from compound **4**, which reacts with 2-bromopyridine to insert the pyridyl group in the alpha-position of thiophene through a Suzuki-Miyaura reaction. The final product (**6**) was obtained as a beige solid with a 66% yield.
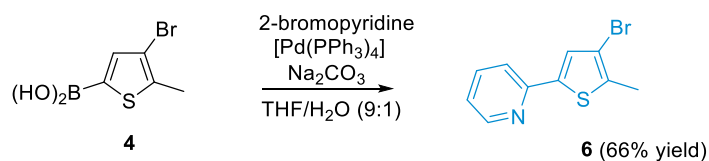
Scheme 2.3. Synthesis of compounds **6**.

The purity and identity of this compound was confirmed by ^{1}H-NMR spectroscopy. Figure 2.3 shows the spectrum obtained for compound **6**. The expected 2-pyridyl aromatic signals are observed in addition to a singlet assigned the thiophene aromatic proton at 7.41 ppm. A singlet is also observed at the aliphatic region, which is associated with the methyl group.
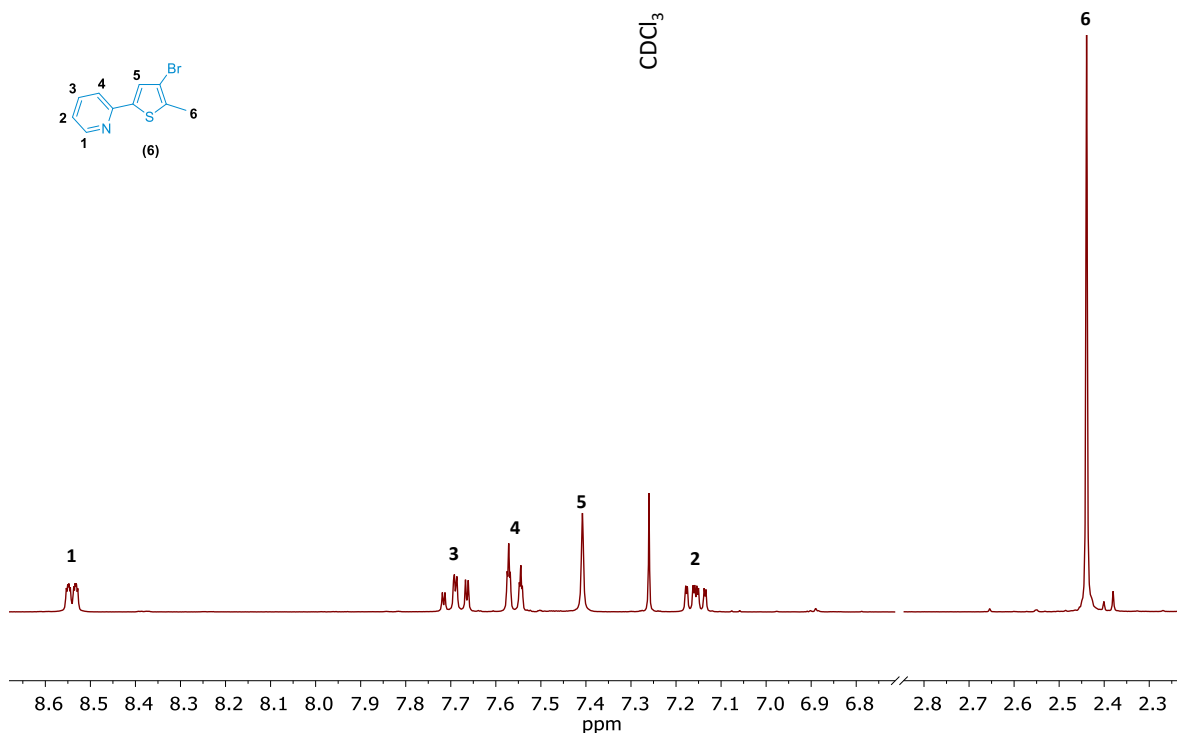
Figure 2.3. ^{1}H-NMR spectrum of compound **6**. (CDCl$_3$, 300 MHz).

Compound **9** was obtained through a less direct synthetic route, as depicted in Scheme 2.4. The synthesis starts with commercially available 3-bromo-5-methylthiophene. It was reacted with n-BuLi in dry Et$_2$O. After 30 minutes at -78 °C, B(O^{i}Pr)$_3$ was added dropwise, obtaining intermediate **7'** as a white precipitate after removing volatiles under reduced pressure. Intermediate **7'** was subsequently used in a Suzuki-Miyaura coupling, using a mixture THF/H$_2$O (10:1, v/v) to obtain compound **7**. After workup, the reaction residue was purified by column chromatography, using CH$_2$Cl$_2$ as eluent (See experimental section). Intermediate **7** was then brominated with an excess of NBS using acetic acid as solvent. Dibromo compound **8** was obtained as a brownish oil with a 48% yield after a basic treatment and extractions in CH$_2$Cl$_2$/H$_2$O. The last reaction step consisted of a lithiation of the most reactive bromine using 1.2 equivalents of *n*-BuLi (-78 °C, dry THF), followed by quenching of the lithiated intermediate with water. After workup, compound **9** was obtained as a colorless oil with an 81% yield.
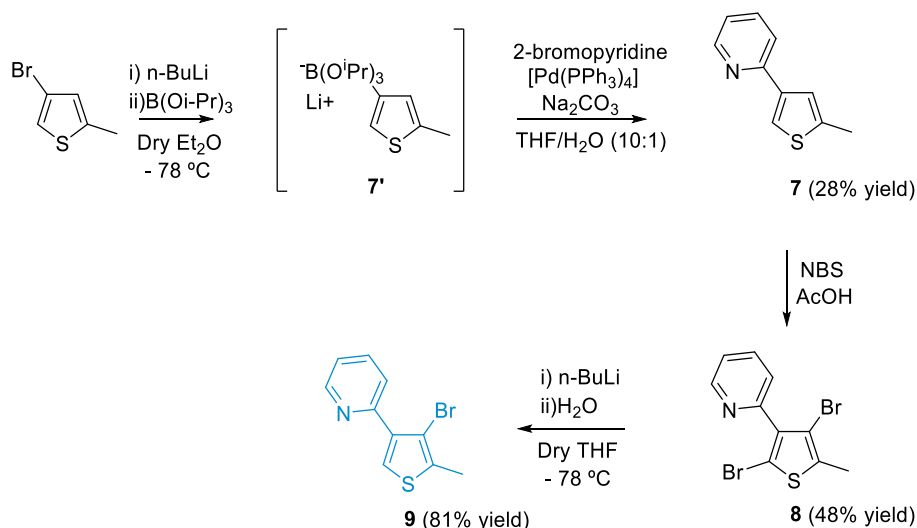
Scheme 2.4. Synthetic route of non-coordinative thiophene **9**.

The purity and identity of these compounds was confirmed by ^{1}H-NMR spectroscopy. Figure 2.4 shows the spectra obtained for the different intermediates during the synthesis of compound **9**. All compounds (**7-9**) present the general pattern of resonances associated with the 2-pyridyl group, consisting of two double doublets and two double triplets, and the presence of the methyl group of thiophene in higher fields of the NMR spectrum. To identify the compounds, attention was focused on the presence of signals associated with the aromatic protons of the thiophene group. In the case of compound **7**, two signals were observed. A singlet at 7.51 ppm corresponding to the H_6 proton, which appears at lower fields and may be due to the presence of the sulfur atom. On the other hand, a pseudo triplet, corresponding to H_5, is observed at somewhat higher fields. This characteristic signal might be due to residual coupling of the proton H_5 with the protons H_7 of the methyl group (which resolve into a doublet). Next, in green, the presence of compound **8** is verified due to the disappearance of the signals associated with the aromatic protons of thiophene. Accordingly, the methyl signal appears as the expected singlet integrating by 3H. Finally, in red, the presence of compound **9** is confirmed by the appearance of a new signal at 7.51 ppm, associated with the H_5 aromatic proton. In the aliphatic region, it is observed, integrating by three protons, the signal assigned to the methyl group of compound **9**.
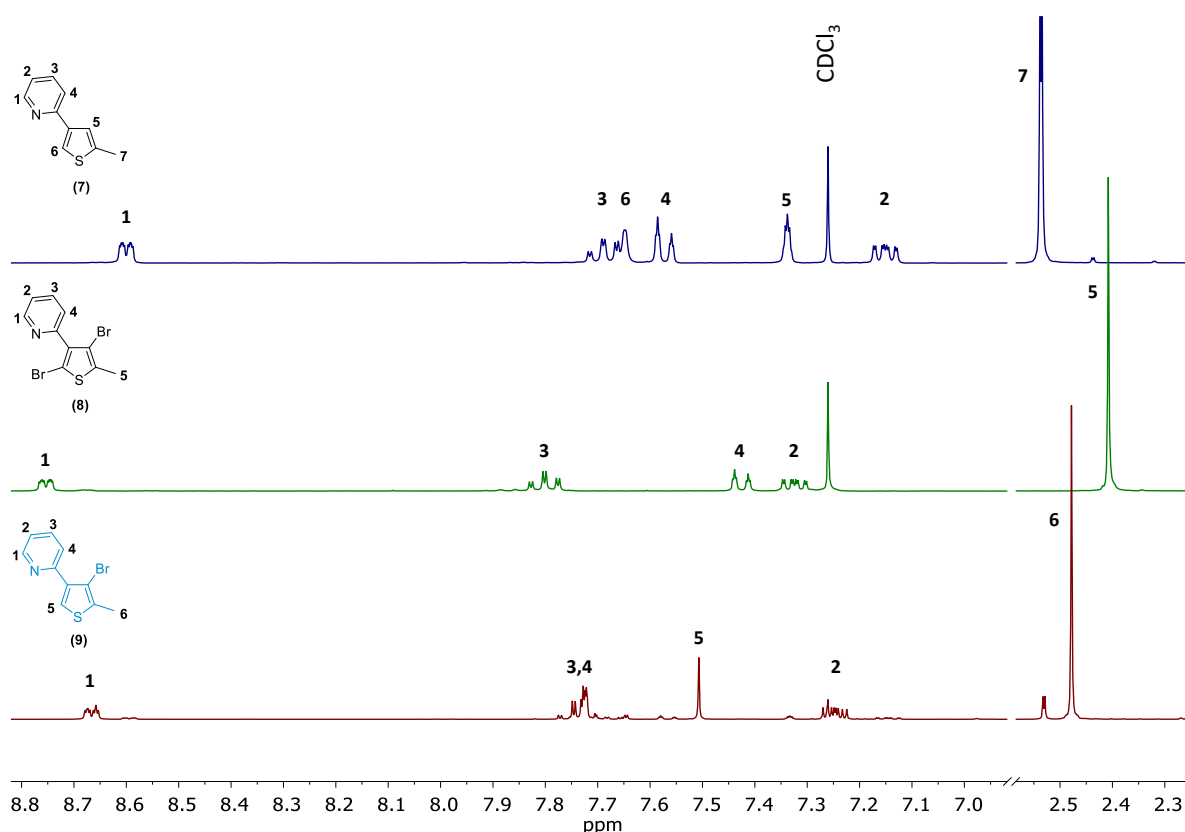
Figure 2.4. ^{1}H-NMR spectra of compounds **7-9**. (CDCl$_3$, 300 MHz).

2.1.3 THIENYLETHENE DERIVATIVES

As shown in Figure 2.1, all the synthetic routes towards non-symmetric DTEs involve forming an intermediate thienlylheptafluorocyclopentene (thienylethene, TE). This section will describe the synthesis of one coordinating TE (**10**) and one non-coordinating TE (**11**) as representative examples. Both compounds were synthesized similarly, following standard literature procedures.[5,6]
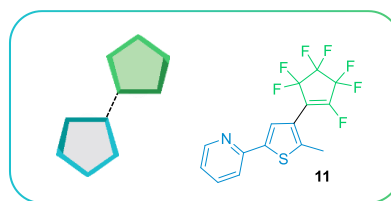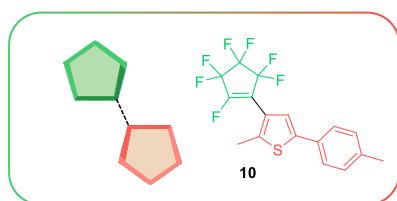
These TEs were obtained by lithiation of the corresponding 2-bromothiophene using *n*-BuLi (-78 °C, dry THF). While keeping the temperature at -78 °C, the highly reactive lithiothiophene intermediate solution was added to a cold solution of octafluorocyclopentene in THF (Scheme 2.5). After workup, all the compounds were purified by column chromatography over silica gel, eluting with hexane, and obtained with low-to-moderate yields (28–40%).
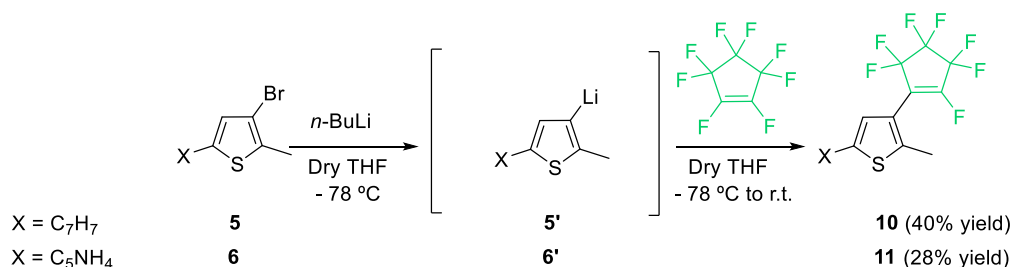
Scheme 2.5. Syntheses of TEs **10** and **11**.

These compounds were identified by ^{1}H-NMR (Figure 2.5) spectroscopy. The spectra obtained were in agreement with the published spectroscopic data.[4,5] Compound **10** presents two characteristic signals in the aromatic region, a doublet at lower fields (7.40 ppm) and a multiplet at 7.18 ppm, which is the superposition of singlet (H_5) and the second doublet corresponding to the toluene group. In the aliphatic zone, a singlet can be observed (integrating for 3H) corresponding to the toluene methyl fragment and a doublet (2.46 ppm), associated with the methyl at the 5-position of the thiophene, which presents a splitting due to the interaction with a fluorine atom of the heptafluorocyclopentene. In the case of intermediate **11**, the characteristic group of signals corresponding to the pyridyl fragment can be distinguished in the aromatic region together with the singlet associated with the aromatic proton of thiophene. At higher fields, like its homolog **10**, the splitting of the methyl group into a doublet is observed, and it is attributed again to the interaction with a fluorine atom of the heptafluorocyclopentene. This coupling will be analyzed in more detail in *Chapter 3* (*See section 3.1.1.4 THIENYLETHENE DERIVATIVES of Chapter 3*).
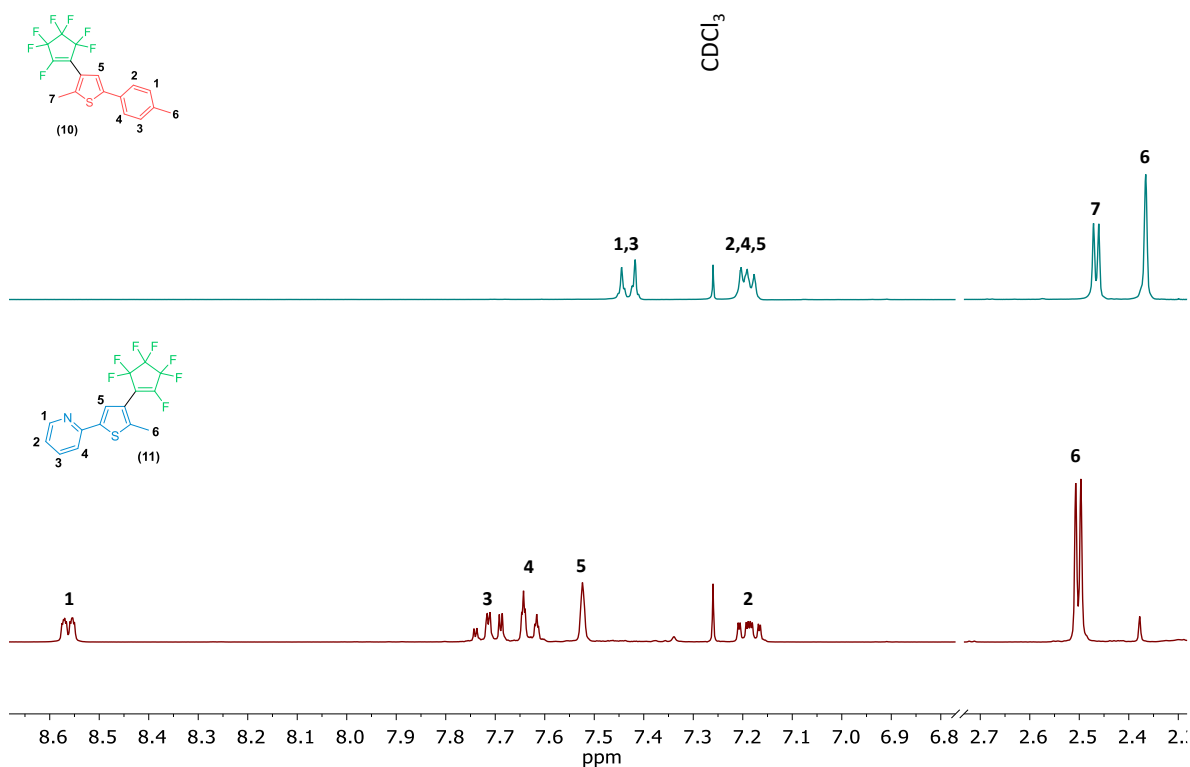
Figure 2.5. ^{1}H-NMR spectra of TEs **10** (blue line) and **11** (red line). (CDCl₃, 300 MHz).

2.1.4 DITHIENYLETHENE LIGANDS

   This section presents the synthesis and characterization of the DTE ligands. One can distinguish two types of ligands: on the one hand, we have **L1-A** as the only symmetric ligand of this family of photoswitches, possessing two coordinating pyridyl branches. This ligand could act as a bridge between two iridium centers, or as monodentate ligand, depending on the Ir/DTE ratio. On the other hand, we synthesized three non-symmetric ligands (**L1-B**, **L1-C** and **L1-D**) which contain a coordinating pyridyl fragment and a non-coordinating functionalized thiophene group.

2.1.4.1. SYMMETRIC DTE LIGANDS.
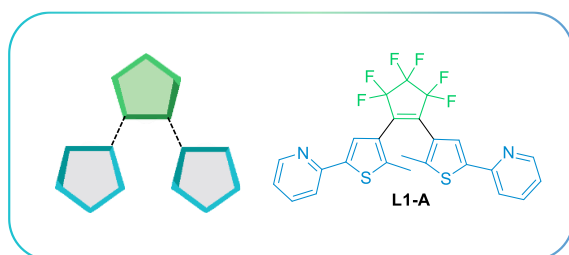
   DTE **L1-A** is the only symmetric ligand synthesized within this project which was obtained following the synthetic procedure described in the literature for the same compound.[7] It was obtained by lithiation of the corresponding 2-pyridyl-4-bromo-methylthiophene (**6**) using *n*-BuLi (-78 °C, dry THF). While keeping the temperature at -78 °C, a solution octafluorocyclopentene in THF was transferred by cannula to the solution of **6'** (Scheme 2.6). After workup, the final compound **L1-A** was obtained as a beige greenish solid after purification by column chromatography over silica gel, eluting with hexane (65% yield).
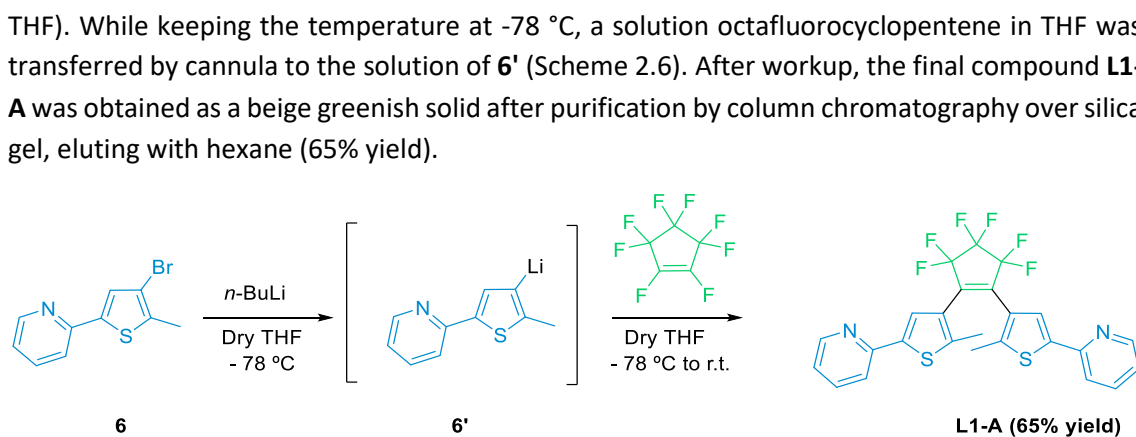
Scheme 2.6. Syntheses of **L1-A**.

   The purity and identity of compound **L1-A** were confirmed by ^{1}H-NMR spectroscopy. The obtained spectrum was in agreement with the data published in the literature.[7] The ^{1}H-NMR (Figure 2.6) showed five aromatic signals, as expected due to its C_2 symmetry in solution. Compound **L1-A** exhibits the set of signals observed previously for the 2-pyridyl-containing intermediates: one doublet of doublets, a triplet of doublets, a doublet of triplets, a double-double of doublets (assigned to the pyridyl protons), and a singlet assigned to the thiophene aromatic proton.
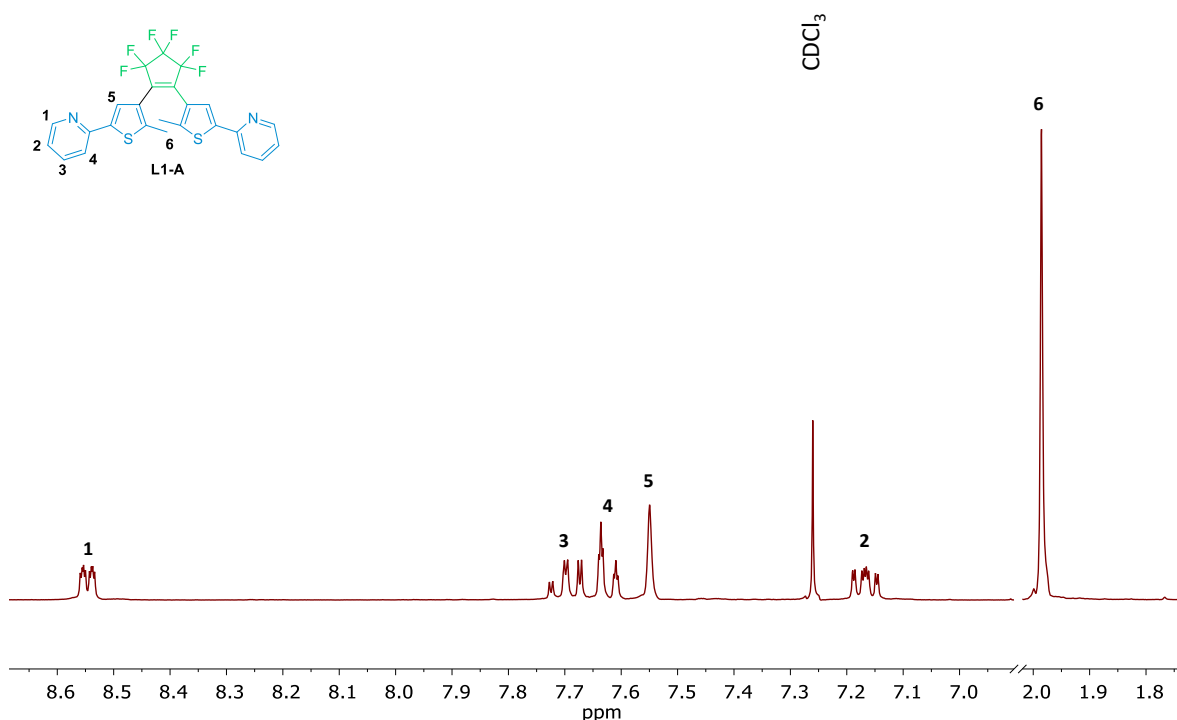
Figure 2.6. ^{1}H-NMR spectrum of compound **L1-A**. (CDCl₃, 300 MHz).

2.1.4.2. NON-SYMMETRIC DTE LIGANDS.
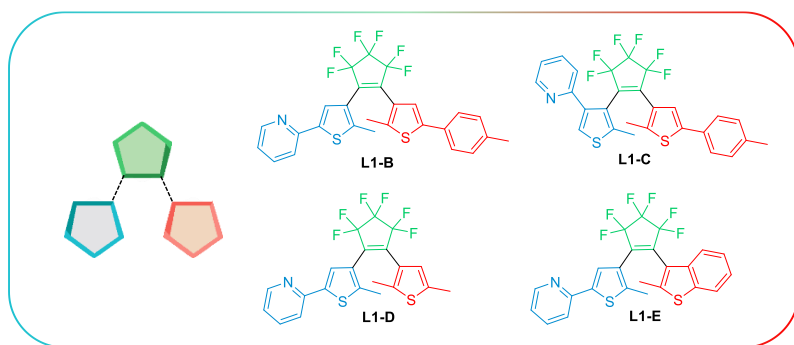
A series of non-symmetric DTE ligands containing a single coordinating fragment were synthesized to be used as ligands for the synthesis of mononuclear metal complexes. Ligands **L1-B** and **L1-C** were synthesized following the protocols described in the literature. The synthesis of ligand **L1-D**, (not described in the literature) was attempted using similar procedures as those described for the known ligands.[8,9] The synthesis of non-symmetric ligands varies significantly compared to that reported for symmetric DTE ligands. In the formation of these ligands, a lithiation is carried out on the simple "arm" (**1**, **2**, **5** or **9**) at -78 °C, to which a solution of the corresponding TE ligand (**10** or **11**) is added (Scheme 2.7). After workup, all the final DTE ligands were purified by column chromatography over silica gel, and the target DTE molecules **L1-B–L1-D** were obtained in moderate to low yields (5-50%).

72
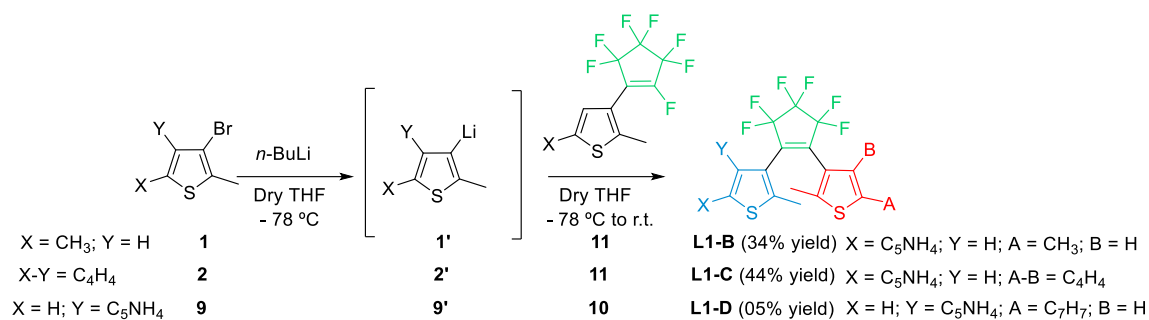
Scheme 2.7. Syntheses of **L1-B, L1-C** and **L1-D**.

The isolated final DTE ligands **L1-B–L1-D** were analyzed by ^{1}H-NMR spectroscopy. In the stacked spectrum, the different DTE ligands obtained can be observed. In blue and green, the spectra obtained for the ligands **L1-B** and **L1-C** are observed, which are in agreement with the data published in the bibliography[8,9]. Finally, in red, the ligand **L1-D** also shows the signals corresponding to the pyridyl group (H$_1$-H$_4$) and two broad doublets at 7.25 ppm and 7.17 ppm, corresponding to the aromatic protons of the toluene fragment. A singlet corresponding to the H$_5$ proton is seen at 6.18 ppm, while the H$_6$ is overlapped with one of the aromatic doublets of toluene (7.25 ppm). In the aliphatic zone, the appearance of three singlets can be seen, integrating to 9H in total, which corresponds to the methyl of pyridyl-thiophene (H$_{11}$), the homologue of the toluene-thiophene fragment (H$_{12}$), and the methyl of the toluene fragment (H$_{13}$).
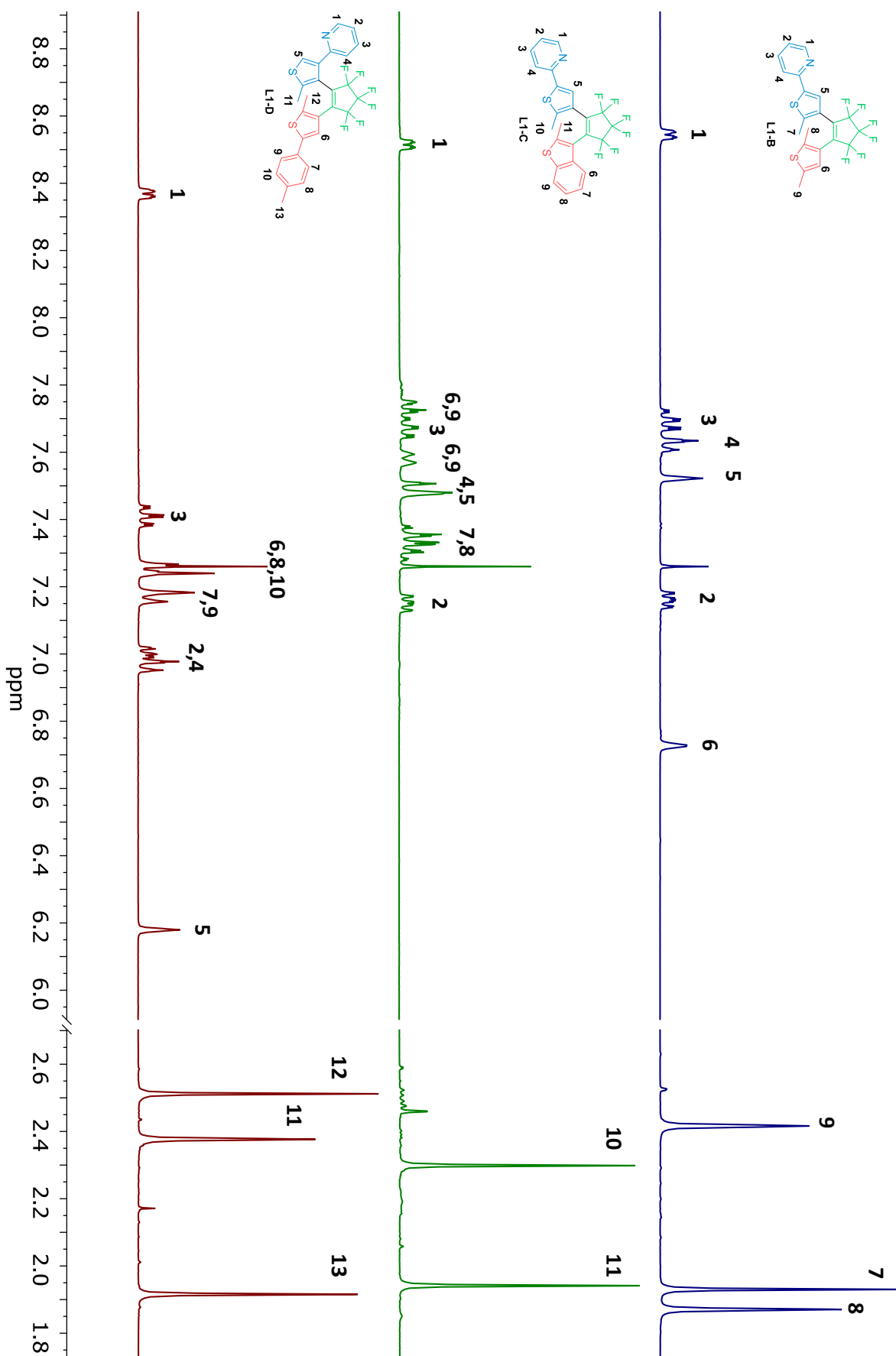
Figure 2.7. ^{1}H-NMR spectra of **L1-B − L1-D**. (CDCl$_3$, 300 MHz).

2.2 COMPLEXES

DTE ligands **L1-A**, **L-B**, **L1-C**, and **L1-D** were intended to be used as C-N cyclometalating ligands for the synthesis of heteroleptic tris-cyclometalated Ir(III) complexes. The ligands were designed to coordinate through the pyridyl fragment and cyclometalate through C-H activation of the thiophene, either C_α or C_β, depending on the specific ligand (See Figure 2.8).
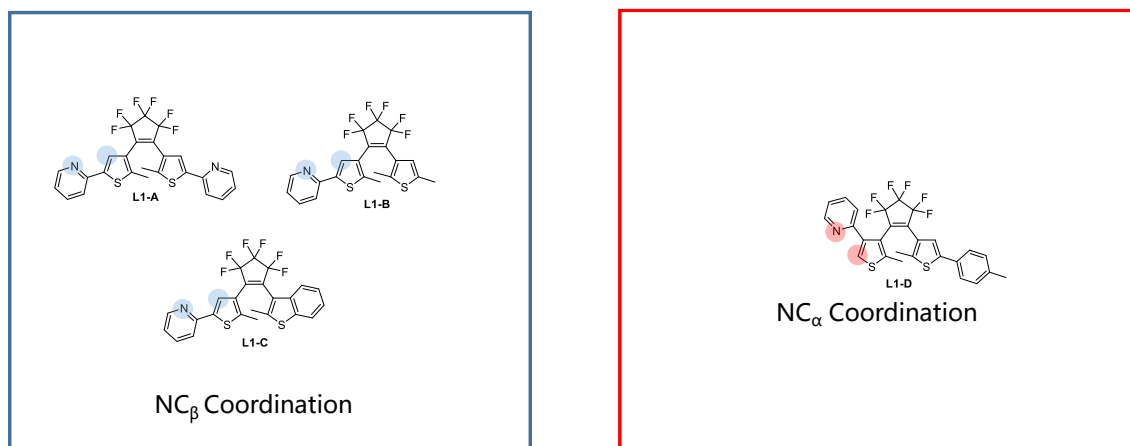
Figure 2.8. Expected coordination sites for the different synthesized DTEs.

2.2.1 TRIS-CYCLOMETALATED RACEMIC IR(III) COMPLEXES

Taking into account the bibliographic precedents, initial coordination experiments were attempted using **L1-A** trying to reproduce the example described by Tian's group using a similar DTE containing a non-fluorinated cyclopentene bridge.[10] These authors published the synthesis of an heteroleptic Ir(III) compound based on two coordinating symmetric DTEs, and an acetylacetonate as third ligand ([Ir(DTE)$_2$(acac)]). The synthesis proposed by Tian et al. is presented in Scheme 2.8. The synthesis consisted of reacting the commercially available IrCl$_3$·3H$_2$O with the corresponding DTE ligand in refluxing 2-ethoxyethanol for twenty-four hours. In situ cleavage of the chloride bridges was achieved in a subsequent step by addition of base rendering the desired [Ir(DTE)$_2$(acac)] complex containing two cyclometalated symmetric DTE ligands.
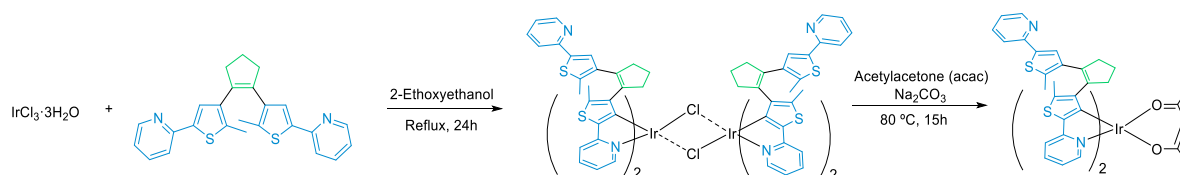
Scheme 2.8 Published synthesis of [Ir(DTE)$_2$(acac)] described by Tian's group.[10]

Initially, **L1-A** was reacted following the same synthetic protocol (Scheme 2.9). IrCl$_3$·3H$_2$O was reacted with the ligand **L1-A** in 2-ethoxyethanol overnight at 135 °C. Afterwards, Na$_2$CO$_3$ and two equivalents of acac were added to the reaction mixture, and the reaction mixture was refluxed overnight. After cooling the reaction mixture down to room temperature, it was treated with CH$_2$Cl$_2$/H$_2$O, obtaining a brown solid after removing the solvent from the organic layer. Figure 2.9 presents the ^{1}H-NMR spectrum of the solid obtained. As it can be seen, only the signals

for the **L1-A** DTE ligand are observed, showing that the synthesis of the complexes **C1'** was unsuccessful.
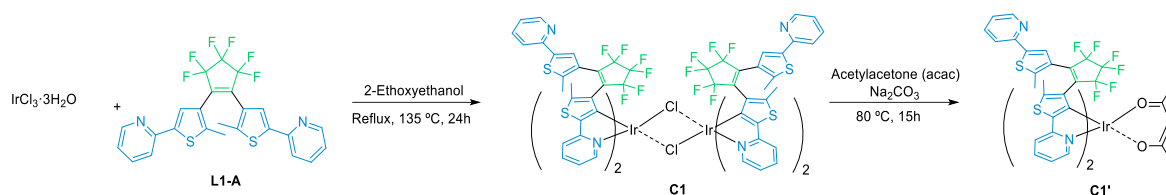
Scheme 2.9. Synthetic route for compounds **C1** and **C1'**.
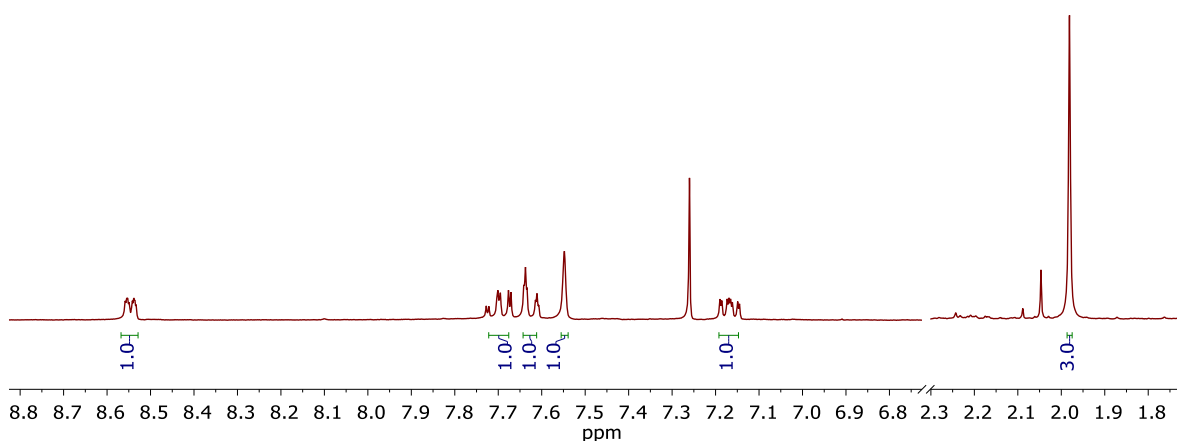
Figure 2.9. ^{1}H-NMR spectrum of **L1-A** obtained for the synthesis of **C1'**. (CDCl$_3$, 300 MHz).

Taking into account that the synthesis of the model compound [Ir(ppy)$_2$(Cl)]$_2$ is usually performed in mixtures of 2-ethoxyethanol/H$_2$O (3:1, v/v)[11], a new synthesis was attempted using these conditions. IrCl$_3$·3H$_2$O was reacted with **L1-A** in 2-ethoxyethanol/H$_2$O (3:1, v/v) overnight at 120 °C. NMR spectroscopy experiments where done during the reaction on different aliquots (after 1 hour and 24 hours) to follow the reaction progress. Only free ligand **L1-A** was observed in the different measured aliquots, see Figure 2.10, suggesting that either the reaction did not work as expected or that the final product was not soluble and could not be measured. After cooling the reaction mixture down to room temperature, a green-brownish precipitate was observed. Under a nitrogen atmosphere, this solid was filtered off and washed with 40 mL of Et$_2$O and 40 mL of H$_2$O to eliminate possible impurities, obtaining a final brown solid. NMR spectroscopy experiments on the solid obtained showed the presence of free ligand together with sets of unidentified signals that did not match those associated with the expected complex (Figure 2.10). Another reason why it was concluded that this synthetic route had not been successful was the possible isomerization of the compounds because, after performing thin layer

chromatography methodologies (TLC), only the spot corresponding to the free ligand **L1-A** produced a color change under UV irradiation.
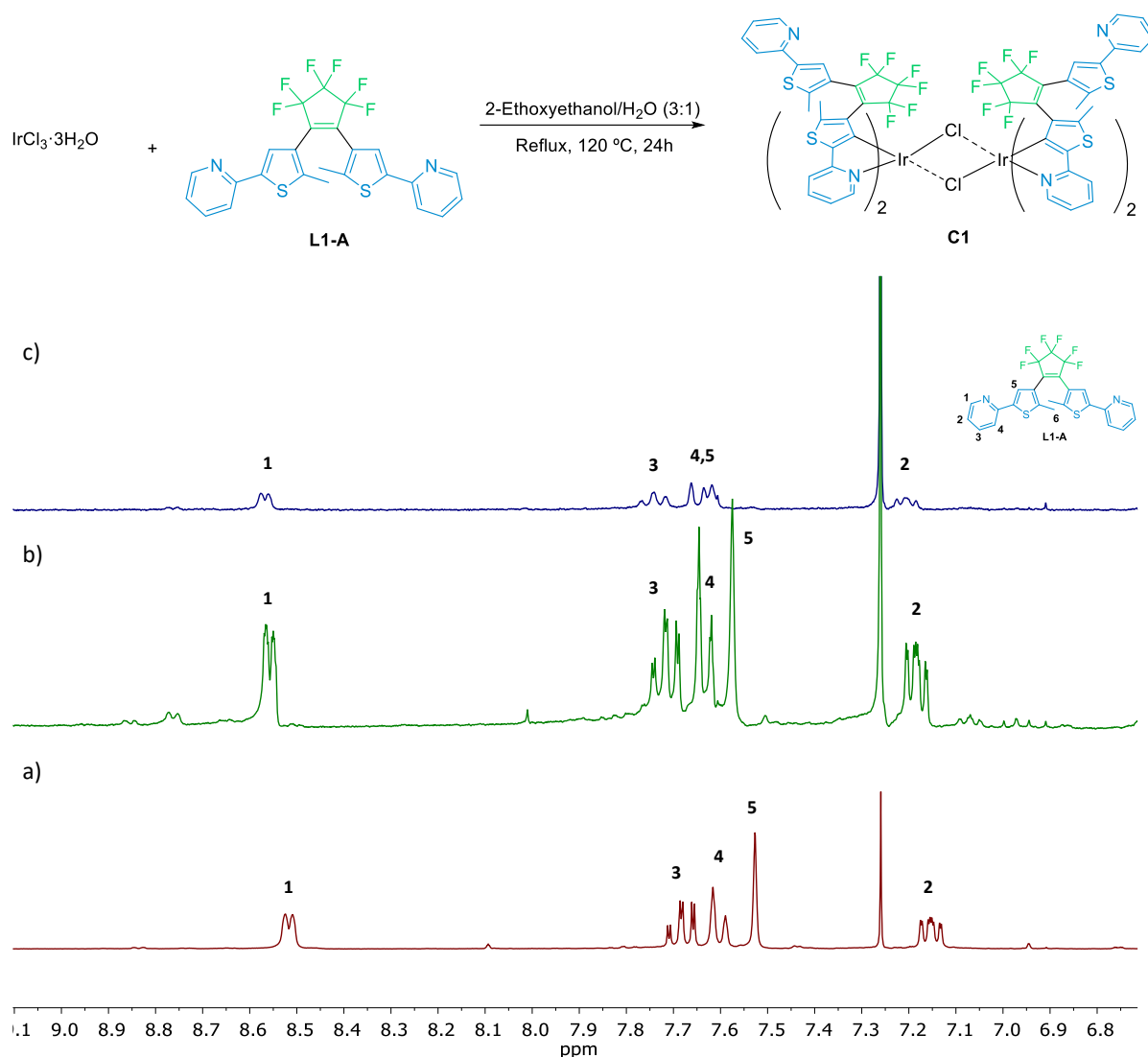
Figure 2.10. a) ^{1}H-NMR spectrum of the reaction after 1 hours b) ^{1}H-NMR spectrum of the reaction after 24 hours. c) ^{1}H-NMR spectrum of the reaction after work-up. (CDCl$_3$, 300 MHz).

In view of the discouraging results obtained, it was decided to verify that the cyclometalation of a 2-thienylpyridine actually occurs under these experimental conditions. For this purpose, compound **6** was used as cyclometalating ligand. Compound **6** was reacted with the iridium metal precursor (IrCl$_3$·3H$_2$O) in a mixture of 2-ethoxyethanol/H$_2$O (3:1, v/v) refluxing for twenty-four hours, following the synthetic protocols published by Qin[12] and Marcaccio[13], carrying out some modifications in it. After refluxing the reaction for twenty-four hours, an orange precipitate was observed. It was filtered off and washed with 40 mL of Et$_2$O and 40 mL of H$_2$O to eliminate possibilities of free ligand or metallic precursor traces. Attempts to identify the solid obtained by ^{1}H-NMR spectroscopy were unsuccessful due to the insolubility of the product in the different deuterated solvents assayed (DMSO, CDCl$_3$, MeOD, Acetone-d_6, or THF-d_8). The identification of the reaction product was carried out through elemental analysis of the sample, which showed values in agreement with the expected molecular formula. Table 2.1 shows the results obtained.

Table 2.1. *Elemental analysis of compound* **C2** *($C_{40}H_{28}Br_4Cl_2Ir_2N_4S_4$)*

	C%	H%	N%	S%
Theoretical value	32.73%	1.92%	3.82%	8.74%
Experimental value	33.66%	2.56%	3.49%	7.68

   To corroborate the results obtained from the elemental analysis and that the coordination of compound **6** occurred through cyclometallation, a bipyridine group was inserted as the third ligand. The racemic target complex was obtained with a similar synthetic procedure to that described by Marcaccio *et al.*[13] As Scheme 2.10 shows, to a solution of **C2** in CH_2Cl_2/MeOH (1:1, v/v), two equivalents of bpy were added to obtain compound **C3**. After the volatiles were removed, the resultant solid was washed with 20 mL H_2O and 20 mL of diethyl ether (Et_2O) to eliminate free thy/bpy. Finally, the desired product precipitated from Et_2O, obtaining the final product as an orange solid (57% yield).
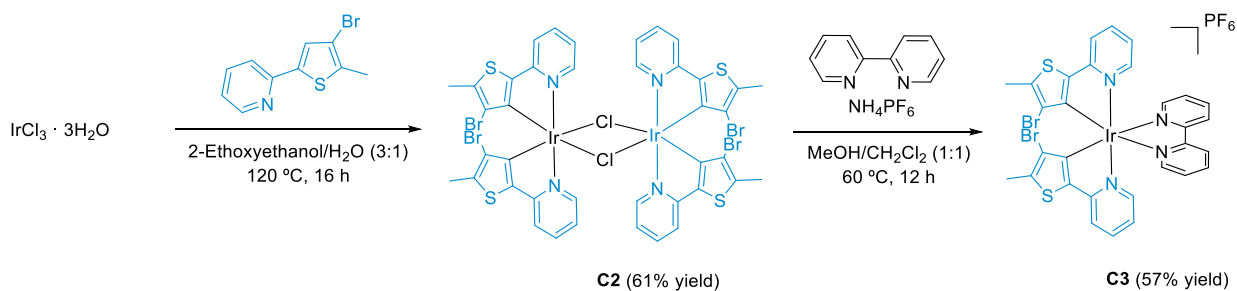
Scheme 2.10. Synthetic route for compounds **C2** and **C3**.

   The isolated compound **C3** was analyzed by ^{1}H-NMR spectroscopy. The ^{1}H-NMR spectrum shown in Figure 2.11 shows one singlet in the aliphatic region of the spectra assigned to the methylgroups of the 2-thienylpyridine ligand. Regarding the aromatic region, the characteristic pattern assigned the pyridine group can be distinguished (doublet, triplet, triplet, doublet). The number of signals and relatively simple spectra reflects the C_2 symmetry of the complex in solution.
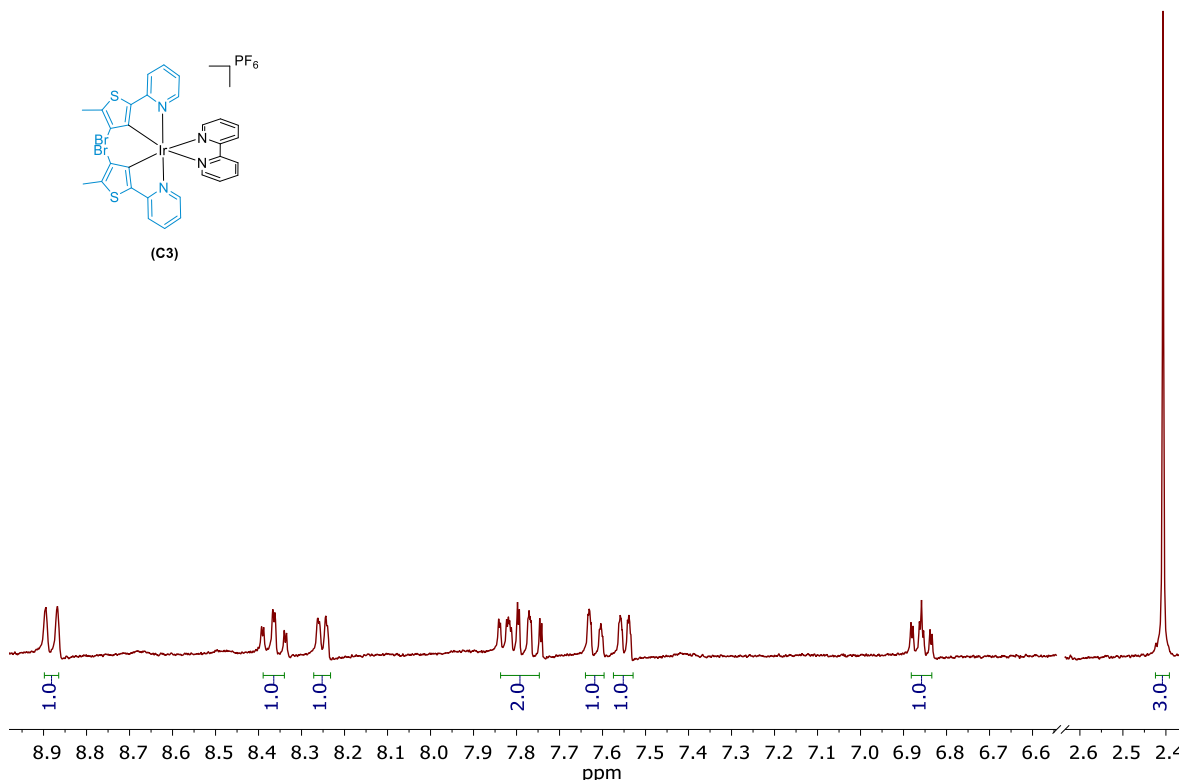
Figure 2.11. ^{1}H-NMR spectra of compounds **C3**. (Acetone-d_6, 300 MHz).

The results obtained using compound **6** as bis-cyclometalated ligand demonstrate that the NC coordination of the coordinating thiophene is obtained satisfactorily. Despite not being able to characterize compound **C2** by NMR spectroscopy, due to the insolubility of the compound in the different deuterated solvents, a third ligand could be introduced testing the cyclometalation of **6**. However, even observing the cyclometalation of the coordinating thiophene of the final DTE in the dimer generation, the results for the coordination of the **L1-A** ligand were not satisfactory since it did not show any indication of coordination. It should be noted that this type of coordination was tested by Tian's research group in 2009, using a DTE similar to **L1-A**, differing only in the presence of the fluorine groups of the cyclopentene "bridge". The presence of these fluorine groups may be justify the lack of coordination, as they could prevents an approach by the thiophene to the metal center. The only example in which they show a cyclometallation of a DTE ligand with a hexafluorocyclopentene group as a bridge is the one described by Pu group in 2020[14], which introduced a phenyl group between pyridine and the DTE fragment (ppy group), moving the molecule away switch of the metallic center, managing to avoid the interaction of the fluorine groups with the metallic center. The conclusions obtained from these experiments are schematically represented in Scheme 2.12.
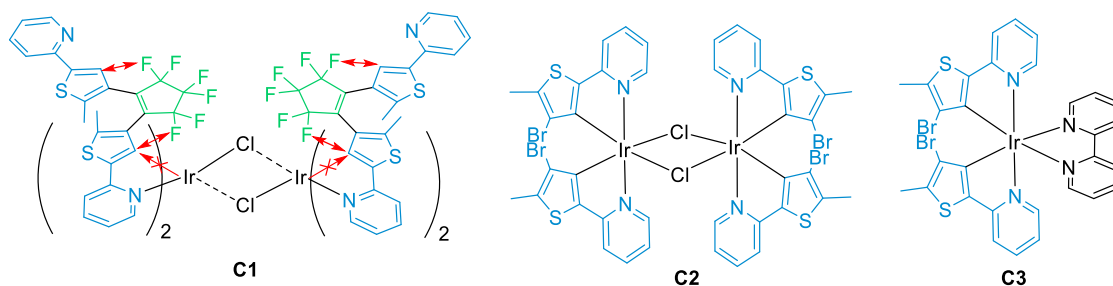
Scheme 2.12. Representative drawings of the obtained experimental conclusions.

   In view of the above-described difficulties, we considered the synthesis of heteroleptic bis-phenylpyridyl complexes containing only one coordinated DTE as third ligand. For this purpose, the chloride-bridged dimeric precursor **C4** was synthesized using the standard procedure described by Watts in 1984.[15] Commercially available $IrCl_3.H_2O$ and 2-phenylpyridine were refluxed (120 °C) overnight in a solvent mixture of ethoxyethanol/water (3:1). After filtering and washing the reaction residue, the desired product was obtained as a bright yellow solid with a 66% yield. Compound **C4** was identified using ^{1}H-NMR spectroscopy, where the signals obtained agreed with the spectroscopic information reported in the literature.[11]
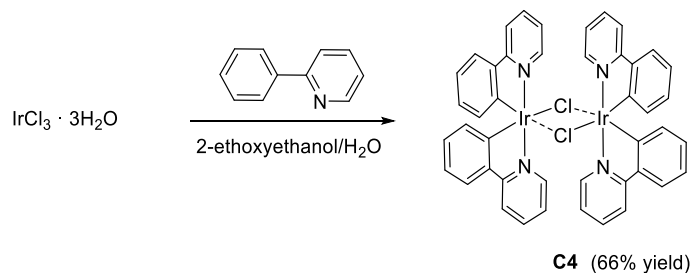
Scheme 2.13. Synthetic route for metallic precursor **C4**.

   The introduction of a cyclometalated DTE as a third ligand was initially attempted using a standard procedure used previously in our laboratory (Scheme 2.14).[iError! Marcador no definido.] **C4** was reacted under a nitrogen atmosphere, dissolving the metallic precursor in degassed acetone in the presence of AgOTf. The resulting yellow solution was heated for two hours at 60 °C. After this time, a precipitate was observed (AgCl) and filtered off through a celite pad. In another schlenk, a DTE ligand (**L1-A**) and Et_3N (acting as a base) were dissolved in degassed acetone. The yellow filtrate containing the metal precursor was transferred, via cannula, into the green/brown ligand solution and refluxed overnight. The reaction was followed by ^{1}H-NMR spectroscopy through evaporated aliquots of the reaction. As shown in Figure 2.12 the spectra of the measured aliquots did not show significant variations with time, and only signals corresponding to the free ligand **L1-A** and a small group of signals, which correspond to the iridium precursor, showed that it was not coordinated with the iridium metal precursor.
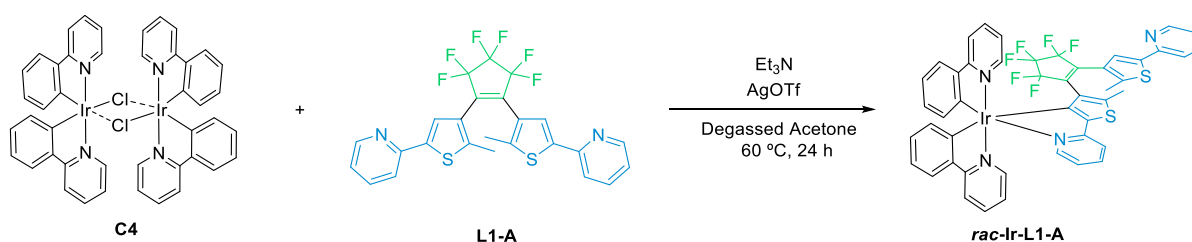
Scheme 2.14. Synthetic route for complex *rac*-**Ir-L1-A**.
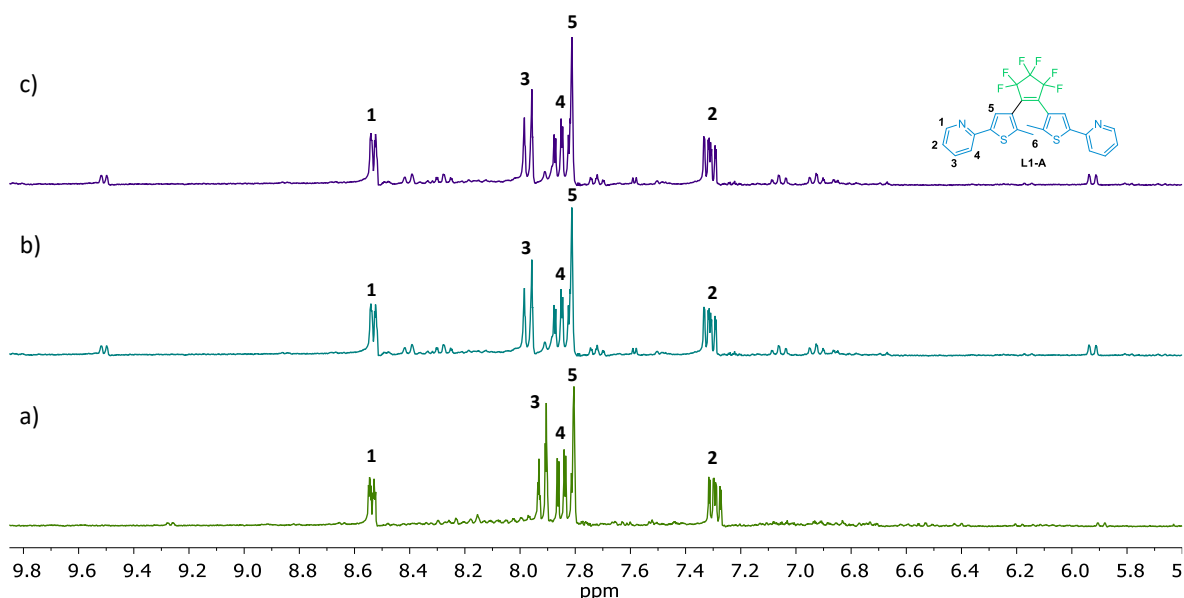
Figure 2.12. a) ^{1}H-NMR spectrum of the reaction between **C4** and **L1-A** after 3 hours b) ^{1}H-NMR spectrum of the reaction between **C4** and **L1-A** after 8 hours. c) ^{1}H-NMR spectrum of the reaction between **C4** and **L1-A** after 24 hours. (Acetone-d_6, 300 MHz).

These results indicated that DTE was not susceptible to undergo cyclometalation using the traditional methodologies for introducing a third cyclometalated ligand to build meridional heteroleptic iridium complexes. Besides, the synthetic methodologies for the construction of the facial compounds (thermodynamic product) were also dismissed due to the high temperatures used in the synthetic protocols, which are not compatible with the future intended synthesis of enantiopure metal complexes. Alternative reaction conditions to the classic synthesis protocols to obtain Ir(III) *fac/mer* complexes include the work published by Mann and collaborators in 2007.[16] They report the cyclometalation of both phenylpyridine (ppy) and pyridylthiophene (thpy) ligands to Ir(III) metal centers to form both *fac* and *mer* complexes starting from different organometallic precursors under mild reaction conditions (Scheme 2.15). Mann proposed that the kinetic product (*mer*) can be obtained from a reaction in *o*-dichlorobenzene, refluxing the reaction at 100 °C from an iridium dimer with hydroxy bridges (*Route A* in Scheme 2.15).

On the other hand, they report the use of an iridium bis-cyclometalated bis-acetonitrile precursor to generate the thermodynamic product (*fac*). From this precursor, the facial product can be obtained by two different routes. The direct route (*Route B* in Scheme 2.15) requires refluxing in *o*-dichlorobenzene at 100 °C. The alternative route (*Route C* in Scheme 2.15, valid only for 2-pyridylthiophene ligands) consists of a two-step reaction in which coordination occurs initially through the nitrogen and sulfur atoms. The conditions of this type of reaction are relatively milder compared to the previous ones described, using acetone as a solvent and heating the reaction to 60 °C. In the final step, interconversion of the Ir-S bond occurs to generate the desired cyclometalation by heating the reaction to higher temperatures (80-100 °C). It should be noted that Mann's research group observed the interconversion of the N-S coordination to the C-N cyclometalation but did not observe the direct reorganization of the ligands when heating the kinetic product (*mer*) to obtain the thermodynamic product (*fac*).
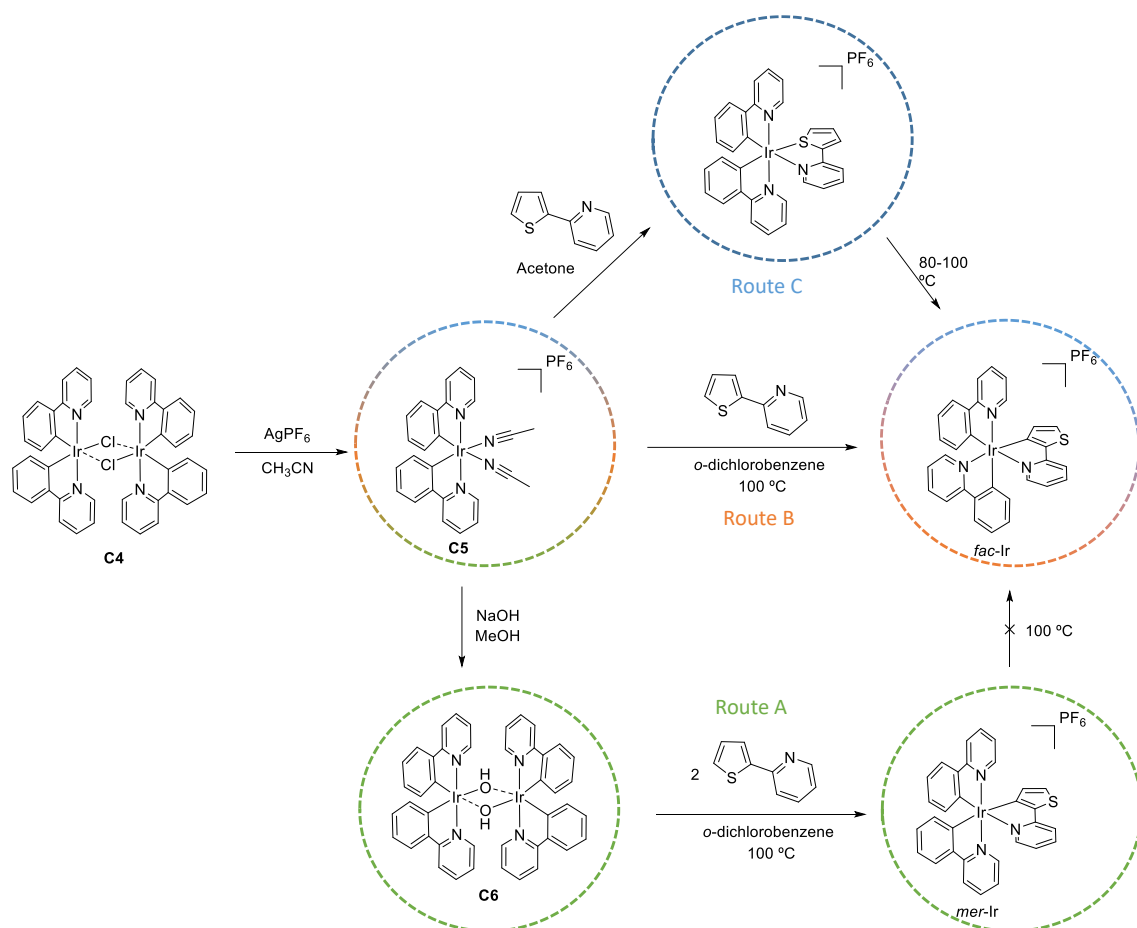
Scheme 2.15. Synthesis of *fac/mer* heteroleptic iridium complexes proposed by Mann.[16]

In order to reproduce Mann's methodology, the required metallic precursors were synthesized. To synthesize complex **C5**, **C4** was refluxed in acetonitrile with a silver salt, used as halide abstractor (AgOTf). The use of the silver salt drives the chloride bridge scission due to the precipitation of AgCl in the reaction media. The salt formed was filtered through a celite pad at the end of the reaction. **C5** was obtained as a yellow solid in a 70% yield.
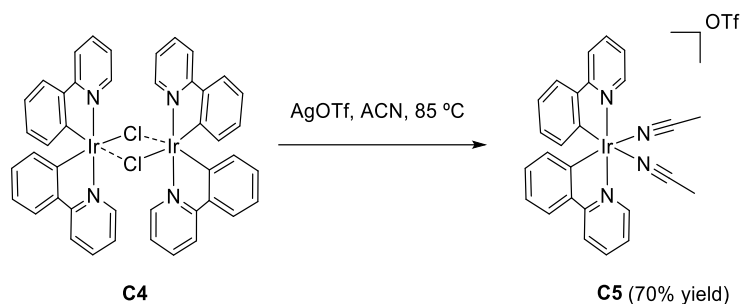
Scheme 2.16. Synthesis of iridium precursors **C5**.

C5 was analyzed by ^{1}H-NMR spectroscopy. Figure 2.13 shows the ^{1}H-NMR spectrum of **C5** in deuterated dichloromethane (CD$_2$Cl$_2$). The C$_2$ symmetry of the compound is reflected in the simplicity of the spectra, showing only one set of signals assigned to the coordinated 2-phenylpyridine and acetonitrile ligands, which agreed with the characterization published in literature.[17]
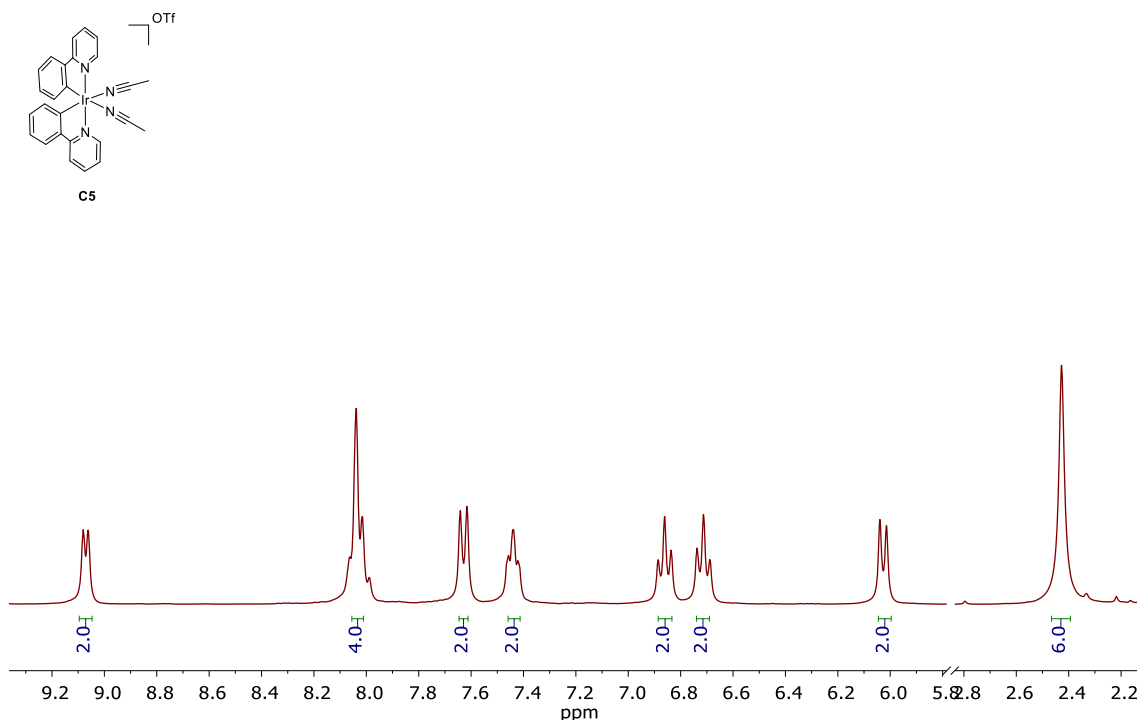
Figure 2.13. ^{1}H-NMR spectrum of **C5**. (CD$_3$CN, 300 MHz).

On the other hand, compound **C6** was synthesized following the protocol described by Mann (Scheme 2.17). **C5** was stirred in methanol in the presence of NaOH for twenty-four hours. After this period, an orange solid precipitates, and this precipitate was filtered off and washed with methanol to eliminate possible impurities. Compound **C6** was obtained as an orange solid in 32 % yield. The generation of this hydroxy precursor provides a feasible route to the *mer* isomers without the need to add a base since the metallic intermediate itself introduces the basic character.
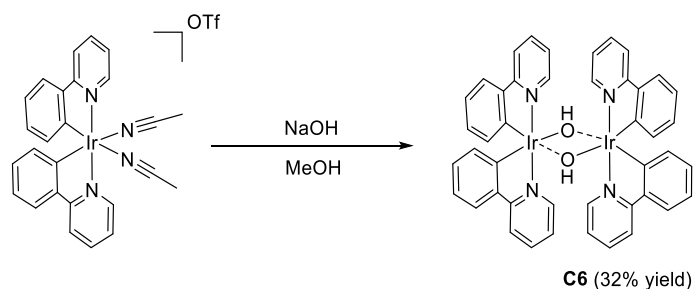
Scheme 2.17. Synthesis of iridium precursor **C6**.

The purity and identity of compound **C6** were analyzed by ^{1}H-NMR spectroscopy. The signals obtained agree with the spectroscopic information reported in the literature.[18] Figure 2.14 shows the ^{1}H-NMR spectrum of **C6** in deuterated dichloromethane (CD$_2$Cl$_2$). The C$_2$ symmetry of

the compound shows one set of signals assigned to the coordinated 2-phenylpyridine and hydroxy groups.
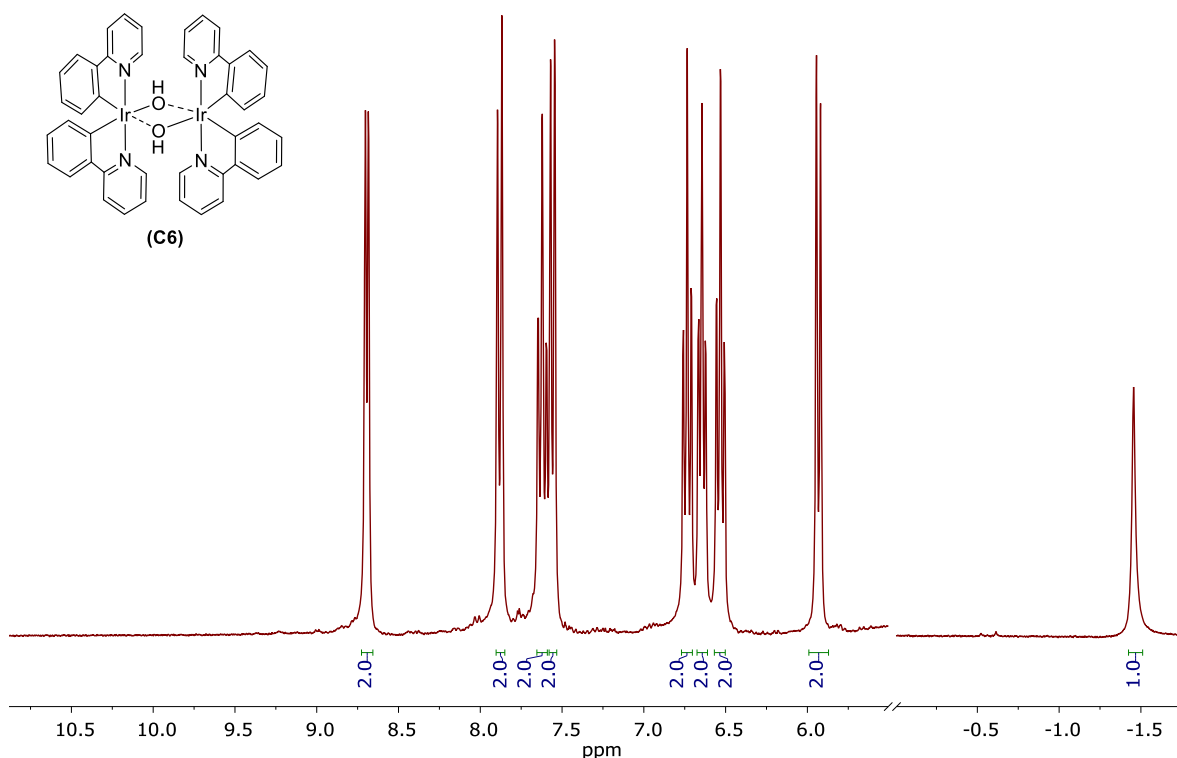
Figure 2.14. ^{1}H-NMR spectrum of **C6**. (CD$_2$Cl$_2$, 300 MHz).

The feasibility of Mann's route for the cyclometalation of thienylpyridines containing a bulky substituent were initially tested using compound **6** as ligand. This 2-methyl-3-bromo-5-(2-pyridyl)thiophene ligand was selected as a model of a bulky DTE ligand.

Initially, the *route A* in Scheme 2.18 was attempted. The iridium precursor **C6** was reacted with ligand **6** in *o*-dichlorobenzene at 100 °C for 48 hours, obtaining a yellowish-orange solution. After removing the volatiles and precipitating the final compound with Et$_2$O, the metal compound was identified using ^{1}H-NMR spectroscopy. The spectrum (shown in Figure 2.15), although not fully assigned, showed a spectroscopic pattern compatible with the expected cyclometalated product.
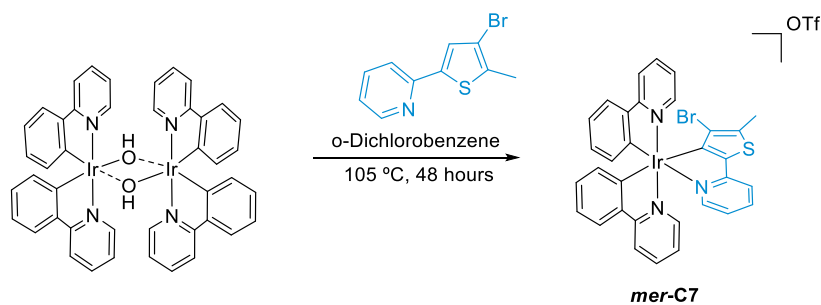
Scheme 2.18. Synthesis of iridium complex *mer*-**C7**.
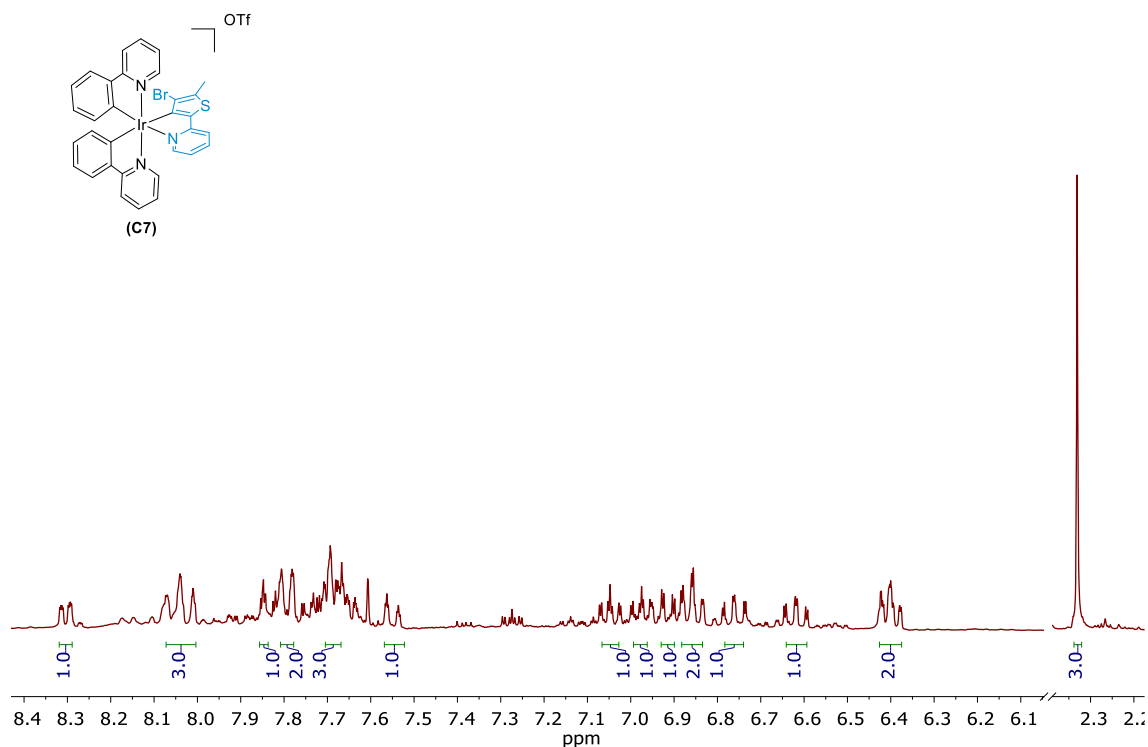
Figure 2.15. Obtained ^{1}H-NMR spectrum of ***mer*-C7**. (Acetone-d_6, 300 MHz).

Additionally, the coordination of **6** under the conditions described to obtain the *fac* isomers was also attempted (*route B* in Scheme 2.19). Under nitrogen, **C5** was reacted with **6** in *o*-dichlorobenzene (reflux, 100 °C) for six days. At the beginning of the reaction, the reaction mixture presented a yellowish colour. After six days of reaction, a muddy yellow solution could be observed. The resultant yellow solution was evaporated under vacuum, obtaining a yellow-brown residue. Subsequently, the final compound was obtained after washing the resultant residue with Et$_2$O, obtaining a pale-yellow solid.
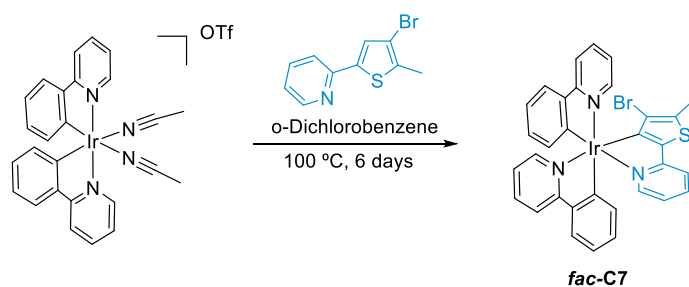
Scheme 2.19. Synthesis of iridium complex ***fac*-C7**.

The solid obtained was analyzed by ^{1}H-NMR spectroscopy in acetone-d_6. (Figure 2.16). It is worth mentioning that there are no signals associated with the free ligand. Instead, different signals corresponding to coordinated phenylpyridine fragments and consistent with **6** but shifted from its original position were observed. For instance, a singlet assigned to the methyl group of the complex was observed in the aliphatic region (2.48 ppm) but it was shifted compared to the position of the free ligand. The most indicative signal of the coordination mode of the ligand is the singlet at 7.62 ppm. This signal could correspond to the aromatic proton of the thiophene for compound **6**, but not in its free form. According to these signals, and the

resemblance of the spectra with the ones described by Mann for a pyridylthiophene complexes we propose that the compound contains a N-S coordinated ligand **6**.
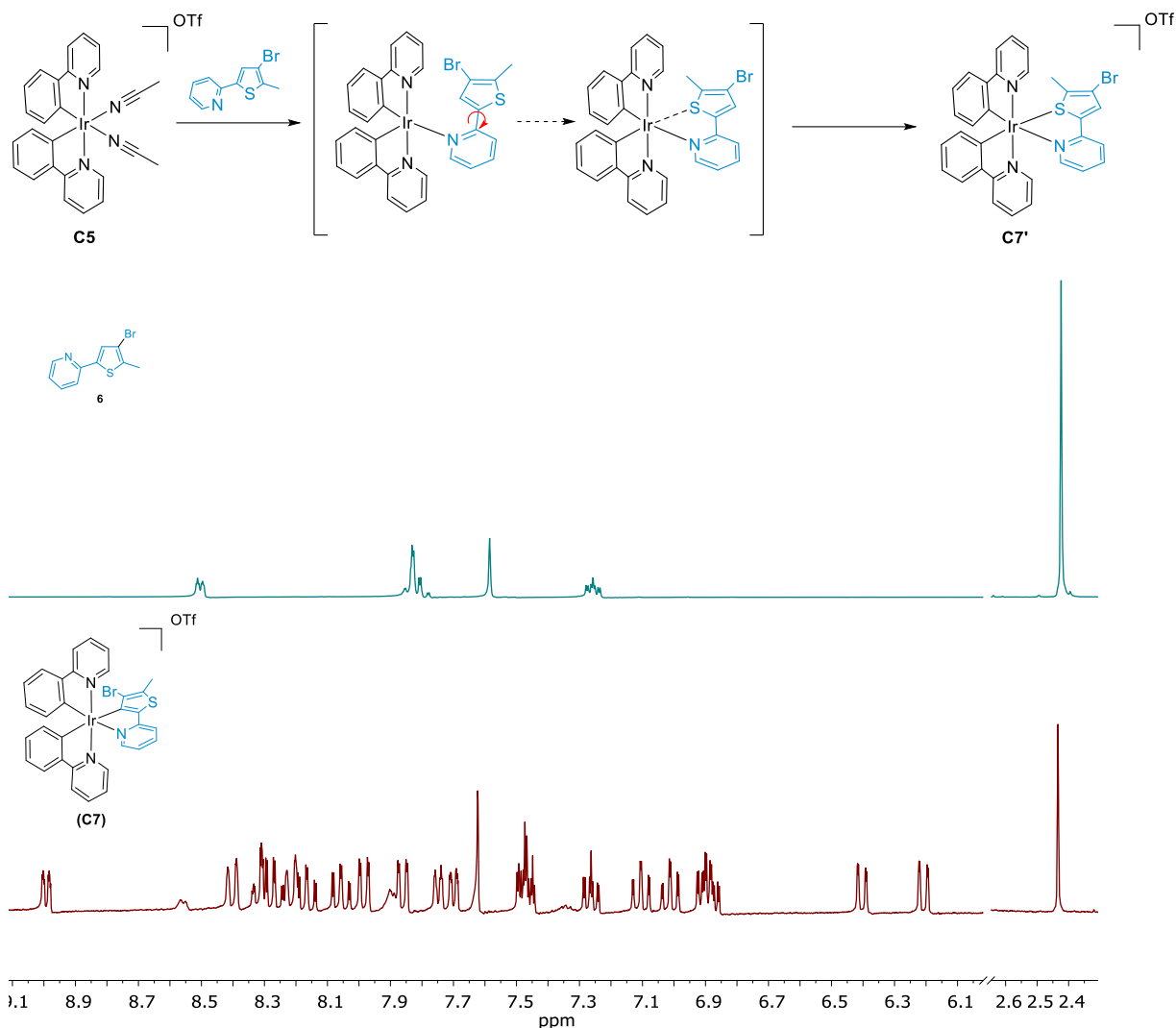
Figure 2.16. ^{1}H-NMR spectra and possible mechanism for the N-S coordination between **C5** and compound **6**. (Acetone-d_6, 300 MHz).

In an effort to obtain the cyclometalation of pyridylthiophene ligand **6** in a *fac* complex, several reaction conditions were screened: different solvents, from *o*-dichlorobenzene to di-fluorobenzene (higher boiling point), higher reaction temperatures (120-130 °C) and extended reaction times (up to 7 days). In spite of the harsher reaction conditions, the same results were consistently obtained, being the N-S coordinated complex the only reaction product. The identity of this compound was confirmed by comparison with a sample obtained following the synthetic processes suggested by Mann for the N-S coordinated derivative under milder condition (*route C* in Scheme 2.20). **C5** was reacted with **6** in acetone at room temperature for 72 hours. The resulting reaction solution was filtered through celite to remove acetone-insoluble impurities, yielding a clear yellow solution. Volatiles were removed under vacuum, and the **C7'** complex was purified washing the residue with Et$_2$O, obtaining a pale-yellow solid.
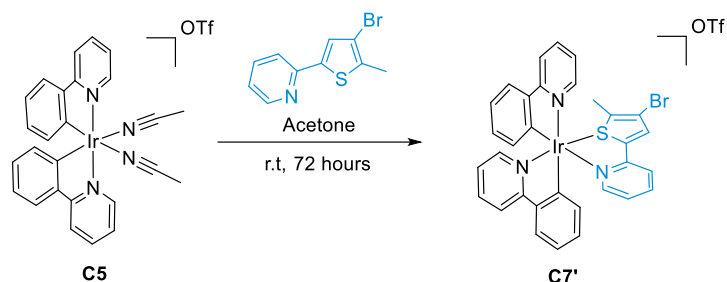
Scheme 2.20. Synthesis of iridium complex **C7'**.

   Compound **C7'** was characterized by ^{1}H-NMR spectroscopy. The spectra was identical to that obtained following *route B* (intended for the cyclometalation of the ligand to form a *fac* complex). This compound was fully characterized by multidimensional NMR spectroscopy, confirming the N-S coordination of the ligand (The complete characterization of this complex is included in the experimental section).

   As in the original publication by Mann they propose that the cyclometallation of a pyridylthiophene to form a *fac* complex can be accomplished starting from the N-S chelated derivative (*Route C* in Scheme 2.15), we tested this reaction also. **C7'** was refluxed in *o*-dichlorobenzene for 6 days at 100 °C. Unfortunately, unreacted **C7'** was the only product observed in the reaction mixture.

   After the various preliminary studies carried out with thiophene **6** and the different metal precursors, it was concluded that cyclometalation was strongly inhibited when using phenylpyridyl ligands containing bulky fragments in position 3 of the thiophene, and could only be accomplished starting from **C5** at high temperatures (*Route A* in Scheme 2.15). Instead, N-S coordination was easily observed starting from **C5** using very mild conditions. Therefore, we considered that coordination of the DTE ligands as neutral N-S chelates would be a more appropriate strategy due to the milder conditions required. Additionally, this coordination mode would not be inhibited by the bulkiness of the fluorinated octafluorobenzene and eventually would render compound with the methyl group of the thiophene close to the iridium center. It is worth mentioning that this methyl group is bonded to the stereogenic carbon generated upon photo-induced ring-closure of the DTE.

   DTE based ligands **L1-A**, **L1-B**, and **L1-C**, were initially considered as ligands for the N-S coordination studies. Ligand **L1-A** was the preferred candidate due to the possibility of creating complexes of the monomer or dimer type. **L1-B** and **L1-C** ligands were designed to avoid the possible bridging coordination mode of symmetric **L1-A**, whilst maintaining one coordinating pyridylthiophene fragment. Scheme 2.21 shows the synthetic route followed. It consisted of reacting the precursor **C5** and the corresponding ligand in degassed acetone, under a nitrogen atmosphere, for 7–24 hours. After this time, an orange-reddish coloration of the reaction mixture was observed.
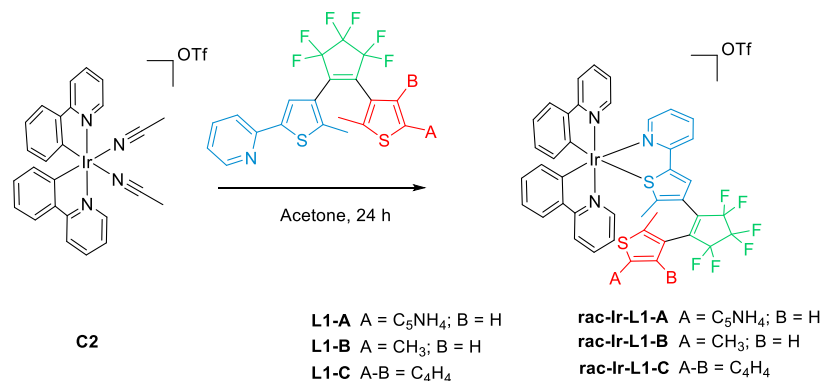
Scheme 2.21. Synthesis of complexes *rac-L1-A*, *rac-Ir-L1-B*, and *rac-Ir-L1-C*.

The purification of the products was carried out through various classical purification techniques (precipitation of the product or through a chromatographic column). In the case of the reaction with **L1-A**, the product obtained was purified by washing the reaction residue with hexane. The solid obtained was purified through a chromatographic column using as eluents, first CH_2Cl_2, and later acetone with an excess of KPF_6 to carry out counter ion exchange, obtaining a green solid. The product was analyzed by ^{1}H-NMR spectroscopy. The spectrum obtained, presented in Figure 2.17, shows a spectroscopic pattern compatible with the desired compound. The broad singlet at 7.56 ppm, could correspond to the aromatic proton of a N-S coordinated thiophene.
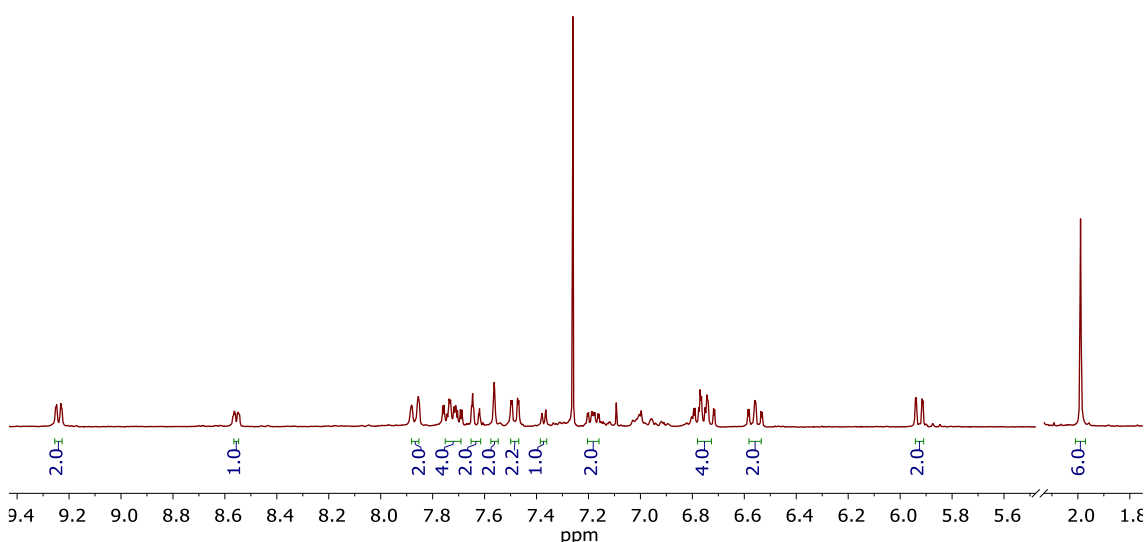
Figure 2.17. ^{1}H-NMR spectrum *rac-Ir-L1-A*. (Acetone-d_6, 300 MHz).

The next step was the coordination of ligand **L1-C**, using the same reaction conditions for the successful coordination of ligand **L1-A**. The compound obtained from the reaction was

precipitated using mixtures of CH_2Cl_2/Et_2O and hexane/MeOH, obtaining a final red solid. The solid was identified employing ^{1}H-NMR spectroscopy, as shown in Figure 2.18. In red, the spectrum measured for the red solid is shown, and different groups of signals were obtained indicating the presence of more than one compound in the solution, probably a mixture of final compound *rac*-Ir-L1-C and free ligand L1-C. Therefore, in an attempt to get the final compound *rac*-Ir-L1-C, the reaction product was purified through a chromatographic column, using silica as the stationary phase and CH_2Cl_2 as eluent. The blue spectrum shows the product resulting from the second workup. Significant decomposition of the product was observed with the appearance of a multitude of unidentified new signals.

b)

a)
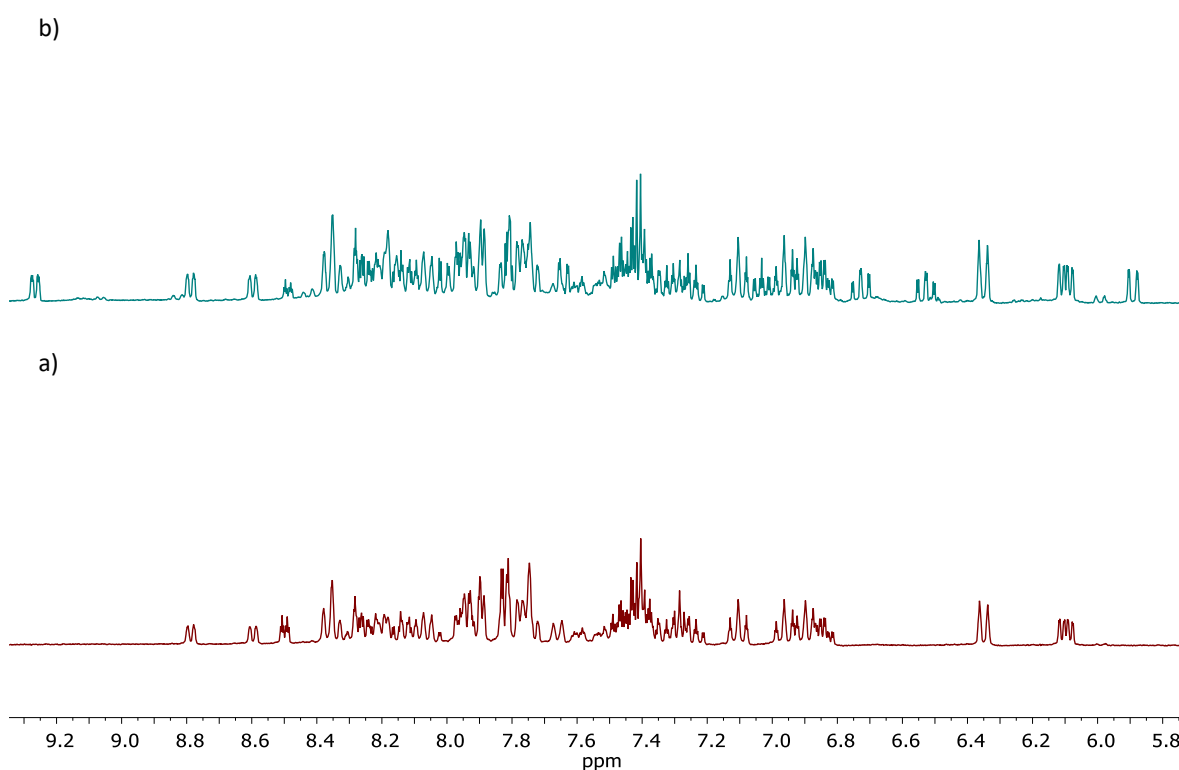
Figure 2.18. a) ^{1}H-NMR spectrum of compound *rac*-Ir-L1-C after precipitation with CH_2Cl_2/Et_2O, b) ^{1}H-NMR spectrum of compound *rac*-Ir-L1-C after purification through chromatography column. (Acetone-d_6, 300 MHz).

During the synthesis of **rac-Ir-L1-B**, other methodologies were used to purify the final product. Such as chromatographic columns. Alumina and silica gel were tested as stationary phases, using CH_2Cl_2 as eluent, varying the polarity with CH_2Cl_2/MeOH mixtures (9:1, v/v) to purify the desired products. Figure 2.19 shows the progress of the reaction between the metallic precursor **C5** and the ligand **L1-B**. In green, two possible compounds are seen, marked with arrows in the upper part of the image. Marked with red arrows, the signals of the free ligand **L1-B** can be observed, the evolution of which can be observed as the reaction progresses and subsequent purification are carried out. After completion of the reaction, two possible compounds could be identified (blue spectrum). At the same time, once an attempt was made to separate them, new unidentified signals appeared in the spectrum. The presence of a free ligand could be explained because the chelation of the DTE ligands occurs weakly, promoting the lack of coordination of the DTE ligand and the possible insertion of solvent molecules. Regarding the unidentified

signals, it could be a compound generated by the coordination of molecules of the solvent used as eluent, creating a bis-solvate precursor due to the lack of coordination of the photoswitchable ligand.
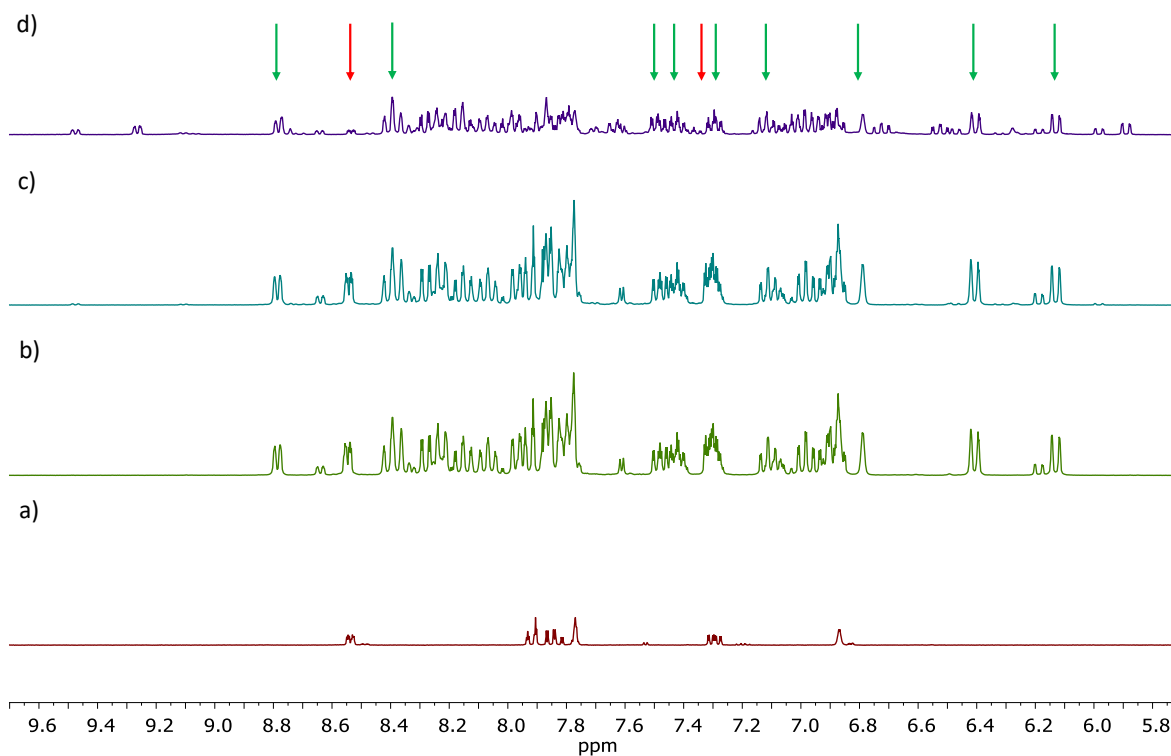
Figure 2.19. a) ^{1}H-NMR spectrum of free ligand **L1-B;** b) ^{1}H-NMR spectrum of compound **_rac_-Ir-L1-B** after 1 hour of reaction; c) ^{1}H-NMR spectrum of compound **_rac_-Ir-L1-B** after 24 hours of reaction; d) ^{1}H-NMR spectrum of compound **_rac_-Ir-L1-B** after purification through column chromatography. (Acetone-d_6, 300 MHz).

After the numerous studies carried out, it has been confirmed that the N-S coordination of fragment **6** to the Ir(III) center occurred effectively, reproducing the results described by Mann. Similarly, the coordination of ligand **L1-A** to precursor **C5** could be observed. Likewise, promising results were obtained for ligands **L1-B** and **L1-C**, even though the purification problems observed. It could also be concluded that the cyclometallation of the **L1-A-L1-C** ligands could not be carried out, probably due to a steric hindrance related to the fluorine groups of the DTE ligands. For this reason, the DTE cyclometalation was studied from another perspective. For this, a new DTE ligand (**L1-D**) was designed. Ligand **L1-D** differs from the rest of **L1** ligands in the position of the coordination site within the thiophene fragment. Therefore, the **L1-D** ligand was used as a candidate to act as a third cyclometalated ligand, using the metallic precursor **C5**. Initially, compound **7** was studied as model ligand to study the cyclometalation of a 5-pyridylthiophene ligand. The metallic precursor **C5** was reacted with compound **7** in excess of base (K_2CO_3) in methanol. The reaction was stirred at room temperature for thirty minutes. After that time, a yellow/gray precipitate was observed. The volatiles were removed, and the resulting solid was washed first with methanol and, secondly, dissolved in acetone, thus eliminating the gray part of the solid, which was filtered off. After removing the volatiles, compound **C8** was obtained as a yellow solid with a yield of 29%.
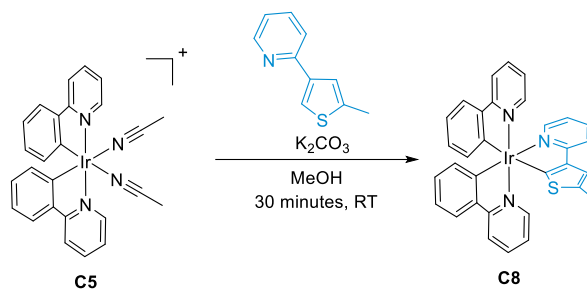
Scheme 2.22. Synthesis of **C8**.

The isolated compound **C8** was analyzed by ^{1}H-NMR spectroscopy. Figure 2.20 shows the ^{1}H-NMR spectrum of complex **C8** where different signal groups could be observed. Despite incomplete complete assignment of ensemble of the numerous different signals, it has been possible to observe a consistent relationship between the number and integration of the signals with the proposed structure for **C8**.
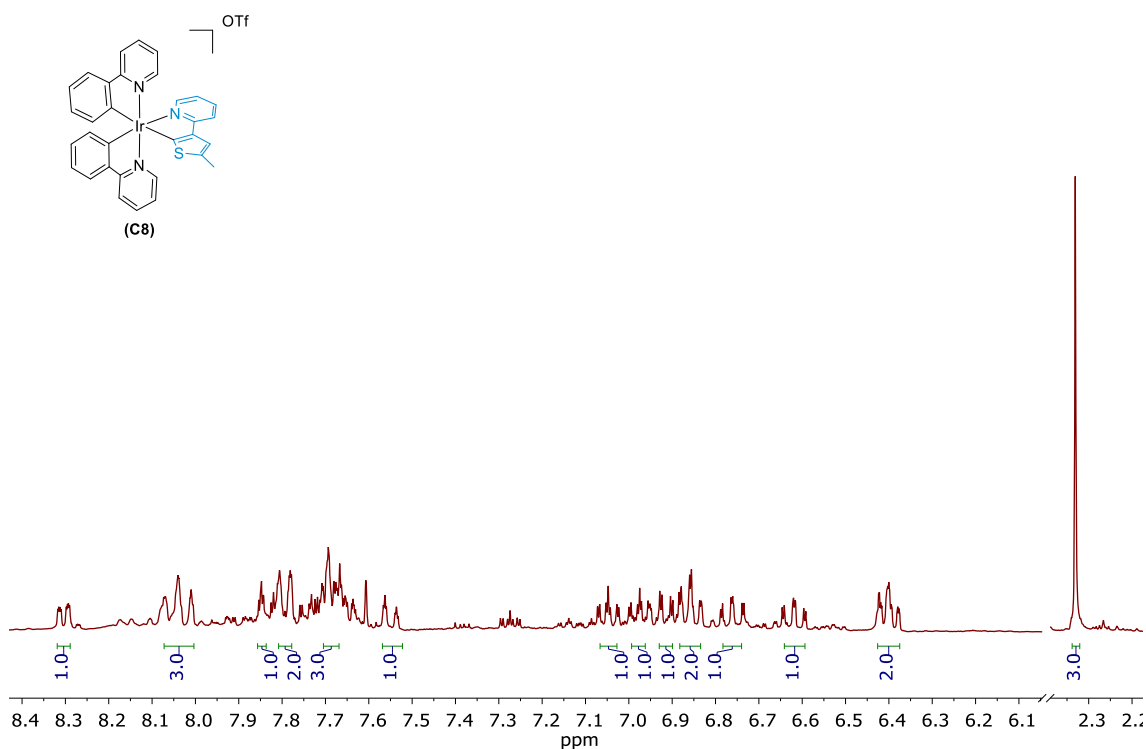
Figure 2.20. ^{1}H-NMR spectra of compounds **C8**. (Acetone-d_6, 300 MHz).

After verifying the coordination of compound **7** to the metal center, the reaction was attempted using **L1-D** (Scheme 2.23). **C5** and **L1-D** were dissolved in 0.5 mL of MeOH in the presence of K_2CO_3, stirring the reaction mixture for 30 minutes. The reaction mixture consisted of a black solid and a yellow solution. The black solid was filtered off through a celite pad and the yellow solution was purified through column chromatography using CH_2Cl_2 as eluent. Figure 2.21 shows the spectrum of the two eluted fractions. The spectrum showed that unreacted **L1-D** and precursor **C5** were obtained from the reaction mixture.

Scheme 2.23. Synthesis of iridium complex *rac*-**Ir-L1-D**.
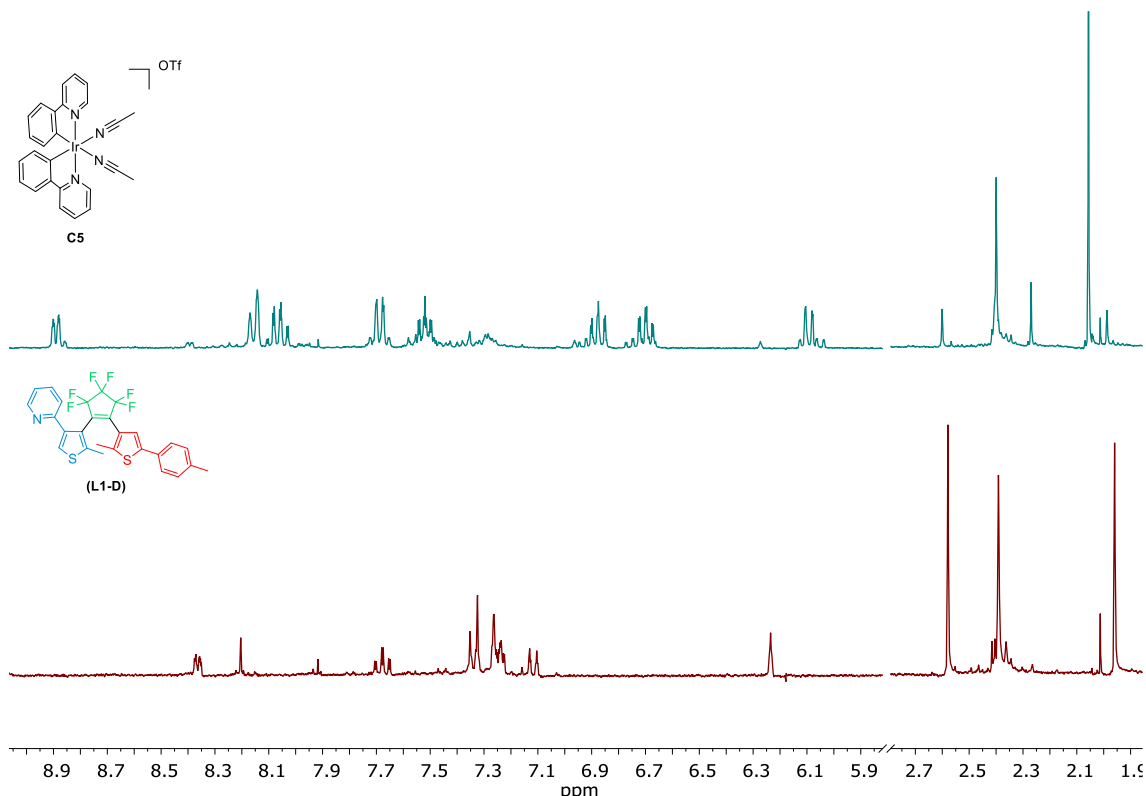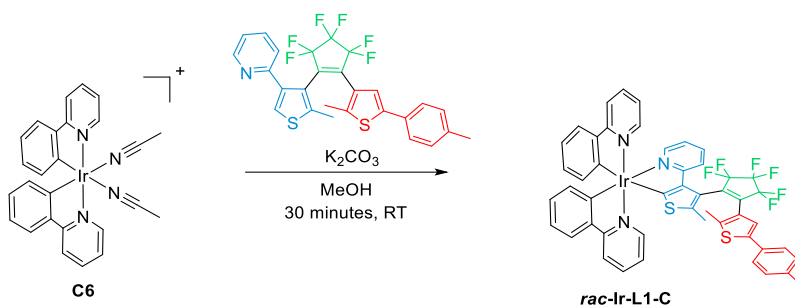
Figure 2.21. ^{1}H-NMR spectrum of **C5** (blue) and[1]H-NMR spectrum of **L1-D** (red) after purification. (Acetone-d_6, 300 MHz).

This experiment suggests that there is also a problem in coordinating **L1-D**, presumably due to steric problems of the ligand.

After all the data obtained, it was concluded that the cyclometalation of DTE ligands synthesized in this section, either for the generation of mono- or bis-cyclometalated photoswitchable complexes was strongly inhibited. Alternatively, N-S coordination was observed, but the final compounds decomposed during the purification process. Nevertheless, it is worth mentioning that these reactions were performed on small scales. Therefore, this research line remains open for future projects of the group, varying the synthetic strategy to be followed or using alternative procedures for the purification of the products.

2.3 REFERENCES

[1] J. Moreno, F. Schweighöfer, J. Wachtveitl, S. Hecht, *Chem. Eur. J.*, **2016**, *22*, 1070-1075.

[2] B. Oruganti, P. P. Kalapos, V. Bhargav, G. London, B. Durbeej, *J. Am. Chem. Soc.*, **2020**, *142*, 13941-13953.

[3] G. Liu, S. Pu, X. Wang, W. Liu, T. Yang, *Dyes and Pigments*, **2011**, *90*, 71-81.

[4] G. Liu, M. Liu, S. Pu, C. Fan, S. Cui, *Dyes and Pigments*, **2012**, *95*, 553-562.

[5] H. Liu, S. Pu, G. Liu, B. Chen, *Dyes and Pigments*, **2014**, *102*, 159-168.

[6] B. Li, J-Y. Wang, H-M. Wen, L-X. Shi, Z-N. Chen, *J. Am. Chem. Soc.*, **2012**, *134*, 16059-16067.

[7] M. Munakata, J. Han, A. Nabei, T. Kuroda-Sowa, M. Maekawa, Y. Suenaga, N. Gunjima, *Inorganica Chimica Acta,* **2006**, *359*, 4281-4288.

[8] M. Liu, G. Liu, S. Cui, *Adv. Mat. Res.*, **2012**, *455*, 41-44.

[9] S. Cui, S. Pu, W. Liu, G. Liu, *Dyes and Pigments*, **2011**, *91*, 435-441.

[10] W. Tan, Q. Zhang, J. Zhang, H. Tian, *Org. Lett.*, **2009**, *11*, 161-164.

[11] V. E. Pritchard, D. Rota Martir, E. Zysman-Colman, M. J. Hardie, *Chem. Eur. J.,* **2017**, *23*, 8839-8849.

[12] M-X. Song, Y. Li, R-P. Deng, F-Q. Bai, Z-K. Qin, *RSC Adv.*, **2016**, *6*, 68960-68963

[13] M. Bandini, M. Bianchi, G. Valenti, F. Piccinelli, F. Paolucci, M. Monari, A. Umani-Ronchi, M. Marcaccio, *Inorg. Chem.*, **2010**, *49*, 1439-1448.

[14] Y. Guo, D. Zhang, J. Wang, H. Lu, S. Pu., *Dyes and Pigments*, **2020**, *175*, 108191.

[15] S. Sprouse, K. A. King, P. J. Spellane, R. J. Watts, *J. Am. Chem. Soc.*, **1984**, *106*, 6647-6653.

[16] K. A. McGee, K. R. Mann, *Inorg. Chem.*, **2007**, *46*, 7800-7809.

[17] N. Wu, J-J. Cao, X-W. Wu, C-P. Tan, L-N. Ji, Z-W. Ma, *Dalton Trans.*, **2017**, *46*, 13482-13491.

[18] F. Scarpelli, A. Ionescu, L. Ricciardi, P. Plastina, I. Aiello, M. La Deda, A. Crispini, M. Ghedini, N. Godbert, *Dalton Trans.*, **2016**, *45*, 17264-17274.

CHAPTER 3

BIPYRIDYL-CONTAINING DITHIENYLETHENES: SYNTHESIS AND COORDINATION TO IR(III)
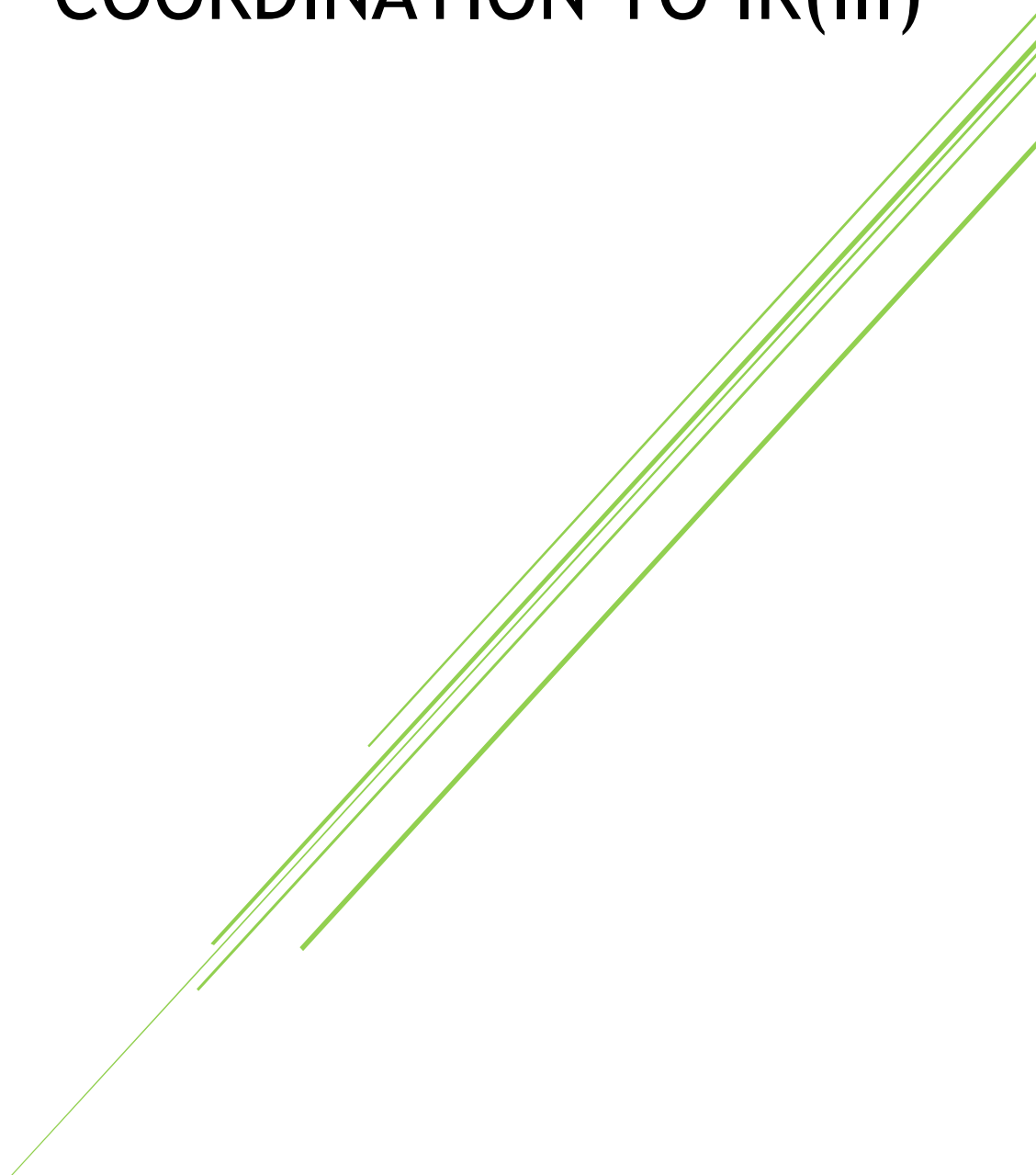
3.1 SYNTHESIS

In the previous chapter, the cyclometallation of different DTE ligands to Ir(III) metallic precursors was studied, observing that the coordination via C-N was not feasible for the designed DTE ligands. Despite the absence of C-N cyclometallation, a new coordination form, not previously described for DTEs, could be observe. The N-S coordination offers a coordination where the photocyclization point is close to the metal center, which, a priori, could significantly influence the induction of selective photoisomerization. Despite observing the N-S coordination, the lability of the bond generated between the ligand and Ir(III) causes the purification and subsequent study of the isomerization of these cationic complexes not yet been optimized.

Due to the results obtained, other ways through which photoswitch ligands coordinate were explored. As studied in *Chapter 1*, the generation of cationic Ir(III) complexes incorporating a bipyridine ligand as an ancillary ligand has been described in depth in the academy over the last decades. Based on the stability and reliability offered by the coordination of these groups to Ir(III) precursors, different DTEs were designed that incorporate bipyridines in their structure, to be used as the coordination fragment.

3.1.1 LIGANDS

This chapter describes the synthesis of racemic and enantiopure (chiral-at-metal) bis-cyclometalated Ir(III) complexes containing a DTE-based auxiliary ligand containing a bipyridyl coordinating fragment. In particular, a bipyridyl fragment was used as the coordinating unit because of the facile synthesis of the corresponding cationic complexes of the type $[Ir(C-N)_2(bpy)]^+$ (C-N = cyclometalating ligand, bpy = bipyridyl ligand). These compounds can be obtained by reacting an iridium-dimeric precursor with the corresponding bipyridyl ligand at room temperature. These mild reaction conditions will preclude the racemization of the metallic center when the reactions are performed in an enantiopure manner (*See section 3.1.2.2*). Therefore, four different DTE-bipyridyl ligands have been designed and synthesized (**L2-A**, **L2-B**, **L3-A,** and **L3-B**, in Scheme 3.1). Ligands **L2** contain an ethynyl spacer between the DTE and the coordinating fragment, whereas ligands **L3** are intended to locate the photochromic fragment closer to the metallic center. Additionally, two different thiophenes (designed as **A**, and **B**), widely used to construct photoresponsive DTEs, have been used as non-coordinating components of the ligands. In all the examples, hexafluorocyclopentene was chosen as bridging-ethene.

L2-A

L2-B

L3-A

L3-B
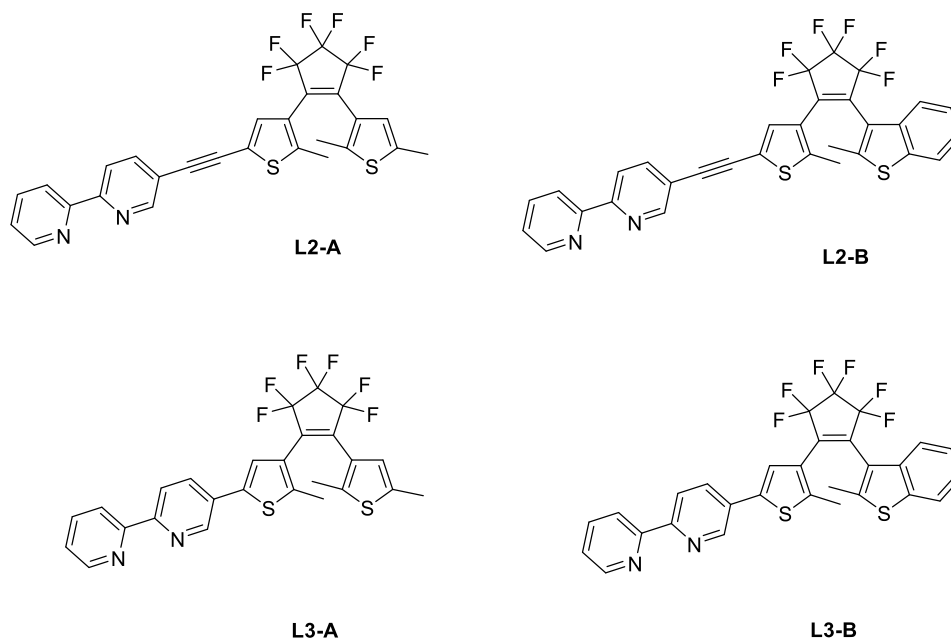
Scheme 3.1. Asymmetric DTE-bipyridyl ligands synthesized.

From a synthetic perspective, these ligands can be considered modular. They can be obtained from the appropriate starting components through several synthetic routes. Some of these alternative reaction paths and the modularity of the ligands are depicted in Figure 3.1. Each of the ligands (**L2-A**, **L2-B**, **L3-A**, and **L3-B**) has been obtained through different synthetic routes obtaining identical final compounds. In the following sections, representative examples of each of the different steps involved in the different routes and the synthesis of the required intermediates will be described.
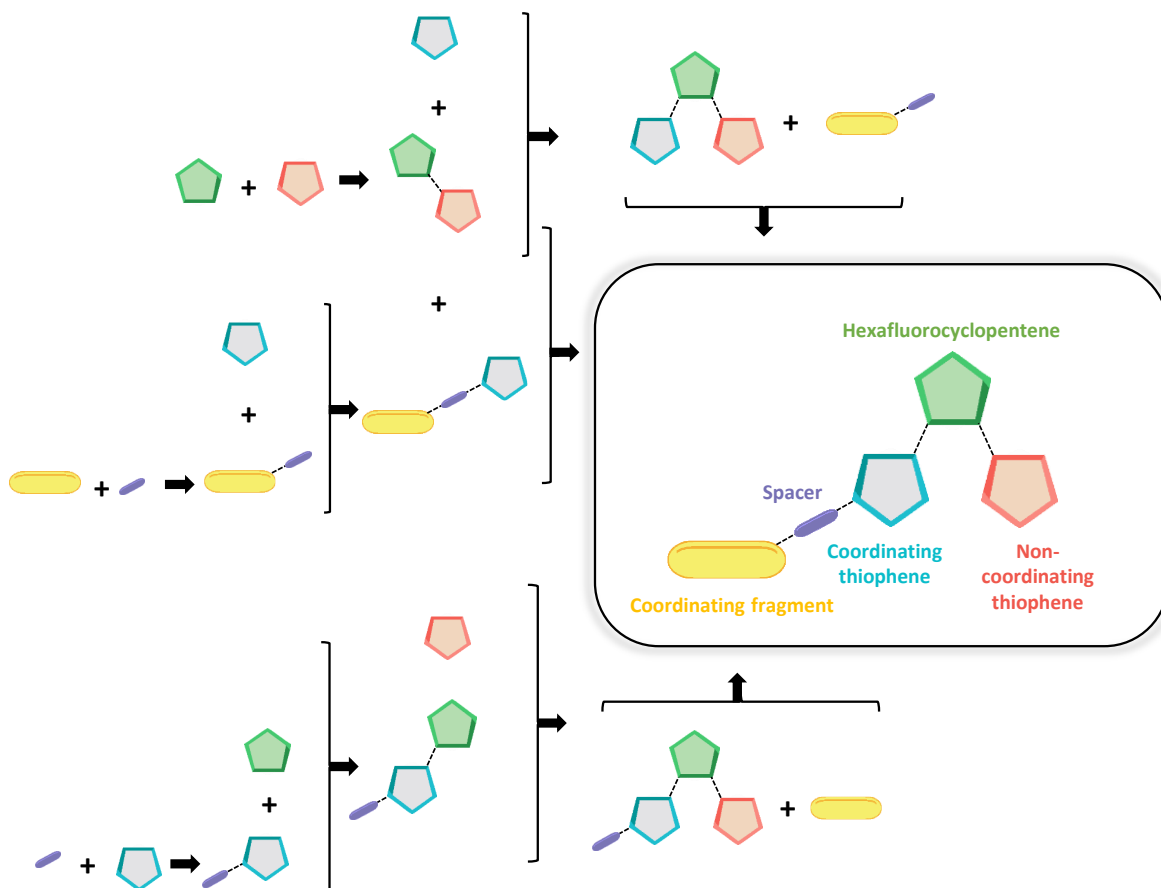
Figure 3.1. Conceptual drawing showing the modularity of the DTEs synthesized and some of the different synthetic routes explored.

3.1.1.1. NON-COORDINATING THIOPHENE

As it was presented in *Chapter 2*, different non-coordinative thiophenes were chosen to create the new asymmetric DTE families. The choice of the 2,5-dimethylthiophene and 2-methylbenzo[*b*]thiophene-based bromothiophenes (**1** and **2**) is mainly due to the relative ease of synthesizing both compounds. As the synthetic procedure was studied and discussed in the previous section, Scheme 3.2 is shown only as a reminder of the synthesis of these.
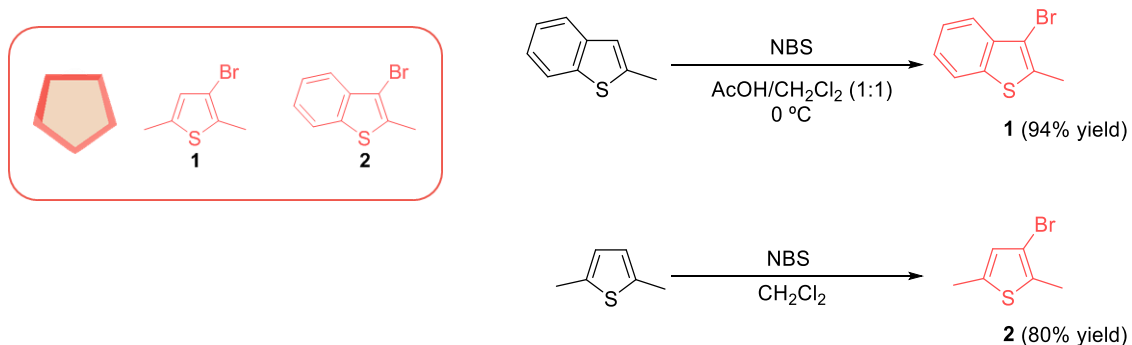
Scheme 3.2. Synthesis of non-coordinating thiophenes **1** and **2**.

3.1.1.2. COORDINATING THIOPHENE

As described in Figure 3.1, different synthetic routes can be envisaged to construct the final DTEs. Some of them require molecular modules containing a thiophene unit appended with the appropriate functional groups. The synthesis of these fragments will be described in this section.
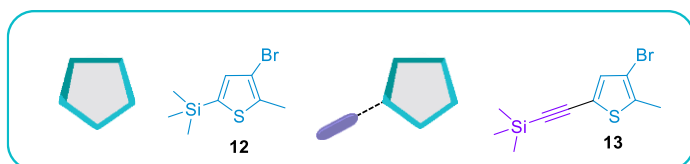
For the synthesis of asymmetric DTE ligands **L3** (without spacer) and **L2** (with an ethynyl spacer), derivatives **12** and **13** were prepared. They contain a bromine atom in position 2, which will be used in a coupling reaction to link the fragment to the central cyclopentene, and a TMS protecting group. The latter will be cleaved at a later stage to allow the incorporation of the coordinating bipyridyl unit. The synthesis of these derivatives (shown in Scheme 3.3) was described in the literature.[1,2] Similarly to compound **5**, both compounds were synthesized starting from commercially available 2-methylthiophene, through a double bromination using NBS.
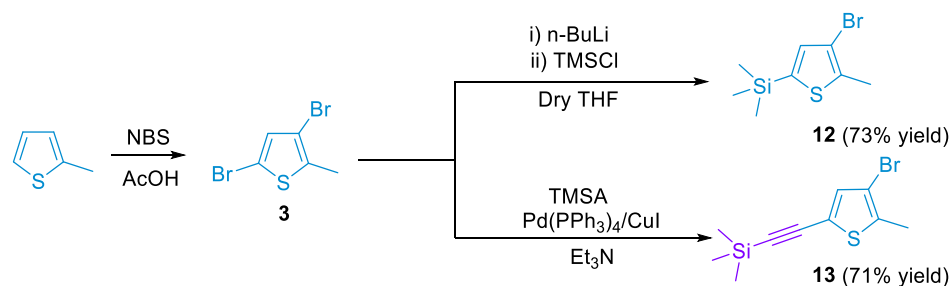
Scheme 3.3. Syntheses of compounds **4** and **5**.

In the case of compound **12**, the most reactive bromine of intermediate **3** was protected with a tetramethylsilyl group (TMS) by lithiation using one equivalent of *n*-BuLi (-78 °C, dry THF), followed by *in situ* reaction of the lithiated intermediate with tetramethylchlorosilane (TMSCl). After workup and purification by column chromatography in petroleum ether, the expected compound was obtained as a colorless oil with a 73% yield.[1]

Compound **13** was obtained by Sonogashira coupling[2,3] of intermediate **3** with tetramethylsilylacetylene (TMSA) using Pd(Ph$_3$)$_4$ and CuI as catalysts in basic media (NEt$_3$). The compound was obtained, after workup and purification by column chromatography in hexane, as a yellow oil (71% yield).

The purity and identity of these compounds were confirmed by ^{1}H NMR spectroscopy. The spectra obtained were in agreement with the published spectroscopic data.[1,2] They showed only one singlet in the aromatic region (assigned to the thiophene proton) and two singlets at high fields of the spectra (integrating for 3 and 9 protons, respectively), assigned to the methyl groups of the thiophene and the TMS protecting group.

3.1.1.3 BIPYRIDINE FRAGMENTS

14   **16**   **17**
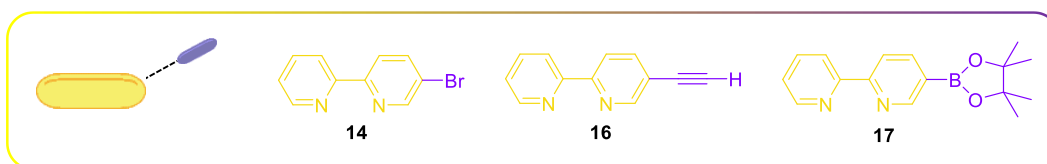
As mentioned above, this chapter aims to develop and study a new family of DTE derivatives incorporating bipyridine as a coordinating fragment. Therefore, as shown in Figure 3.1, the synthesis of the different bipyridine-containing intermediates with the appropriate functional groups was needed. The starting bromo-bipyridine precursor **14** was synthesized following a described procedure.[4] It was obtained by palladium-catalyzed Negishi coupling of the commercially available 2-iodo-5-bromopyridine and 2-pyridylzinc bromide (r.t, THF/H_2O) as shown in Scheme 3.4. After workup, compound **14** was purified by column chromatography (hexane). The product was obtained as a white solid with a 52% yield. ^1H NMR spectroscopy confirmed the identity of the resultant product.[5]
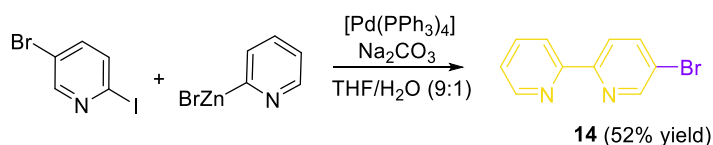
Scheme 3.4. Synthesis of compound **14**.

Compound **14** could be used either as a direct module or further modified to create other bipyridyl-containing synthons **16** and **17**. The syntheses of both compounds were already described in the literature.[6,7,8]

Compound **16** was obtained through two reaction steps (Scheme 3.5): Initially, the starting compound (**14**) was reacted with TMSA by Sonogashira coupling using palladium and copper catalysts. The reaction residue after workup was purified by column chromatography (see the experimental section for details), obtaining compound **15**. Eventually, the acetylene group was deprotected in a basic medium (K_2CO_3/MeOH). After workup and purification, **16** was obtained as a beige solid in an overall yield of 74%.

In the case of compound **17**, the synthetic procedure, described by Beves *et al.,* consisted of three consecutive synthetic steps executed in a one-pot process (Scheme 3.5).[8] The reaction started by a lithiation of compound **14** (-78 °C, dry Et_2O). Once the lithium intermediate was formed, tributyl borate was added, and the reaction mixture was warmed up to room temperature. Finally, pinacol was added to the reaction medium to form the corresponding boronic ester. After workup, the expected compound was obtained as a brown solid with a 49% yield. Several attempts to use the corresponding boronic acid (bpy-B(OH)$_2$) showed that it was a highly unstable compound. Therefore, **17**, the corresponding pinacol borate, was chosen for further reactions.
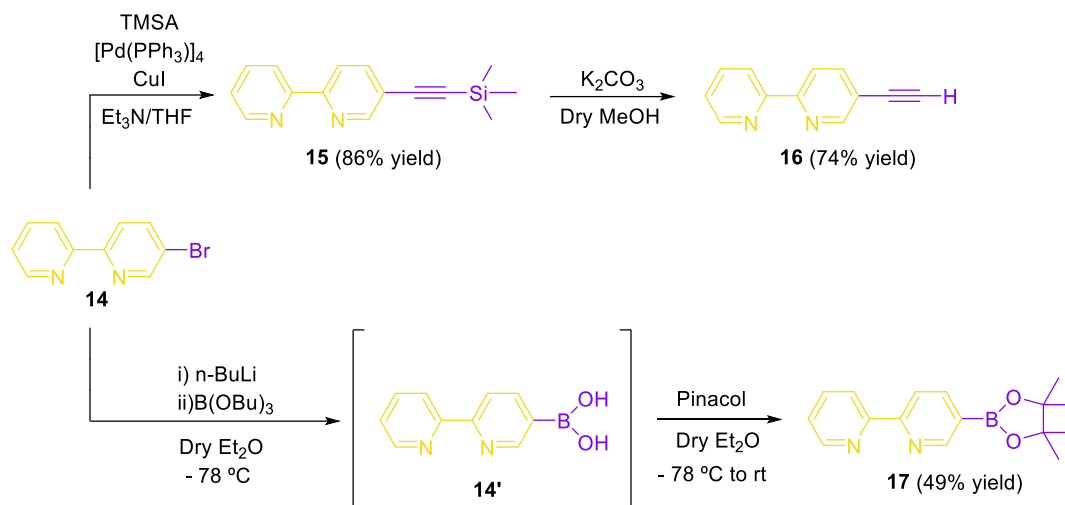
Scheme 3.5. Synthesis of compounds **16** and **17**.

The purity of these compounds was confirmed by ^{1}H NMR spectroscopy (Figure 3.2). The spectra obtained were in agreement with the published spectroscopic data.[6-8] At the aromatic region of the spectra they showed the characteristic pattern of a 5-monosubstituted bipyridine (two triplets and five doublets). More distinctive signals could be observed at the high-field region of the spectra. In the case of compound **15** (in blue), an intense singlet (integrating for 9 nuclei) corresponding to the trimethylsilyl group was observed. Instead, in the case of compound **16** (in green) a singlet integrating for 1 proton was observed at lower fields, and it was assigned to the acetylene proton. The ^{1}H NMR spectrum of compound **17** (in red) showed an intense singlet (integrating for 12 nuclei) in the aliphatic region, which was assigned to the methyl groups of the pinacol borate.
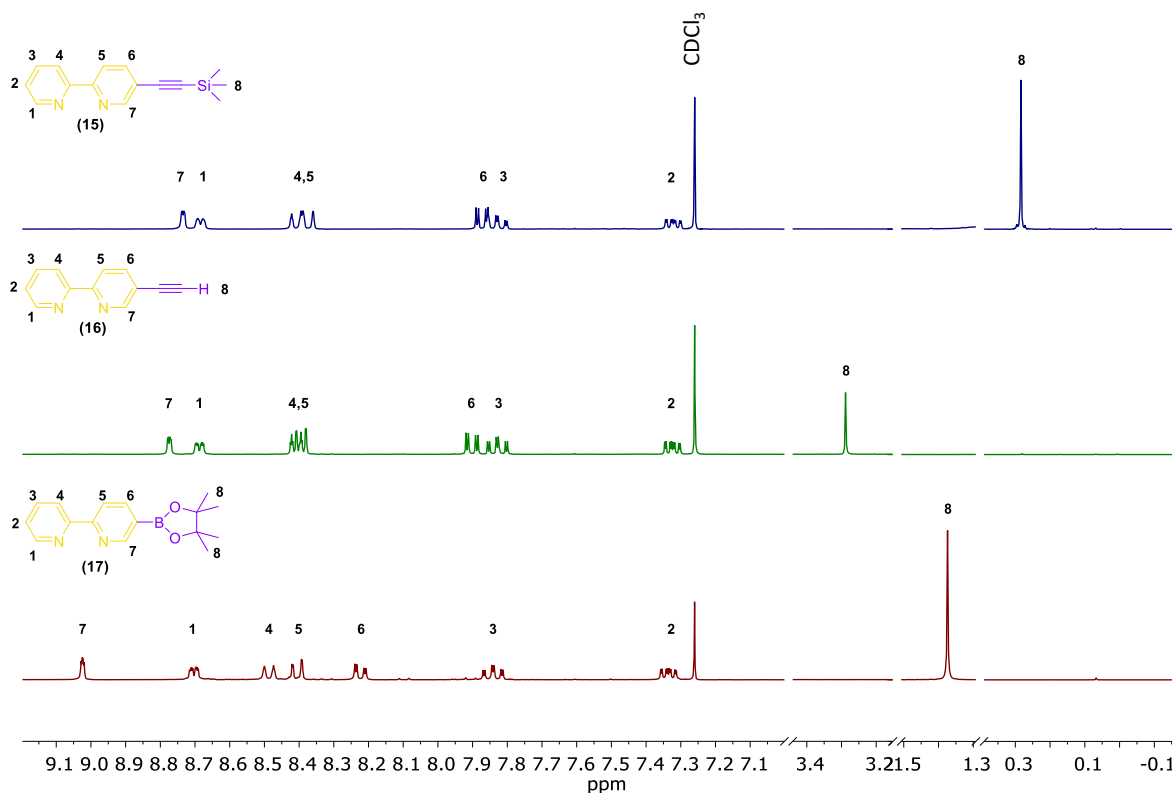
Figure 3.2. ^{1}H NMR spectra of compounds **15-17**. (CDCl$_3$, 300 MHz).
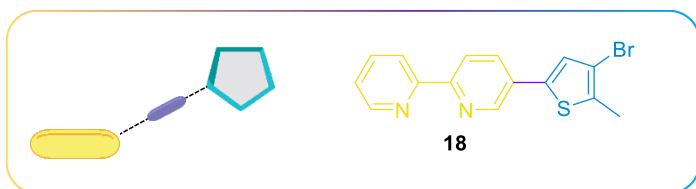
As described in Figure 3.1, some synthetic routes towards DTEs required the synthesis of a complete coordinating branch (containing both bipyridyl and thiophene units). This convergent synthetic strategy was of particular interest for the synthesis of the **L3** ligands, since it provides a direct bond between the thiophene and the coordinating bipyridine fragment, this approach would provide a direct synthesis of the **L3** ligands. For this purpose, compound **18** was synthesized, starting from the well-known intermediate **3** (Scheme 3.6). Initially, boronic acid intermediate **4** was obtained by reaction with *n*-BuLi and triisopropyl borate at -78 °C in THF and subsequent workup.[9] The intermediate **4** was obtained as a brown solid (60% yield). Compound **4**, was subsequently reacted with 5-bromo-2,2'-bipyridine **14** by palladium-catalyzed Suzuki cross-coupling, as reported in the literature.[10] After workup and purification through column chromatography using silica gel as the stationary phase (petroleum ether/AcOEt (9:1, v/v)), the desired product was obtained as a beige solid with a 49% yield. The purity of the compound was confirmed by ^{1}H NMR spectroscopy.[10]
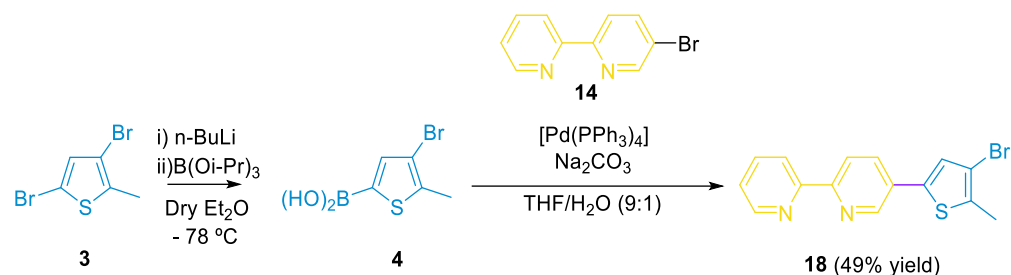
Scheme 3.6. Synthetic route for compound **18**.

3.1.1.4 THIENYLETHENE DERIVATIVES

As shown in Figure 3.1 and previously presented in *Chapter 1*, all the synthetic routes towards asymmetric DTEs involve forming an intermediate thienlylheptafluorocyclopentene (thienylethene, TE). The synthesis of two new coordinating TEs (**19** and **20**) and the two non-coordinating TEs (**21** and **22**) will be presented for the new DTE families. All these compounds were synthesized similarly, following standard literature procedures.[11-14]
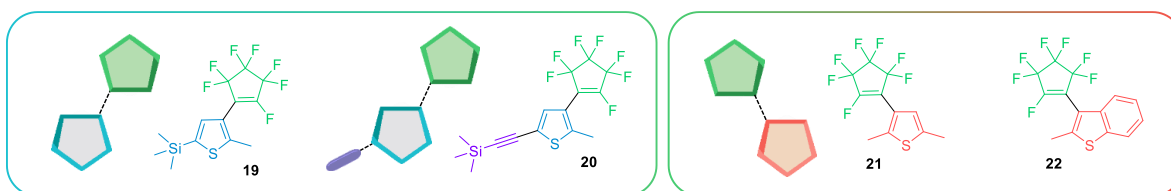
The synthesis of the TE compound started by lithiation of the corresponding 2-bromothiophene using *n*-BuLi (-78 °C, dry THF). While keeping the temperature at -78 °C, the corresponding reactive lithiothiophene intermediate solution was added via cannula to a solution of octafluorocyclopentene in THF (Scheme 3.7). This "inverse" addition order is required to minimize the formation of the undesired symmetric DTE. After workup, all the compounds were purified by column chromatography over silica gel, eluting with hexane, and obtained with good-to-moderate yields (49–70%).

X = SiTMS; Y = H	**12**	**12'**	**19** (70% yield)
X = C$_2$SiTMS; Y = H	**13**	**13'**	**20** (64% yield)
X = CH$_3$; Y = H	**1**	**1'**	**21** (58% yield)
X-Y = C$_4$H$_4$	**2**	**2'**	**22** (49% yield)
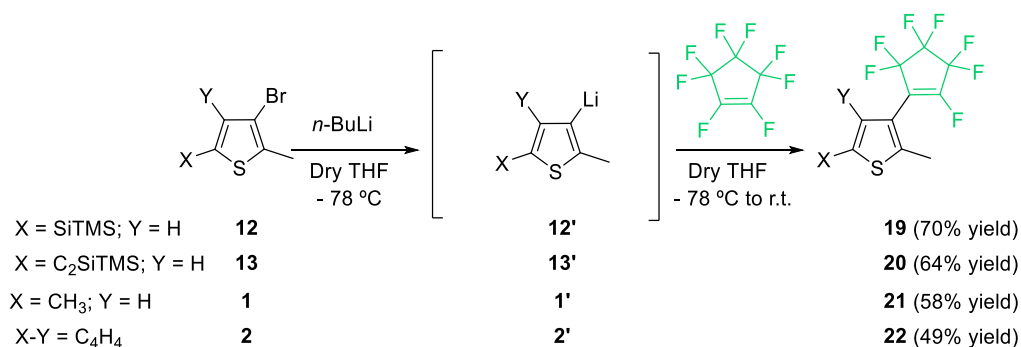
Scheme 3.7. Syntheses of TEs **19–22**.

These compounds were characterized by ^{1}H NMR (Figure 3.3), and ^{19}F NMR (Figure 3.4) spectroscopies. Compounds **19**, **20**, and **21** show, as expected, only one singlet in the aromatic region of the ^{1}H NMR spectra due to the thiophene proton, whereas the characteristic pattern of the benzothiophene is observed in the case of derivative **22**. The most characteristic signature of these spectra is the doublet observed for the methyl in position 2 of the thiophene, in the case of compounds **19–21**. To unravel the origin of this coupling, a {^{19}F}^{1}H NMR spectrum was recorded for one of the simplest compounds of the series (**20**) and was compared to its ^{1}H NMR spectrum (Figure 3.3). This experiment showed that the methyl that appeared as a doublet (J = 3.1 Hz) in the ^{1}H NMR spectrum collapsed into a singlet in the fluorine-decoupled spectrum. Additionally, the broad signal observed for the thiophene proton also sharpened. ^{19}F NMR spectra were also recorded to confirm this H–F coupling. The {^{1}H}^{19}F NMR spectrum (Figure 3.4) showed a broad triplet at -126.7 ppm. A more complex signal was observed in the corresponding ^{19}F NMR spectra assigned to the additional H–F coupling. These results confirmed that the multiplicity observed for the methyl signal in the ^{1}H NMR was due to the coupling (most probably through space) with the fluorine atom of the fluorinated ethene. In the case of compound **22**, the absence of this coupling is most probably due to a different conformational arrangement of the compound due to the larger steric hindrance of the benzothiophene unit. The mentioned behavior was also observed during the synthesis of intermediate compounds **10** and **11** in Chapter 2 (*See section 2.1.3 THIENYLETHENE DERIVATIVES of Chapter 2*), strengthening the hypothesis of the methyl-fluorine coupling.
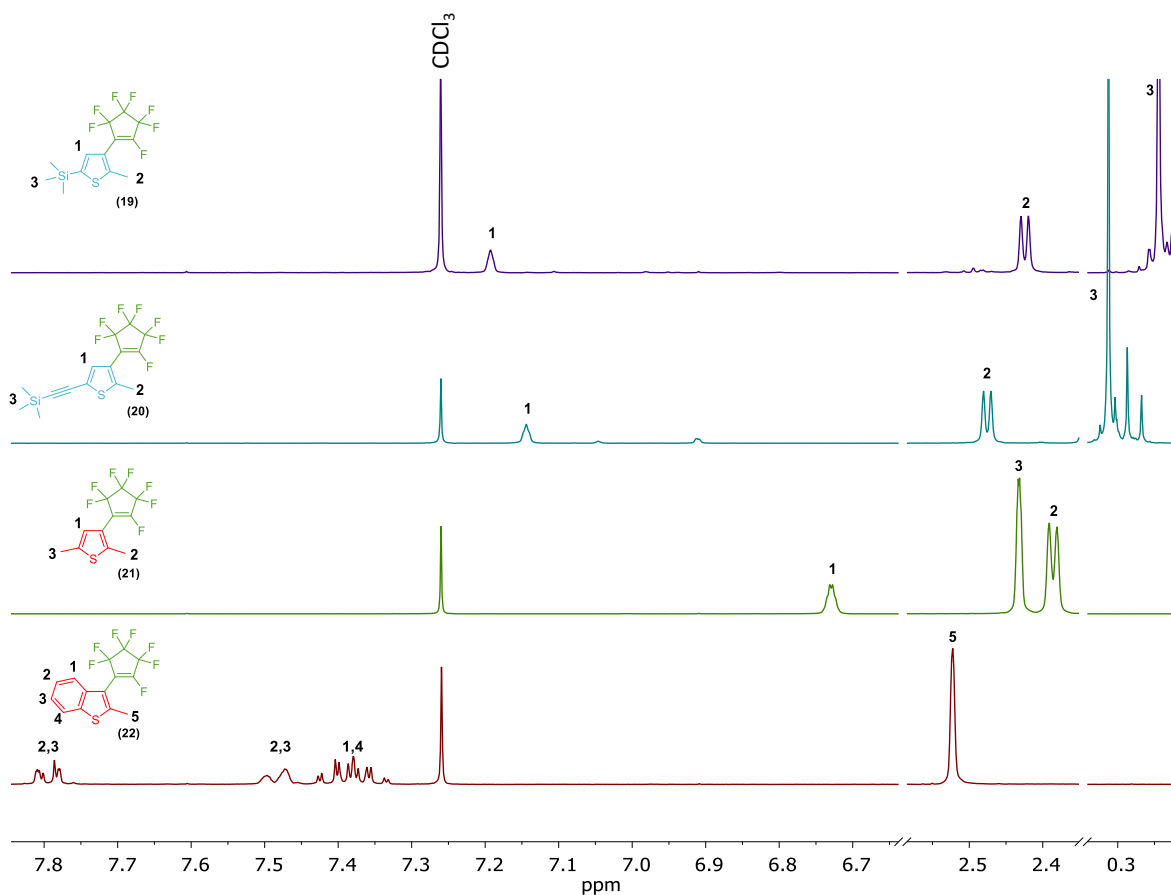
Figure 3.3. ¹H-NMR spectra of TEs **19** (purple line), **20** (blue line), **21** (green line), and **22** (red line). (CDCl₃, 300 MHz).
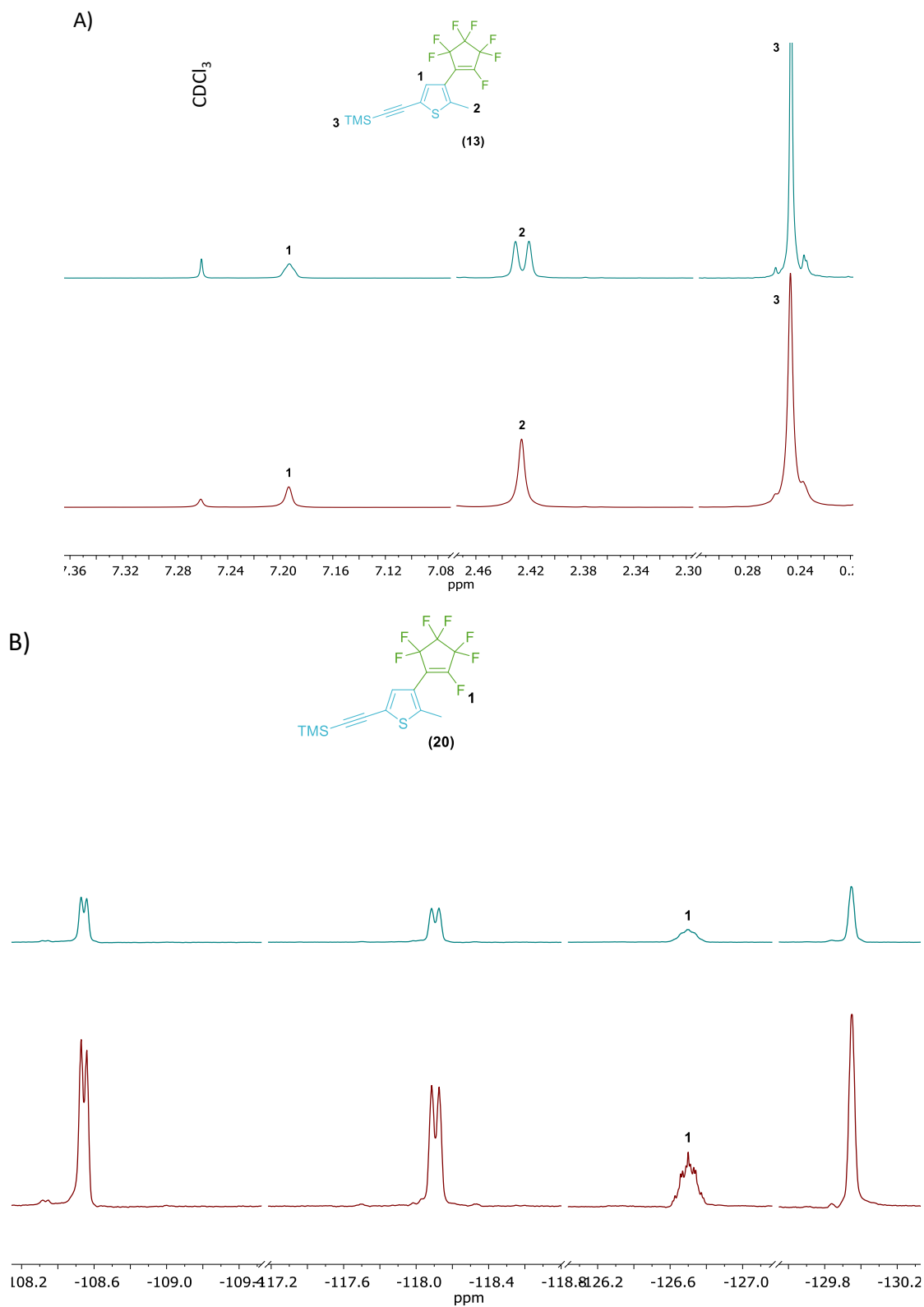
Figure 3.4. A) ^{1}H NMR (blue) and {^{19}F}^{1}H NMR (red) spectra of compound **20**. B) . {^{1}H} ^{19}F NMR (blue) and ^{19}F NMR (red) spectra of compound **20**. (CDCl$_3$, 300 MHz).

3.1.1.5 DITHIENYLETHENE PRECURSORS AND LIGANDS

  Several synthetic routes can be considered to construct the final DTE derivatives. In this section, the synthesis of four DTE scaffolds will be described. Two of them (**18** and **19**) are intended for the construction of **L2**-type ligands, and the other two (**22** and **23**) for the synthesis of **L1**-type ligands. The synthesis of the final DTE_bipyridyl ligands will also be described here. All these DTEs were synthesized in a similar manner, following standard literature procedures for related compounds.[15,16] For the sake of clarity, the synthesis of both families of DTEs will be explained separately.

3.1.1.5.1. L3-TYPE LIGANDS.
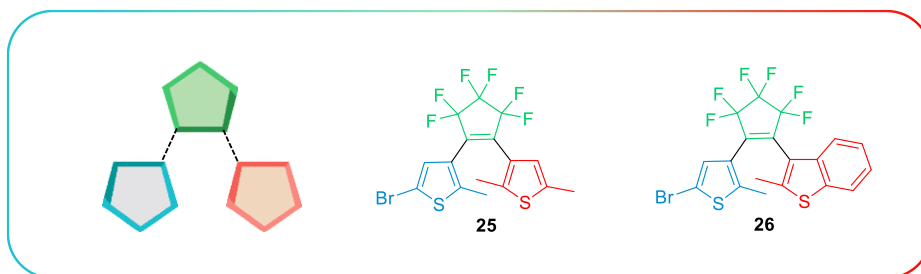
  DTEs **23** and **24**, intended to be used for the synthesis of direct **L3**-type ligands, were obtained by lithiation of the corresponding TMS-protected thiophene (**12**) using *n*-BuLi (-78 °C, dry THF). While keeping the temperature at -78 °C, a cold solution of the corresponding TE derivative (**21** or **22**) was transferred by cannula to the solution of the highly reactive lithium-thiophene intermediate (**12'**) (Scheme 3.8). After workup, intermediates **23** and **24** were purified by column chromatography over silica gel, eluting with hexane and were obtained with similar yields (circa 50-55%).
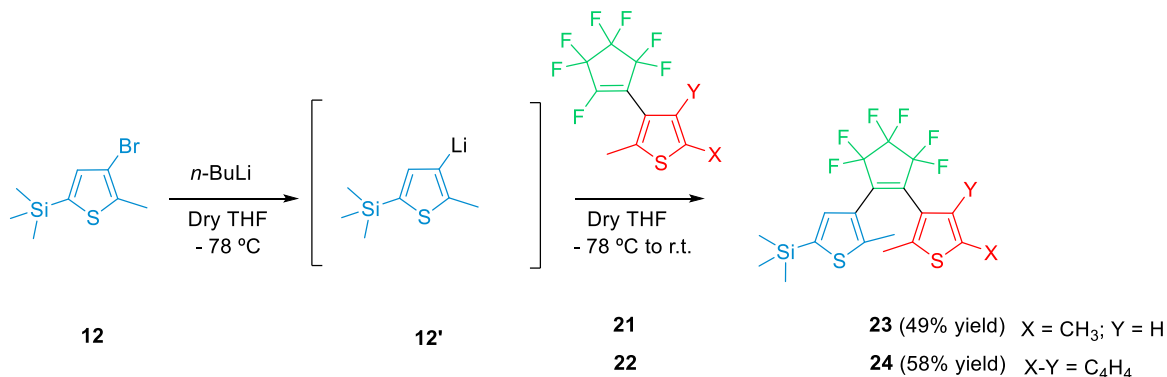
Scheme 3.8. Syntheses of **23-24**.

  The purity and identity of compound **23** was confirmed by ^{1}H NMR spectroscopy, as the spectrum obtained was in agreement with the published spectroscopic data for the same compound.[16] In the

case of derivative **24**, the ^{1}H NMR (Figure 3.5) showed four signals in the aromatic region, two doublet of doublets, two overlapped triplets of doublets (assigned to the benzothiophene protons), and a singlet assigned to the coordinating thiophene aromatic proton. At high fields of the spectrum, two singlets (integrating for 3 nuclei each) assigned to the methyl group of the thiophenes, and a singlet corresponding to the trimethylsilyl fragment (integrating for 9 nuclei) were observed.
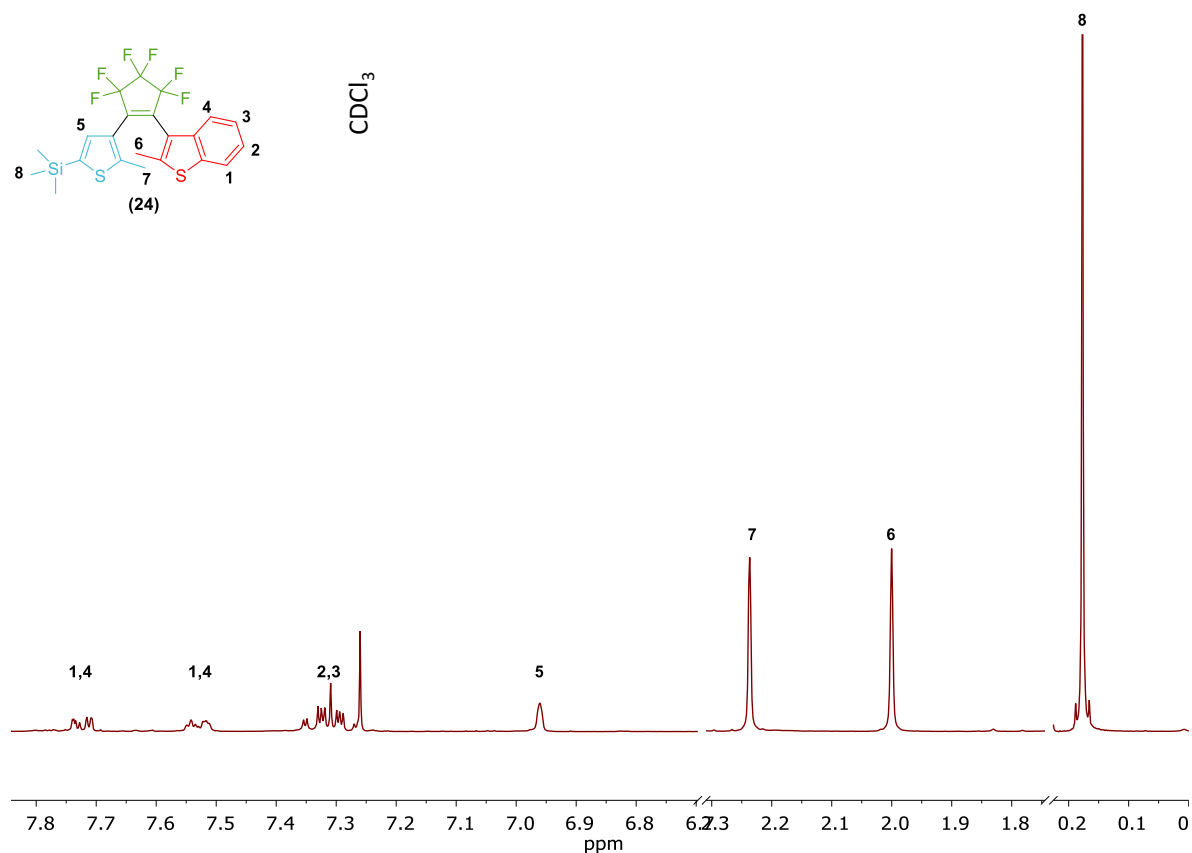
Figure 3.5. ^{1}H NMR spectrum of compound **24**. (CDCl$_3$, 300 MHz).

The target DTE molecules **25** and **26** were obtained by bromination of TMS-protected intermediates **23** and **24** by a procedure slightly modified from the one described in the literature (Scheme 3.9).[16] After workup, intermediates **25** and **26** were purified by column chromatography over silica gel, eluting with hexane. The final compounds were obtained in good to moderate yields.
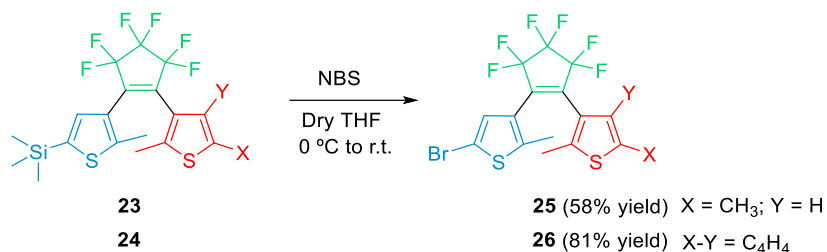
Scheme 3.9. Syntheses of **25** and **26**.

The isolated compounds **25** and **26** were analyzed by ^{1}H NMR spectroscopy. The measured spectrum of compound **25** was in agreement with the described spectroscopic data.[16] Compound **26** (not described in the literature) was fully characterized by multinuclear NMR spectroscopy (See experimental section). The ^{1}H NMR spectra shows in Figure 3.6 the comparison between precursor **24** and compound **26**, observing a similar pattern between them. In red, the effectiveness of the bromination reaction was confirmed by the disappearance of the singlet assigned to the TMS groups present in the precursor **24**. A slight displacement of the aromatic signals of the DTE towards lower fields can also be observed.
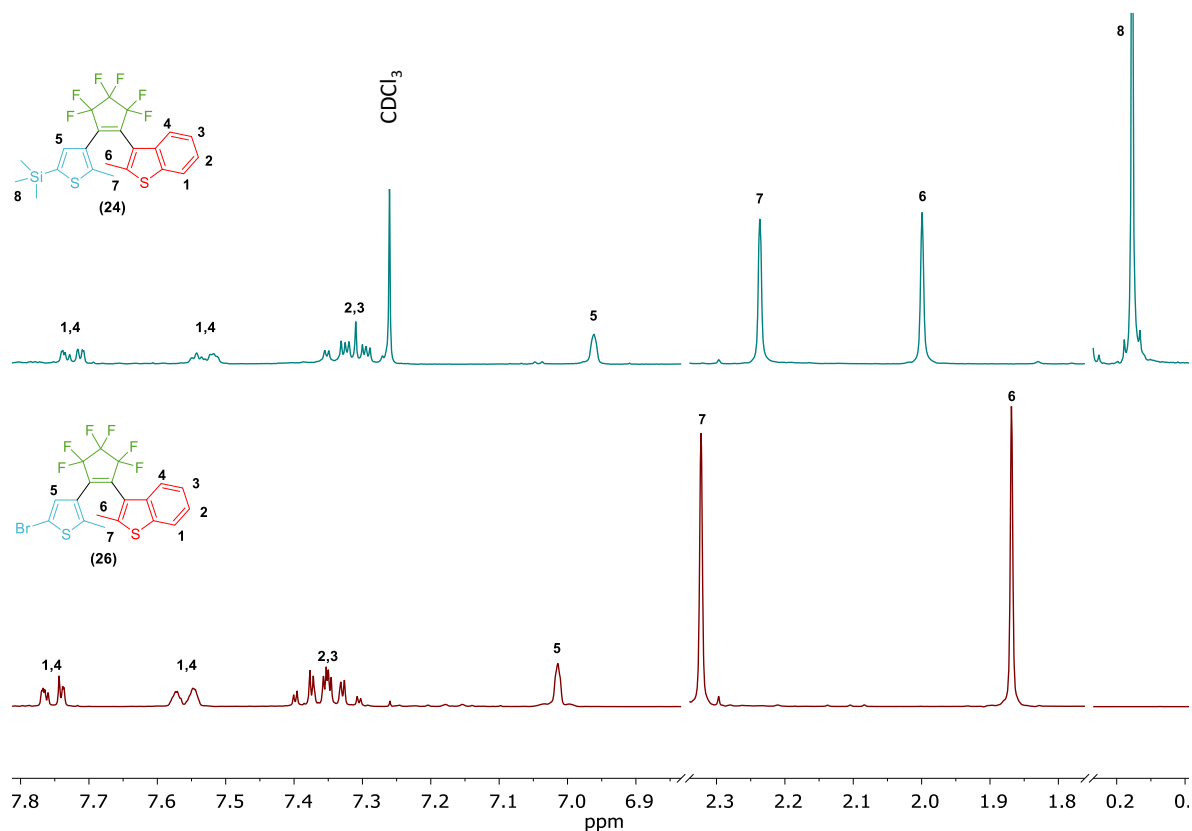
Figure 3.6. ^{1}H NMR spectrum of compound **26**. (CDCl₃, 300 MHz).
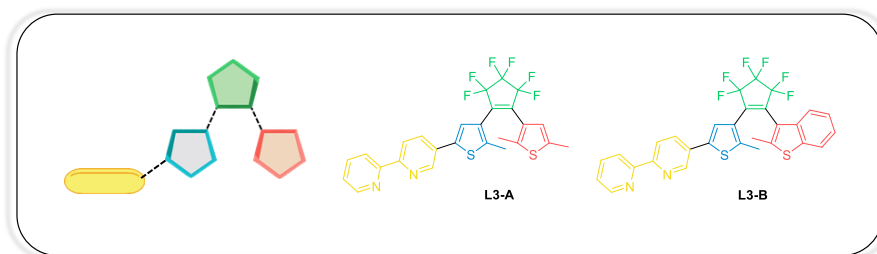
DTE ligands **L3-A** and **L3-B** were not described in the literature. The synthetic methodology was initially optimized for the derivative **L3-A**, before applying it to **L3-B**. Two different synthetic routes were envisaged based on slightly modified synthetic procedures compared to those described in the literature for related DTEs (Scheme 3.10).[17] *Route 1* involved a lithiation of the corresponding bipyridine-thiophene coordinating fragment (**18**) using *n*-BuLi (-78 °C, dry THF). While keeping the temperature at -78 °C, a cold solution of the corresponding TE derivative (**21**) was added to the solution of the highly reactive lithium intermediate (**18'**). After workup, the residue was purified by column chromatography over silica gel eluting with CH_2Cl_2, obtaining ligand **L3-A** with only poor yields (9%). *Route 2* was designed to increase the reaction yields. It consisted of a palladium-catalyzed cross-coupling of the bipyridyl pinacol ester **17** with the brominated DTE **25**. After workup and purification through column chromatography in CH_2Cl_2, the final product was obtained as a brown powder with a 60% yield.
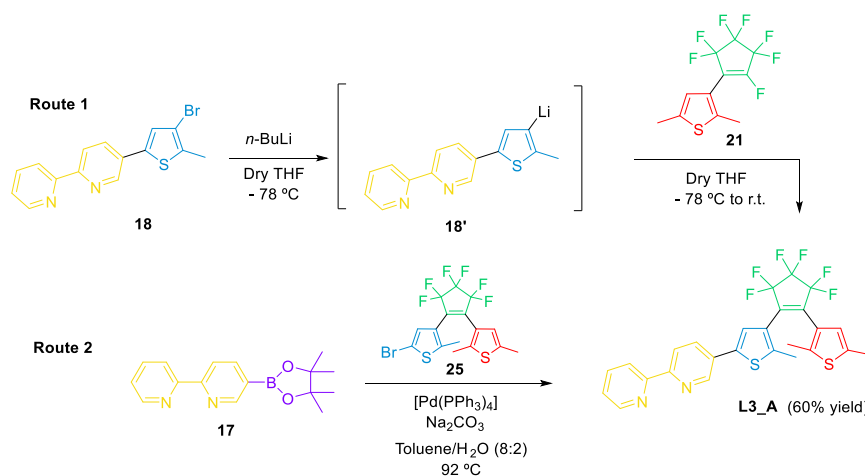
Scheme 3.10. Syntheses of **L3-A**.

L3-A was fully characterized by multinuclear NMR spectroscopy (*See Experimental Section*). The ^{1}H NMR (Figure 3.7) showed at low fields two doublets, two doublets of doublets, a triplet of doublets, and a doublet of doublets of doublets, assigned to the bipyridyl fragment of the ligand. In this region of the spectrum, two singlets attributed to the thiophene aromatic protons were also observed. Three singlets (integrating for 3 nuclei each) and assigned to the methyl groups were observed at the aliphatic region of the spectrum.
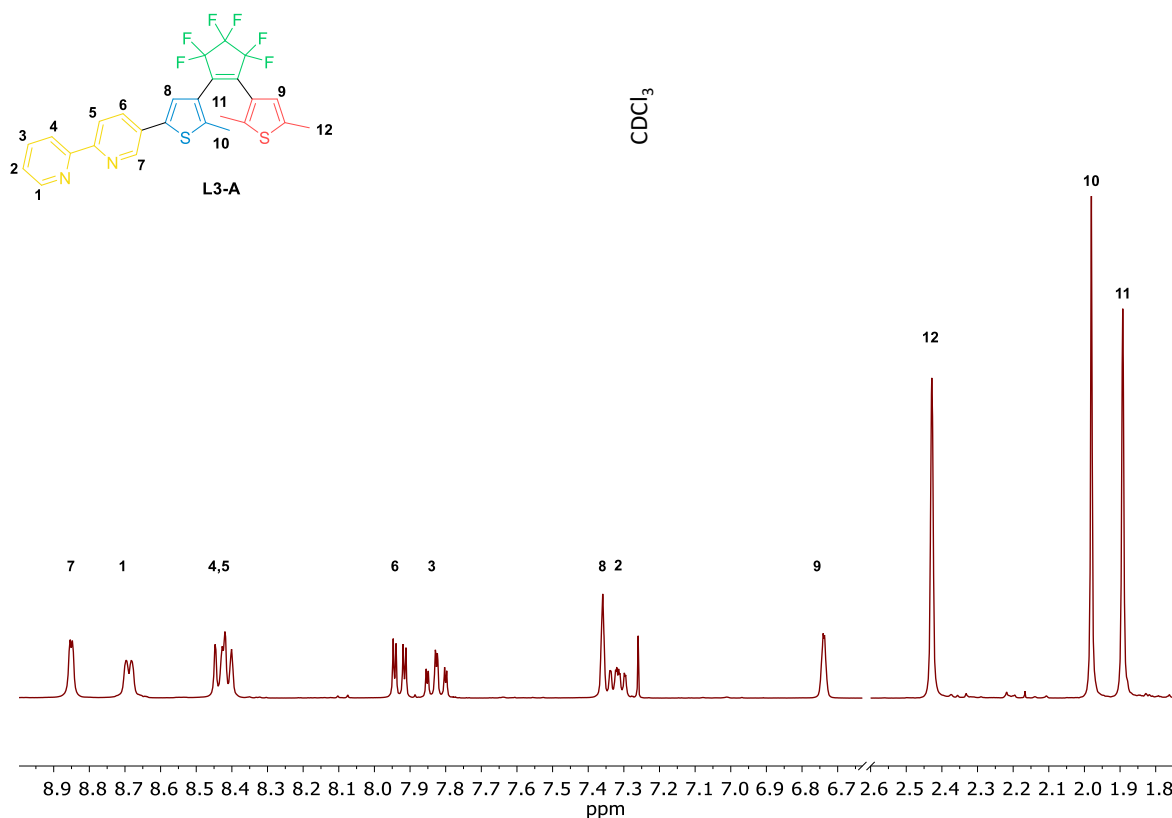
Figure 3.7. ^{1}H NMR spectrum of **L3-A**. (CDCl$_3$, 300 MHz).

Given the good yields obtained through *Route 2*, an analogous cross-coupling procedure was used to synthesize ligand **L3-B**, using intermediates **17** and **26** as coupling partners (Scheme 3.11). After workup and purification through column chromatography over silica gel, eluting with CH$_2$Cl$_2$, the final product was obtained as a brown powder with a 40% yield.
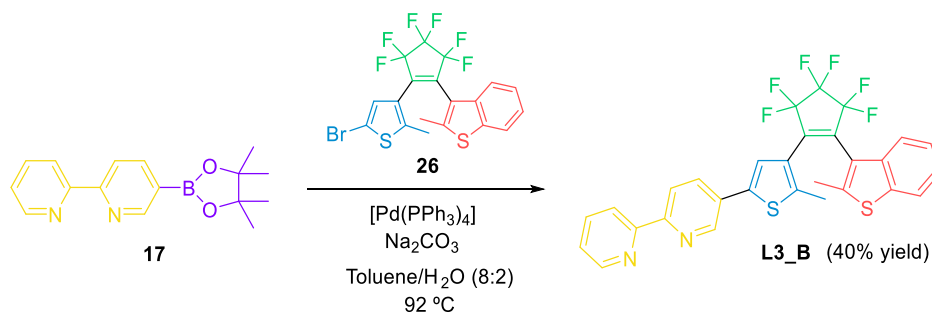
Scheme 3.11. Synthesis of **L3-B**.

L3-B was characterized by means of multinuclear NMR spectroscopy (*See Experimental Section*). The ^{1}H NMR spectrum of **L3-B** was more complex than that of **L3-A** due to the overlap of aromatic

signals of the bipyridyl and benzo[*b*]thiophene fragment, but it could be assigned unequivocally to the desired compound (Figure 3.8).
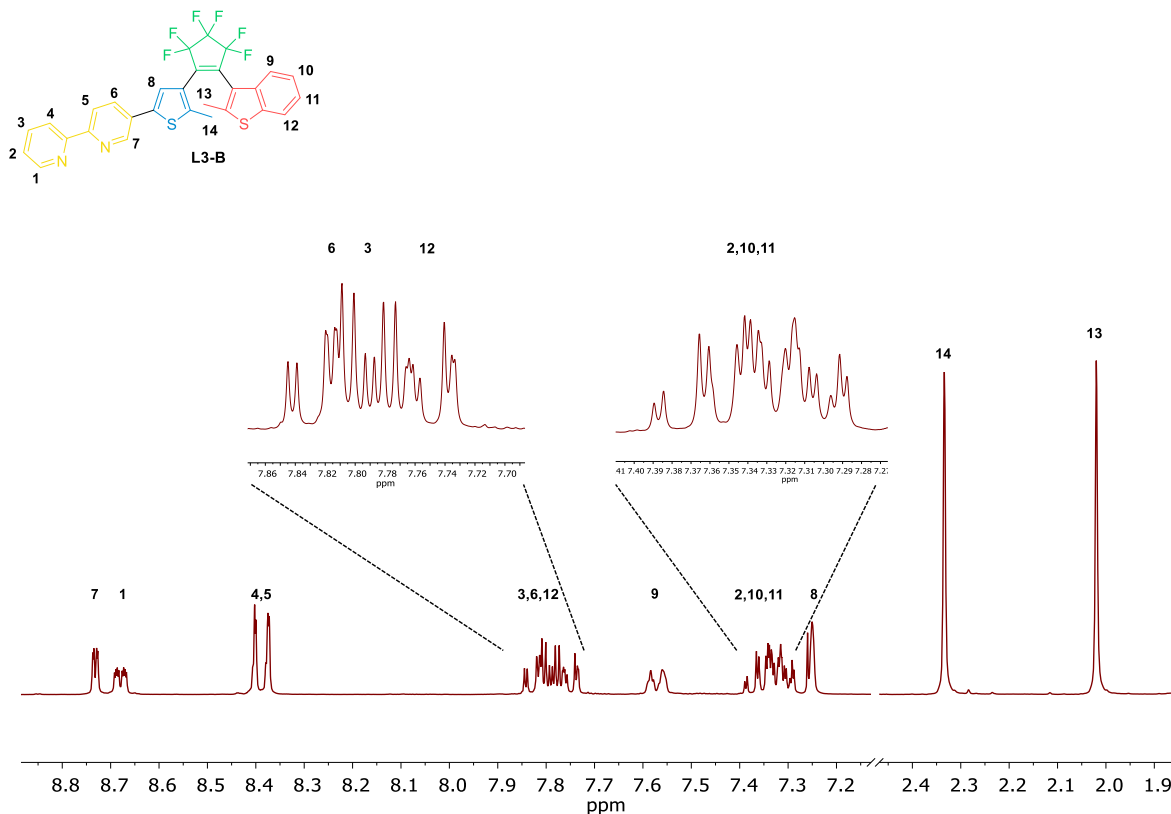
Figure 3.8. ^{1}H NMR spectrum of **L3-B**. (CDCl$_3$, 300 MHz).

3.1.1.5.2. L2-TYPE LIGANDS.
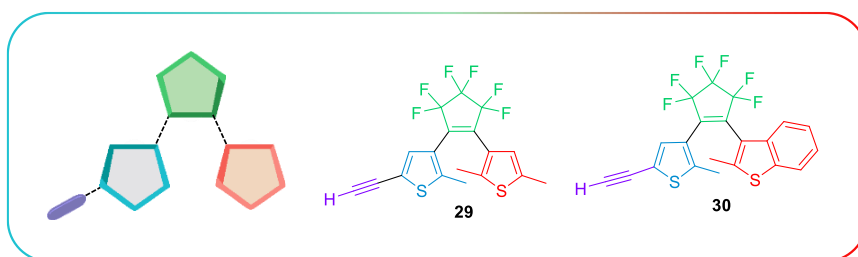
Concerning DTE modules containing the alkyne spacer, the first part of the synthesis is similar to the one already described for compounds **21** and **22** (See Scheme 3.12).[15,18] The corresponding TMS-protected DTE intermediates were obtained via lithiation (-78 °C, dry THF) of intermediate **13** and *in situ* addition of the corresponding TE solution. After workup and purification, compounds **27** and **28** were obtained in low to moderate yields (62% and 30%, respectively).
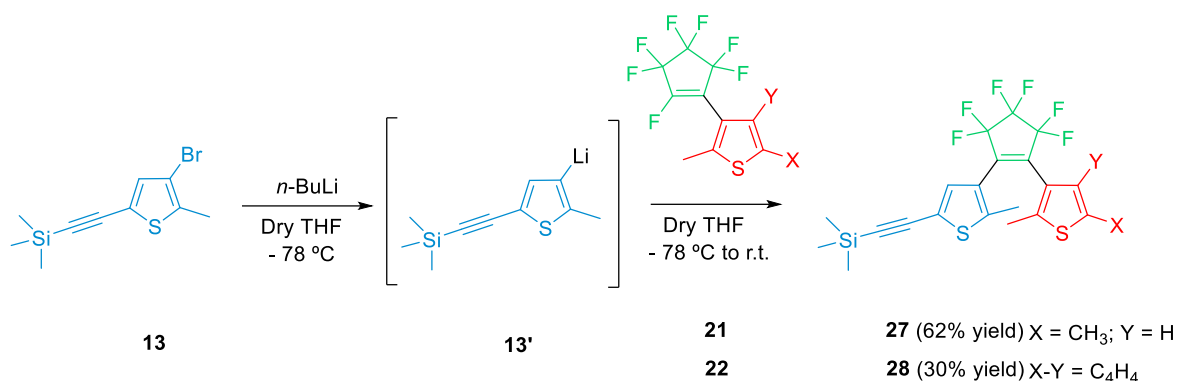
Scheme 3.12. Synthesis of compounds **27** and **28**.

The purity and identity of these compounds were confirmed by ^{1}H NMR spectroscopy. The spectra obtained were in agreement with the published spectroscopical data.[18,19] Compound **27** showed only two singlets in the aromatic region (assigned to the thiophene protons), four singlets at high fields of the spectra (three integrating for 3 nuclei each and one integrating for 9), assigned to the methyl groups of the thiophene and the TMS protecting group, respectively. Compound **28** instead presented the characteristic benzothiophene group of signals (two doublets and two triplets integrating for 1 nucleus each), plus one singlet, assigned to the coordinating thiophene aromatic proton. The expected four singlets integrating 3:3:3:9, respectively, were observed in the aliphatic region of the spectra.

The synthesis of the acetylene derivatives **29** and **30** was accomplished by deprotection of the TMS-intermediates **27** and **28**, by a procedure slightly modified from that described in the literature.[15] The reaction was performed in a basic media in a MeOH/THF solvent mixture. After workup, compounds **29** and **30** were purified by column chromatography over silica gel, eluting with hexane. The final compounds were obtained with moderate yields (30-48% yield).
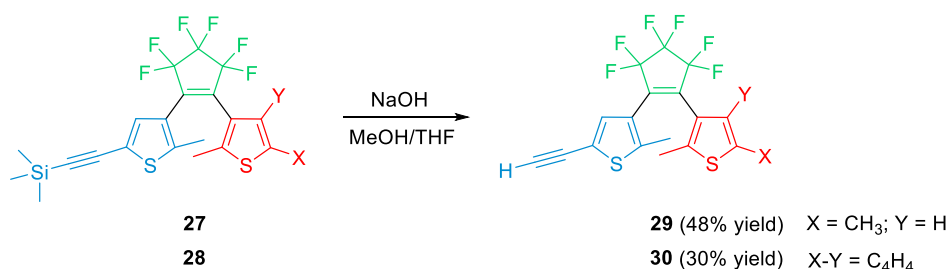
Scheme 3.13. Synthetic route for compounds **29-30**.

The alkyne derivatives **29-30** were identified by ^{1}H NMR spectroscopy. The measured spectrum for compound **30** was in agreement with the described spectroscopic data.[15] Compound **29** (Figure 3.9), as expected, was similar to that of the parent compound **27**, but the characteristic acetylene proton can be observed at 3.3 ppm, and in the aliphatic region, only three singlets (integrating for 3 nuclei each) assigned to the methyl groups of the thiophenes were observed.
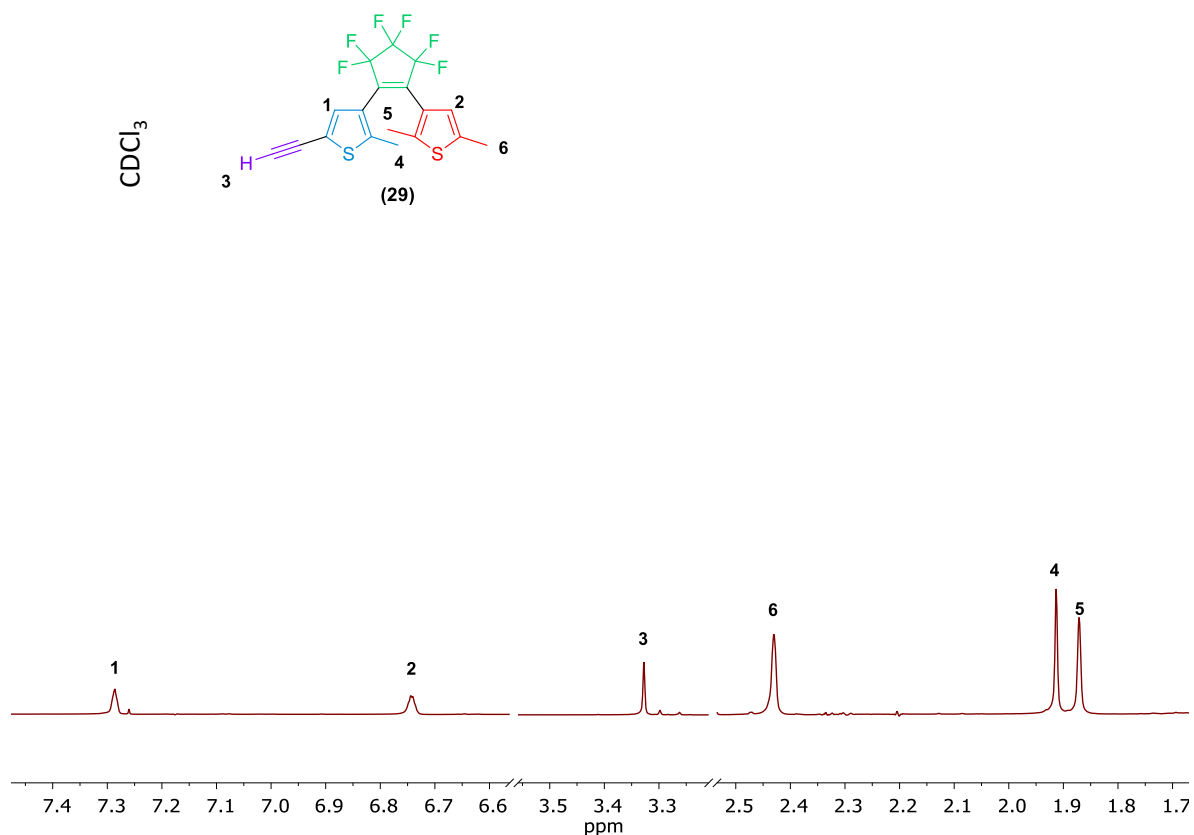
Figure 3.9. ^{1}H NMR spectrum of compound **29**. (CDCl$_3$, 300 MHz)
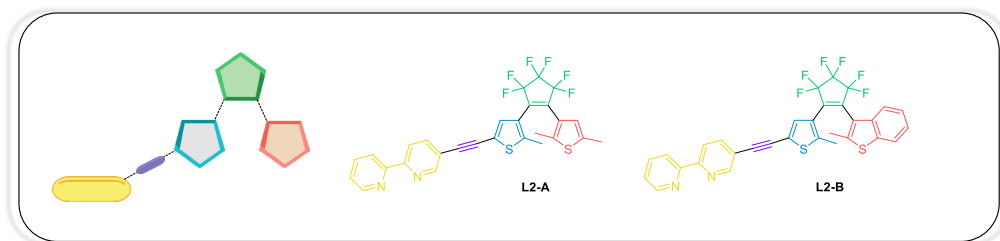
The DTE-bipyridyl ligands **L2-A** and **L2-B** were synthesized by Sonogashira coupling. Two possible synthetic routes can be envisaged depending on the coupling partners. Both of them were interchangeably used depending only on the availability of the starting reagents, both routes giving similar yields. After workup and purification through chromatography column over silica gel, eluting with CH$_2$Cl$_2$, the final products were obtained as a beige solid with a 47% yield for **L2-A** and brown solid with a 40% yield for **L2-B**.
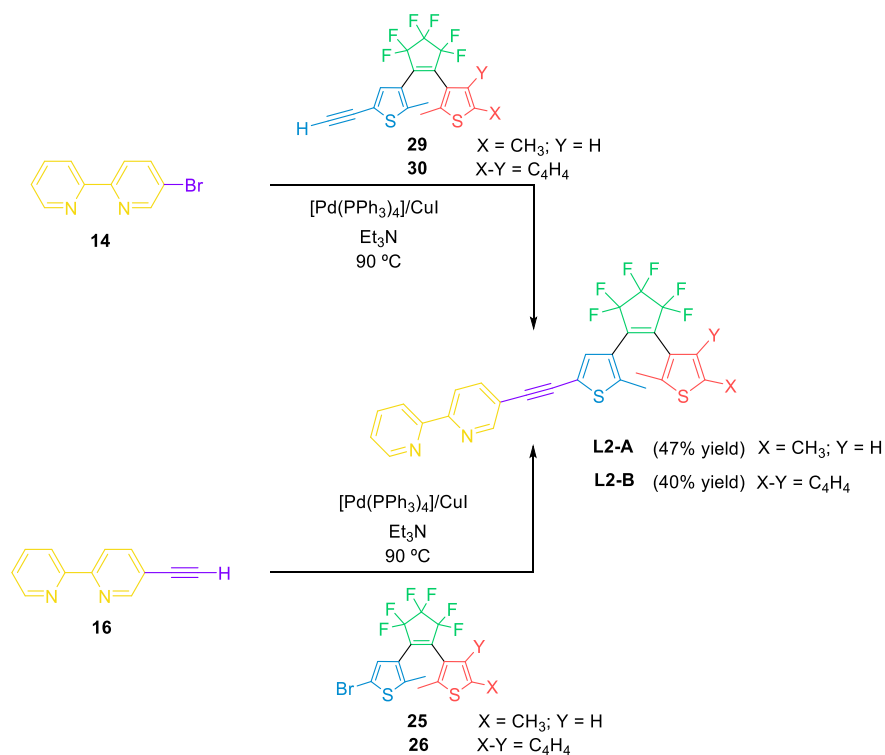
Scheme 3.14. Synthetic routes for the synthesis of **L2-A** and **L2-B** DTE ligands.

Compound **L2-A** was identified by ^{1}H NMR spectroscopy. The ^{1}H NMR spectra (Figure 3.10) showed a spectroscopic pattern in the aromatic region consistent with a substituted bipyridine unit and two singlets assigned to the aromatic thiophene protons. Three singlets assigned to the methyl groups of the thiophenes were observed in the aliphatic region.
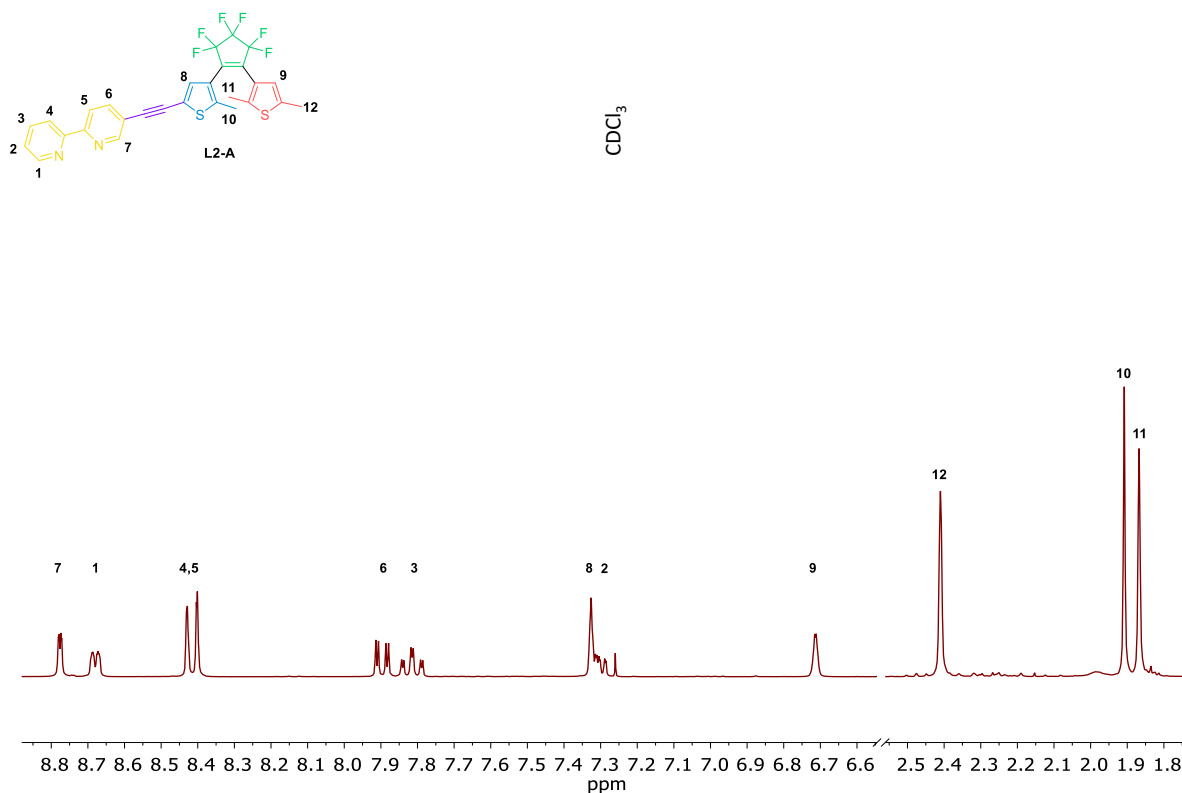
Figure 3.10. ^{1}H NMR spectrum of **L2-A**. (CDCl$_3$, 300 MHz).

Ligand **L2-B** was fully characterized by means of multinuclear NMR spectroscopy (*See Experimental Section*). The ^{1}H NMR spectrum (Figure 3.11) presented, as expected, a more complex spectroscopic pattern compared to that observed for **L2-A**. It showed multiple aromatic signals, consistent with the proposed structure containing a bipyridyl and a benzo[*b*]thiophene units, in addition to the two singlets assigned to the aromatic thiophene protons. In the aliphatic region, the singlets assigned to the methyl substituents could be identified.
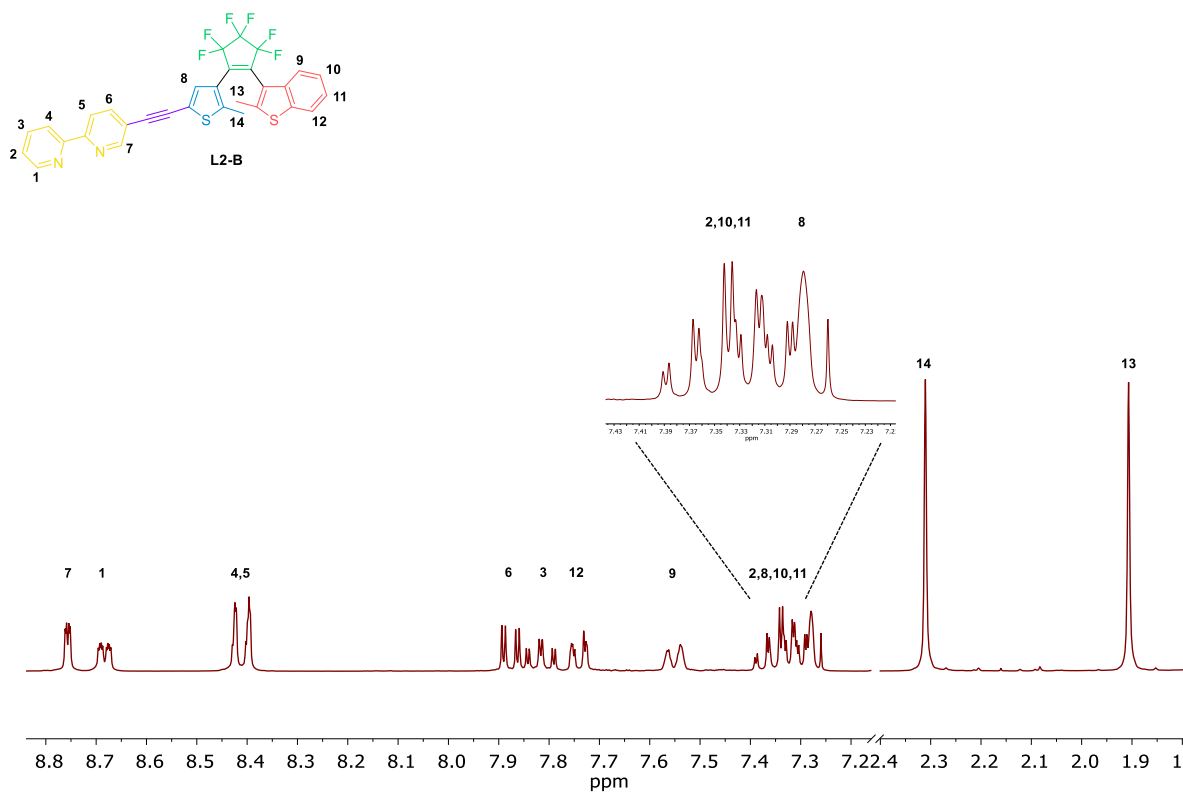
Figure 3.11. ^{1}H NMR spectrum of **L2-B**. (CDCl$_3$, 300 MHz).

To conclude this section, the spectra of the four ligands are collected in Figure 3.12.
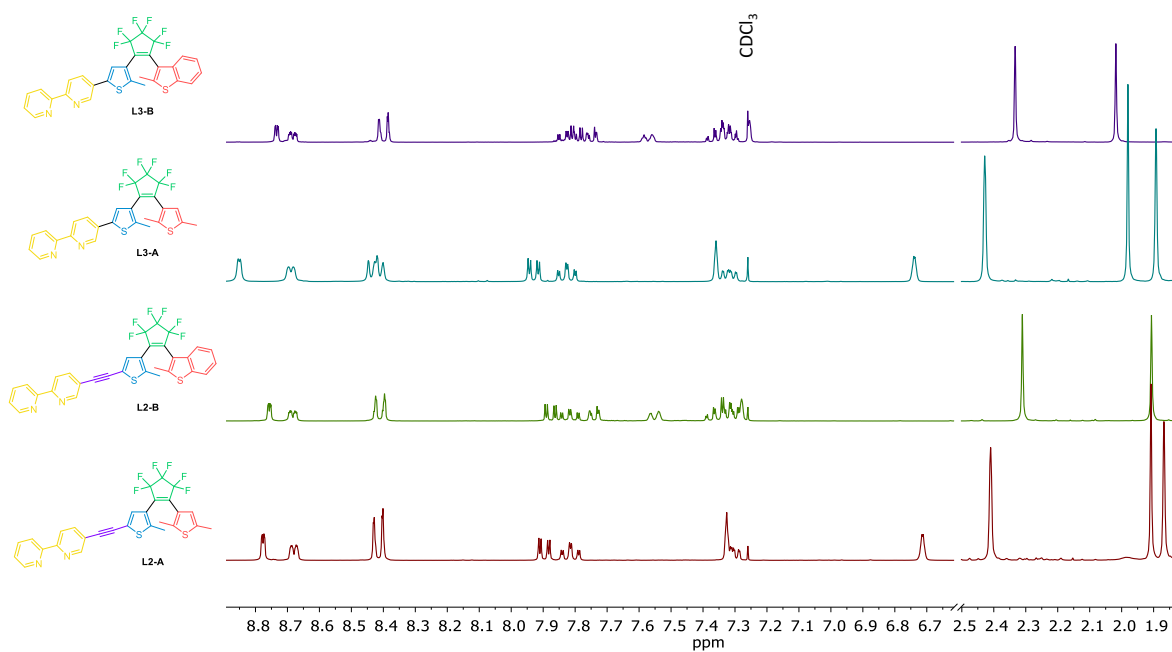
Figure 3.12. ^{1}H-NMR spectra of synthetized ligands (**L2-A**, **L2-B**, **L3-A** and **L3-B**). (CDCl$_3$, 300MHz).

117

3.1.1.6 .X-RAY CHARACTERIZATION FOR L2 AND L3-TYPE LIGANDS.

  The described structures by NMR spectroscopy for the **L2** ligand family could be corroborated from the single crystal X-ray diffraction studies. The crystalline structures were obtained through slow evaporation of the solvent media (hexane or methanol), obtaining colorless-yellowish crystals, which changed to a purple color after being irradiated at λ = 370 nm. Observing both structures in Figure 3.13 for the ligands **L2-A** and **L2-B**, it can be seen that the ligand **L2-A** crystallized an orthorhombic system ($P2_12_12_1$), where all the unit cell angles are 90 ° (α = β = γ), while the lengths are all different (a ≠ b ≠ c), while the **L2-B** crystallized a triclinic system (P-1) (α ≠ β ≠ γ, a ≠ b ≠ c).
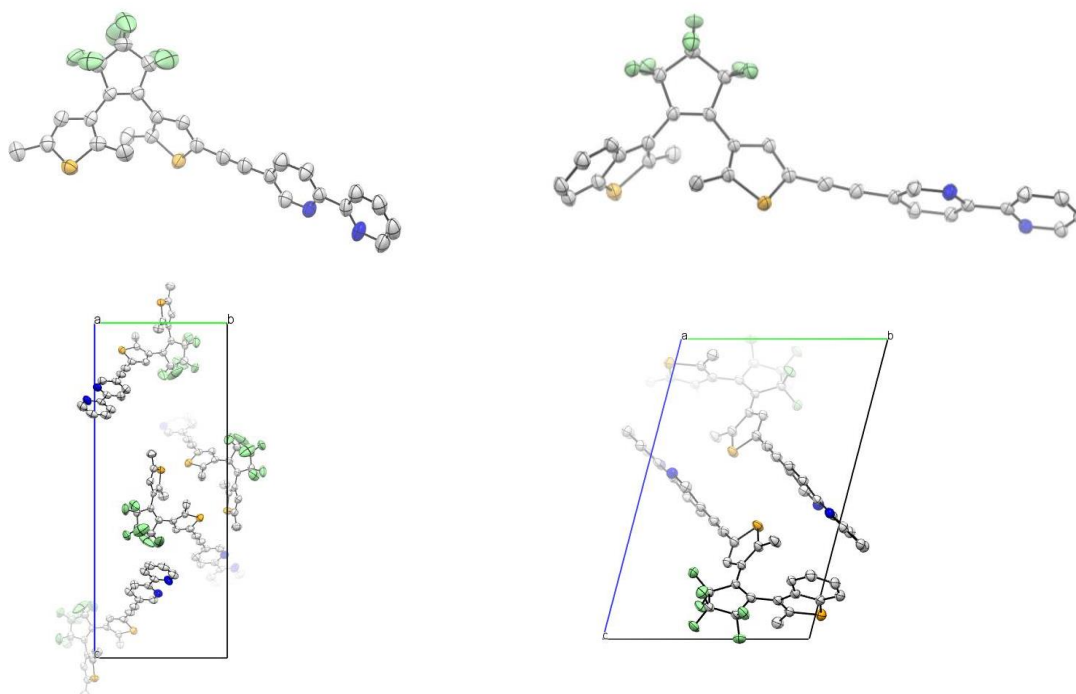
Figure 3.13. Molecular structure derived from single crystal X-ray crystal analyses and crystal unit cells for ligands **L2-A** and **L2-B**.

  Likewise, as in previous literature reports, the solid-state structures of the open form of DTEs can give an indication of the feasability of the photocycling process of the photoswitch molecules in their crystalline form. First, it is essential to know the molecular sub-unit orientation in the crystal (which is different than in solution). Figure 3.13 shows how the antiparallel orientation is predominant for both ligands, thus increasing the possibilities of presenting a photochromic character in the crystalline state. Second, the distance between the reactive carbons of the DTEs is decisive to know if photocyclization is feasible or not. Different studies determined that if the distance between reactive positions is less than 0.42 nm, the pericyclic reaction can be observed, while if it is greater than 0.42 nm, the probabilities of observing the photochromic character of the compounds decrease.[20,21] Therefore, the distances between reactive carbons of both ligands were measured, obtaining a distance of 0.358 nm for **L2-A** ligand and 0.393 nm for **L2-B**. In other words, the photocyclization reaction of the DTEs for the **L2** family of ligands is, in principle, possible.

As described for the **L2** family, the crystal structures for the **L3** compounds were also obtained (Figure 3.14). The compound **L3-A** crystallized a monoclinic crystalline system ($P2_1/c$), where all the distances of the unit cell are different (a ≠ b ≠ c), while two of its angles are 90 ° and a third different from 120 °. In the case of **L3-B**, it presents a unit cell with a triclinic system (P-1) (α ≠ β ≠ γ, a ≠ b ≠ c), as its alkyne counterpart **L2-B**.
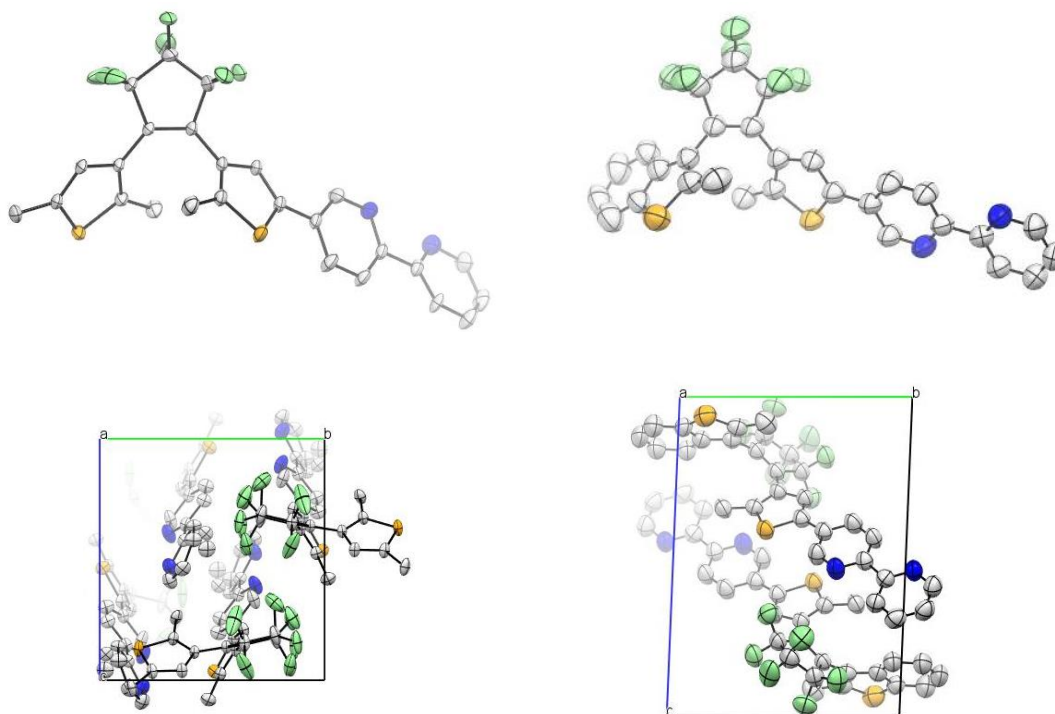
Figure 3.14. Molecular structure derived from single crystal X-ray crystal analyses and crystal unit cells for ligands **L3-A** and **L3-B**.

Like the **L2** ligands, the crystals obtained for the **L3** family present an antiparallel orientation and distances of less than 0.4 nm between the reactive carbons during the photocyclization process, 0.353 nm for **L3-A**, and 0.362 nm for **L3-B**.

Once the crystalline structures of the ligands had been obtained, some of the most relevant data were compared to predict the possible photochromic behavior. Table 3.1 shows values of intermolecular distances between different atoms of the crystalline structures, as well as angles of the molecule that could influence future photochromic studies. The data that have been considered most relevant are the distances between the reactive carbons C_1-C_1*and the different torsion angles present in the hexafluorocyclopentene bridge since they directly affect the photocyclization process. As previously mentioned, the four synthesized ligands show distances between reactive carbons of less than the photoswitching threshold distance of 0.4 nm. Similarly, it is observed that the ligands with the dimethylthiophene group as non-coordinating thiophene show shorter distances (0.358 nm and 0.353 nm for **L2-A** and **L3-A**, respectively), which could be conducive with a higher quantum cyclization yield of these ligands in the solid-state. In addition, the torsion angle

generated between both thiophene groups through the hexafluorocyclopentene group affects the distance of C_1-C_1*, so they should be studied for greater consistency in the prediction of the isomerization process. It can be seen how the angles for **LA** ligands (dimethylthiophene), the torsion of these groups is lower than for **LB** ligands, so it fits that the distances between C_1-C_1* are shorter, while for **LB**, this distance is more remarkable, increasing the mentioned distance.

Table 3.1. Crystallographic data obtained from the crystal structures of **L2-A**, **L2-B**, **L3-A** and **L3-B**.
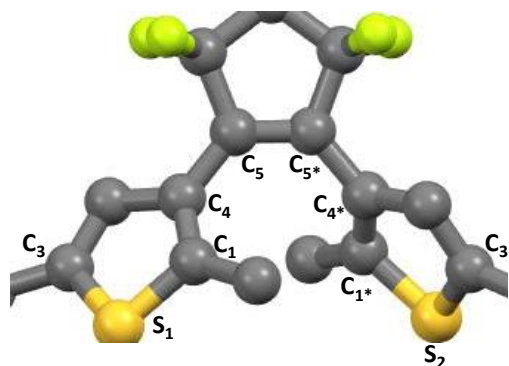
	L2-A	*L2-B*	*L3-A*	*L3-B*
C_1-C_1*	0.358 nm	0.393 nm	0.353 nm	0.368 nm
S_1-C_1	0.172 nm	0.174 nm	0171 nm	0.172 nm
C_1-C_3	0.172 nm	0.173 nm	0.173 nm	0.175 nm
C_1-C_4	0.138 nm	0.138 nm	0.137 nm	0.136 nm
C_4-C_5	0.146 nm	0.148 nm	0.147 nm	0.147 nm
S_2-C_1*	0.173 nm	0.172 nm	0.172 nm	0.171 nm
S_2-C_3*	0.173 nm	0.173 nm	0.172 nm	0.172 nm
C_1*-C_4*	0.136 nm	0.137 nm	0.138 nm	0.137 nm
C_4*-C_5*	0.147 nm	0.147 nm	0.146 nm	0.146 nm
C_1-S_1-C_3	93.25 °	92.39 °	93.22 °	91.49 °
C_1-C_4-C_5	124.396 °	121.30 °	123.73 °	121.30 °
C_1*-S_2-C_3*	91.93 °	124.77 °	93.32 °	93.38 °
C_1*-C_4*-C_5*	125.01 °	92.64 °	124.63 °	124.29 °
C_4-C_5-C_5*	129.29 °	129.24 °	129.92 °	128.46 °
C_4*-C_5*-C_5	129.53 °	129.71 °	129.89 °	129.72 °
C_4-C_5-C_5*-C_4*	4.8 °	-12.0 °	-6.0 °	10.3 °

   Once the crystalline structures of the ligands were determined, they were compared with different compounds described in the literature to study the possibility of their use as molecular switches in the solid-state. This comparison aimed to check if the synthesized ligands are within the range allowed to be studied as potential photoswitch systems in the solid-state. Table 3.2 lists the bond distances between the reactive carbons (C_1-C_1*) described in the literature. As shown in Table 3.2, the distances between the reactive carbons of the four ligands are consistent with distances found in DTE-based photochromism investigations in the crystalline state. Irradiation of crystals resulted in a loss of crystallinity.

Table 3.2. Comparison of the C_1-C_1* distances between the synthesized ligands and compounds described in the literature.[22,23]
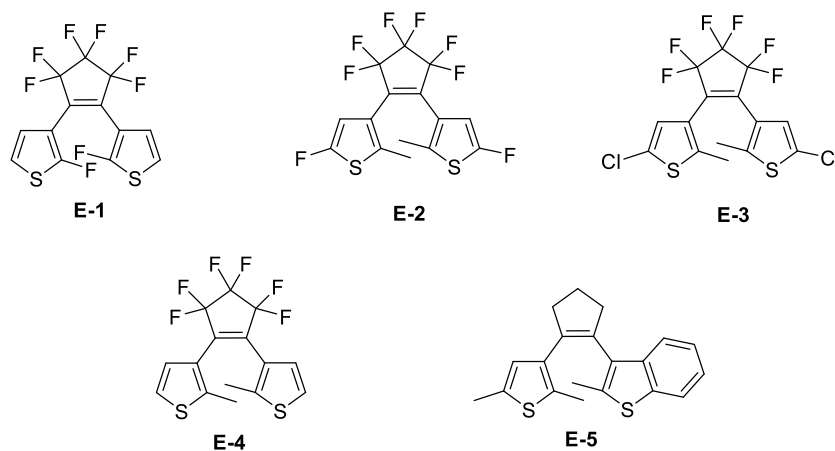
Compound	Distance C_1-C_1* (nm)
E-1	0.323
E-2	0.334
E-3	0.360
E-4	0.358
E-5	0.384
L2-A	0.358
L2-B	0.393
L3-A	0.353
L3-B	0.368

   Finally, it is interesting to mention how the crystalline structures of the **LB** ligands show a π-π stacking between the molecules of the unit cell. This behavior did not seem like the specific case of ligands **LA**, where the π-π stacking interactions were not observed. Figure 3.15 shows the unit cells of both ligands. The left image shows how the **L2-B** molecules crystallized in an antiparallel

orientation between them, with a distance between them of 4.69 Å. Similarly, the angle between planes and distances for the **L3-B** ligand were obtained, observing significantly shorter distances between molecules (3.95 Å). The intermolecular π-π stacking interaction can inhibit the photocyclization process because an inhibition of the free rotation bonds of the thiophene in the solid-state. Therefore, the isomerization process of the synthesized DTE ligands may show interesting significant differences.
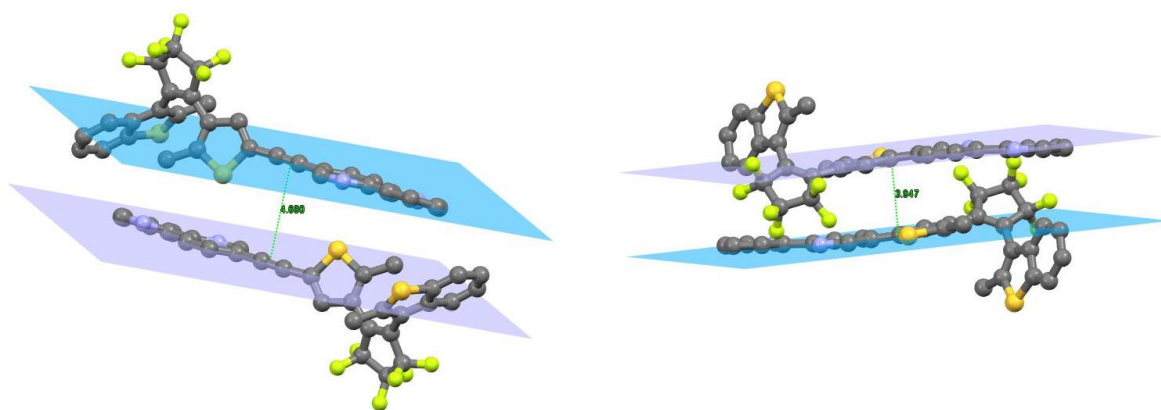
Figure 3.15 Unit cell π-π stacking for ligands **L2-B** and **L3-B**.

To sum up, four new four new asymmetric DTEs containing a bipyridyl coordinating fragment have been synthesized through different synthetic routes. Several possible reaction pathways to the target molecules reflect the modularity of the ligands.

3.1.2 COMPLEXES

In this section, the synthesis and characterization of racemic and enantiopure (chiral-at-metal) bis-cyclometalated Ir(III) complexes containing the already described bipyridyl DTE-based ancillary ligands will be described. The simplest derivatives (based on phenylpyridyl cyclometalated ligands) were intended to be used as model compounds. The chemical structure of these complexes (**Ir-L2-A**, **Ir-L2-B**, **Ir-L3-A,** and **Ir-L3-B**) is shown in Scheme 3.15.

Ir-L2-A

Ir-L2-B

Ir-L3-A

Ir-L3-B
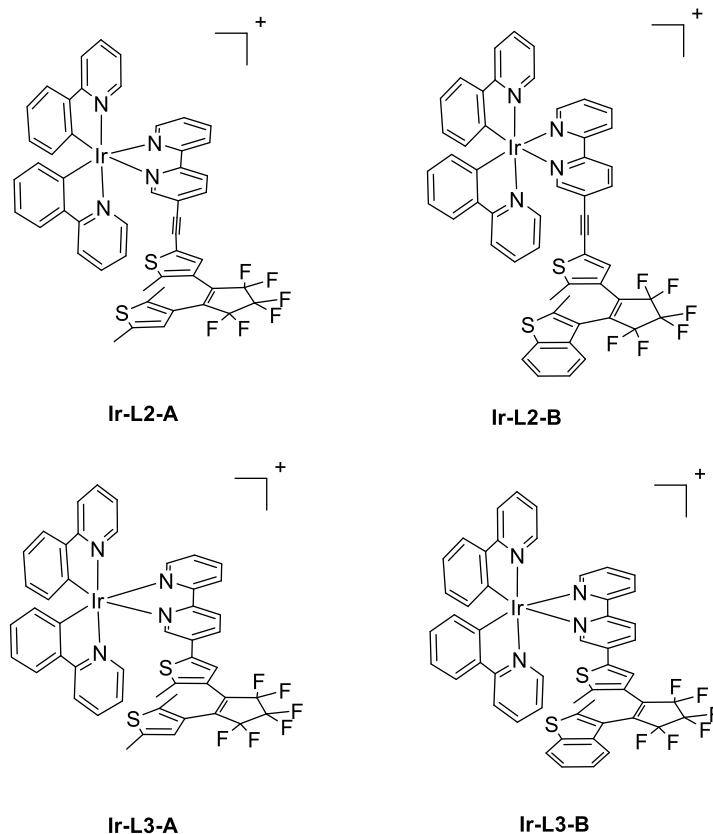
Scheme 3.15. DTE-bipyridyl based Ir(III) complexes synthesized in this work (counter anions and stereochemical information are omitted).

3.1.2.1 RACEMIC IRIDIUM(III) COMPLEXES

The synthesis of bis- and tris-cyclometalated octahedral Ir(III) complexes has been studied extensively during the last decades.[24] There are multiple synthetic routes to obtain this type of metal complex depending on the ligands required in the structure. In our case, we are interested in cationic bis-cyclometalated ligands containing a bipyridyl derivative as auxiliary ligand. The different processes described to obtain this type of compound (racemic and enantiopure) will be detailed. Scheme 3.16 shows several of the synthetic routes employed to obtain these complexes, as described in the literature. The most frequently used synthetic pathway consists of refluxing the well-known chloride-bridged bis-cyclometalated iridium dimer precursor in a mixture of $CH_2Cl_2/MeOH$, with the corresponding bipyridine-based ligand.[25-27] These compounds can also be obtained using ethylene glycol as solvent, as was described in the literature.[28,29] These reactions are followed (when required) by salt metathesis to introduce specific, desired counterions. This may play an important role in solubility, for example.
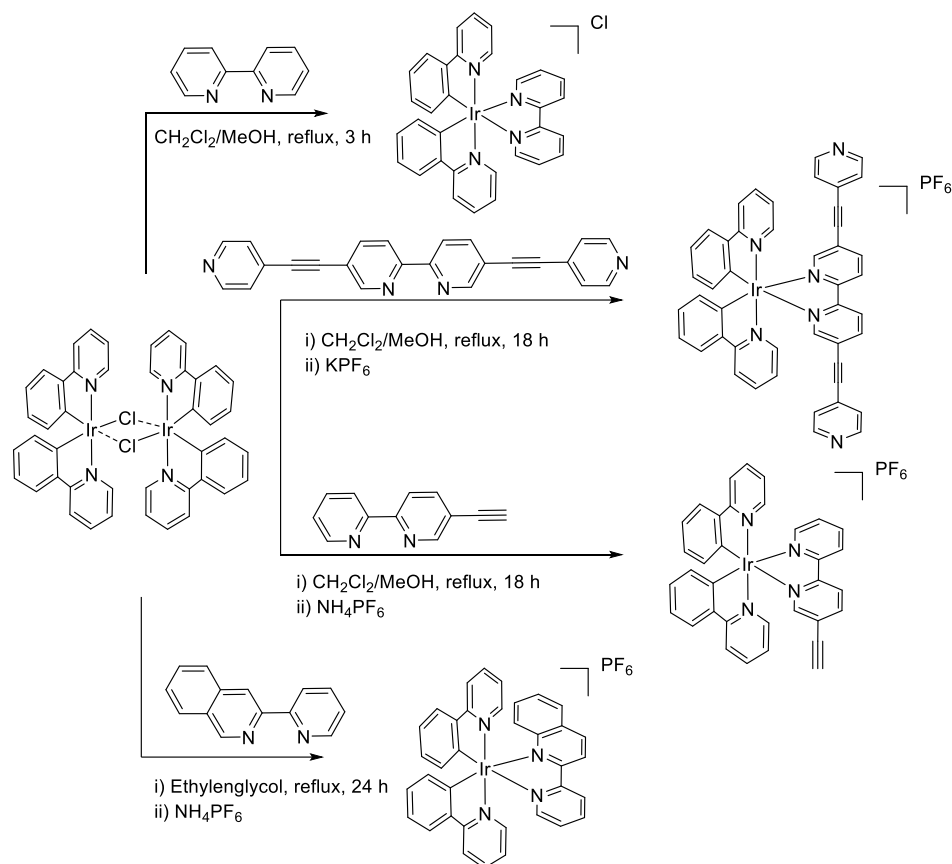
Scheme 3.16. Representative examples of the synthetic routes to obtained cationic [Ir(ppy)$_2$(NN)]$^+$ complexes (ppy = 2-phenylpyridyl, NN = bipyridyl ligand).

These methodologies imply refluxing the reaction mixture in a given solvent. Alternatively, these complexes can be obtained through a two-step reaction. These procedures are based on the synthesis of an intermediate complex with two coordinating vacancies occupied by solvent molecules; (MeOH, acetonitrile, etc.),[30,31] favoring the coordination of the bipyridyl ligand in a subsequent step. This methodology avoids using high temperatures. (See Scheme 3.17)
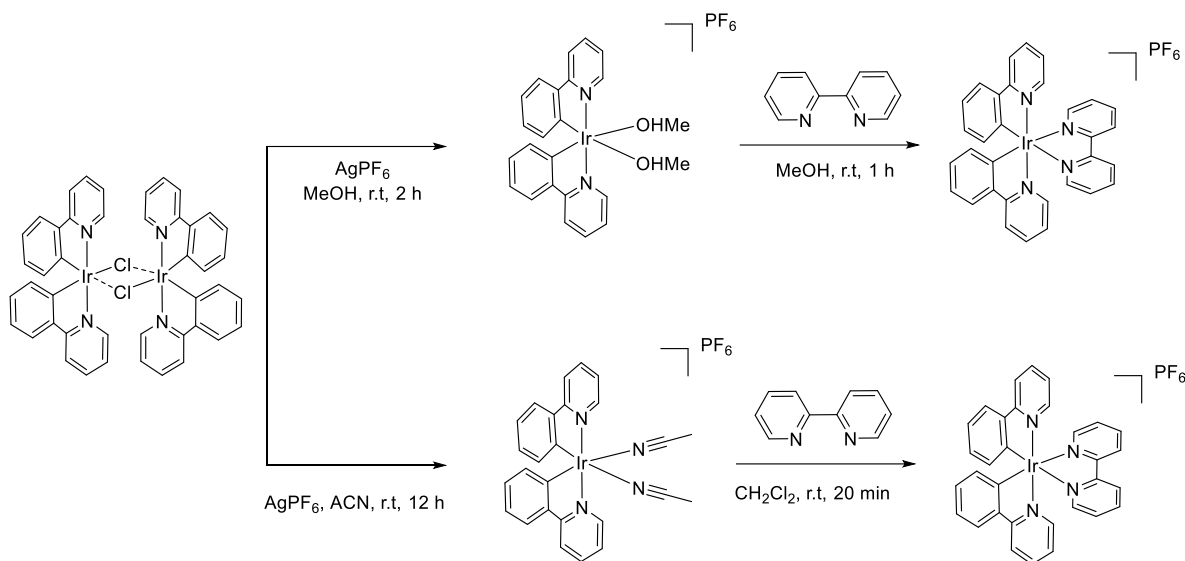
Scheme 3.17. Representative examples of synthetic routes to obtain bipyridine derivatives-based complexes through a two-step reaction.[30,31]

Taking into account that the ultimate goal is the synthesis of chiral-at-metal enantiopure complexes, the two-step (milder) reaction route was chosen to minimize the potential risk of racemization of the chiral center during the process. Therefore, chiral-at-metal enantiopure bis-acetonitrile compounds were chosen as iridium precursors. Their synthesis will be described in a later section.

Initially, to test the synthetic viability, we attempted the synthesis of the racemic derivatives, using the metallic precursor **C5** described in the previous chapter. To confirm the coordinating ability of the obtained bipyridyl DTE ligands, a reaction was attempted using **L2-A** as a model compound, following a synthetic procedure similar to that described above for related bipyridyl derivatives.[31] The precursor **C2** was reacted with the ligand **L2-A** in CH_2Cl_2 at room temperature overnight. The solvent was removed and the blue residue was purified through column chromatography eluting with CH_2Cl_2. The product was obtained as a blue solid in a 69% yield. It should be noted that the blue color of the complex must be attributed to photoinduced cyclization of the coordinated DTE ligand as it was not protected from light during the synthetic procedure (See Scheme 3.18). As described in a later section, the complexes can be obtained as a blue (closed form, **CF**) or yellow (open form, **OF**) products depending on the open-closed state of the coordinated ligand. To optimize the quantity of **OF** present and thereby obtain better characterization, the compound was irradiated with red light (590 nm) to get *rac*-**Ir-L2-A** in the **OF**.
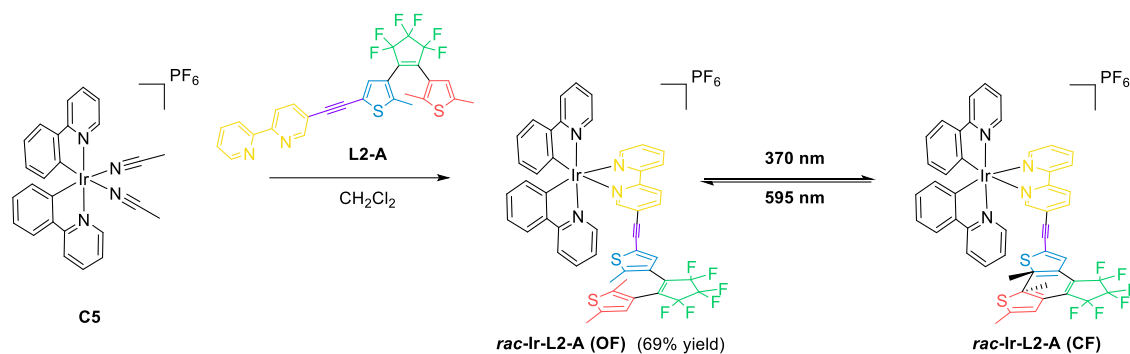
Scheme 3.18. Synthesis of *rac*-**Ir-L2-A** complex.

Complex *rac*-**L1-A** was identified by multinuclear NMR spectroscopy (*See Experimental Section*). Taking into account its C_1 symmetry, up to twenty-eight different proton signals were expected in the ^{1}H NMR spectra, and up to 50 carbon signals in the ^{13}C NMR spectra. Although the complexity of the spectra hampered its full assignment, the spectrum was consistent with the proposed structure. The most characteristic signals are the protons of the thiophene groups (at 7.30 ppm and 6.71 ppm) and the three singlets corresponding to the methyl substituents at the high field region of the spectra (Figure 3.16). Additionally, the identity of the compound was confirmed by desorption ionization mass spectrometry.
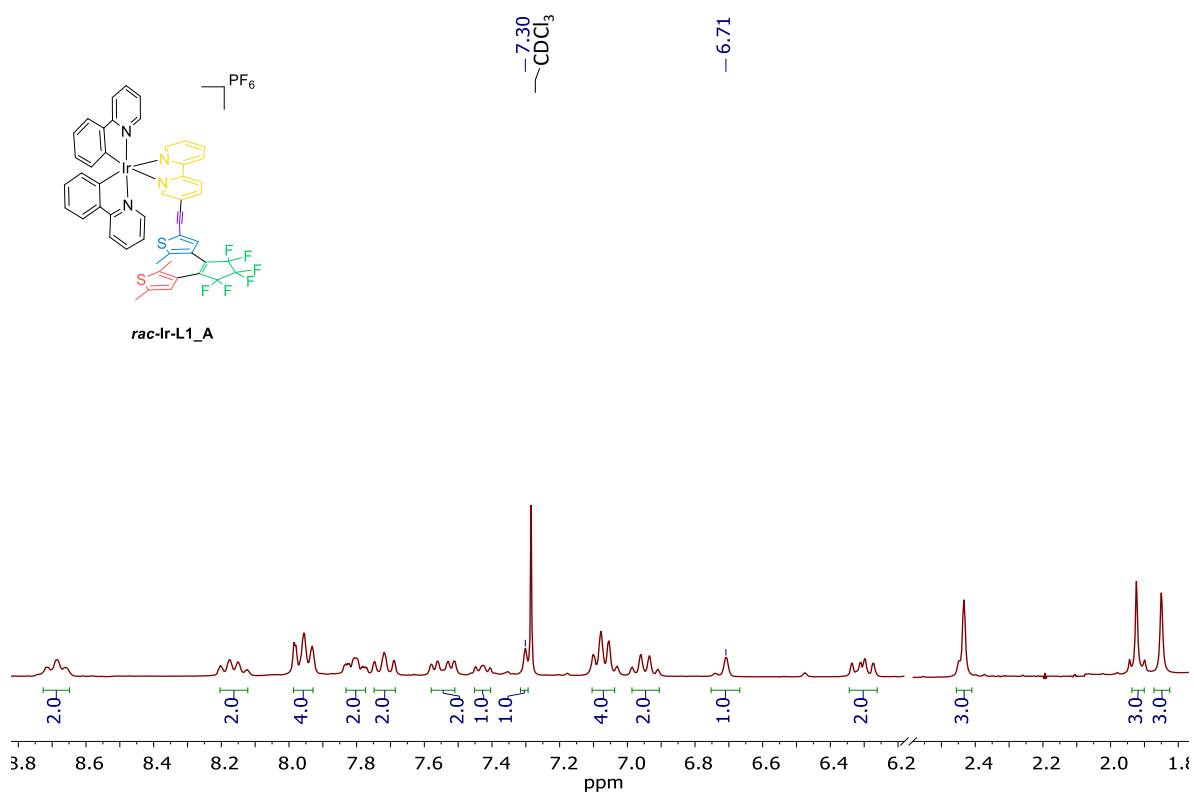
Figure 3.16. ^{1}H NMR spectrum of **rac-Ir-L2-A**. (CDCl₃, 300 MHz).

Once the obtaining of *rac*-**Ir-L2-A** was confirmed, the synthetic study was carried out for the rest of the synthesized ligands (**L2-B**, **L3-A**, and **L3-B**), using the classic reaction conditions described in the literature.

3.1.2.2 ENANTIOPURE IRIDIUM(III) COMPLEXES

Having confirmed the synthetic viability of the proposed route towards the DTE-containing complexes, the next step was the synthesis of chiral-at-metal enantiopure derivatives. This requires the synthesis of a chiral-at-metal enantiopure **C5** precursor. It must be kept in mind that **C5** was synthesized as a racemic mixture of the **Δ** and **Λ** enantiomers. As mentioned in the introduction, there are different methodologies to synthesize this type of compound in their enantiopure forms. A resolution methodology is required, which ranges from semi-preparative chiral HPLC,[32,33] fractional precipitation technique with chiral counterions,[34] or using an auxiliary chiral ligand as a resolution agent. The latter one - chiral resolution through an auxiliary chiral ligand - will be used throughout this section. For this purpose, we followed the methodology published by E. Meggers,[35] that gives rise to enantiopure chiral-at-metal complexes with a high enantiomeric excess (>99%) in a reproducible manner. Typical chiral auxiliary ligands for these methodologies are salicylthiazolines and salicyloxazolines, or commecially available amino acids, such as proline, α-methylproline, serine, or β-phenylalanine. The strategy consists of coordinating a chiral ligand as a third ligand to a bis-cyclometallated chiral complex that exists as a racemic mixture (**Δ** and **Λ**, Figure 3.17). Therefore, coordination of a third chiral ligand (for example *R* configuration) causes the formation of diastereoisomers (**Δ*R*** and **Λ*R***), which can be easily separated by conventional methodologies (column chromatography, precipitation, etc.). Eventually, the auxiliary ligand is removed (recovering the chiral resolution agent), yielding the chiral-at-metal enantiopure compound.
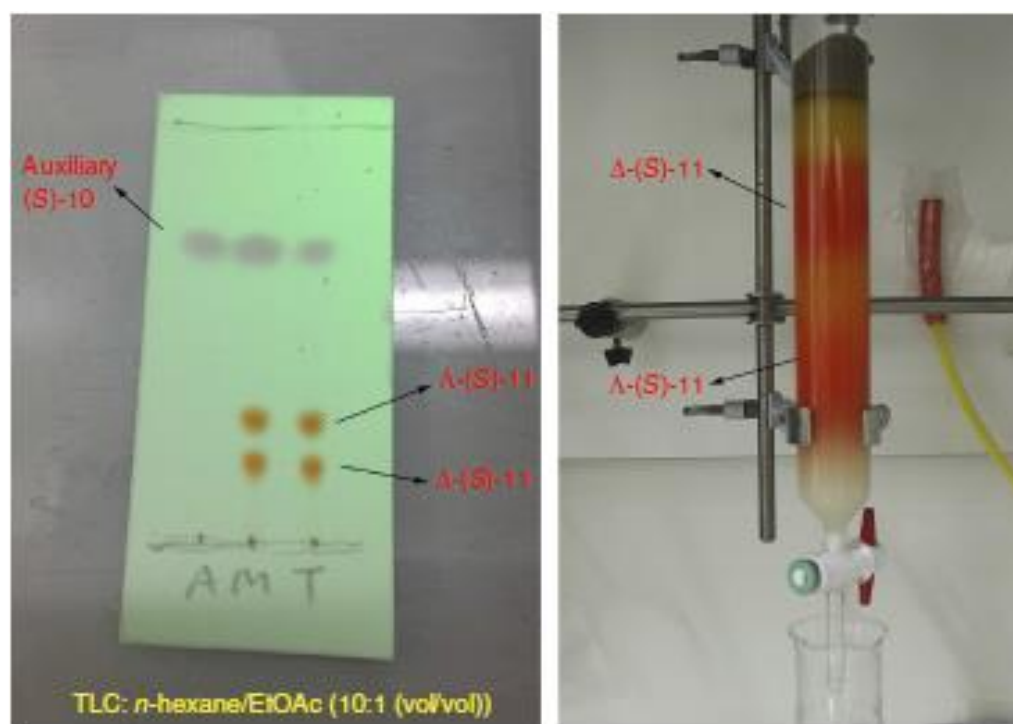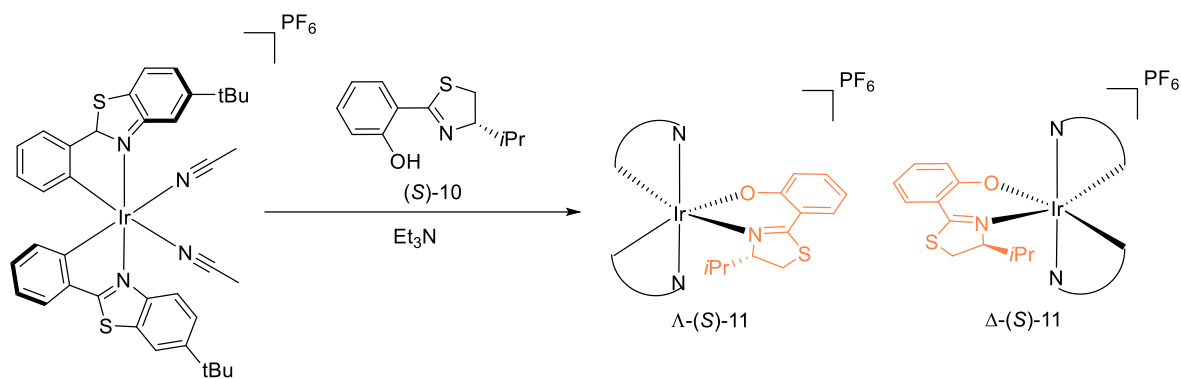
Figure 3.17. Example of chiral resolution via a chiral agent.[35]

The methodology described by E. Meggers *et al*. that was employed in the current work started from the racemic precursor, **C4**. It was reacted with a chiral amino acid as the resolution agent. Initially commercially available *L*-proline was used as a chiral resolution agent (Scheme 3.19).[36] After refluxing a mixture of **C4**, K_2CO_3, and *L*-proline at 85 °C in distilled methanol inside a sealed high-pressure tube, a yellow precipitate was obtained. After filtering and subsequently washing with EtOH, **Λ*L*$_{proline}$-C9** was obtained as a yellow solid. **Δ*L*$_{proline}$-C9** was obtained treating the combined mother liquor of the reaction. The resultant yellow solution was concentrated to dryness under vacuum and the residue was dissolved in CH_2Cl_2. The insoluble precipitate (*L*-proline and Na_2CO_3 excess) was filtered through a celite pad. The solvent was removed under vacuum again obtaining **Δ*L*$_{proline}$-C9** as a yellow solid. Following these procedures, **Λ*L*$_{proline}$-C9** and **Δ*L*$_{proline}$-C9** isomers were obtained with 35% and 23% yields, respectively.
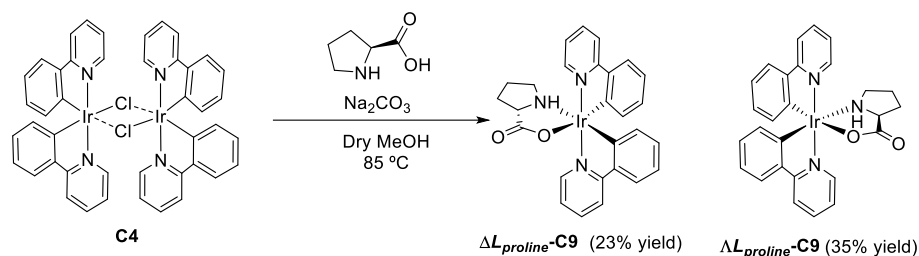
Scheme 3.19. Synthesis of **ΔL_proline-C9/ΛL_proline-C9** complexes.

The presence and the purity of the diastereoisomers were studied by ^{1}H-NMR spectroscopy. The signals obtained are consistent with those described in the literature.[37] The ^{1}H-NMR spectra of both compounds are shown in the Figure 3.18. It shows a different shifting for several of the signals, as can be seen in the two doublets present at lower fields of the spectra. In blue, **ΔL_proline-C9** shows a characteristic doublet at 9.05 ppm, while in red (**ΛL_proline-C9**), the corresponding signal is observed at higher fields (8.57 ppm). This behavior was expected because of the different configuration between them, making them distereoisomeric complexes.
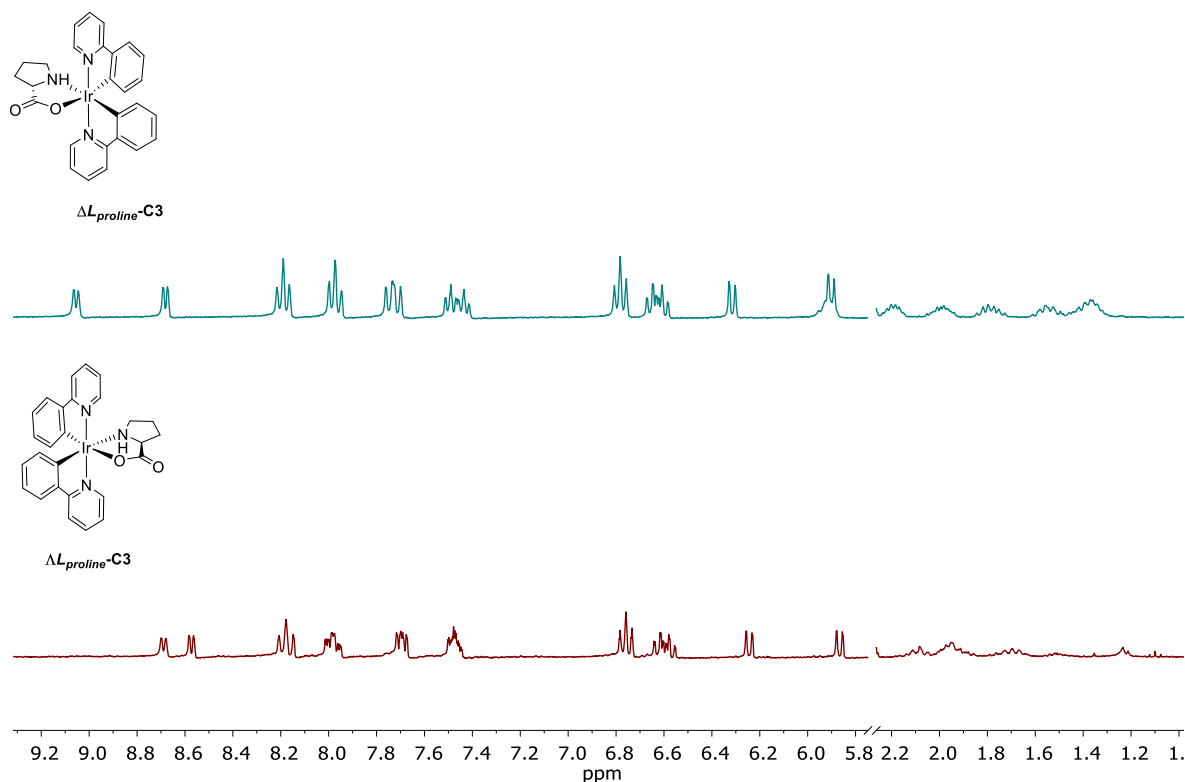
Figure 3.18. ^{1}H NMR comparison of **ΔL_proline-C9** and **ΛL_proline-C9**. (DMSO, 300 MHz).

Due to the relatively low yields obtained when using *L*-proline as a resolution agent, an attempt was made using serine as a chiral auxiliary ligand. This procedure was also described in the

literature.[38] In this case, we used both isomers of serine (*L/D*) depending on the desired chiral-at-metal enantiomer (Scheme 3.20). The reaction consists of reacting the **C4** precursor with the selected serine isomer, stirring in methanol overnight at 45 °C in the presence of Na_2CO_3. After filtration, the solid was washed with MeOH and dissolved in CH_2Cl_2. This purification method, developed in our research group by PhD Student A. Pazos, has not yet been described in the literature. The new method greatly simplifies the purification process, avoiding column chromatography. The solid was washed with MeOH in order to eliminate possible traces of unreacted starting material or other impurities. Similarly, by dissolving the resultant solid in CH_2Cl_2, the excess of serine present in the medium can easily be filtered out. After filtering, the yellow solution was evaporated to dryness, obtaining **Λ*L_serine*-C10** and **Δ*D_serine*-C10** complexes as a yellow solid in yields of 71% and 43%, respectively. It can be seen that, even being issued from the same reaction, there is a wide difference between the reactions yields while using different chiral agents. This fact was studied in the laboratory, determining that the scaling of the reaction influenced in the final yield. A greater amount of initial reagent (300 mg of **C4**) obtained lower reaction yields, not higher than 43%, while in smaller quantities (100 mg) the reaction yields showed a significant increase (71%).
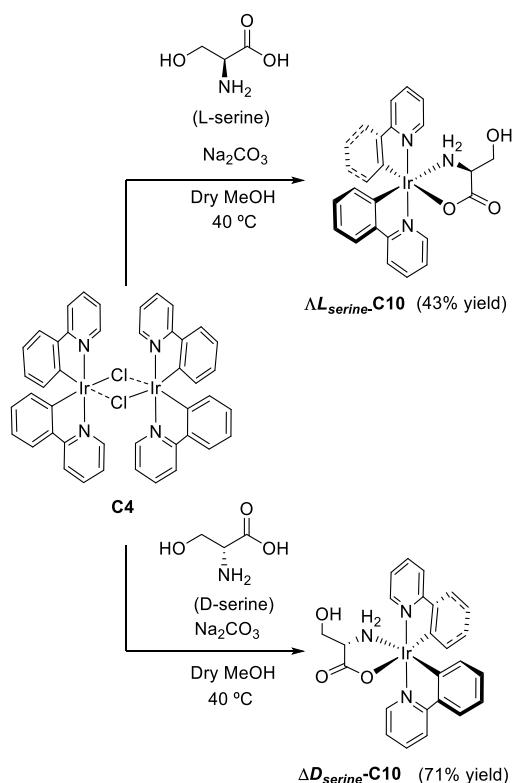
Scheme 3.20. Synthesis of **ΔD_serine-C10** and **ΛL_serine-C10** complexes.

The purity and identity of the precursors were studied by ^{1}H-NMR spectroscopy.[38] The spectra obtained for the complexes were compared with the data reported in the literature (Figure 3.19). As expected, the enantiomeric compounds show identical NMR spectra.
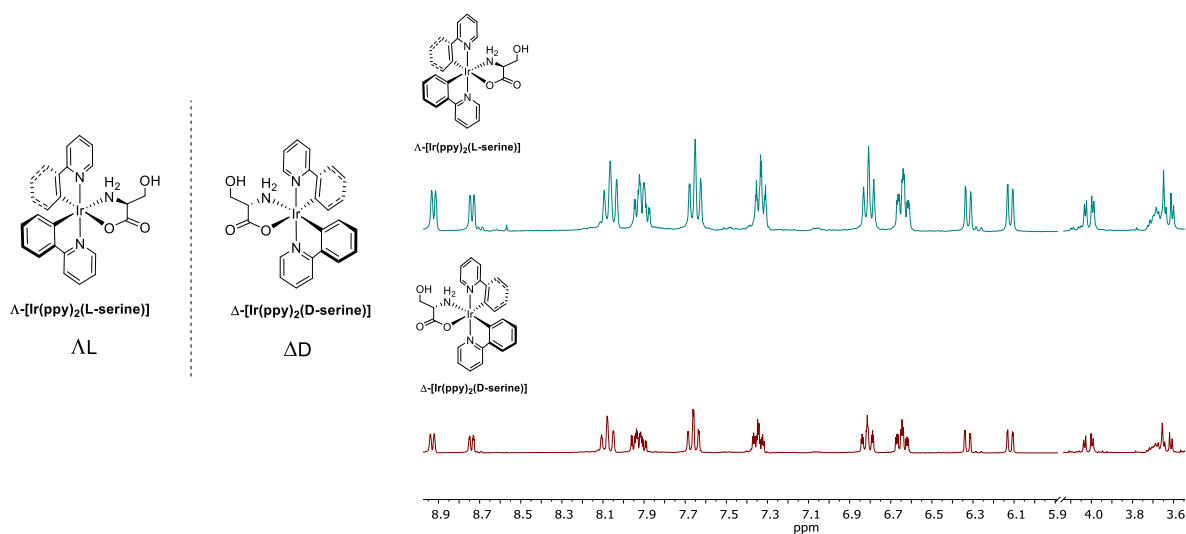
Figure 3.19. Comparison of ^{1}H-NMR **ΔD$_{serine}$-C10** and **ΛL$_{serine}$-C10**. (MeOD, 300 MHz)

The synthesis of enantiopure chiral-at-metal **C5** requires removing the chiral resolution agent from enantiopure **C9** and **C10** derivatives. This reaction was performed, following published methodologies.[24,39,40] A suspension of **ΛL$_{proline}$-C9** was stirred in acetonitrile. TFA is added to the reaction to promote the removal of the chiral agent. The resultant free coordination vacancies are filled by solvent (CH$_3$CN). After that, the reaction solvent was removed under vacuum and an aliquot of saturated ammonium salt is added to carry out a counter ion change (PF$_6^-$). The reaction mixture was purified through column chromatography, using acetonitrile as eluent. The desired product was obtained as a yellow solid with a 61% yield. As shown in Scheme 3.21, the methodology used to obtain **C5** precursor can be used in the same way to change the ligands starting from the serine intermediates (**ΛL$_{serine}$-C10**).
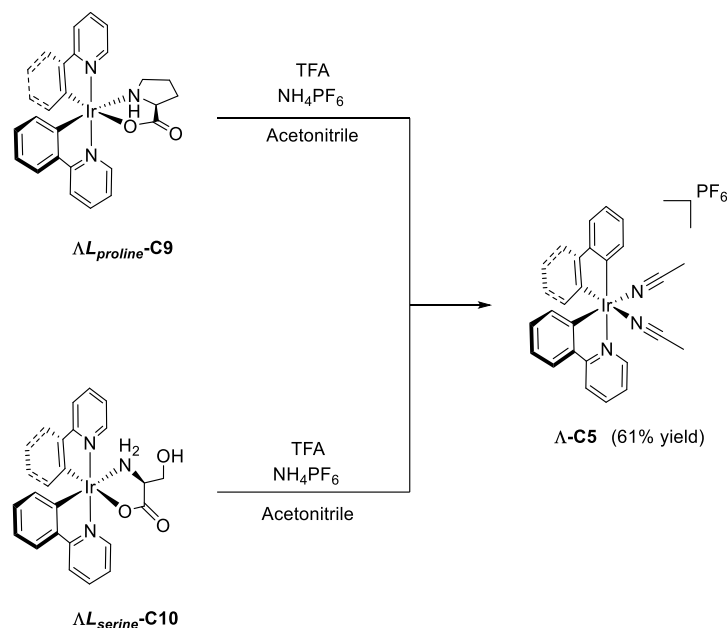
Scheme 3.21. Synthesis of **Λ-C5** enantiopure complexes.

The purity of the compound was analyzed by NMR spectroscopy. Figure 3.20 shows the comparison between the spectra **Λ-C5** and **Δ-C5**, as well as the formerly described racemic **C5**. As expected, the three compounds show identical spectra. To corroborate that the complex still maintained the chiral at metal properties, circular dichroism (CD) measurements were performed. Circular dichroism, (*See Experimental Section*), measures the enantiomeric excess of the sample. This means that, in a sample where there is a 1:1 mixture of **Λ/Δ** isomers, a dichroic signal will not be obtained. Figure 3.21 shows the comparison between the three possible complexes (***rac*-C5**, **Λ-C5** and **Δ-C5**). The theoretical measurement for a ***rac*-C5** complex appears in green. No signal is observed due to the 1:1 (**Λ/Δ**) ratios of the complex. In orange, the measurement obtained for the **Λ-C5** complex is presented. In this case, a signal is observed in the dichroism spectrum. This signal is drawn due to the fact that in the sample there is a greater quantity of one of the isomers, in this case the lambda (**Λ**>**Δ**). And finally, in blue, we have the signal obtained after the **Δ-C5** measurement. As with its **Λ**-counterpart, a signal is obtained indicating an enantiomeric excess. Because both isomers are opposite, their signal will be inversed (*See Chapter 4*), being mirror images of each other.

132
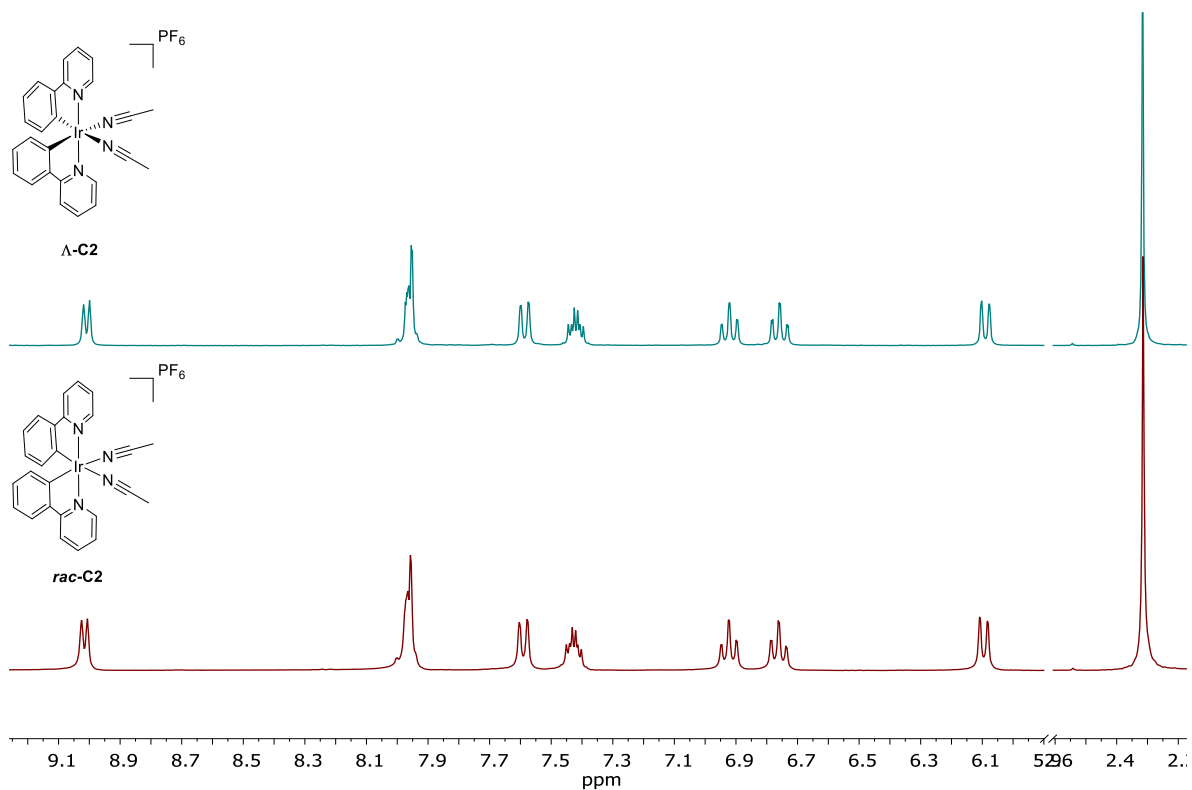
Figure 3.20. ¹H NMR comparison of *rac*-**C5** and **Λ-C5**. (CDCl₃, 300 MHz).
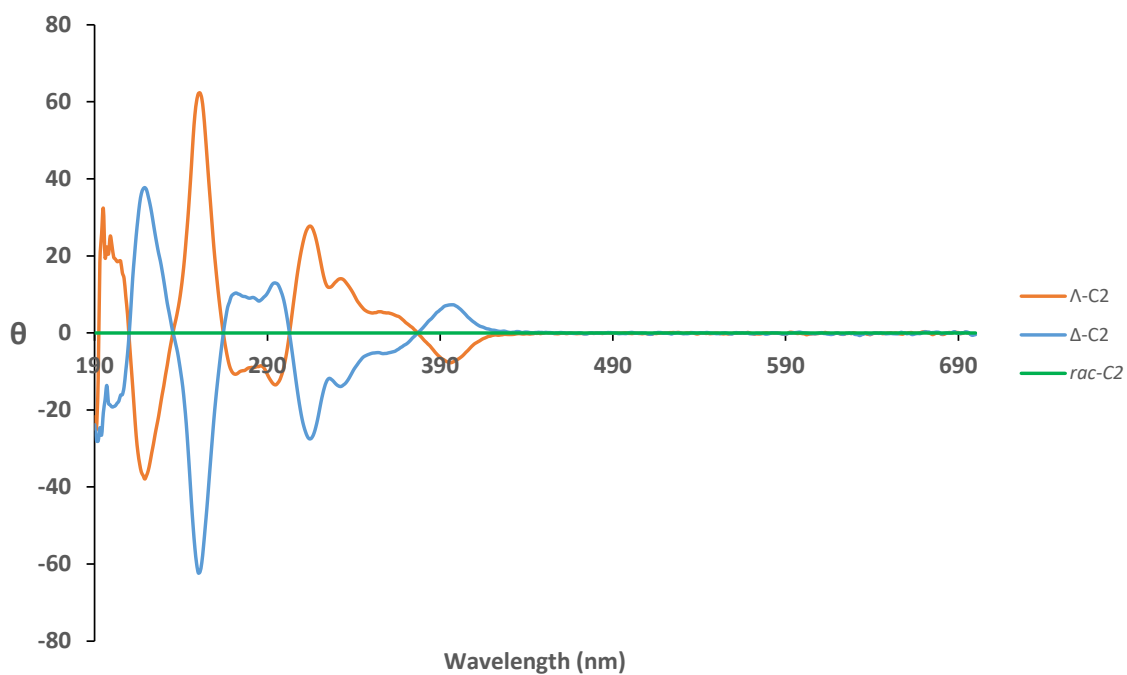
Figure 3.21. Circular Dichroism (CD) spectra for *rac*-**C5**, **Λ-C5** and **Δ-C5** (CH₃CN).

Enantiopure bis-acetonitrile **C5** derivatives were used to attempt the synthesis of chiral-at-metal enatiopure DTE derivatives. For this purpose, we followed the same methodology descrived above for the racemic compounds. Complexes **Λ-Ir-L2-A** and **Λ-Ir-L2-B** were obtained by stirring the corresponding DTE ligands (**L1-A** and **L1-B**) in CH_2Cl_2 solution of **Λ-C2** (Scheme 3.22).[40] After workup, final complexes **Λ-Ir-L2-A** and **Λ-Ir-L2-B** were purified by column chromatography in CH_2Cl_2. The final complexes were obtained as blue solids, with yields of 61% for **Δ-Ir-L2-A** and 56% for **Δ-Ir-L2-B**. **Δ-Ir-L2-A** and **Δ-Ir-L2-B** isomers were obtained after a process identical to that described above. The photoswitching process was tested directly on the solid. By applying light (595 nm) on the solid, it loses its blue color and turns beige.
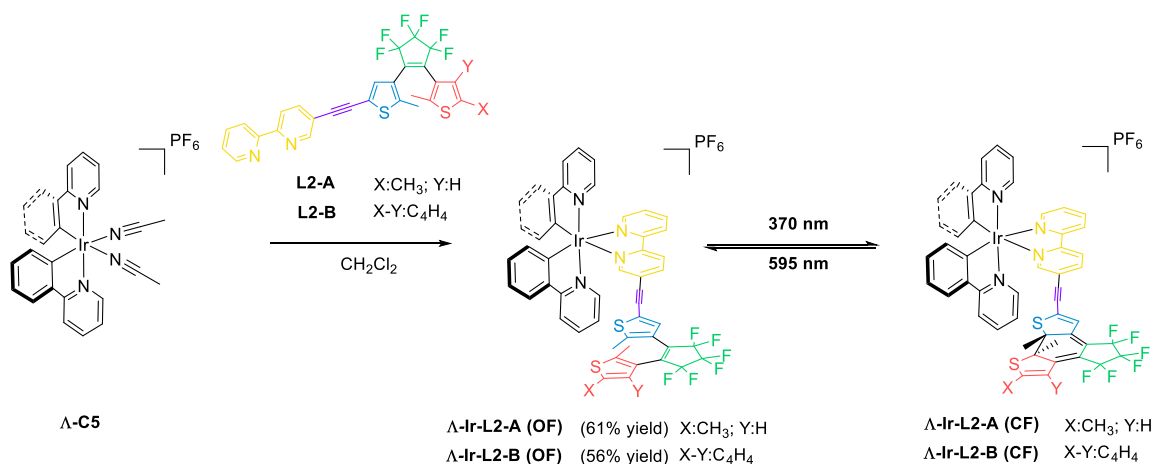
Scheme 3.22. Synthesis of **Λ-Ir-L2-A** and **Λ-Ir-L2-B**.

Once the **Λ-Ir-L2-A** and **Λ-Ir-L2-B** complexes were obtained, a comparison was made between the racemic and enantiopure complexes to verify if there is any significant difference in the NMR spectra. As shown in Figure 3.22, both complexes (**Λ-Ir-L2-A** and *rac*-**Ir-L2-A**) spectra are identical, so it can be deduced that being coordinated to the enantiopure metal center in its open form does not produce any significant effect on the spectrum by NMR. This result can be striking, since a DTE ligand in its open form (**OF**) could also be chiral, provided that the conversion between the *P* and *M* isomers was restricted (as explained in *Chapter 1*). The reason for not observing a splitting of the synthesized complexes signals lies in a rapid interconversion between the *P* and *M* configurations of the antiparallel form of the **OF-DTE** when it is in solution.
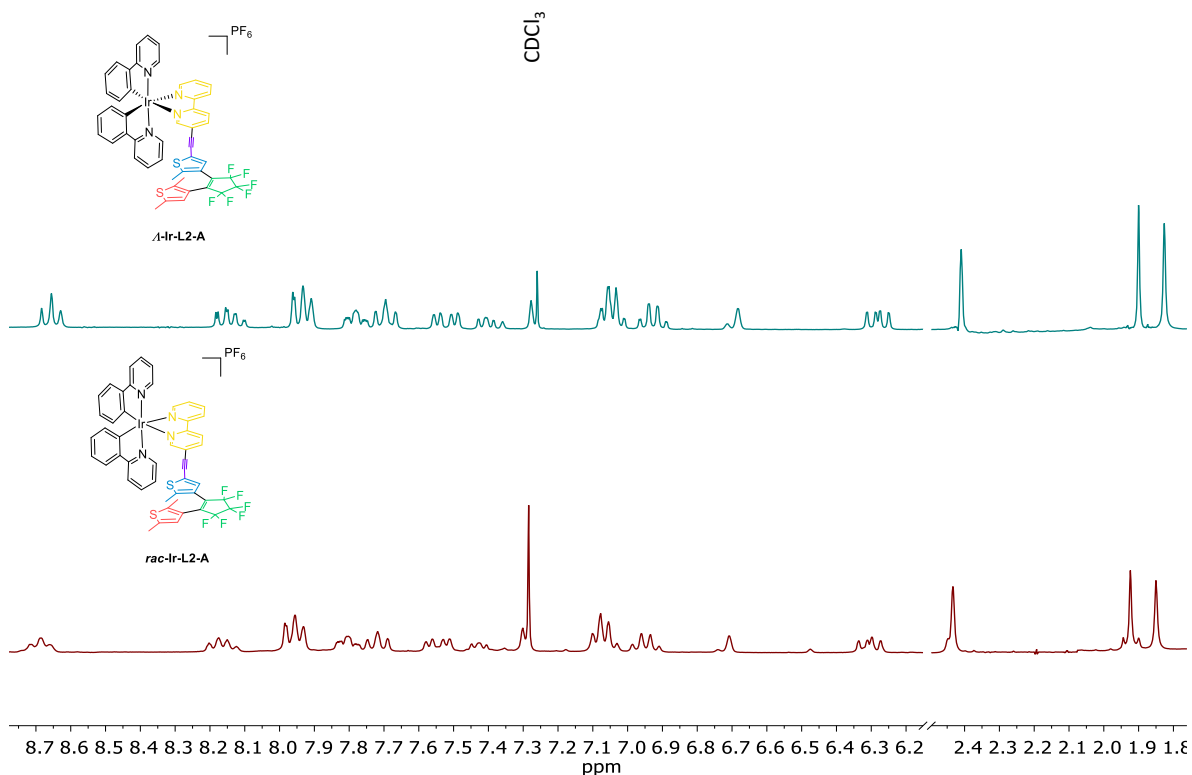
Figure 3.22. ^{1}H NMR spectra comparing of *rac*-**Ir-L2-A** and **Λ-Ir-L2-A**. (CDCl$_3$, 300 MHz).

Once the complexes incorporating an alkyne spacer DTE fragment were synthesized, the synthesis of the complexes with the ligands **L3-A** and **L3-B** was performed. The target enantiopure complexes **Λ-Ir-L3-A** and **Λ-Ir-L3-B** were obtained with a similar synthetic procedure as complexes **Λ-Ir-L2-A** and **Λ-Ir-L2-B**. As Scheme 3.23 shows, to a solution of **Λ-C5** in CH$_2$Cl$_2$, 1.1 equivalents of **L3-A** or **L3-B** were added to obtain **Λ-Ir-L3-A** or **Λ-Ir-L3-B**, respectively. After purification through alumina chromatography column, using CH$_2$Cl$_2$ as eluent, final complexes **Λ-Ir-L3-A** and **Λ-Ir-L3-B** were obtained as blue solids, with good to moderate yields (66% for **Δ-Ir-L3-A** and 60% for **Δ-Ir-L3-B**). **Δ-Ir-L3-A** and **Δ-Ir-L3-B** isomers were obtained after a process identical to that described above.

135
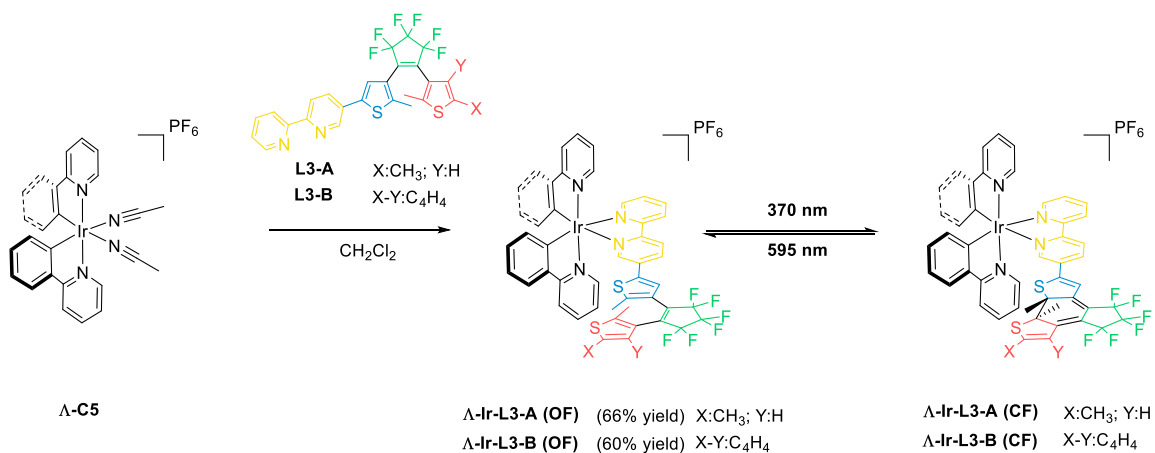
These new complexes were identified through NMR spectroscopy. Figure 3.23 shows the spectra obtained via ^{1}H-NMR spectroscopy. The pattern of the spectrum obtained previously for the **Λ-Ir-L2-A** complex proved to be very similar to those obtained for these complexes. This is because the presence of the alkyne group does not significantly affect the multiplicity of the different signals. In red, the spectrum obtained for the **Λ-Ir-L3-A** complex is shown. The proof of this is the presence of the three methyl groups at high fields of the spectrum. The blue spectrum shows the signals obtained for **Λ-Ir-L3-B** after purification. The presence of two methyls in the high field region is striking because one of the methyls appears as a doublet. This splitting can be caused by the proximity of the coordinated phenylpyridines to the metal. This effect is not observed when the ligand **L3-B** alone is studied. This effect may be because, due to the proximity of the DTE to the metal center and the steric hindrance generated by the benzo[*b*]thiophene group, the formation of diastereomers occurs in the **OF-DTE**. This hypothesis could be supported by the appearance of splitting in various signals of the ^{1}H-NMR of **Λ-Ir-L3-B**, associated with the diastereomers ***P*-Λ-Ir-L3-B** and ***M*-Λ-Ir-L3-B**, since for the complex that introduces the ligand **L3-A**, no mentioned effect is observed. This would be explained due to the inhibition of the interconversion between the antiparallel configurations of the **Λ-Ir-L3-B** complex. In contrast, for **Λ-Ir-L3-A**, this inhibition is not produced by the presence of less bulky groups.
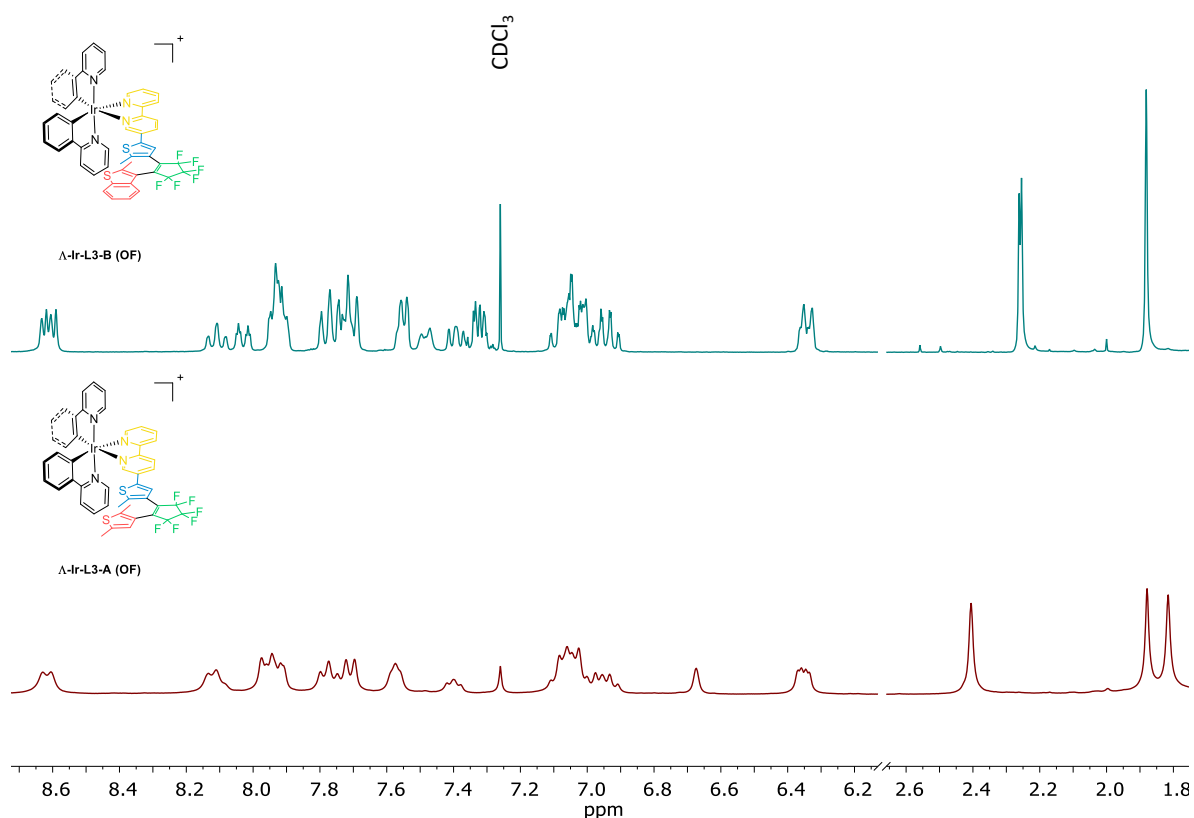
Figure 3.23. ^{1}H NMR spectrum of **Λ-Ir-L3-A** and **Λ-Ir-L3-B**. (CDCl₃, 300 MHz).

As a summary of this chapter, it can be indicated that they have been able to synthesize four new DTE ligands based on a bipyridine structure. On the other hand, the coordination of ligands **L2** and **L3** to a metallic precursor of Ir(III) (**C5**) was successfully confirmed. Likewise, by reproducing the synthetic protocols described by E. Meggers, it was possible to synthesize enantiopure metal intermediates (**Λ/Λ-C5**), from which DTE-based enantiopure Ir(III) complexes were obtained for the first time.

3.2 REFERENCES

[1] D. Becker, N. Konertz, M. Böhning, J. Schmidt, A. Thomas, *Chem. Mater*., **2016**, *28*, 8523-8529.

[2] J. Ma, X. Cu, F. Wang, X. Wu, J. Zhao, X. Li, *J. Org. Chem*., **2014**, *79*, 10855-10866.

[3] R. Chinchilla, C. Nájera, *Chem. Rev*., **2007**, *107*, 874-922.

[4] J. Chen, M. Kuss-Petermann, O. S. Wenger, *Chem. Eur. J*., **2014**, *20*, 4098-4104.

[5] A. J. Scott, J. Vallejo, A. Sarkar, L. Smythe, E. R. Martí, G. S. Nichol, W. T. Klooster, S. J. Coles, M. Murrie, G. Rajaraman, S. Piligkos, P. J. Lusby, E. K. Brechin, *Chem. Sci*., **2021**, *12*, 5134.

[6] S. Dey, C. L. Rühl, A. Jäschke, *Chem. Eur. J*., **2017**, *23*, 12162-12170.

[7] W. Wu, J. Sun, X. Cui, J. Zhao, *J. Mater. Chem. C*., **2013**, *1*, 4577-4589.

[8] E. T. Luis, H. Irasnmanesh, K. S. A. Arachchige, W. A. Donald, G. Quach, E. G. Moore, J. E. Beves, *Inorg. Chem*., **2018**, *57*, 8476-8486.

[9] J. von Irmer, F. Frieβ, D. Herold, J. Kind, C. M. Thiele, M. Gallei, *J. Mater. Chem. C*., **2019**, *7*, 14088-14097.

[10] M. Kamila, G. Cosquer, B. K. Breedlove, M. Yamashito*, Bull. Chem. Soc. Jpn*., **2017**, *90*, 595-603.

[11] V. Valderrey, A. Bonasera, S. Fredrich, S. Hecht*, Angew. Chem. Int. Ed*., **2017**, *56*, 1914-1918.

[12] S. Fredrich, A. Bonasera, V. Valderrey, S. Hecht*, J. Am. Chem. Soc*., **2018**, *140*, 6432-6440.

[13] H. Wang, H. Lin, W. Xu, D. Zhu, *Chem. Eur. J*., **2013**, *19*, 3366-3373.

[14] Y-M. Hervault, C. M. Ndiaye, L. Norel, C. Lagrost, S. Rigaut., *Org Lett*., **2012**, *14*, 4454-4457.

[15] F. Sun, S. Cui, S. Pu, *Adv. Mat. Res*., **2014**, *952*, 79-83.

[16] H. Zhao, E. Garoni, T. Roisnel, A. Colombo, C. Dragonetti, D. Marinotto, S. Righetto, D. Roberto, D. Jacquemin, J. Boixel, V. Guerchais, *Inorg. Chem*., **2018**, *57*, 7051-7063.

[17] R. T. F. Jukes, V. Adamo, F. Hartl. P. Belser, L. De Cola, *Inorg. Chem*., **2004**, *43*, 9, 2779-2792.

[18] B. Li, H-M. Wen, J-Y. Wang, L-X. Shi, Z-N. Chen, *Inorg. Chem*. **2013**, *52*, 12511-12520.

[19] L. Ma, H. Xu, G. Liu, *Adv. Mat, Res*., **2014**, *1003*, 35-38.

[20] Y. Asano, A. murakami, T. Kobayashi, S. Kobatake, M. Irie, S. Yabushita, S. Nakamura, *J. Mol. Struc*., **2003**, *625*, 227-234.

[21] S. Kobatake, K. Uchida, E. Tsuchida, M. Irie, *Chem. Commun*., **2002**, 2804-2805.

[22] K. Higashiguchi, K. Matsuda, Y. Asano, A. Murakami, S. Nakamura, M. Irie, *Eur. J. Org. Chem*., **2005**, 91-97.

[23] V. A. Migulin, M. M. Krayushkin, V. A. Barachevsky, O. I. Kobeleva, T. M. Valova, K. A. Lyssenko, *J. Org. Chem,* **2012**, *77*, 332-340.

[24] E. C. Constable, *Coord. Chem. Rev*., **1990**, *98*, 251-277

[25] M. Mauro, K. C. Schuermann, R. Prétôt, A. Hafner, P. Mercandelli, A. Sironi, L. De Cola*., Angew. Chem. Int. Ed*., **2010**, *49*, 1222-1226.

[26] A. M. Soliman, D. Fortin, P. D. Harvey, E. Zysman-Colman, *Chem. Commun*., **2012**, *48*, 1120-1122.

[27] C. Xu, A. Guenet, N. Kyritsakas, J-M. Planeix, M. W. Hosseini, *Chem. Commun*., **2015**, *51*, 14785-14788.

[28] R. Liu, N. Dandu, J. Chen, Y. Li, Z. Li, C. Wang, S. Kilina, B. Kohler, W. Sun, *J. Phys. Chem. C*., **2014**, *118*, 23233-23246.

[29] C. Lentz, O. Schott, T. Auvray, G. Hanan, B. Elias, *Inorg. Chem*., **2017**, *56*, 10875-10881.

[30] A. M. Bünzli, E. C. Constable, C. E. Housecroft, A. Prescimone, J. A. Zampese, G. Longo, L. Gil-Escrig, A., Pertegás, E. Orti, H. J. Bolink, *Chem. Sci*., **2015**, *6*, 2843-2852.

[31] N. A. Till, L. Tian, Z. Dong, G. D. Scholes, D. W. C. MacMillan, *J. Am. Chem. Soc*., **2020**, *142*, 15830-15841.

[32] B-J. Zhang, W-W. Fu, R. Wu, J-L. Yang, C-Y. Yao, B-X. Yan, H-S. Tan, C-W. Zheng, Z-J. Song, H-X. Xu, *Bioorganic Chemistry*, **2019**, *82*, 274-283.

[33] K. H. Kim, D. S. Kim, S-P. H, O. S. Keon, *Arch. Pharm. Res.,* **2000**, *23*, 26-30.

[34] C. Q. Kabes, W. J. Maximuck, S. K. Ghosh, A. Kumar, N. Bhuvanesh, J. A. Gladysz, *ACS Catal*., **2020**, *10*, 3249-3263.

[35] J. Ma, X. Zhang, X. Huang, S. Luo, E. Meggers, *Nature protocols*, **2018**, *13*, 605-632.

[36] M. Helms, C. Wang, B. Orth, K. Harms, E. Meggers., *Eur. J. Inorg. Chem.,* **2016**, 2896-2901.

[37] L-P. Li, S-Y. Yao, Y-L. Ou, L-Q. Wei, B-H. Ye., *Organometallics*, **2017**, *36*, 3257-3265.

[38] O. Chepelin, J. Ujma, X. Wu, A. M. Z. Slawin, M. B. Pitak, S. J. Coles, J. Michel, A. C. Jones, P. E. Barran, P. J. Lusby, *J. Am. Chem. Soc*., **2012**, *134*, 19334-19337.

[39] L. Gong, S. P. Mulcahy, K. Harms, E. Meggers, *J. Am. Chem. Soc*., **2009**, *131*, 9602-9603.

[40] S-Y. Yao, Y-L. Ou, B-H. Ye, *Inor. Chem*., **2016**, *55*, 6018-6026.

CHAPTER 4

PHOTOPHYSICAL MEASUREMENTS: INDUCTION OF DIASTEREOMERIC ISOMERIZATION
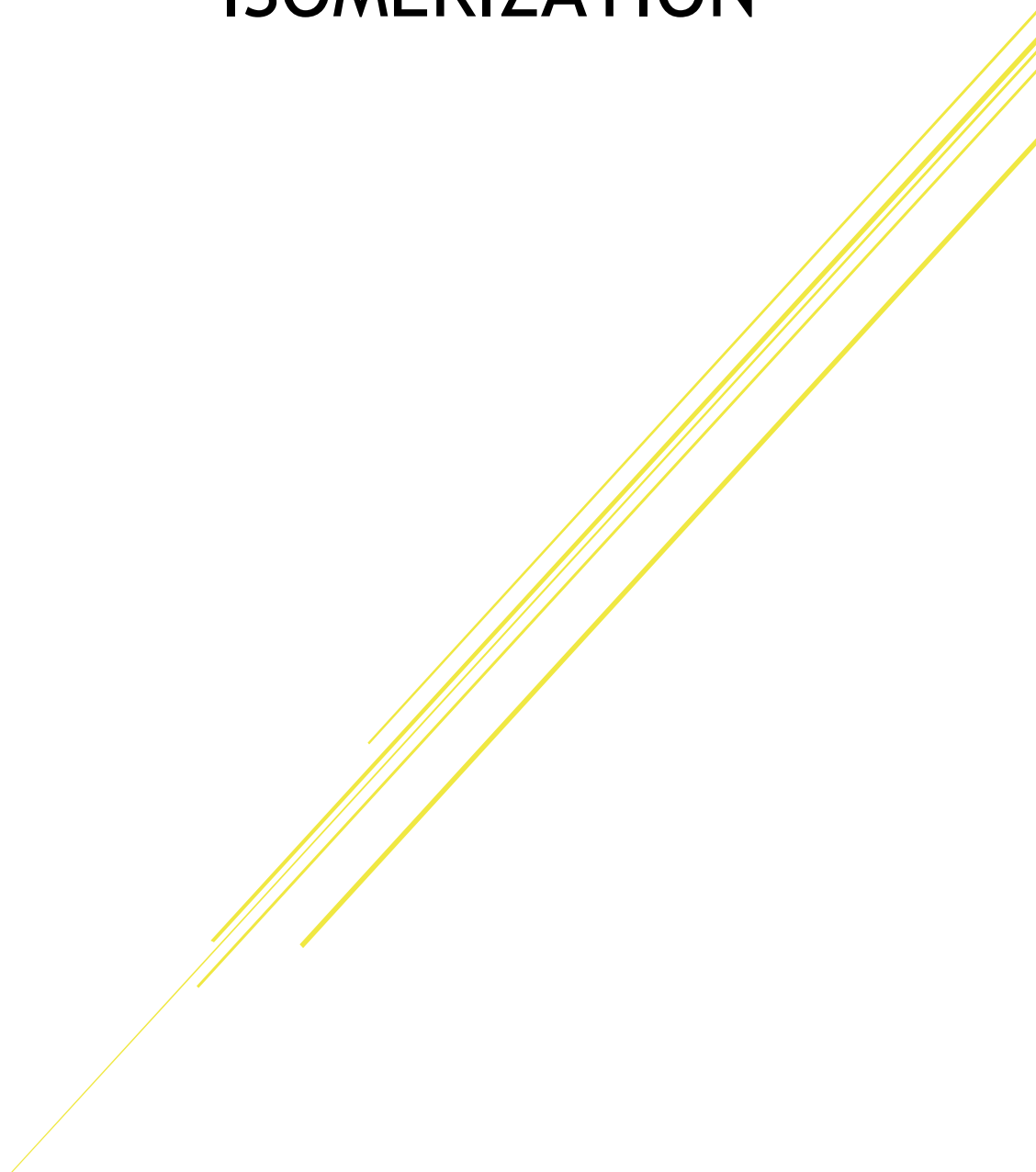
4.1 PHOTOCHEMISTRY STUDIES

4.1.1 LIGANDS

This section will present studies of the photoreactivity of the DTE unit within the free ligands, primarily by electronic absorption spectroscopy. These results will be used as reference data to determine the effect of the ligand coordination to the metal center in governing photoreactivity, particularly the photocyclization process. The introduction described the light-triggered DTE open-to-closed photocyclization, where both forms are thermally stable, and the photochemical process can be reversed only by photoirradiation (photocycloreversion). UV-Vis spectroscopy offers a convenient method to optically monitor photoinduced change in dilute solution due to the different spectra characteristic of each form. Scheme 4.1. shows the primary photoswitching processes that were studied for the four new synthesized DTE ligands
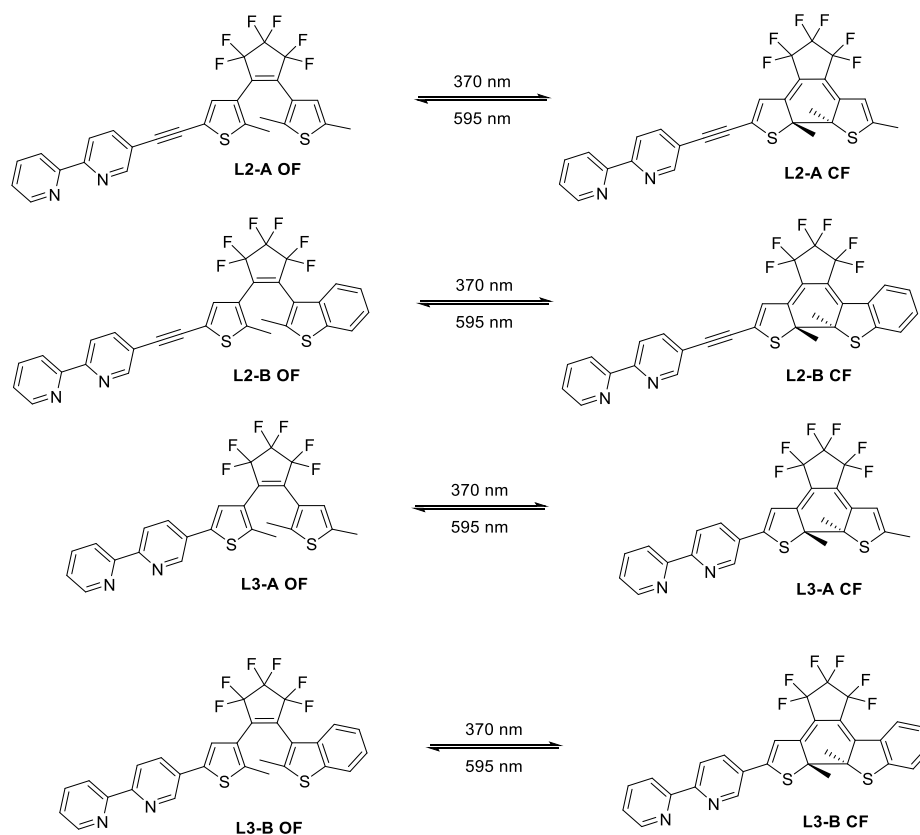
Scheme 4.1. Reversible photocyclization processes for **L2-A**, **L2-B**, **L3-A** and **L3-B**.

The primary photochemical behavior of DTE derivatives can, typically, be satisfactorily described by two processes:- i) a photocyclization reaction and, ii) a photocycloreversion reaction. These processes can only occur through light irradiation; as such, these dyes may be considered bistable "P-type" photochromes. The photocyclization reaction occurs due to the excitation resulting from the absorption of a photon in the ultraviolet spectral region. Absorption of this energy, provided by a suitable light source, causes the open form of the DTE to pass from its ground state (S_0) to its excited state (S_1), before undergoing a cyclization reaction. As explained in the introduction, the photocycling of DTE compounds is based on an electrocyclic transformation to form a single bond between the terminal ends of a linear system containing $n\pi$ electrons. This transformation depends on the symmetry of the HOMO-LUMO orbitals, which predicts whether the electrocyclization process will occur through a disrotatory

or conrotatory mechanism. As defined by Woodward-Hoffman, in the case of carrying out the process in the excited state (photochemical process), the reaction proceeds via a conrotatory mechanism.[1,2]

The π-conjugation in DTEs in their open-form is mainly restricted to each thiophene-based group. However, when photocyclization process occurs (giving the closed isomer), the π-conjugation of the ligand is extended and delocalized through the molecule. As a consequence, the HOMO-LUMO gap becomes energetically smaller. As a result of this electronic change, the absorption bands in the electronic absorption spectrum shift to longer wavelengths. This effect can be monitored through UV-Vis absorption spectroscopy due to the different sets of spectroscopic bands for each isomer (**OF** and **CF**). When a DTE isomerizes, the absorption band attributed to the π-π* transition shifts to longer wavelengths, generally giving broader, less intense bands. Figure 4.1 shows the photoswitching behaviour of **L2-A** in solution. The spectrum corresponding to the open form **OF L2-A** is shown in orange. Two absorption maxima at the UV spectral region are observed (λ_{max} = 250 nm and λ_{max} = 330 nm), and are associated with electronic transitions centred on the thiophene units. The purple line shows the spectrum of the **CF** after irradiation at 370 nm for a specific time (30 s), which gives a significant change in the absorption bands. The **OF** isomer absorption band, attributed to a π-π* band decreases in intensity, and a new broad band at 561 nm assigned to the **CF** is identified. This broad band in the visible region of the spectra is the most characteristic band of the closed isomers of DTEs.
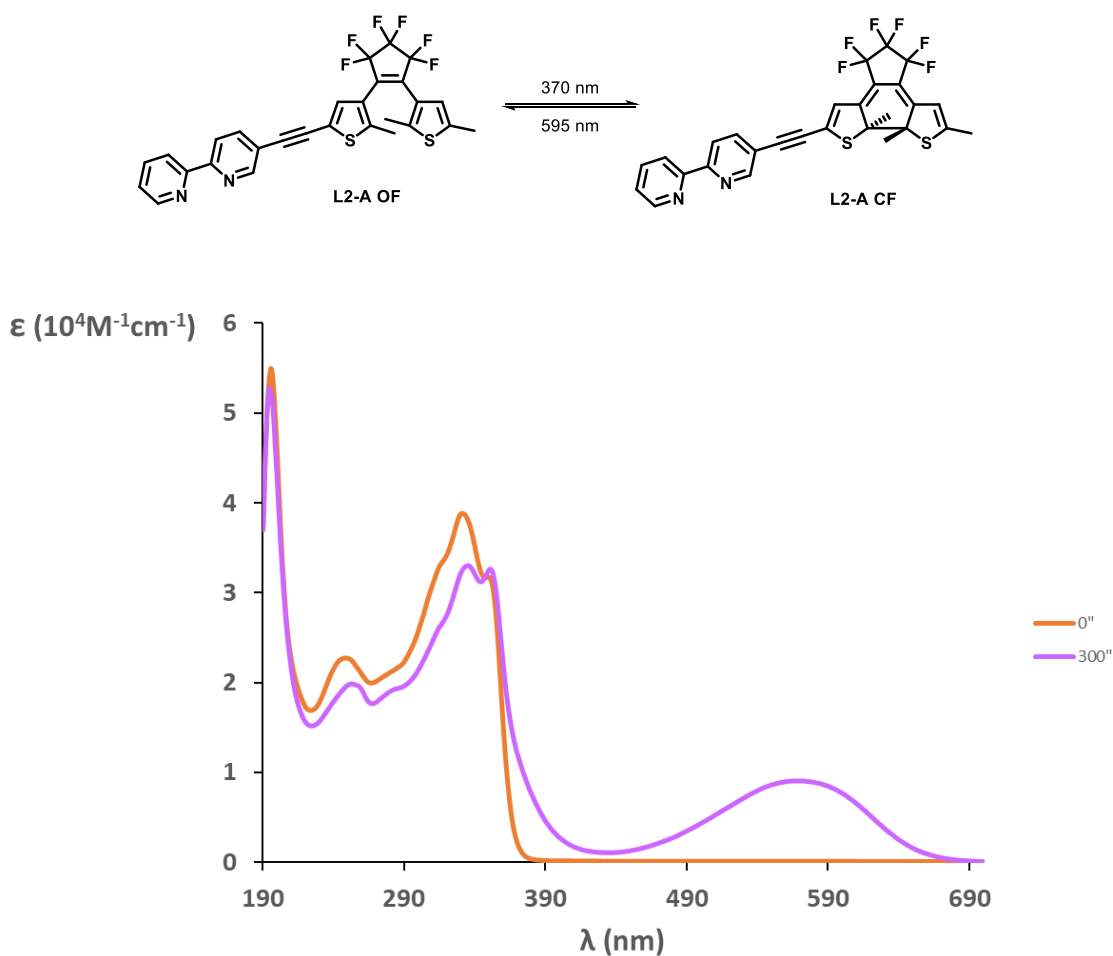
Figure 4.1. Absorption spectra of **L2-A OF** and **L2-B CF** obtained after 300 seconds of irradiation at 370 nm. (5·10^{-5} M solution in CH$_3$CN).

The photochromism of DTEs can also be studied through other spectroscopic techniques such as NMR spectroscopy. In this case, the identification of individual resonances allows unambiguous determination and quantification of the species present in solution, albeit at higher concentrations than those compatible with optical methods. Figure 4.2 shows the different ^{1}H NMR spectra measured for ligand **L2-A**, before and after irradiating the sample (370 nm). The spectrum of **OF L2-A** is shown in red. Several of the signals which were chosen to study the isomerization process are marked in orange. They correspond to the two aromatic protons of the thiophene groups (7.32 ppm and 6.72 ppm) and to the three methyl groups present in the ligand **L2-A** (2.41 ppm, 1.91 ppm and 1.87 ppm), respectively. The mixture of species obtained by irradiating the sample at 370 nm is shown in purple. It can be seen how the signals assigned to the aromatic protons, marked in orange, decrease while two new signals appear at higher fields of the spectrum, marked in purple. The same effect was observed studying the methyl group signals. As the target sample is irradiated, there is a decrease in these signals, giving rise to the appearance of a new singlet and a doublet (overlap of two singles), marked in purple. After four hours of irradiation, the experiment was stopped because the PSS of the sample was reached. As can be seen, there is a coexistence between both **OF** and **CF L2-A** species.
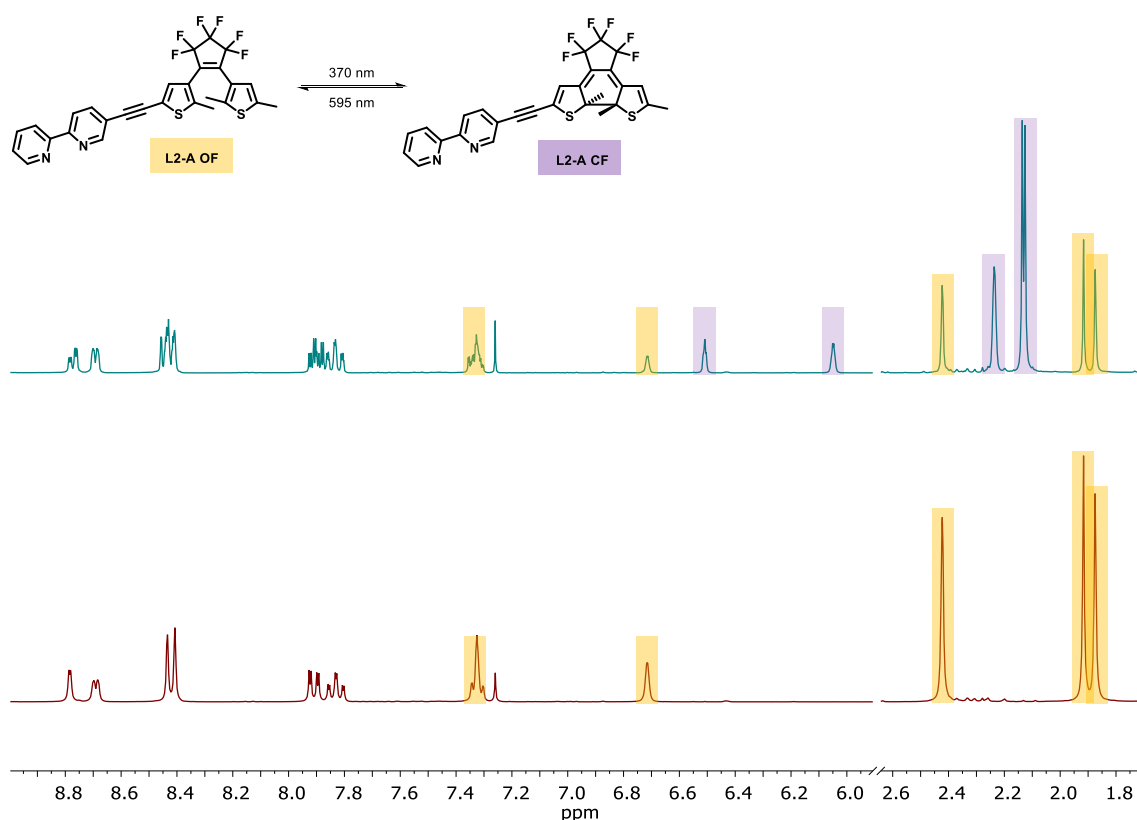
Figure 4.2. ^{1}H-NMR spectra of **L2-A** before (bottom) and after photocyclization (top). (300 MHz, CDCl$_3$).

The same types of analyses were performed for the rest of the ligands (Figure 4.3). The UV-vis spectra show that all the DTE ligands synthesized showed a photochromic behaviour. It is observed how the bands that present the different isomers in their open form are centered in the UV region (250–400 nm), and they experience an evident bathochromic shift upon photocyclization, being characterized by a broad band centered at 552–569 nm.
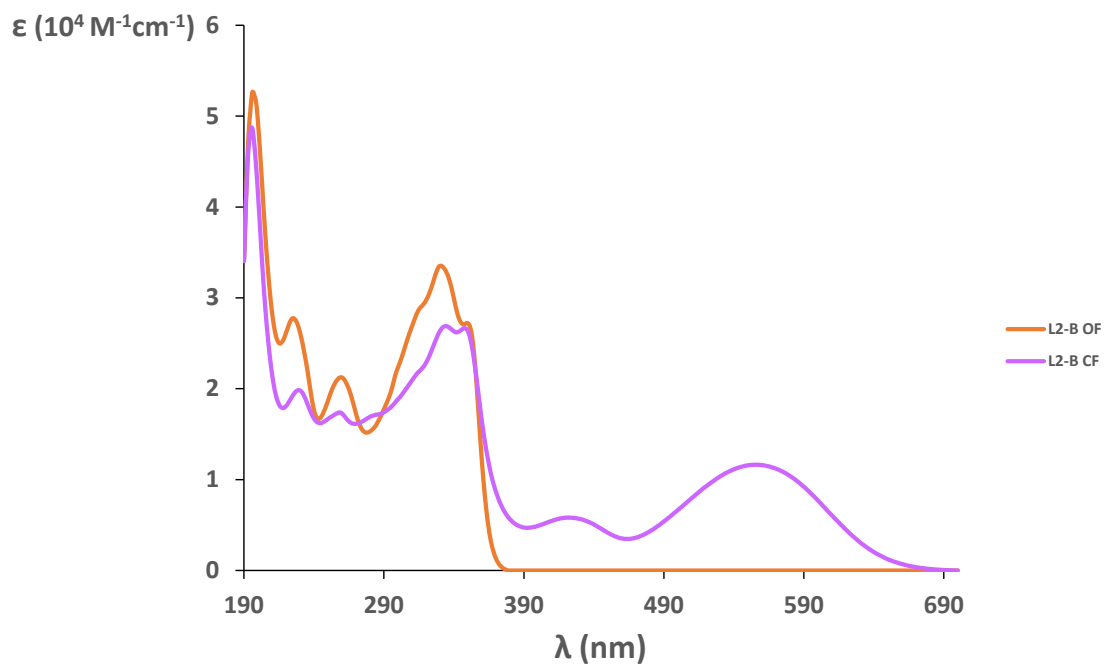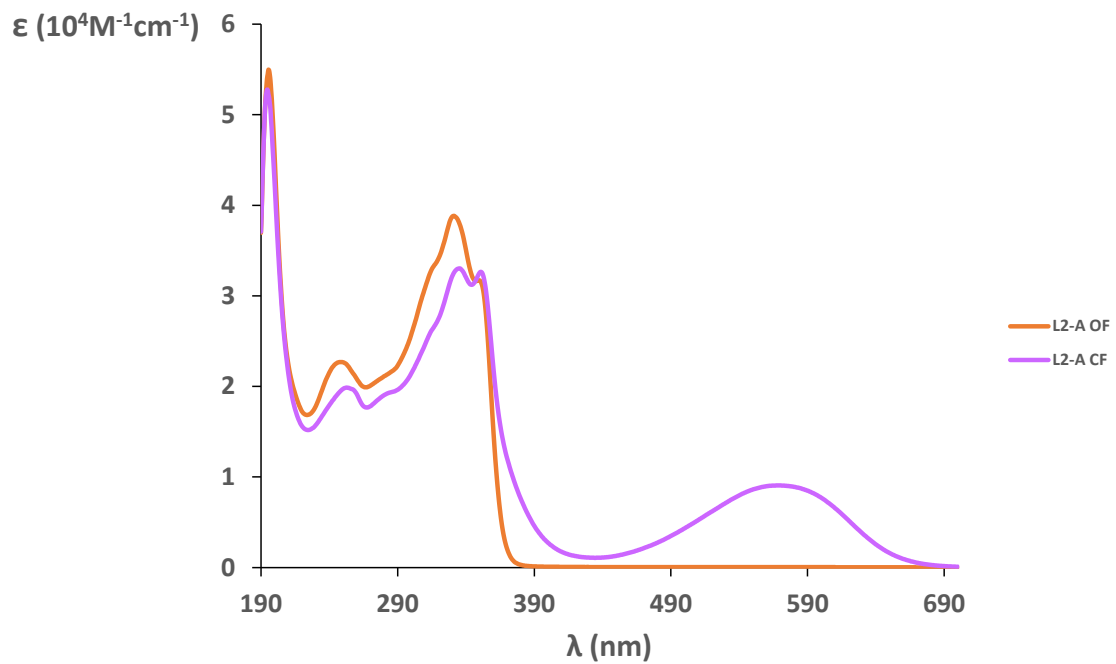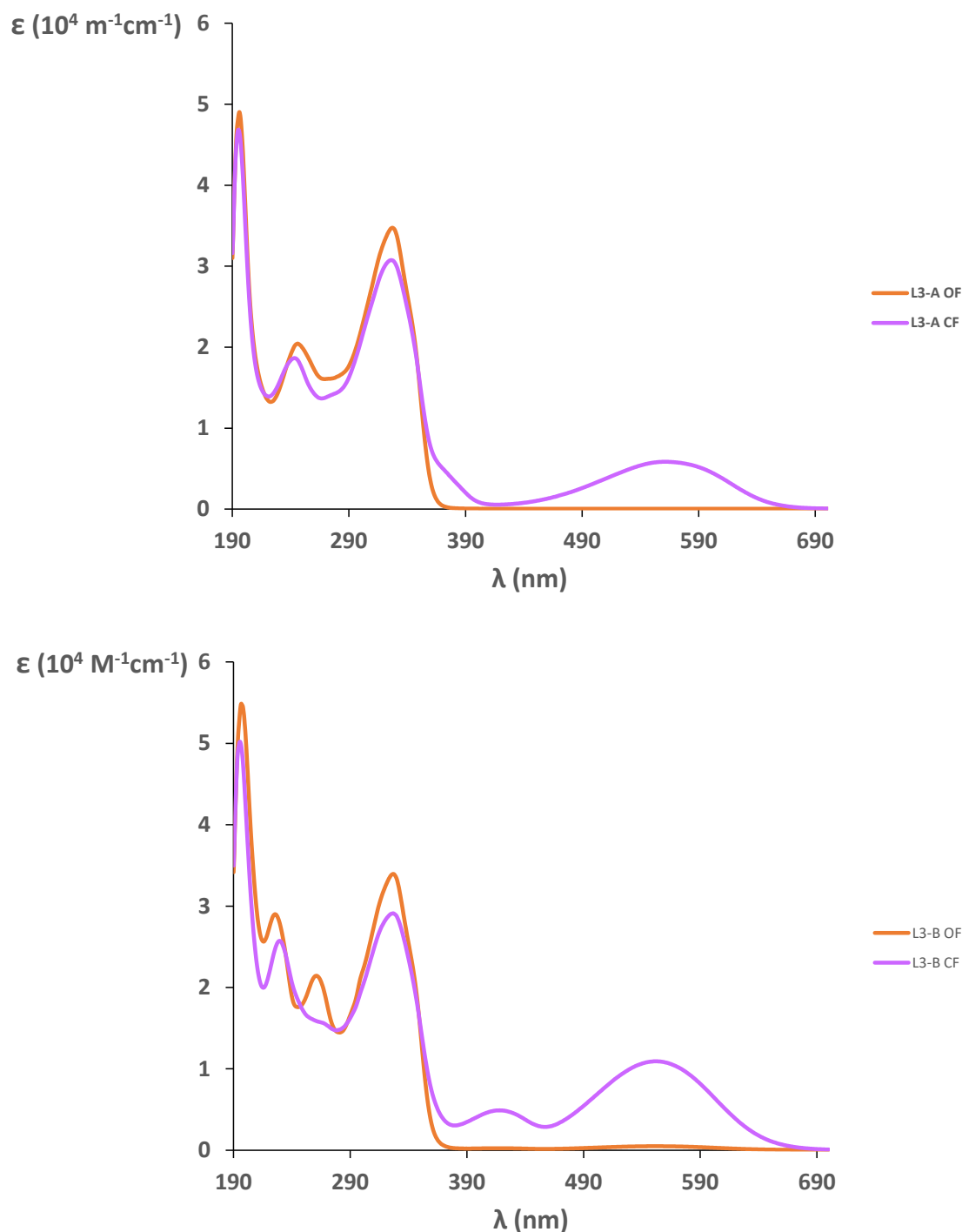
Figure 4.3. Electronic absorption spectra of DTE ligands synthesized before and after photocyclization. (5·10⁻⁵ M solution in CH₃CN).

Comparing the different spectra obtained for the closed isomers, some differences can be observed between the ligands, which are presented in Table 4.1. On one hand, the **L2-B** and **L3-B** ligands have higher intensity bands than the **L2-A** and **L3-A** ligands. The presence of benzo[*b*]tiophene group generates another difference, which is the appearance of an additional band of low intensity in the visible region of the spectra (420-430 nm). It should also be noted that upon, photocyclization, the less energetic absorption band of dimethyl ligands (**L2-A** and **L3-A**) is red-shifted with respect to their benzothiophene counterparts (**L2-B** and **L3-B**). This

effect does not correspond with the concept described in the literature, which indicates that the greater the electronic conjugation of the system, the greater bathochromic effect would be obtained.[3]

Table 4.1. *Absorption data comparison for free ligand.*

Entry	Compound	λ OF-isomer maxima (nm)	λ OF-isomer maxima (cm^{-1})	ε OF-isomer maxima (M^{-1}cm^{-1})	λ CF-isomer maxima (nm)	λ CF-isomer maxima (cm^{-1})
1	L2-A	331	30210	38840	569	17570
2	L2-B	330	30300	33520	555	18020
3	L3-A	327	30580	34740	560	17860
4	L3-B	326	30670	33900	552	18120

For comparative purposes, Scheme 4.2 and Table 4.2 collect the data of several published DTEs compared to the ones studied in this work. It presents two symmetrical DTEs (entries 1 and 2) and several non-symmetric ones (entries 3-12). The photocycling reaction of symmetric DTEs results in a low-energy band of the closed isomer centered close to 500 nm. A more significant bathochromic shift occurs in the case of symmetric benzothiophene DTE, compared to dimethyl DTE, which would be in agreement with the generally accepted trend mentioned above. On the other hand, when non-symmetric structures are compared (entries 3, 5, 7, and 9 vs entries 4, 6, 8, and 10) DTEs possessing the dimethyl branch exhibit a greater bathochromic effect than those with benzothiophene in the structure. Therefore, one can conclude that the DTEs synthesized behave similarly to other published non-symmetric DTEs.

Table 4.2. *Absorption maxima of the less energetic band of **CF DTE** isomer for symmetric/non-symmetric DTEs.*

ENTRY	COMPOUND	λ CF-ISOMER MAXIMA (nm)	SOLVENT
1	E-1[4]	503	Hexane
2	E-2[5]	515	Hexane
3	E-3[6]	541	Hexane
4	E-4[7]	536	Hexane
5	E-5[8]	563	Hexane
6	E-6[7]	546	Hexane
7	E-7[9]	549	Hexane
8	E-8[7]	534	Hexane
9	E-9[10]	545	Hexane
10	E-10[7]	541	Hexane
11	E-11[11]	548	Acetonitrile
12	E-12[12]	612	Acetonitrile

4

CF λ = 503 nm
E-1

CF λ = 515 nm
E-2

CF λ = 541 nm
E-3

CF λ = 536 nm
E-4

CF λ = 563 nm
E-5

CF λ = 546 nm
E-6

CF λ = 549 nm
E-7

CF λ = 534 nm
E-8

CF λ = 545 nm
E-9

CF λ = 541 nm
E-10

CF λ = 548 nm
E-11

CF λ = 612 nm
E-12
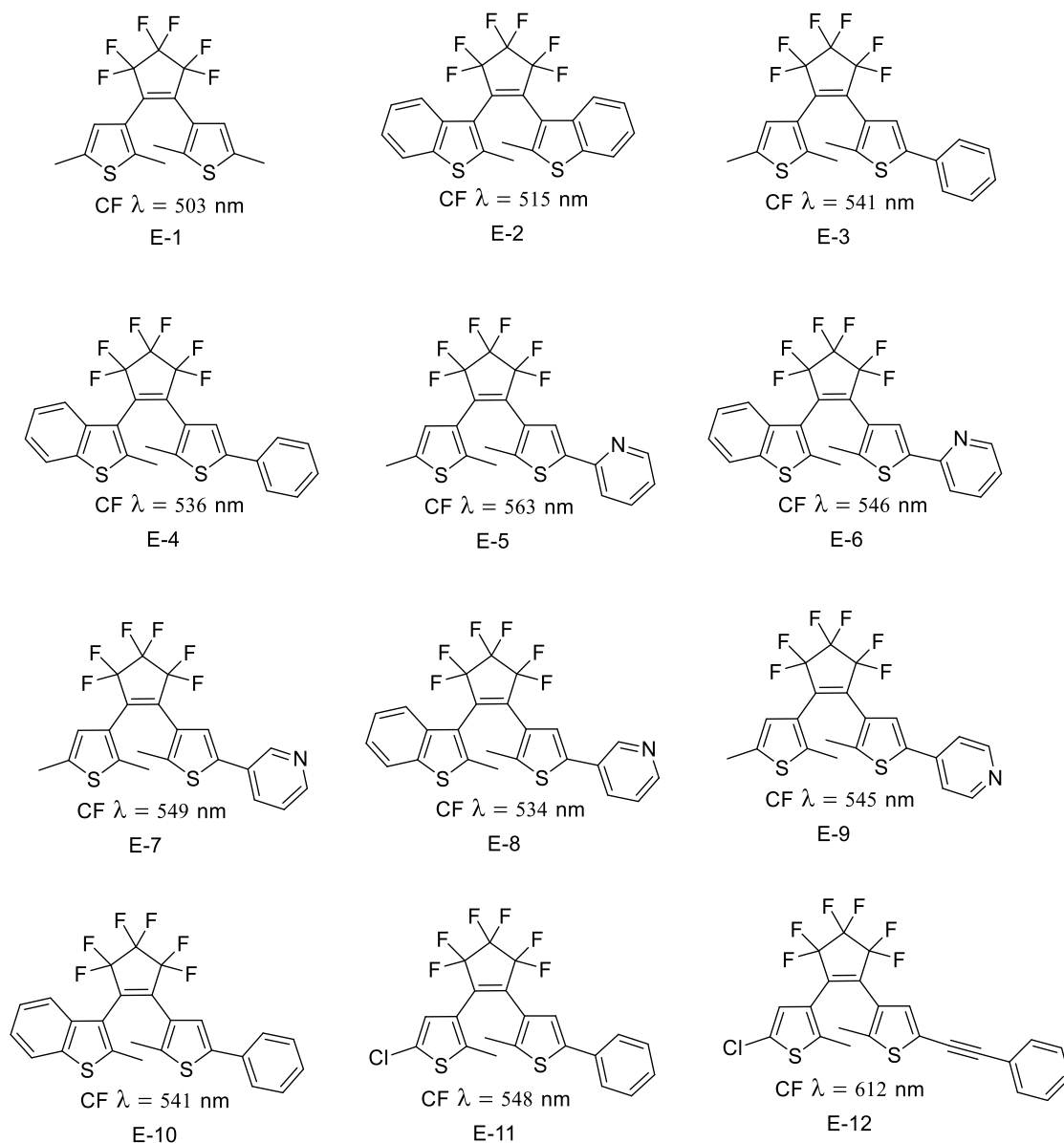
Scheme 4.2. Less energetic band maxima of several closed isomers of published DTE.

Additionally, the effect caused by the presence/absence of an alkyne spacer in published examples can be exemplified by comparing entries 11 and 12. The insertion of the alkyne spacer in the structure generates a bathochromic effect of the **CF-DTE** bands after the photocyclization process. The same effect is seen for the characteristic band of **CF-DTEs** (λ = 500-600 nm) synthesized in this study, corroborating the theory of the greater conjugation at the molecule the greater redshifting.
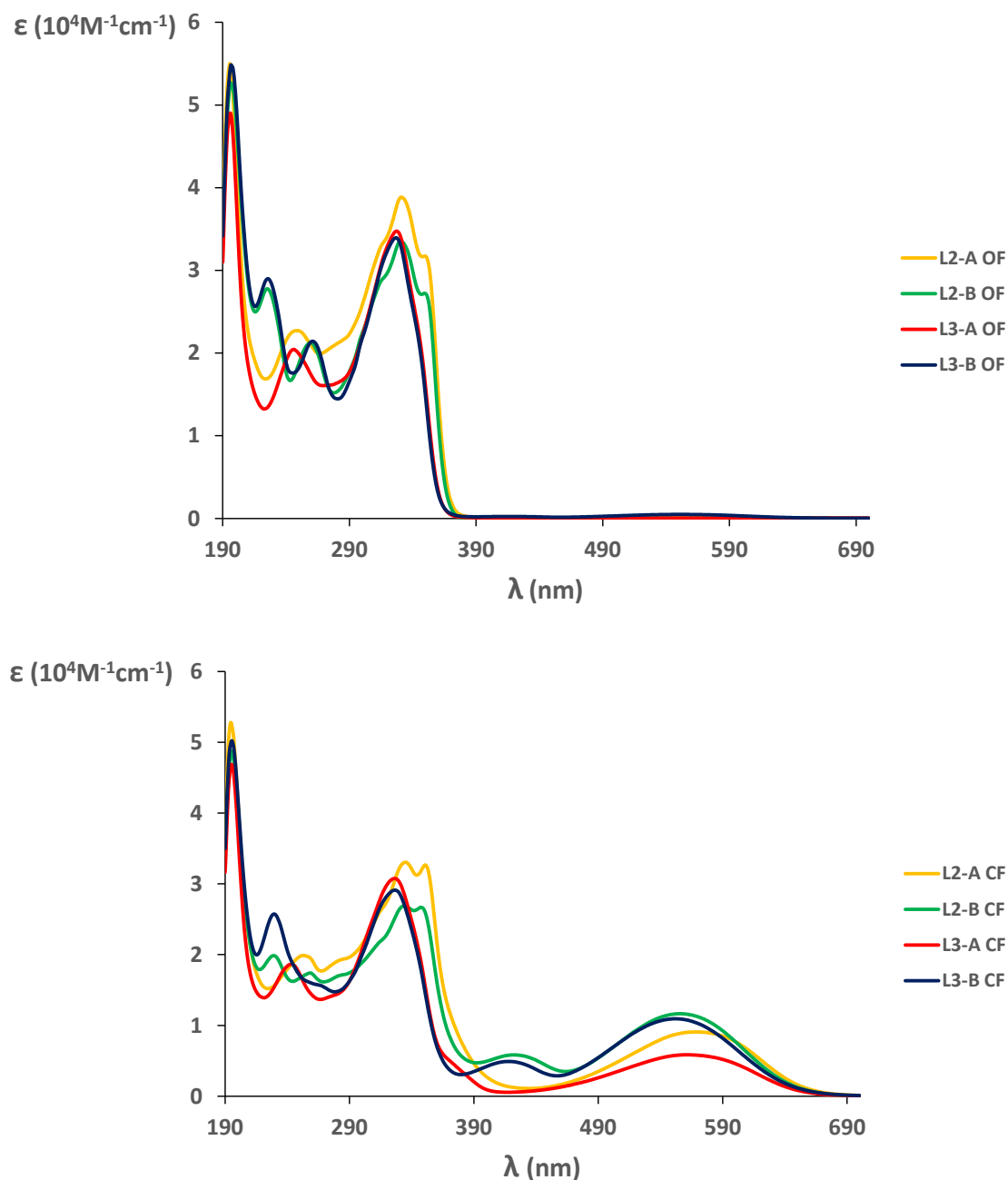
Figure 4.4. UV-Vis spectra of DTE ligands synthesized (**OF** and **CF**). ($5 \cdot 10^{-5}$ M solution in CH_3CN).

To get a deeper insight on the photochemical process, initially, the time needed to reach the PSS was evaluated using UV-vis spectroscopy. A commercial Kessil Led Photoredox light PR160 lamp (370 nm; 43 W) with an intensity setting of 25% was used for this preliminary kinetic study. Before this measurement, the ligand solution was irradiated for one minute with an orange-red LED (595 nm) to ensure that the sample was entirely in its **OF**. Indeed, at this wavelength, only the **CF** absorbs the excitation light, allowing full closed-to-open conversion. In Figure 4.5, the effect of irradiation on a sample of **L2-A** is presented. As it can be observed, DTE **L2-A** exhibits good photochromic properties and can be toggled between its colorless **OF** isomer and colored **CF** isomer by alternate irradiation with appropriate wavelengths of UV and visible light.
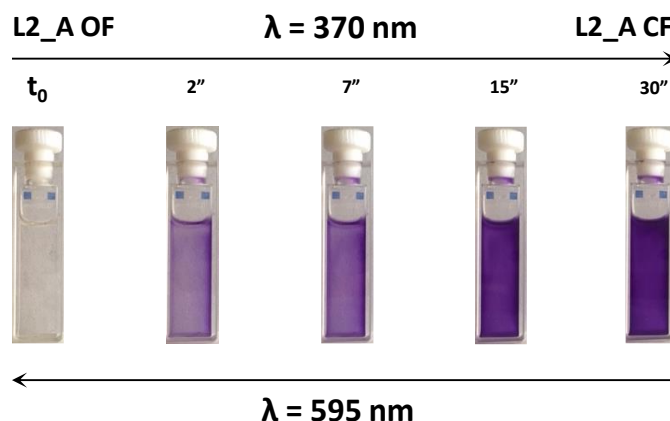
Figure 4.5. Colour changes during the isomerization process of **L2-A** in CH$_3$CN solution.

Figure 4.6 shows the absorption spectral changes of **L2-A** in acetonitrile (c = 5 × 10^{-5} mol L^{-1}). The absorption maximum of compound **L2-A** was observed at 250 nm and 330 nm (ε = 2.3 × 10^4 L mol^{-1} cm^{-1}; ε = 3.8 × 10^4 L mol^{-1} cm^{-1}), which are attributed to $\pi \rightarrow \pi^*$ transitions of the thiophene rings. Upon irradiation with 370 UV light, the colorless solution turned purple, and a new visible absorption band centered at 569 nm (ε = 0.9 × 10^4 L mol^{-1} cm^{-1}) emerged while the original bands with maxima at 250 nm and 330 nm decreased, indicating the formation of the closed-ring isomer **CF L2-A**, reaching with the purple spectrum (300 s) the photostationary state of the compound (PSS). The PSS is a steady state reached by a reacting chemical system when light has been absorbed by at least one of the components. At this state, the rates of formation and disappearance are equal for each of the transient molecular entities formed. The composition of the PSS for a specific compound depends on the molar absorptivity of each isomer at the wavelength of the irradiation and on the quantum yield of the forward and reverse processes (Equation 4.1).

Photocyclization process: $\quad\quad v_{O \rightarrow C} \sim C_O \cdot \varepsilon_O \cdot \Phi_{O \rightarrow C}$

Photocycloreversion process: $\quad v_{C \rightarrow O} \sim C_c \cdot \varepsilon_c \cdot \Phi_{C \rightarrow O}$

At the PSS, both rates ($v_{O \rightarrow C}$ and $v_{C \rightarrow O}$) are equal

$$v_{C \rightarrow O} = v_{O \rightarrow C}$$

Therefore, the PSS must obey the following equation.

$$C_c \cdot \varepsilon_c \cdot \Phi_{C \rightarrow O} = C_O \cdot \varepsilon_O \cdot \Phi_{O \rightarrow C}$$

$$\frac{C_C}{C_O} = \frac{\varepsilon_O \cdot \Phi_{O \rightarrow C}}{\varepsilon_C \cdot \Phi_{C \rightarrow O}} \quad\quad\quad\quad \textbf{Equation 4.1.}$$
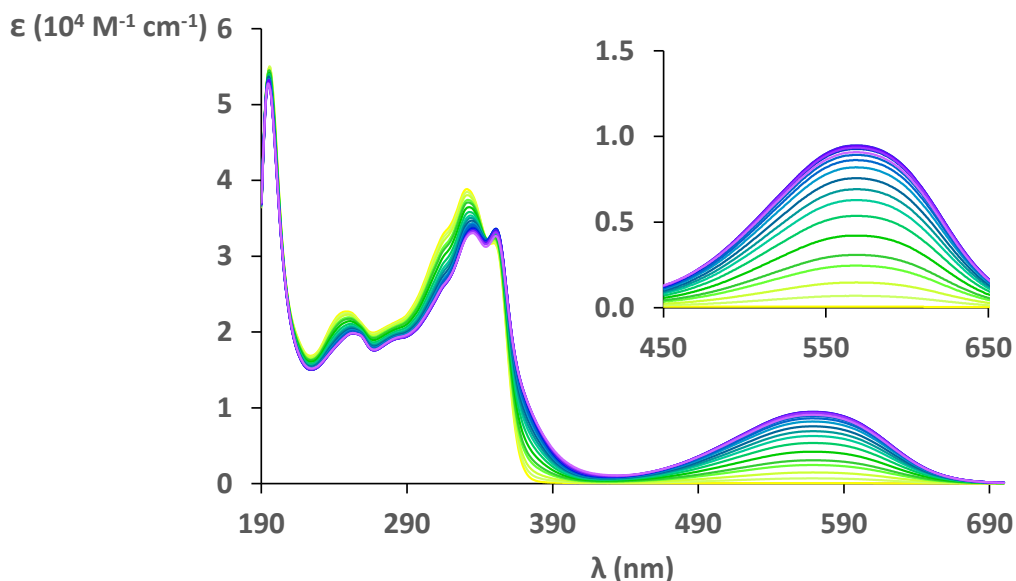
Figure 4.6. UV-Vis spectral changes of ligand **L2-A** on irradiation ($5 \cdot 10^{-5}$ M solution in CH₃CN).

To measure the rate at which the PSS is reached, the absorption at the position of the characteristic band of the **CF** isomer is plotted against irradiation time to observe the conversion from the **OF** to the **CF** of the DTEs. The chosen wavelength was 569 nm for **L2-A**, shown as a model compound. The study was carried out similarly for the rest of the ligands (see experimental section). Figure 4.7 shows the comparison between the different ligands. The results obtained showed that **L2** ligands (alkyne linker in its structure) reach the PSS state faster than **L3** ligands. Additionally, it can be seen how the DTE ligands that contain the dimethylthiophene group as non-coordinating thiophene reach the PSS at a higher rate than those with the coupled benzo group. Even though there are slight differences in their isomerization rate, all the ligands reach the PSS within four minutes of irradiation.
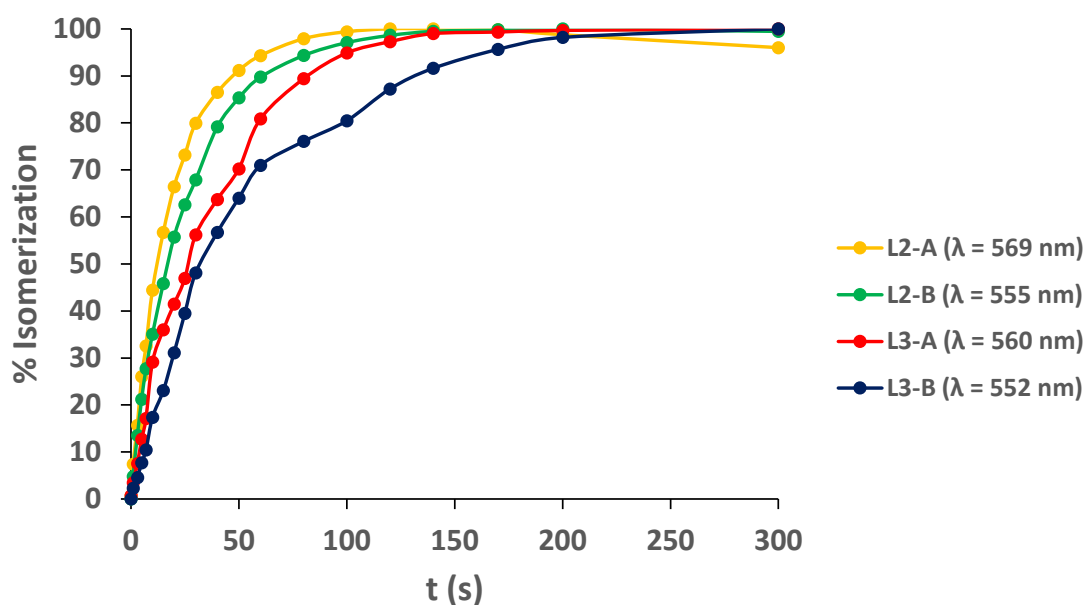
Figure 4.7. Percentage of isomerization of the **CF** specific band wavelength versus time plot obtained for the **OF** → **CF** isomerization process of synthesized DTEs. ($5 \cdot 10^{-5}$ M solution in CH_3CN, irradiation at 370 nm).

The fact that the ligands reach the PSS faster does necessarily mean that the isomerization process is more efficient. As explained above, the PSS is an equilibrium reached between two species, which may be different depending on the studied ligand. The isomerization processes for the DTEs consist of two different reactions, photocyclization reaction and a photocycloreversion process. The efficiency of the isomerization process (photocyclization or photocycloreversion) can be quantified through their corresponding isomerization quantum yields (Φ). In the simplest case, the quantum yield of a photoreaction considers the number of molecules transformed from A to B (Isomer A → Isomer B), divided by the number of photons absorbed by the sample according to Equation 4.2.

$$\Phi = \frac{N^{\underline{o}}\ transformed\ molecules}{N^{\underline{o}}\ photons\ absorbed}$$

Equation 4.2.

Each stage has a specific quantum yield value, where $\Phi_{O \to C}$ is for the photocyclization reaction, and $\Phi_{C \to O}$ is for the photocycloreversion reaction. Equation 4.1 showed the relationship between the quantum yields ($\Phi_{O \to C}$ and $\Phi_{C \to O}$), with the concentrations of both isomers in the PSS (open isomer concentration C_O and closed isomer concentration C_C) and the respective values of the molar absorptivity coefficient of the isomers (ε_O and ε_C). Therefore, to calculate the specific quantum yields, it is necessary to know the ratio of isomers in the PSS, and the extinction coefficients of pure **OF** and **CF** isomers at the irradiation wavelength.

To calculate the relative fractions of each species at the PSS, a complementary technique to UV-Vis spectroscopy is needed to quantify the exact amount of both species in the equilibria. For this, studies were performed analyzing the intensities of selected signals by ^{1}H-NMR spectroscopy. The experiment is based on irradiating a sample of a known concentration of the **OF** photoswitch system until no more changes were observed in the spectra. Knowing the corresponding signals for the **OF** of the DTE, those of the **CF** can be assigned. This experiment is exemplified with **L2-A** (Figure 4.8). A 53 mM solution of ligand **L2-A** in $CDCl_3$ was irradiated with the orange-red LED (595 nm) for 5 minutes, to ensure that all the compound is in the **OF**. Then, under constant irradiation with a lamp Kessil Led Photoredox PR160 lamp (370 nm; 43 W) with an intensity setting of 75%, measurements were made using ^{1}H-NMR spectroscopy every 20 minutes. It can be seen how as the sample is irradiated, the signals corresponding to the **OF** of the DTE, marked in orange, begin to decrease while, in blue, new signals associated with the DTE's **CF** grow. Focusing only on the spectrum corresponding to the PSS of **L2-A** (Figure 4.9), the integration corresponding to the methyl groups can be observed. The obtained values determined that 63% of the sample is in the **CF** in the equilibrium, while 37% remains in its **OF**.
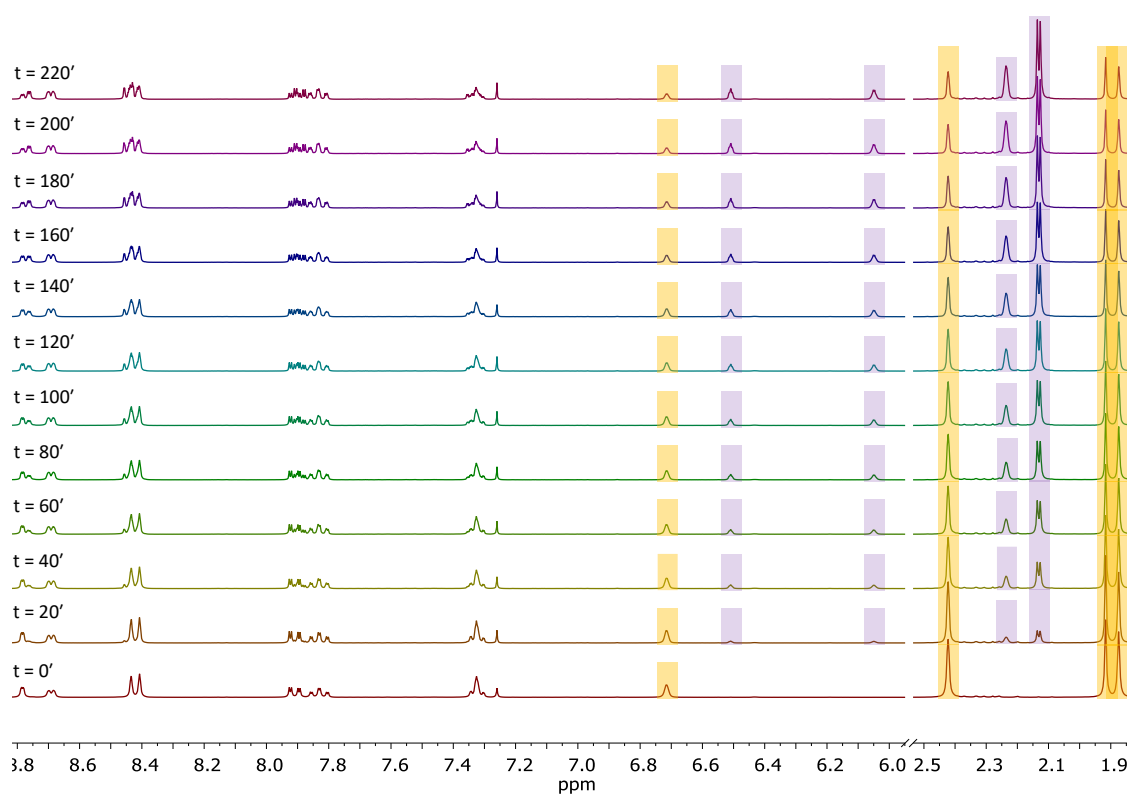
Figure 4.8. ^{1}H-NMR spectra for **L2-A** upon different irradiation times. (53 mM solution in CDCl$_3$).
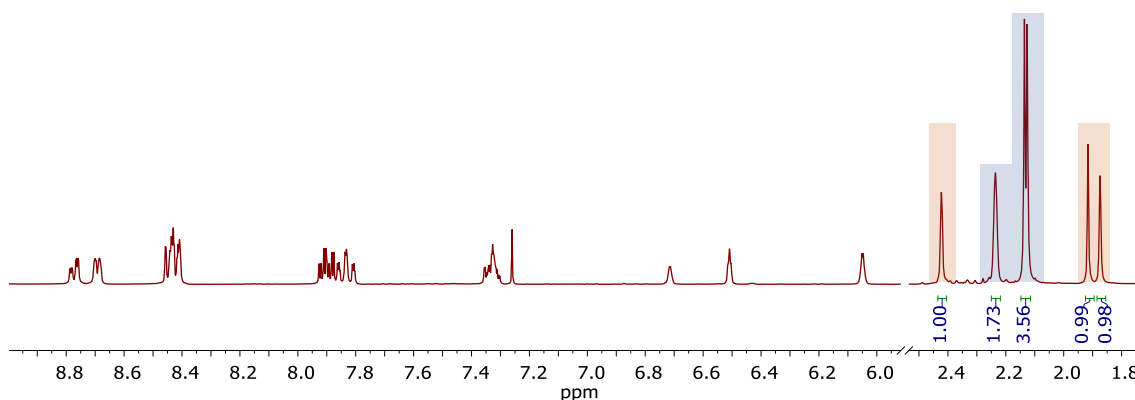
Figure 4.9. ^{1}H-NMR spectrum of the PSS of **L2-A** on irradiating at 370 nm. (0.053 M solution in CDCl$_3$).

The study described here for **L2-A** was repeated for the other ligands (See experimental section). The data obtained from these experiments are collected in the Table 4.3.

Table 4.3. Photostationary state (PSS) calculated ratios for DTEs free ligands.

Compound	[M]	mol	mol OF (PSS)	mol CF (PSS)
L2-A	0.053	$2.67 \cdot 10^{-5}$	$0.99 \cdot 10^{-5}$ (37%)	$1.68 \cdot 10^{-5}$ (63%)
L2-B	0.050	$2.51 \cdot 10^{-5}$	$0.63 \cdot 10^{-5}$ (25%)	$1.88 \cdot 10^{-5}$ (75%)
L3-A	0.055	$2.79 \cdot 10^{-5}$	$1.81 \cdot 10^{-5}$ (65%)	$0.98 \cdot 10^{-5}$ (35%)
L3-B	0.052	$2.61 \cdot 10^{-5}$	$1.07 \cdot 10^{-5}$ (41%)	$1.54 \cdot 10^{-5}$ (59%)

The data obtained for the PSS of the synthesized ligands mostly resemble the percentages obtained for other DTEs, where compound **L2-B** reaches 75% of the **CF** at the PSS[4]. A general trend can be observed in which ligands with the non-coordinating benzo[*b*]thiophene present a higher percentage of the **CF**-DTE isomer in the PSS than the dimethyl-DTE homologs. The composition of the mixture in the PSS through NMR, allows subsequent calculation of the absorption spectrum of the **CF** isomer, knowing that the UV-vis spectrum for the PSS is a weighted average of that of both forms. (Note. The spectrum of the pure open form is experimentally available). This is shown in detail for **L2-A** in Figure 4.10. The yellow spectrum corresponds to the **CF L2-A** spectrum of the ligands, while blue shows the **OF** spectrum. Additionally, in orange and grey, the closed DTE fraction and open DTE fraction's contribution to the spectrum obtained in the PSS is presented. The absorption differences observed in the spectra resides in both isomers' absorption capacity at the irradiation length (370 nm). At this wavelength for the studied cases, both isomers can absorb light, causing the mixture of species in the PSS to be similar. After calculating the spectrum for the **CF L2-A**, the same calculation was performed for the rest of the ligands, as can be seen in Figure 4.10.
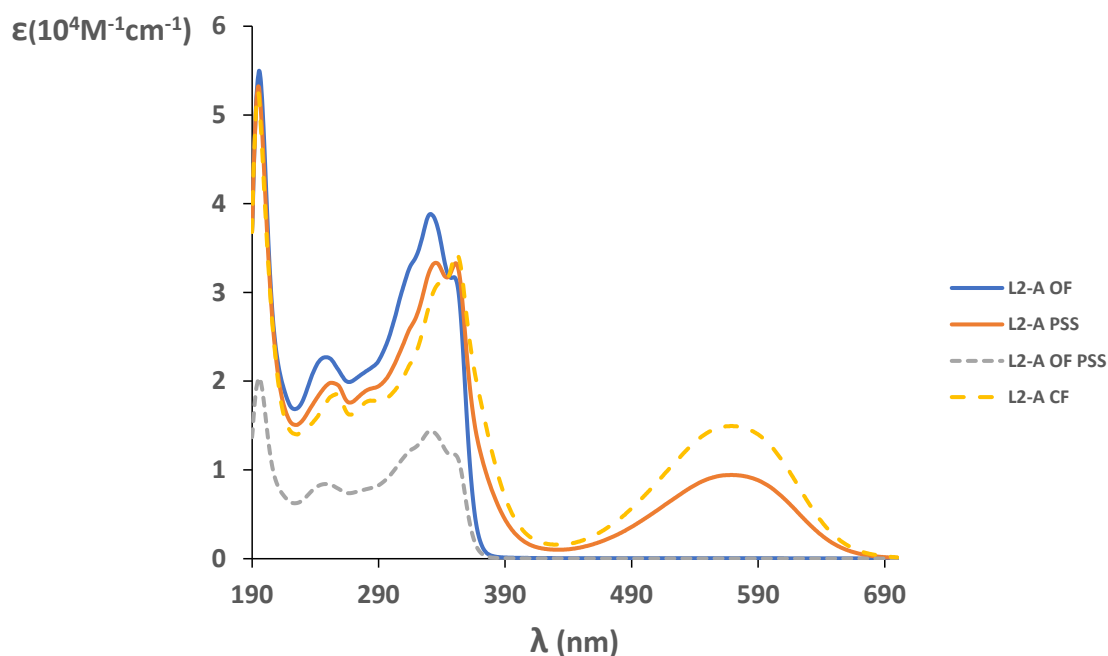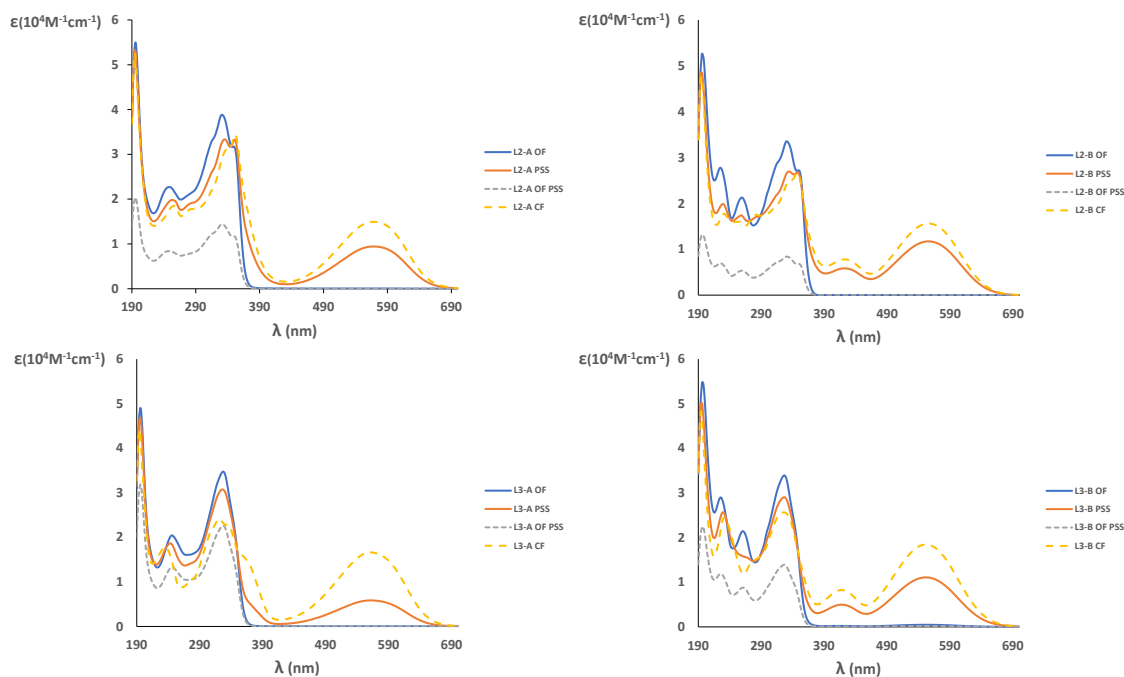
Figure 4.10. Calculated contribution of the **OF** and **CF** ligand isomers to the PSS and calculated spectrum obtained for the closed form.

Once the concentrations of both isomers and the molar absorptivity value of the species in both states (**OF** and **CF**) at 370 nm can be determined, as Table 4.4 shows, the next step is the calculation of the quantum yields of both processes. To do this, we decided to evaluate experimentally $\Phi_{C \to O}$, since it is a one-species process because only one of the species can generate the ring-opening process. Determination of the quantum yield is further facilitated due to the selective absorption of the closed form in the visible spectral region.

Table 4.4. *Molar absorptivities for **OF/CD-DTE** at 370 nm.*

Compound	ε OF at 370 nm ($M^{-1}cm^{-1}$)	ε CF at 370 nm ($M^{-1}cm^{-1}$)
L2-A	2140	18240
L2-B	1340	11130
L3-A	440	13700
L3-B	600	6090

This interconversion study was developed using an automated system, implemented in the research group at the University of Bordeaux, which is required to study multi-cycle switching and resulting potential fatigue. For a better understanding of the measurement, a scheme of the system is presented in Figure 4.11.
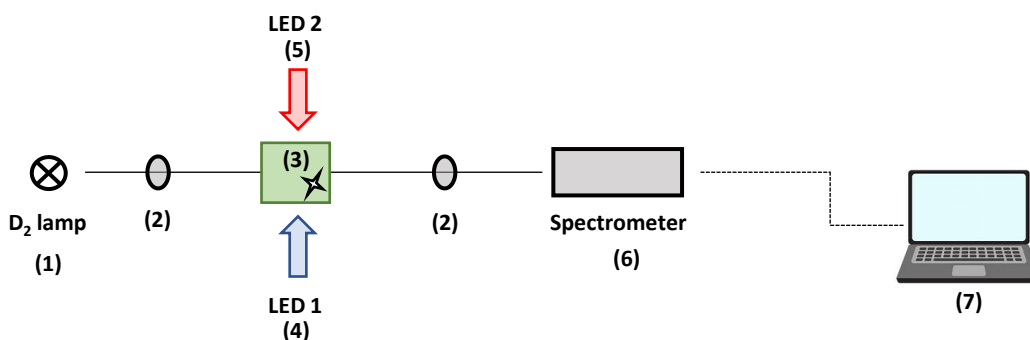
Figure 4.11. Automated electronic absorption spectroscopy system piloted in a Labview environment, involved a low intensity continuous monitoring light and high intensity LEDs for alternate excitation of each photochrome form.

This measurement-irradiation system consists of: **(1)** a low-intensity deuterium lamp, for continuous monitoring of the state of the photochrome; cell holder for the sample with magnetic agitation to assure homogeneous irradiation of the solution, **(2)** optical lenses to optimize monitoring light and recovery of transmitted light; **(3)** spectrometric cuvette; **(4)** LED for UV irradiation (λ = 370 nm), placed close to the sample so that the maximum emitted light passes through the cell containing the sample. The LED could be switched on and off and the duration of irradiation was controlled by Labview. Output energy was measured using a power meter (Coherent). (Note: While 370 nm is not an ideal excitation wavelength, it represents one of the shortest-wavelength affordable LED irradiation sources, and is considered adequate for the current study). **(5)** LED for visible (red) irradiation (λ = 595 nm) subject to same conditions as **(4)**; **(6)** an Aventis spectrometer with simultaneous detection across the UV-vis-NIR spectral domains (200 nm – 1150 nm; time resolution 3 ms). **(7)** PC piloting Labview which, via an in-house developed virtual instrument, could control LED pulse sequences, irradiation time (or threshold parameters), and recover data.

The main idea is to constantly measure the absorption spectrum of a sample, throughout each step of the irradiation cycle. The study of the photocycloreversion process was the first to be studied, because only one of the isomers (**CF**) responds to an irradiation of wavelength λ = 595 nm, facilitating obtaining the quantum yield of the photocycloreversion process ($\Phi_{C\rightarrow O}$). Before carrying out the measurement, the photon flux of the 595 nm LED must be known precisely. This photon flux can be calculated in two different ways. On the one hand, through chemical actinometry, according to the standard procedure developed by Hatchard and Parker in 1956[13], where conversion of a photochemical standard of known reactivity is used. Typically, this technique uses a stock solution of a ferrioxylate $Fe(C_2O_4)_3^{3-}$ complex, several aliquots of which are irradiated for a series of specific times with the light to be measured. After irradiation, a determined volume of a stock solution of phenanthroline is added. The photochemical reaction product reacts with the phenanthroline stock solution, generating a new coordination complex $Fe(phen)_3^{2+}$, which can be quantified by electronic absorption spectroscopy due to its characteristic MLCT band of known absorptivity, whose absorption maximum is at 510 nm. From a calibration line and subsequent calculation, the photon flux can be obtained. Limitations associated with this technique are the limited number of wavelengths at which the reaction quantum yield of the actinometer has been determined, as well as absorption of this reference. On the other hand, the incident irradiation photon flux can be measured from its power, divided by the energy associated with a photon of light of a given wavelength. In all cases, the volume of the irradiated sample and its concentration should be known. During the measurements, both

techniques were used, the second being the one used for the final calculation of the quantum cycloreversion yields. Once all the parameters were known, the various measurements were carried out. The ring-opening reaction kinetics for ligand **L2-A** is presented in Figure 4.12.
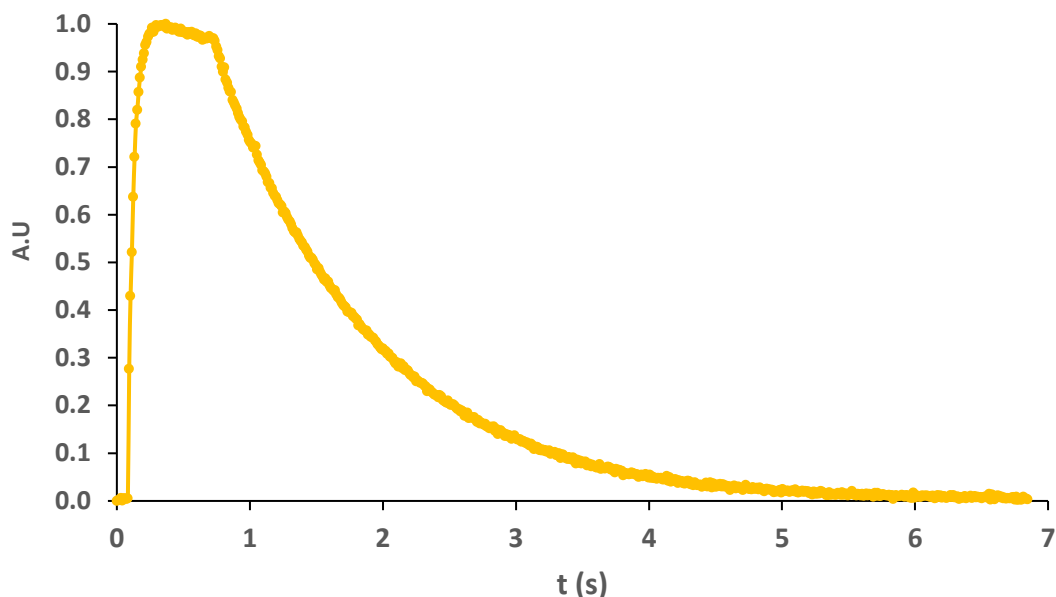
Figure 4.12. Cycloreversion kinetics for **L2-A** measuring at 569 nm (CH$_3$CN. $3.3 \cdot 10^{-5}$ M).

The $\Phi_{C \to O}$ values were calculated from monoexponential fits of the experimental data recorded when irradiating the closed form at 595 nm, using the following Equation 4.3.

$$y(t) = y_0 \times \exp\left(-\frac{\Phi_{C \to O} \times N_{hvt} \times \ln 10 \times \varepsilon_C(595) \times l}{V} \times t\right) + constant \qquad \textbf{Equation 4.3}$$

Where $y(t)$ corresponds to the absorption at a given time (t), while y_0 corresponds to the initial absorbance. N_{hvt} is the number of moles of photons going through the sample per second, l is the pathlength, t is irradiation time, V is the volume. The quantum yields of photocycloreversion were calculated for all the ligands following this same method. Table 4.5 shows the different values obtained. The values are consistent with the previously described properties of the ligands, where a more pronounced redshift was established for the closed isomers of the ligands **L2-A** and **L3-A**. The bathochromic shift reflects directly in the quantum yield value. The proximity of the absorption maxima for **CF L2-A** and **CF L3-A** to the used LED wavelength is consistent with higher quantum yield values than for **CF L3-A** and **CF L-B**.

Table 4.5. *Photocycloreversion quantum yields ($\Phi_{C \to O}$) for free DTE ligands*

Compound	L2-A	L2-B	L3-A	L3-B
$\Phi_{C \to O}$	0.083	0.027	0.045	0.021

Once the values of the $\Phi_{C \to O}$ are known, $\Phi_{O \to C}$ can be determined using data obtained at the PSS obtained from 370 nm irradiation and the corresponding values of $\Phi_{C \to O}$, C_O, C_C, ε_O, and ε_C, according to Equation 4.1. Table 4.6 presents the values obtained for $\Phi_{C \to O}$ and $\Phi_{O \to C}$ for the

synthesized DTEs. The data obtained show that the most efficient ligand for the open-to-close isomerization process at 370 nm is **L2-A**, while the least efficient is **L3-B**.

Table 4.6. *Summarizes table for photocyclization/cycloreversion quantum yields.*

Compound	C_O/C_C	ε_O (370 nm)	ε_C (370 nm)	$\Phi_{O \to C}$	$\Phi_{C \to O}$
L2-A	0.59	2140	18240	1.2	0.083
L2-B	0.33	1340	11130	0.66	0.027
L3-A	1.86	440	13700	0.76	0.045
L3-B	0.69	600	6090	0.31	0.021

The data obtained for the quantum yields of photocyclization and photocycloreversion of the synthesized DTEs in this project slightly exceed or maintain agreement with values obtained from the literature. These data evidence that for all the DTE ring-opening isomerization is more efficient than ring-closure at 370 nm by at least one order of magnitude, which is in agreement with the values reported in the literature for related DTEs (Table 4.7).

Table 4.7. *DTE photocyclization/photocycloreversion quantum yields.*

Compound	$\Phi_{O \to C}$	$\Phi_{C \to O}$
E-7	0.25	0.036
E-4	0.16	0.020
E-6	0.53	0.012
E-8	0.40	0.020
E-10	0.34	0.023

It is worth mentioning that the value obtained for the photocyclization reaction of the ligand **L2-A** is striking, this being $\Phi_{O \to C}$ = 1.2. This value cannot be supported by itself since it would imply that the efficiency of the unimolecular photoswitching reaction is over 1.0. This result can be rationalized if we take into account the possible generation of a reaction by-product, which would hamper the accurate determination of the PSS and, consequently, the determined quantum yield. As explained in the introduction, the generation of a by-product is possible due to a non-reversible cyclization of the DTE (Scheme 4.3). This reaction by-product can possess absorption bands similar to those of the photocyclization product with different molar absorptivities.
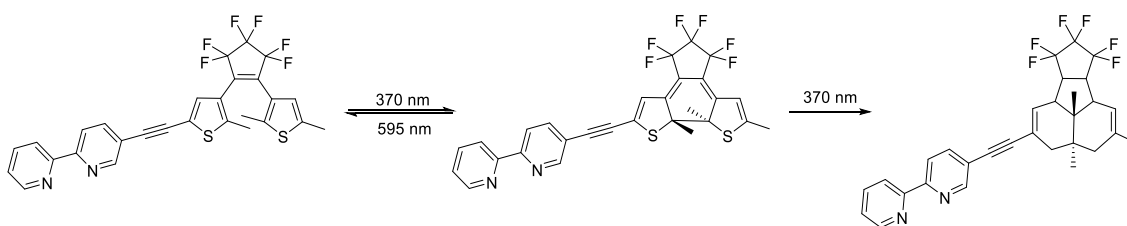
Scheme 4.3. Possible by-product for **L2-A**.

Once the efficiency of the photocyclization and photocycloreversion processes was studied, other aspects necessary for the creation of an effective molecular switch were studied. One of the essential properties of DTE ligands is their high fatigue resistance. Fatigue resistance indicates how many times a molecular switch can undergo an isomerization process without presenting significant decomposition (circa 20%). In this context, the synthesized ligands were studied. Both LEDs (370 nm and 595 nm) were programmed to irradiate the sample with

intervals of determined time between them, using the automated irradiation system described above. The process was monitored using the maximum absorbance of the characteristic band of the closed isomer in the PSS as a reference. First, the irradiation time required to reach the PSS of each sample using a 370 nm LED and the time required for the photocycloreversion process (595 nm LED) was calculated. Once the isomerization cycle time was determined, the system was programmed to alternate the irradiation of each LED. Figure 4.13 shows the resistance of **L2-A** over 50 isomerization cycles, which shows a significant decomposition after the first ten cycles since its decomposition exceeds 20% of the initial value.
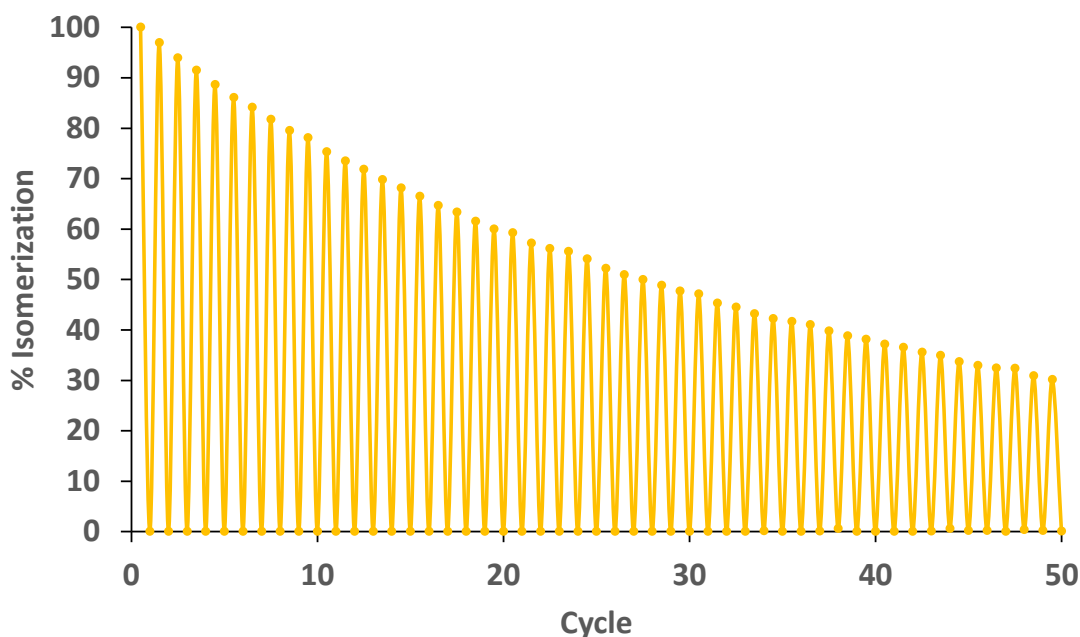
Figure 4.13. Photocyclization (λ_{irr} = 370 nm)-photocycloreversion (λ_{irr} = 595 nm) cycles of **L2-A**, showing photoinduced-decomposition in CH$_3$CN.

Fatigue resistance was further studied for ligands **L2-B**, **L3-A**, and **L3-B**. Figure 4.14 shows the representation of the maxima obtained for the PSS of each ligand in each isomerization cycle. It can be seen how the ligands with the alkyne group as linker (**L2-A** and **L2-B**) show a higher decomposition, obtaining values below 80% of the initial absorbance value after the first ten isomerization cycles. Ligand **L2-A** shows a progressive decomposition reaching values lower than 80% of the initial absorbance after 30 cycles. On the other hand, ligand **L3-B** seems the best candidate among the different synthesized ligands. Indeed, the stability of the ligand remains intact after the first 50 cycles, presenting a high fatigue resistance. A second measurement was performed, increasing the number of isomerization cycles to verify the results obtained. Figure 4.15 confirms that ligand **L3-B** maintained maximum absorbance for 100 cycles.
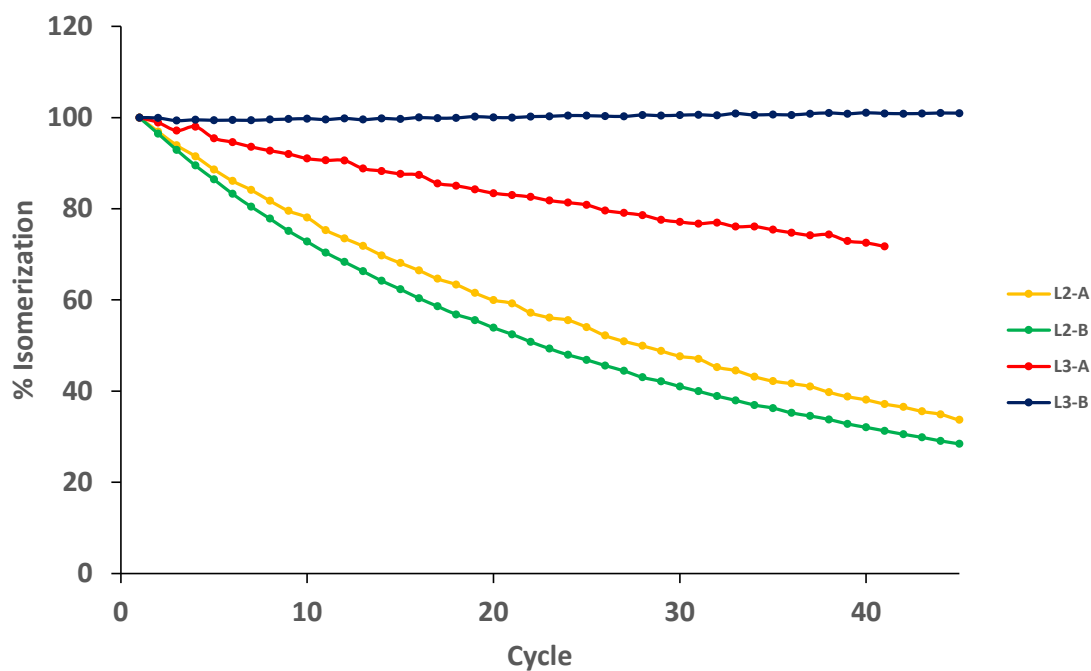
Figure 4.14. Absorption maxima in each isomerization cycle for the CF DTEs characteristic band.
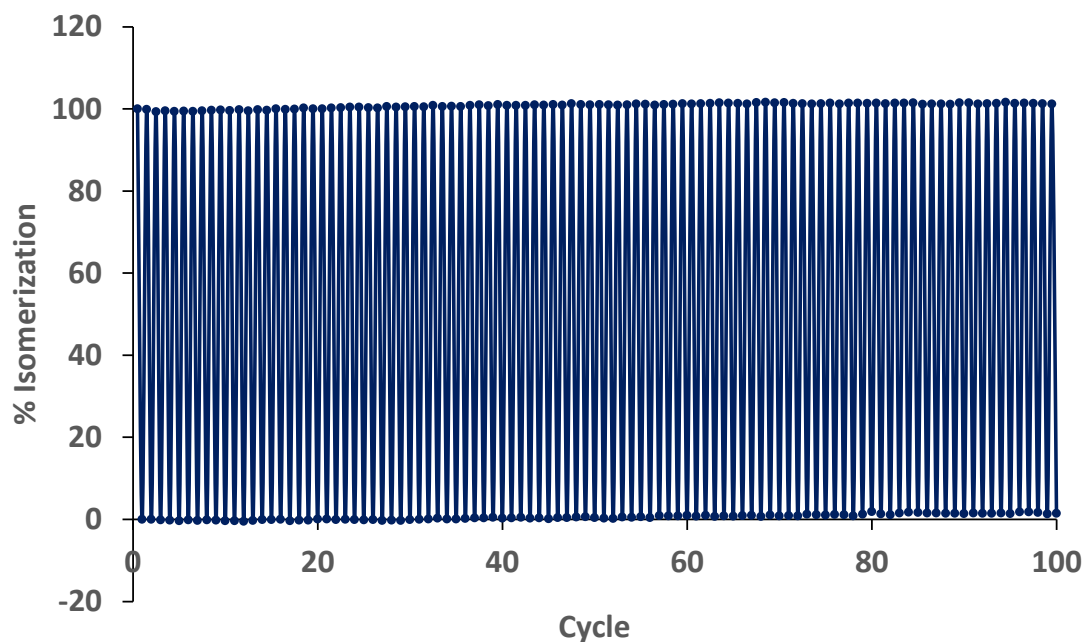
Figure 4.15. Photocyclization (λ_{irr} = 370 nm)-photocycloreversion (λ_{irr} = 595 nm) cycles of **L3-B**, showing high fatigue resistance in CH$_3$CN.

Another important aspect to determine the potential applications of a molecular photoswitch is to prove that the isomerization reactions are governed exclusively by a photochemical process. As explained in the introduction, there are two types of chromophores, type T and type P. DTEs (DAEs) are classified as type P chromophores, which generate the cycling and cycloreversion processes only through light irradiation. An experiment was designed to study the thermal stability of the metastable form of the ligands (**CF**). To carry out this experiment, 5·10^{-5} M solutions were prepared in toluene for each of the ligands. They were irradiated with UV light (λ = 370 nm) until reaching the PSS. Then, UV-Vis spectra were measured in 15-minute intervals at

a specified temperature for 10 hours. The measurement was replicated at different temperatures (30 °C, 40 °C, 50 °C and 70 °C) to monitor possible changes in the absorption spectrum. For an appropriate control of the temperature, a spectrometer with a sample chamber with a built-in Peltier was used from which the temperature of the cell of the UV-Vis cuvette is controlled. If the initial spectrum changes during the experiment, it would indicate that our DTE ligands have some thermochromic character, which would mean that the activation barrier between the DTE open and closed form is lower than expected. The results obtained did not show any thermochromic process of the DTEs, as shown in Figure 4.16 for **L3-B**. As shown in the graph, only an insignificant change in the spectrum of ultraviolet spectroscopy is observed, which is attributed to partial evaporation of the solvent due to prolonged exposure to a specific temperature. No isosbestic point was observed throughout the spectra obtained, thus confirming that only one species is absorbing, corroborating the absence of processes derived from temperature. Same experiments were carried out for the rest of the synthetized ligands, observing the same behavior as for **L3-B**.
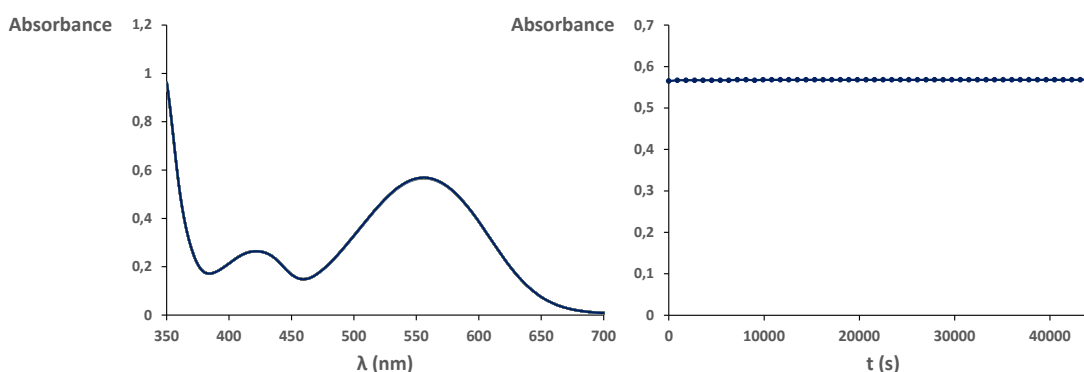
Figure 4.16. Electronic absorption spectrum of **L3-B** (PSS) in toluene (left) and absorbance at 556 nm as a function of time at 70°C.

Once the efficiency of the photocyclization/photocycloreversion processes had been studied, these processes were studied in greater detail using transient absorption (TA) spectroscopy on different time scales. This type of spectroscopy allows to follow, following excitation, molecular evolution in the fundamental (S_0) and excited (S_n) states in short times (sub-picosecond (sub-ps), picoseconds (ps) - nanoseconds (ns)).

Figure 4.17 shows a schematic representation of the system used to measure processes on the nanoscecond and sub-nanosecond times scales. (Note: ultrafast processes were measured on a different set-up following excitation with 50 fs pulsed and an alternative detection system[14]). It is a system that uses a wavelength tunable pulsed excitation (pump) & white light source (probe) with streak camera detection. Nd-YAG lasers equipped with OPG (30 ps FWHM pulse) or OPO (5 ns FWHM pulse) were used as the excitation source, exciting the lower energy absorption bands.

The white light probes the excited sample and gives information on differing absorption with respect to the molecule in the ground state (having removed contributions due to fluorescence, ground state absorption and background).

Pertinent processes are:

- Ground state bleaching (ground state depopulation: ground-state absorption is reduced → signal is negative)

- Stimulated emission located at the wavelengths of fluorescence (transition from excited singlet state to state basic singlet)
- Absorption of excited or transient states ($S_1 \rightarrow S_N$, $T_1 \rightarrow T_N$, other multiplicities of states is not excluded)
- Absorption of generated radical states

Thus, the streak camera makes it possible to record a complete matrix, creating a TA data map (signal intensity vs. wavelength vs. delay time) in a single experiment for a specific time range.
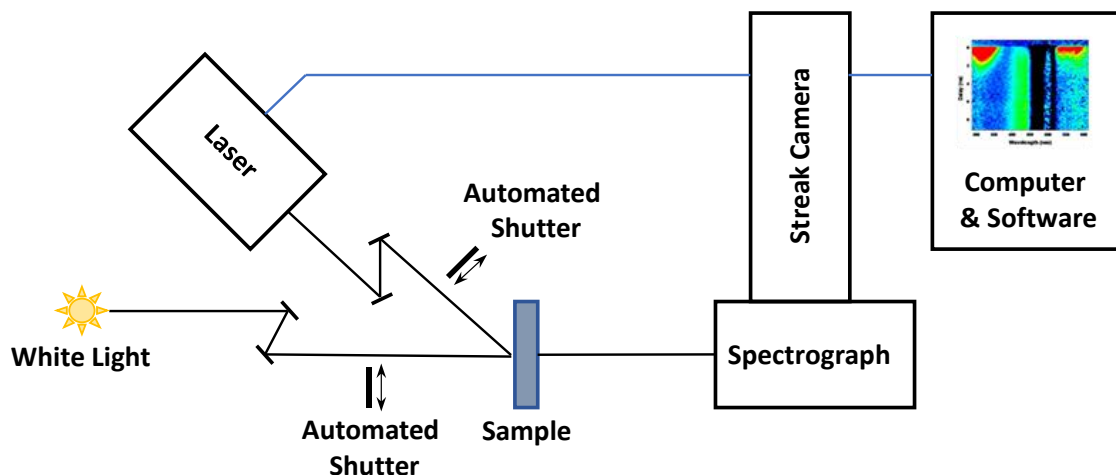
Figure 4.17. Representation of the TA system used for the study.[1]

The ultrafast study began by studying the cyclization process of the ligand **L3-B**, chosen for this study due to its high stability, both thermal and against the fatigue of the process. For this, **L3-B** sample was excited at an excitation centered at 345 nm (3.5×10^{-4}M in CH_3CN), in a 2 mm pathlength cell (with continuous flow from a reservoir of solution irradiated with a 1W CW power white LED to avoid photoproduct build-up). The spectral map presented in Figure 4.18 was obtained. Each spectrum obtained in this stroboscopic method corresponds to an incremental increase in delay time with respect to excitation. It is observed in Figure 4.18 how as the number of spectra increases (Y axis), there is a signal change in the region close to the maximum absorption of **CF-L3-B** (red-yellow-green). The color change is associated with a greater or lesser change in the signal collected, the change observed is substantial, indicating the rapid generation of **CF-L3-B**.

As the sample becomes populated with **CF** isomers, the signal's color will begin to change (yellow and green). From this measurement, it can be extracted that the process occurs mainly in the first moments of irradiation. Likewise, after observing that only a change occurs after excitation, it was possible to observe how the maximum absorption of displacement at the beginning of the experiment until it fell at 525 nm. This displacement may be due to fast dynamic solvation (Figure 4.18 right). The observed displacement is 500 cm^{-1} with a time constant of 280 fs. This effect can be associated with the constant orientational time constant of CH_3CN (260 fs) reported by Maroncelli.[15] The solvent's effect is the only observable change, indicating that only one state is visible after 30 ps, which remains constant after solvent reorganization. This

---

[1] Transient absorption spectroscopy studies were performed by Dr. Gediminas Jonusauskas at the "Institut Laboratoire Ondes et Matière d'Aquitaine" at the University of Bordeaux.

phenomenon is related to vibrational relaxation and a solvent reorganization around a new dipole on an excited molecule.
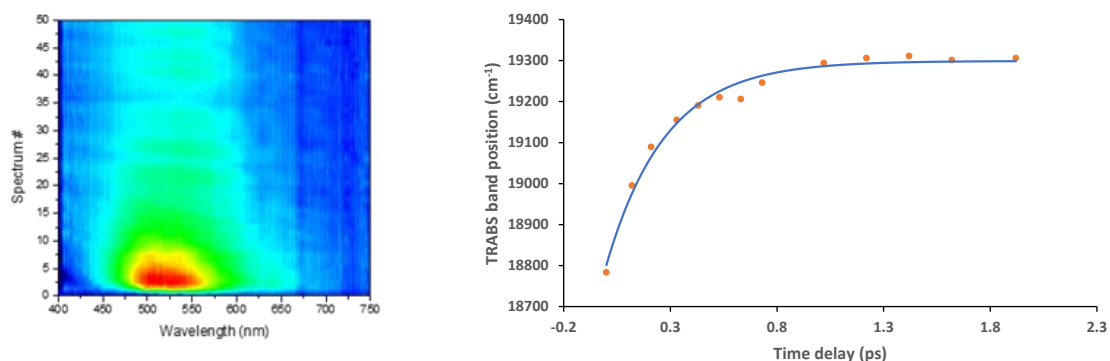
Figure 4.18. Transient absorption spectroscopy map for the photocyclization process for **L3-B** and effect of the solvation of CH_3CN on the absorption maximum.

The ring-closing kinetics (TRABS vs. Time delay) present in Figure 4.19 can be represented by the maximum absorption obtained after solvation. The kinetics obtained agrees with a level 2 kinetic, which shows a fast relaxation time constant (τ) of 1.1 ps. It could also be observed that the kinetic ratio at the maximum of TA, at the moment of excitation, after 10 ps, provided a **CF-L3-B** ratio close to 30%, which corroborates the quantum efficiency of photocyclization ($\Phi_{O \to C}$ = 0.31). Thus it can be concluded that in free ligand DTEs the fast photoreaction occurs in a few picoseconds accompanied by solvent reorganisation.
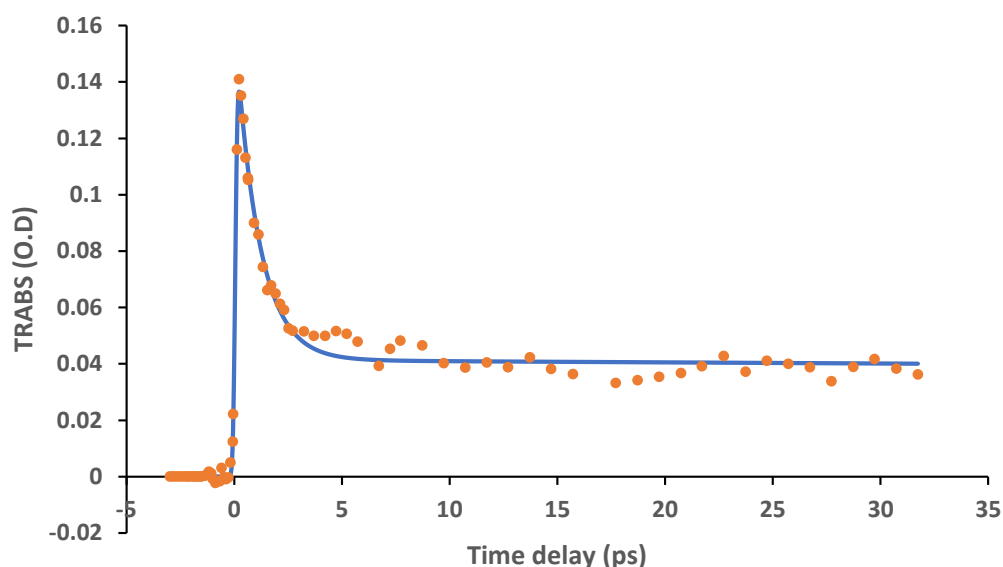
Figure 4.19. Optical difference kinetics observed at 525 nm associated with the photocyclization process.

In the same way that photocyclization was studied, measurements were made to study the process of photocycloreversion. The sample was irradiated with an excitation centered at 570 nm (while fresh closed sample was ensured by exciting the reservoir of stock solution using a 100 mW CW UV-LED). Decoloration of the molecule was observed, specifically the characteristic **CF-L3-B** band between 380-500 nm. Taking 440 nm as a reference, it was observed that the

system relaxed with a time constant of 1.2 ps, very similar to that observed for the photocyclization process (τ = 1.1 ps).
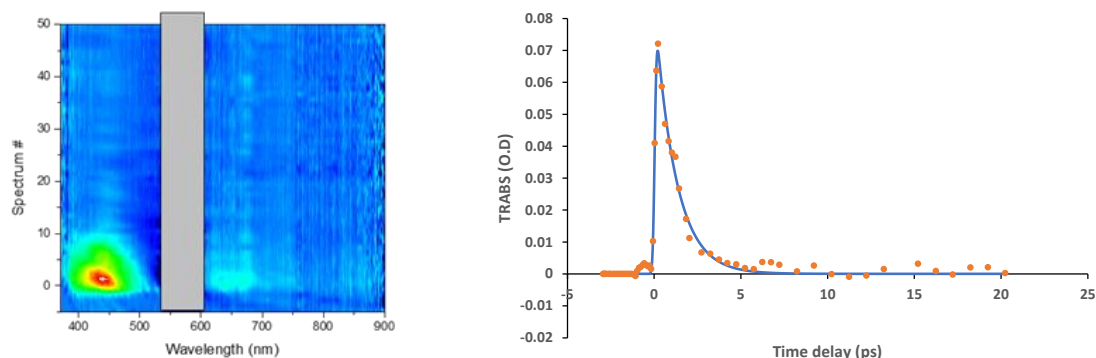
Figure 4.20. Transient absorption spectroscopy map for the photocycloreversion process for **L3-B** and photocycloreversion kinetics at 440 nm.

Figure 4.21 represents the disappearance of the excited state for the closed form of **L3-B**. A negative spectral characteristic can be observed for the molecule at 525 nm (Orange dots) that represents the change of the ground state for the closed isomer; that is, it explains how the photocycloreversion process changes for **L3-B**, which fits on the representation of the absorbance at 440 nm at each moment. Taking into account the relaxation of positive band with the time constant 1.2 ps (green curve), a tentative fit of the kinetic at 525 nm is presented above. The ratio of remaining negative signal at the end of kinetic to the maximum depopulation (most negative amplitude of blue curve) gives a value of 0.16, corresponding to the $\Phi_{C \to O}$ of the process.
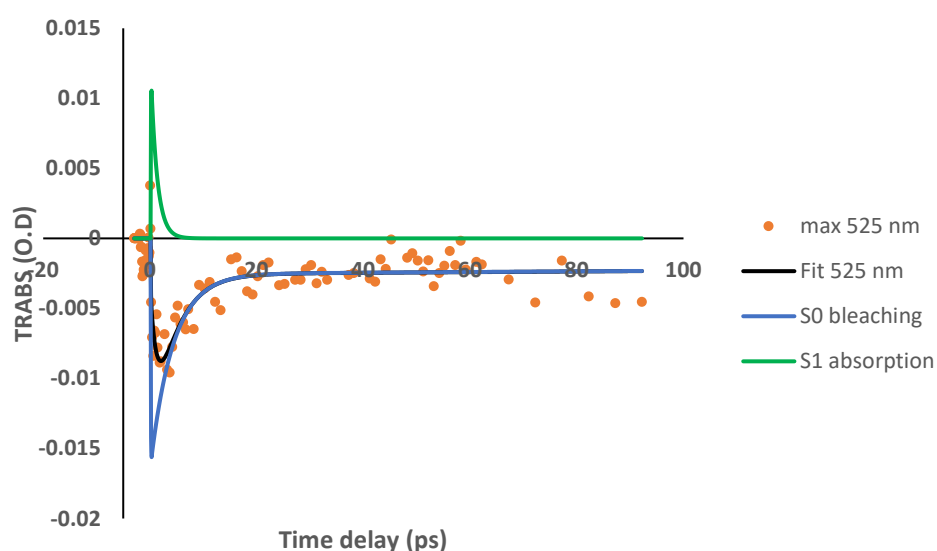
Figure 4.21. General representation of photocycloreversion kinetics for **L3-B**.

The MOPAC simulation of the potential surfaces of the ground and excited states when the distance between thiophene C atoms (next to methyls) is changed is presented in Figure 4.22. The energies of the transitions $S_0 \to S_1$ are represented as vertical red (**CF**) and black (**OF**) arrows.

The energies are overestimated slightly compared with the experimental data of PSS absorption. The energetic barrier on the ground state between closed and open form was found to be 1.8 eV which formally corresponds to 20000 K needed to overcome it, explaining the high thermal stability of **L3-B.**
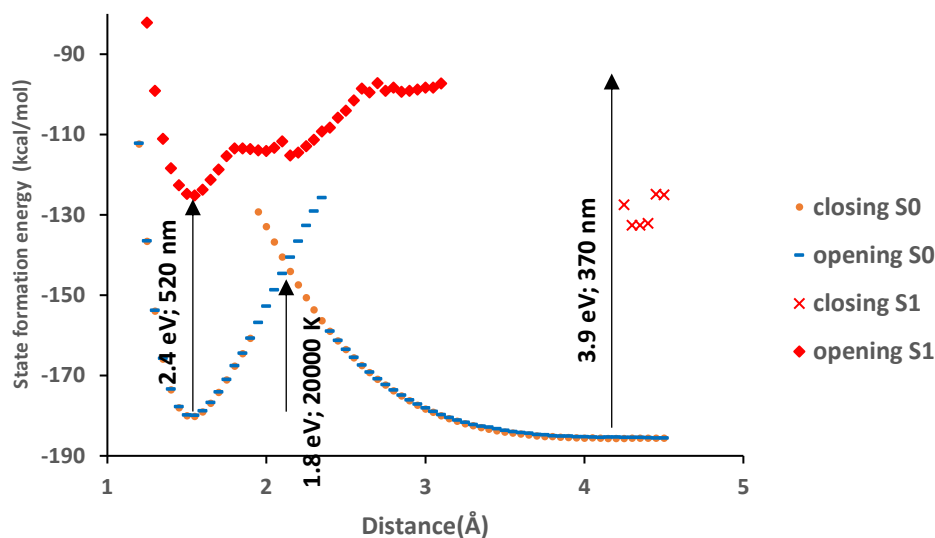
Figure 4.22. Potential energy surface for compound **L3-B**.

In this section it has been possible to study in detail the characteristics and properties of the different DTEs synthesized. On the one hand, the dithienylethene ligands synthesized for this project present the typical photochromic character described for DTE ligands, observing how the characteristic band of the ring-closed DTEs increases as the ring-opened form is irradiated. Photoreaction kinetics were carried out using different techniques (NMR spectroscopy and ultraviolet-visible spectroscopy) to determine the efficiency of the photocyclization and photocycloreversion processes. From these techniques, the percentages for the different species were calculated in the PSS, observing significant differences between them. Such differences were attributed to each ligand's absorption capacity (ring-closed form and ring-opened form) at the chosen irradiation length (λ=370 nm), and the corresponding quantum yields of the ring-opening and ring-closing process. The efficiency of the photocyclization and photocycloreversion processes and possible side-reactions were calculated using an automated spectrophotometer. In general, the values obtained for the quantum yields of both processes correlate to a greater or lesser extent with those described by other research groups in the literature. On the other hand, possible decomposition of the DTEs was studied through the isomerization cycle repetition, observing an evident decomposition in all of them except in the ligand **L3-B**, which demonstrated an outstanding resistance to decomposition due to fatigue. Finally, it was proved that the ligands obtained in this project do not have a thermochromic character, corroborating that the isomerization process of these molecular switches occurs only through light irradiation.

4

4.1.2 COMPLEXES

As seen previously in the introductory section, several known organometallic compounds contain a photoswitchable DTE ligand in their structure, which encounter practical use in various applications. Among them, a group that draws special attention is the set of compounds that contain a metal center in an octahedral geometry. Various examples are known where DTEs have different coordination natures to these metal ions, which can be direct coordination, as the case presented by Tian[16,17] and Pu[18] for an Ir(III) complex, or through highly coordinating groups, such as pyridines, as the examples presented by de Cola and Belser[19] among others for ruthenium or osmium compounds.

This section will present the various studies carried out for the complexes synthesized during this project. These organometallic complexes contain DTE ligands coordinated through bipyridine groups, thus obtaining cationic Ir(III) compounds. Scheme 4.4 shows the different compounds obtained using the ligands **L2-A**, **L2-B**, **L3-A** and **L3-B**.

Ir-L2-A   **Ir-L2-B**

Ir-L3-A   **Ir-L3-B**
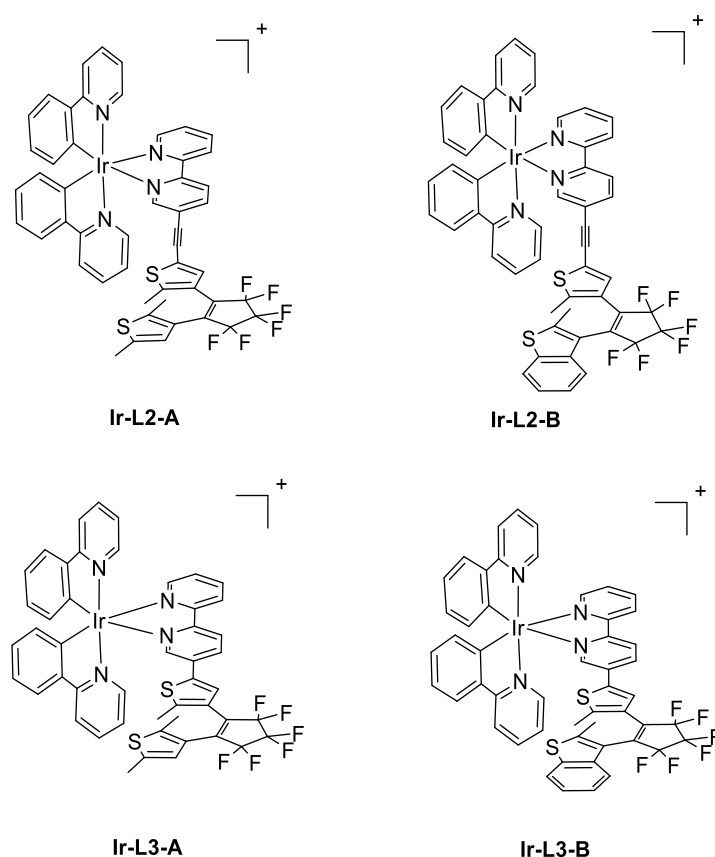
Scheme 4.4. Cyclometalated Ir(III) complexes synthesized in this work.

The efficiency of the photocycling and photocycloreversion processes for the synthesized compounds was studied, and the properties of the complexes obtained were examined. Taking into account the results obtained for the free ligands, the **Ir-L3-B** complex was taken as a model complex for these studies. This choice is due to the high resistance to fatigue in multiple photochemical cycles observed for the **L3-B** ligand, which was much higher than with the rest of the ligands, even knowing that the efficiency of the isomerization processes (photocyclization and photocycloreversion) was not ideal. The first study was intended to verify that the coordination of the DTE ligand to the metal center does not inhibit the photocycling process.

Indeed, fast metal-centred deexcitation processes may be competitive with the switching process.[20]

Irradiating a sample of **Ir-L3-B** in acetonitrile (λ_{ex} = 370 nm) lead to an instantaneous change from a colorless solution to a dark blue solution. This visual change was further measured using UV-Vis spectroscopy. Figure 4.23 shows the spectra obtained for the **OF Ir-L3-B** and **CF Ir-L3-B** complex after 300 seconds. In orange, the spectrum associated with the open form of the complex can be observed, while the blue spectrum shows the PSS where the closed-form of the complex is predominant after irradiation.
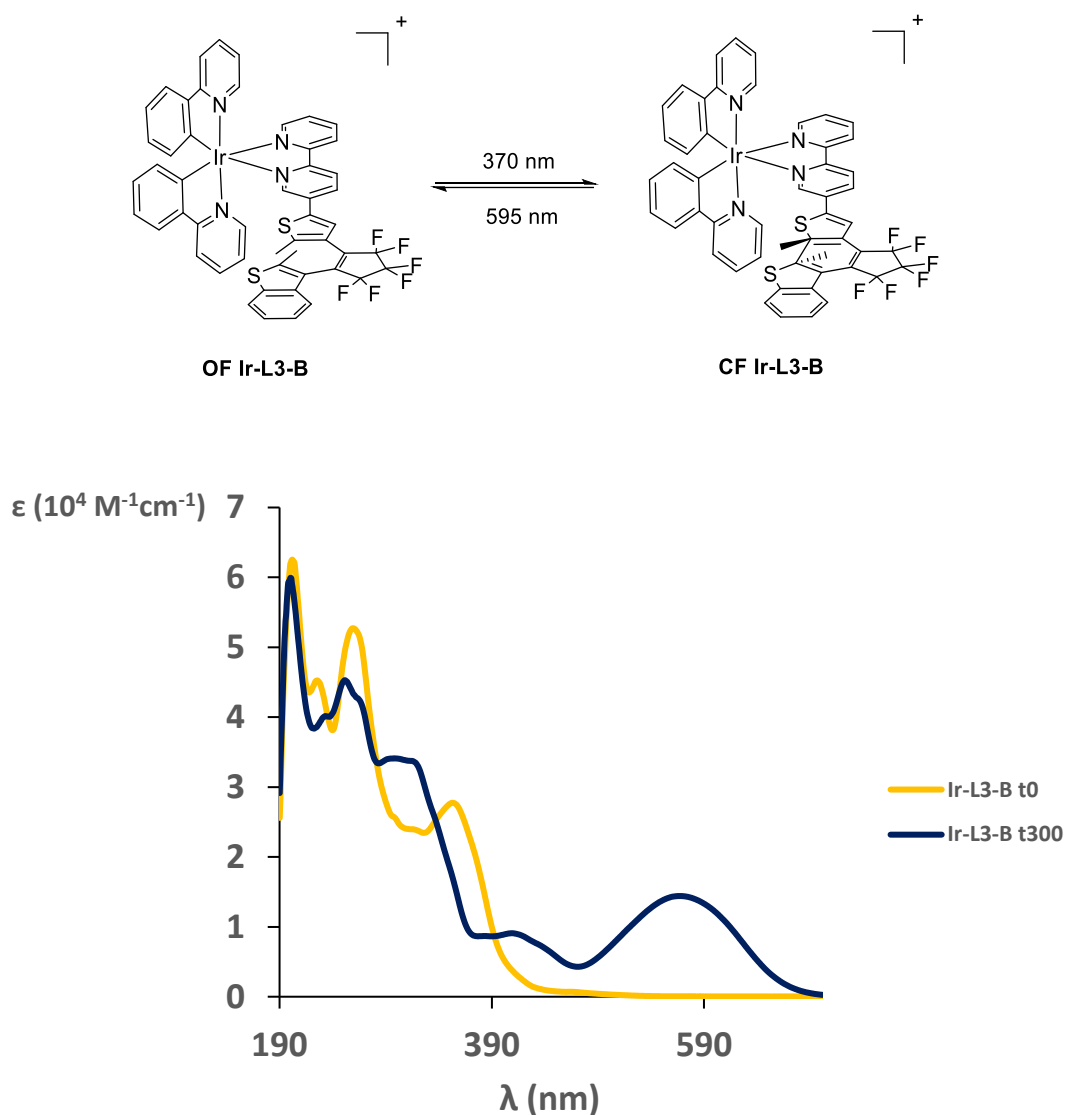
Figure 4.23. Top) Photoswitching of complex **Ir-L3-B**; Bottom) Electronic absorption spectra of open form and PSS (mainly closed form).

The photochromic behaviour of the complex **Ir-L3-B** was also studied by NMR spectroscopy, allowing the identification of the different isomers formed and their distribution in solution. Figure 4.24 shows the spectra corresponding to the **Ir-L3-B** complex before and after irradiation (370 nm). In red, the spectrum of complex **Ir-L3-B** in its open form is shown. Representative complex signals were marked in orange, chosen for the subsequent study of isomerization of the compound. The signals selected correspond to the methyl groups present **Ir-L3-B** (2.26 ppm

and 1.88 ppm). El desdoblamiento observado en diversas señales del ^{1}H-NMR spectrum paara **OF-Ir-L3-B** puede deberse a la generación de diastereoisomeros, tal y como se explicó en el Capitulo 3. The mixture of species obtained by irradiating the sample at 370 nm is shown in blue. It can be seen how the signals assigned to **OF Ir-L3-B** decrease as the irradiation time increases. While some signals disappear, new signals assigned to **CF Ir-L3-B** grow up, (marked in blue). The displacement of one of the methyls to higher fields and the other to lower fields is observed (2.01 ppm and 1.99 ppm), while a characteristic aromatic proton displaces to higher fields (6.29 ppm). The residual quantity of the **OF Ir-L3-B** in the PSS may be due to the possible parallel orientation of the coordinated DTE, or to the fact that **CF Ir-L3-B** is also capable of absorbing at 370 nm, activating the cycloreversion process.
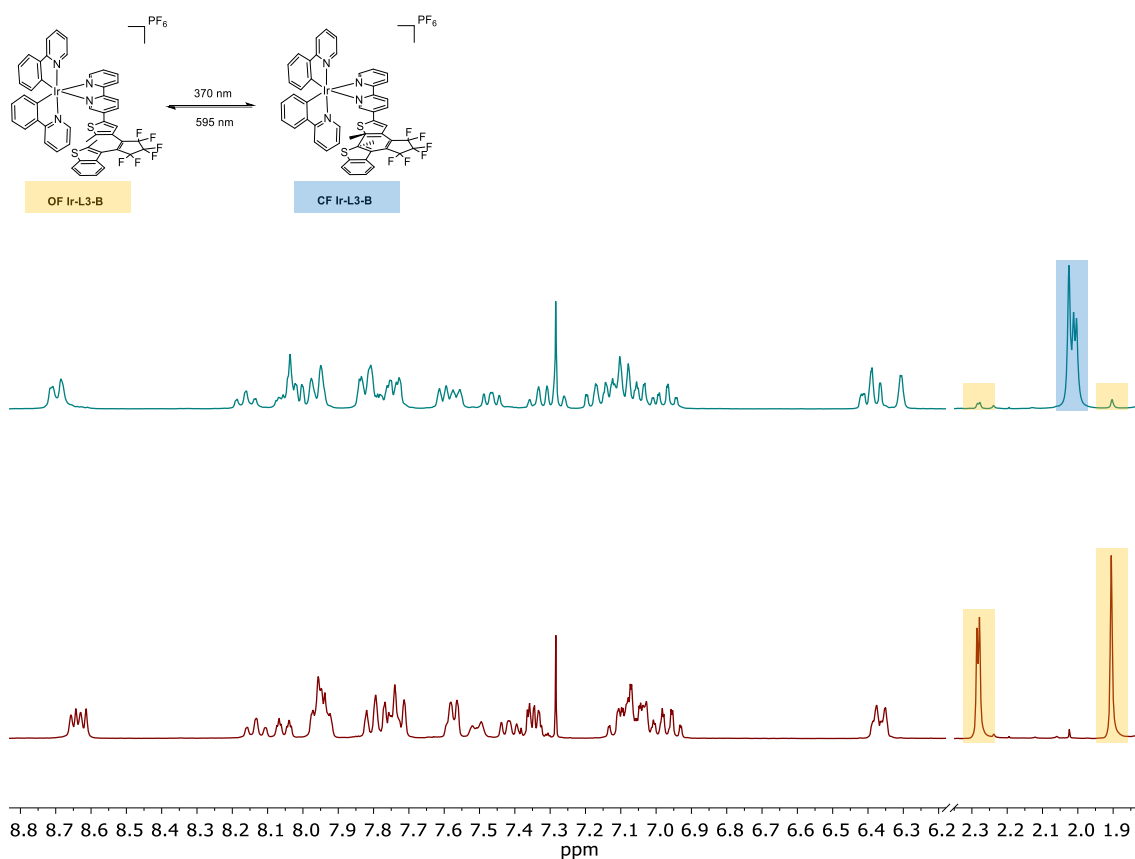
Figure 4.24. ^{1}H-NMR spectra of **Ir-L3-B** before and after photocyclization. (300 MHz, CDCl$_3$).

After having verified that the iridium complex **Ir-L3-B** showed photochromic behaviour, the same study was replicated for the rest of the complexes synthesized (Figure 4.25). All the complexes showed photochromic behaviour, following the same pattern submitted for **Ir-L3-B**. It is observed, as in the free DTE ligands, how the bands that the different complexes present in their open form are centered in the UV region (250-400nm). When the complexes are irradiated with UV light (370 nm), the appearance of new bands is observed in the region around 590 nm.
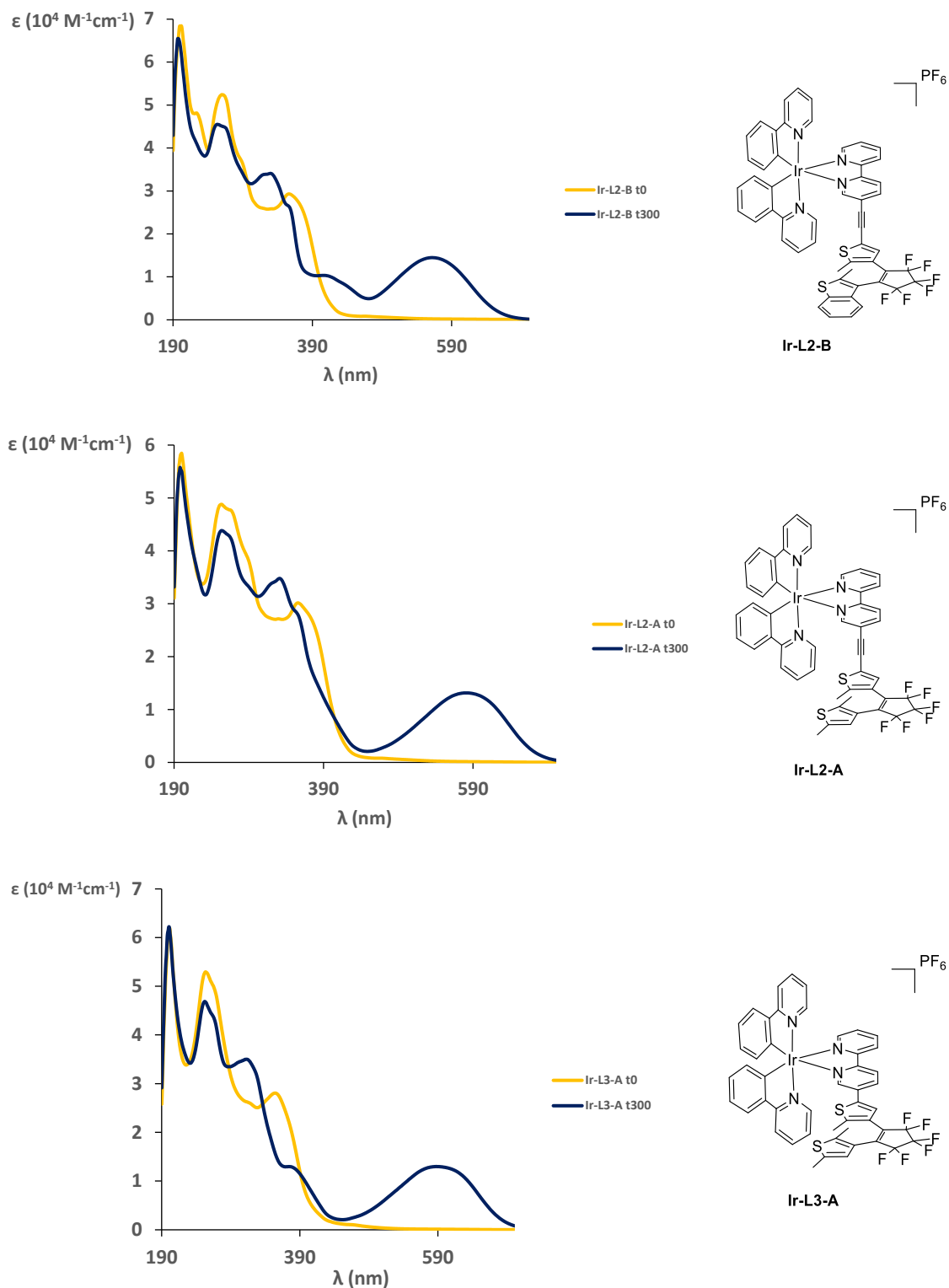
Figure 4.25. Electronic absorption spectra of **Ir-L2-A**, **Ir-L2-B** and **Ir-L3-A** before (orange line) and after (blue line) irradiation.

The similarities described above can be better seen in the ligands by observing the stacked absorption spectra as a function of the isomer (open or closed). The coordination of the ligands to the metal centers does not change the trend observed for the free ligands studied. The more significant bathochromic effect previously present in the ligands with the non-coordinating

thiophene compared to the ligands with the non-coordinating benzothiophene is again present (Figure 4.26).
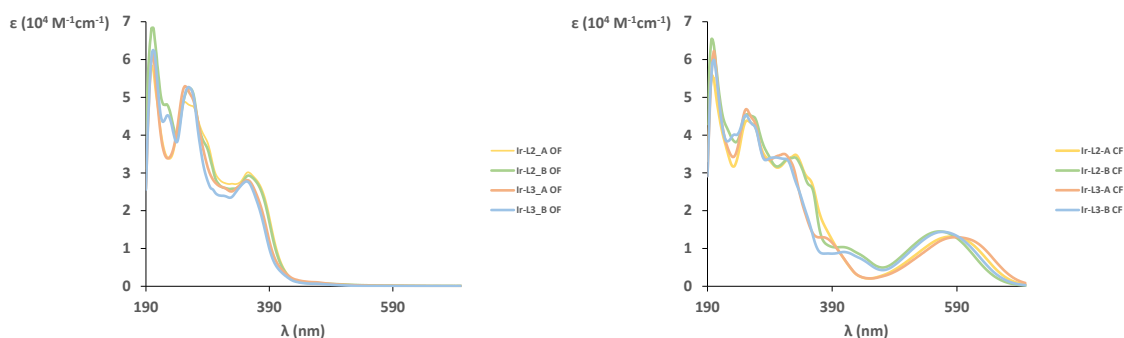
Figure 4.26. UV-Vis spectra of synthesized DTE complexes: left- **OF** and right- **CF**(PSS). ($5 \cdot 10^{-5}$ M solution in CH_3CN).

Differences in the absorption maxima are observed, comparing the spectra obtained for the free ligand **L3-B** and its corresponding iridium complex. The **OF Ir-L3-B** complex exhibits a red-shift of the signal at 327 nm for the free ligand, towards longer wavelengths (359 nm). This effect is also observed after the cyclization reaction of **CF Ir-L3-B** (552 nm **L3-B** → 567 nm **Ir-L3-B**).
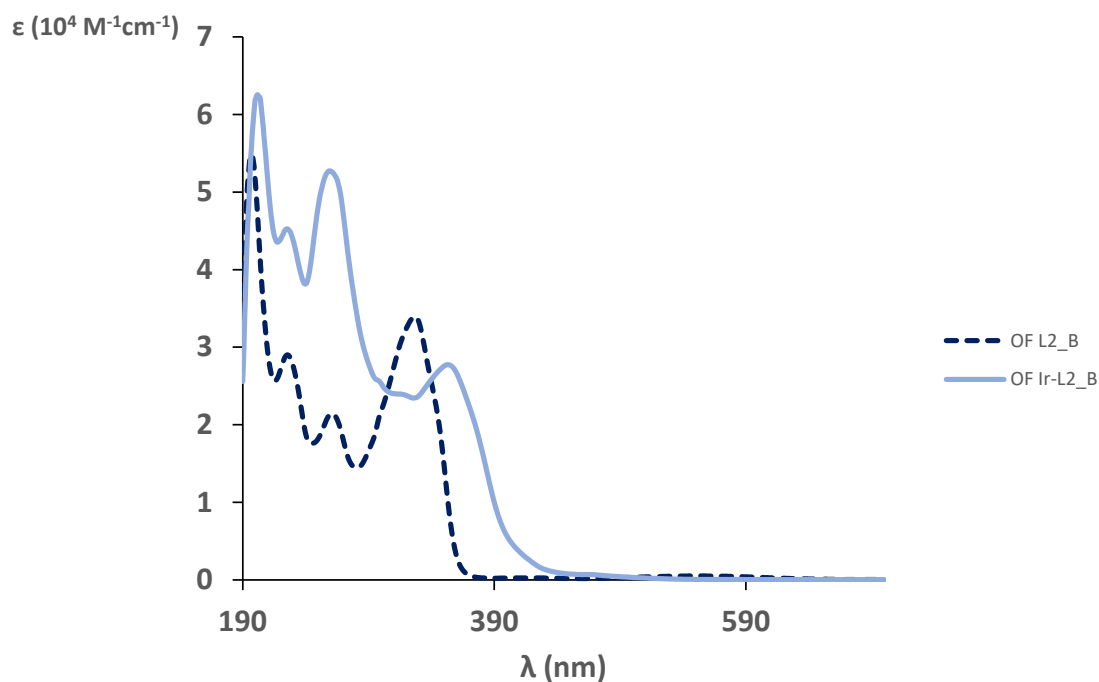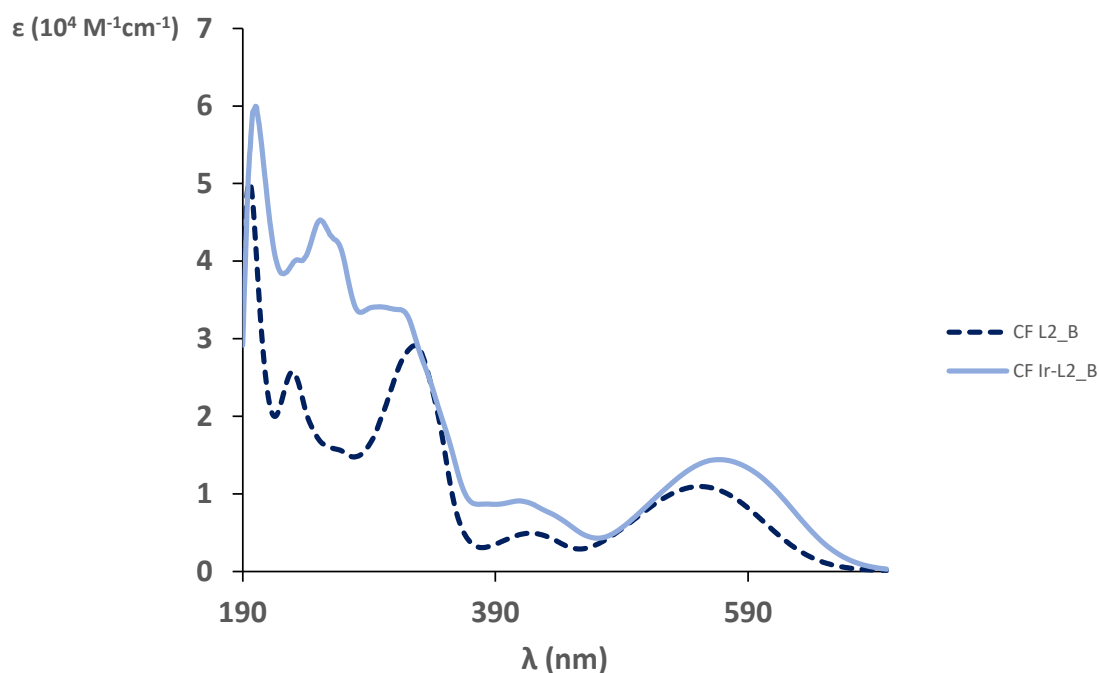
Figure 4.27. UV-Vis spectra comparing free ligand **L3-B** and iridium complex **Ir-L3-B** in open form (above) and closed form (PSS; below).

Table 4.8 summarizes the data obtained for all the compounds synthesized. The red-shift character present in the **Ir-L3_B** complex is confirmed after comparing the results obtained for the absorption maximum of the band of closed metal isomers located in the ultraviolet spectrum's 560-580 nm region.

Table 4.8. Summarised table for UV-Vis absorption band shifting.

Entry	Compound	λ OF-isomer maxima (nm)	λ OF-isomer maxima (cm⁻¹)	ε OF-isomer maxima (M⁻¹cm⁻¹)	λ CF-isomer maxima (nm)	λ CF-isomer maxima (cm⁻¹)
1	Ir-L2-A	356	28090	30160	581	17210
2	Ir-L2-B	356	28090	29300	562	17790
3	Ir-L3-A	354	28250	28060	588	17010
4	Ir-L3-B	353	28330	27720	567	17640

Figure 4.28 shows the progressive changes in the absorption spectra of complex **Ir-L3-B** in acetonitrile (c = 5×10^{-5} M). The absorption maximum of compound **OF Ir-L3-B** was observed at 353 nm ($\varepsilon = 2.8 \times 10^4$ L·mol⁻¹·cm⁻¹), which was attributed, similarly to the free ligand, to a $\pi \rightarrow \pi^*$ transition. Upon irradiation with 370 nm UV light, the colorless solution turned dark blue, and a new visible absorption band centered at 567 nm ($\varepsilon = 1.44 \times 10^4$ L·mol⁻¹·cm⁻¹) emerged while the original band with maxima at 353 nm decreased, indicating the formation of the closed-ring isomer **CF Ir-L3-B**, reaching with the violet spectrum (300 s) to the PSS.
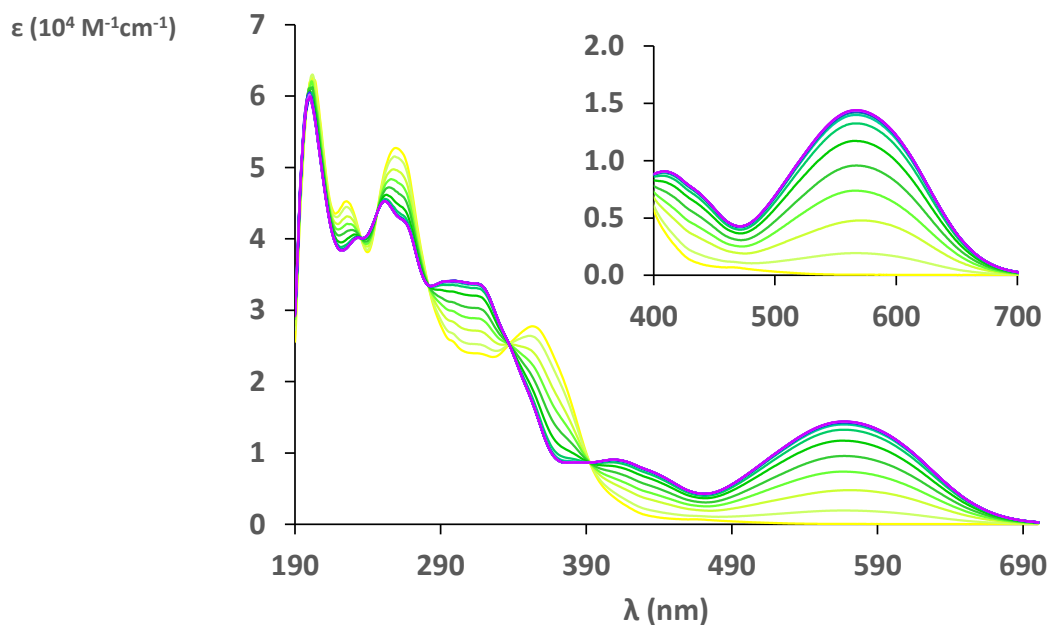
Figure 4.28. UV-Vis spectra of ligand **Ir-L3-B** upon prolonged irradiation times (λ_{ex}= 370 nm; $5 \cdot 10^{-5}$ M solution in CH$_3$CN).

The values obtained for the maximum absorption of the characteristic CF-band for the iridium compound were represented for each measurement time to study the required time to reach the PSS in each case, obtaining the graph shown in Figure 4.29. It can be seen that the observed behavior for free ligands differs significantly from the one observed for complexes. In the case of free ligands, those aligned with the alkyne linker reached an equilibrium between species faster, while the ligands with the direct bipy-DTE link required a longer irradiation time. Meanwhile, in the case of iridium complexes, this behavior is reversed. **L3** family complexes reach species equilibrium in 20 seconds, while alkyne homologs (**Ir-L2**) take twice as long (40 s).
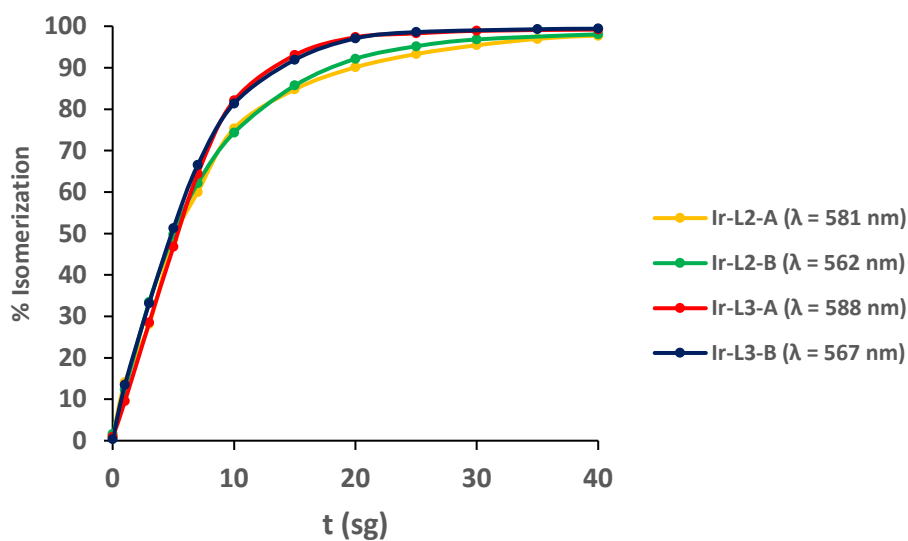
Figure 4.29. Percentage of isomerization of the **CF** versus time plot obtained for the **OF → CF** isomerization process of synthesized DTE complexes. ($5 \cdot 10^{-5}$ M solution in CH$_3$CN, irradiation at 370 nm).

Next, the composition of the PSS is being studied. As described before for the free ligands, to accurately express the rate of the photocyclization reaction, the proportions of the different species in the PSS, and the molar absoptivity of the pure **CF** isomer must be known. The composition of the PSS was obtained through ^{1}H-NMR spectroscopy, and it is explained in detail for **Ir-L3-B**. A 0.027 M solution of the **Ir-L3-B** was irradiated at 30-minute intervals with a Kessil Led Photoredox PR160 lamp (370 nm; 43 W) with an intensity setting of 75%. Figure 4.30 shows the stacking of ^{1}H-NMR spectroscopy obtained throughout the kinetic study. In red, the spectrum obtained for the ring-opened **Ir-L3-B**. The signals corresponding to the methyl of the molecule (marked in orange, 2.26 ppm doublet, and 1.88 ppm singlet) were taken as reference signals to control the isomerization process efficiently. As the sample was irradiated, it was possible to observe how the signals marked in orange corresponding to **OF Ir-L3-B** decrease while indications of a new species are noted in the aliphatic region. The growing of new signals associate to **CF Ir-L3-B** can be observed throughout the entire ^{1}H-NMR spectrum, the singlet located at 6.29 ppm being one of the clearest signals. This signal is assigned to the aromatic proton of the thiophene of the coordinating branch of the ligand **L3-B**, which moves to higher fields after the isomerization process. The PSS is sown in the violet spectrum, where the signals of the **OF Ir-L3-B** methyls have almost completely disappeared. Instead, a singlet (2.01 ppm) and a doublet (1.99 ppm) can be clearly seen corresponding to the ring-closed isomer. Integrating the signals obtained for the PSS, the proportions of the different isomers are obtained.
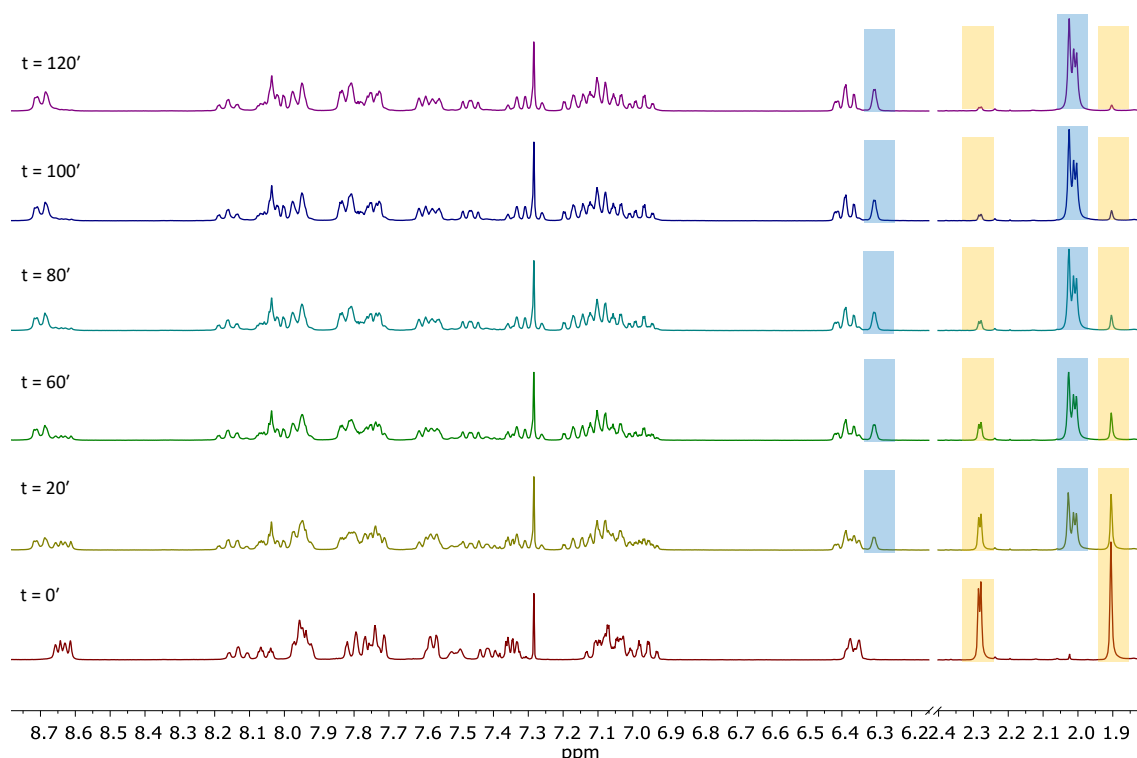
Figure 4.30. ^{1}H-NMR spectra of **Ir-L3-B** after different irradiation times (0.027 M solution in CDCl$_3$).

Table 4.9 shows the percentages calculated for the free ligands and the organometallic complexes. As a general trend, metallic complex contributions to the PSS are higher than free ligands. Based on the data obtained for the **Ir-L3-B** model complex, the the **CF Ir-L3-B** isomer is the predominant species at the PSS. This result differs from the one obtained for its free ligand **L3-B**, where only 59% of the solution molecules were in the **CF**. This different behavior may be because the ring-closed form of the complexes absorb fewer photons at the irradiation

wavelength than the open form, promoting an equilibrium in which the proportion of closed isomers is bigger. On the contrary, as previously observed for the free ligands, both isomers have very similar molar absorptivity coefficients at 370 nm.

Table 4.9. Photostationary state (PSS) calculated ratios for DTE compounds.

Compound	[M]	mol	mol OF (PSS)	mol CF (PSS)
L2-A	0.053	$2.67 \cdot 10^{-5}$	$0.99 \cdot 10^{-5}$ (37%)	$1.68 \cdot 10^{-5}$ (63%)
Ir-L2-A	0.018	$0.91 \cdot 10^{-5}$	$0.06 \cdot 10^{-5}$ (6%)	$0.86 \cdot 10^{-5}$ (94%)
L2-B	0.050	$2.51 \cdot 10^{-5}$	$0.63 \cdot 10^{-5}$ (25%)	$1.88 \cdot 10^{-5}$ (75%)
Ir-L2-B	0.024	$1.21 \cdot 10^{-5}$	$0.02 \cdot 10^{-5}$ (2%)	$1.19 \cdot 10^{-5}$ (98%)
L3-A	0.055	$2.79 \cdot 10^{-5}$	$1.81 \cdot 10^{-5}$ (65%)	$0.98 \cdot 10^{-5}$ (35%)
Ir-L3-A	0.016	$0.835 \cdot 10^{-5}$	$0.03 \cdot 10^{-5}$ (3%)	$0.81 \cdot 10^{-5}$ (97%)
L3-B	0.052	$2.61 \cdot 10^{-5}$	$1.07 \cdot 10^{-5}$ (41%)	$1.54 \cdot 10^{-5}$ (59%)
Ir-L3-B	0.027	$1.40 \cdot 10^{-5}$	$0.07 \cdot 10^{-5}$ (5%)	$1.33 \cdot 10^{-5}$ (95%)

Knowing the values of each species at the PSS, the theoretical UV-Vis spectra of the closed isomers are estimated for the iridium complex **Ir-L3-B** (Figure 4.31). The yellow spectrum corresponds to the theoretical spectrum of the ligands in their full closed-form, while blue shows the DTE **OF** spectrum. Additionally, in orange and grey, the closed DTE fraction and opened DTE fraction's contribution to the spectrum obtained in the PSS, respectively, is presented. The difference of band's intensity between the PSS absorption spectrum (orange) and the theoretically calculated **CF** spectrum (dashed yellow line) is minimal, corroborating the large contribution of the **CF**-isomer at the PSS. After calculating the theoretical spectra for the **CF Ir-L3-B**, the same calculation was performed for the rest of the complexes, as shown in Figure 4.31.
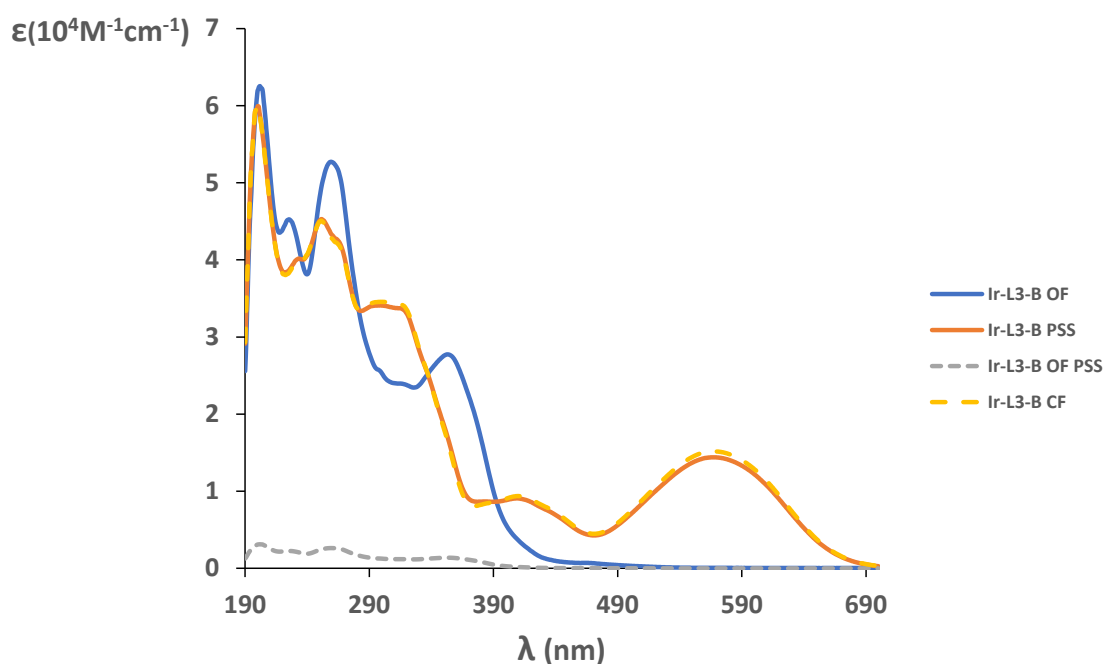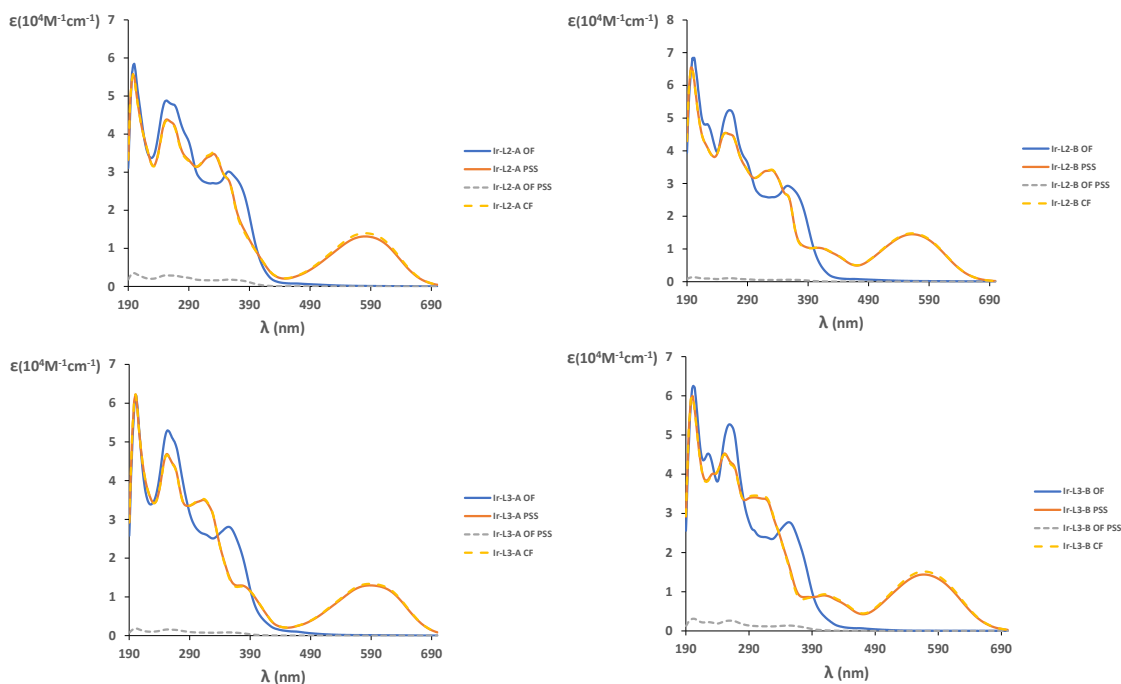
Figure 4.31. Calculated contribution of the **OF** and **CF** complex isomers to the PSS and calculated spectrum obtained for the closed form.

Having demonstrated that the new complexes with DTE fragments in the structure possess the characteristic photochromic character of the dithienylethenes switches and their behavior in the PSS was studied (giving the percentage of each of the isomers at equilibrium) we proceeded to study the efficiency of the photocyclization and photocycloreversion processes for these compounds. For this, using the same system for calculating the quantum isomerization yields for the free ligands, the corresponding experiments were carried out for the iridium complexes. From the measurements carried out, it was possible to obtain the curve of the ring-opening for the **Ir-L3-B** complex, shown below in Figure 4.32.

176
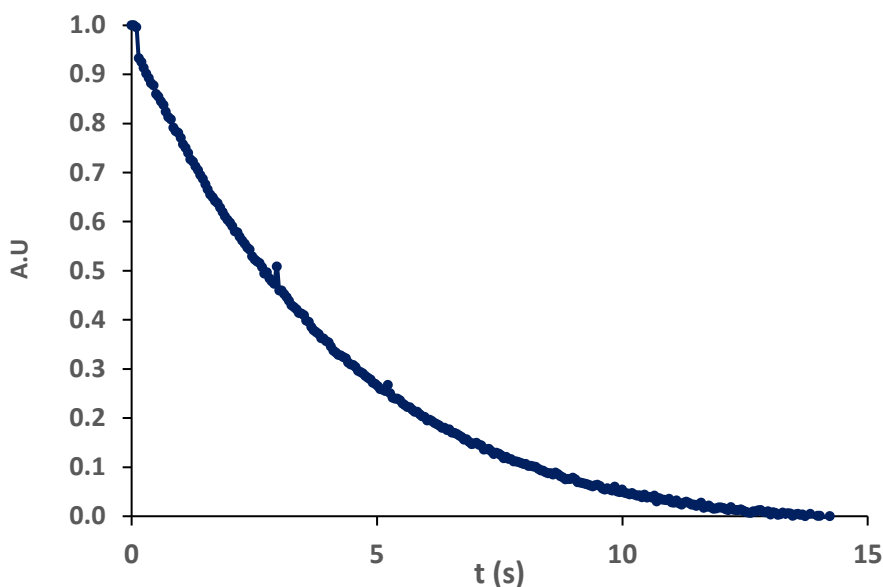
Figure 4.32. Cycloreversion kinetic for **Ir-L3-B** (CH$_3$CN, 1.9 · 10^{-5} M).

From monitoring the opening process of the DTE fragment, the values of the quantum yield can be obtained. The same strategy used for free ligands was followed. It consists of initially evaluating the photocycloreversion process taking into account that only one process is involved during visible irradiation. The value obtained for the photocycloreversion quantum yield for the **Ir-L3_B** was $\Phi_{C\rightarrow O}$ = 0.017. This result does not differ substantially from that obtained for the free ligand **L3_B** ($\Phi_{C\rightarrow O}$ = 0.021), which implies that the coordination of the DTE fragment to the iridium metal center did not imply significant changes in the photocycloreversion process for this specific case. The Equation 4.1, shown above, was used to calculate the cyclization quantum yield, obtaining a value of $\Phi_{O\rightarrow C}$ =0.12. This last process does present a significantly lower value than that obtained for the free ligand ($\Phi_{O\rightarrow C}$ = 0.31). A comparison of the different values for the isomerization quantum yields obtained for all the complexes, following the same procedure described for **Ir-L3_B** is presented in Table 4.10. The values obtained for $\Phi_{C\rightarrow O}$ and $\Phi_{O\rightarrow C}$ of **Ir-L3_B** complex are significantly lower than those obtained for the rest of the complexes. Additionally, it is appreciated that the complexes that incorporate the non-coordinating thiophene 2,5-dimethylthiophene show greater efficiency in both processes than the ones with the non-coordinating benzothiophene. Comparing the results obtained with the examples described in the literature for octahedral iridium complexes that incorporate DTE fragments in their structure, it can be concluded that the synthesized complexes generally present greater efficiency in the photocycling and photocycloreversion processes, since the bibliographic values for the compound Ir[(py-DTE)$_2$(acac)] are $\Phi_{O\rightarrow C}$=0.2 for the photocycling process and $\Phi_{O\rightarrow C}$=0.01 for the photocycloreversion process.[21]

Table 4.10. *DTE organometallics photocyclization/photocycloreversion quantum yields*.

Compound	C_O/C_c	ε_O (370 nm)	ε_C (370 nm)	$\Phi_{O\rightarrow C}$	$\Phi_{C\rightarrow O}$
Ir-L2-A	0.064	28000	18640	0.70	0.067
Ir-L2-B	0.020	27380	14600	0.66	0.025
Ir-L3-A	0.031	23980	12600	0.78	0.046
Ir-L3-B	0.053	22420	8360	0.12	0.017

As described before for the **L3-B** ligand, the processes for the corresponding iridium complex (**Ir-L3-B**) were studied by transient absorption spectroscopy. Figure 4.33 shows the study carried out for the photocyclization process, using an excitation of 440 nm in a picosecond regime. As can be seen in the map, following the explanations made previously, different changes in the spectrum are observed as a function of the relaxation time. On the one hand, in the 350-375 nm region, we can observe a negative signal (blue color), corresponding to the fading of the ground state (S$_0$) of the molecule in its open form. Similarly, a new positive signal appears at the same time in the 450-500 nm region. This new signal is associated with a ^{3}MLCT excited state. Finally, with a delay time of 30 ns, a new absorption band can be seen in the region of 550-600 nm. This last band is the one that was associated with the generation of the closed-form of the complex (**CF-Ir-L3-B**). In the blue spectrum, it can be seen that at 6 ns, the spectrum obtained shows the band generated by the excitation of the metal, while as the relaxation time increases, it generates the orange spectrum, collected at 45 ns, which agrees with the closed-form of **Ir-L3-B**.[2]

---

[2] Transient absorption spectroscopy studies were performed by Dr. Gediminas Jonusauskas at the "Institut Laboratoire Ondes et Matière d'Aquitaine" at the University of Bordeaux.
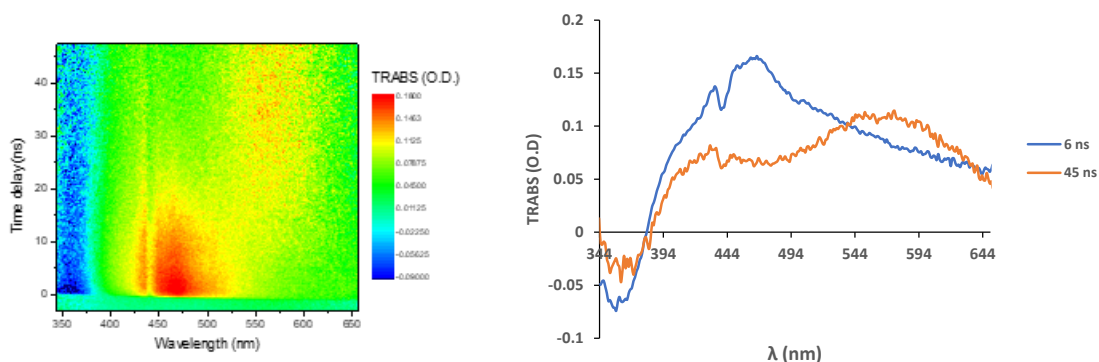
Figure 4.33. Transient absorption spectroscopy map for the photocyclization process for **Ir-L3-B**

From these data, it has been possible to represent the kinetics of both processes (MLCT excitation and photocyclization), represented in Figure 4.34. The global fit of the whole map produces the value of the time constant associated with the decay of ^{3}MLCT and the formation of the closed-form equal to 23 ns. Finally, it is evident that the photocyclization process of the **Ir-L3-B** complex occurs in two consecutive processes. Photocyclization begins with the excitation of S_0 to ^{1}MLCT. This excited state relaxes through ISC to ^{3}MLCT in a time of 200 fs, finally relaxing to the S_0 state of the closed-form of the complex in 23 ns.
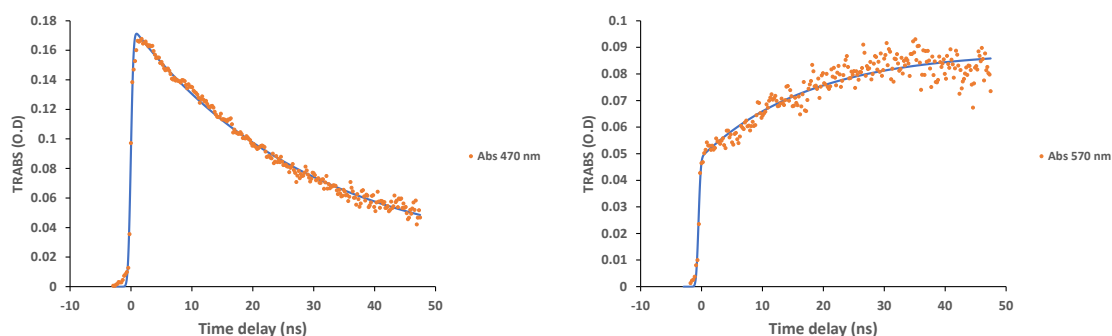
Figure 4.34. 2 step-kinetic for photocyclization process for **Ir-L3-B** (left) kinetic associated to $S_0 \rightarrow {}^1$MLCT transition. (right) kinetic for ^{3}MLCT $\rightarrow S_0$ relaxation.

In the same way, the cycloreversion process was studied, as shown in Figure 4.35, where two simultaneous processes can be seen: A process of disappearance (blue color) and a process of appearance of absorption (red color). The spectrum on the right shows the TA spectrum associated with this map, observing how negative absorption corresponds to the disappearance of molecules from the ground state of **CF-Ir-L3-B**, while absorption is observed in the excited state (positive absorbance signal). This behavior indicates that only one process is being developed due to the absence of different changes in the TA map.
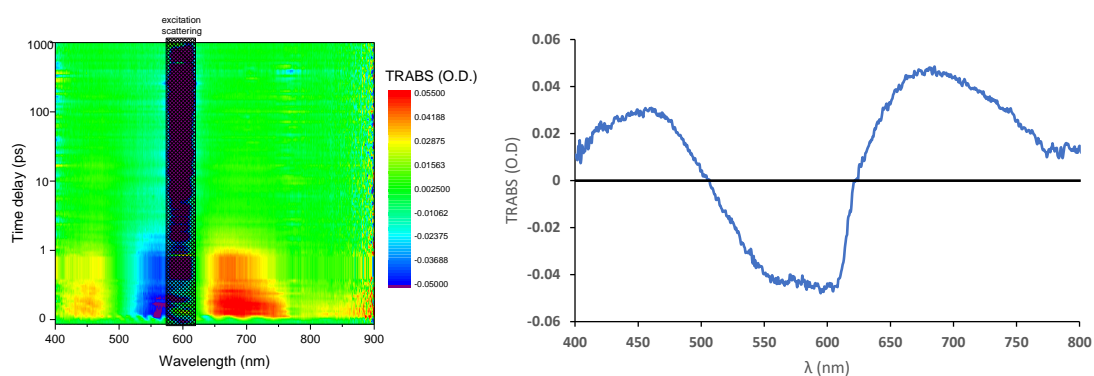
Figure 4.35. Transient absorption spectroscopy map for the photocyclizationn process for **Ir-L3-B**

From the obtained data, the kinetics of both processes can be represented, taking the maximum of 560 nm for the **CF** molecule's population loss in the ground state and 700 nm as the maximum for their appearance in the excited state. From the kinetics obtained, it is possible to calculate a relaxation time of the excited state (τ = 5 ps) and a quantum yield of photocycloreversion close to 0.20, obtained from the disappearance of molecules in S_0, with similar value to the one obtained previously ($\Phi_{C \to O}$ = 0.17).
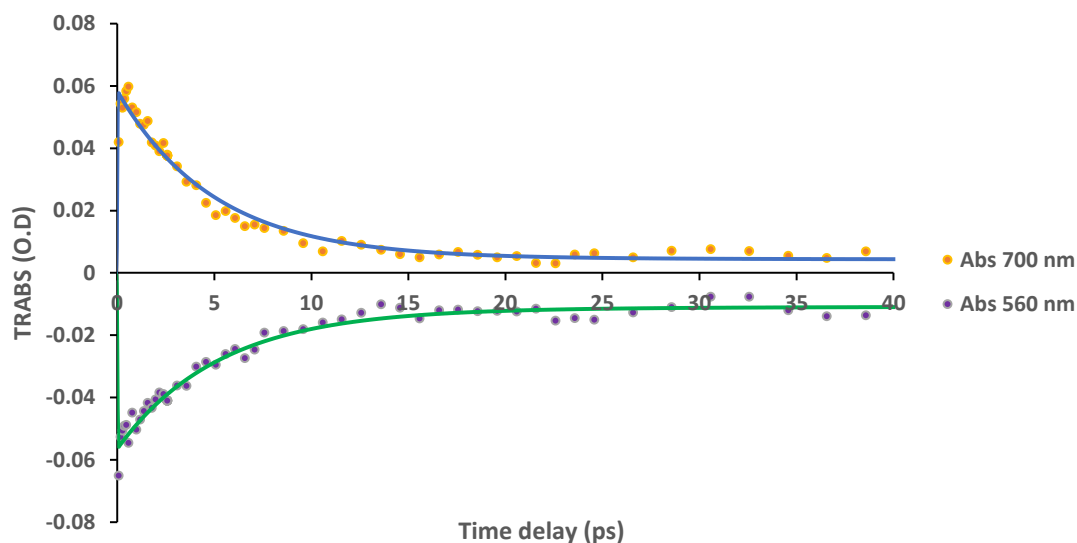
Figure 4.36. Obtained kinetics for S_0 bleaching (560 nm) and S_1 appearance (700 nm)

As for the DTE ligands, it is necessary to know the capacity of the iridium organometallic complexes against the fatigue produced by the repetition of the isomerization process. This property was studied for **Ir-L3-B** to study the effect of DTE ligands' coordination on the metal complex on the resistance to fatigue. Figure 4.37 shows the study carried out for **Ir-L3-B** showing a high resistance to fatigue, which is consistent with the results obtained for **L3-B**, where no decomposition was observed after 100 cycles. Figure 4.37 presents a comparison between **Ir-L3-B** (light blue dashed line) and **L3-B** (dark blue continuous line) showing that the of both compounds is identical.
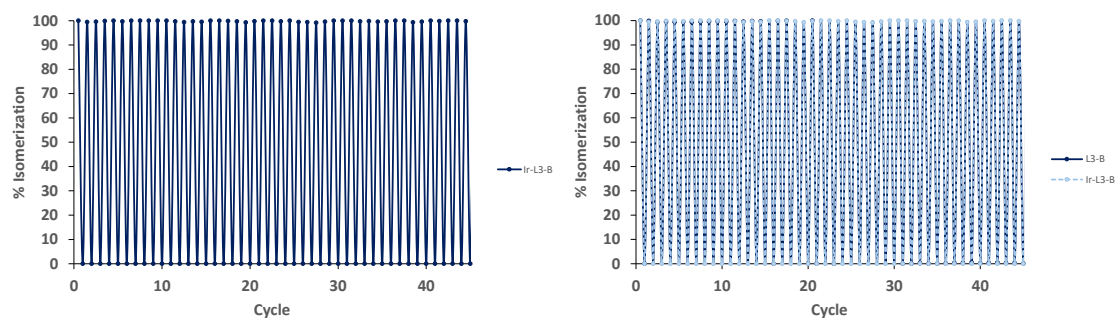
Figure 4.37. Fatigue resistance / multi-cycling experiment for **Ir-L3-B**.

This study was also performed with the rest of the compounds. Figure 4.38 shows the results obtained, showing that the compounds containing the **L1** ligands have a lower resistance to fatigue than those iridium complexes with the DTEs directly linked to bipyridine. Despite showing decomposition, it can be indicated that this is minimal since, after 45 ring-closing-ring-opening isomerization cycles, only a maximum loss of 8% is reached in the maximum absorbance, suggesting a high resistance to fatigue of the synthesized complexes.
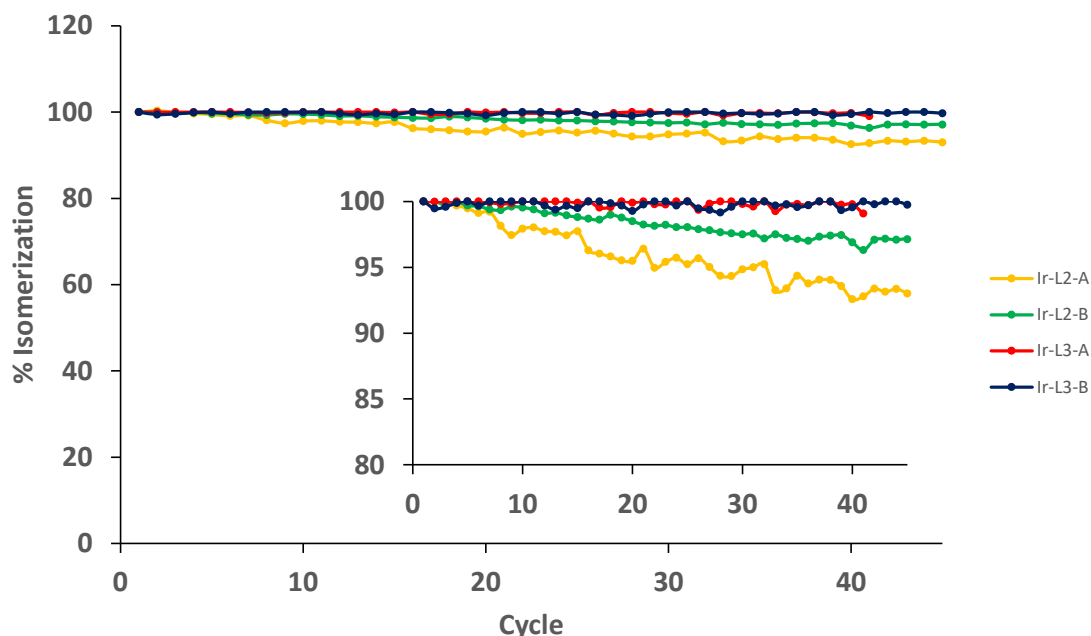
Figure 4.38. Representation for the absorption maxima in each isomerization cycle for the CF DTEs complexes characteristic band.

The results obtained for the complexes were compared with those of free ligands (Figure 4.39), showing that metal center provides additional resistance for the photoswitching process against the decomposition of the photoswitchable fragment compared to the free ligand, being most significant for **L2** derivatives.
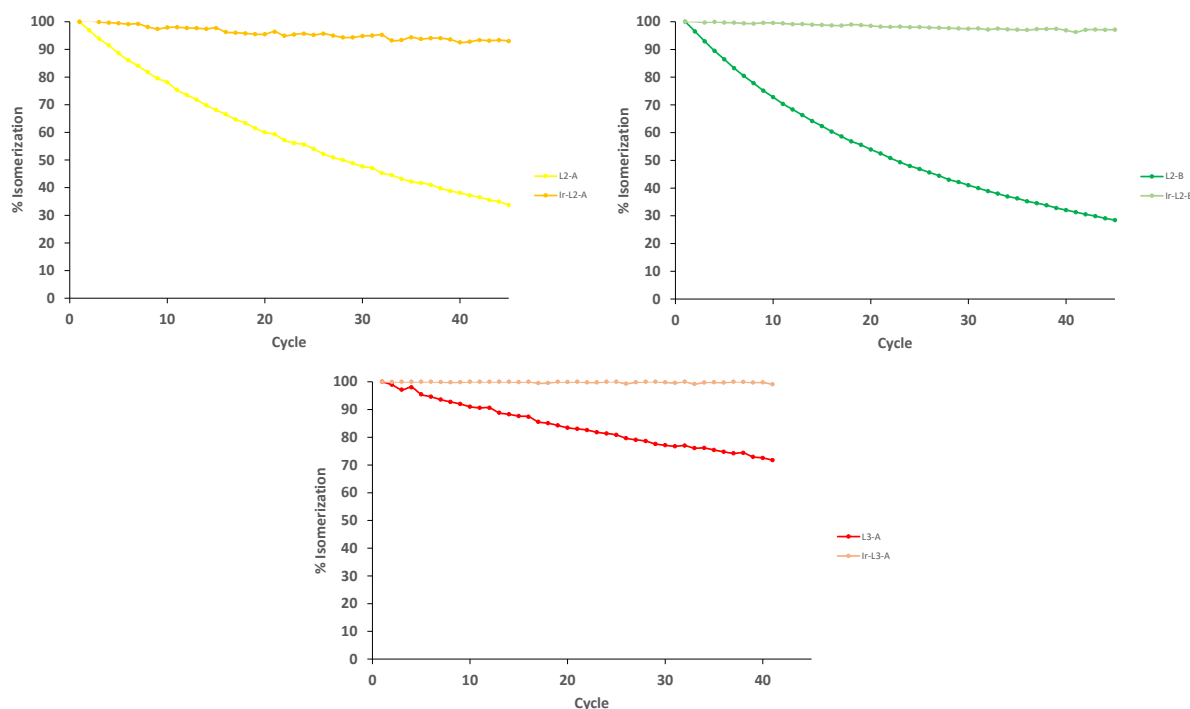
Figure 4.39. Fatigue resistance comparison between free ligands (**L2-A, L2-B** and **L3-A**) and DTE complexes (**Ir-L2-A**, **Ir-L2-B** and **Ir-L3-A**).

In summary, throughout this section, the effect of the metal coordination on the photophysical processes of DTEs has been studied. The results obtained showed that the complexes that incorporate a DTE fragment reach the corresponding PSSs faster than the free DTE ligands. Additionally, the percentage of **CF** isomers in the PSS is almost 100%. These two facts can be attributed to the molar absorptivity coefficients of the complexes at the irradiation wavelength. The origin of this effect is red-shift observed in the absorption spectra upon coordination of the DTEs. On the other hand, the efficiency of the photocycling/photocycloreversion process of metal compounds was studied, obtaining similar values of quantum yields to those obtained for free ligands, indicating that the presence of the metal center does affect the efficiency of the isomerization process. Additionally, transient absorption spectroscopy studies showed that the photocyclization process could be generated through metal to ligand charge transfer mechanism, causing the cyclization of the fragment to occur in a two-step process. Finally, it has been possible to verify that the coordination of the DTE ligands to the iridium center increases the resistance of the compound against fatigue, as has been observed during the different experiments carried out.

4.2 CIRCULAR DICHROISM STUDIES

This section will discuss the circular dichroism results. These measurements were performed on the different enantiopure complexes synthesized in the previous chapter and the free DTE ligands, for comparative purposes. The study aims to demonstrate the posibility of a diastereoselective photoisomerization of a coordinated DTE using the iridium chiral center as chiral inductor in the photocyclization process. As shown in Scheme 4.5, a racemic octahedral complex, which has a photoisomerizable DTE ligand in its structure, will generate four isomers

after performing the cyclization reaction. The hypothesis being studied is whether the presence of an enantiopure chiral central metal could direct the photoisomerization of the DTE ligand inserted in the coordination sphere of the complex forming an enantioenriched mixture of CF. Various groups have already demonstrated this effect using DTEs containing stereogenic carbon centers, DNA strains as chiral inductors, or when the sample was dissolved in a chiral media (Andréasson in 2013[22], Sun in 2018[23], and Clever in 2019[24]). To the best of our knowledge, there is no example in the literature in which a stereogenic metal center (chiral only-at-metal complex) has been used as source of chiral induction.
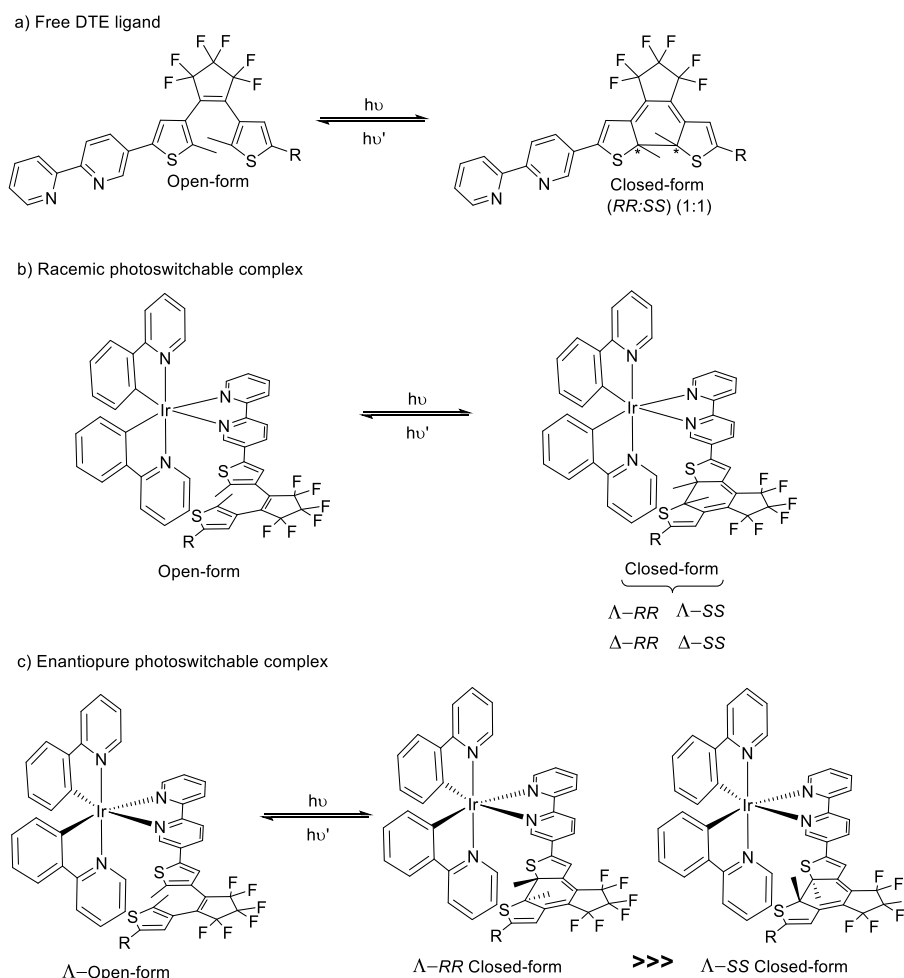
Scheme 4.5. a) Photocyclization process for free DTE ligands b) Photocyclization process for racemic photoswitchable complexes c) Hypothesis for photocyclization process for enantiopure complexes.

The study of selective isomerization began with the study of free ligands. The objective of measuring free ligands is to confirm that no trace/impurity generates chirality in the sample, altering the final results. The free DTE ligand, being a non-chiral molecule in its open-form (or a racemic mixture of P,M antiparallel and parallel isomers), does not produce a signal in circular dichroism spectroscopy. The closed form contains chiral centres (RR and SS) but both enantiomers are produced in equal quantities, no net signal would be observed. Using this as reference, different free DTE samples were prepared, and the dichroic signal was measured both in its open (**OF**) and closed-form (**CF**) of the ligand. Figure 4.40 shows the results obtained for these experiments, confirming the absence of signal for free DTE ligands.
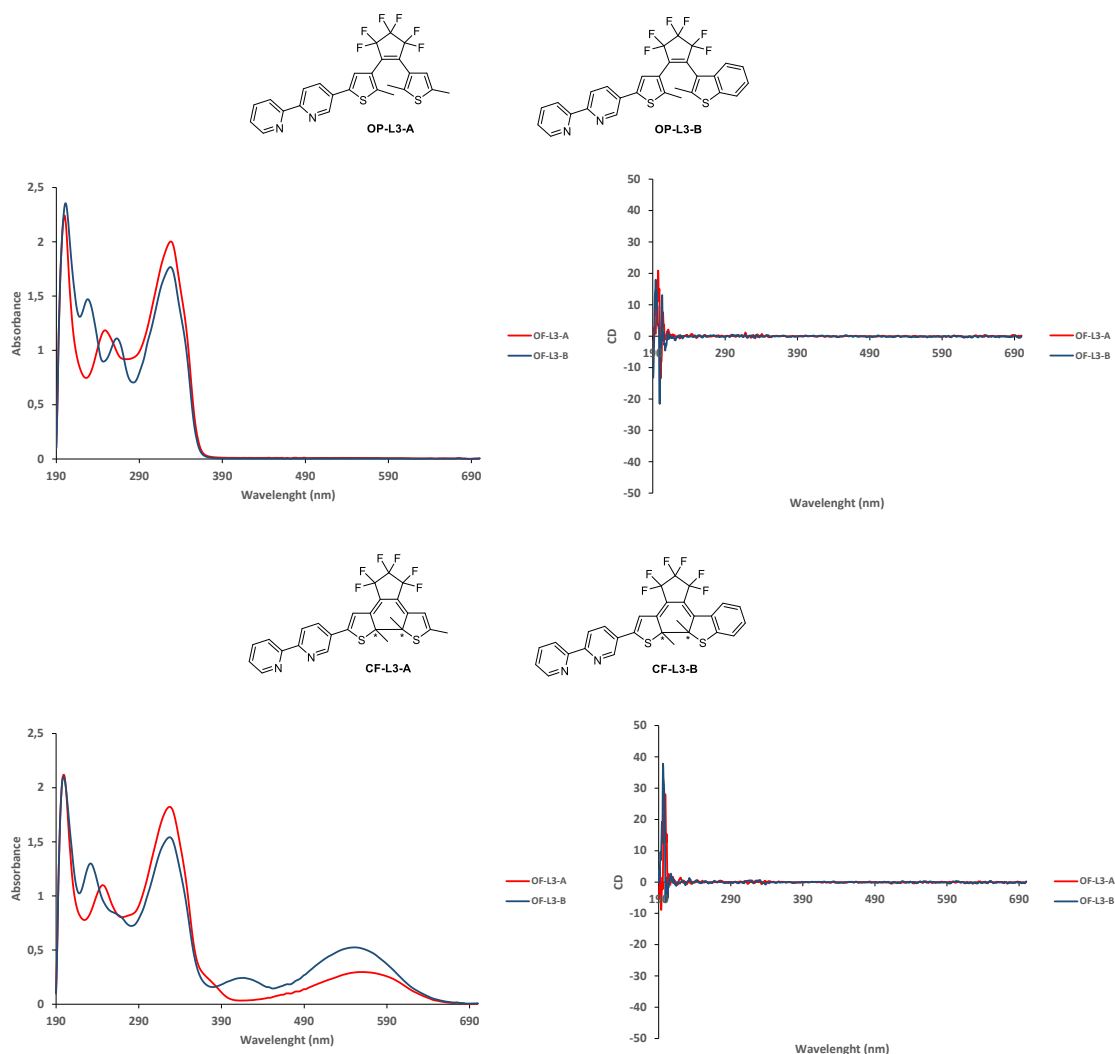
Figure 4.40. (Top) CD measurement for **OF L3-A** and **OF L3-B** in CH$_3$CN (5·10^{-5}); Bottom) CD measurement for **CF L3-A** and **CF L3-B** in CH$_3$CN (5·10^{-5}).

The next step was the measurement of CD spectra of enantiopure chiral-at-metal complexes without coordinated DTEs. For this purpose, we used the [Ir(ppy)$_2$(ACN)$_2$]PF$_6$ (**Λ/Δ-C5**), used as precursors for the enantiopure DTE complexes. These spectra were acquired to confirm the enantiopurity of these derivatives and were used as reference. As a reminder of the synthesis of these enantiopure compounds Scheme 4.6 is shown, where the chiral resolution of the metallic precursor **Λ/Δ-C5** is presented from the reaction of compound **C4** with a chiral agent (*L*-proline or *L/D*-serine).
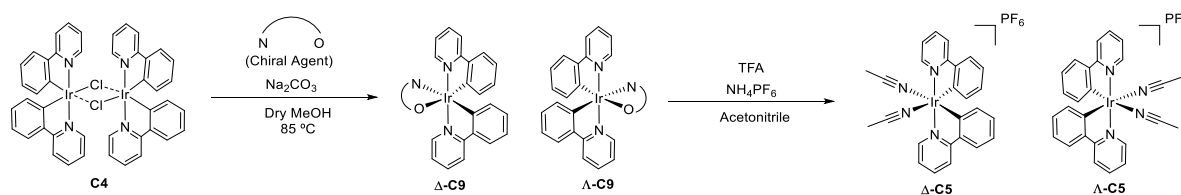
Scheme 4.6. Synthesis of **Λ/Δ-C5** enantiopure complexes.

The UV-vis and CD spectra obtained are shown in Figure 4.41. In this case, since the central metal is a chiral center, signals of the same intensity but opposite sign are expected in the UV region of the spectrum, agreeing with the absorption bands generated by the compounds (see UV-inset). As predicted, the UV-vis spectra of both compounds are identical, observing various maxima at λ = 254 nm and 370 nm.

rac-**C5** was also measured, as blank spectra (green line Figure 4.41). As could be expected, no signal was observed, as non-chiral or racemic mixtures do not generate signal in a CD spectrum.
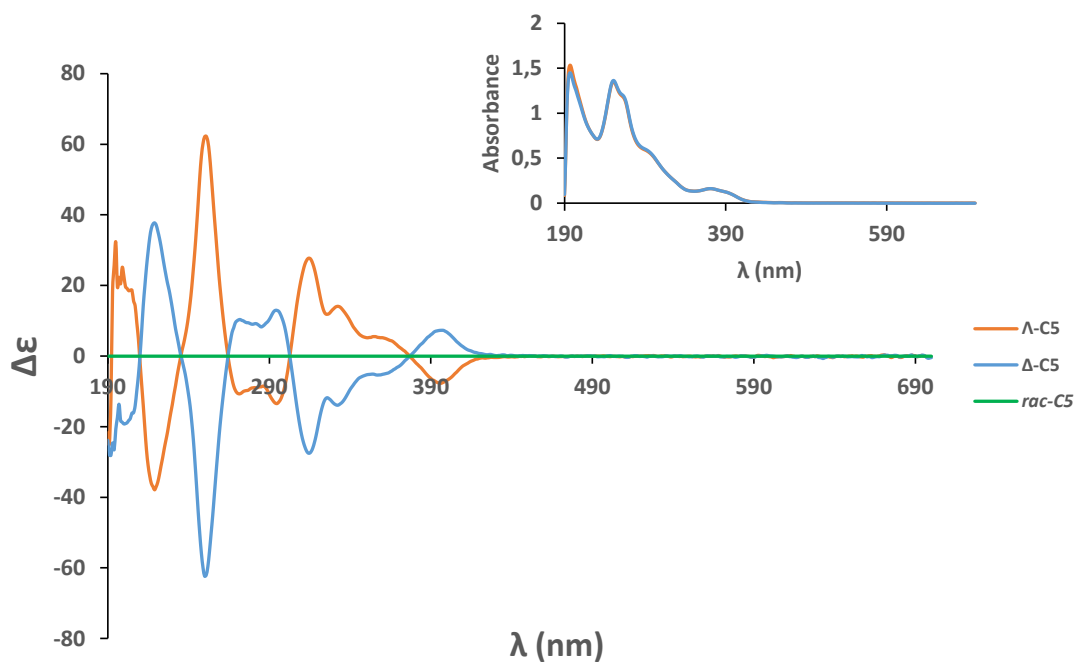
Figure 4.41. Circular dichroism spectra for **Δ-C5** (blue), **Λ-C5** (orange) **and** *rac*-**C5** (green) in CH$_3$CN (5·10^{-5} M).

Once the enantiopure iridium precursors were measured by CD spectroscopy, the enantiopure final complexes were studied by CD spectroscopy. As a reminder, Scheme 4.7 shows the enantiopure synthetic protocol for the obtaining of enantiopure Ir(III) complexes.
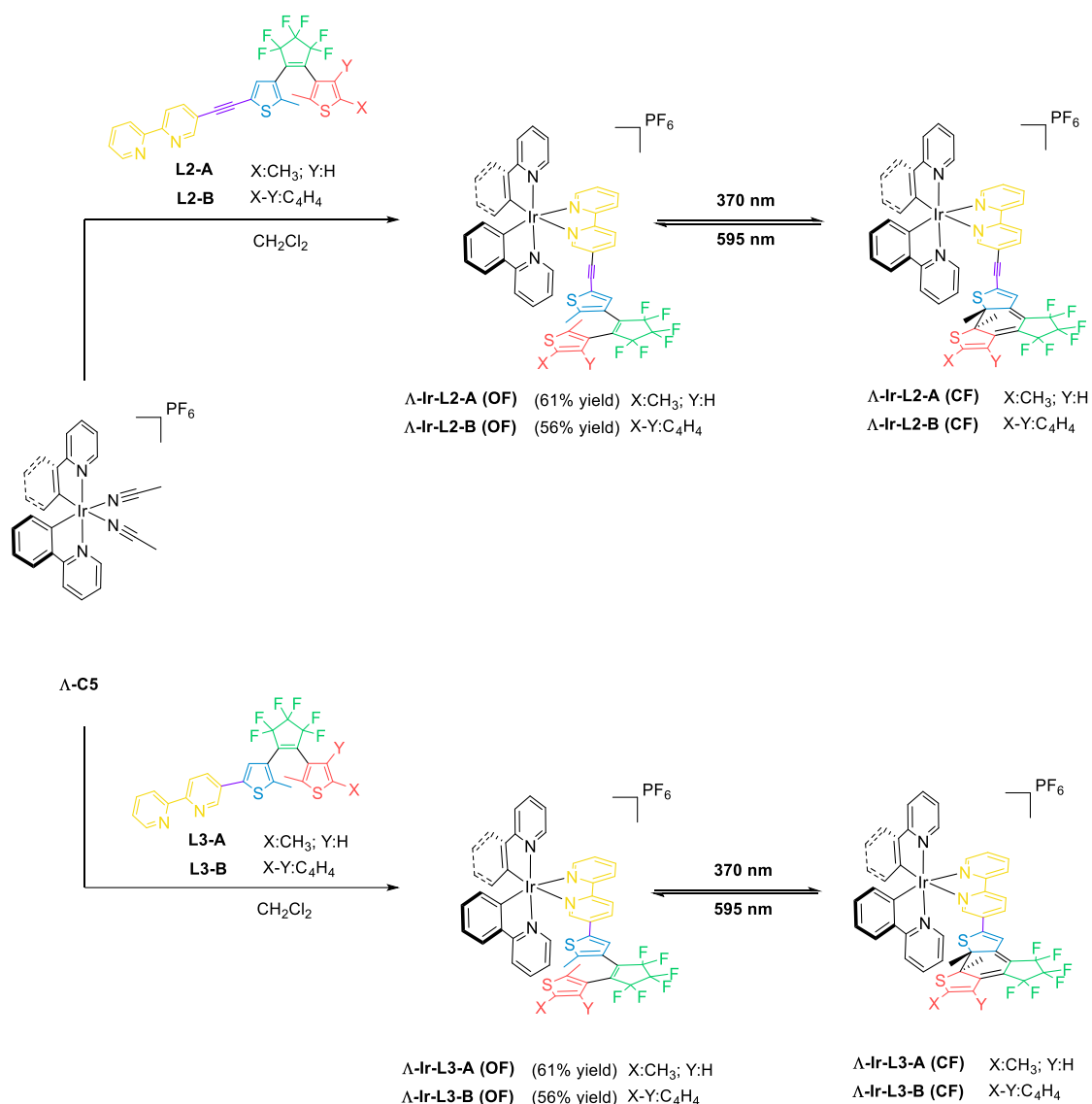
Scheme 4.7. Reaction scheme for the synthesis of enantiopure DTE-containingiridium octahedral complexes.

For each of the enantiomers two different concentrations were employed ($3.5 \cdot 10^{-5}$ M and $8 \cdot 10^{-5}$ M). The fact of measuring two different concentrations for each complex is due to the saturation suffered by the CD equipment with solutions with a concentration higher than ($5 \cdot 10^{-5}$ M); Therefore, in order to observe the 450-650 nm region, the most concentrated solution was chosen, narrowing the measurement specifically to that region of the spectrum.

The complexes will first be measured in their open form. If we assume a fast equilibration between the *P* and *M* parallel forms of the coordinated DTE, it is expected to observe only the dichroic signal of the central metal, as it was observed in the enantiopure metallic precursors **Λ/Δ C5**. Figure 4.42 shows the CD spectra of **Λ-Ir-L3-B** and **Δ-Ir-L3-B** complexes after an irradiation period of two minutes at 530 nm. The dichroic signal can be observed in the UV regions of the spectrum, which are consistent with the UV-Vis signals of the compound. The same measurements were performed for the different complexes, observing similar results.
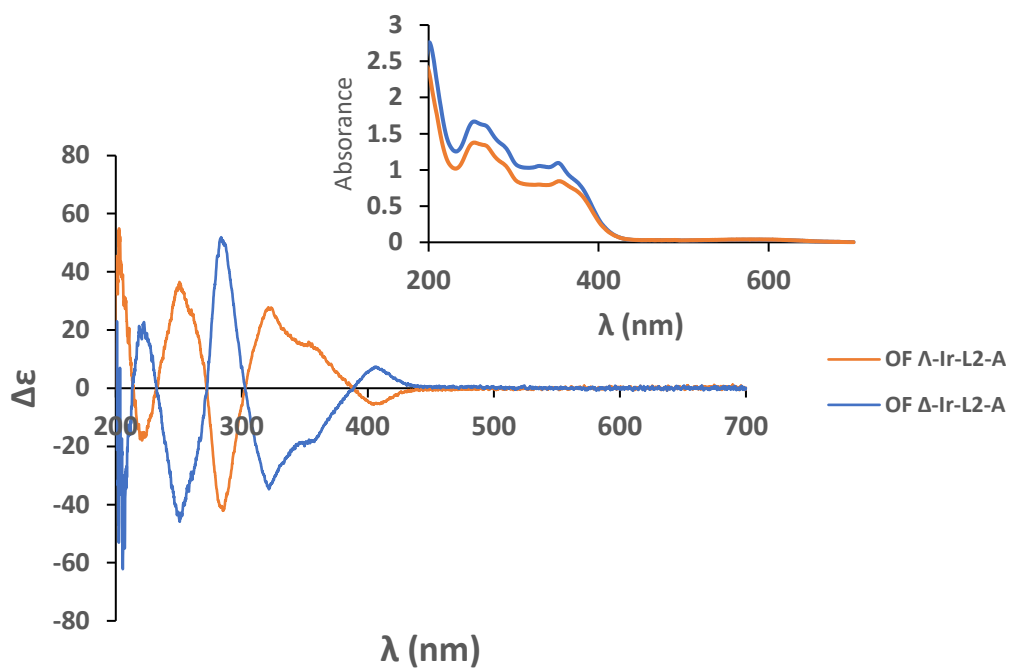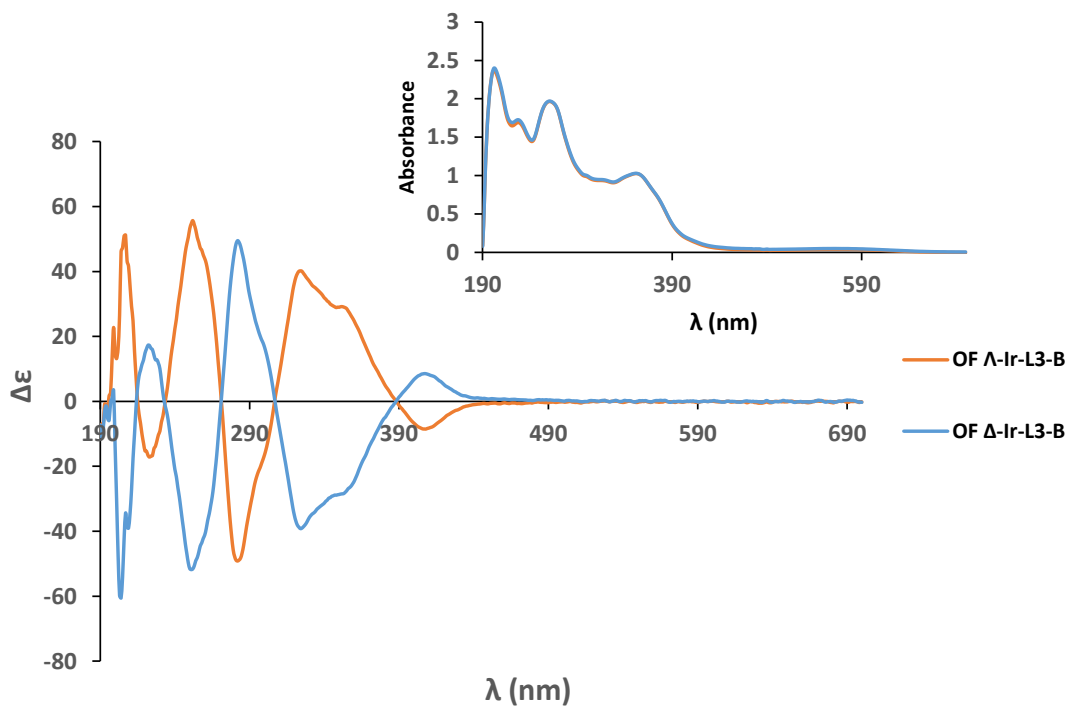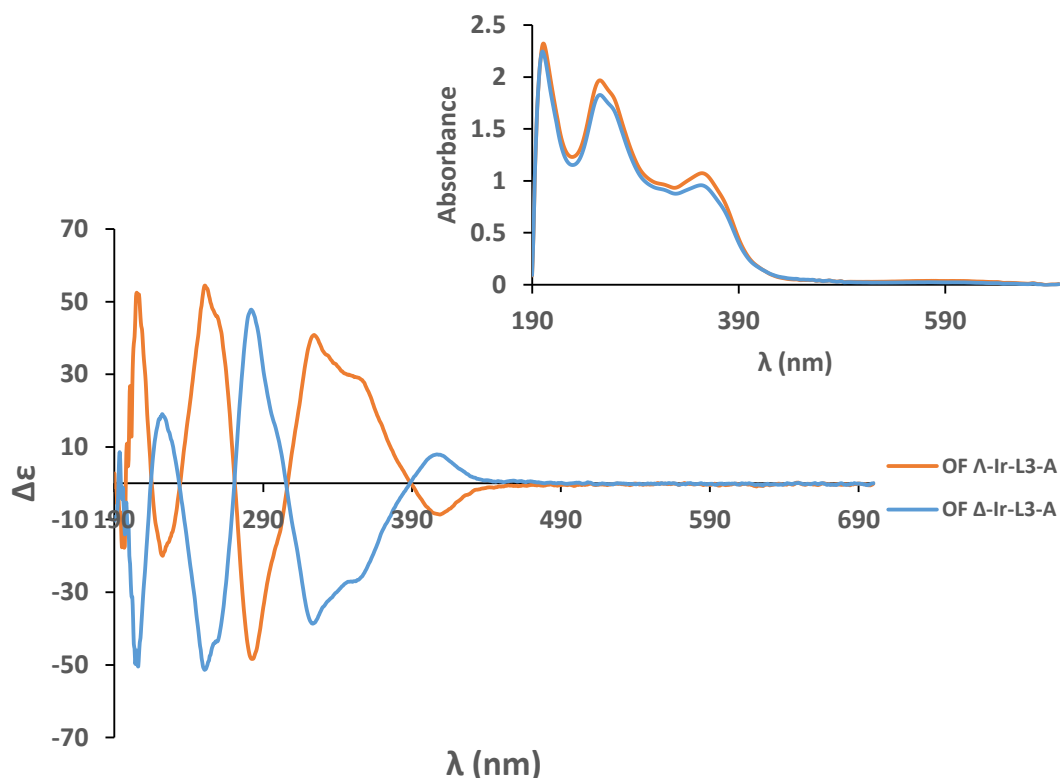
Figure 4.42. CD spectra of **OF-Λ/Δ-Ir-L2-A**, **OF-Λ/Δ-Ir-L2-B**, **OF-Λ/Δ-Ir-L3-A** and **OF-Λ/Δ-Ir-L3-B** in CH$_3$CN. (3.5 · 10^{-5}M).

The complementary dichroic signals obtained for all the complexes confirm their enantiopurity. The next experiment consists of measuring solutions of these compounds in their PSS (mostly **CF** isomers, as explained before). Solutions of the complexes were irradiated at 370 nm for two minutes. This irradiation time should suffice to reach the PSS of the sample (as explained in the previous section). The spectra obtained for **CF-Λ/Δ-Ir-L3-B** are shown in Figure 4.43. Two significant changes can be observed compared to the **OF** spectra. On the one hand, the CD signal shows intensity changes in the 250 nm and 350 nm signals. This change is associated with the electronic change generated by the photocyclization process in the molecule. On the other hand, in the 500-600 nm region, the barely visible appearance of a broad band can be observed. This new "shoulder" may be due to the characteristic band for the closed shape of DTE compounds.
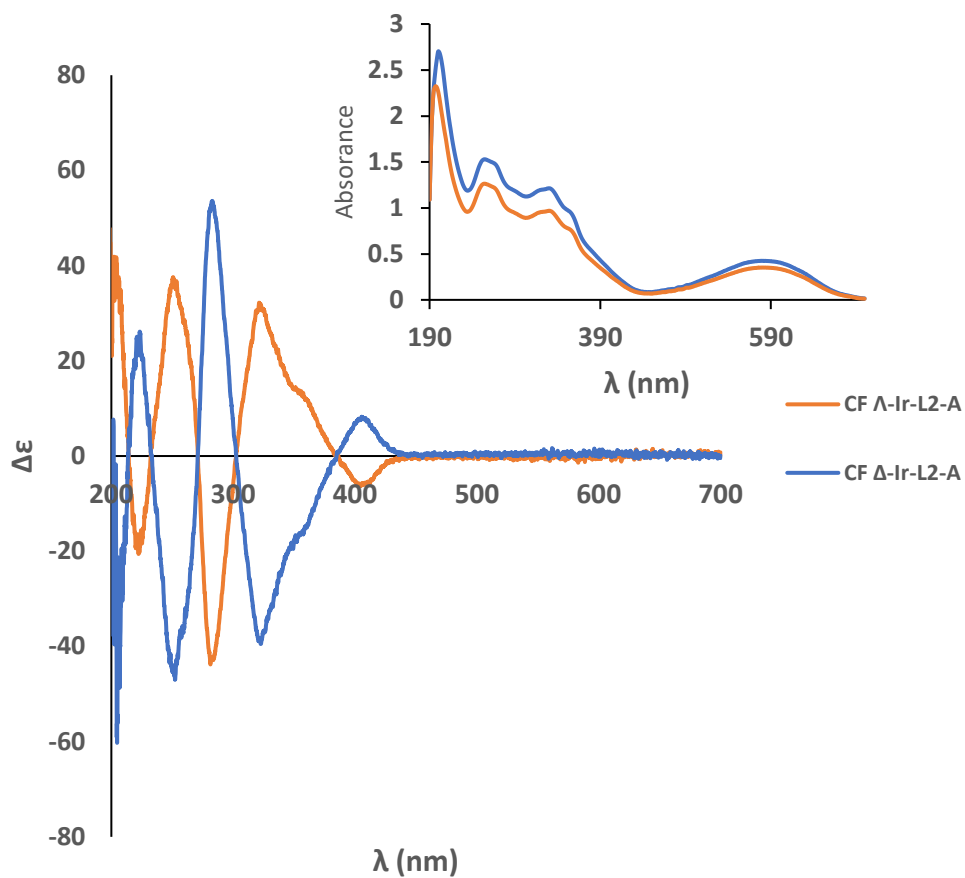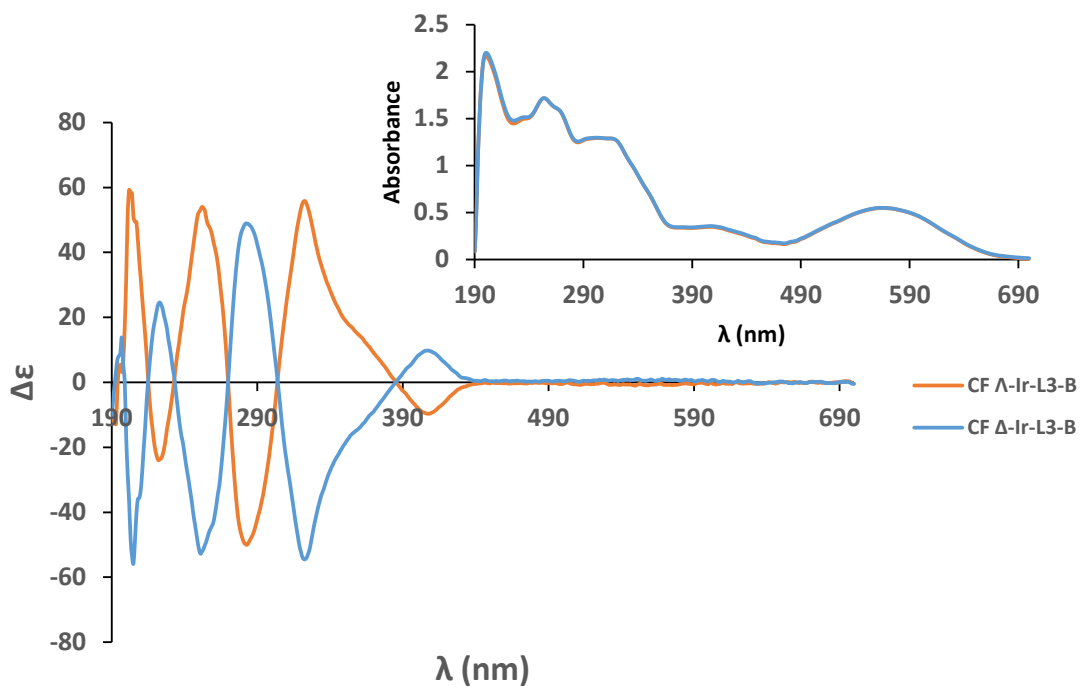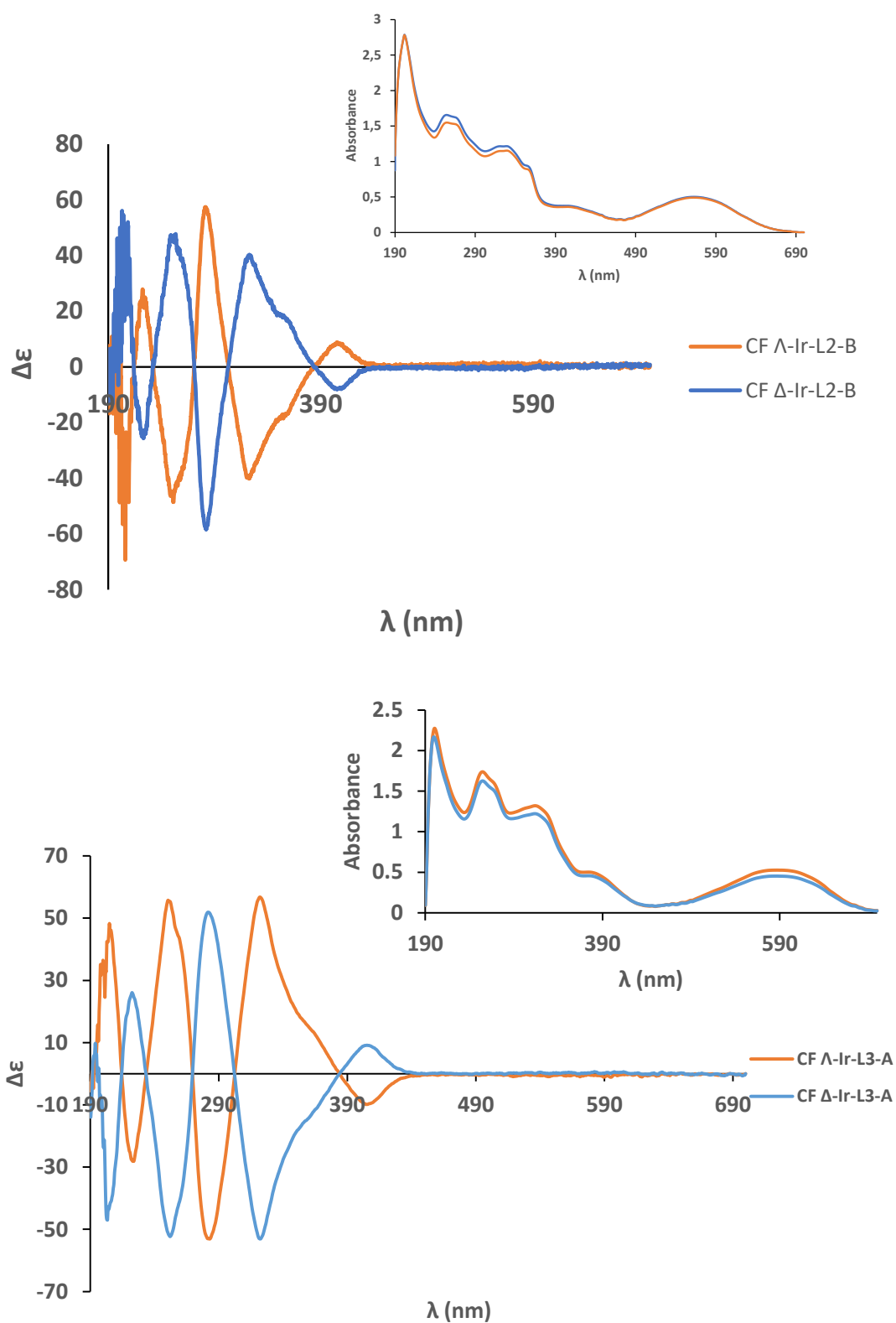
Figure 4.43. CD spectroscopy of **CF-Λ/Δ-Ir-L2-A**, **CF-Λ/Δ-Ir-L2-B**, **CF-Λ/Δ-Ir-L3-A** and **CF-Λ/Δ-Ir-L3-B** in CH₃CN. (3.5 · 10⁻⁵M).

To confirm that this apparent shoulder was a true signal, and not just an artifact, the measurement was repeated on a more concentrated sample (8 · 10⁻⁵ M), scanning only the visible region of the spectra for both compounds in their **OF** and **CF**. Figure 4.44 shows the results

obtained. The upper graph shows a new signal in the dichroism spectrum, corresponding to the DTE fragment in its closed form compared to the same compound in the open form. In turn, in the lower graph, it can be seen that for each of the measured isomers, the signal is opposite, indicating that the chiral configuration of the metal center directly affects the photocyclization process, thus generating a diastereoselective photocyclization process.

4
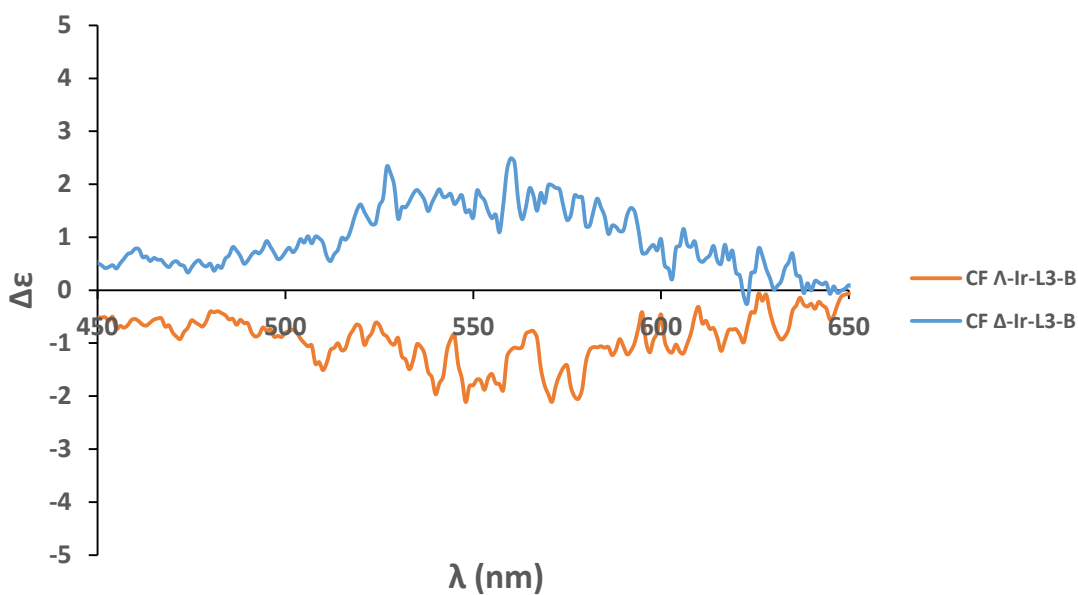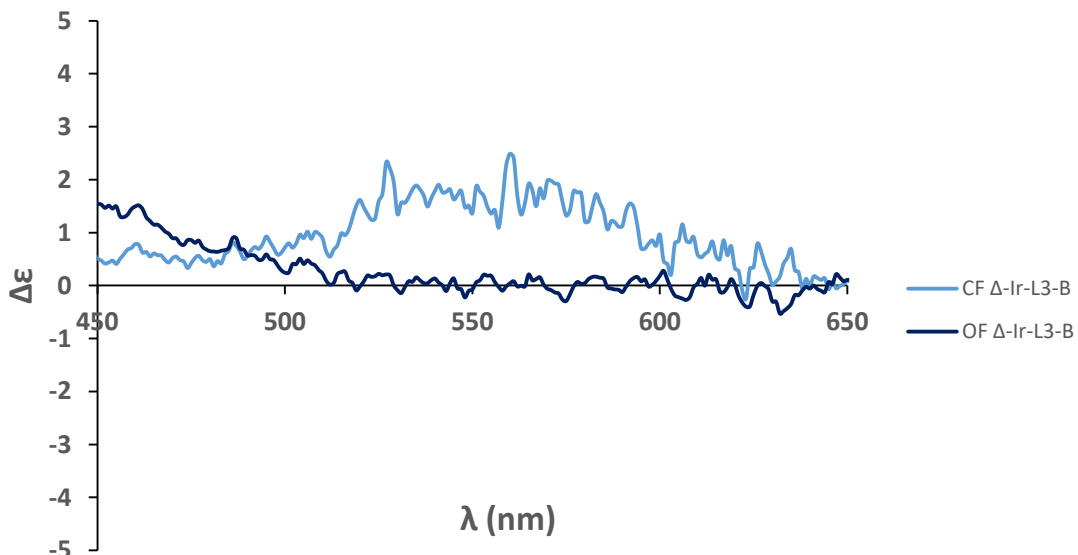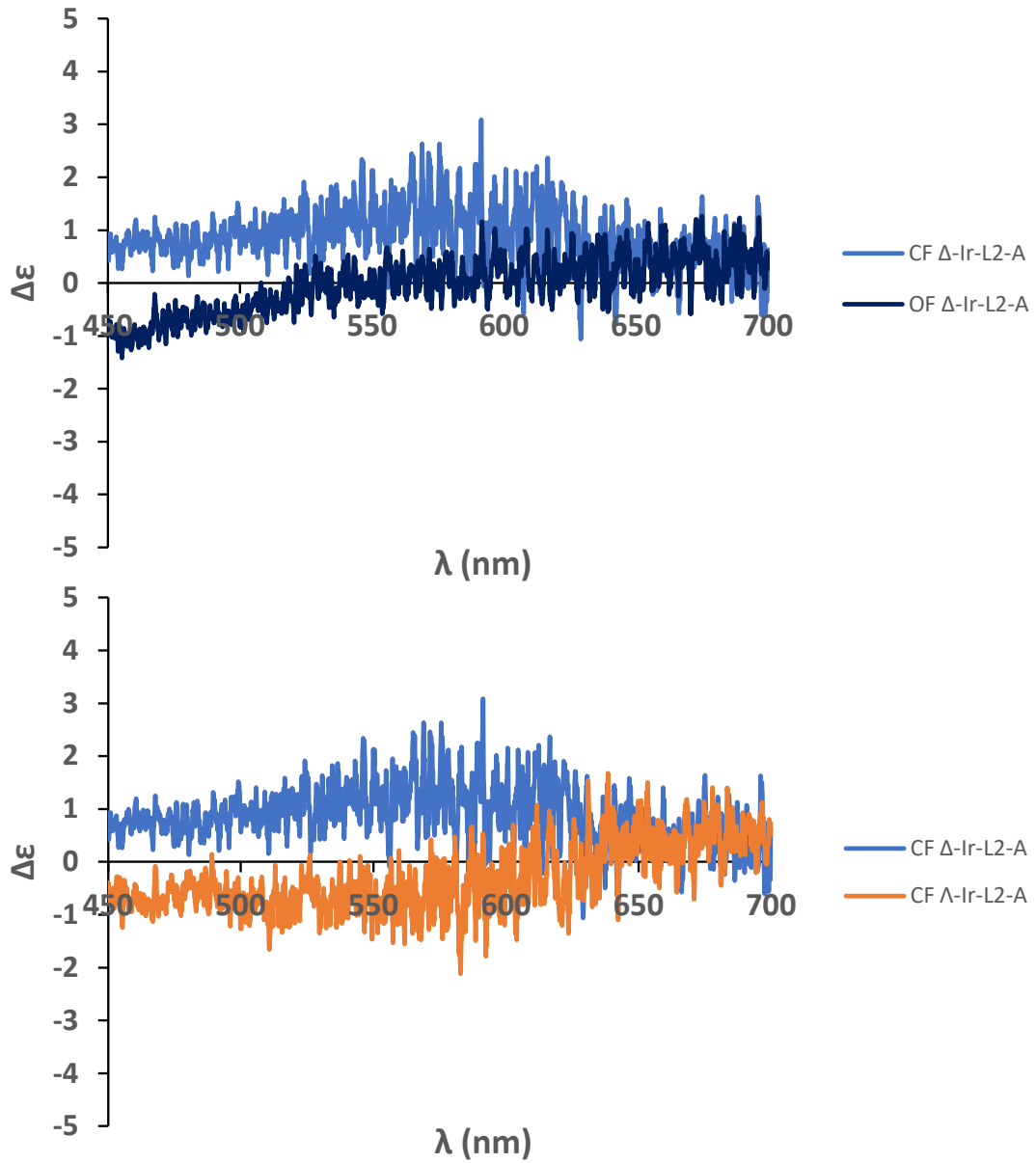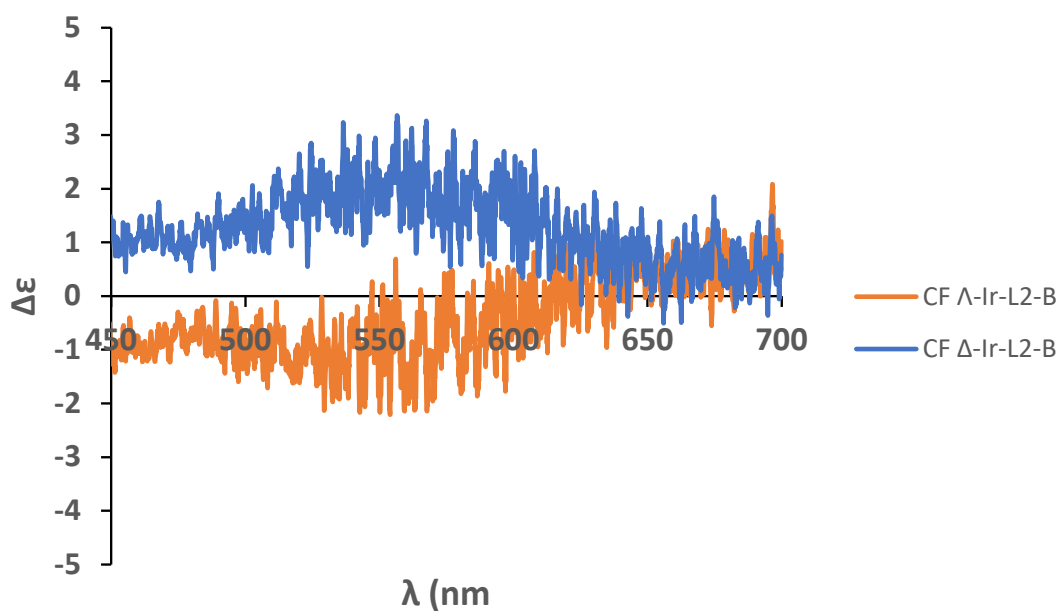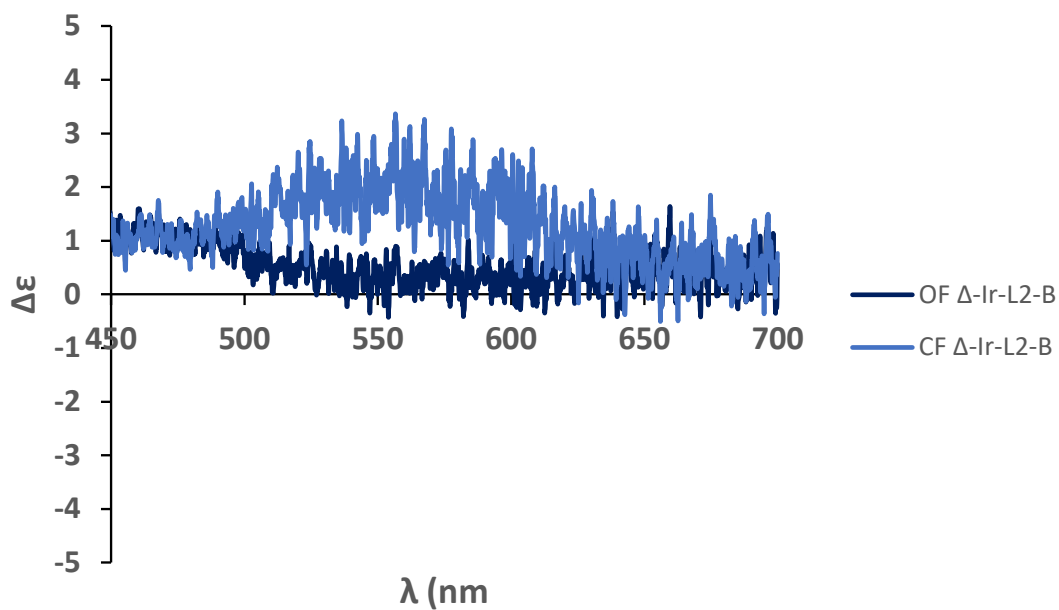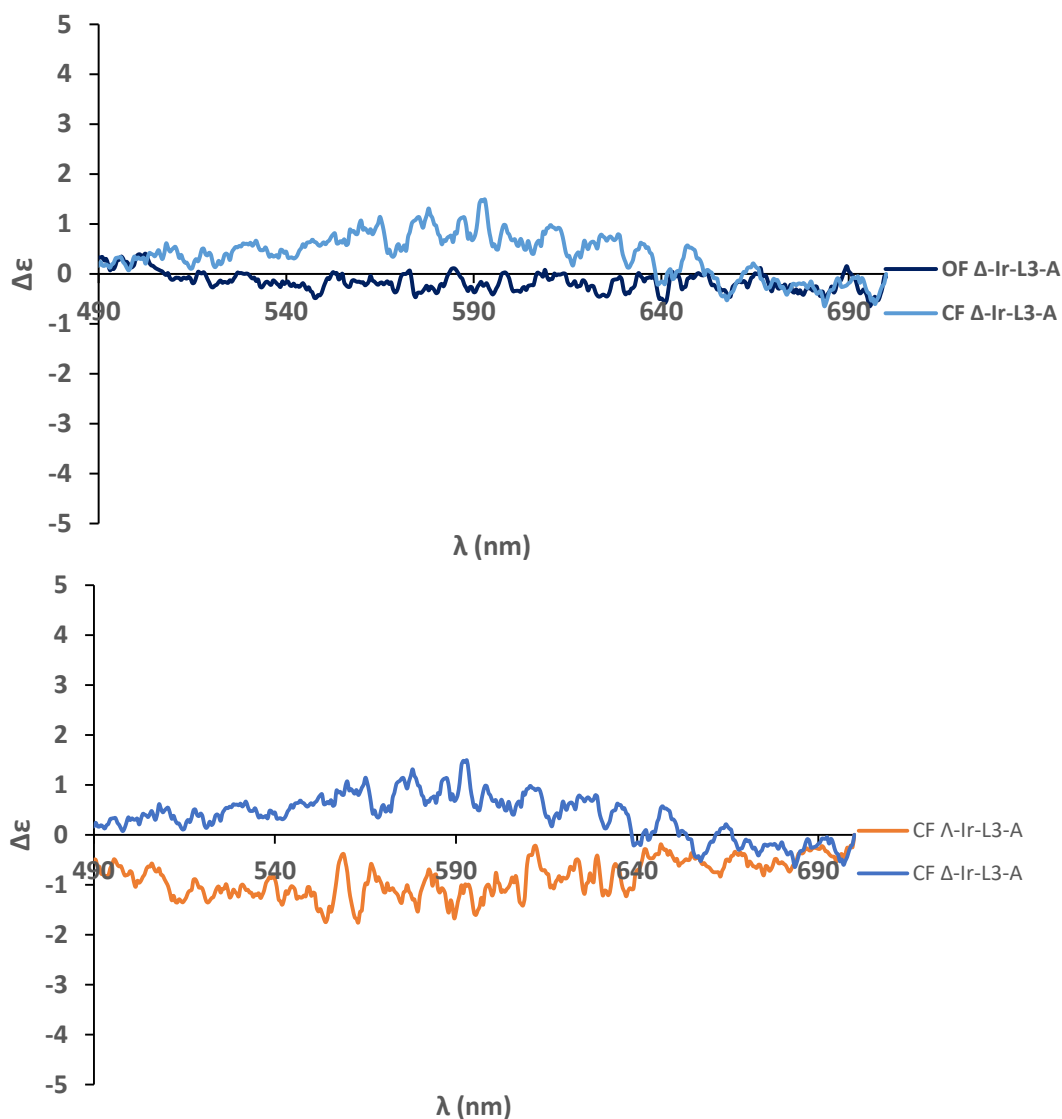
Figure 4.44. CD spectroscopy comparing **OF/CF-Δ and Δ/Λ** of **Ir-L2-A**, **Ir-L2-B**, **Ir-L3-A** and **Ir-L3-B** at 450-650 nm region in CH$_3$CN. (8 · 10^{-5}M).

Therefore, in this section, it has been found that a chiral central metal can act as a chiral inducer for diastereoselective ring-closure of a coordinated DTE ligand. Unfortunately, the chiral induction is very modest according to the weak dichroic signal. Most probably, this is due to the long distance between the chiral center and the stereogenic carbon atoms created upon ring-closure. Further ligand designs in which the sterogenic centers of the DTE are closer to the metal center are currently under development in our laboratory.

4.3 REFERENCES

[1] R. B. Woodward, R. Hoffmann, *Angew. Chem. Int. Ed.*, **1969**, *8*, 781-932.

[2] R. B. Woodward, R. Hoffmann, *J. Am. Chem. Soc.*, **1969**, *87*, 395-397.

[3] G. Pariani, M. Quintavalla, L. Colella, L. oggioni, R. Castagna, F. Ortica, C. Bertrarelli, A. Bianco, *J. Phys. Chem.,* **2017**, *121*, 23592-23598.

[4] H. Xu, S. Wei, C. Fan, G. Liu, S. Pu, *Tetrahedron*, **2017**, *73*, 6479-6485.

[5] A. J. Vazquez, N. S. Nudelman, *J. Phys. Org. Chem.*, **2012**, *25*, 925-932.

[6] S. Pu, L. Yan, Z. Wen, G. Liu, L. Shen*, J. Photochem. Photobiol. A.*, **2008**, *196*, 84-93.

[7] G. Liu, M. Liu, S. Pu, C. Fan, S. Gui, *Dyes and Pigments*, **2012**, *95*, 553-562.

[8] S. Cui, S. Pu, W. Liu, G. Liu, *Dyes and Pigments*, **2011**, *91*, 435-441.

[9] S. Cui, S. Pu, G. Liu, W. Liu, *Adv. Mat. Res.*, **2011**, *156*, 462-466.

[10] M. Liu, G. Liu, S. Cui, *Applied Mechanics and Materials*, **2012**, *164*, 239-242.

[11] W. R. Browne, J. J. D. de Jong, T. Kudernac, M. Walko, L. N. Lucas, K. Uchida, J. H. van Esch, B. L. Feringa, *Chem. Eur. J.*, **2005**, *11*, 6430-6441.

[12] G. Sevez, J-L. Pozzo, *Dyes and Pigments*, **2011**, *89*, 246-253.

[13] C. G. Hatchard, C. A. Parker, *Proc. R. Soc. Lond. A*, **1956**, *235*, 518-536.

[14] Y. Leydet, P. Batat, G. Jonusauskas, S. Denisov, J. C. Lima, A. J. Parola, N. D. McClenaghan, F. Pina, *J. Phys. Chem. A.*, **2013**, *17*, 4167-4173.

[15] M. L. Horng, J. A. Gardecki, A. Papazyan, M. Maroncelli, *J. Phys. Chem.*, **1995**, *99*, 17311-17337.

[16] W. Tan, J. Zhou, F. Li, T. Yi, H. Tian, *Chem. Asian J.*, **2011**, *6*, 1263-1268.

[17] S. Monaco, M. Semeraro, W. tan, H. Tian, P. Ceroni, A. Credi, *Chem. Commun.*, **2012**, *48*, 8652-8654.

[18] Y. Guo, D. Zhang, J. Wang, H. Lu, S. Pu, *Dyes and Pigments*, **2020**, *175*, 108191.

[19] R. T. F. Jukes, V. Adamo, F. Hartl, P. Belser, L. de Cola, *Inorg. Chem.*, **2004**, *43*, 2779-2792.

[20] A. Telleria, J. Pérez-Miqueo, A. Altube, E. Garcia-Lecina, A. de Cózar, Z. Freixa, *Organometallics*,**2015**, *34*, 5513-5529.

[21] W. Tan, Q. Zhang. J. Zhang, H. Tian, *Org. Lett.*, **2009**, *11*, 161-164.

[22] T. C. S. Pace, V. Müller, S. Li, P. Lincoln, J. Andréasson, *Angew. Chem. Int. Ed.*, **2013**, *52*, 4393-4396.

[23] L-X. Cai, L-L. Yan, S-C. Li, L-P. Zhou, Q-F. Sun, *Dalton Trans.*, **2018**, *47*, 14204-14210.

[24] R-J. Li, J. J. Holstein, W. G. Hiller, J. Andréasson, G. H. Clever, *J. Am. Chem. Soc.*, **2019**, *141*, 2097-2103.

CHAPTER 5

GENERAL CONCLUSIONS AND FUTURE PERSPECTIVES
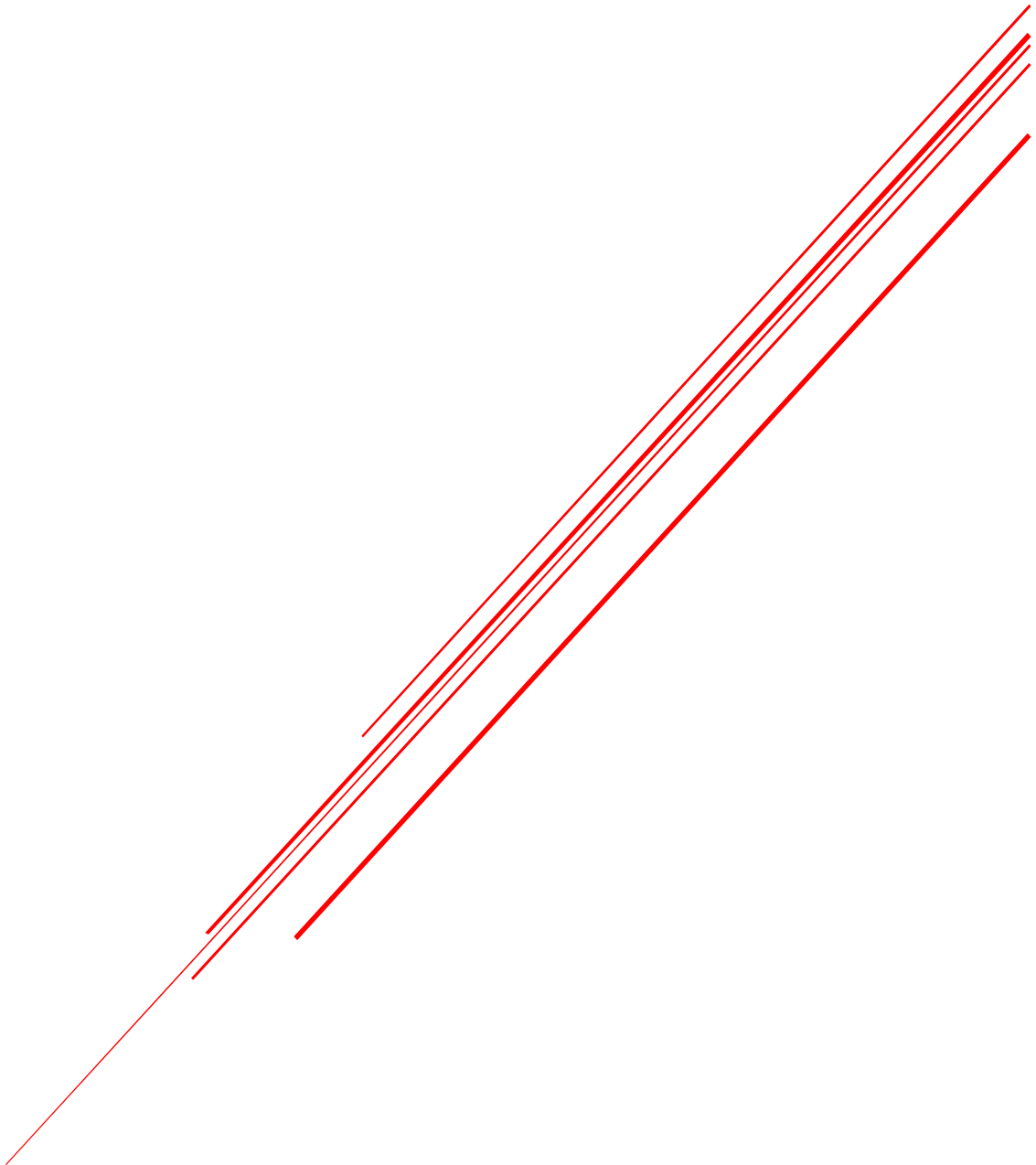
According to the main objectives proposed during the thesis, the general conclusions and future perspectives are presented in this chapter.

CHAPTER 2

- ✓ The synthesized ligands were used in studies of cyclometalation to Ir(III) precursors. Effective coordination of these DTEs via C-N coordination could not be observed. It was concluded that the lack of C-N coordination of the DTEs is due to steric problems generated between the fluorine groups of the hexafluorocyclopentene "bridge" and the coordinating thiophene during the approximation of the ligand to the metal center.

- ✓ The C-N cyclometallation of coordinating thiophene fragments was demonstrated. Various Ir(III) complexes were generated that introduce intermediate **6** as a bis-cyclometalated ligand and its insertion as a third cyclometalated ligand.

- ✓ A new type of coordination has been demonstrated for the synthesized DTE compounds. The coordination occurs via N-S, bringing the stereogenic center of the closed DTE ligand and the central metal significantly close together.

- ✓ Despite observing N-S coordination, the lability of the covalent bond between the ligand and the metal center prevented the purification and study of this new family of ligands.

- 🞣 **Future perspectives:** We will try to optimize the synthesis and purification of the N-S complexes, deepen the study of the N-S coordination of the DTE ligands to metal centers, and study the photocyclization/photocycloreversion processes for this new family of Ir(III) complexes.

CHAPTER 3

- ✓ A new synthetic procedure was developed to obtain bipyridine-based on dithienylethenes.

- ✓ Four non-described DTE-containing bipyridine ligands were synthetized, which differ in the bond between the bipyridine and the photoswitch fragment, which can be a direct bond or an alkyne spacer.

- ✓ Ligands **L2** and **L3** were coordinated with different enantiopure precursors of Ir(III), obtaining for the first time enantiopure complexes of Ir(III) that incorporate DTE fragments in their structure.

- ✓ The complexes **Δ-[Ir(ppy)₂(L3-B)]** and **Λ-[Ir(ppy)₂(L3-B)]** showed the possible formation of diastereomeric compounds in the open form of the DTE (**OF-L3- B**). This effect may be due to the proximity of the DTE fragment to the metal center, which in turn has a more significant steric hindrance due to the presence of the benzo[*b*]thiophene group as a non-coordinating group.

- **Future perspectives**: Synthesize compounds based on **L2** and **L3**, where the thiophene groups (coordinating and non-coordinating) are oxidized. Oxidation of the sulfur atoms of the thiophene groups gives DTEs luminescent properties.

CHAPTER 4

- ✓ The photochromic behavior of the new dithienylethene ligands and the corresponding metal complexes was successfully studied, observing a red-shift effect of the absorption bands after coordination to the metallic center Ir(III).

- ✓ The photostationary state of the photoswitch compounds was studied, observing how the percentage of **CF-isomer** for the complexes (**CF-Ir**) was much higher than that observed for the free ligands (**CF-L**). This behavior was associated with a lower **CF-Ir** absorption at the irradiation length for the photocyclization process.

- ✓ Using the spectra obtained for the **OF-DTE** forms and the proportions of the isomers in the PSS, it was possible to calculate the theoretical **CF-DTE** spectra for each compound, both free ligands and metal complexes.

- ✓ Quantum yields were calculated to determine the efficiency of the photocyclization ($\Phi_{o\to c}$) and photocycloreversion ($\Phi_{c\to o}$) processes, finding that the free DTE ligands coordination to the metal center does not significantly affect the efficiency of the photophysical processes, except in the specific case of **L3-B** and **Ir-L3-B**, where it is found that the coordination of the ligand decreases the efficiency of both processes.

- ✓ Preeliminary transient absorption spectroscopy studies suggest that for the **Ir-L3-B** metal complex, the photocyclization process occurs via charge transfer from the metal to the DTE fragment.

- ✓ The study of fatigue resistance proposes **L3-B** as the best candidate for application in systems due to the absence of fatigue during the first 100 cycles. Incorporating the DTE fragment into the organometallic complex (**Ir-DTE**) improves the fatigue resistance property of the DTE, observing a minimum decomposition of the photoswitch complexes compared to the free DTE ligands.

- ✓ The study by circular dichroism spectroscopy showed satisfactory results concerning a diastereoselective photoinduction of the photocyclization process of the **Ir-DTE** complexes, observing signals with a positive/negative Cotton effect in the region of 450-600 nm, corresponding to the **CF-DTE** fragments absorption band.

- **Future perspectives**: It is intended to study the photocyclization processes for the **Ir-L2-A**, **Ir-L2-B**, and **Ir-L3-A** complexes to confirm the activation of the photocyclization process via MLCT observed for **Ir-L3- B**. In turn, it is intended to study the selective induction of the photocyclization process for complexes with N-S coordination due to the high probability of observing a more significant effect than that observed for bipyridine-based complexes. In addition, from the oxidative ligands presented in future perspectives of *Chapter 3*, new Ir(III) compounds can be generated, which could be

presented as excellent candidates as luminescent complexes, activating/deactivating luminescence utilizing light.

EXPERIMENTAL SECTION

Chiral-at-metal Iridium(III) Complexes Containing Dithienylethene-Based Photoswitchable Ligands

Euskal Herriko Unibertsitatea UPV-EHU

Donostia (Gipuzkoa), 2022

TABLE OF CONTENTS

1. GENERAL EXPERIMENTAL CONDITIONS AND INSTRUMENTATION

All solvents were dried and purified by known procedures and freshly distilled under nitrogen from appropriate drying agents prior to use. All manipulations and reactions involving air and/or moisture-sensitive organometallic compounds were performed under an atmosphere of dry nitrogen using standard Schlenk techniques.

NMR spectra were recorded on a Bruker Avance DPX 300 MHz and 400 MHz (University of the Basque Country, UPV-EHU) and Bruker Avance NEO 300 MHz, Bruker Avance III 300 MHz, Bruker Avance II 400 MHz and Bruker Avance III 600 MHz (University of Bordeaux, UB).

Elemental Analysis were performed on a microanalizer Leco CHNS-932.

Field Desorption (FD) experiments were carried out on an AccuToF Mass Spectrometer (Jeol) is a GC-TOF type mass spectrometer.

UV-Vis Measurements.

UV-Vis absorption measurements were performed with a Shimadzu RF-540 fluorimeter spectrophotometer utilizing 10 mm cell-path cuvettes (110 QS). Measurements of photocyclization were performed using $5 \cdot 10^{-5}$ M solutions of CH_3CN. Using a Shimadzu RF-540 fluorimeter, a 3 mL portion of each sample at $\lambda = 370$ nm at different times until reach the PSS. Temperature was controlled with a HP 89090A Peltier temperature control accessory.

Photocyclization/Photocycloreversion Quantum Yield.

Isomerization measurements were performed with an Aventis spectrometer with simultaneous detection across the UV-vis-NIR spectral domains (200 nm – 1150 nm; time resolution 3 ms), utilizing 10 mm cell-path cuvettes. Measurements of photocyclization/photocycloreversion were performed using $2 \cdot 10^{-5}$ - $5 \cdot 10^{-5}$ M solutions of CH_3CN.

Circular Dichroism Studies

Circular dichroism measurements were performed with a Jasco J-815 spectrometer utilizing 10 mm cell-path cuvettes. Measurements of Circular Dichroism were performed using $3.5 \cdot 10^{-5}$ M and $8 \cdot 10^{-5}$ M solutions of CH_3CN. Measurements for compounds CF-isomer were carried out after 3 minutes of irradiation at $\lambda = 370$ nm.

X-ray Crystallography

Intensity data were collected on a Rigaku FRX diffractometer. The crystals were kept at 140-293 K during data collection. Using Olex2[1], the structure was solved with the SHELXT[2] structure solution program using Intrinsic Phasing and refined with the SHELXL[2] refinement package using Least Squares minimisation.

2. SYNTHESIS AND CHARACTERIZATION

2.1 Ligands

2.1.1 Compound 3-bromo-2,5-dimethylthiophene (1):
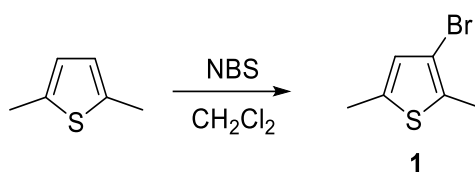
Compound **1** was synthesized following a slightly modified reported procedure[3]. NBS (20 mmol, 3.48 g) was added slowly over a solution of 2,5-dimethylthiophene (18 mmol, 2.04 mL) in CH_2Cl_2 (50 mL), and stirred at r.t. for 15 h. The solvent was removed and the residue was suspended in diethyl ether (50 mL), and filtered. The filtrate was partitioned using CH_2Cl_2/H_2O and dried over $MgSO_4$. After evaporation of the solvent from the organic layer, the residue was purified by silica gel column chromatography (hexane, Rf = 0.85), and it was obtained as a colourless oil (2.8 g, 80% yield). The spectroscopic data are consistent with those reported in the literature.

^{1}H NMR (300 MHz, CDCl$_3$): δ 6.55 (d, J_{Br-H} = 1.2 Hz, 1H, CH$_{ar}$), δ 2.40 (d, J_{Br-H} = 1.35 Hz, 3H, CH$_3$), δ 2.32 (s, 3H, CH$_3$).
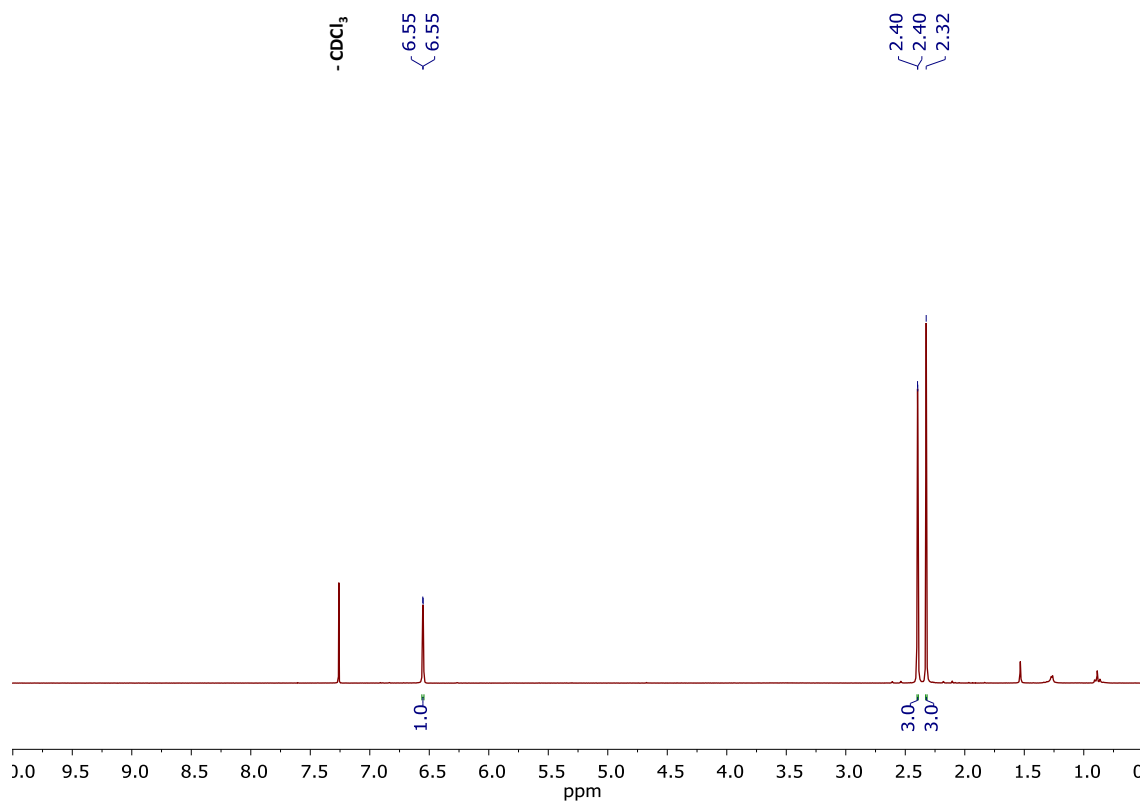
Figure S1. ^{1}H NMR of 3-bromo-2,5-dimethylthiophene (**1**). (CDCl$_3$, 300 MHz).

2.1.2 Compound 3-bromo-2-methylbenzo[*b*]thiophene (2):
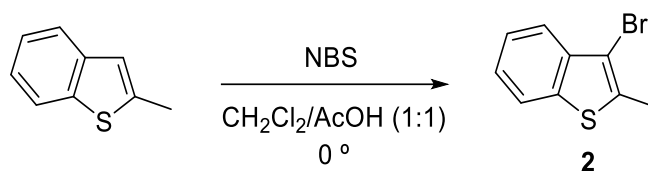
Compound **2** was synthesized following a reported procedure[4]. NBS (10 mmol, 1.72 g) was added slowly over a solution of 3-bromo-2-methylbenzo[*b*]thiophene (9 mmol, 1.31 mL) in a mixture of glacial acetic acid/CH$_2$Cl$_2$ (1:1, 50 mL), at 0 °. The reaction mixture was stirred for 15 h quenched with 100 mL of a sat. aqueous Na$_2$S$_2$O$_3$. The organic layer was washed with H$_2$O, dried over MgSO$_4$ and after removal of the solvent the residue was purified by silica gel column chromatography (cyclohexane, Rf = 0.85). The product was obtained as a colourless oil (1.6 g, 94% yield). The spectroscopic data are coincident with those reported in the literature.

^{1}H NMR (300 MHz, CDCl$_3$): δ 7.74–7.73 (m, 1H, CH$_{ar}$), δ 7.72–7.70 (m, 1H, CH$_{ar}$), δ 7.44–7.36 (ddd, J$_{H-H}$ = 7.89 Hz, J$_{H-H}$ = 6.99 Hz, J$_{H-H}$ = 0.9 Hz, 1H, CH$_{ar}$), δ 7.35–7.30 (ddd, J$_{H-H}$ = 8.25 Hz, J$_{H-H}$ = 7.11 Hz, J$_{H-H}$ = 1.14 Hz, 1H, CH$_{ar}$), δ 2.56 (s, 3H, CH$_3$).

7.74
7.70
7.44
7.44
7.42
7.41
7.39
7.39
7.36
7.35
7.33
7.31
7.30

- CDCl₃

2.56

2.0
1.0
1.0

3.0

0.0 9.5 9.0 8.5 8.0 7.5 7.0 6.5 6.0 5.5 5.0 4.5 4.0 3.5 3.0 2.5 2.0 1.5 1.0 0.5 0
ppm
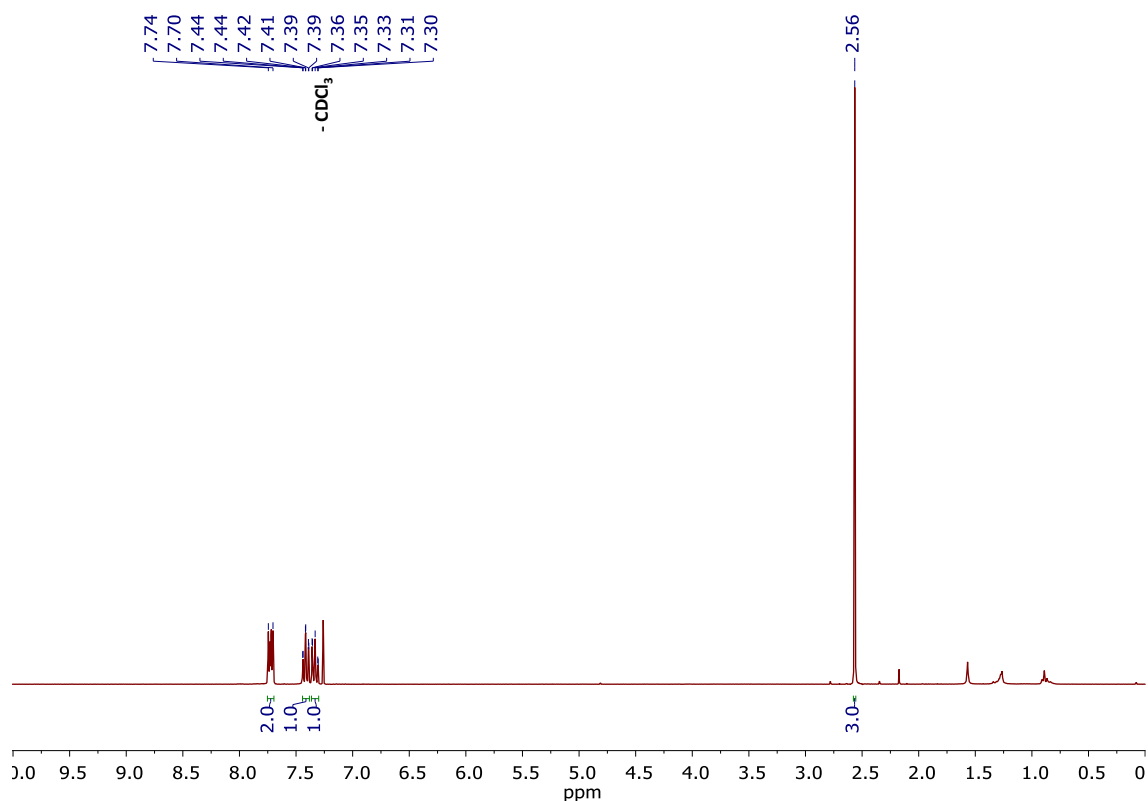
Figure S2. ^{1}H NMR of 3-bromo-2-methylbenzo[*b*]thiophene (**2**). (CDCl₃, 300 MHz).

2.1.3 Compound 2,4-dibromo-5-methylthiophene (3):
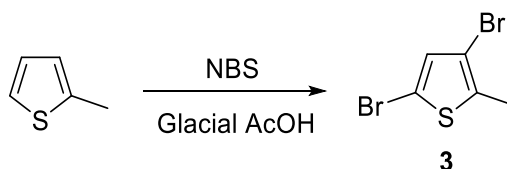
Compound **3** was synthesized following the literature procedure, slightly modified[5]. 2-methylthiophene (40 mmol, 3.92 mL) was dissolved in glacial acetic acid (50 mL). NBS (80 mmol, 15.20 g) was added slowly over the pale yellow solution. The colour changed to red and finally to orange. The reaction mixture was stirred overnight, and neutralized to pH 6-7 with aqueous NaOH (15%). The desired product was extracted with CH₂Cl₂, and the organic layer washed with H₂O. After evaporation of the solvent of the organic phase, the product was obtained as a red liquid (8.7 g, 85%). The spectroscopic data are in agreement with those reported in the literature.

^{1}H NMR (300 MHz, CDCl₃): δ 6.86 (s, 1H, *CH$_{ar}$*), δ 2.34 (s, 3H, *CH$_3$*).
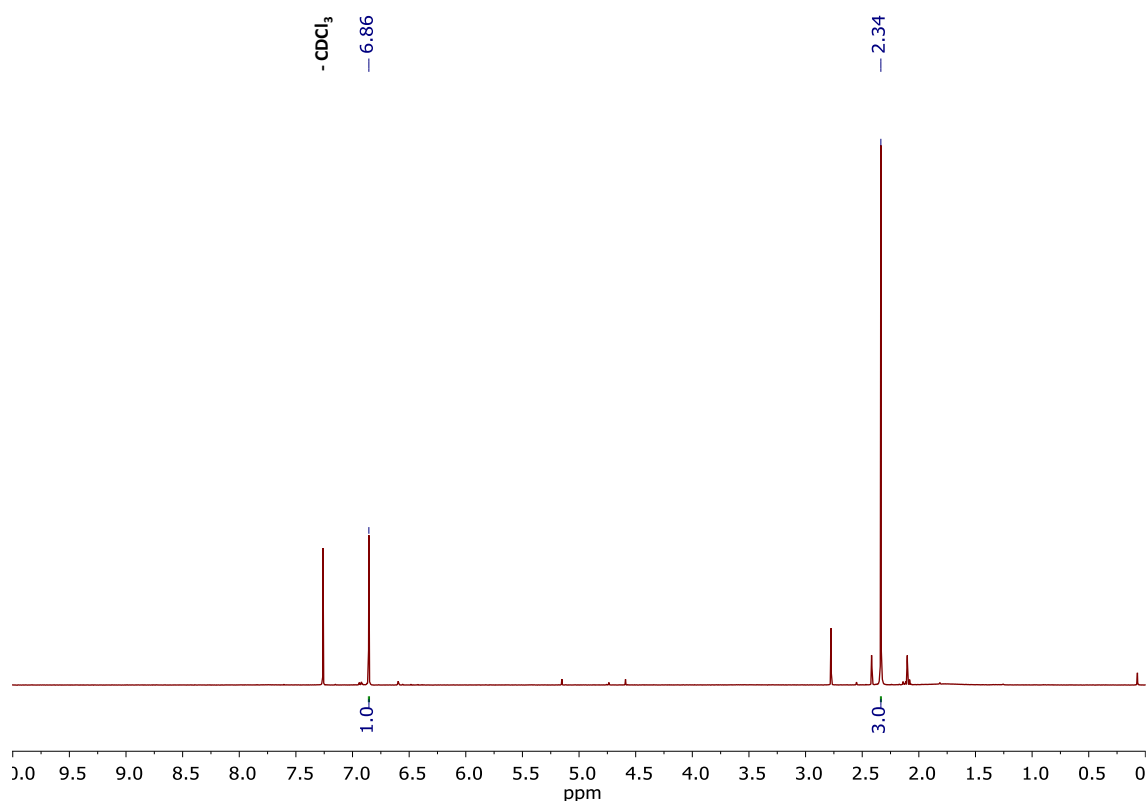
Figure S3. ^{1}H NMR of 2,4-dibromo-5-methylthiophene (**3**). (CDCl$_3$, 300 MHz).

2.1.4 Compound 2-boronic acid-4-bromo-5-methylthiophene (4):
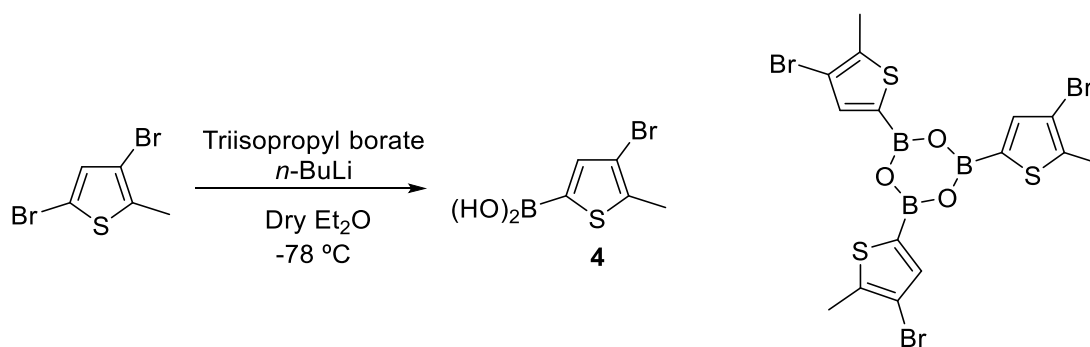
Compound **4** was synthesized following a reported procedure[6]. Under N$_2$, 2,4-dibromo-5-methylthiophene (16 mmol, 4.20 g) were dissolved in freshly distilled diethyl ether (80 mL). The solution was cooled down to – 78 °C. At this temperature, n-BuLi (20 mmol, 7.84 mL, 2.5 M) was added to the solution dropwise.The reaction was stirred for 30 minutes at – 78 °C and triisopropil borate (41 mmol, 9.46 mL) was added. The reaction was warmed slowly overnight to R.T. The reaction was quenched with HCl and stirred for 30 minutes. The organic layer was washed with aq. NaOH (1.2 M). In an ice bath, the aqueous layers were combined and concentrated HCl was added until the pH was turned to 1. At this point, a precipitate was observed. The solid was filtered under vacuum, washed with H$_2$O and dried under vacuum. The product was obtained as a pale brown solid. (1.99 g, 60% Yield). The spectroscopic data are coincident with those reported in the literature.

^{1}**H NMR (CDCl$_3$)**: δ 7.75 (s, 1H, CH$_{ar}$), δ 7.34 (s, 1H, CH$_{ar}$), δ 2.51 (s, 3H, CH$_3$), δ 2.45 (s, 3H, CH$_3$).

213
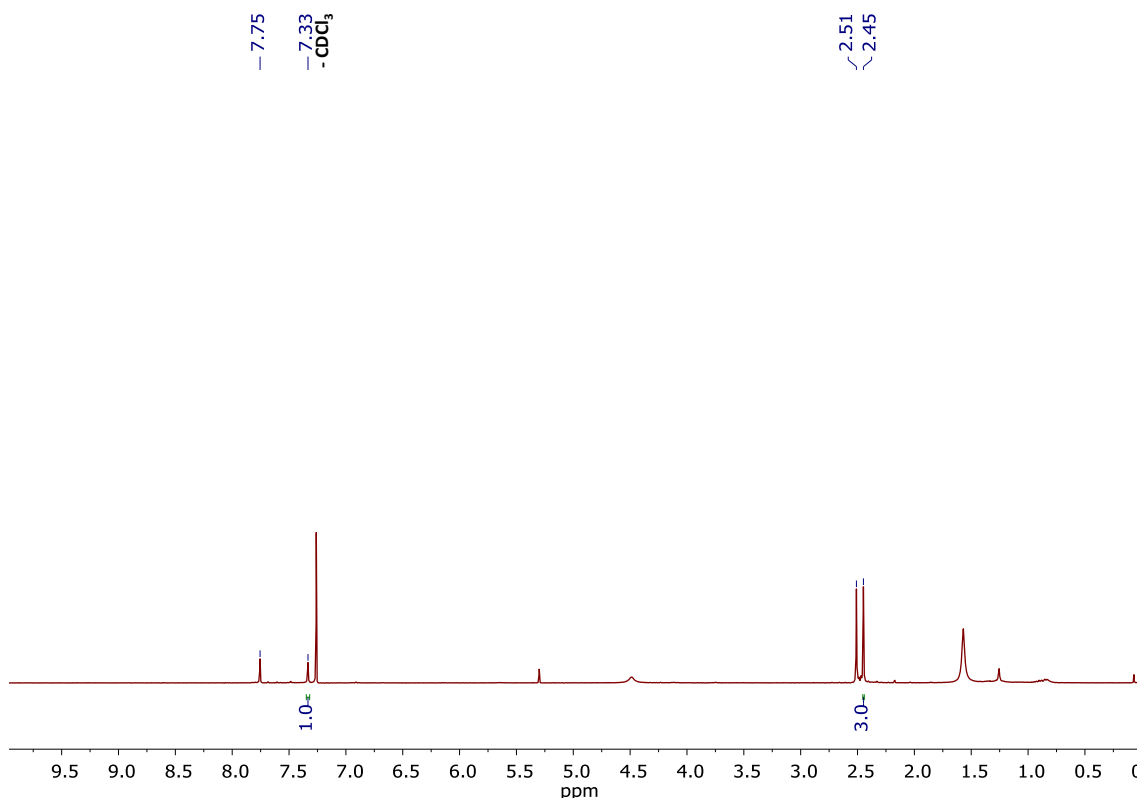
Figure S4. ^{1}H NMR of 2-boronic acid-5-methylthiophene (**4**). (CDCl₃, 300 MHz).

2.1.5 Compound 3-bromo-2-methyl-5-(*p*-tolyl)thiophene (5):
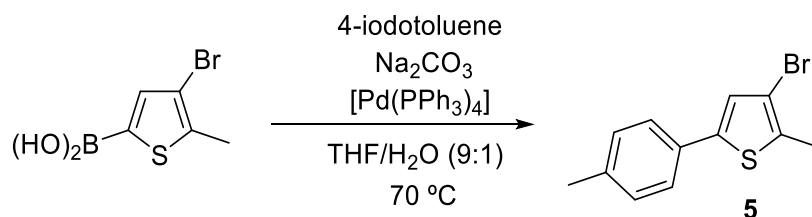
Compound **5** was synthesized following a reported procedure[7]. Under N₂, 2-boronic acid-5-methylthiophene (11.3 mmol, 2.5 g), 2-iodotoluene (8.71 mmol, 1.89 g), Na2CO3 (23.07 mmol, 2.44 g) and [Pd(PPh₃)₄] (0.17 mmol, 0.2 g) were dissolved in a degassed mixture of THF/H₂O (9:1) (200 mL). The reaction was stirred overnight at room temperature. To the reaction solution, 40 mL of H₂O and CH₂Cl₂ were added. The organic layer was washed with H₂O and dried over MgSO₄ and after removal of the solvent the residue was purified by silica gel column chromatography (Hexane, Rf = 0.77). The product was obtained as a beige solid. (1.52 g, 66% Yield). The spectroscopic data are coincident with those reported in the literature

^{1}H NMR (CDCl₃): δ 7.40 (d, J_{H-H} = 8.19 Hz, 2H, CH$_{ar}$), δ 7.17 (d, J_{H-H} = 7.95 Hz, 1H, CH$_{ar}$), δ 7.05 (s, 1H, CH$_{ar}$), δ 2.41 (s, 3H, CH₃), δ 2.36 (s, 3H, CH₃).
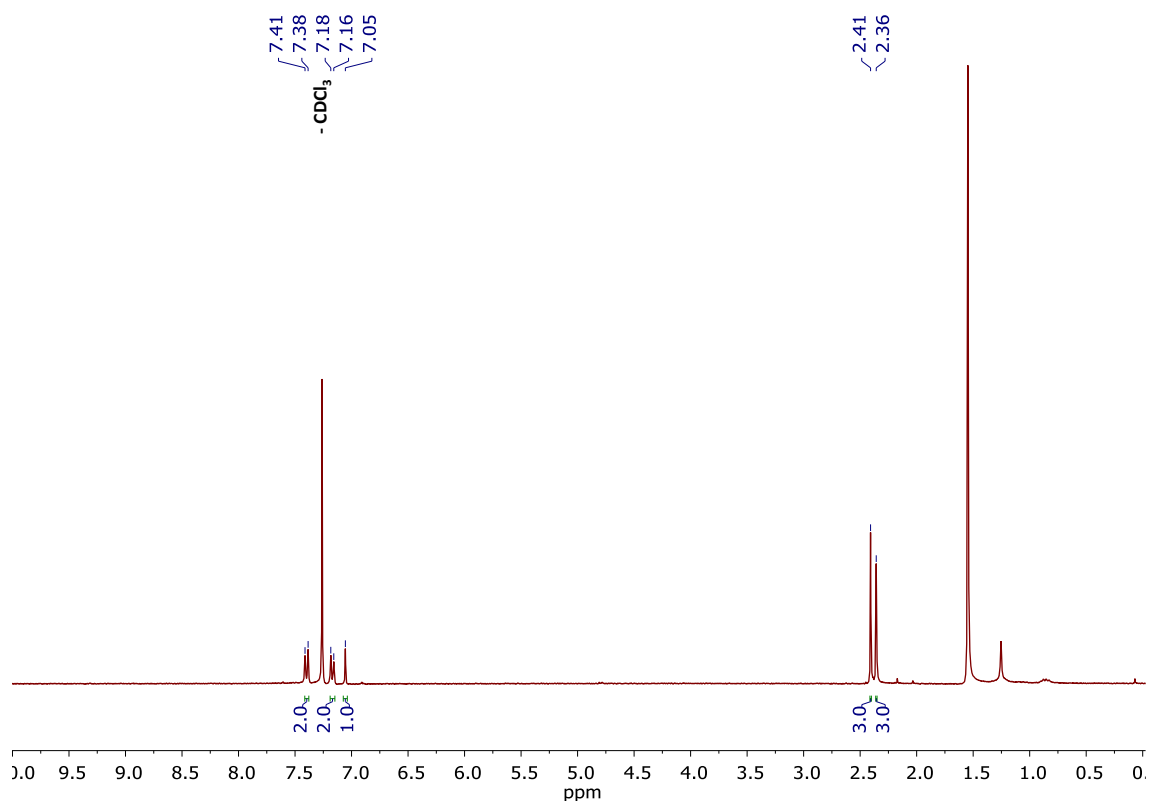
Figure S5. ¹H NMR of 3-bromo-2-methyl-5-(*p*-tolyl)thiophene (**5**). (CDCl₃, 300 MHz).

2.1.6 Compound 2-(4-bromo-5-methylthiophen-2-yl)pyridine (6):
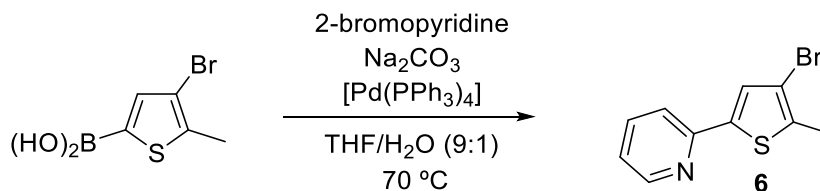
Compound **6** was synthesized following a reported procedure[8]. Under N₂, 2-boronic acid-4-bromo-5-methylthiophene (9.05 mmol, 2 g), 2-bromopyridine (9.05 mmol, 0.86 mL), [Pd(PPh₃)₄] (0.14 mmol, 0.17 g, 1.5%) and Na₂CO₃ (38.78 mmol, 4.11 g) were dissolved in a degassed mixture of THF/H₂O (9:1) (50 mL). The reaction was refluxed overnight at 70 °C. To the reaction solution, 40 mL of H₂O and Et₂O were added. The organic layer was washed with H₂O and dried over MgSO₄ and after removal of the solvent the residue was purified by silica gel column chromatography (Hexane/AcOEt (95:5), Rf = 0.38). The product was obtained as a beige solid. (1.52 g, 66% Yield). The spectroscopic data are coincident with those reported in the literature.

¹H NMR (CDCl₃): δ 8.54 (ddd, J$_{H-H}$ = 1.0 Hz, J$_{H-H}$ = 1.70 Hz, J$_{H-H}$ = 4.90 Hz 1H, CH$_{ar}$), δ 7.68 (td, J$_{H-H}$ = 1.77 Hz, J$_{H-H}$ = 7.95 Hz, 1H, CH$_{ar}$), δ 7.58(dt, J$_{H-H}$ = 1.02 Hz, J$_{H-H}$ = 8.01 Hz, 1H, CH$_{ar}$), δ 7.41 (s, 1H, CH$_{ar}$), δ 7.15 (ddd, , J$_{H-H}$ = 1.10 Hz, J$_{H-H}$ = 4.90 Hz, J$_{H-H}$ = 7.40 Hz, 1H, CH$_{ar}$), δ 2.44 (s, 3H, CH₃).
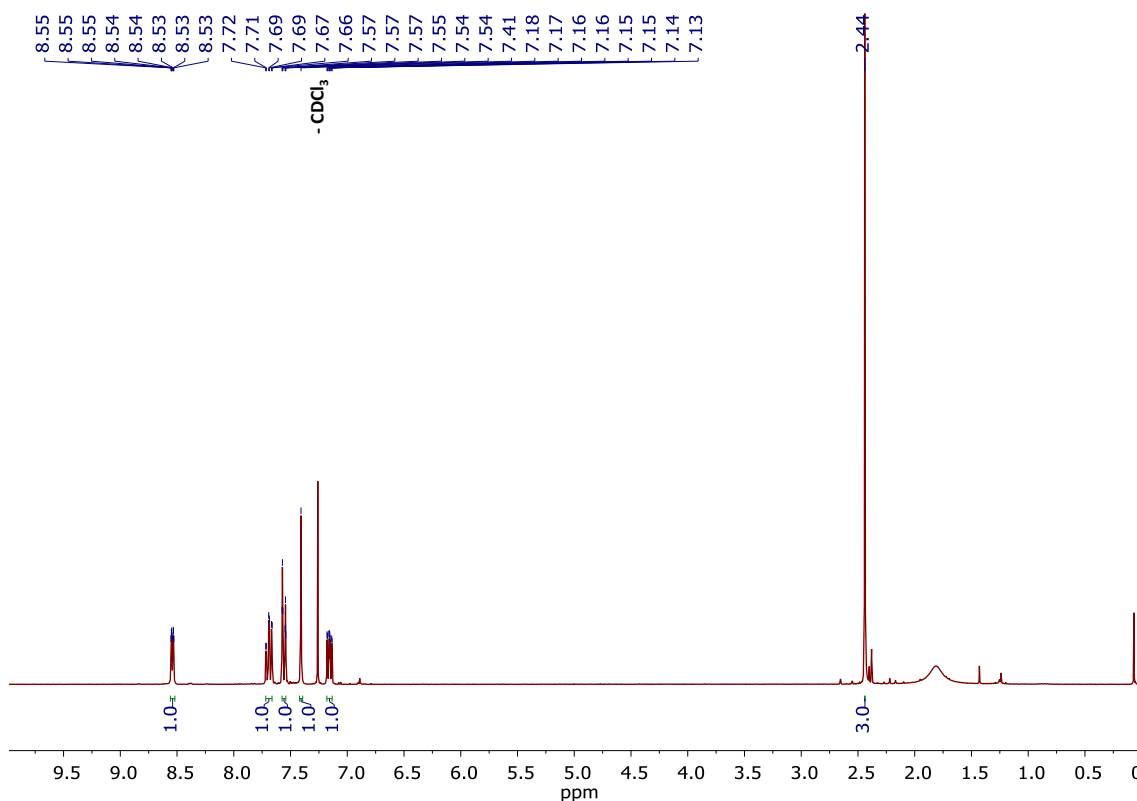
Figure S6. ^{1}H NMR of 2-(4-bromo-5-methylthiophen-2-yl)pyridine (**6**). (CDCl$_3$, 300 MHz).

2.1.7 Compound 2-(5-methylthiophen-3-yl)pyridine (7):
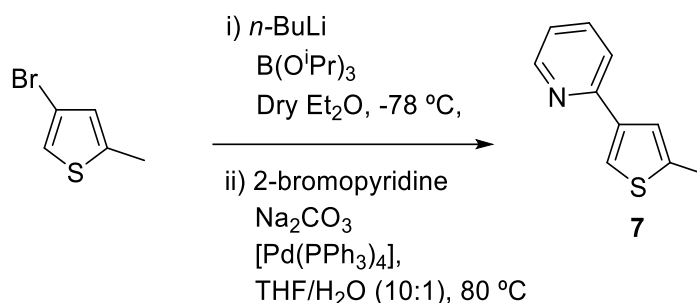
Under N$_2$, 4-bromo-2-methylthiophene (2.68 mmol, 0.3 mL) were dissolved in freshly distilled diethyl ether (25 mL). The solution was cooled down to − 78 °C. At this temperature, n-BuLi (3.2 mmol, 2 mL, 1.6 M) was added to the solution dropwise. The reaction was stirred for 30 minutes at − 78 °C and triisopropil borate (3.5 mmol, 0.8 mL) was added. The cold bath was removed after 10 minutes, allowed the reaction to warm up to R.T, observing the appearance of a white solid. Volatiles were removed under reduced pressure. Under N$_2$ [Pd(PPh$_3$)$_4$] (2,5 mol%; 0,067 mmol, 0,077 g) and Na$_2$CO$_3$ (5,36 mmol, 0,568 g) were added to the reaction crude. The reagents were dissolved in a degassed mixture of THF/H$_2$O (10:1) (27.5 mL). The reaction was refluxed overnight at 80 °C. To the reaction solution, 40 mL of H$_2$O and the mixture was extracted was extracted with Et$_2$O, dried over MgSO$_4$ and after removal of the solvent the residue was purified by silica gel column chromatography (CH$_2$Cl$_2$, Rf = 0.3). The product was obtained as colourless crystals. (0.13 g, 28% yield).

¹H NMR (CDCl₃): δ 8.60 (ddd, J_{H-H} = 0.90 Hz, J_{H-H} = 1.80 Hz, J_{H-H} = 4.90 Hz 1H, CH$_{ar}$), δ 7.68 (td, J_{H-H} = 1.80 Hz, J_{H-H} = 7.86 Hz, 1H, CH$_{ar}$), δ 7.65 (s, 1H, CH$_{ar}$), δ 7.58(dt, J_{H-H} = 1.02 Hz, J_{H-H} = 7.98 Hz, 1H, CH$_{ar}$), δ 7.34 (m, 1H, CH$_{ar}$), δ 7.15 (ddd, , J_{H-H} = 1.10 Hz, J_{H-H} = 4.90 Hz, J_{H-H} = 7.40 Hz, 1H, CH$_{ar}$), δ 2.54 (d, J_{H-H} = 1.10 Hz, 3H, CH₃).
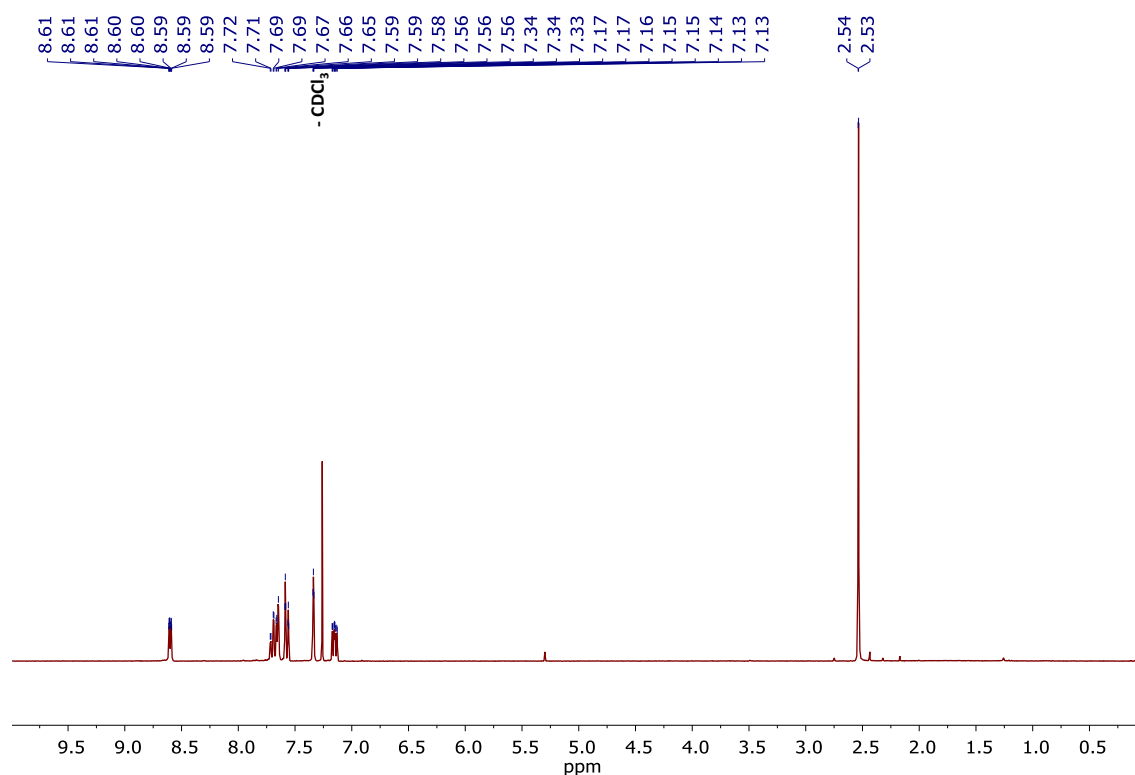
Figure S7. ¹H NMR of 2-(5-methylthiophen-3-yl)pyridine (**7**). (CDCl₃, 300 MHz).

2.1.8 Compound 2-(2,4-dibromo-5-methylthiophen-3-yl)pyridine (8):
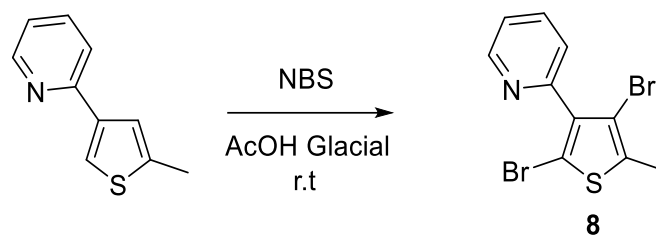
Under air, 2-(5-methylthiophen-3-yl)pyridine (0.63 mmol, 0.11g) were dissolved in glacial AcOH (2 mL). NBS (2.21 mmol, 0.392g) was added portionwise and stirred for 3 hours. The mixture was quenched with KOH (aq) solution, extracted with CH₂Cl₂, dried over MgSO₄. Final compound was obtained as a brown oil (0.1 g, 48% yield). The resultant product was used in the next step without furthermore purification.

¹H NMR (CDCl₃): δ 8.75 (ddd, J_{H-H} = 0.93 Hz, J_{H-H} = 1.77 Hz, J_{H-H} = 4.89 Hz 1H, CH$_{ar}$), δ 7.80 (td, J_{H-H} = 1.80 Hz, J_{H-H} = 7.71 Hz, 1H, CH$_{ar}$), δ 7.43 (dt, , J_{H-H} = 2.91 Hz, J_{H-H} = 7.83 Hz, 1H, CH$_{ar}$), δ 7.327 (ddd, J_{H-H} = 1.17 Hz, J_{H-H} = 4.89 Hz, J_{H-H} = 6.06 Hz, 1H, CH$_{ar}$), δ 2.41 (s, 3H, CH₃).
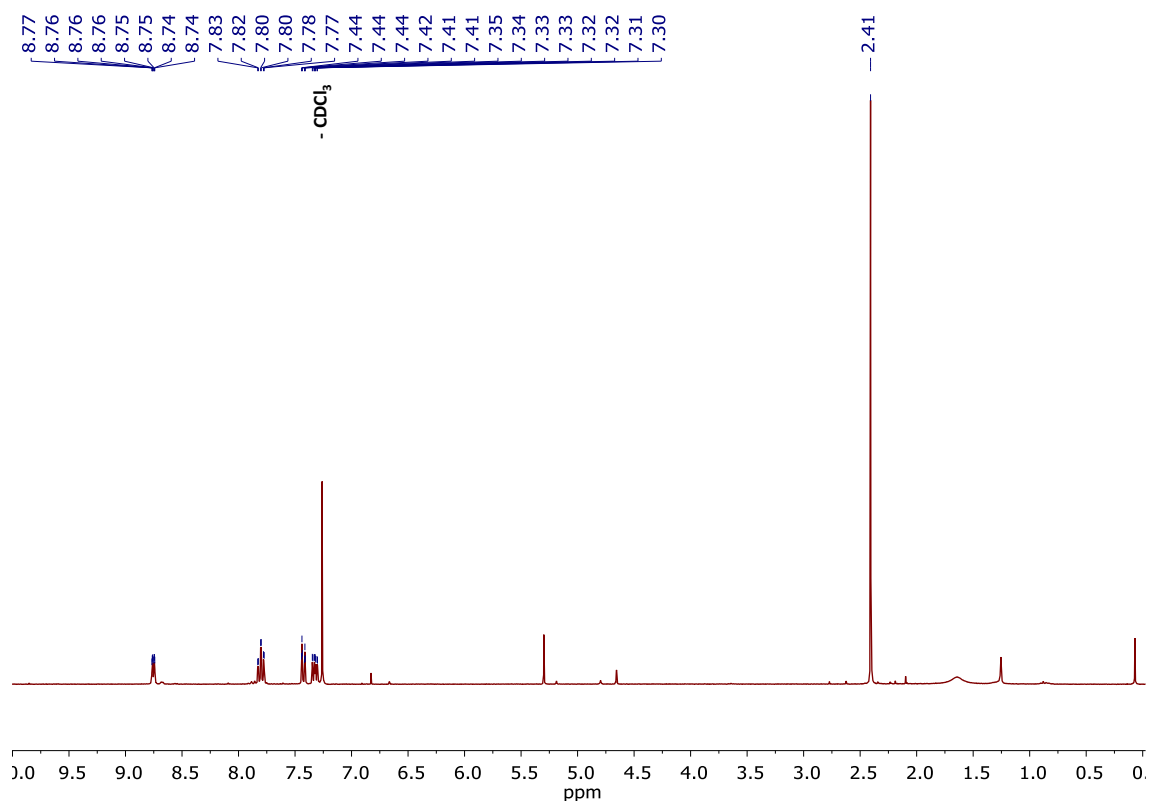
Figure S8. ^{1}H NMR of 2-(2,4-dibromo-5-methylthiophen-3-yl)pyridine (**8**). (CDCl$_3$, 300 MHz).

2.1.9 Compound 2-(4-bromo-5-methylthiophen-3-yl)pyridine (9):
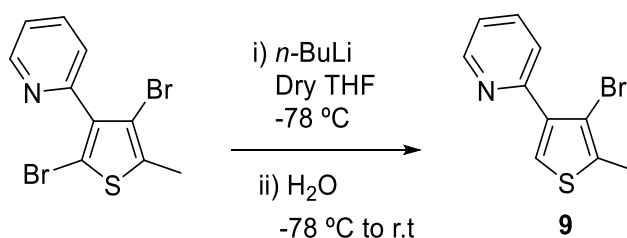
Under N$_2$, 2-(2,4-dibromo-5-methylthiophen-3-yl)pyridine (0.3 mmol, 0.1g) were dissolved in dry THF (10 mL). The solution was cooled down to − 78 °C. At this temperature, n-BuLi (0.36 mmol, 0.36 mL, 1.6M) was added to the solution dropwise. The yellow solution was kept at -78 °C for 30 min and water (5 drops) was added. After 10 min, the cold bath was removed and the reaction allowed to warm up to room temperature. White solid precipitated and volatiles were removed under reduced pressure. H$_2$O and Et$_2$O were added. The mixture was extracted with Et$_2$O, dried over MgSO$_4$, and volatiles removed. The crude product was used without further purification in the next step. The final compound was obtained as a colorless oil (0.06 g, 81% yield)

^{1}H NMR (CDCl$_3$): δ 8.69 (ddd, J$_{H-H}$ = 1.08 Hz, J$_{H-H}$ = 1.68 Hz, J$_{H-H}$ = 4.86 Hz 1H, CH$_{ar}$), δ 7.77-7.74 (m, 2H, CH$_{ar}$), δ 7.53 (s, 1H, CH$_{ar}$), δ 7.27 (ddd, , J$_{H-H}$ = 0.96 Hz, J$_{H-H}$ = 4.71 Hz, J$_{H-H}$ = 7.20 Hz, 1H, CH$_{ar}$), δ 2.50 (s, 3H, CH$_3$).
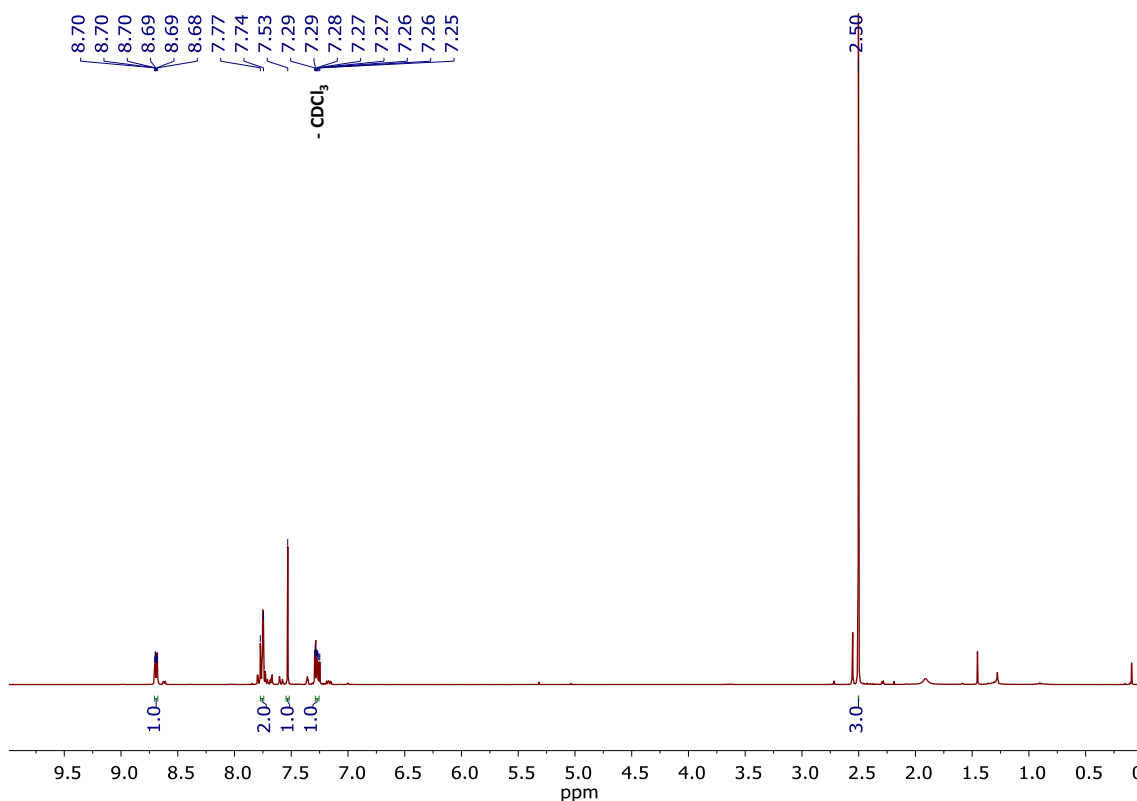
Figure S9. ^{1}H NMR of 2-(4-bromo-5-methylthiophen-3-yl)pyridine (**9**). (CDCl$_3$, 300 MHz).

2.1.10 Compound 2-methyl-3-(perfluorocyclopent-1-en-1-yl)-5-(p-tolyl)thiophene (10):
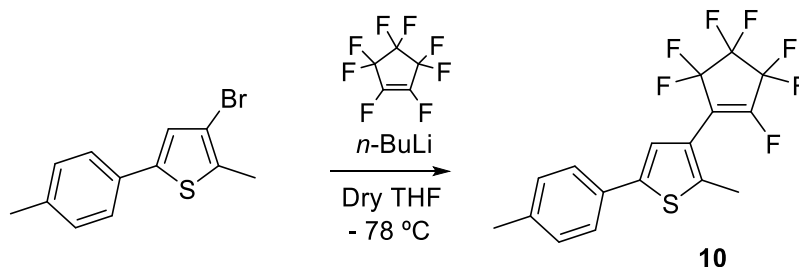
Compound **10** was synthesized following a reported procedure[9]. Under N$_2$, 3-bromo-2-methyl-5-(*p*-tolyl)thiophene (2.99 mmol, 0.8 g) were dissolved in freshly distilled THF (40 mL). In another flask, octafluorocyclopentene (12 mmol, 1.66 mL) were dissolved in freshly distilled THF (40 mL). Both solutions were cooled down to − 78 °C. Then, n-BuLi (3.59 mmol, 2.24 mL, 1.6 M) were added dropwise over the thiophene solution. The reaction was stirred for 30 minutes at − 78 °C. Then, via cannula, the lithiated reaction was added over the octafluorocyclopentene solution. The reaction was stirred for 30 minutes at this temperature and, after that, warmed up slowly to R.T overnight. The reaction was quenched with aq. HCl. The product was extracted with CH$_2$Cl$_2$, dried over MgSO$_4$ and after removal of the solvent the residue was purified by silica gel column chromatography (hexane, Rf = 0.43). The product was obtained as a brown-greenish solid. (0.31 g, 28% yield). The spectroscopic data are coincident with those reported in the literature.

^{1}**H NMR (CDCl$_3$)**: δ 7.44 (d, J$_{H-H}$ = 8.2 Hz, 2H, CH$_{ar}$), δ 7.20 (d, J$_{H-H}$ = 8.4 Hz, 2H, CH$_{ar}$), δ 7.19 (s, 1H, CH$_{ar}$), δ 2.47 (d, J$_{H-F}$ = 3.1 Hz, 3H, CH$_3$), δ 2.37 (s, 3H, CH$_3$).
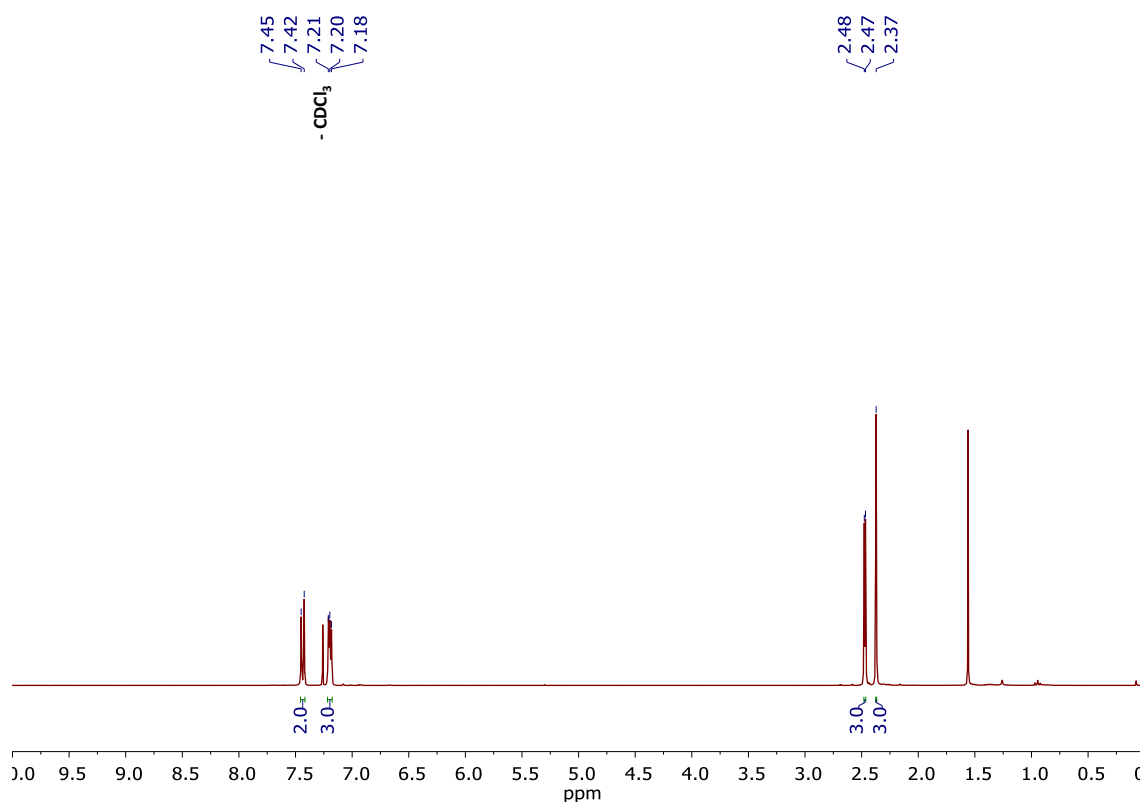
Figure S10. ^{1}H NMR of 2-methyl-3-(perfluorocyclopent-1-en-1-yl)-5-(p-tolyl)thiophene (**10**). (CDCl$_3$, 300 MHz).

2.1.11 Compound (4-bromo-5-methylthiophen-2-yl)trimethylsilane (12):
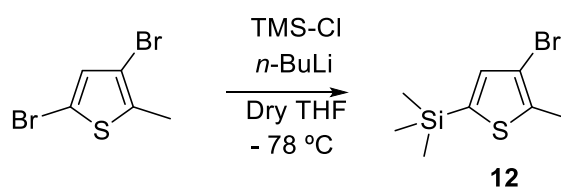
The title compound was synthesized following a reported procedure[10]. Under N$_2$, 2,4-dibromo-5-methylthiophene (4 mmol, 1 g) were dissolved in freshly distilled THF (15 mL). The solution was cooled down to – 78 °C. At this temperature, n-BuLi (5 mmol, 2.90 mL, 1.6M) was added to the solution dropwise. The reaction was stirred for 30 minutes and then, TMS-Cl (8 mmol, 1 mL) was added. The reaction was warmed slowly overnight to R.T). The reaction mixture was quenched with aqueous HCl. The organic layer was washed with H$_2$O, dried over MgSO$_4$ and after removal of the solvent the residue was purified by silica gel column chromatography (petroleum ether, Rf = 0.85). The product was obtained as a colourless oil. Yield: 73%. The spectroscopic data are coincident with those reported in the literature.

^{1}H NMR (300 MHz, CDCl$_3$): δ 7.00 (s, 1H, CH$_{ar}$), δ 2.42 (s, 3H, CH$_3$), δ 0.28 (s, 9H, 3(CH$_3$)).
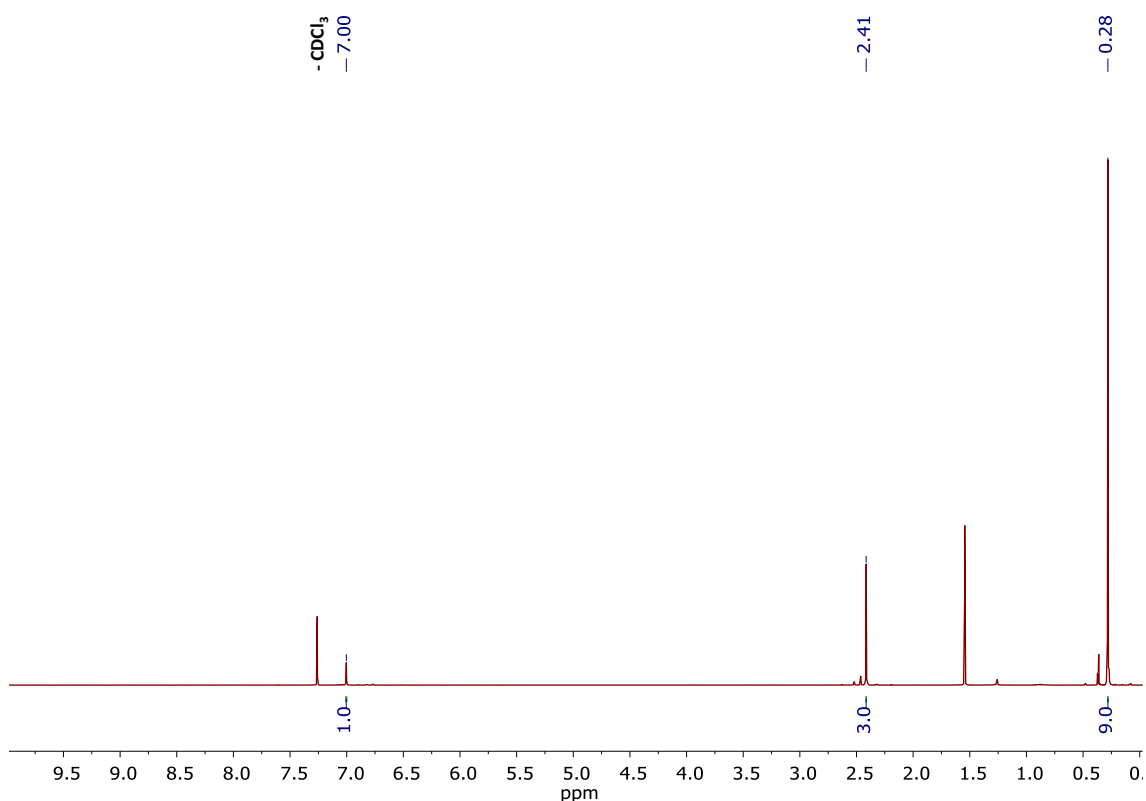
Figure S11. ^{1}H NMR of(4-bromo-5-methylthiophen-2-yl)trimethylsilane (**12**). (CDCl$_3$, 300 MHz).

2.1.12 Compound ((4-bromo-5-methylthiophen-2-yl)ethynyl)trimethylsilane (13):
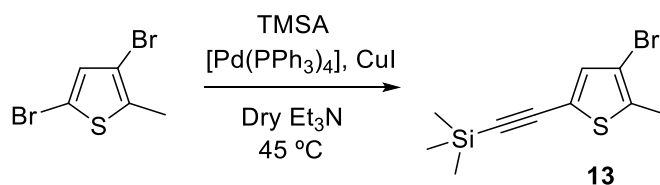
The title compound was synthesized following a reported procedure, slightly modified.[11] Under N$_2$, 2,4-dibromo-5-methylthiophene (18 mmol, 4.57 g) was dissolved in dry Et$_3$N (50 mL). To this solution, TMSA (21 mmol, 3.00 mL), [Pd(PPh$_3$)$_4$] (0.5 mmol, 0.37 g), and CuI (0.0 mmol, 5%, 0.17 g) were added. The reaction was stirred at 45 °C for 15 h. After removal of the solvent, the black residue was extracted with hexane to obtain a yellow solution. After evaporation of the solvent at reduced pressure, the residue was dissolved in CH$_2$Cl$_2$ and washed with H$_2$O and dried over MgSO$_4$. The product was obtained after evaporation of the solvent from the organic layer and purification by silica gel column chromatography (hexane, Rf = 0.83) as a yellow oil (3.46 g, 71% yield). The spectroscopic data are coincident with those reported in the literature.

^{1}H NMR (300 MHz, CDCl$_3$): δ 7.02 (s, 1H, CH$_{ar}$), δ 2.36 (s, 3H, CH$_3$), δ 0.23 (s, 9H, 3(CH$_3$)).

221
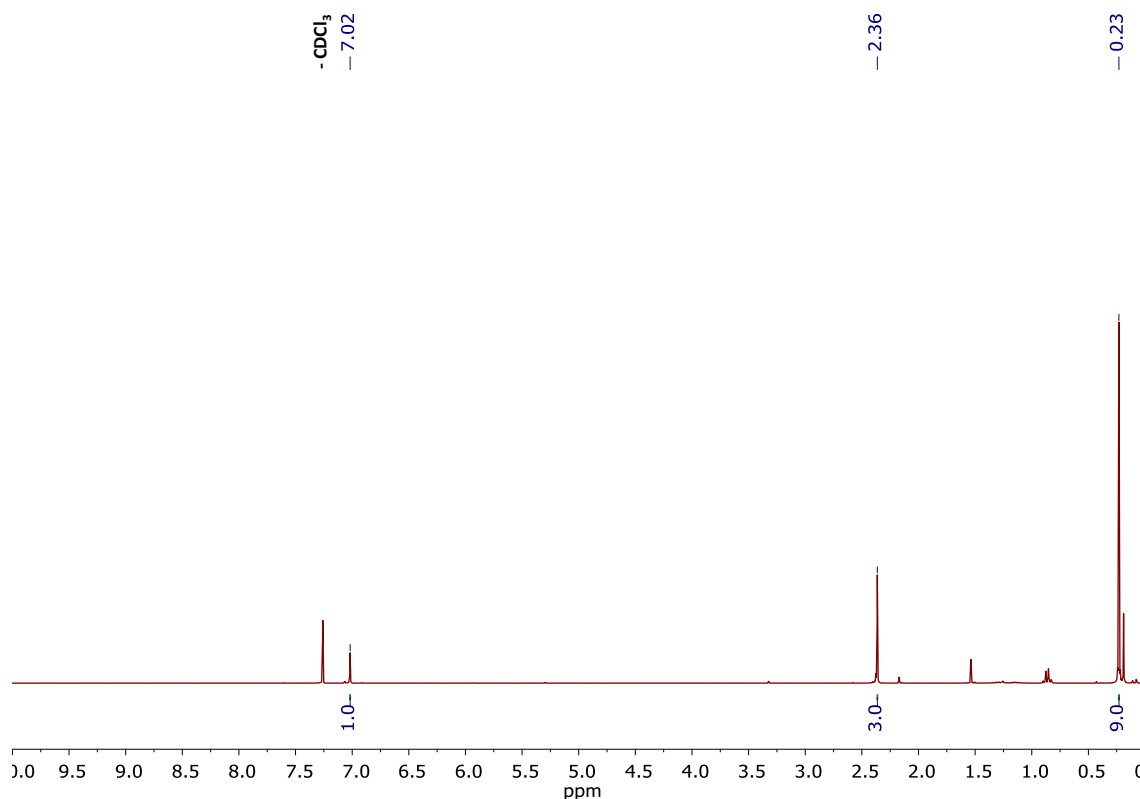
Figure S12. ^{1}H NMR of ((4-bromo-5-methylthiophen-2-yl)ethynyl)trimethylsilane (**13**). (CDCl₃, 300 MHz).

2.1.13 Compound 5-bromo-2,2'-bipyridine (14):
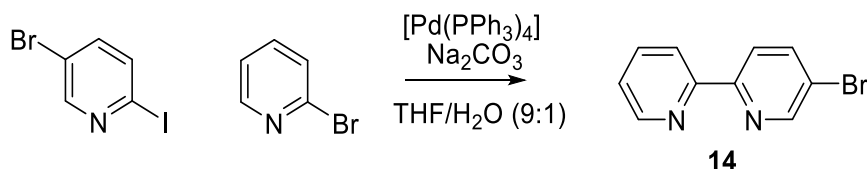
The title compound was synthesized following slightly modified literature procedures.[12] Under N_2, 2-iodo-5-bromopyridine (29 mmol, 8.23 g) were dissolved in freshly distilled THF (40 mL). In another flask, under N_2, [Pd(PPh₃)₄] (0.29 mmol, 0.34 g) were dissolved in bromozinc-pyridine (29 mmol, 58.00 mL). Both solutions were bubbled with N_2 for 5 minutes. Then, the 2-iodo-5-bromopyridine solution was added via cannula over the black reaction. The reaction was stirred at R.T overnight. 200 mL of a solution of EDTA (0.25 M) and NaOH (1 M) was added and stirred for 30 minutes. After that, 100 mL of sat. Na_2CO_3 was added. The product was extracted with CH_2Cl_2, dried over $MgSO_4$ and after removal of the solvent the residue was purified by silica gel column chromatography (petroleum ether/ ethyl acetate (95:5, 9:1, 8:2), Rf = 0.53). The product was obtained as a white solid (3.54 g, 52% yield). The spectroscopic data are coincident with those reported in the literature.

^{1}H NMR (CDCl₃): δ 8.72 (dd, J_{H-H} = 0.48 Hz, J_{H-H} = 2.31 Hz, 1H, CH$_{ar}$), δ 8.67 (ddd, J_{H-H} = 0.87, J_{H-H} = 4.8 Hz, 1H, CH$_{ar}$), δ 8.37 (dt, J_{H-H} = 0.99 Hz, J_{H-H} = 8.01 Hz, 1H, CH$_{ar}$), δ 8.33 (dd, J_{H-H} = 0.54 Hz, J_{H-H} = 8.49 Hz, 1H, CH$_{ar}$), δ 7.93 (dd, J_{H-H} = 2.37 Hz, J_{H-H} = 8.52 Hz, 1H, CH$_{ar}$), δ 7.81 (dt, J_{H-H} = 1.8 Hz, J_{H-H} = 7.65 Hz, 1H, CH$_{ar}$), δ 7.33 (ddd, J_{H-H} = 1.17 Hz, J_{H-H} = 4.8 Hz, J_{H-H} = 5.97, 1H, CH$_{ar}$).
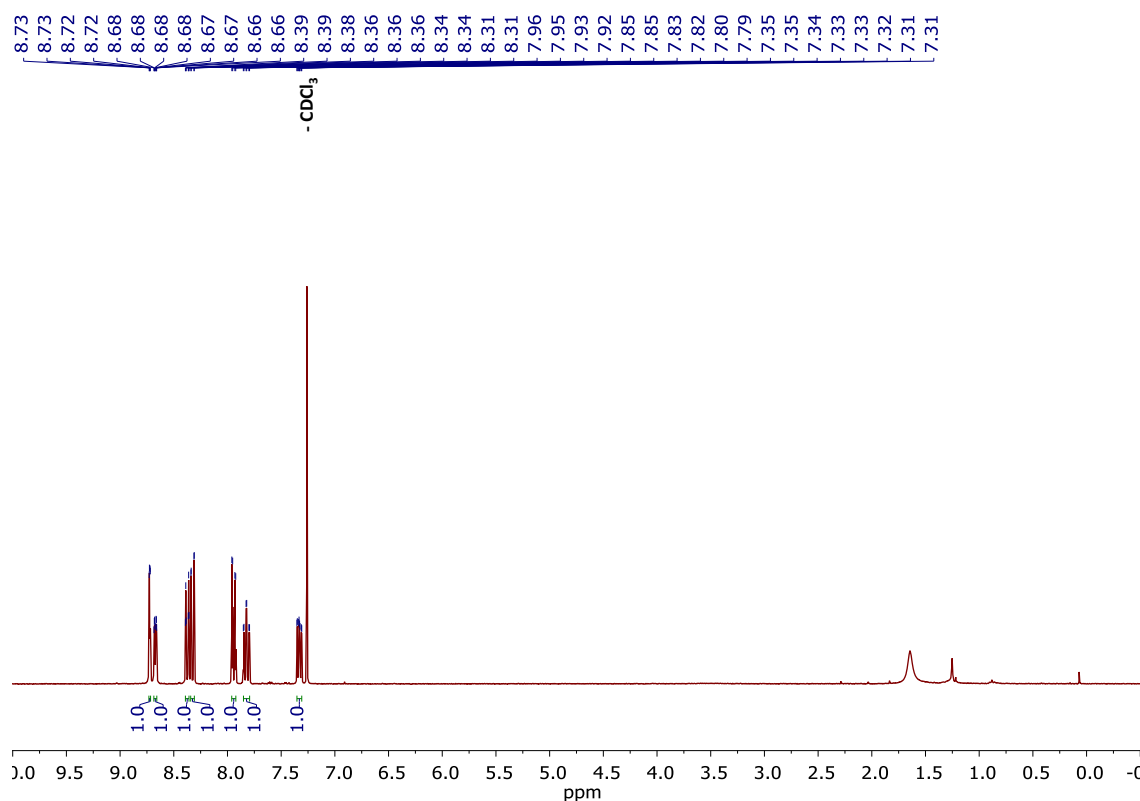
Figure S13. ^{1}H NMR of 5-bromo-2,2'-bipyridine (**14**). (CDCl$_3$, 300 MHz).

2.1.14 Compound 5-((trimethylsilyl)ethynyl)-2,2'-bipyridine (15):
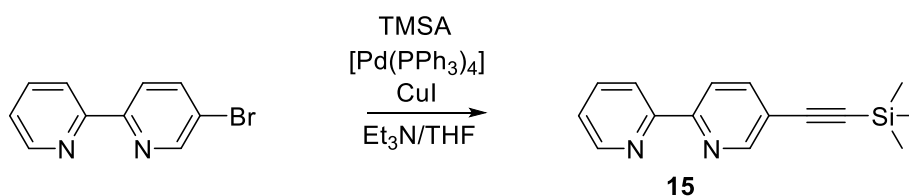
The title compound was synthesized following slightly modified literature procedures.[13] Under N$_2$, 5-bromo-2,2'-bipyridine (0.64 mmol, 0.15 g), [Pd(PPh$_3$)$_4$] (0.032 mmol, 0.037 g, 5%), CuI (0.096 mmol, 0.019 g, 15%) were dissolved in a degassed mixture of dry Et$_3$N/THF (8 mL). Then, TMSA (0.7 mmol, 0.1 mL) were added. The reaction was refluxed overnight at 40 °C. The resultant brown solution was evaporated under vacuum. The brown residue was washed several time with CH$_2$Cl$_2$ and with a mixture of NH$_3$ and EDTA. The product was extracted with CH$_2$Cl$_2,$ dried over MgSO$_4$ and after removal of the solvent, the residue was purified by silica gel column chromatography (hexane/AcOEt (9:1), Rf = 0.43). The product was obtained as a brown solid. (0.14 g, 86 % yield). The spectroscopic data are consistent with those reported in the literature.

^{1}H NMR (CDCl$_3$): δ 8.73 (dd, J_{H-H} = 0.69 Hz, J_{H-H} = 2.01 Hz, 1H, CH$_{ar}$), δ 8.69 (ddd, J_{H-H} = 0.75, J_{H-H} = 1.56 Hz, J_{H-H} = 4.74, 1H, CH$_{ar}$), δ 8.40 (dt, J_{H-H} = 0.90 Hz, J_{H-H} = 7.98 Hz, 1H, CH$_{ar}$), δ 8.37 (dd, J_{H-H} = 0.63, J_{H-H} = 8.30, Hz, 1H, CH$_{ar}$), δ 7.87 (dd, J_{H-H} = 2.13 Hz, J_{H-H} = 8.25 Hz, 1H, CH$_{ar}$), δ 7.82 (td, J_{H-H} = 7.92 Hz, J_{H-H} = 4.8 Hz, J_{H-H} = 5.94 Hz, 1H, CH$_{ar}$), δ 7.32 (ddd, J_{H-H} = 1.17, J_{H-H} = 4.83 Hz, J_{H-H} = 7.50, 1H, CH$_{ar}$), δ 0.28 (s, 9H, 3(CH$_3$).
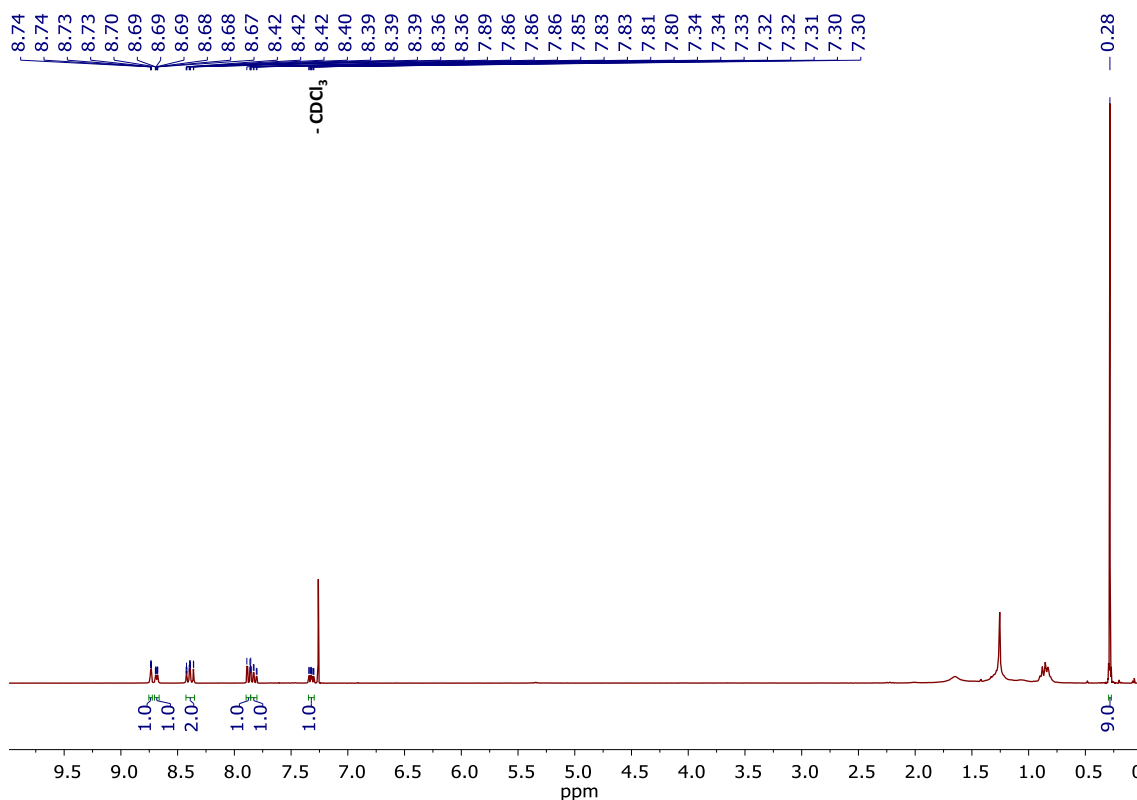
Figure S14. ^{1}H NMR of 5-((trimethylsilyl)ethynyl)-2,2'-bipyridine (**15**). (CDCl$_3$, 300 MHz).

2.1.15 Compound 5-ethynyl-2,2'-bipyridine (16):
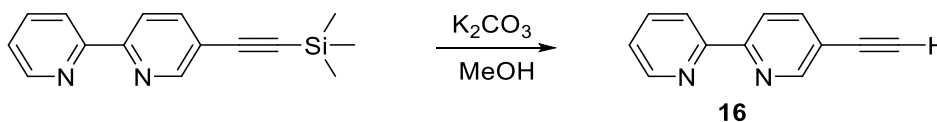
The title compound was synthesized following slightly modified literature procedures.[14] Under N$_2$, 5-((trimethylsilyl)ethynyl)-2,2'-bipyridine (3.05 mmol, 0.77 g), was dissolved in 20 mL of dry MeOH. K$_2$CO$_3$ (9.15 mmol, 1.26 g) were added. The white suspension was stirred overnight. The reaction was washed with H$_2$O and Et$_2$O. The organic layer was dried over MgSO$_4$ and after removal of the solvent the product was obtained as a beige solid. (0.49 g, 86 % yield). The spectroscopic data are consistent with those reported in the literature.

^{1}H NMR (CDCl$_3$): δ 8.77 (d, J_{H-H} = 1.38 Hz, 1H, CH$_{ar}$), δ 8.69 (dd, J_{H-H} = 0.81, J_{H-H} = 1.59 Hz, 1H, CH$_{ar}$), δ 8.41 (m, 1H, CH$_{ar}$), δ 7.90 (d, J_{H-H} = 2.13 Hz, 1H, CH$_{ar}$), δ 7.84 (dt, J_{H-H} = 1.77 Hz, J_{H-H} = 7.68 Hz, 1H, CH$_{ar}$), δ 7.34 (ddd, J_{H-H} = 1.14 Hz, J_{H-H} = 4.8 Hz, J_{H-H} = 5.94 Hz, 1H, CH$_{ar}$), δ 3.29 (s, 1H).

Figure S15. ^{1}H NMR of 5-ethynyl-2,2'-bipyridine (**16**). (CDCl$_3$, 300 MHz).

2.1.16 Compound 5-(4,4,5,5-tetramethyl-1,3,2-dioxaborolan-2-yl)-2,2'-bipyridine (17):

The title compound was synthesized following slightly modified literature procedures.[15] Under N$_2$, 5-bromo-2,2'-bipyridine (13.02 mmol, 3.06 g), were dissolved in 150 mL of dry ether. The colourless solution was cooled down to -78 °C. Then, n-BuLi (13.54 mmol, 8.46 mL, 1.6 M) were added dropwise over the 5-bromo-2,2`-bipyridine. The reaction was stirred for 90 minutes. After that, B(OBu)$_3$ (13.54 mmol, 3.6 mL) were added, observing a red brownish colour. The reaction was warmed up slowly to R.T. After two hours, pinacol (16.14 mmol, 1.91 g) was added, instantaneously colour change to bright orange was observed. Then, after 10 minutes, 1 mL of acetic acid was added and the reaction was stirred overnight. The resultant brown suspension was filtered through celite and was washed with CH$_2$Cl$_2$. The solvent was removed and the product was used in the next step without further purification. The product was obtained as a brown solid. (1.8 g, 49% yield). The spectroscopic data are consistent with those reported in the literature.

^{1}H NMR (CDCl$_3$): δ 9.02 (dd, J_{H-H} = 0.96 Hz, J_{H-H} = 1.71 Hz, 1H, CH$_{ar}$), δ 8.69 (ddd, J_{H-H} = 0.9 Hz, J_{H-H} = 1.8 Hz, J_{H-H} = 2.67 Hz, 1H, CH$_{ar}$), δ 8.48 (d, J_{H-H} = 7.98 Hz, 1H, CH$_{ar}$), δ 8.40 (dd, J_{H-H} = 0.93 Hz, J_{H-H} = 7.92 Hz, 1H, CH$_{ar}$), δ 8.22 (dd, J_{H-H} = 1.74 Hz, J_{H-H} = 7.92 Hz, 1H, CH$_{ar}$), δ 7.84 (td, J_{H-H} = 1.8 Hz,

J_{H-H} = 7.92 Hz, 1H, CH$_{ar}$), δ 7.34 (ddd, J_{H-H} = 1.2 Hz, J_{H-H} = 4.83 Hz, J_{H-H} = 6 Hz, 1H, CH$_{ar}$), δ 1.38 (s, 12H, 4CH$_3$).
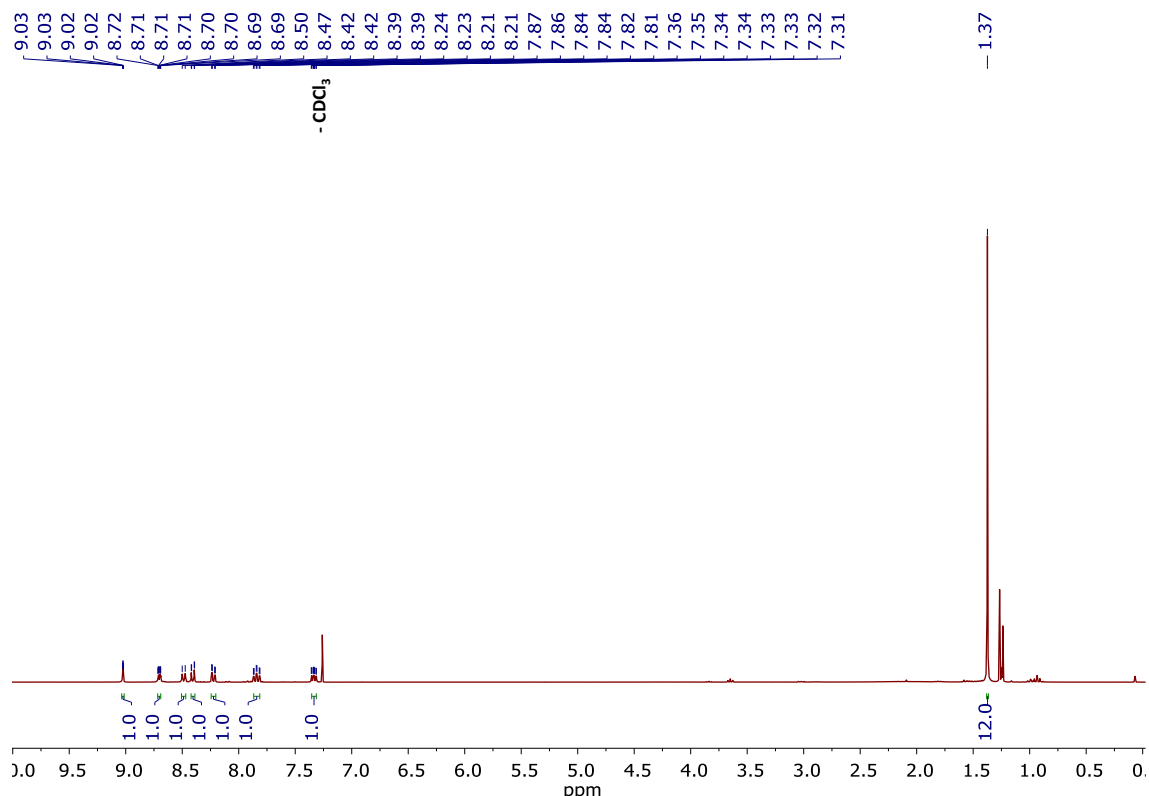
Figure S16. ^{1}H NMR of5-(4,4,5,5-tetramethyl-1,3,2-dioxaborolan-2-yl)-2,2'-bipyridine (**17**). (CDCl$_3$, 300 MHz).

2.1.17 Compound 5-(4-bromo-5-methylthiophen-2-yl)-2,2'-bipyridine (18):
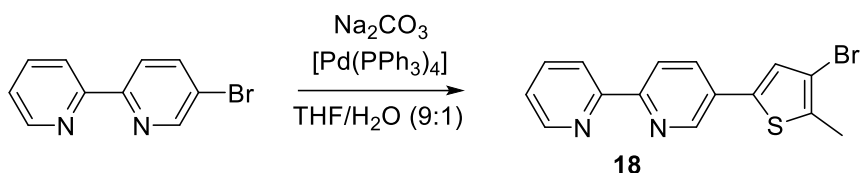
The title compound was synthesized following slightly modified literature procedures.[16] Under N$_2$, 5-bromo-2,2'-bipyridine (4 mmol, 0.86 g), 2-boronic acid-5-methyltiophene (4 mmol, 1.00 g), [Pd(PPh$_3$)$_4$] (0.12 mmol, 0.14 g, 3%) and Na$_2$CO$_3$ (4 mmol, 0.43 g) were dissolved in a degassed mixture of THF/H$_2$O (9:1) (50 mL). The reaction was refluxed overnight at 85 °C. To the reaction solution, 50 mL of sat. aqueous NH$_4$Cl were added and stirred for 15 minutes. The product was extracted with CH$_2$Cl$_2$ and after removal of the solvent the residue was purified by silica gel column chromatography (hexane/ ethyl acetate (9:1, 8:2). The product was obtained as a beige solid. (0.65 g, 49% yield).

^{1}H NMR (CDCl$_3$): δ 8.79 (dd, J_{H-H} = 0.69 Hz, J_{H-H} = 2.37, 1H, CH$_{ar}$), δ 8.63 (ddd, 1H), δ 8.37 (dd, J_{H-H} = 0.69 Hz, J_{H-H} = 8.31 Hz, 1H, CH$_{ar}$), δ 8.36 (dt, J_{H-H} = 0.99 Hz, J_{H-H} = 8.01 Hz, 1H, CH$_{ar}$), δ 7.85 (dd, J_{H-H} = 2.4 Hz, J_{H-H} = 8.34 Hz, 1H, CH$_{ar}$), δ 7.76 (dt, J_{H-H} = 1.83 Hz, J_{H-H} = 7.62 Hz, 1H, CH$_{ar}$), δ 7.26 (ddd, J_{H-H} = 1.17 Hz, J_{H-H} = 4.83 Hz, J_{H-H} = 6.00 Hz, 1H, CH$_{ar}$), δ 7.18 (s, 1H), δ 2.40 (s, 3H),
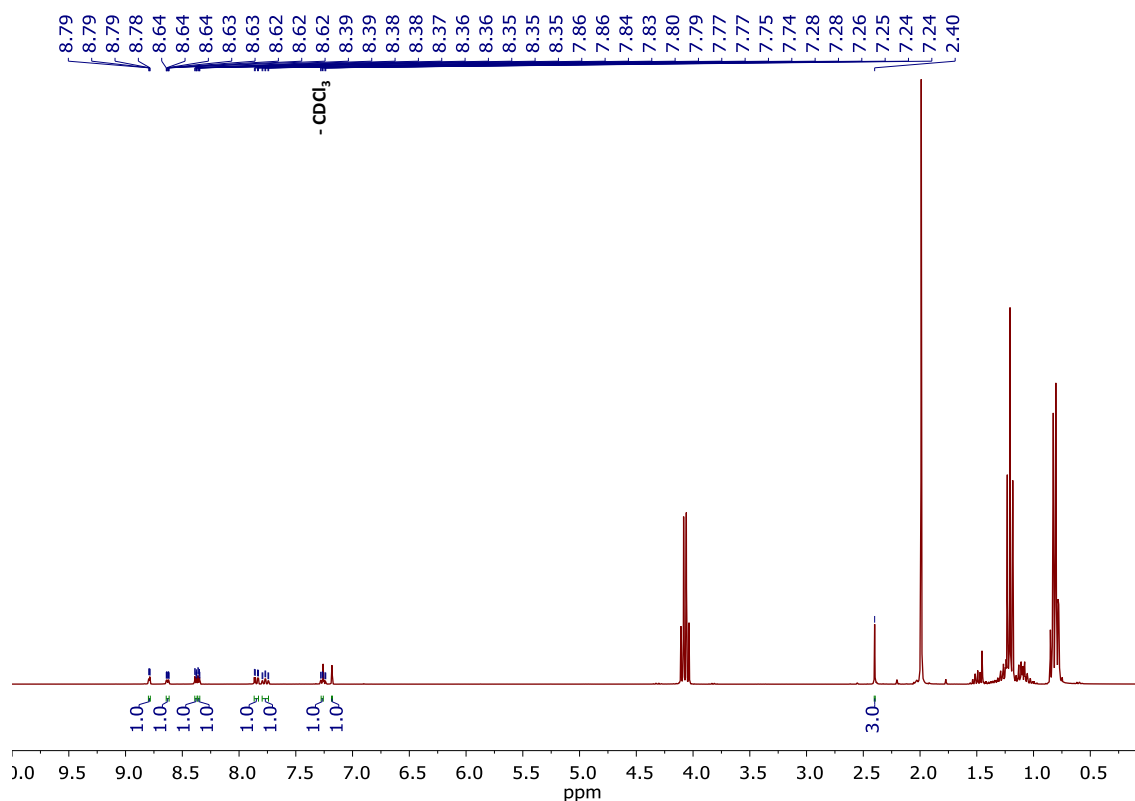
Figure S17. ^{1}H NMR of5-(4-bromo-5-methylthiophen-2-yl)-2,2'-bipyridine (**18**). (CDCl$_3$, 300 MHz).

2.1.18 Compound trimethyl(5-methyl-4-(perfluorocyclopent-1-en-1-yl)thiophen-2-yl)silane (19):
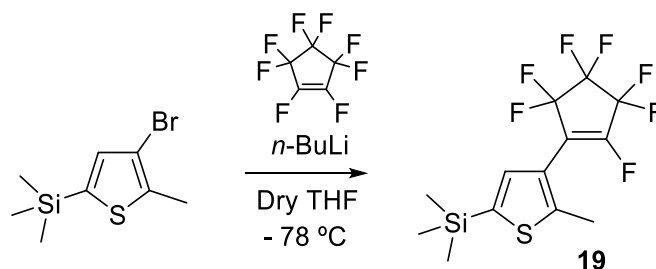

The title compound was synthesized following slightly modified literature procedures.[17] Under N$_2$, (4-bromo-5-methylthiophen-2-yl)trimethylsilane (12.8 mmol, 3.2 g) were dissolved in freshly distilled THF (60 mL). In another flask, octafluorocyclopentene (14.1 mmol, 1.9 mL) were dissolved in freshly distilled THF (20 mL). Both solutions were cooled down to – 78 °C. Then, n-BuLi (15.37 mmol, 9.6 mL, 1.6 M) were added dropwise over the thiophene solution. The reaction was stirred for 30 minutes at – 78 °C. Then, via cannula, the lithiated reaction was added over the octafluorocyclopentene solution. The reaction was stirred for 30 minutes at this temperature and, after that, warmed up slowly to R.T overnight. The reaction was quenched with aq. HCl. The product was extracted with CH$_2$Cl$_2$ and after removal of the solvent the residue was purified by silica gel column chromatography (hexane, Rf = 0.8). The product was obtained as a colourless oil. (3.2 g, 70% yield). The spectroscopic data are consistent with those reported in the literature.

^{1}H NMR (CDCl$_3$): δ 7.14 (s, 1H, CH$_{ar}$), δ 2.47 (d, J$_{H-F}$ = 3.03 Hz, 3H), δ 0.31 (s, 9H, 3(CH$_3$)).

227
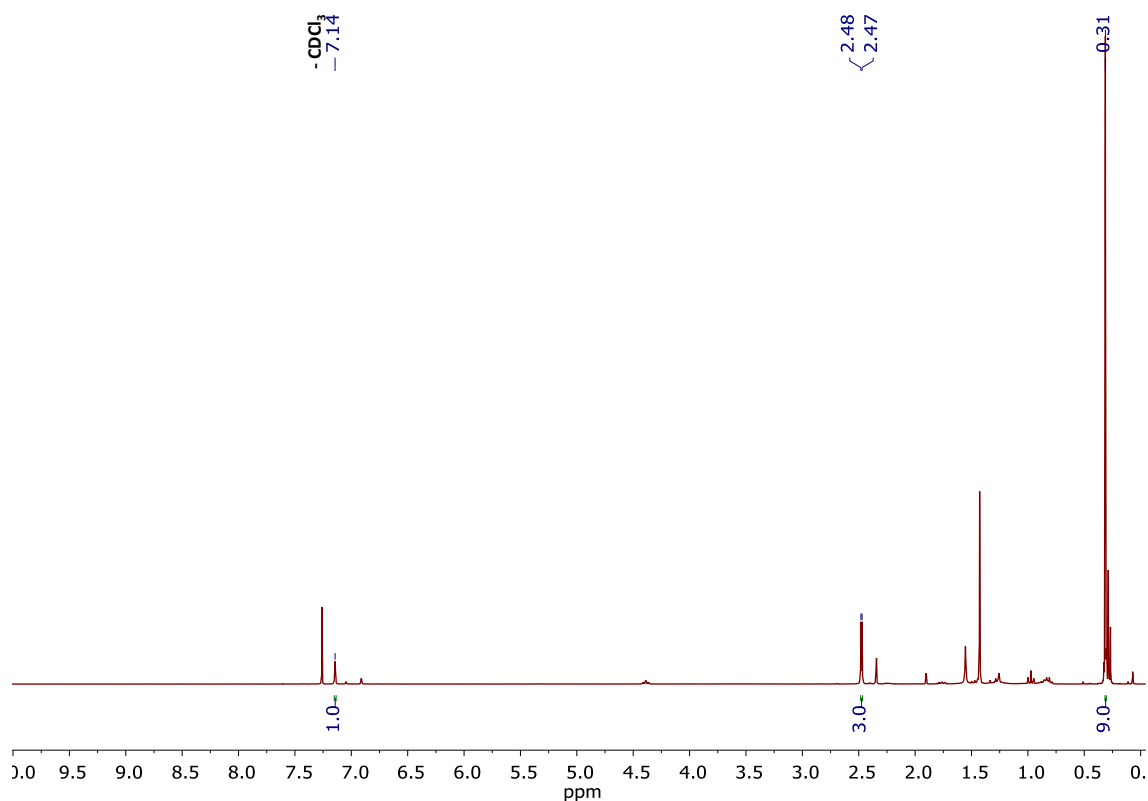
Figure S18. ¹H NMR of trimethyl(5-methyl-4-(perfluorocyclopent-1-en-1-yl)thiophen-2-yl)silane (**19**). (CDCl₃, 300 MHz).

2.1.19 Compound trimethyl((5-methyl-4-(perfluorocyclopent-1-en-1-yl)thiophen-2-yl)ethynyl)silane (20):
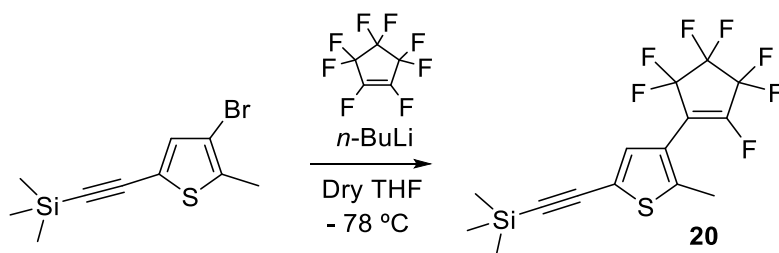
The title compound was synthesized following slightly modified literature procedures.[18] Under N₂, ((4-bromo-5-methylthiophen-2-yl)ethynyl)trimethylsilane (11 mmol, 3.08 g) were dissolved in freshly distilled THF (50 mL). In another flask, octafluorocyclopentene (12 mmol, 1.66 mL) were dissolved in freshly distilled THF (5 mL). Both solutions were cooled down to − 78 °C. Then, n-BuLi (14 mmol, 5.40 mL, 2.5 M) were added dropwise over the thiophene solution. The reaction was stirred for 30 minutes at − 78 °C. Then, via cannula, the lithiated reaction was added over the octafluorocyclopentene solution. The reaction was stirred for 30 minutes at this temperature and, after that, warmed up slowly to R.T overnight. The reaction was quenched with aq. HCl. The product was extracted with CH₂Cl₂ and after removal of the solvent the residue was purified by silica gel column chromatography (hexane, Rf = 0.73). The product was obtained as a yellow oil. (2.76 g, 64% yield). The spectroscopic data are coincident with those reported in the literature. The spectroscopic data are consistent with those reported in the literature.

¹H NMR (CDCl₃): δ 7.19 (s, 1H, CH$_{ar}$), δ 2.42 (d, J_{H-F} = 3.09 Hz, 1H, CH₃), δ 0.24 (s, 9H, 3(CH₃)).
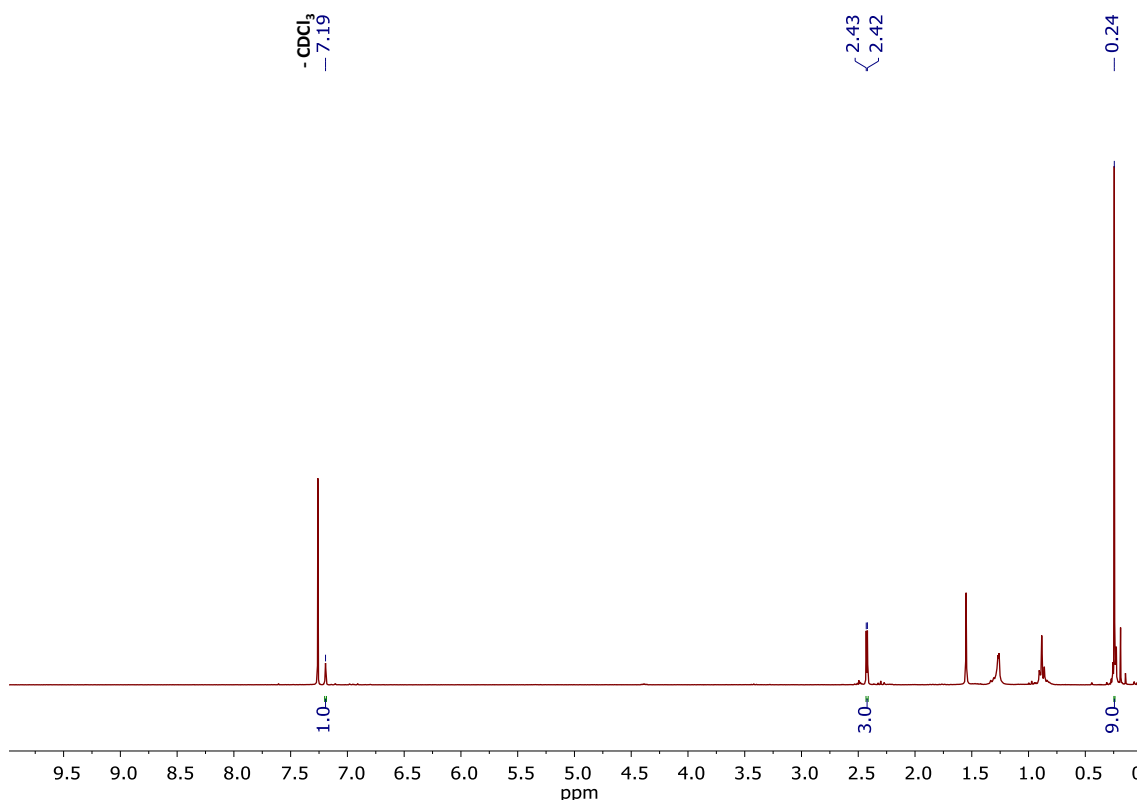
Figure S19. ¹H NMR of trimethyl((5-methyl-4-(perfluorocyclopent-1-en-1-yl)thiophen-2-yl)ethynyl)silane (**20**) . (CDCl₃, 300 MHz).

2.1.20 Compound 2,5-dimethyl-3-(perfluorocyclopent-1-en-1-yl)thiophene (21):
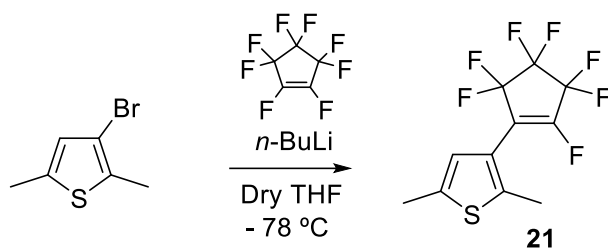
The title compound was synthesized following slightly modified literature procedures.[19] Under N₂, 3-bromo-2,5-dimethylthiophen (5 mmol, 1.06 g) were dissolved in freshly distilled THF (25 mL). In another flask, octafluorocyclopentene (6 mmol, 0.82 mL) were dissolved in freshly distilled THF (10 mL). Both solutions were cooled down to − 78 °C. Then, n-BuLi (7 mmol, 2.64 mL, 2.5 M) were added dropwise over the thiophene solution. The reaction was stirred for 30 minutes at − 78 °C. Then, via cannula, the lithiated reaction was added over the octafluorocyclopentene solution. The reaction was stirred for 30 minutes at this temperature and, after that, warmed up slowly to R.T overnight. The reaction was quenched with aq. HCl. The product was extracted with CH₂Cl₂ and after removal of the solvent the residue was purified by silica gel column chromatography (cyclohexane, Rf = 0.86). The product was obtained as a yellow oil. (1.62 g, 58% yield). The spectroscopic data are coincident with those reported in the literature.

229

^{1}H NMR (CDCl$_3$): δ 6.73 (d, J$_{H-F}$ = 0.99, 1H, CH$_{ar}$), δ 2.43 (s, 1H), δ 2.45 (s, 3H, CH$_3$), δ 2.39 (d, J$_{H-F}$ = 3.3 Hz, 3H, CH$_3$).
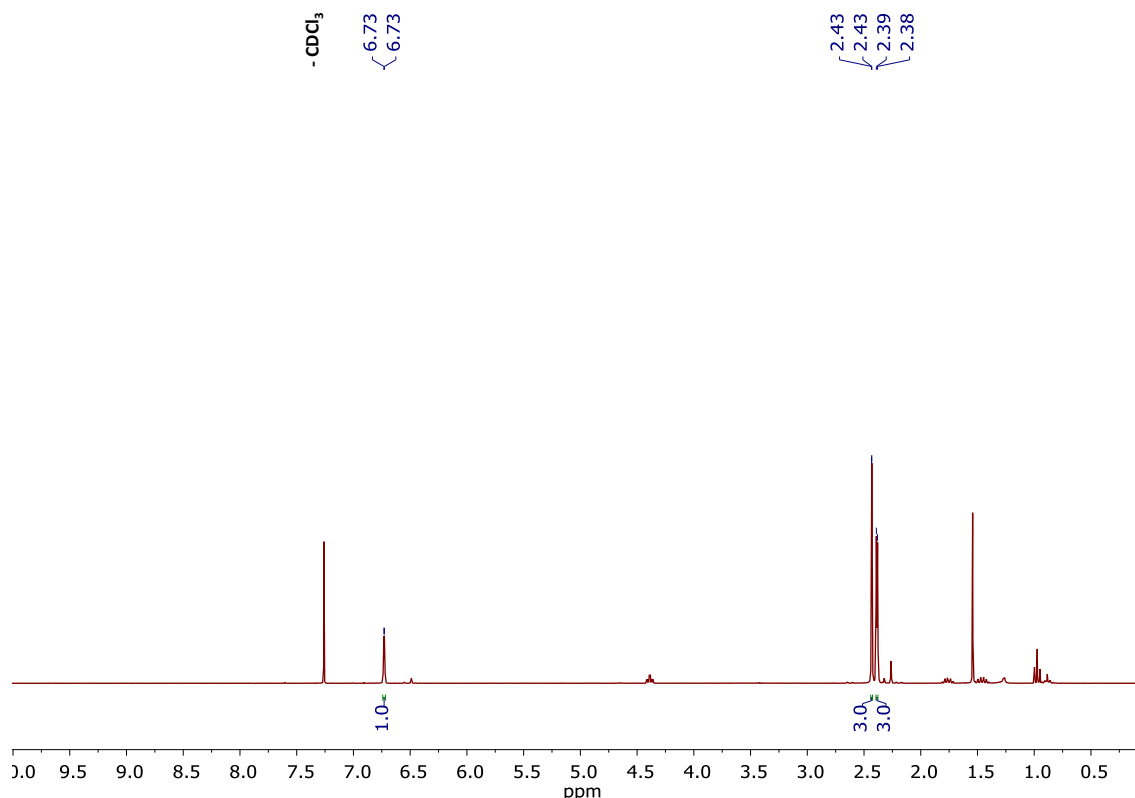
Figure S20. ^{1}H NMR of 2,5-dimethyl-3-(perfluorocyclopent-1-en-1-yl)thiophene (**21**). (CDCl$_3$, 300 MHz).

2.1.21 Compound 2-methyl-3-(perfluorocyclopent-1-en-1-yl)benzo[*b*]thiophene (22):
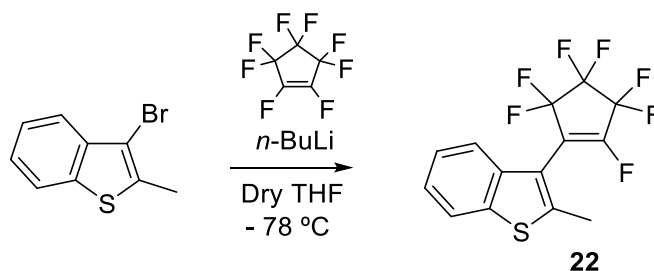
The title compound was synthesized following slightly modified literature procedures.[20] Under N$_2$, 3-bromo-2-methylbenzo[*b*]thiophene (7 mmol, 1.62 g) were dissolved in freshly distilled THF (50 mL). In another flask, octafluorocyclopentene (8 mmol, 1.06 mL) were dissolved in freshly distilled THF (10 mL). Both solutions were cooled down to − 78 °C. Then, n-BuLi (9 mmol, 3.42 mL, 2.5 M) were added dropwise over the thiophene solution. The reaction was stirred for 30 minutes at − 78 °C. Then, via cannula, the lithiated reaction was added over the octafluorocyclopentene solution. The reaction was stirred for 30 minutes at this temperature and, after that, warmed up slowly to R.T overnight. The reaction was quenched with aq. HCl. The product was extracted with CH$_2$Cl$_2$ and after removal of the solvent the residue was purified by silica gel column chromatography (cyclohexane, Rf = 0.75). The product was obtained as a white powder. (1.08 g, 45% yield). The spectroscopic data are coincident with those reported in the literature.

¹H NMR (CDCl₃): δ 7.82 – 7.78 (m, 1H, CH$_{ar}$), δ 7.50 – 7.47 (m, 1H, CH$_{ar}$), δ 7.43 – 7.33 (m, 2H, CH$_{ar}$), δ 2.52 (s, 3H, CH₃).
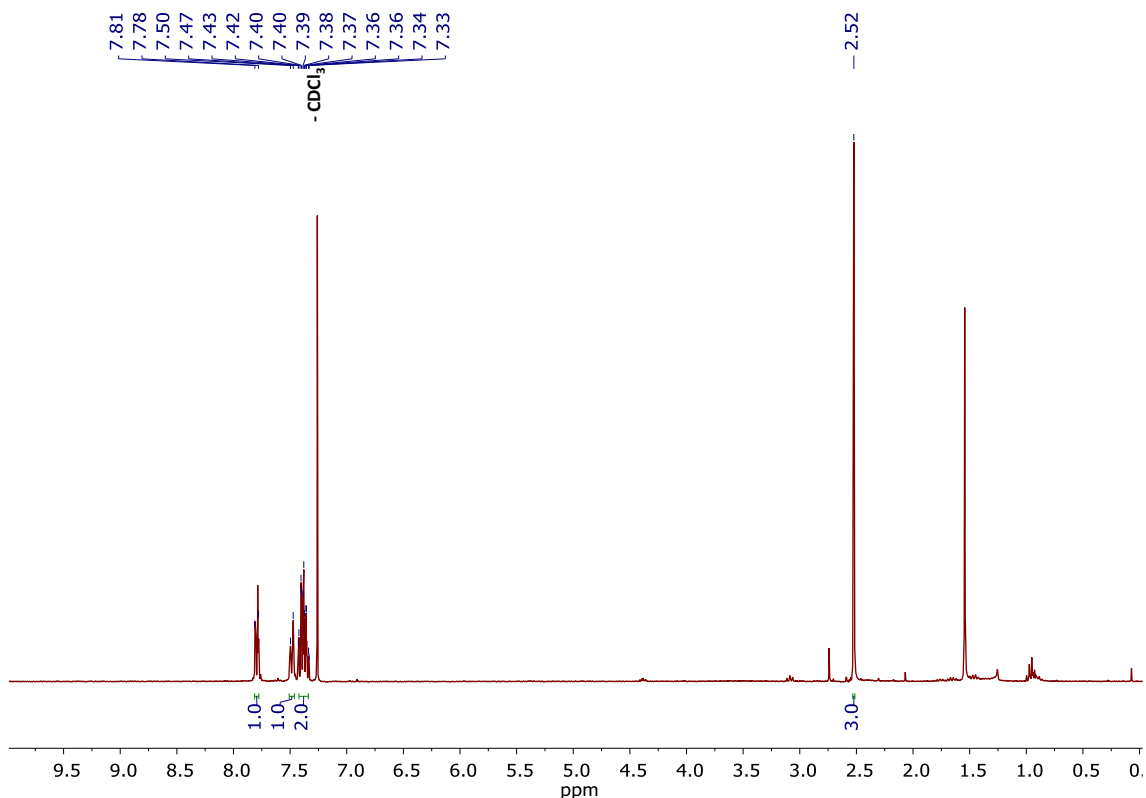
Figure S21. ¹H NMR of 2-methyl-3-(perfluorocyclopent-1-en-1-yl)benzo[*b*]thiophene (**22**). (CDCl₃, 300 MHz).

2.1.22 Compound (4-(2-(2,5-dimethylthiophen-3-yl)-3,3,4,4,5,5-hexafluorocyclopent-1-en-1-yl)-5-methylthiophen-2-yl)trimethylsilane (23):
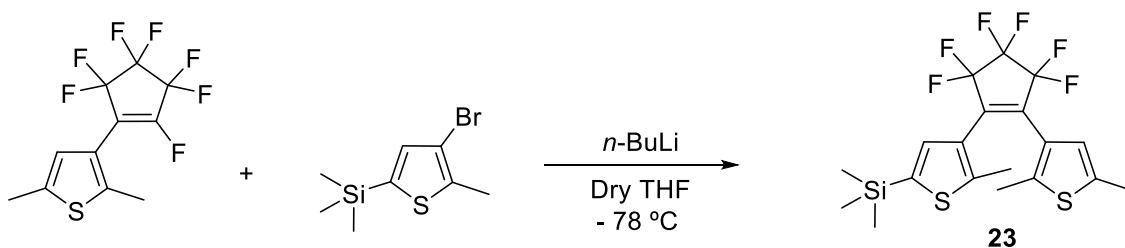
The title compound was synthesized following slightly modified literature procedures.[21] Under N₂, 2,5-dimethyl-3-(perfluorocyclopent-1-en-1-yl)thiophene (4.04 mmol, 1.23 g) were dissolved in freshly distilled THF (25 mL). In another flask, (4-bromo-5-methylthiophen-2-yl)trimethylsilane (4.4 mmol, 1.1 g) were dissolved in freshly distilled THF (25 mL). Both solutions were cooled down to – 78 °C. Then, n-BuLi (1.95 mmol, 1.22 mL, 1.6 M) were added dropwise over , (4-bromo-5-methylthiophen-2-yl)trimethylsilane solution. The reaction was stirred for 30 minutes at – 78 °C. Then, via cannula, the 2,5-dimethyl-3-(perfluorocyclopent-1-en-1-yl)thiophene solution was added over the lithiated reaction. The reaction was stirred for 30 minutes at this temperature and, after that, warmed up slowly to R.T overnight. The reaction was quenched with H₂O. The product was extracted with CH₂Cl₂ and after removal of the solvent

the residue was purified by silica gel column chromatography (hexane, Rf = 0.5). The product was obtained as a pale pink oil. (1.06 g, 58% yield). The spectroscopic data are coincident with those reported in the literature.
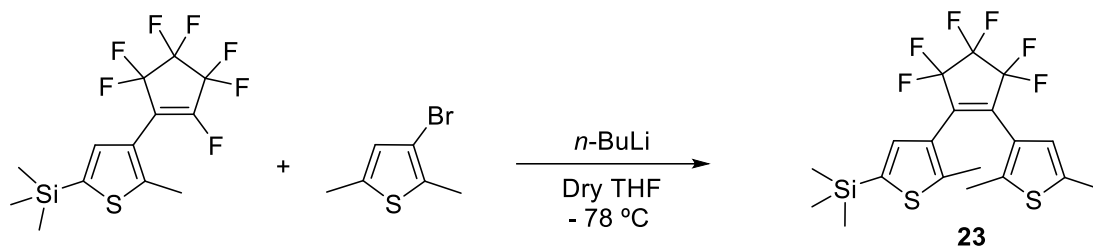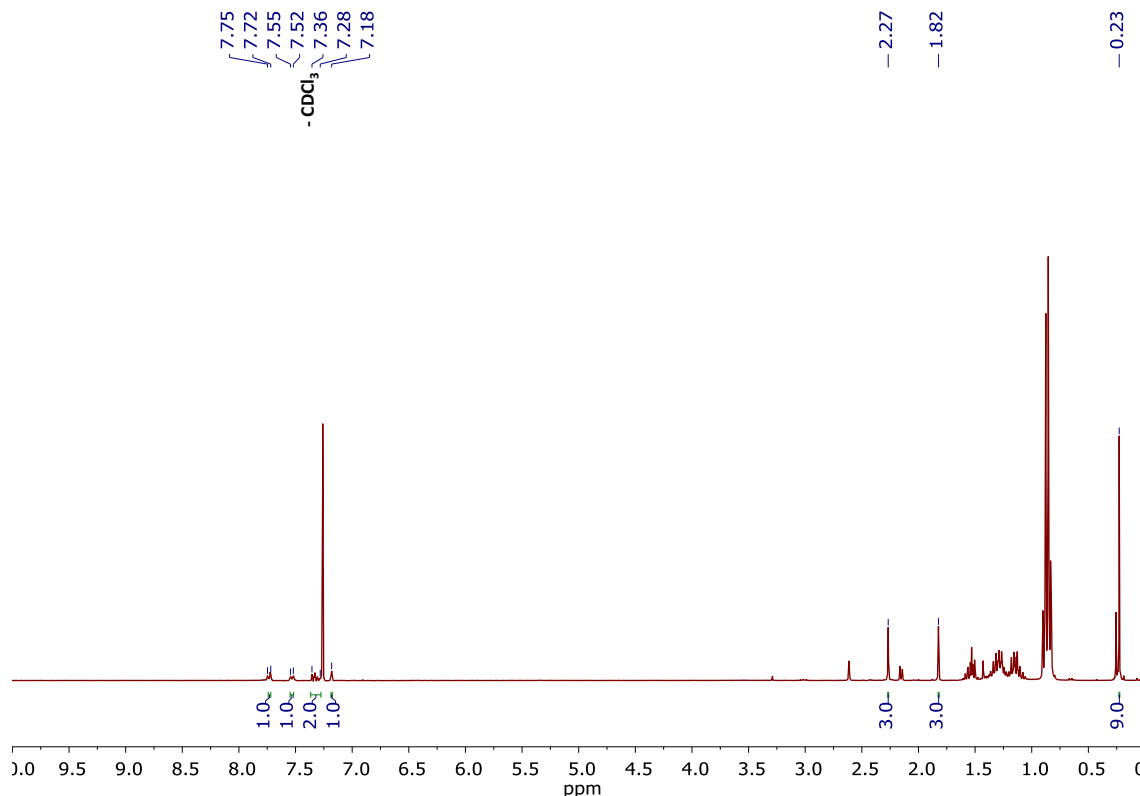

The title compound was synthesized following slightly modified literature procedures. Under N_2, trimethyl(5-methyl-4-(perfluorocyclopent-1-en-1-yl)thiophen-2-yl)silane (3.31 mmol, 1.2 g) were dissolved in freshly distilled THF (20 mL). In another flask, 3-bromo-2,5-dimethylthiophene (3.31 mmol, 0.64 g) were dissolved in freshly distilled THF (20 mL). Both solutions were cooled down to – 78 °C. Then, n-BuLi (3.97 mmol, 2.48 mL, 1.6 M) were added dropwise over , 3-bromo-2,5-dimethylthiophene solution. The reaction was stirred for 30 minutes at – 78 °C. Then, via cannula, the trimethyl(5-methyl-4-(perfluorocyclopent-1-en-1-yl)thiophen-2-yl)silane solution was added over the lithiated , 3-bromo-2,5-dimethylthiophene solution. The reaction was stirred for 30 minutes at this temperature and, after that, warmed up slowly to R.T overnight. The reaction was quenched with H_2O. The product was extracted with CH_2Cl_2 and after removal of the solvent the residue was purified by silica gel column chromatography (hexane, Rf = 0.56). The product was obtained as a pale pink oil. (0.68 g, 45% yield). The spectroscopic data are coincident with those reported in the literature.

¹H NMR (CDCl₃): δ 7.12 (s, 1H, CH$_{ar}$), δ 6.73 (d, J$_{H-H}$ = 1.17 Hz, 1H, CH$_{ar}$), δ 2.43 (d, J$_{H-H}$ = 0.45 Hz, 3H, CH₃), δ 1.96 (s, 3H, CH₃), δ 1.75 (s, 3H, CH₃), δ 0.30 (s, 9H, 3(CH₃).
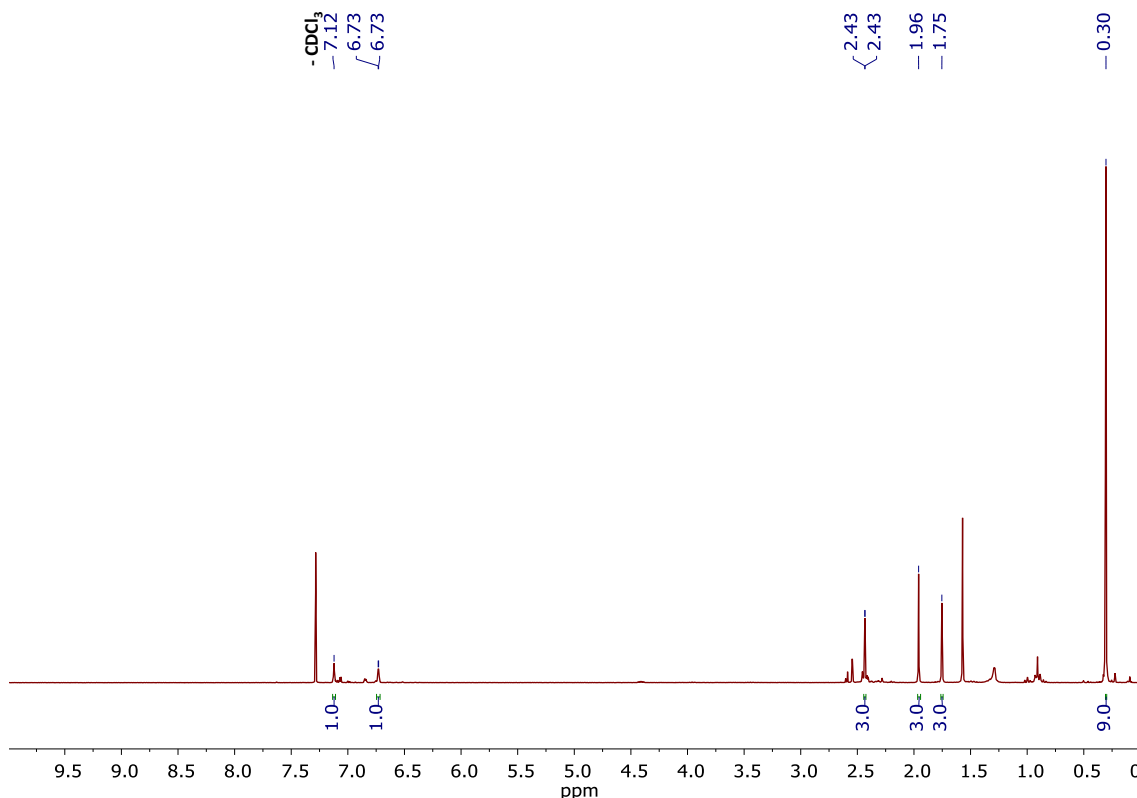
Figure S22. ^{1}H NMR of (4-(2-(2,5-dimethylthiophen-3-yl)-3,3,4,4,5,5-hexafluorocyclopent-1-en-1-yl)-5-methylthiophen-2-yl)trimethylsilane (**23**). (CDCl$_3$, 300 MHz).

2.1.23 Compound (4-(3,3,4,4,5,5-hexafluoro-2-(2-methylbenzo[b]thiophen-3-yl)cyclopent-1-en-1-yl)-5-methylthiophen-2-yl)trimethylsilane (24):
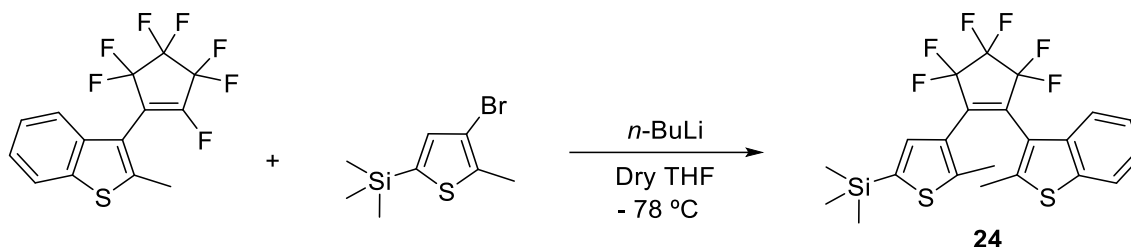
The title compound was synthesized following slightly modified literature procedures.[21] Under N$_2$, 2-methyl-3-(perfluorocyclopent-1-en-1-yl)benzo[*b*]thiophene (4.7 mmol, 1.6 g) were dissolved in freshly distilled THF (20 mL). In another flask, (4-bromo-5-methylthiophen-2-yl)trimethylsilane (5.17 mmol, 1.29 g) were dissolved in freshly distilled THF (40 mL). Both solutions were cooled down to − 78 °C. Then, n-BuLi (6.11 mmol, 3.8 mL, 1.6 M) were added dropwise over the (4-bromo-5-methylthiophen-2-yl)trimethylsilane solution. The reaction was stirred for 30 minutes at − 78 °C. Then, via cannula, the 2-methyl-3-(perfluorocyclopent-1-en-1-yl)benzo[*b*]thiophene solution was added over the lithiated (4-bromo-5-methylthiophen-2-yl)trimethylsilane solution. The reaction was stirred for 30 minutes at this temperature and, after that, warmed up slowly to R.T overnight. The reaction was quenched with H$_2$O. The product was extracted with CH$_2$Cl$_2$ and after removal of the solvent the residue was purified by silica gel column chromatography (hexane, Rf = 0.50). The product was obtained as a pale pink oil. (0.99 g, 43% yield).
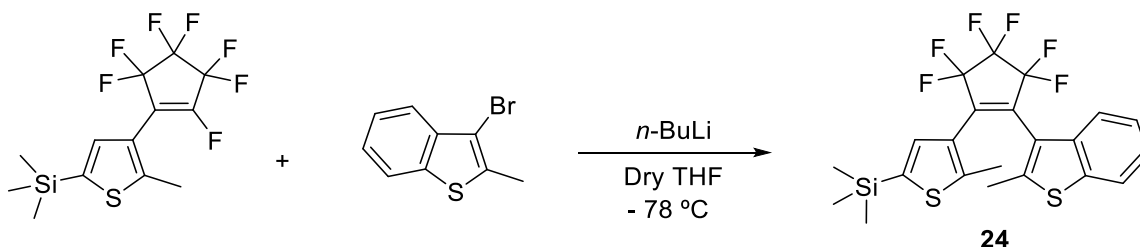
The title compound was synthesized following slightly modified literature procedures. Under N$_2$, trimethyl(5-methyl-4-(perfluorocyclopent-1-en-1-yl)thiophen-2-yl)silane (1.77 mmol, 0.64 g) were dissolved in freshly distilled THF (10 mL). In another flask, 3-bromo-2-methylbenzo[*b*]thiophene (1.77 mmol, 0.4 g) were dissolved in freshly distilled THF (30 mL). Both solutions were cooled down to − 78 °C. Then, n-BuLi (1.95 mmol, 1.22 mL, 1.6 M) were added dropwise over the 3-bromo-2-methylbenzo[*b*]thiophene solution. The reaction was stirred for 30 minutes at − 78 °C. Then, via cannula, the trimethyl(5-methyl-4-(perfluorocyclopent-1-en-1-yl)thiophen-2-yl)silane solution was added over the lithiated 3-bromo-2-methylbenzo[*b*]thiophene solution. The reaction was stirred for 30 minutes at this temperature and, after that, warmed up slowly to R.T overnight. The reaction was quenched with H$_2$O. The product was extracted with CH$_2$Cl$_2$ and after removal of the solvent the residue was purified by silica gel column chromatography (hexane, Rf = 0.50). The product was obtained as a pale pink oil. (0.35 g, 40% yield).

¹H NMR (CDCl₃): δ 7.74 – 7.71 (m, 1H, CH_{ar}), δ 7.55 -(7.52m, 1H, CH_{ar}), δ 7.35 – 7.25 (m, 1H, CH_{ar}), δ 7.31 (s, 1H, CH_{ar}), δ 6.96 (s, 1H, CH_{ar}), δ 2.24 (s, 3H, CH₃), δ 2.00 (s, 3H, CH₃), δ 0.18 (s, 9H, 3(CH₃)).
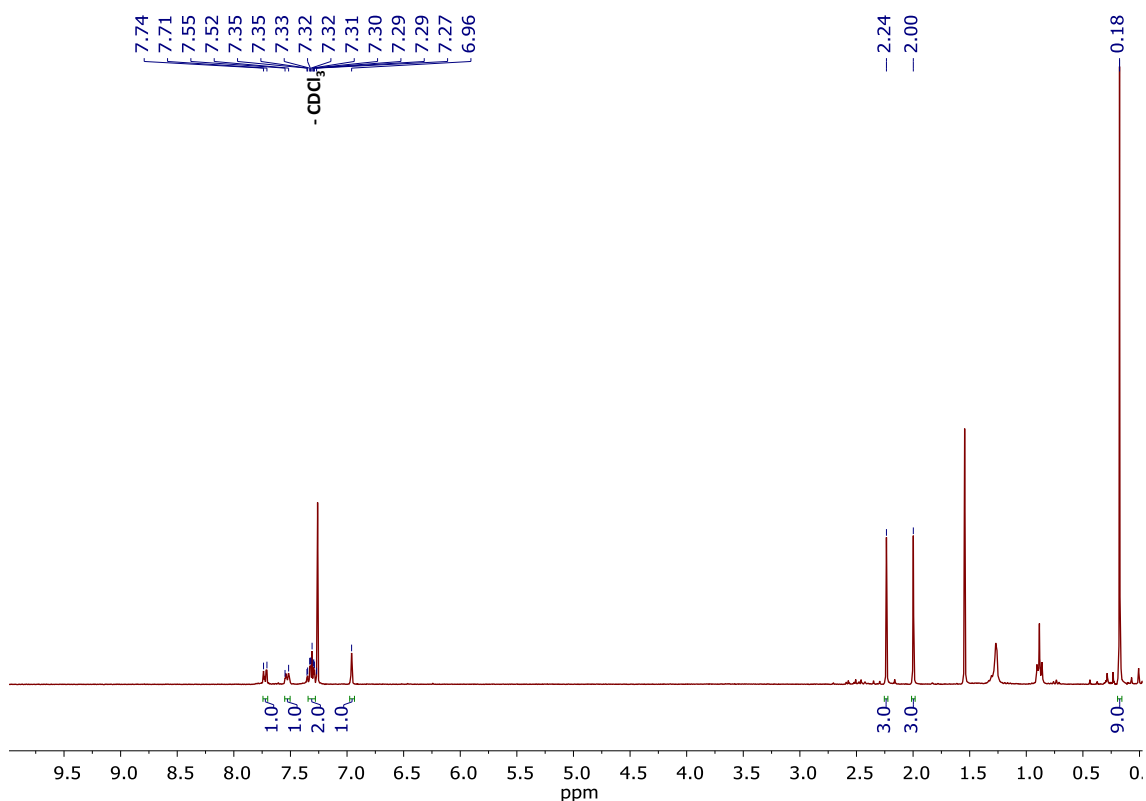
Figure S23. ¹H NMR of (4-(3,3,4,4,5,5-hexafluoro-2-(2-methylbenzo[b]thiophen-3-yl)cyclopent-1-en-1-yl)-5-methylthiophen-2-yl)trimethylsilane (**24**). (CDCl₃, 300 MHz).

2.1.24 Compound 5-bromo-3-(2-(2,5-dimethylthiophen-3-yl)-3,3,4,4,5,5-hexafluorocyclopent-1-en-1-yl)-2-methylthiophene (25):
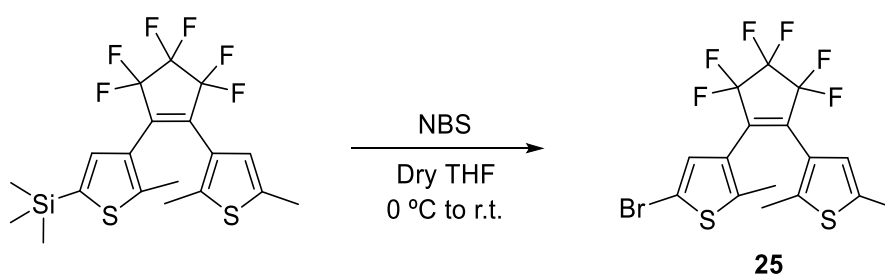
The title compound was synthesized following slightly modified literature procedures.[21] Under N₂, (4-(2-(2,5-dimethylthiophen-3-yl)-3,3,4,4,5,5-hexafluorocyclopent-1-en-1-yl)-5-methylthiophen-2-yl)trimethylsilane (5.27 mmol, 2.4 g), NBS (5.8 mmol, 1.03 g) were dissolved in freshly distilled THF (30 mL). The reaction was cooled down to 0 °C and stirred overnight. The product was extracted with CH₂Cl₂ and after removal of the solvent the residue was purified by silica gel column chromatography (hexane, Rf = 0.6). The product was obtained as a pale pink oil. (1.4 g, 58% yield). The spectroscopic data are coincident with those reported in the literature.

^{1}H NMR (CDCl$_3$): δ 7.02 (s, 1H, CH$_{ar}$), δ 6.69 (d, J$_{H-H}$ = 1.17 Hz, 1H, CH$_{ar}$), δ 2.41 (d, J$_{H-H}$ = 0.51 Hz, 3H, CH$_3$), δ 1.86 (s, 3H, CH$_3$), δ 1.84 (s, 3H, CH$_3$).
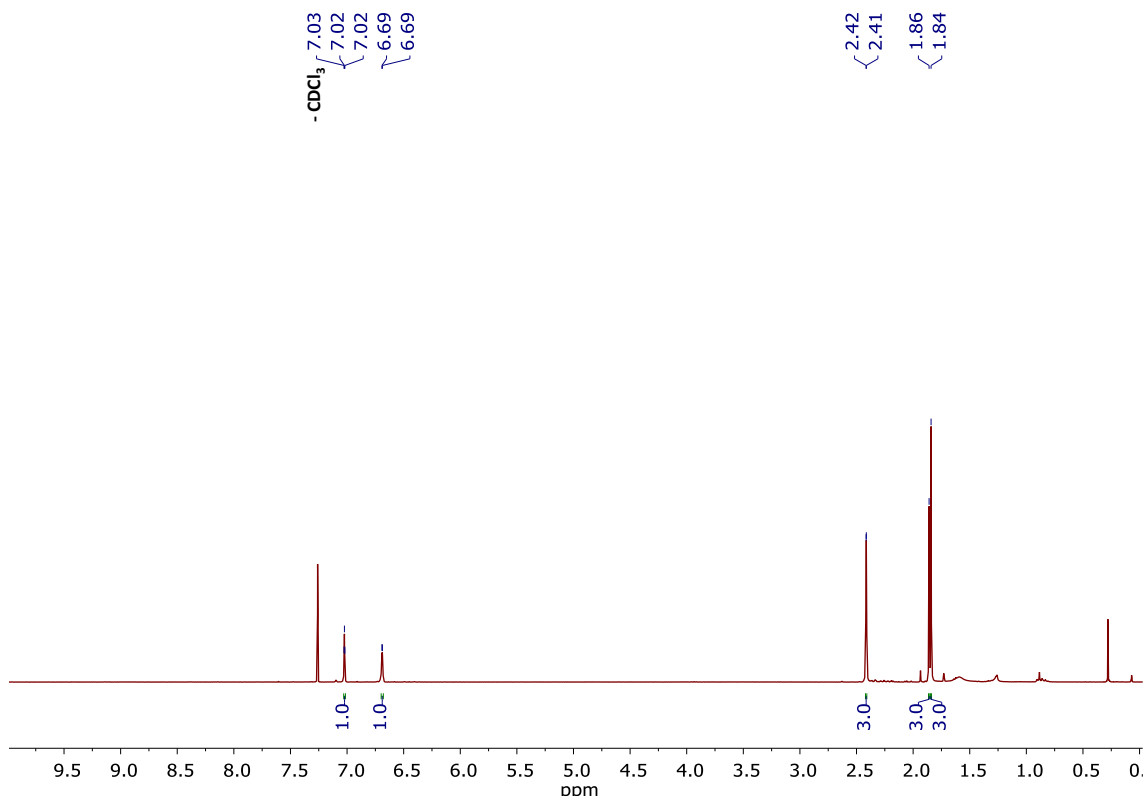
Figure S24. ^{1}H NMR of (4-(3,3,4,4,5,5-hexafluoro-2-(2-methylbenzo[b]thiophen-3-yl)cyclopent-1-en-1-yl)-5-methylthiophen-2-yl)trimethylsilane **(24)**. (CDCl$_3$, 300 MHz).

2.1.25 Compound 3-(2-(5-bromo-2-methylthiophen-3-yl)-3,3,4,4,5,5-hexafluorocyclopent-1-en-1-yl)-2-methylbenzo[*b*]thiophene (26):
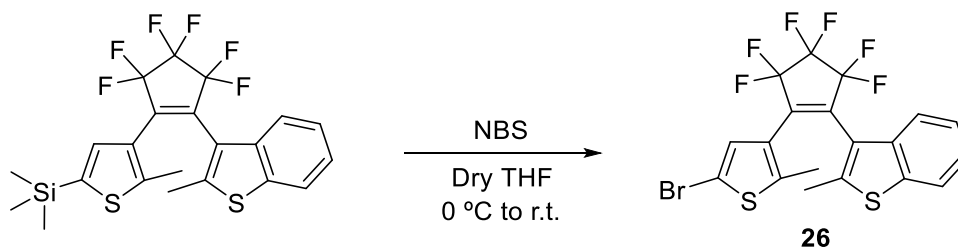
Under N$_2$, trimethyl(5-methyl-4-(perfluorocyclopent-1-en-1-yl)thiophen-2-yl)silane (2.44 mmol, 1.2 g), NBS (4.88 mmol, 0.86 g) were dissolved in freshly distilled THF (40 mL). The reaction was cooled down to 0 °C and stirred overnight. The product was extracted with CH$_2$Cl$_2$, dried over MgSO$_4$ and after removal of the solvent the residue was purified by silica gel column chromatography (hexane, Rf = 0.29). The product was obtained as a pale pink oil. (0.98 g, 81% yield).

^{1}H NMR (CDCl$_3$): δ 7.77 – 7.74 (m, 1H, CH$_{ar}$), δ 7.56 (d, J$_{H-H}$ = 7.59 Hz, 1H, CH$_{ar}$), δ 7.40 – 7.30 (m, 2H, CH$_{ar}$), δ 6.96 (s, 1H, CH$_{ar}$), δ 2.32 (s, 3H, CH$_3$), δ 1.87 (s, 3H, CH$_3$).

¹³C NMR (CDCl₃): δ 143.80 (C_quat), δ 142.74 (C_quat), δ 138.12 (C_quat), δ 129.38 (C_quat), δ 125.13 (CH), δ 124.72 (CH), δ 122.230 (CH), δ 122.15 (CH), δ 120.09 (C_quat), δ 119.76 (C_quat), δ 119.44 (C_quat), δ 116.35 (C_quat), δ 116.04 (C_quat), δ 109.76 (C_quat), δ 14.95 (CH₃), δ 14.71 (CH₃)

Figure S25. ¹H NMR of 3-(2-(5-bromo-2-methylthiophen-3-yl)-3,3,4,4,5,5-hexafluorocyclopent-1-en-1-yl)-2-methylbenzo[b]thiophene (**26**). (CDCl₃, 300 MHz).
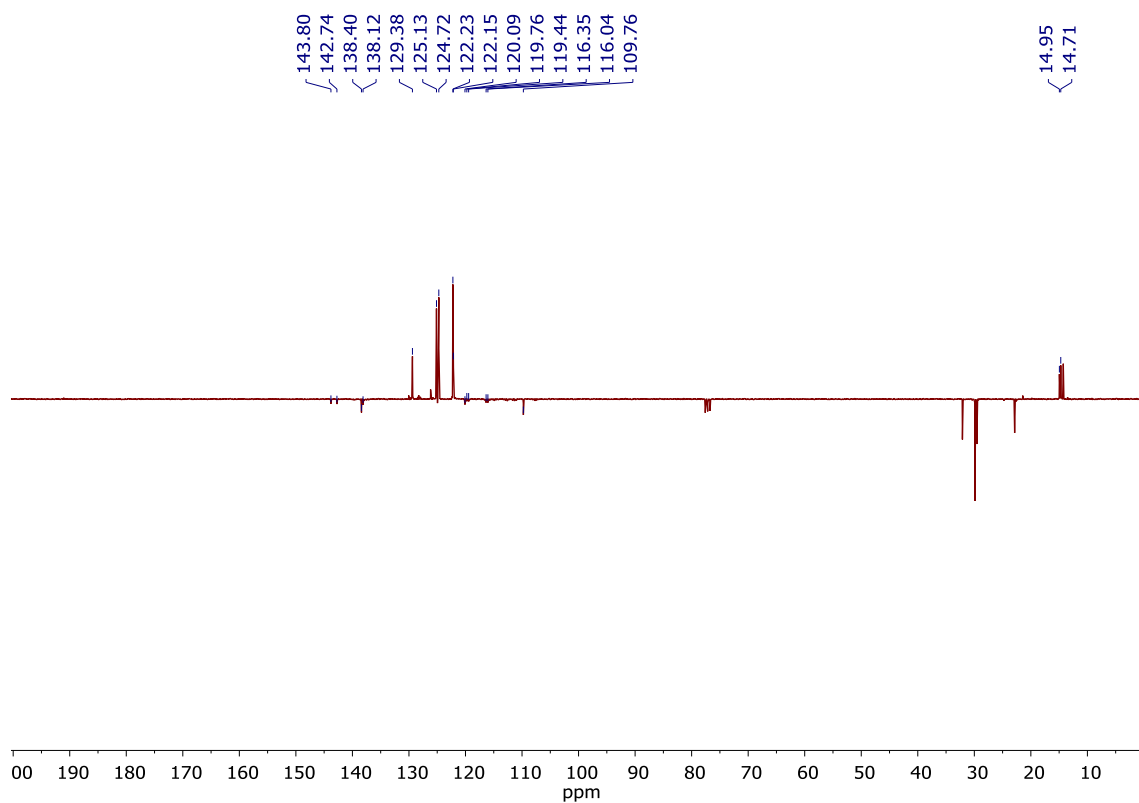
Figure S26. ^{13}C NMR of 3-(2-(5-bromo-2-methylthiophen-3-yl)-3,3,4,4,5,5-hexafluorocyclopent-1-en-1-yl)-2-methylbenzo[b]thiophene (**26**). (CDCl$_3$, 300 MHz).
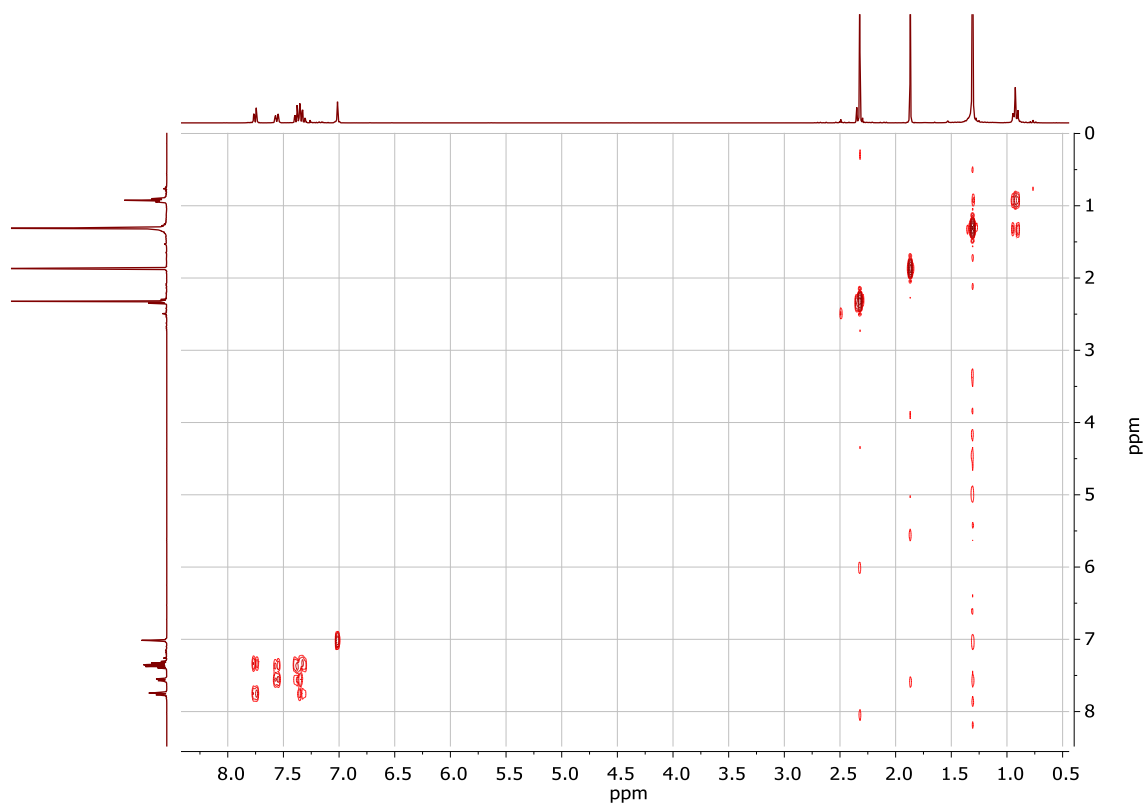
Figure S27. COSY NMR of 3-(2-(5-bromo-2-methylthiophen-3-yl)-3,3,4,4,5,5-hexafluorocyclopent-1-en-1-yl)-2-methylbenzo[b]thiophene (**26**). (CDCl$_3$, 300 MHz).

237
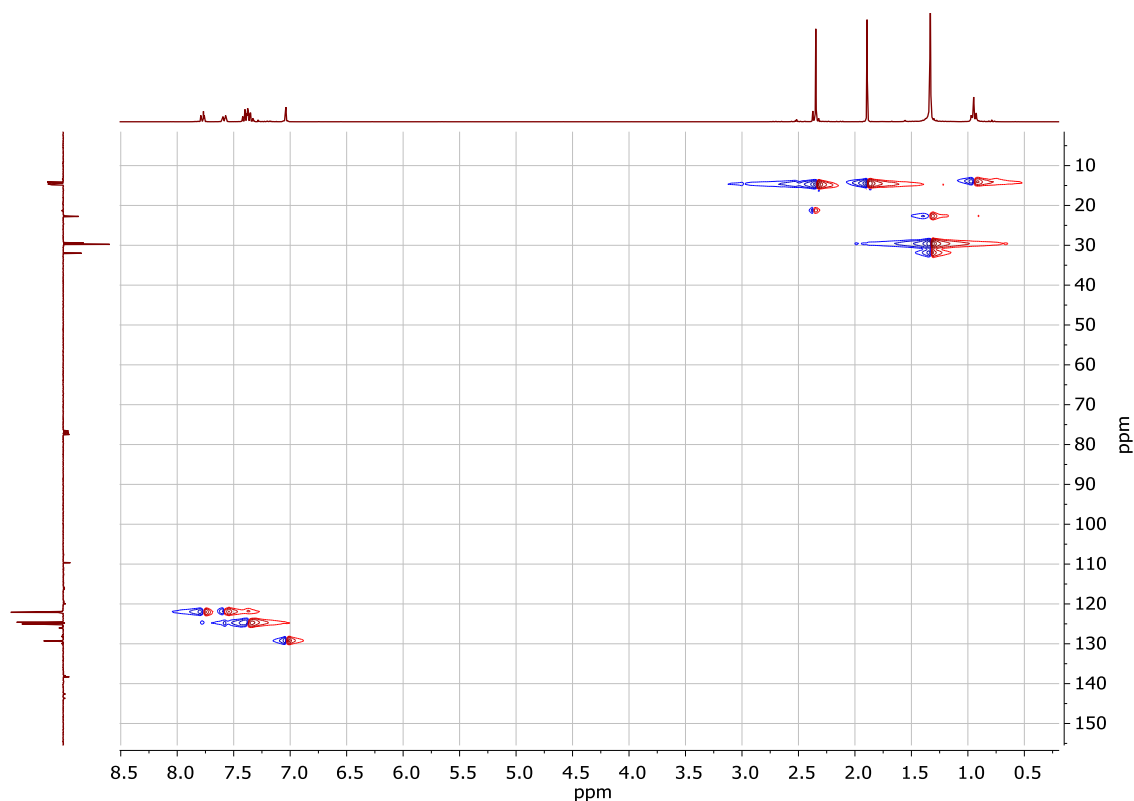
Figure S28. HSQC NMR of 3-(2-(5-bromo-2-methylthiophen-3-yl)-3,3,4,4,5,5-hexafluorocyclopent-1-en-1-yl)-2-methylbenzo[b]thiophene (**26**). (CDCl$_3$, 300 MHz).

2.1.26 Compound ((4-(2-(2,5-dimethylthiophen-3-yl)-3,3,4,4,5,5-hexafluorocyclopent-1-en-1-yl)-5-methylthiophen-2-yl)ethynyl)trimethylsilane (27):
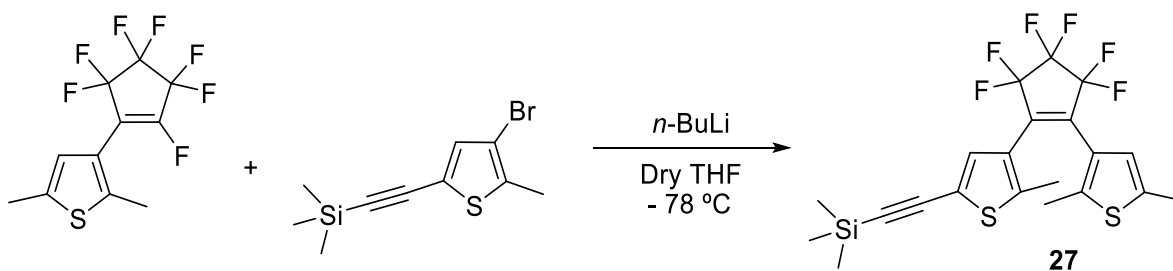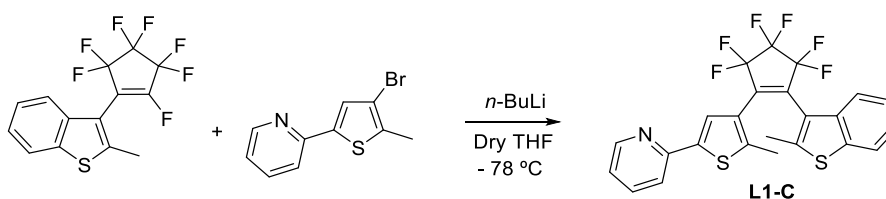

The title compound was synthesized following slightly modified literature procedures.[22] Under N$_2$, 2,5-dimethyl-3-(perfluorocyclopent-1-en-1-yl)thiophene (5.06 mmol, 1.54 g), were dissolved in 10 mL of dry THF. Under N$_2$, ((4-bromo-5-methylthiophen-2-yl)ethynyl)trimethylsilane (4.2 mmol, 1.15 g), were dissolved in 55 mL of dry THF. The colourless solutions was cooled down to -78 °C. Then, n-BuLi (5.46 mmol, 3.4 mL, 1.6 M) were added dropwise over ((4-bromo-5-methylthiophen-2-yl)ethynyl)trimethylsilane. The reaction was stirred for 30 minutes. After that, the 2,5-dimethyl-3-(perfluorocyclopent-1-en-1-yl)thiophene was added over the lithiated ((4-bromo-5-methylthiophen-2-yl)ethynyl)trimethylsilane solution, observing a brownish colour. The reaction was warmed up slowly to R.T. The reaction was quenched with H$_2$O. The product was extracted with CH$_2$Cl$_2$, dried over MgSO$_4$ and after removal of the solvent the residue was purified by silica gel column chromatography (hexane, Rf = 0.42). The product was

obtained as a pale pink oil. (1.04 g, 52% yield). The spectroscopic data are coincident with those reported in the literature.
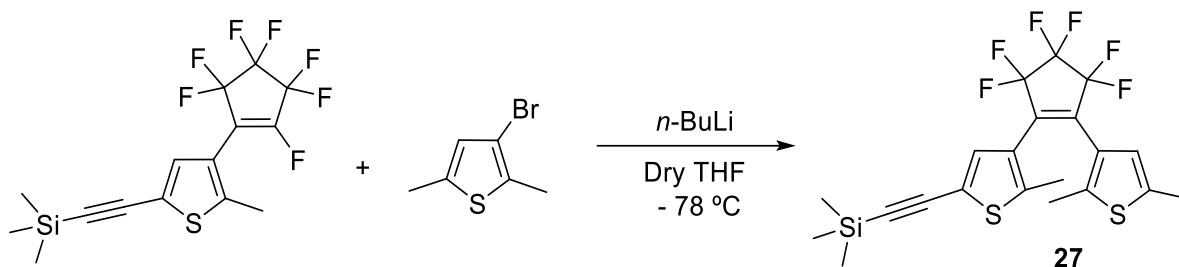
The title compound was synthesized following slightly modified literature procedures[22]. Under N₂, trimethyl((5-methyl-4-(perfluorocyclopent-1-en-1-yl)thiophen-2-yl)ethynyl)silane (1.16 mmol, 0.45 g), were dissolved in 5 mL of dry THF. Under N₂, 3-bromo-2,5-dimethylthiophene (1.16 mmol, 0.22 g), were dissolved in 25 mL of dry THF. The colourless solutions was cooled down to -78 °C. Then, n-BuLi (1.5 mmol, 0.95 mL, 1.6 M) were added dropwise over3-bromo-2,5-dimethylthiophene. The reaction was stirred for 60 minutes. After that, the trimethyl((5-methyl-4-(perfluorocyclopent-1-en-1-yl)thiophen-2-yl)ethynyl)silane was added over the lithiated 3-bromo-2,5-dimethylthiophene solution, observing a brownish colour. The reaction was warmed up slowly to R.T. The reaction was quenched with H₂O. The product was extracted with CH₂Cl₂, dried over MgSO₄ and after removal of the solvent the residue was purified by silica gel column chromatography (cyclohexane, Rf = 0.40). The product was obtained as a pale pink oil. (0.35 g, 62% yield). The spectroscopic data are coincident with those reported in the literature.

^{1}H NMR (CDCl₃): δ 7.24 (s, 1H, CHar), δ 6.71 (d, J_{H-H} = 0.9 Hz, 1H, CHar), δ 2.43 (s, 3H, CH₃), δ 1.87 (s, 3H, CH₃), δ 1.86 (s, 3H, CH₃), δ 0.27 (s, 9H, (CH₃)₃.
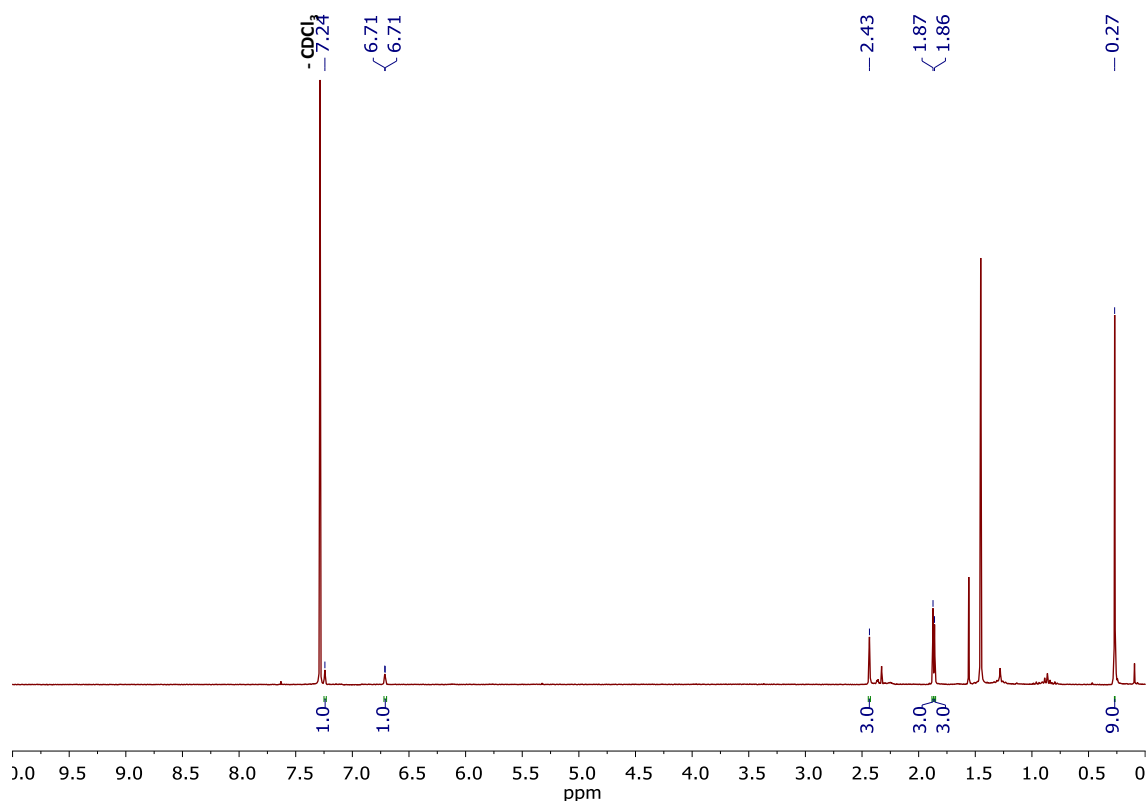
Figure S29. ^{1}H NMR of((4-(2-(2,5-dimethylthiophen-3-yl)-3,3,4,4,5,5-hexafluorocyclopent-1-en-1-yl)-5-methylthiophen-2-yl)ethynyl)trimethylsilane (**27**). (CDCl$_3$, 300 MHz).

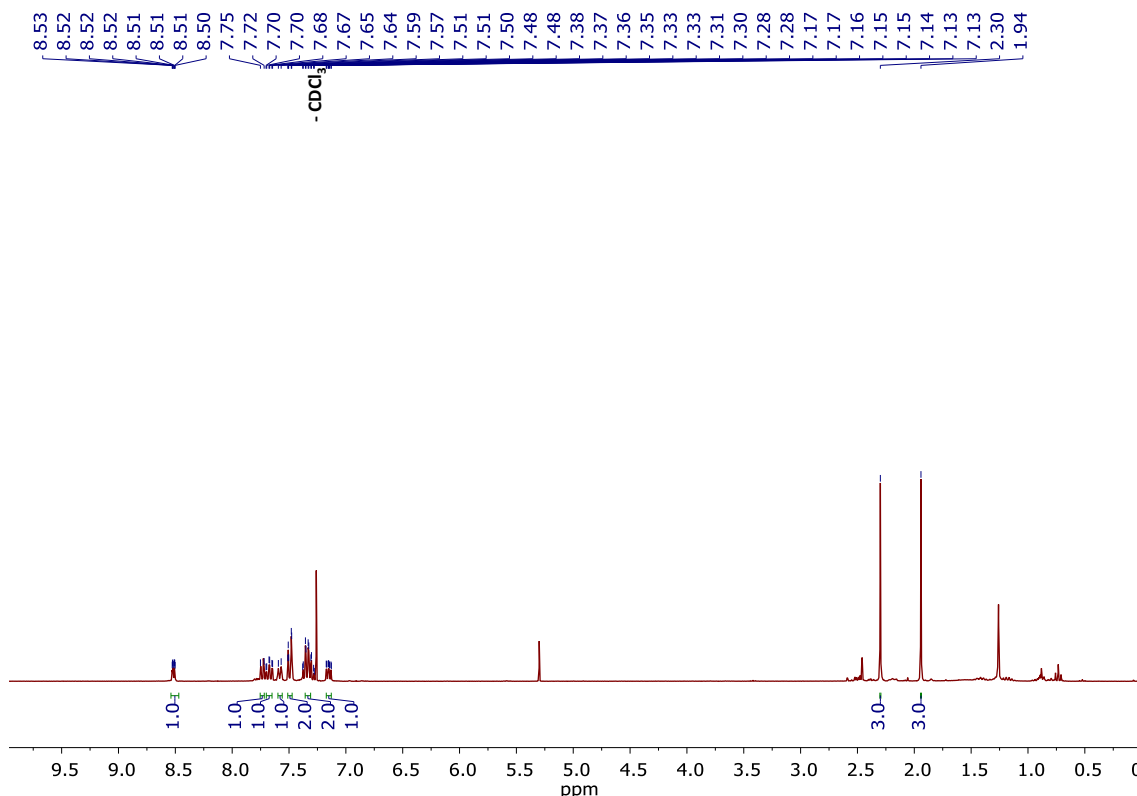### 2.1.27 Compound ((4-(3,3,4,4,5,5-hexafluoro-2-(2-methylbenzo[b]thiophen-3-yl)cyclopent-1-en-1-yl)-5-methylthiophen-2-yl)ethynyl)trimethylsilane (28):
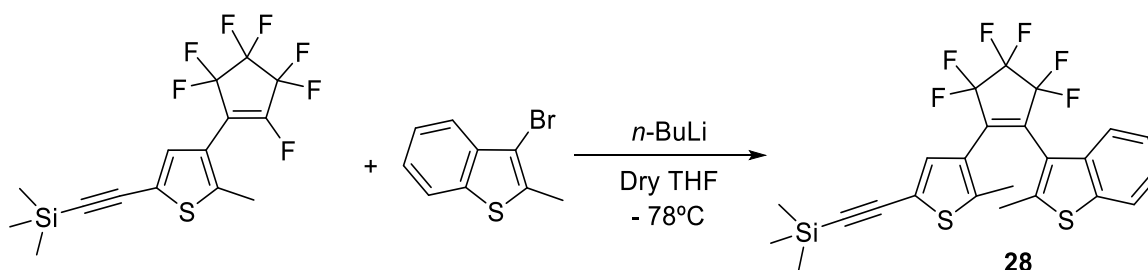
The title compound was synthesized following slightly modified literature procedures.[23] Under N$_2$, trimethyl((5-methyl-4-(perfluorocyclopent-1-en-1-yl)thiophen-2-yl)ethynyl) (1.29 mmol, 0.5 g) were dissolved in 5 mL of dry THF. Under N$_2$, 3-bromo-2-methylbenzo[b]thiophene (1.41 mmol, 0.32 g), were dissolved in 20 mL of dry THF. The colourless solutions was cooled down to -78 °C. Then, n-BuLi (1.67 mmol, 0.67 mL, 2.5 M) were added dropwise over 3-bromo-2-methylbenzo[b]thiophene. The reaction was stirred for 60 minutes. After that, via cannula the trimethyl((5-methyl-4-(perfluorocyclopent-1-en-1-yl)thiophen-2-yl)ethynyl) was added over the lithiated 3-bromo-2-methylbenzo[b]thiophene solution, observing a brownish colour. The reaction was warmed up slowly to R.T. The reaction was quenched with H$_2$O. The product was extracted with CH$_2$Cl$_2$, dried over MgSO$_4$ and after removal of the solvent the residue was purified by silica gel column chromatography (petroleum ether, Rf = 0.40). The product was

240

obtained as a pale pink oil. (0.2 g, 30% yield). The spectroscopic data are coincident with those reported in the literature.

¹H NMR (CDCl₃): δ 7.75 − 7.72 (m, 1H, CH$_{ar}$), δ 7.55 − 7.52 (m, 1H, CH$_{ar}$), δ 7.38 − 7.36 (m, 2H, CH$_{ar}$), δ 7.18 (s, 1H, CH$_{ar}$), δ 2.27 (s, 3H, CH₃), δ 1.82 (s, 3H, CH₃), δ 0.23 (s, 9H, 3(CH₃)).

Figure S30. ¹H-NMR of ((4-(3,3,4,4,5,5-hexafluoro-2-(2-methylbenzo[b]thiophen-3-yl)cyclopent-1-en-1-yl)-5-methylthiophen-2-yl)ethynyl)trimethylsilane (**28**). (CDCl₃, 300 MHz).

2.1.28 Compound 3-(2-(2,5-dimethylthiophen-3-yl)-3,3,4,4,5,5-hexafluorocyclopent-1-en-1-yl)-5-ethynyl-2-methylthiophene (29):
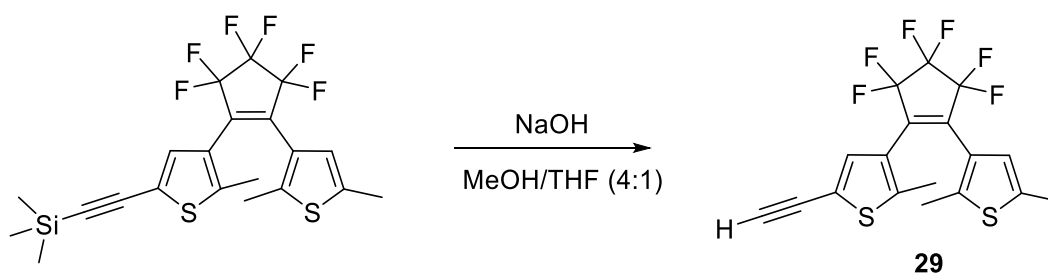
The title compound was synthesized following slightly modified literature procedures[24]. ((4-(2-(2,5-dimethylthiophen-3-yl)-3,3,4,4,5,5-hexafluorocyclopent-1-en-1-yl)-5-methylthiophen-2-yl)ethynyl)trimethylsilane (4.9 mmol, 2.38 g), were dissolved in 100 mL of a sat. NaOH (MeOH/THF (4:1)). The brown solution was stirred for 48 hours at r.t. After that, the product was extracted with CH₂Cl₂, washed with H₂O and dried over MgSO₄ . The solvent was removed and the product was purified by silica gel column chromatography (cyclohexane, Rf = 0.37). The product was obtained as a pale pink oil. (0.97 g, 48% yield).

^{1}H NMR (CDCl$_3$): δ 7.29 (s, 1H, CH$_{ar}$), δ 6.74 (d, J$_{H-H}$ = 1.1 Hz, 1H, CH$_{ar}$), δ 3.33 (s, 1H, CH$_{ar}$), δ 2.43 (d, J$_{H-H}$ = 0.36 Hz, 3H, CH$_3$), δ 1.91 (s, 3H, CH$_3$), δ 1.87 (s, 3H, CH$_3$).
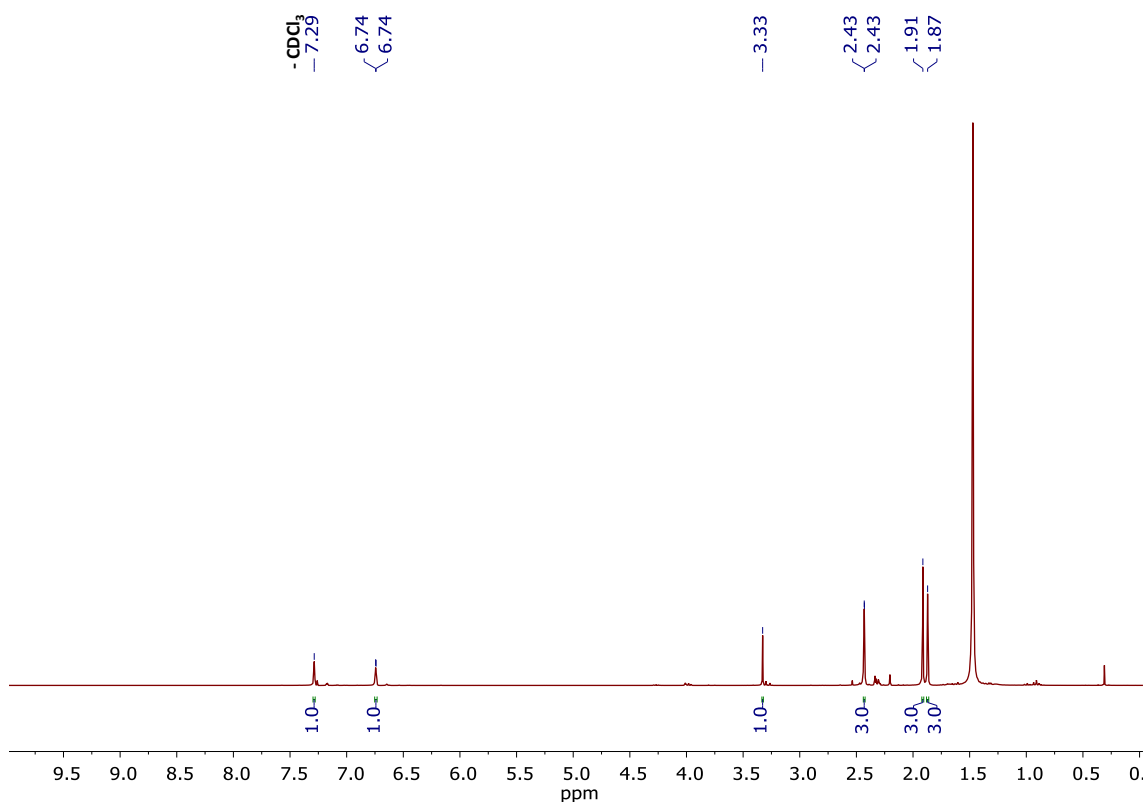
Figure S31. ^{1}H-NMR of 3-(2-(2,5-dimethylthiophen-3-yl)-3,3,4,4,5,5-hexafluorocyclopent-1-en-1-yl)-5-ethynyl-2-methylthiophene (**29**). (CDCl$_3$, 300 MHz).

2.1.29 Compound 3-(2-(5-ethynyl-2-methylthiophen-3-yl)-3,3,4,4,5,5-hexafluorocyclopent-1-en-1-yl)-2-methylbenzo[b]thiophene (30):
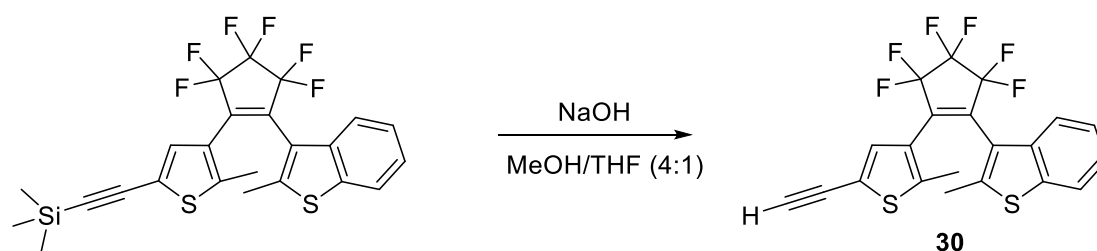
The title compound was synthesized following slightly modified literature procedures.[24] ((4-(3,3,4,4,5,5-hexafluoro-2-(2-methylbenzo[b]thiophen-3-yl)cyclopent-1-en-1-yl)-5-methylthiophen-2-yl)ethynyl)trimethylsilane (1.64 mmol, 0.79 g), were dissolved in 100 mL of a sat. NaOH (MeOH/THF (4:1)). The brown solution was stirred for 48 hours at r.t. After that, the product was extracted with CH$_2$Cl$_2$, washed with H$_2$O and dried over MgSO$_4$. The solvent was removed and the product was purified by silica gel column chromatography (hexane, Rf = 0.33). The product was obtained as a pale pink oil. (0.20 g, 30% yield). The spectroscopic data are coincident with those reported in the literature.

¹H NMR (CDCl₃): δ 7.75 − 7.72 (m, 1H, CH$_{ar}$), δ 7.53 − 7.50 (m, 1H, CH$_{ar}$), δ 7.38 − 7.28 (m, 1H, CH$_{ar}$), δ 7.18 (s, 1H, CH$_{ar}$), δ 3.30 (s, 1H, CH$_{ar}$), δ 2.28 (s, 3H, CH₃), δ 1.88 (s, 3H, CH₃).
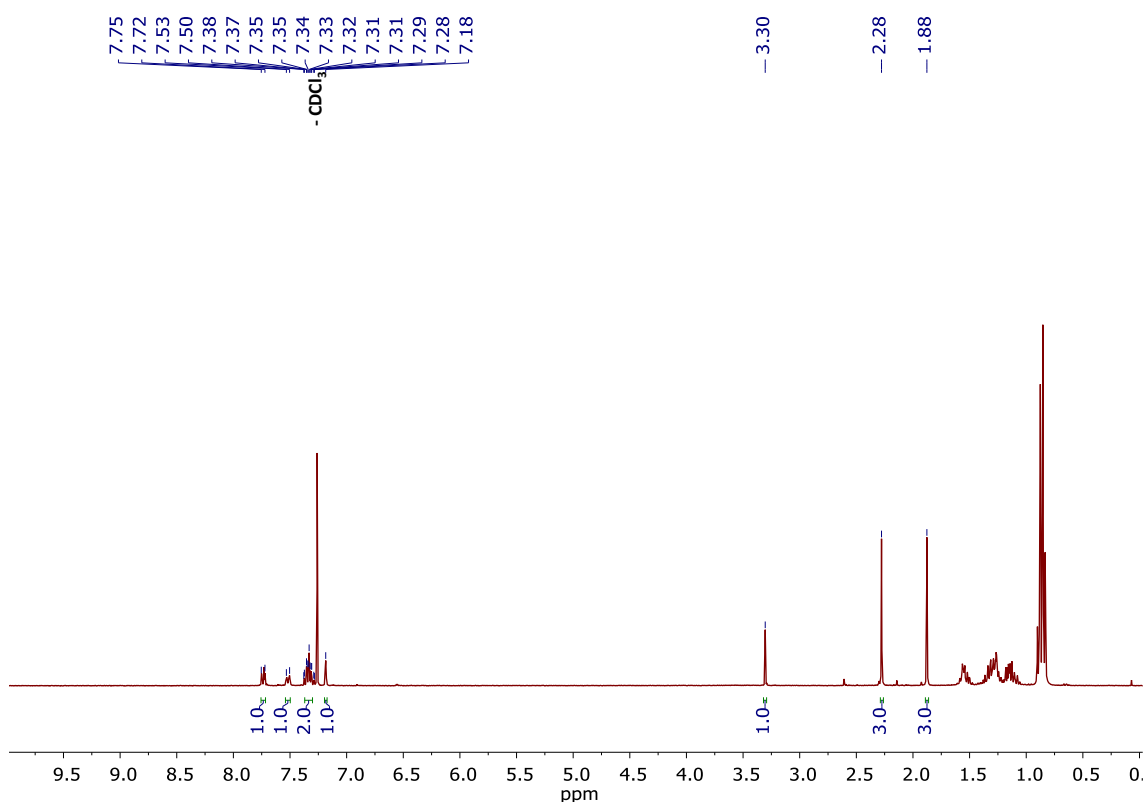
Figure S32. ¹H NMR of 3-(2-(5-ethynyl-2-methylthiophen-3-yl)-3,3,4,4,5,5-hexafluorocyclopent-1-en-1-yl)-2-methylbenzo[b]thiophene (**30**). (CDCl₃, 300 MHz).

2.1.30   Compound   2,2'-((perfluorocyclopent-1-ene-1,2-diyl)bis(5-methylthiophene-4,2-diyl))dipyridine (L1-A):
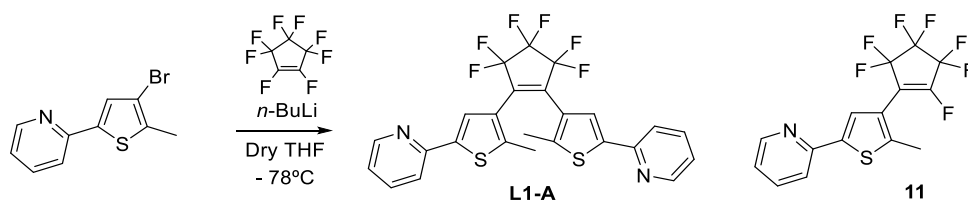
The title compound was synthesized following slightly modified literature procedures.[25] Under N₂, 2-(4-bromo-5-methylthiophen-2-yl)pyridine (3.94 mmol, 1 g) were dissolved in freshly distilled THF (60 mL). In another flask, octafluorocyclopentene (1.79 mmol, 0.37 mL) were dissolved in freshly distilled THF (10 mL). Both solutions were cooled down to − 78 °C. Then, n-BuLi (3.94 mmol, 2.46 mL, 1.6 M) were added dropwise over the thiophene solution. The reaction was stirred for 30 minutes at − 78 °C. Then, via cannula, the lithiated reaction was added over the octafluorocyclopentene solution. The reaction was stirred for 30 minutes at this temperature and, after that, warmed up slowly to R.T overnight. The reaction was quenched with aq. HCl. The product was extracted with CH₂Cl₂ and after removal of the solvent the residue was purified by silica gel column chromatography (CH₂Cl₂, Rf = 0.29). The product was obtained

as a white powder. (1.08 g, 45% yield) and compound 11 was obtained as a sub product.[26] The spectroscopic data are coincident with those reported in the literature.

¹H NMR (CDCl₃): δ 8.55 (ddd, J_{H-H} = 1.0 Hz, J_{H-H} = 1.7 Hz, J_{H-H} = 4.90 Hz, 1H, CH$_{ar}$), δ 7.7 (td, J_{H-H} = 5.9 Hz, J_{H-H} = 7.7 Hz, 1H, CH$_{ar}$), δ 7.62 (dt, J_{H-H} = 1.14 Hz, J_{H-H} = 8.01 Hz, 1H, CH$_{ar}$), δ 7.54 (s, 1H, CH$_{ar}$), δ 7.16 (ddd, J_{H-H} = 1.23 Hz, J_{H-H} = 4.89 Hz, J_{H-H} = 7.26 Hz, 1H, CH$_{ar}$), δ 1.99 (s, 3H, CH₃).
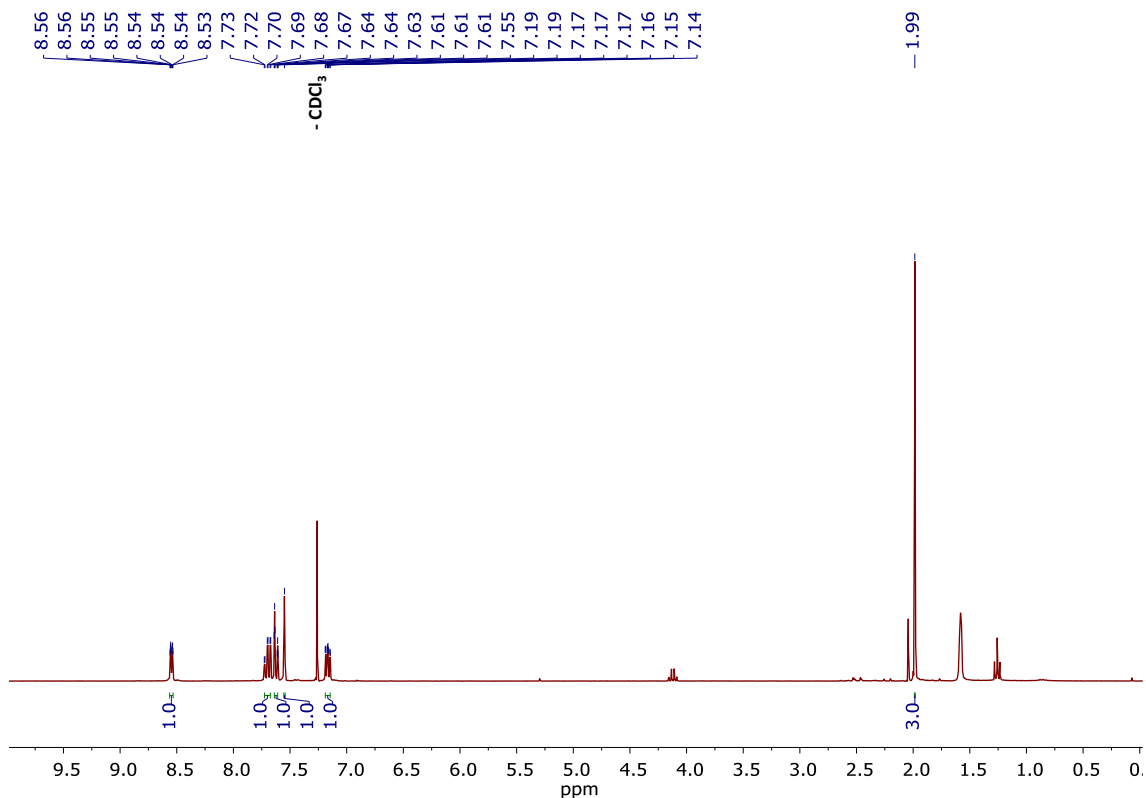
Figure S33. ¹H-NMR of 2,2'-((perfluorocyclopent-1-ene-1,2-diyl)bis(5-methylthiophene-4,2-diyl))dipyridine (**L1-A**). (CDCl₃, 300 MHz).

¹H NMR (CDCl₃): δ 8.56 (ddd, J_{H-H} = 1.0 Hz, J_{H-H} = 1.7 Hz, J_{H-H} = 4.90 Hz, 1H, CH$_{ar}$), δ 7.71 (td, J_{H-H} = 1.77 Hz, J_{H-H} = 7.98 Hz, 1H, CH$_{ar}$), δ 7.62 (dt, J_{H-H} = 1.05 Hz, J_{H-H} = 7.95 Hz, 1H, CH$_{ar}$), δ 7.52 (s, 1H, CH$_{ar}$), δ 7.18 (ddd, J_{H-H} = 1.2 Hz, J_{H-H} = 4.89 Hz, J_{H-H} = 8.55 Hz, 1H, CH$_{ar}$), δ 2.50 (d, J_{H-F} = 3.12 Hz, 3H, CH₃).
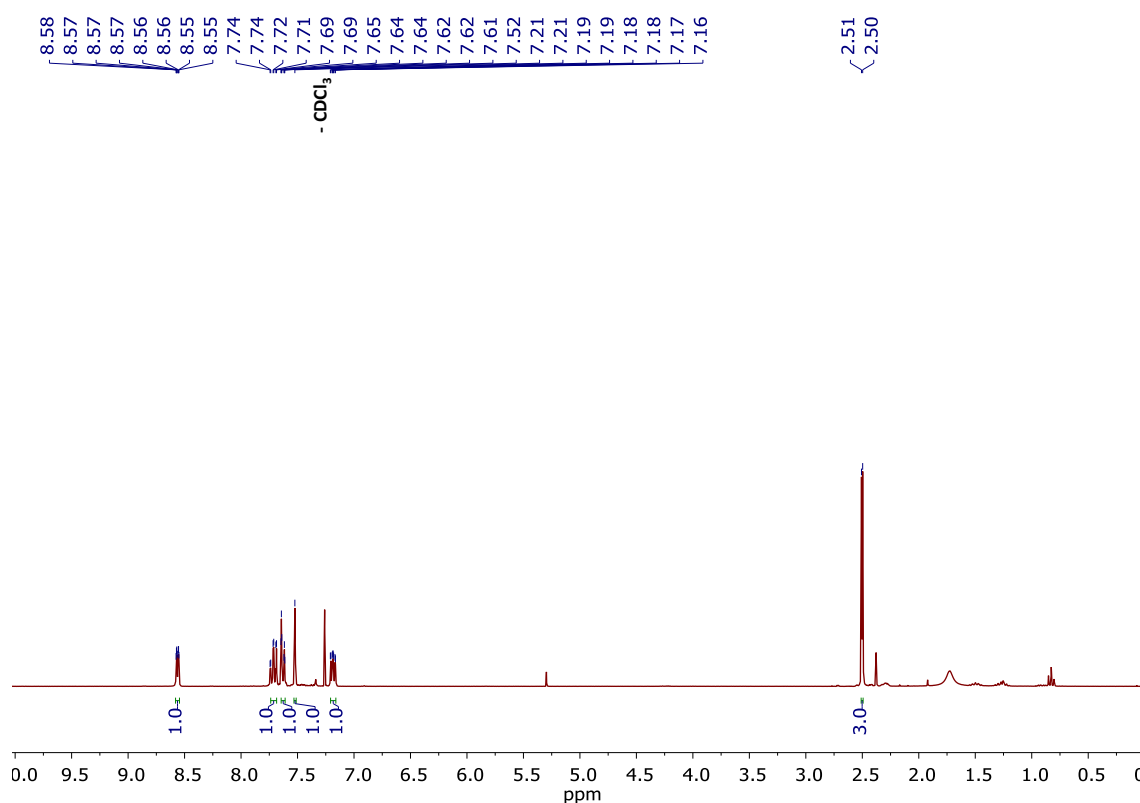
Figure S34. ¹H NMR of 2-(5-methyl-4-(perfluorocyclopent-1-en-1-yl)thiophen-2-yl)pyridine (**11**). (CDCl₃, 300 MHz).

2.1.31 Compound 2-(4-(2-(2,5-dimethylthiophen-3-yl)-3,3,4,4,5,5-hexafluorocyclopent-1-en-1-yl)-5-methylthiophen-2-yl)pyridine (L1-B):
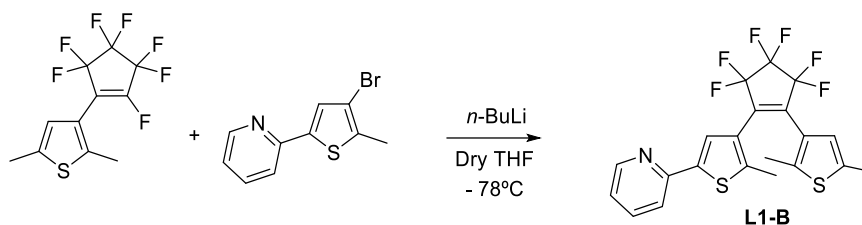
The title compound was synthesized following slightly modified literature procedures.[27] Under N₂, 2,5-dimethyl-3-(perfluorocyclopent-1-en-1-yl)thiophene (1.98 mmol, 0.6 g) were dissolved in freshly distilled THF (7 mL). In another flask, (2-(4-bromo-5-methylthiophen-2-yl)pyridine (1.8 mmol, 0.61 g) were dissolved in freshly distilled THF (15 mL). Both solutions were cooled down to – 78 °C. Then, n-BuLi (2.16 mmol, 1.35 mL, 1.6 M) were added dropwise over the (2-(4-bromo-5-methylthiophen-2-yl)pyridine solution. The reaction was stirred for 30 minutes at – 78 °C. Then, via cannula, the 2,5-dimethyl-3-(perfluorocyclopent-1-en-1-yl)thiophene solution was added over the lithiated (2-(4-bromo-5-methylthiophen-2-yl)pyridine solution. The reaction was stirred for 30 minutes at this temperature and, after that, warmed up slowly to R.T overnight. The reaction was quenched with H₂O. The product was extracted with CH₂Cl₂ and after removal of the solvent the residue was purified by silica gel column chromatography (CH₂Cl₂, Rf = 0.50). The product was obtained as a pale brown oil. (0.28 g, 34% yield).
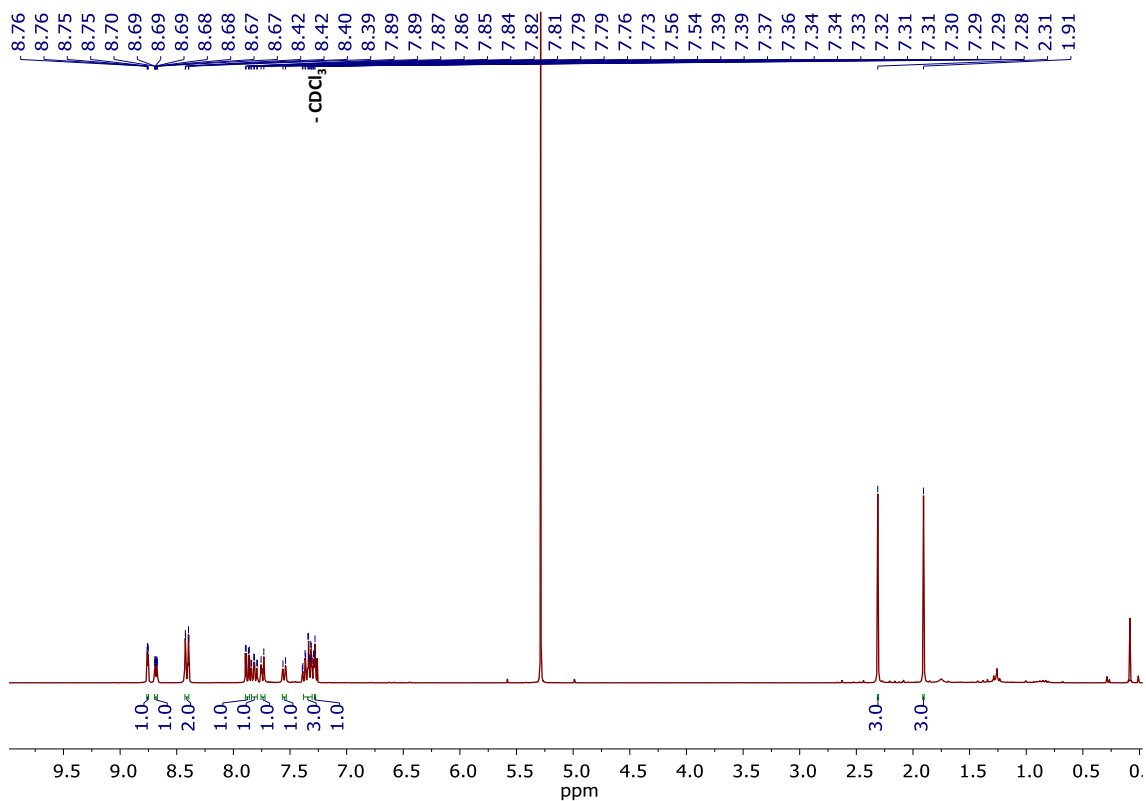
¹H NMR (CDCl₃): δ 8.54 (ddd, J_{H-H} = 0.99 Hz, J_{H-H} = 1.71 Hz, J_{H-H} = 4.89 Hz, 1H, CH$_{ar}$), δ 7.69 (td, J_{H-H} = 1.77 Hz, J_{H-H} = 7.98 Hz, 1H, CH$_{ar}$), δ 7.62 (dt, J_{H-H} = 1.08 Hz, J_{H-H} = 8.01 Hz, 1H, CH$_{ar}$), δ 7.52 (s, 1H, CH$_{ar}$), δ 7.16 (ddd, J_{H-H} = 1.23 Hz, J_{H-H} = 4.92 Hz, J_{H-H} = 7.26 Hz, 1H, CH$_{ar}$), δ 6.72 (d, J_{H-H} = 1.11 Hz, 1H, CH$_{ar}$), δ 2.41 (s, 3H, CH₃), δ 1.93 (s, 3H, CH₃), δ 1.87 (s, 3H, CH₃).
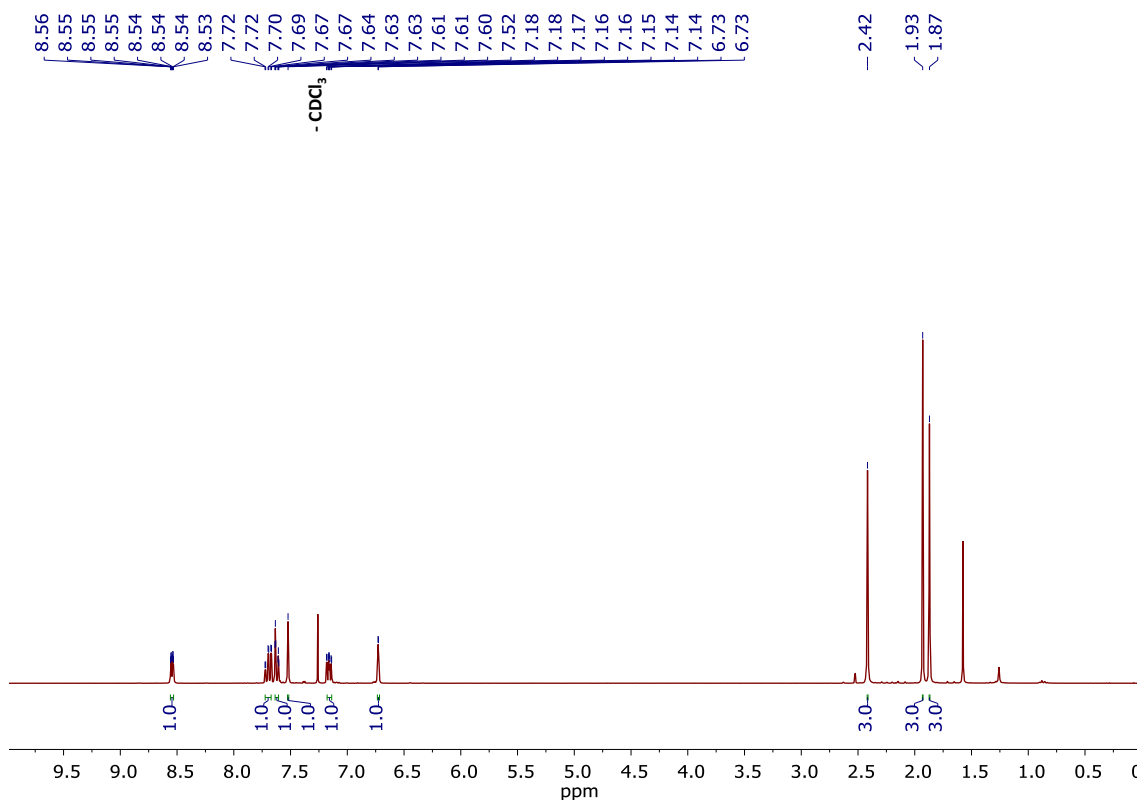
Figure S35. ¹H NMR of 2-(4-(2-(2,5-dimethylthiophen-3-yl)-3,3,4,4,5,5-hexafluorocyclopent-1-en-1-yl)-5-methylthiophen-2-yl)pyridine (**L1-B**) . (CDCl₃, 300 MHz).

2.1.32 Compound 2-(4-(3,3,4,4,5,5-hexafluoro-2-(2-methylbenzo[b]thiophen-3-yl)cyclopent-1-en-1-yl)-5-methylthiophen-2-yl)pyridine (L1-C):

The title compound was synthesized following slightly modified literature procedures.[28] Under N₂, 2-methyl-3-(perfluorocyclopent-1-en-1-yl)benzo[b]thiophene (1.76 mmol, 0.6 g) were dissolved in freshly distilled THF (10 mL). In another flask, (2-(4-bromo-5-methylthiophen-2-yl)pyridine (1.6 mmol, 0.41 g) were dissolved in freshly distilled THF (20 mL). Both solutions were cooled down to – 78 °C. Then, n-BuLi (1.92 mmol, 1.2 mL, 1.6 M) were added dropwise over the (2-(4-bromo-5-methylthiophen-2-yl)pyridine solution. The reaction was stirred for 30 minutes at – 78 °C. Then, via cannula, the 2-methyl-3-(perfluorocyclopent-1-en-1-yl)benzo[b]thiophene solution was added over the lithiated (2-(4-bromo-5-methylthiophen-2-yl)pyridine solution. The reaction was stirred for 30 minutes at this temperature and, after that, warmed up slowly to R.T overnight. The reaction was quenched with H₂O. The product was extracted with CH₂Cl₂ and

after removal of the solvent the residue was purified by silica gel column chromatography (CH₂Cl₂/MeOH (99:1), Rf = 0.71). The product was obtained as a brown oil. (0.35 g, 44% yield).

¹H NMR (CDCl₃): δ 8.51 (ddd, J_{H-H} = 0.9 Hz, J_{H-H} = 1.7 Hz, J_{H-H} = 4.9 Hz, 1H, CH$_{ar}$), δ 7.74 (d, J_{H-H} = 9.8 Hz, 1H, CH$_{ar}$), δ 7.67 (dt, J_{H-H} = 1.77 Hz, J_{H-H} = 7.89 Hz, 1H, CH$_{ar}$), δ 7.57 (d, J_{H-H} = 7.38 Hz, 1H, CH$_{ar}$), δ 7.49 (dt, J_{H-H} = 1.02 Hz, J_{H-H} = 8.04 Hz, 2H, CH$_{ar}$), δ 7.37 – 7.27 (m, 2H, CH$_{ar}$), δ 7.15 (ddd, J_{H-H} = 1.02 Hz, J_{H-H} = 4.92 Hz, J_{H-H} = 7.47 Hz, 1H, CH$_{ar}$), δ 2.30 (s, 3H, CH₃), δ 1.94 (s, 3H, CH₃).

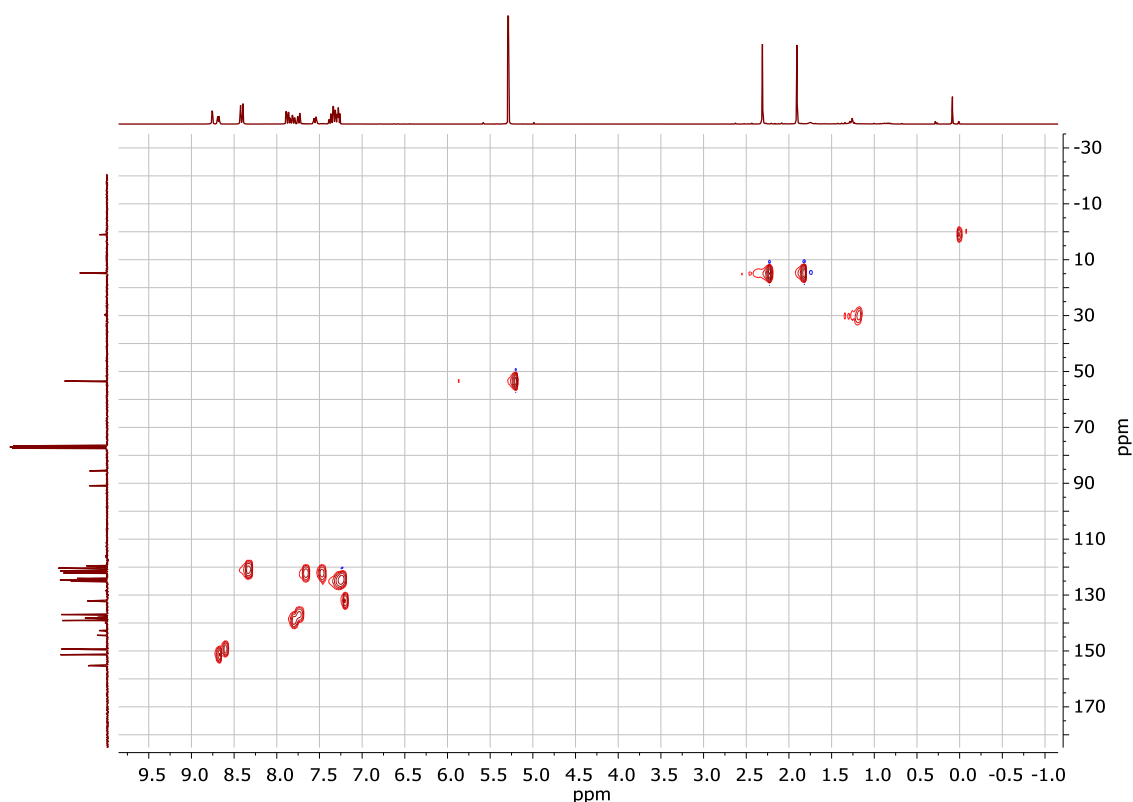**Figure S36.** ¹H NMR of 2-(4-(3,3,4,4,5,5-hexafluoro-2-(2-methylbenzo[b]thiophen-3-yl)cyclopent-1-en-1-yl)-5-methylthiophen-2-yl)pyridine (**L1-C**) (CDCl₃, 300 MHz).

2.1.33 Compound 2-(4-(3,3,4,4,5,5-hexafluoro-2-(2-methyl-5-(p-tolyl)thiophen-3-yl)cyclopent-1-en-1-yl)-5-methylthiophen-3-yl)pyridine (L1-D) : Synthesis
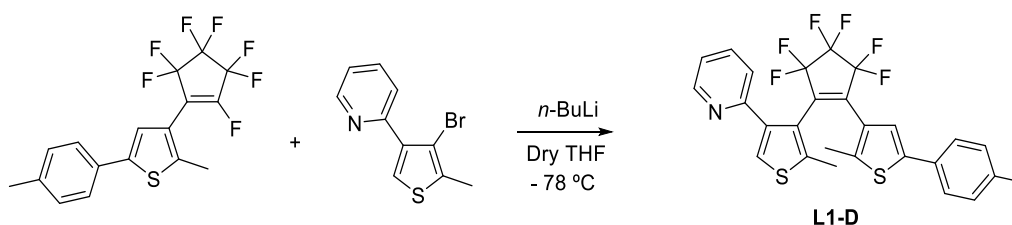
Under N₂, 2-methyl-3-(perfluorocyclopent-1-en-1-yl)-5-(*p*-tolyl)thiophene (0.24 mmol, 0.091 g) were dissolved in freshly distilled THF (3 mL). In another flask, 2-(4-bromo-5-methylthiophen-3-yl)pyridine (0.24 mmol, 0.062 g) were dissolved in freshly distilled THF (7 mL). Both solutions were cooled down to − 78 °C. Then, n-BuLi (0.29 mmol, 0.18 mL, 1.6 M) were added dropwise over the 2-(4-bromo-5-methylthiophen-3-yl)pyridine solution. The reaction was stirred for 30 minutes at − 78 °C. Then, via cannula, the 2-methyl-3-(perfluorocyclopent-1-en-1-yl)-5-(*p*-tolyl)thiophene solution was added over the lithiated 2-(4-bromo-5-methylthiophen-3-

yl)pyridine solution. The reaction was stirred for 10 minutes at this temperature and, after that, warmed up slowly to R.T overnight. The product was purified by silica gel column chromatography (CH$_2$Cl$_2$), Rf = 0.7). The product was obtained as a pale pink oil. (0.005 g, 5% yield).

¹H NMR (CDCl$_3$): δ 8.37 (ddd, J$_{H-H}$ = 1.0 Hz, J$_{H-H}$ = 1.7 Hz, J$_{H-H}$ = 4.8 Hz, 1H, CH$_{ar}$), δ 7.41 (dt, J$_{H-H}$ = 1.8 Hz, J$_{H-H}$ = 7.71 Hz, 1H, CH$_{ar}$), δ 7.25 (m, 3H, CH$_{ar}$), δ 7.17 (d, J$_{H-H}$ = 8.01 Hz, 2H, CH$_{ar}$), δ 7.00 (ddd, J$_{H-H}$ = 1.14 Hz, J$_{H-H}$ = 4.86 Hz, J$_{H-H}$ = 7.62 Hz, 1H, CH$_{ar}$), δ 6.96 (td, J$_{H-H}$ = 1.02 Hz, J$_{H-H}$ = 7.77 Hz, 1H, CH$_{ar}$), δ 6.17 (s, 1H, CH$_{ar}$), δ 2.51 (s, 3H, CH$_3$), δ 2.37 (s, 3H, CH$_3$), δ 1.91 (s, 3H, CH$_3$).
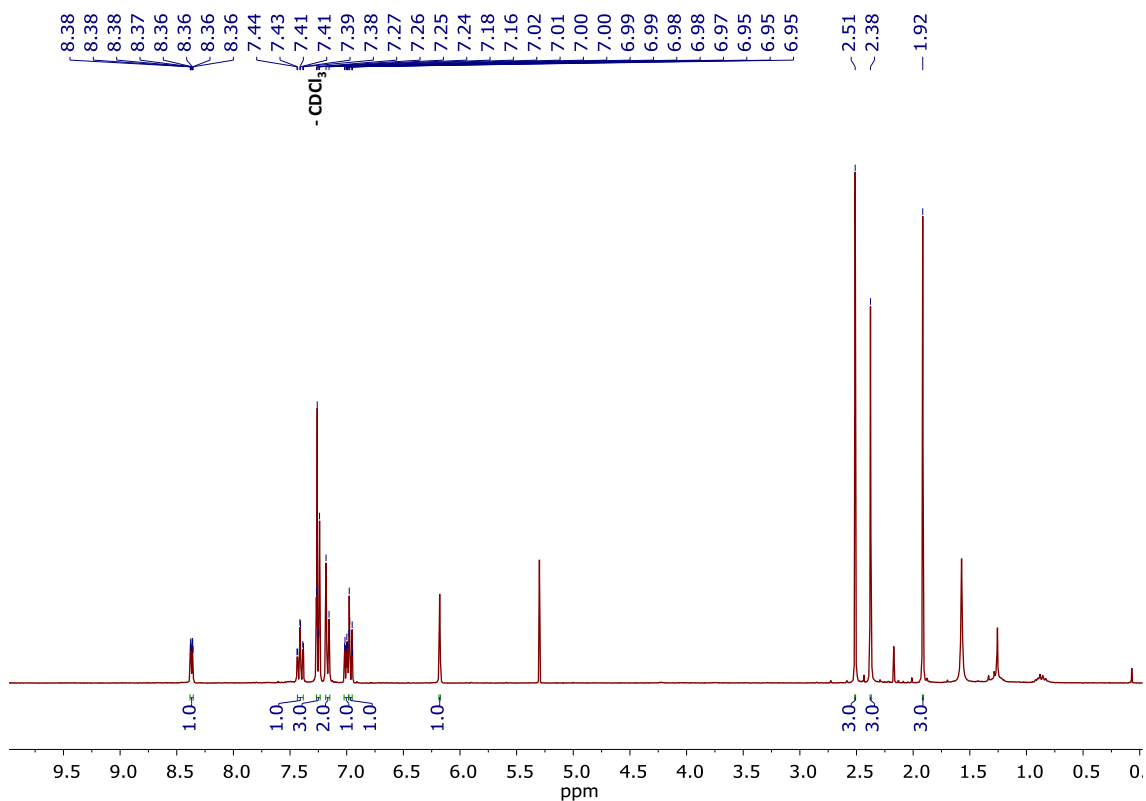
Figure S37. ¹H NMR of 2-(4-(3,3,4,4,5,5-hexafluoro-2-(2-methyl-5-(p-tolyl)thiophen-3-yl)cyclopent-1-en-1-yl)-5-methylthiophen-3-yl)pyridine (**L1-D**). (CDCl$_3$, 300 MHz).

2.1.34 Compound 5-((4-(2-(2,5-dimethylthiophen-3-yl)-3,3,4,4,5,5-hexafluorocyclopent-1-en-1-yl)-5-methylthiophen-2-yl)ethynyl)-2,2'-bipyridine (L2-A):
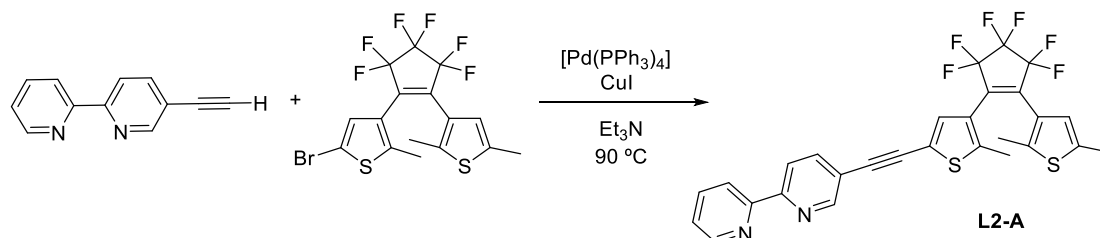

Under N$_2$ 5-ethynyl-2,2'-bipyridine (0.73 mmol, 0.12 g), 5-bromo-3-(2-(2,5-dimethylthiophen-3-yl)-3,3,4,4,5,5-hexafluorocyclopent-1-en-1-yl)-2-methylthiophene (0.92 mmol, 0.42 g), [Pd(PPh$_3$)$_4$] (0.04 mmol, 0.04 g, 5%) and CuI (0.07 mmol, 0.02 g, 10%) were dissolved in 10 mL of degassed Et$_3$N. The brown solution was refluxed for 12 hours at 90 °C. The brown residue was

248

dissolved in CH_2Cl_2 and washed with a mixture of NH_3 and EDTA. The product was extracted with CH_2Cl_2, dried over $MgSO_4$ and after removal of the solvent, the residue was purified by silica gel column chromatography (Hexane/AcOEt (3:1), Rf = 0.3). The product was obtained as a beige solid. (0.2 g, 47% yield).
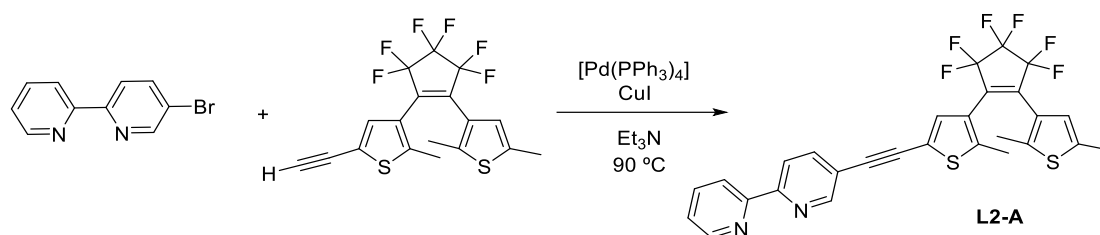
Under N_2 5-bromo-2,2'-bipyridine (2.1 mmol, 0.49 g), 3-(2-(2,5-dimethylthiophen-3-yl)-3,3,4,4,5,5-hexafluorocyclopent-1-en-1-yl)-5-ethynyl-2-methylthiophene (2.31 mmol, 0.94 g), [Pd(PPh$_3$)$_4$] (0.16 mmol, 0.11 g, 7%) and CuI (0.12 mmol, 0.02 g, 5%) were dissolved in 15 mL of degassed Et$_3$N. The brown solution was refluxed for 12 hours at 90 °C. The brown residue was dissolved in CH_2Cl_2 and washed with a mixture of NH_3 and EDTA. The product was extracted with CH_2Cl_2, dried over $MgSO_4$ and after removal of the solvent, the residue was purified by silica gel column chromatography (CH_2Cl_2, Rf = 0.18). The product was obtained as a beige solid. (0.4 g, 34% yield).

**Exact Mass**: FD [$C_{28}H_{18}F_6N_2S_2$]: calculated: m/z = 560.08156, found: m/z = 560.08100.

^{1}H NMR (CDCl$_3$): δ 8.77 (dd, J_{H-H} = 0.72 Hz, J_{H-H} = 2.07 Hz, 1H, CH$_{ar}$), δ 8.67 (ddd, J_{H-H} = 0.78 Hz, J_{H-H} = 1.62 Hz, J_{H-H} = 4.74 Hz, 1H, CH$_{ar}$), δ 8.43 – 8.40 (m, 2H, CH$_{ar}$), δ 7.89 (dd, J_{H-H} = 2.13 Hz, J_{H-H} = 8.25 Hz, 1H, CH$_{ar}$), δ 7.81 (td, J_{H-H} = 1.77 Hz, J_{H-H} = 7.65 Hz, 1H, CH$_{ar}$), δ 7.32 (s, 1H, CH$_{ar}$), δ 7.34 (ddd, J_{H-H} = 1.08 Hz, J_{H-H} = 4.8 Hz, J_{H-H} = 7.47 Hz, 1H, CH$_{ar}$), δ 6.71 (d, J_{H-H} = 1.11 Hz, 1H, CH$_{ar}$), δ 2.41 (s, 3H, CH$_3$), δ 1.90 (s, 3H, CH$_3$), δ 1.86 (s, 3H, CH$_3$).

^{13}C NMR (CDCl$_3$): δ 155.41 (C$_{quat}$), δ 155.21 (C$_{quat}$), δ 151.46 (CH), δ 149.39 (CH), δ 144.11 (C$_{quat}$), δ 140.03 (C$_{quat}$), δ 139.23 (CH), δ 138.18 (C$_{quat}$), δ 137.10 (CH), δ 132.42 (CH), δ 125.55 (C$_{quat}$), δ 124.60 (CH), δ 124.34 (C$_{quat}$), δ 124.13 (CH), δ 121.52 (CH), δ 120.82 (C$_{quat}$), δ 120.49 (CH), δ 129.72 (C$_{quat}$), δ 15.21 (CH$_3$), δ 14.52 (CH$_3$), δ 14.46 (CH$_3$).
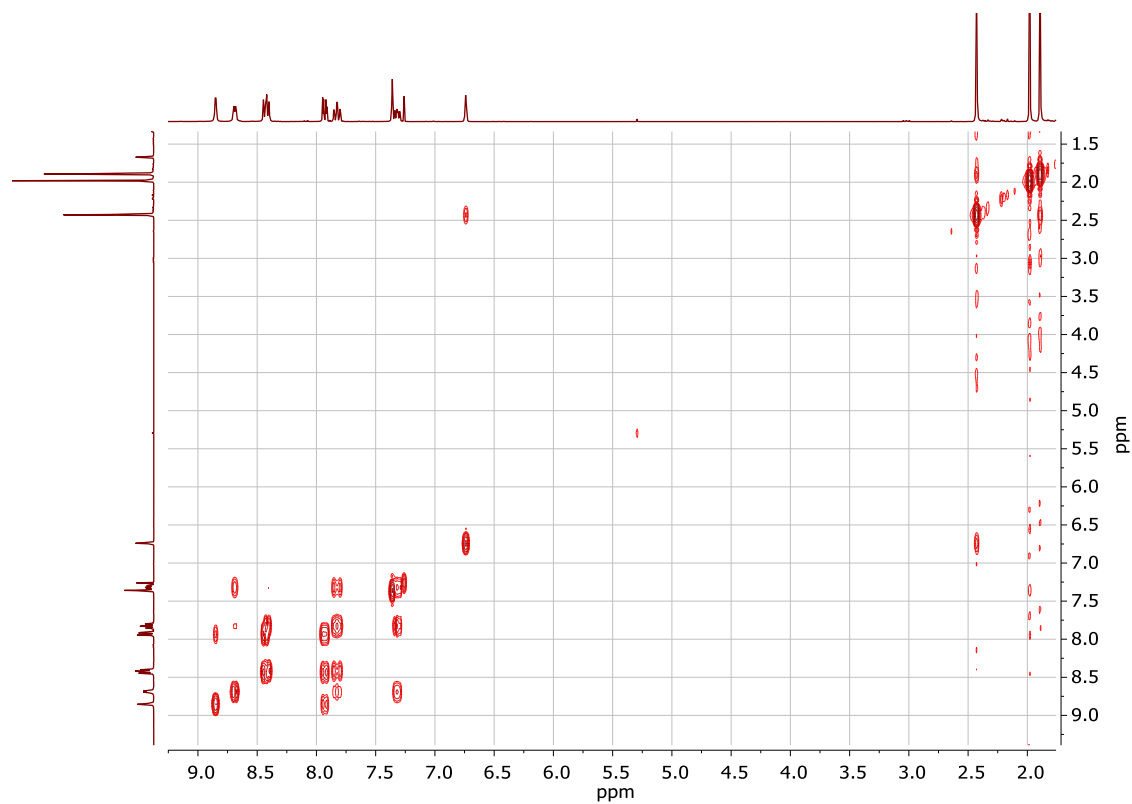
Figure S38. ¹H NMR of 5-((4-(2-(2,5-dimethylthiophen-3-yl)-3,3,4,4,5,5-hexafluorocyclopent-1-en-1-yl)-5-methylthiophen-2-yl)ethynyl)-2,2'-bipyridine (**L2-A**). (CDCl₃, 300 MHz).
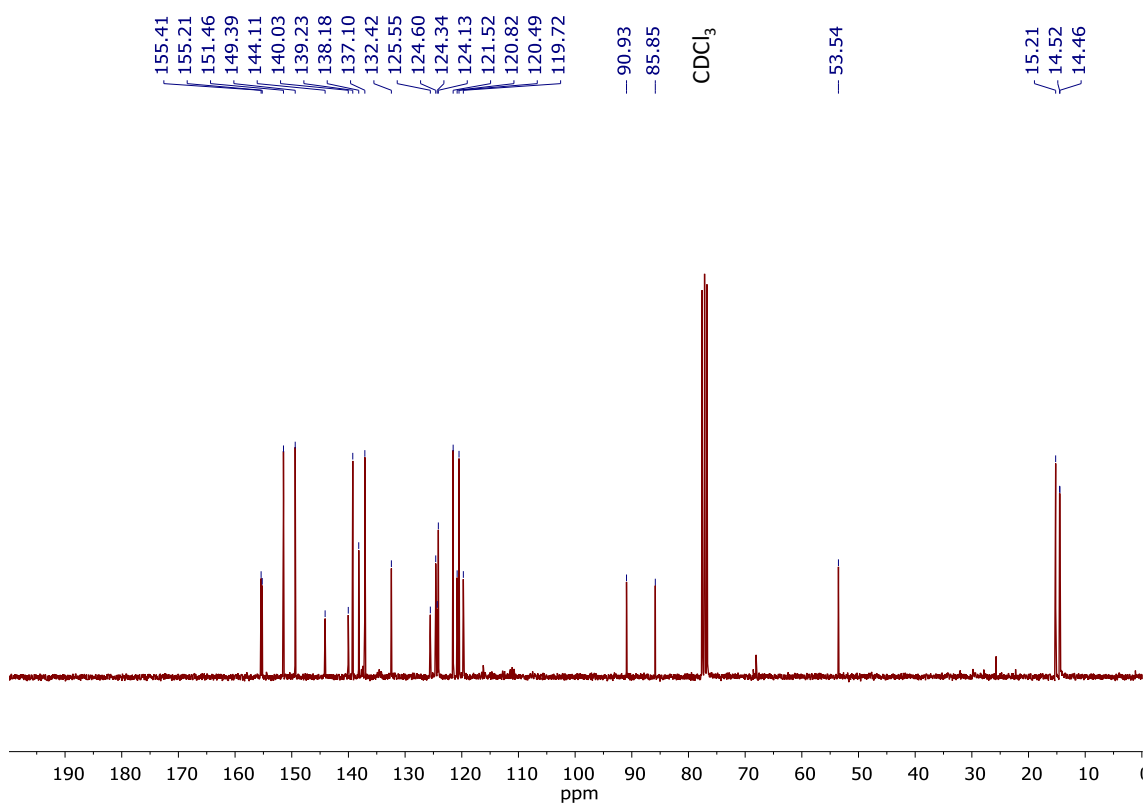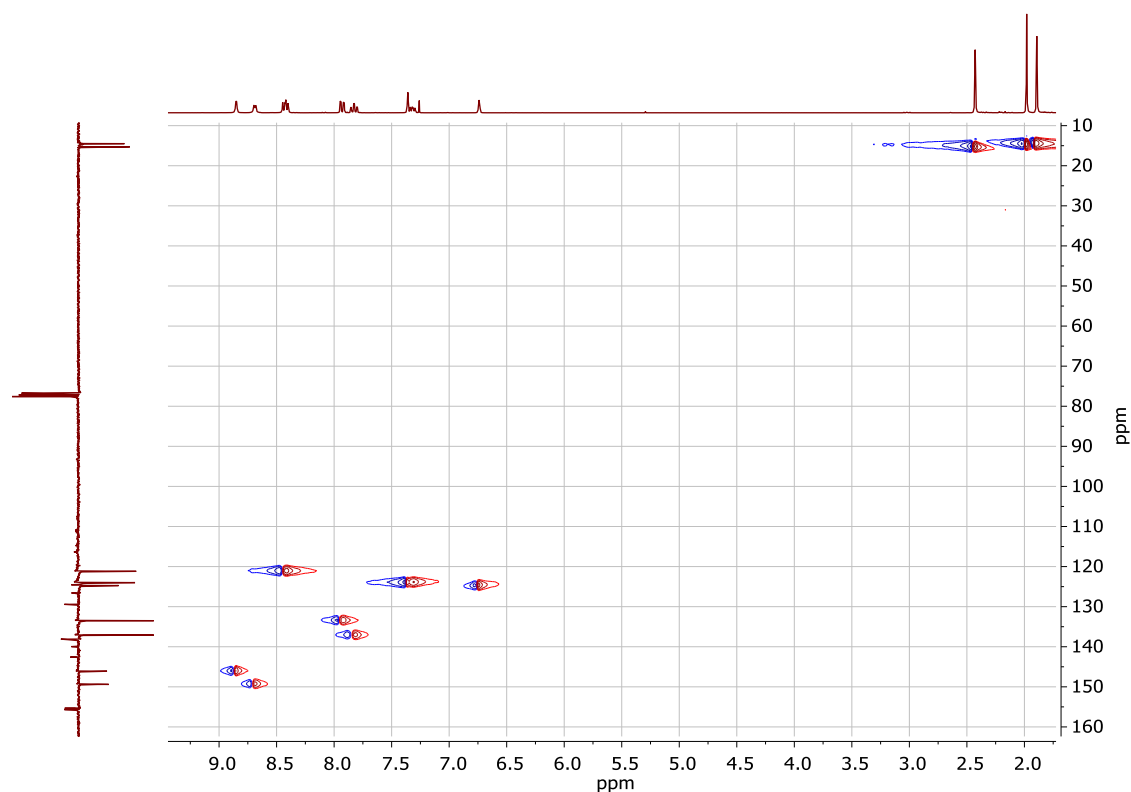

Figure S39. ¹³C NMR of 5-((4-(2-(2,5-dimethylthiophen-3-yl)-3,3,4,4,5,5-hexafluorocyclopent-1-en-1-yl)-5-methylthiophen-2-yl)ethynyl)-2,2'-bipyridine (**L2-A**). (CDCl₃, 300 MHz).
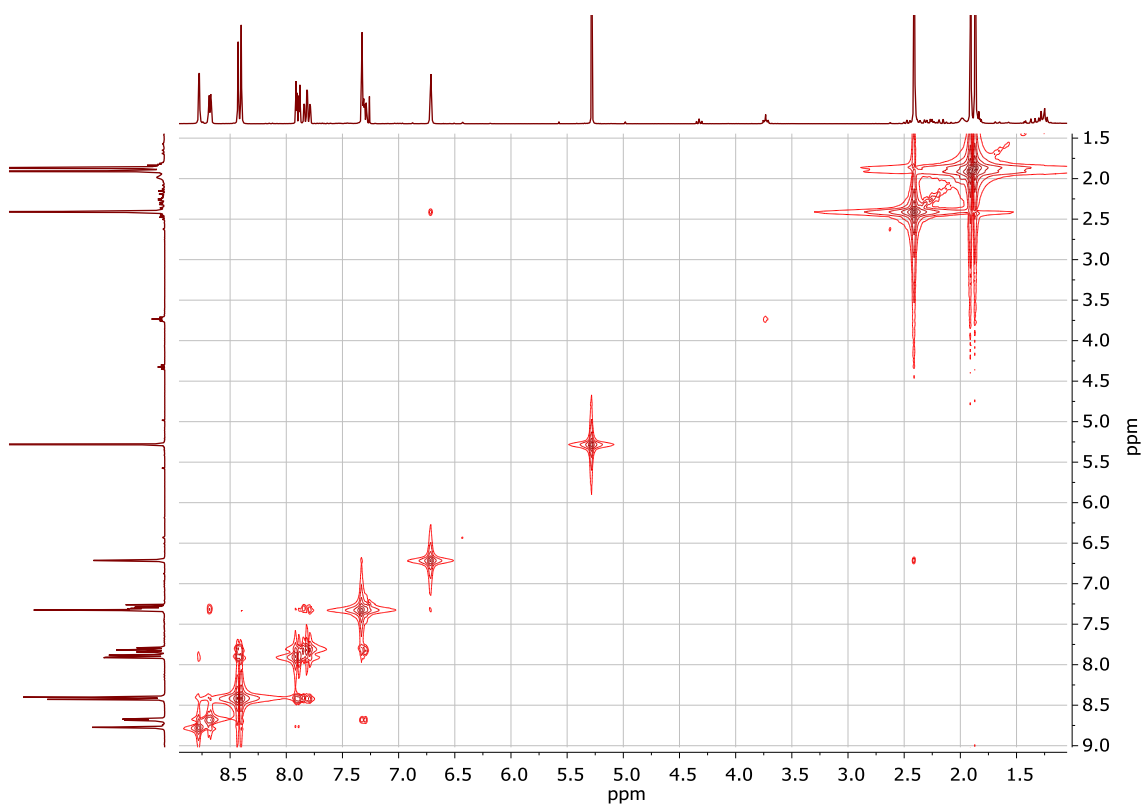
Figure S40. COSY NMR of 5-((4-(2-(2,5-dimethylthiophen-3-yl)-3,3,4,4,5,5-hexafluorocyclopent-1-en-1-yl)-5-methylthiophen-2-yl)ethynyl)-2,2'-bipyridine (**L2-A**). (CDCl$_3$, 300 MHz).
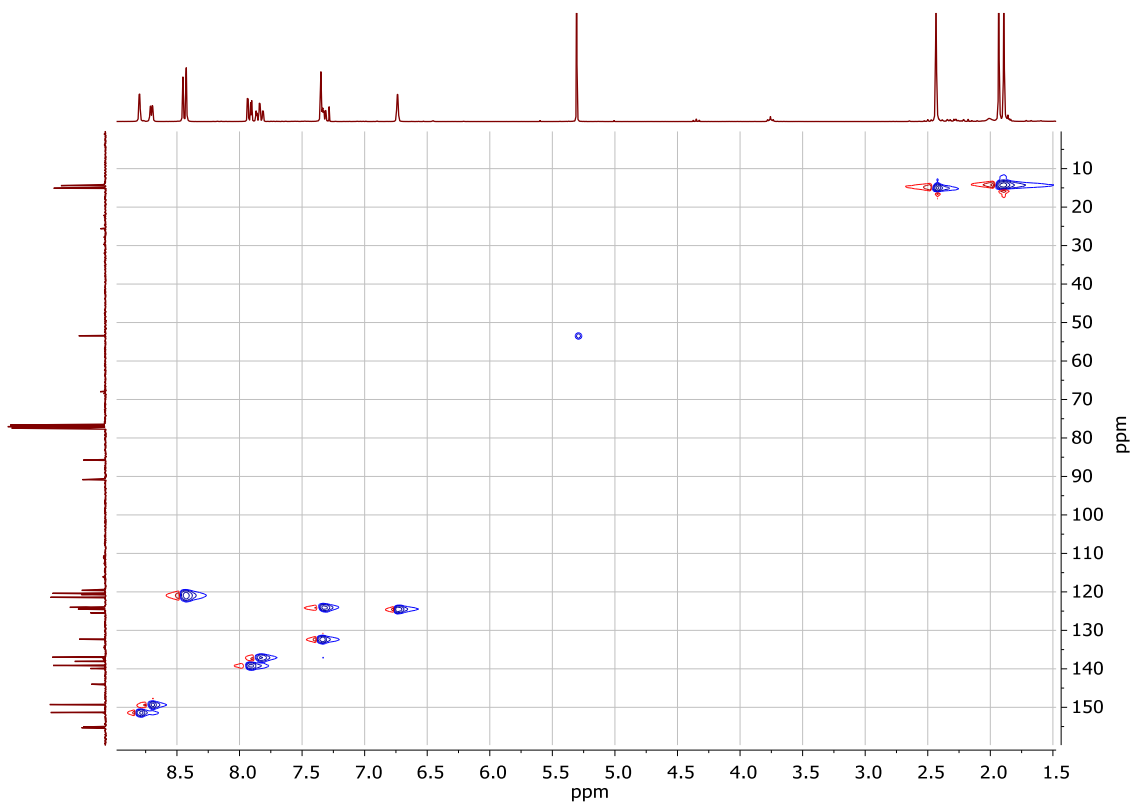
Figure S41. HSQC NMR of 5-((4-(2-(2,5-dimethylthiophen-3-yl)-3,3,4,4,5,5-

hexafluorocyclopent-1-en-1-yl)-5-methylthiophen-2-yl)ethynyl)-2,2'-bipyridine (**L2-A**). (CDCl₃, 300 MHz).

2.1.35 Compound 5-((4-(3,3,4,4,5,5-hexafluoro-2-(2-methylbenzo[b]thiophen-3-yl)cyclopent-1-en-1-yl)-5-methylthiophen-2-yl)ethynyl)-2,2'-bipyridine (L2-B):
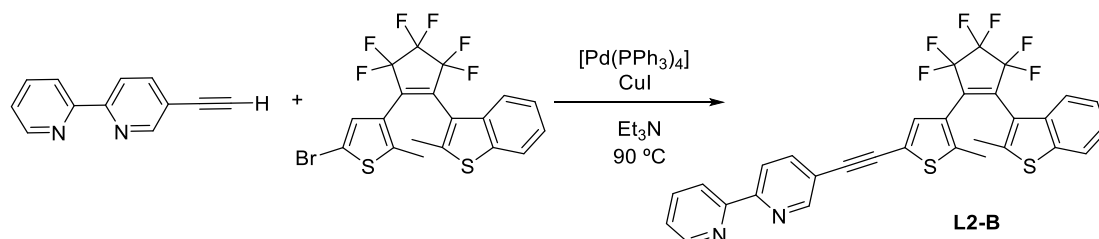
Under N₂ 5-ethynyl-2,2'-bipyridine (0.73 mmol, 0.13 g), 3-(2-(5-bromo-2-methylthiophen-3-yl)-3,3,4,4,5,5-hexafluorocyclopent-1-en-1-yl)-2-methylbenzo[b]thiophene (0.8 mmol, 0.4 g), [Pd(PPh₃)₄] (0.04 mmol, 0.04 g, 5%) and CuI (0.07 mmol, 0.02 g, 10%) were dissolved in 5 mL of degassed Et₃N. The brown solution was refluxed for 12 hours at 90 °C. The brown residue was dissolved in CH₂Cl₂ and washed with a mixture of NH₃ and EDTA. The product was extracted with CH₂Cl₂, dried over MgSO₄ and after removal of the solvent, the residue was purified by silica gel column chromatography (CH₂Cl₂, Rf = 0.2). The product was obtained as a brown solid. (0.07 g, 17% yield).
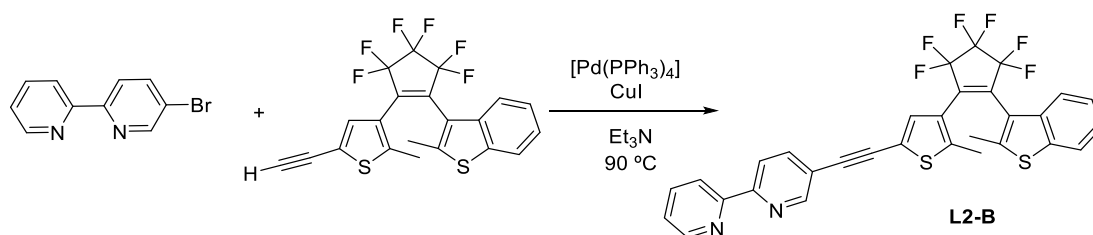
Under N₂ 5-bromo-2,2'-bipyridine (0.43 mmol, 0.1 g), 3-(2-(5-ethynyl-2-methylthiophen-3-yl)-3,3,4,4,5,5-hexafluorocyclopent-1-en-1-yl)-2-methylbenzo[b]thiophene (0.48 mmol, 0.2 g), [Pd(PPh₃)₄] (0.03 mmol, 0.03 g, 7%) and CuI (0.02 mmol, 0.01 g, 5%) were dissolved in 15 mL of degassed Et₃N. The brown solution was refluxed for 12 hours at 90 °C. The brown residue was dissolved in CH₂Cl₂ and washed with a mixture of NH₃ and EDTA. The product was extracted with CH₂Cl₂, dried over MgSO₄ and after removal of the solvent, the residue was purified by silica gel column chromatography (CH₂Cl₂, Rf = 0.22). The product was obtained as a beige solid. (0.06 g, 25% yield).

Exact Mass: FD [C₃₁H₁₈F₆N₂S₂]: calculated: m/z = 560.08156, found: m/z = 560.08224.

¹H NMR (CDCl₃): δ 8.56 (dd, J$_{H-H}$ = 0.81 Hz, J$_{H-H}$ = 2.1 Hz, 1H, CH$_{ar}$), δ 8.67 (ddd, J$_{H-H}$ = 0.9 Hz, J$_{H-H}$ = 1.8 Hz, J$_{H-H}$ = 4.8 Hz, 1H, CH$_{ar}$), δ 8.41 (dd, J$_{H-H}$ = 0.7 Hz, J$_{H-H}$ = 8.4, 2H, CH$_{ar}$), δ 7.88 (dd, J$_{H-H}$ = 2.2 Hz, J$_{H-H}$ = 8.3 Hz, 1H, CH$_{ar}$), δ 7.81 (td, J$_{H-H}$ = 1.8 Hz, J$_{H-H}$ = 7.62 Hz, 1H, CH$_{ar}$), δ 7.74 (d, J$_{H-H}$ = 7.2 Hz, 1H, CH$_{ar}$), δ 7.55 (d, J$_{H-H}$ = 6.9 Hz, 1H, CH$_{ar}$), δ 7.38 – 7.30 (m, 3H, CH$_{ar}$), δ 7.28 (s, 1H, CH$_{ar}$), δ 2.31 (s, 3H, CH₃), δ 1.91 (s, 3H, CH₃).

¹³C NMR (CDCl₃): δ 155.42 (C$_{quat}$), δ 155.26 (C$_{quat}$), δ 151.47 (CH), δ 149.42 (CH), δ 144.52 (C$_{quat}$), δ 142.82 (C$_{quat}$), δ 139.24 (CH), δ 138.36 (C$_{quat}$), δ 138.09 (C$_{quat}$), δ 137.09 (CH), δ 132.19 (CH), δ

125.15 (CH), δ 124.71 (CH), δ 124.14 (CH), δ 122.23 (CH), δ 122.19 (C_quat), δ 122.15 (C_quat), δ 122.11 (C_quat), δ 121.51 (CH), δ 120.75 (C_quat), δ 120.47 (2CH), δ 120.05 (C_quat), δ 119.65 (C_quat), δ 15.03 (CH_3), δ 14.86 (CH_3).

Figure S42. ^{1}H NMR of 5-((4-(3,3,4,4,5,5-hexafluoro-2-(2-methylbenzo[b]thiophen-3-yl)cyclopent-1-en-1-yl)-5-methylthiophen-2-yl)ethynyl)-2,2'-bipyridine (**L2-B**). (CDCl_3, 300 MHz).
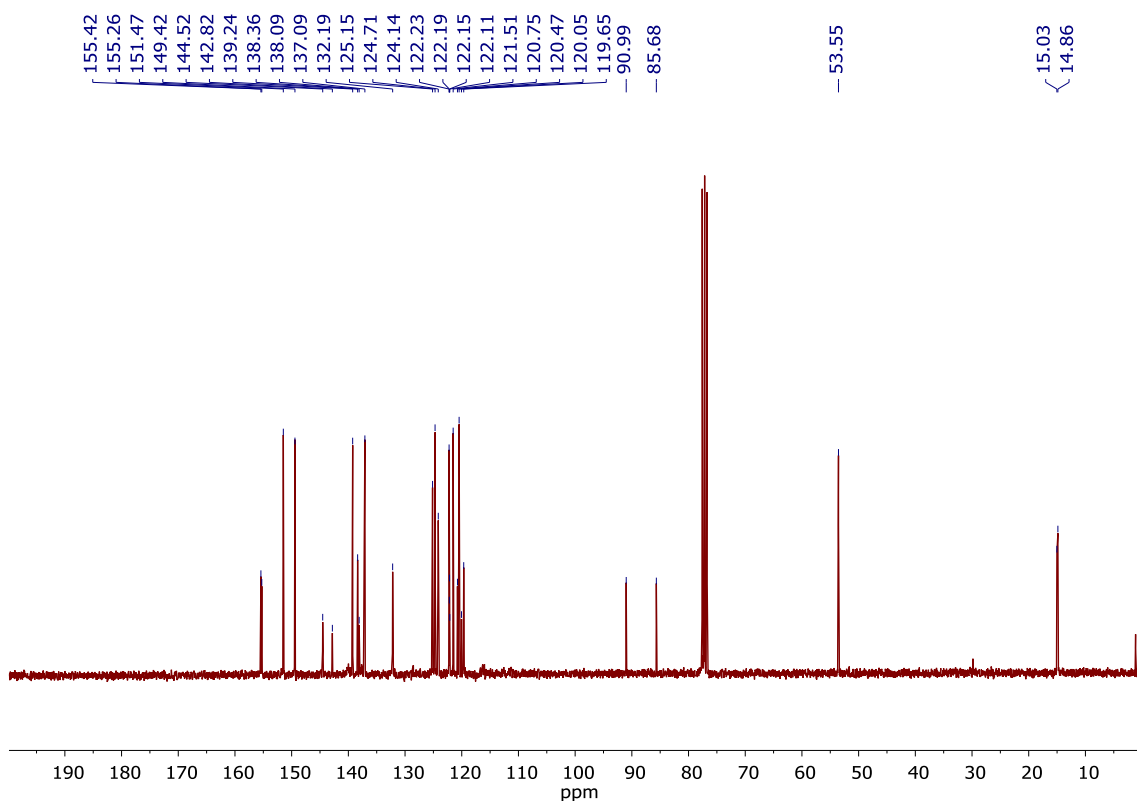
Figure S43. ^{13}C NMR of 5-((4-(3,3,4,4,5,5-hexafluoro-2-(2-methylbenzo[b]thiophen-3-yl)cyclopent-1-en-1-yl)-5-methylthiophen-2-yl)ethynyl)-2,2'-bipyridine (**L2-B**). (CDCl$_3$, 300 MHz).
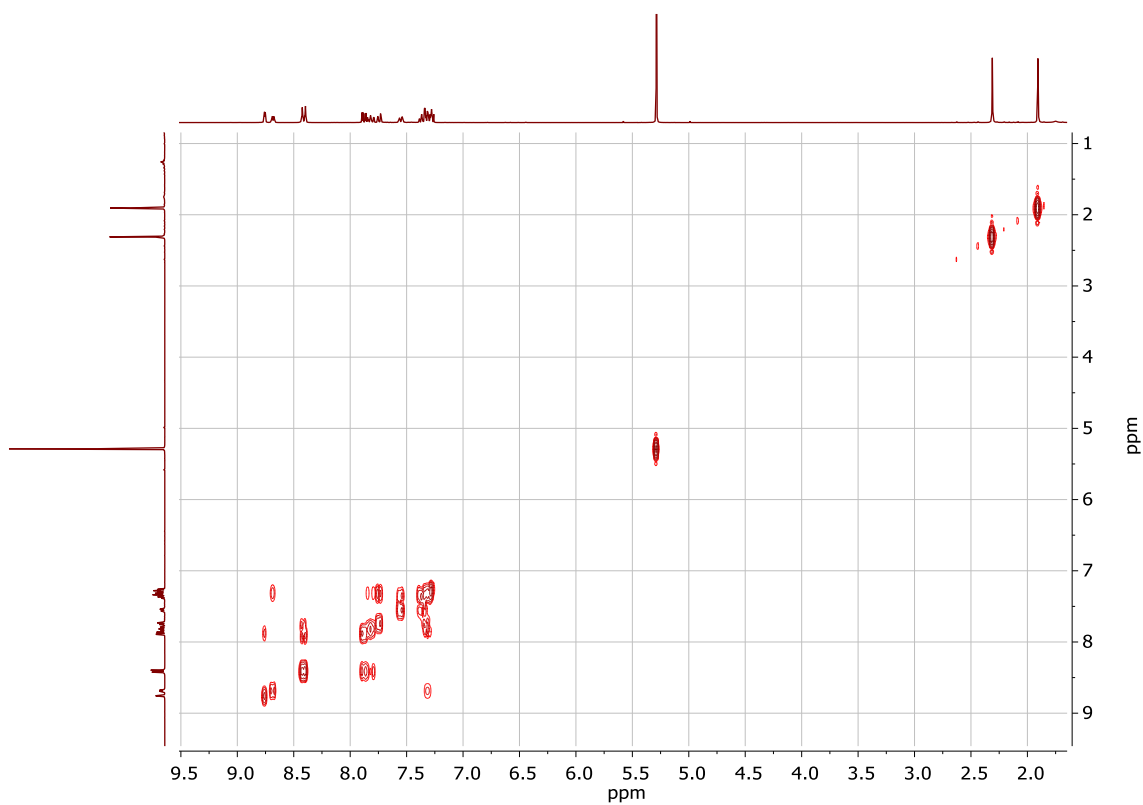
Figure S44. COSY NMR of5-((4-(3,3,4,4,5,5-hexafluoro-2-(2-methylbenzo[b]thiophen-3-yl)cyclopent-1-en-1-yl)-5-methylthiophen-2-yl)ethynyl)-2,2'-bipyridine (**L2-B**). (CDCl₃, 300 MHz).

Figure S45. HSQC NMR of 5-((4-(3,3,4,4,5,5-hexafluoro-2-(2-methylbenzo[b]thiophen-3-yl)cyclopent-1-en-1-yl)-5-methylthiophen-2-yl)ethynyl)-2,2'-bipyridine (**L2-B**). (CDCl₃, 300 MHz).

2.1.36 Compound 5-(4-(2-(2,5-dimethylthiophen-3-yl)-3,3,4,4,5,5-hexafluorocyclopent-1-en-1-yl)-5-methylthiophen-2-yl)-2,2'-bipyridine (L3-A):
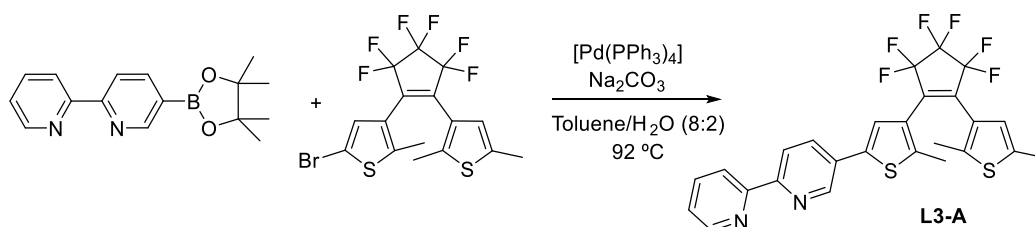
Under N_2 5-(4,4,5,5-tetramethyl-1,3,2-dioxaborolan-2-yl)-2,2'-bipyridine (1.87 mmol, 0.15 g), 3 5-bromo-3-(2-(2,5-dimethylthiophen-3-yl)-3,3,4,4,5,5-hexafluorocyclopent-1-en-1-yl)-2-methylthiophene (0.62mmol, 0.29 g), [Pd(PPh₃)₄] (0.12 mmol, 0.14 g, 20%) and Na_2CO_3 (6.24 mmol, 0.66 g) were dissolved in 20 mL of degassed mixture of toluene/H₂O (8:2). The brown solution was refluxed for 24 hours at 92 °C .The brown solution was extracted with CH₂Cl₂/H₂O. The organic layer was dried over MgSO₄ and after removal of the solvent, the residue was

255

purified by silica gel column chromatography (CH$_2$Cl$_2$, Rf = 0.14). The product was obtained as a beige solid. (0.2 g, 60% yield).

Exact Mass: FD [C$_{26}$H$_{18}$F$_6$N$_2$S$_2$]: calculated: m/z = 536.08156, found: m/z = 536.07967.

^{1}H NMR (CDCl$_3$): δ 8.85 (d, J$_{H-H}$ = 1.9 Hz, 1H, CH$_{ar}$), δ 8.69 (d, J$_{H-H}$ = 4.2 Hz, 1H, CH$_{ar}$), δ 8.42 (dd, J$_{H-H}$ = 5.7 Hz, J$_{H-H}$ = 8.1 Hz, 2H, CH$_{ar}$), δ 7.93 (dd, J$_{H-H}$ = 2.4 Hz, J$_{H-H}$ = 8.3 Hz, 1H, CH$_{ar}$), δ 7.83 (td, J$_{H-H}$ = 1.8 Hz, J$_{H-H}$ = 7.8 Hz, 1H, CH$_{ar}$), δ 7.36 (s, 1H, CH$_{ar}$), δ 7.32 (ddd, J$_{H-H}$ = 1.1 Hz, J$_{H-H}$ = 4.8 Hz, J$_{H-H}$ = 7.4 Hz, 1H, CH$_{ar}$), δ 6.71 (d, J$_{H-H}$ = 1.08 Hz, 1H, CH$_{ar}$), δ 2.43 (s, 3H, CH$_3$), δ 1.98 (s, 3H, CH$_3$), δ 1.89 (s, 3H, CH$_3$).

^{13}C NMR (CDCl$_3$): δ 155.68 (C$_{quat}$), δ 155.34 (C$_{quat}$), δ 149.39 (CH), δ 146.11 (CH), δ 142.60 (C$_{quat}$), δ 139.96 (C$_{quat}$), δ 138.24 (C$_{quat}$), δ 138.11 (C$_{quat}$), δ 137.10 (CH), δ 133.49 (CH), δ 129.43 (C$_{quat}$), δ 126.57 (C$_{quat}$), δ 124.74 (CH), δ 124.54 (CH), δ 124.00 (2CH), δ 121.19 (2CH), δ 15.28 (CH$_3$), δ 14.68 (CH$_3$), δ 14.49 (CH$_3$).
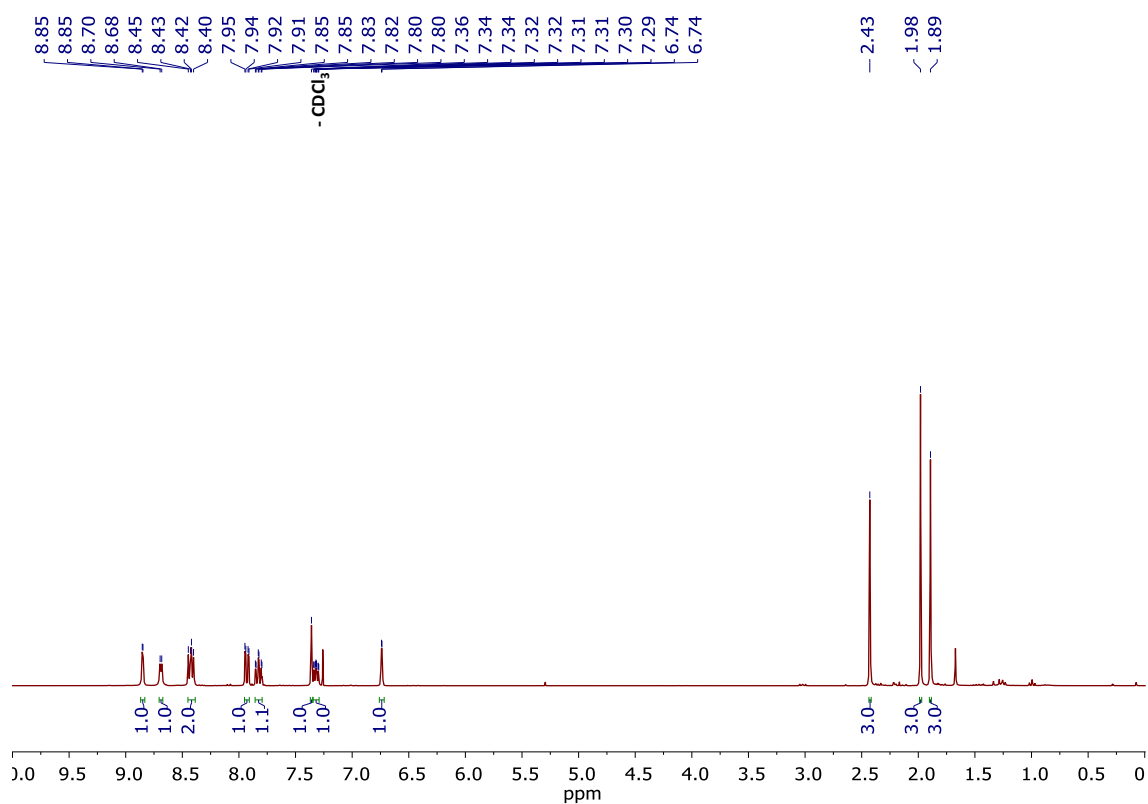
Figure S46. ^{1}H NMR of 5-(4-(2-(2,5-dimethylthiophen-3-yl)-3,3,4,4,5,5-hexafluorocyclopent-1-en-1-yl)-5-methylthiophen-2-yl)-2,2'-bipyridine (**L3-A**). (CDCl$_3$, 300 MHz).
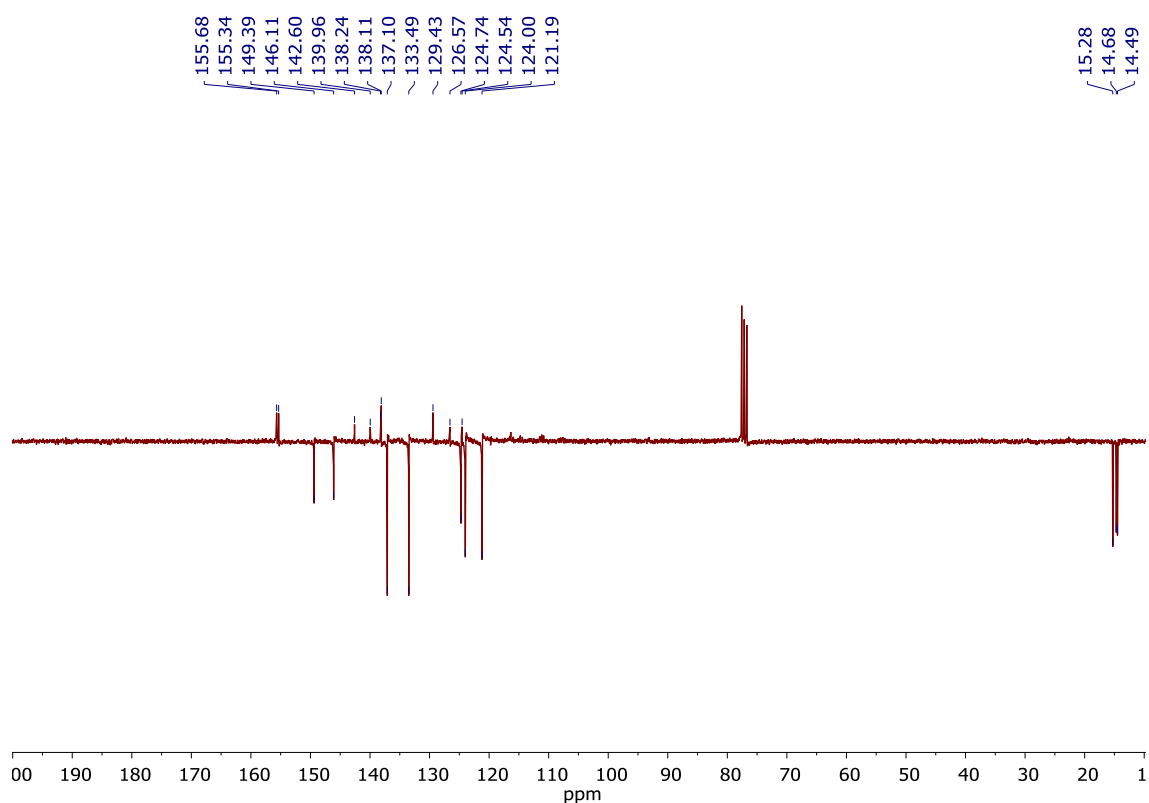
Figure S47. ^{13}C NMR of 5-(4-(2-(2,5-dimethylthiophen-3-yl)-3,3,4,4,5,5-hexafluorocyclopent-1-en-1-yl)-5-methylthiophen-2-yl)-2,2'-bipyridine (**L3-A**). (CDCl$_3$, 300 MHz).

Figure S48. COSY NMR of 5-(4-(2-(2,5-dimethylthiophen-3-yl)-3,3,4,4,5,5-hexafluorocyclopent-1-en-1-yl)-5-methylthiophen-2-yl)-2,2'-bipyridine (**L3-A**). (CDCl$_3$, 300 MHz).

Figure S49. HSQC NMR of 5-(4-(2-(2,5-dimethylthiophen-3-yl)-3,3,4,4,5,5-hexafluorocyclopent-1-en-1-yl)-5-methylthiophen-2-yl)-2,2'-bipyridine (**L3-A**). (CDCl₃, 300 MHz).

2.1.37 Compound 3-(2-(5-bromo-2-methylthiophen-3-yl)-3,3,4,4,5,5-hexafluorocyclopent-1-en-1-yl)-2-methylbenzo[b]thiophene (L3-B):
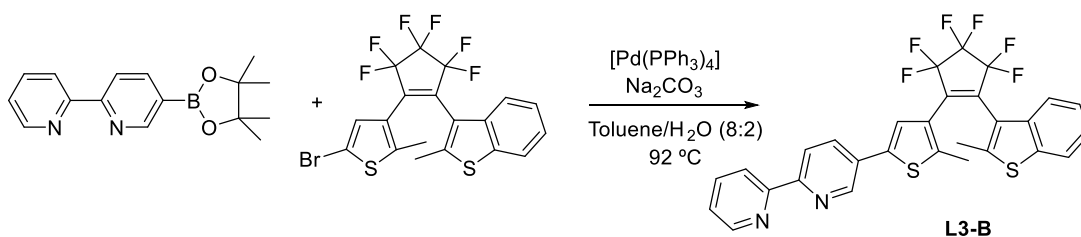
Under N₂ 5-(4,4,5,5-tetramethyl-1,3,2-dioxaborolan-2-yl)-2,2'-bipyridine (4.02 mmol, 0.33 g), 3 5-bromo-3-(2-(2,5-dimethylthiophen-3-yl)-3,3,4,4,5,5-hexafluorocyclopent-1-en-1-yl)-2-methylthiophene (2.01 mmol, 1 g), [Pd(PPh₃)₄] (0.03 mmol, 0.035 g, 15%) and Na₂CO₃ (20.1 mmol, 2.13 g) were dissolved in 80 mL of degassed mixture of toluene/H₂O (8:2). The brown solution was refluxed for 24 hours at 92 °C .The brown solution was extracted with CH₂Cl₂/H₂O. The organic layer was dried over MgSO₄ and after removal of the solvent, the residue was purified by silica gel column chromatography (CH₂Cl₂, Rf = 0.22). The product was obtained as a beige solid. (0.46 g, 40% yield).

Exact Mass: FD [$C_{29}H_{18}F_6N_2S_2$]: calculated: m/z = 572.08156, found: m/z = 572.08261.

¹H NMR (CDCl₃): δ 8.73 (dd, J_{H-H} = 0.8 Hz, J_{H-H} = 2.4 Hz, 1H, CH$_{ar}$), δ 8.67 (ddd, J_{H-H} = 0.9 Hz, J_{H-H} = 1.77 Hz, J_{H-H} = 4.8 Hz, 1H, CH$_{ar}$), δ 8.41 (dd, J_{H-H} = 0.69 Hz, J_{H-H} = 8.19, 2H, CH$_{ar}$), δ 7.82 (td, J_{H-H} = 1.8 Hz, J_{H-H} = 7.56 Hz, 1H, CH$_{ar}$), δ 7.80 (dd, J_{H-H} = 2.4 Hz, J_{H-H} = 8.34 Hz, 1H, CH$_{ar}$), δ 7.76 − 7.74

(m, 1H, CH$_{ar}$), δ 7.57 (d, J$_{H-H}$ = 7.17 Hz, 1H, CH$_{ar}$), δ 7.38 – 7.29 (m, 3H, CH$_{ar}$), δ 7.25 (s, 1H, CH$_{ar}$), δ 2.33 (s, 3H, CH$_3$), δ 2.01 (s, 3H, CH$_3$).

^{13}C NMR (CDCl$_3$): δ 155.50 (C$_{quat}$), δ 155.14 (C$_{quat}$), δ 149.26 (CH), δ 146.02 (CH), δ 143.09 (C$_{quat}$), δ 142.35 (C$_{quat}$), δ 138.37 (C$_{quat}$), δ 138.32 (C$_{quat}$), δ 138.00 (C$_{quat}$), δ 137.24 (CH), δ 133.50 (CH), δ 129.33 (C$_{quat}$), δ 125.68 (C$_{quat}$), δ 125.14 (CH), δ 124.74 (CH), δ 124.00 (CH), δ 122.27 (CH), δ 122.21 (C$_{quat}$), δ 122.15 (C$_{quat}$), δ 121.25 (2CH), δ 120.30 (C$_{quat}$), δ 15.03 (CH$_3$), δ 15.01 (CH$_3$).

Figure S50. ^{1}H NMR of 3-(2-(5-bromo-2-methylthiophen-3-yl)-3,3,4,4,5,5-hexafluorocyclopent-1-en-1-yl)-2-methylbenzo[*b*]thiophene (**L3-B**). (CDCl$_3$, 300 MHz).
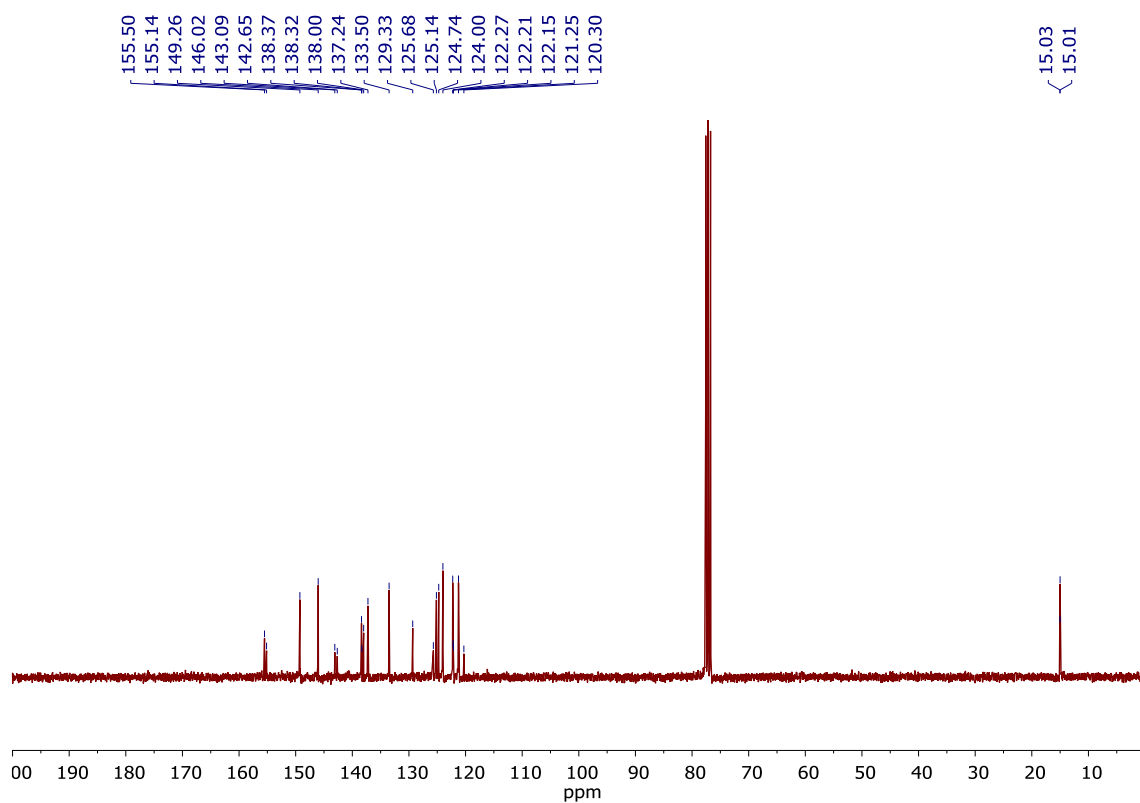
Figure S51. ^{13}C NMR of 3-(2-(5-bromo-2-methylthiophen-3-yl)-3,3,4,4,5,5-hexafluorocyclopent-1-en-1-yl)-2-methylbenzo[*b*]thiophene (**L3-B**). (CDCl$_3$, 300 MHz).
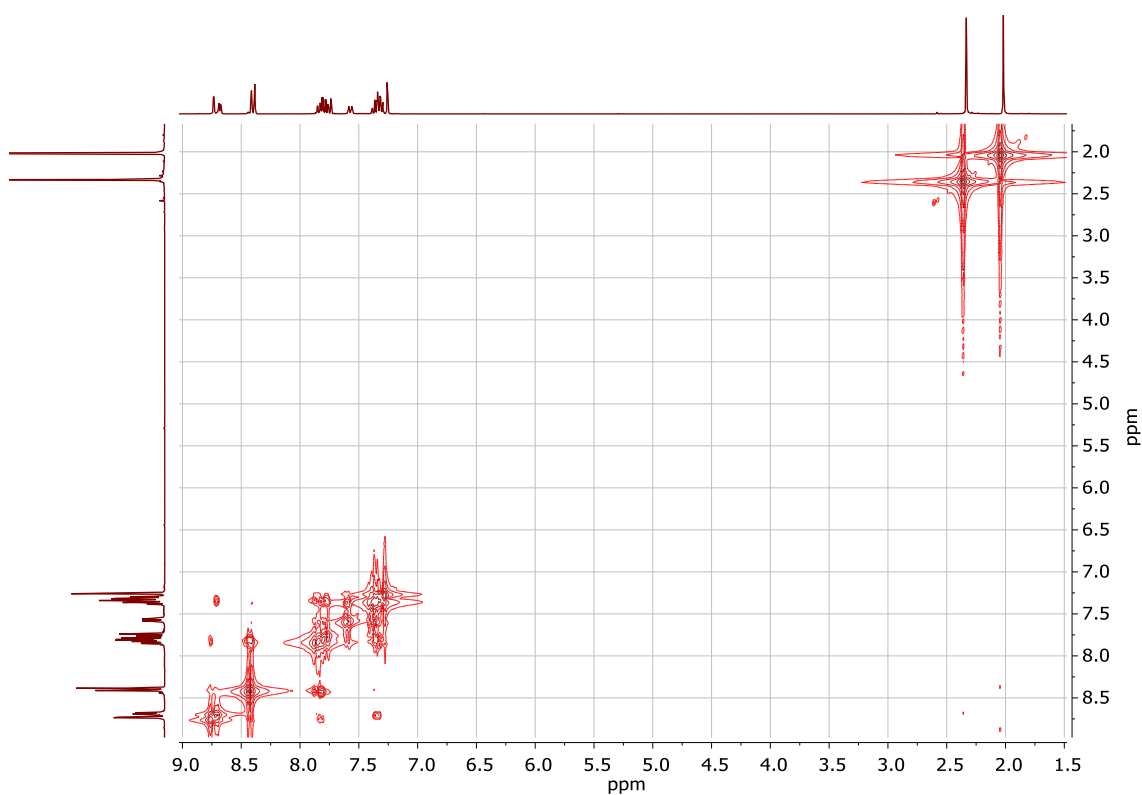
Figure S52. COSY NMR of 3-(2-(5-bromo-2-methylthiophen-3-yl)-3,3,4,4,5,5-hexafluorocyclopent-1-en-1-yl)-2-methylbenzo[*b*]thiophene (**L3-B**). (CDCl$_3$, 300 MHz).
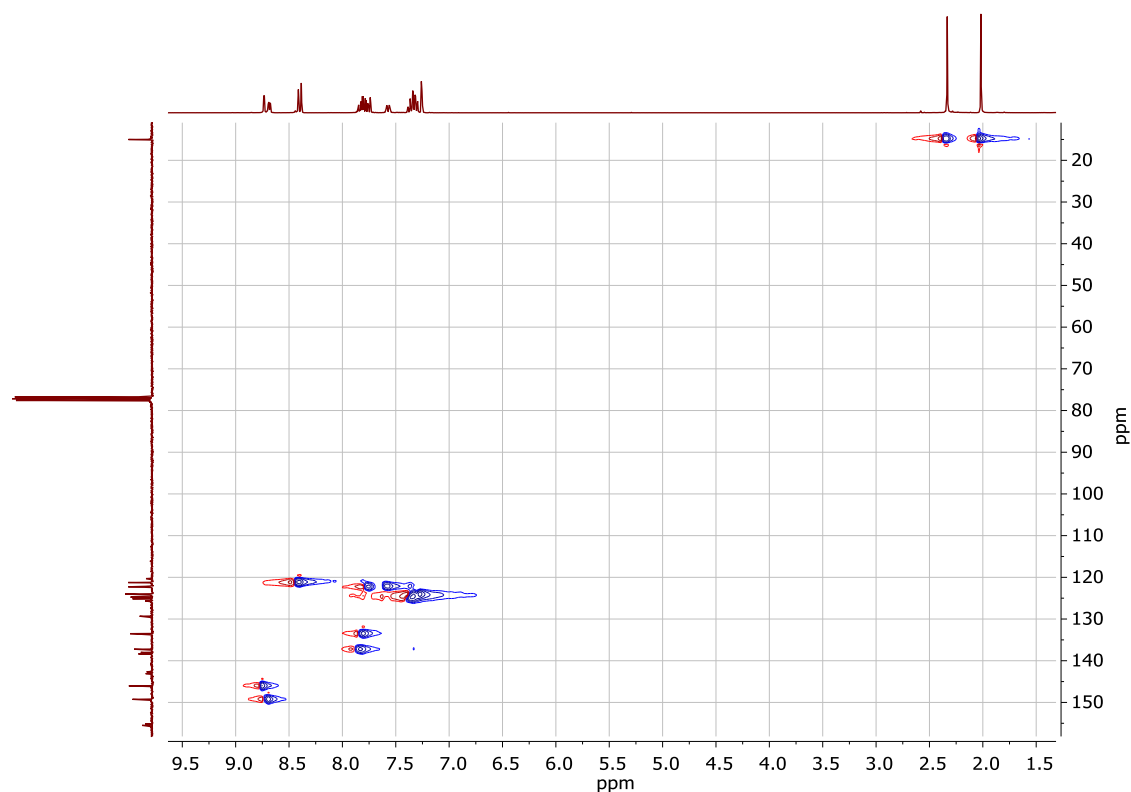
Figure S53. HSQC NMR of 3-(2-(5-bromo-2-methylthiophen-3-yl)-3,3,4,4,5,5-hexafluorocyclopent-1-en-1-yl)-2-methylbenzo[*b*]thiophene (**L3-B**). (CDCl$_3$, 300 MHz).

2.2 COMPLEX

2.2.1 Complex [Ir(2-pyridyl-4-bromo-5-methylthiophene)$_2$Cl]$_2$ (C2):
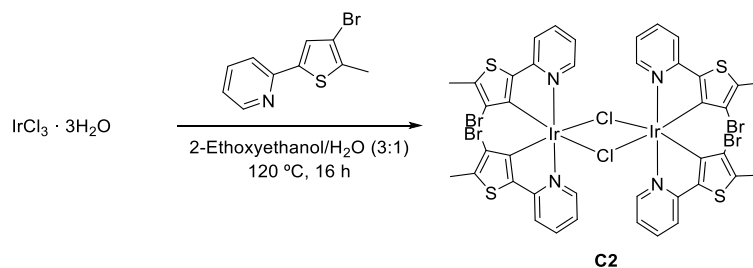
Compound **C2** was synthesized following a slightly modified reported procedure[29]. Under N$_2$, IrCl$_3$·3H$_2$O (0.43 mmol, 0.15 g) and (1.62 mmol, 0.41 g) were dissolved in a 20 mL mixture of 2-ethoxyethanol/H$_2$O (3:1). The brown suspension was refluxed for 16 hours at 120 °C .The orange suspension was filtered under N$_2$ and the resultant orange solid was washed with Et$_2$O (3x20 mL). The product was obtained as an orange solid. (0.19 g, 61% yield). The product was identified employing elemental analysis because the product's low solubility in deuterated solvents.

EA: [C$_{40}$H$_{28}$Br$_4$Cl$_2$N$_4$S$_4$]: Calculated: C: 32.73%, H: 1.92%, N: 3.82%, S: 8.74%; found: C: 33.66%, H: 2.56%, N: 3.49%, S: 7.68%;

2.2.2 Complex [Ir(2-pyridyl-4-bromo-5-methylthiophene)$_2$Cl]$_2$ (C3):
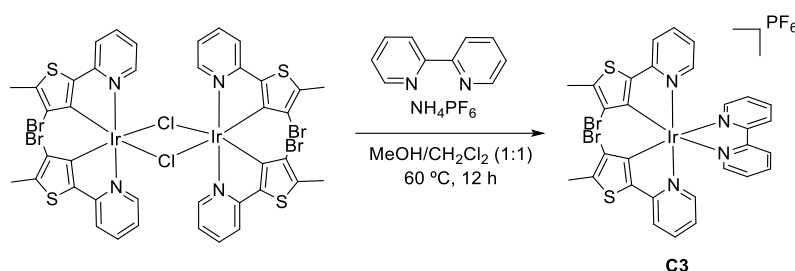
Compound **C3** was synthesized following a slightly modified reported procedure[30]. Under N$_2$, [Ir(6)$_2$Cl]$_2$ (0.14 mmol, 0.05 g) was dissolved in 14 mL of a degassed mixture of MeOH/CH$_2$Cl$_2$ (1:1). 2,2'-bipyridine (0.14 mmol, 0.02 g) was added and the orange suspension was refluxed for 12 hours at 60 °C .To the brown solution NH4PF6 (0.28 mmol, 0.05 g) was added and the reaction was stirred for 24 hours at r.t. Volatiles were removed under vacuum and the resultant solid was washed with H2O (2x10 mL) and Et2O (2x10 mL). The solid was dried under vacuum. The product was obtained as a yellow-brownish solid. 0.06 g, 46% yield).

^{1}H NMR (Acetone-d$_6$): δ 8.88 (d, J_{H-H} = 8.07 Hz, 2H, CH$_{ar}$), δ 8.36 (td, J_{H-H} = 1.47 Hz, J_{H-H} = 7.8 Hz, 2H, CH$_{ar}$), δ 8.25 (dd, J_{H-H} = 1.41 Hz, J_{H-H} = 5.91, 2H, CH$_{ar}$), δ 7.84 – 7.76 (m, 4H, CH$_{ar}$), δ 7.61 (dt, J_{H-H} = 0.81 Hz, J_{H-H} = 8.1 , 2H, CH$_{ar}$), δ 7.54 (dt, J_{H-H} = 0.81 Hz, J_{H-H} = 5.91 Hz, 2H, CH$_{ar}$), δ 2.41 (s, 6H, CH$_3$).
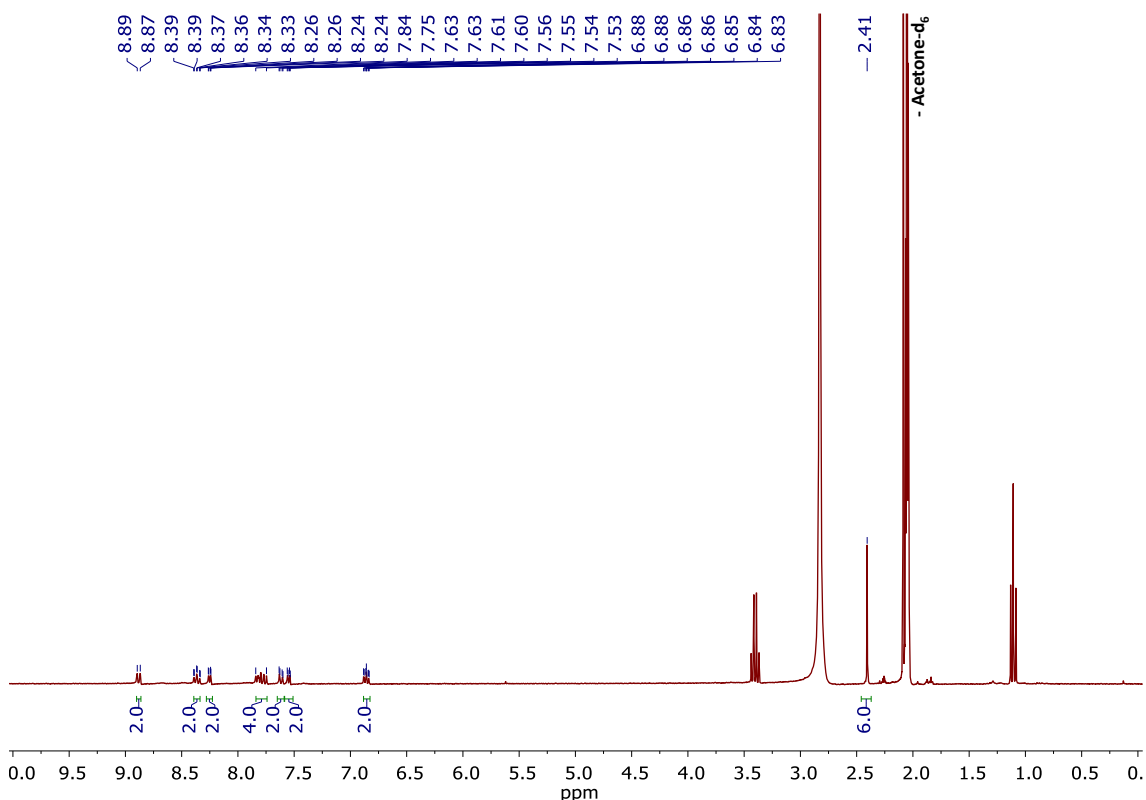
Figure S54. ^{1}H NMR of [Ir(2-pyridyl-4-bromo-5-methylthiophene)$_2$Cl]$_2$ (**C3**) (Acetone-d$_3$, 300 MHz).

2.2.3 Complex [Ir(ppy)$_2$Cl]$_2$ (C4):
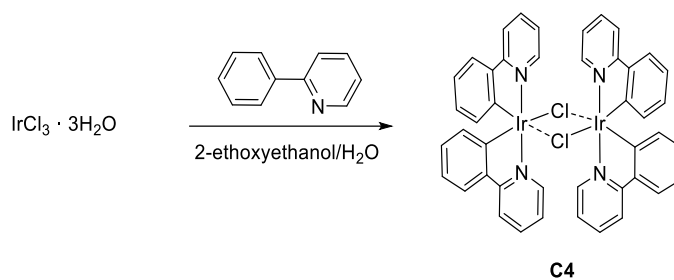
Compound **C4** was synthesized following a slightly modified reported procedure[30]. Under N_2, $IrCl_3 \cdot 3H_2O$ (2.83 mmol, 1 g) were dissolved in 30 mL of 2-ethoxyethanol. To the black solution, phenylpyridine (7.08 mmol, 1 mL) and 10 mL of H_2O were added. The black solution was refluxed for 24 hours at 120 °C .The yellow suspension was filtered under N_2 and the resultant yellow solid was washed with H_2O (3x30 mL). The product was obtained as a yellow solid. (1.08 g, 66% yield).

^{1}H NMR (CDCl$_3$): δ 9.24 (dd, J_{H-H} = 0.81 Hz, J_{H-H} = 5.79 Hz, 4H, CH$_{ar}$), δ 7.87 (d, J_{H-H} = 7.59 Hz, 4H, CH$_{ar}$), δ 7.73 (dt, J_{H-H} = 1.56 Hz, J_{H-H} = 7.38, 4H, CH$_{ar}$), δ 7.48 (dd, J_{H-H} = 1.2 Hz, J_{H-H} = 7.8 Hz, 4H, CH$_{ar}$), δ 6.80-6.71 (m, , 8H, CH$_{ar}$), δ 6.55 (dt, J_{H-H} = 1.38 Hz, J_{H-H} = 7.71 Hz, 4H, CH$_{ar}$), δ 5.93 (dd, J_{H-H} = 0.96 Hz, J_{H-H} = 7.74 Hz, 4H, CH$_{ar}$.
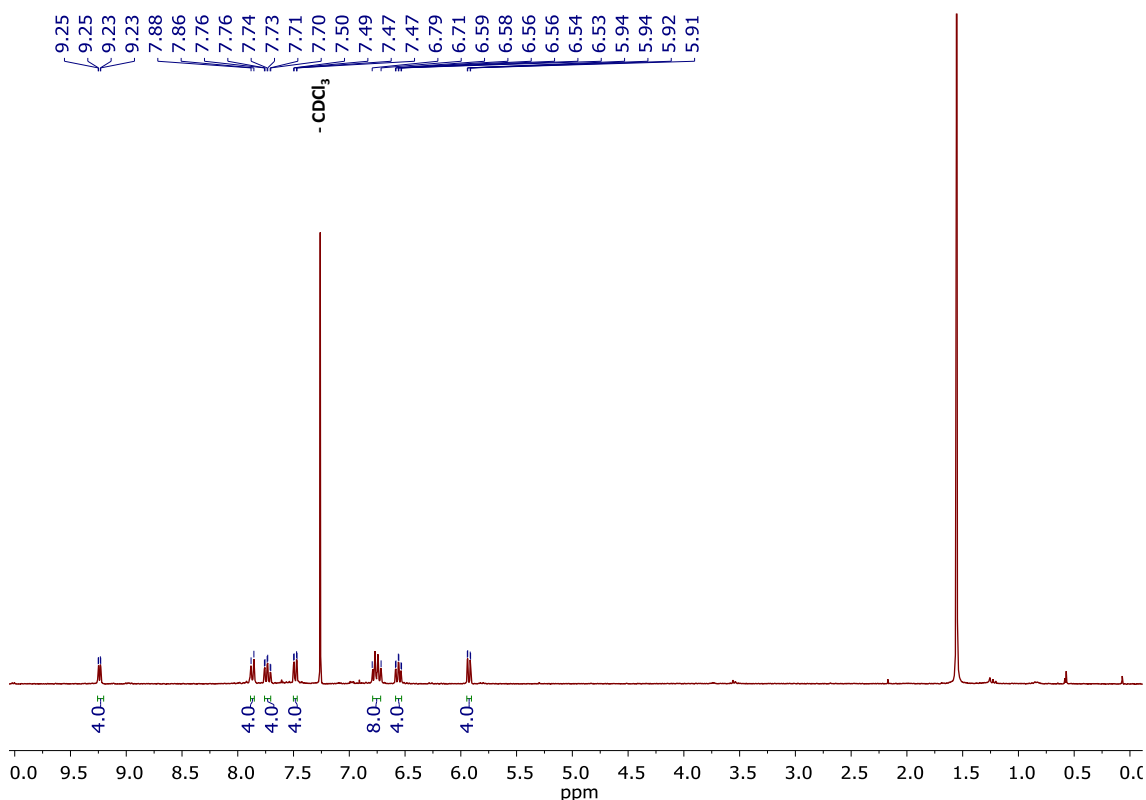
Figure S55. ^{1}H NMR of [Ir(ppy)$_2$Cl]$_2$ (**C4**). (CDCl$_3$, 300 MHz).

2.2.4 Complex [Ir(ppy)$_2$(CH$_3$CN)$_2$] (C5):
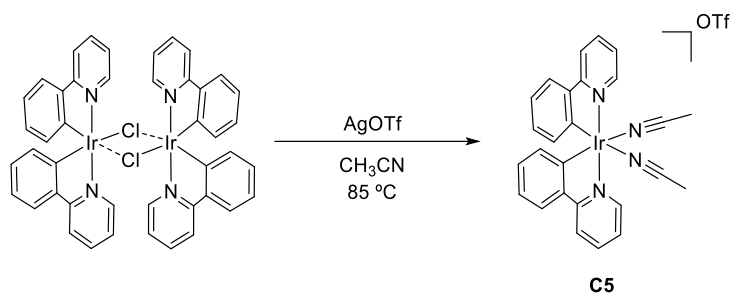
Compound **C5** was synthesized following a reported procedure[31]. Under [Ir(ppy)$_2$Cl]$_2$ (0.149 mmol, 0.16 g) were dissolved in 40 mL of CH$_3$CN. AgOTf (1.49 mmol, 0.38 g) were added to the yellow solution. The resultant yellow solution was refluxed for 16 hours at 82 °C. The yellow solution was filtered through a celite pad, removing traces of AgCl. The product was obtained as a yellow solid. (0.15 g, 70% yield).

^{1}H NMR (CDCl$_3$): δ 9.07 (d, J$_{H-H}$ = 5.49 Hz, 2H, CH$_{ar}$), δ 8.02 (m, 4H, CH$_{ar}$), δ 7.63 (d, J$_{H-H}$ = 7.62 Hz, 2H, CH$_{ar}$), δ 7.44 (t, J$_{H-H}$ = 5.25 Hz, 2H, CH$_{ar}$), δ 6.86 (t, J$_{H-H}$ = 7.32 Hz, 2H, CH$_{ar}$), δ 6.71 (t, J$_{H-H}$ = 7.38 Hz, 2H, CH$_{ar}$), δ 6.02 (d, J$_{H-H}$ = 7.5 Hz, 2H, CH$_{ar}$), δ 2.42 (s, 6H, 2CH$_3$).
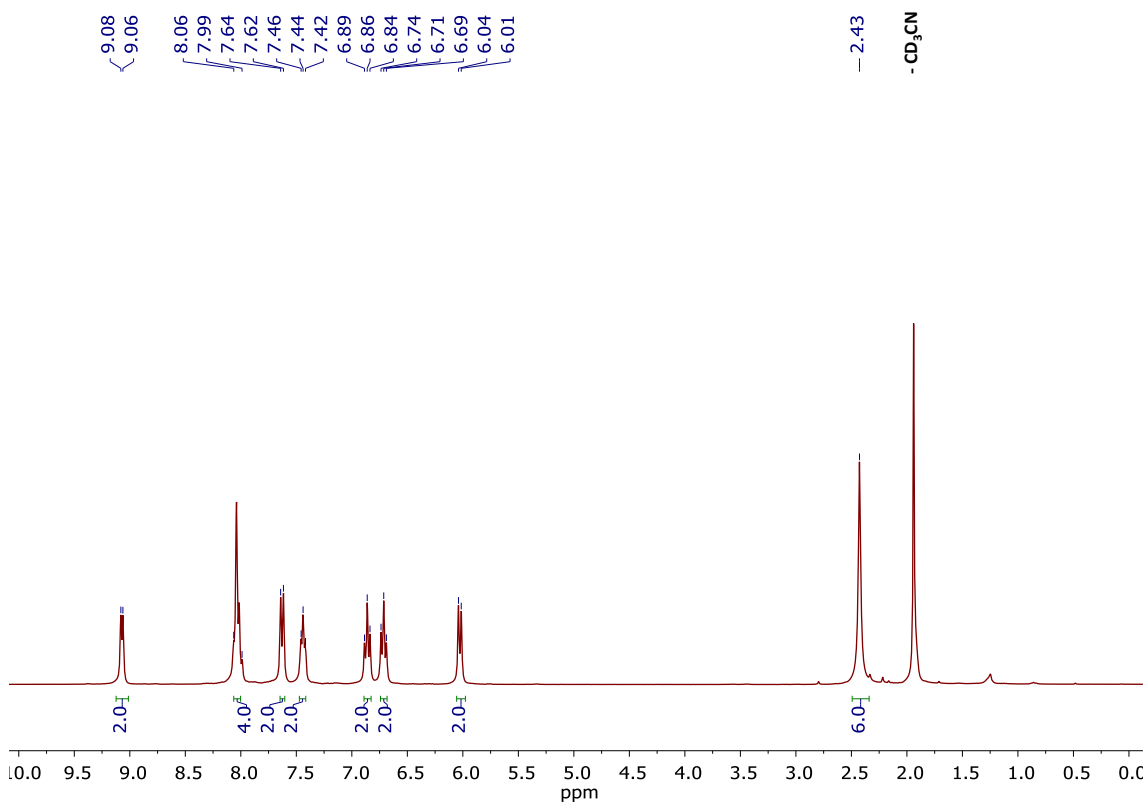
Figure S56. ^{1}H NMR of [Ir(ppy)$_2$(CH$_3$CN)$_2$] (**C5**). (CD$_3$CN, 300 MHz).

2.2.5 Complex [Ir(ppy)$_2$OH]$_2$ (C6):

264

C6
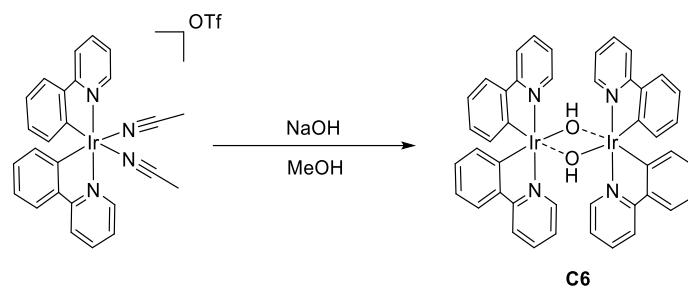
Compound **C6** was synthesized following a reported procedure[31]. Under N$_2$, [Ir(ppy)$_2$(CH$_3$CN)$_2$]OTf (0.14) was dissolved in 40 mL of MeOH. NaOH (1.51 mmol, 0.06g) was added to the yellow solution. The reaction was stirred for 24 hours at r.t. The brown suspension was filtered through a celite pad and the orange solid was dried under vacuum. The product was obtained as a red-orange solid. (0.03 g, 32% yield).

¹H NMR (CD$_2$Cl$_2$): δ 8.69 (dd, J_{H-H} = 0.72 Hz, J_{H-H} = 5.79 Hz, 4H, CH$_{ar}$), δ 7.88 (d, J_{H-H} = 7.98 Hz, 4H, CH$_{ar}$), δ 7.61 (td, J_{H-H} = 1.5 Hz, J_{H-H} = 8.16, 4H, CH$_{ar}$), δ 7.55 (dd, J_{H-H} = 0.87 Hz, J_{H-H} = 7.77 Hz, 4H, CH$_{ar}$), δ 6.73 (dt, J_{H-H} = 1.14 Hz, J_{H-H} = 7.77 Hz, 4H, CH$_{ar}$), δ 6.64 (dt, J_{H-H} = 1.32 Hz, J_{H-H} = 5.94 Hz, 4H, CH$_{ar}$), δ 6.52 (dt, J_{H-H} = 1.29 Hz, J_{H-H} = 7.62 Hz, 4H, CH$_{ar}$), δ 5.93 (dd, J_{H-H} = 0.69 Hz, J_{H-H} = 7.68 Hz, 4H, CH$_{ar}$), δ -1.46 (s, 2H, OH).
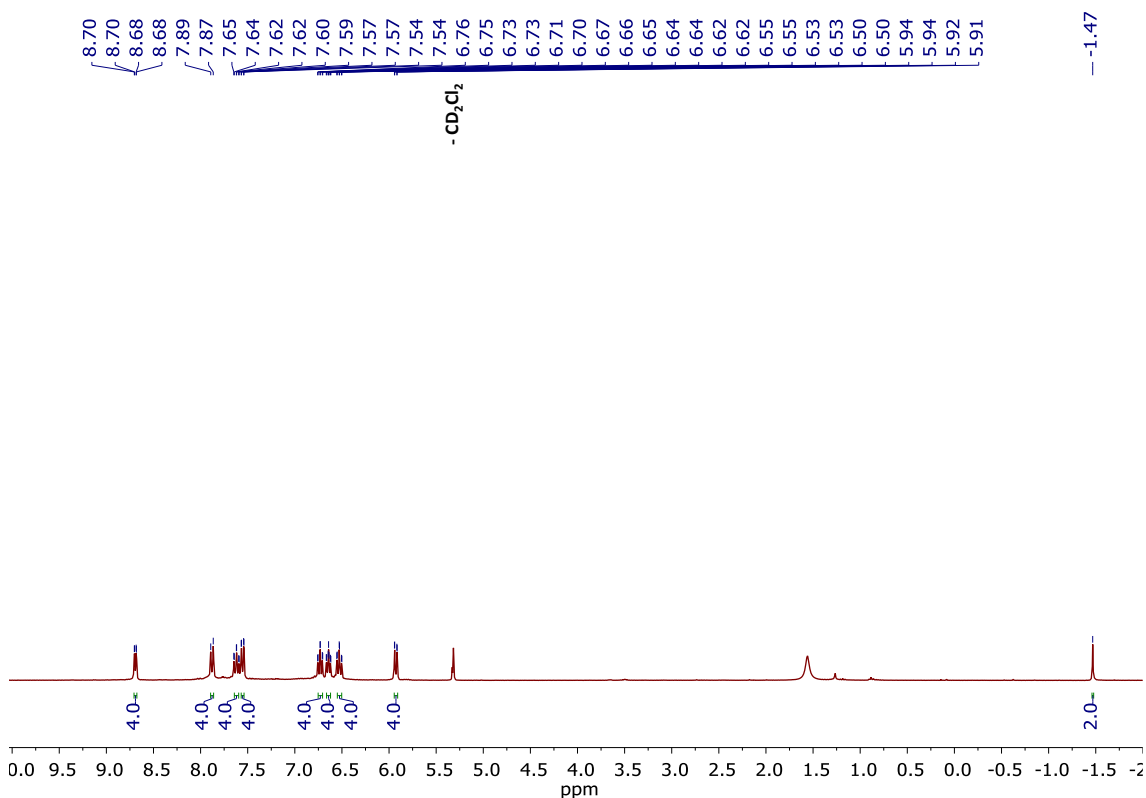
Figure S57. ¹H NMR of [Ir(ppy)$_2$OH]$_2$ (**C6**). (CD$_2$Cl$_2$, 300 MHz).

2.2.6 Complex [Ir(ppy)$_2$(2-pyridyl-4-bromo-5-methylthiophene)] (C7'):
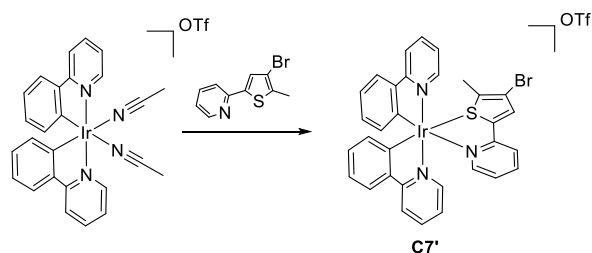
Under N_2, [Ir(ppy)$_2$(CH$_3$CN)$_2$]OTf (0.07 mmol, 0.05 g) was dissolved in 10 mL of degassed acetone. To the yellow solution, 2-pyridyl-4-bromo-5-methylthiophene (0.1 mmol, 0.03 g) was added. The yellow solution was stirred for 72 hours at r.t. The volatiles were removed and the resultant solid was washed with Et$_2$O. The product was obtained as a beige solid. (0.025 g, 40% yield).

^{1}H NMR (Acetone-d$_6$): δ 8.89 (dd, J$_{H-H}$ = 0.6 Hz, J$_{H-H}$ = 5.85 Hz, 1H, CH$_{ar}$), δ 8.39 (d, J$_{H-H}$ = 7.98 Hz, 1H, CH$_{ar}$), δ 8.33-8.30 (m, 1H, CH$_{ar}$), δ 8.27 (dd, J$_{H-H}$ = 1.47 Hz, J$_{H-H}$ = 7.38 Hz, 1H, CH$_{ar}$), δ 8.23-8.13 (m, 3H, CH$_{ar}$), δ 8.05 (td, J$_{H-H}$ = 1.50 Hz, J$_{H-H}$ = 7.53 Hz, 1H, CH$_{ar}$), δ 7.98 (dd, J$_{H-H}$ = 1.23 Hz, J$_{H-H}$ = 7.83 Hz, 1H, CH$_{ar}$), δ 7.85 (dd, J$_{H-H}$ = 1.14 Hz, J$_{H-H}$ = 7.83 Hz, 1H, CH$_{ar}$), δ 7.73 (dt, J$_{H-H}$ = 0.9 Hz, J$_{H-H}$ = 5.55 Hz, 1H, CH$_{ar}$), δ 7.69 (d, J$_{H-H}$ = 0.66 Hz, J$_{H-H}$ = 5.82 Hz, 1H, CH$_{ar}$), δ 7.62 (s, 1H, CH$_{ar}$), δ 7.49-7.43 (m, 2H, CH$_{ar}$), δ 7.26 (dd, J$_{H-H}$ = 1.41 Hz, J$_{H-H}$ = 5.85 Hz, 1H, CH$_{ar}$), δ 7.09 (dd, J$_{H-H}$ = 1.05 Hz, J$_{H-H}$ = 7.71 Hz, 1H, CH$_{ar}$), δ 7.00 (dd, J$_{H-H}$ = 1.2 Hz, J$_{H-H}$ = 7.44 Hz, 1H, CH$_{ar}$), δ 6.92-6.85 (m, 2H, CH$_{ar}$), δ 6.40 (dd, J$_{H-H}$ = 0.78 Hz, J$_{H-H}$ = 7.53 Hz, 1H, CH$_{ar}$), δ 6.20 (dd, J$_{H-H}$ = 0.75 Hz, J$_{H-H}$ = 7.74 Hz, 1H, CH$_{ar}$), δ 1.78 (s, 3H, CH$_3$).

^{13}C NMR (Acetone-d$_6$): δ 168.18 (C$_{quat}$), δ 167.26 (C$_{quat}$), δ 151.77 (C$_{quat}$), δ 151.74 (CH), δ 151.26 (CH), δ 150.13 (CH), δ 147.88 (C$_{quat}$), δ 145.65 (C$_{quat}$), δ 144.96 (C$_{quat}$), δ 143.83 (C$_{quat}$), δ 141.04 (CH), δ 140.43 (CH), δ 140.27 (CH), δ 140.24 (C$_{quat}$), δ 138.02 (C$_{quat}$), δ 135.81 (CH), δ 133.94 (CH), δ 131.60 (CH), δ 131.40 (CH), δ 130.68 (CH), δ 127.13 (CH), δ 126.21 (CH), δ 125.56 (CH), δ 125.44 (CH), δ 125.25 (CH), δ 124.80 (CH), δ 124.45 (CH), δ 124.24 (CH), δ 123.95 (C$_{quat}$), δ 121.49 (CH), δ 120.22 (CH), δ 119.70 (C$_{quat}$), δ 116.70 (C$_{quat}$), δ 14.74 (CH$_3$).

9.00 9.00 8.98 8.98 8.41 8.39 8.30 8.28 8.28 8.26 8.25 8.07 8.05 8.05 8.00 7.99 7.97 7.97 7.87 7.87 7.84 7.84 7.74 7.74 7.73 7.72 7.70 7.70 7.68 7.68 7.62 7.26 7.10 7.10 7.01 7.00 6.98 6.92 6.42 6.41 6.39 6.39 6.22 6.21 6.19 6.19 1.78

- Acetone-d$_6$

Figure S58. ^{1}H NMR of [Ir(ppy)2(2-pyridyl-4-bromo-5-methylthiophene)]. (Acetone-d$_3$, 300 MHz).

168.18 167.26 151.77 151.74 151.26 150.13 147.88 145.65 144.96 143.83 141.04 140.43 140.27 140.24 138.02 135.81 133.94 131.60 131.40 130.68 127.13 126.21 125.56 125.44 125.25 124.80 124.45 124.24 123.95 121.49 120.22 119.70 116.70

— 14.74

Figure S59. ^{13}C NMR of [Ir(ppy)2(2-pyridyl-4-bromo-5-methylthiophene)]. (Acetone-d$_3$, 300 MHz).

267

Figure S60. COSY NMR of [Ir(ppy)2(2-pyridyl-4-bromo-5-methylthiophene)]. (Acetone-d₃, 300 MHz).
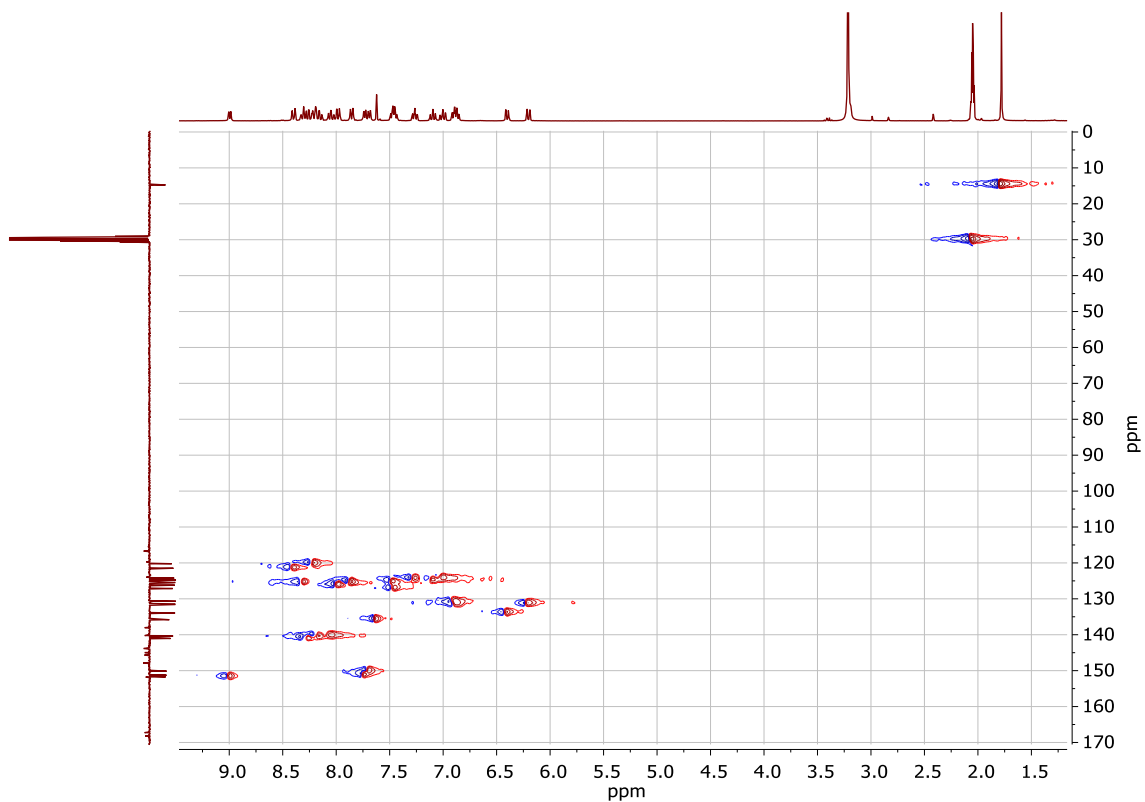
Figure S61. HSQC NMR of of [Ir(ppy)2(2-pyridyl-4-bromo-5-methylthiophene)]. (Acetone-d₃, 300 MHz).

2.2.7/2.2.8 Complexes Λ-[Ir(ppy)₂(L-proline)] (Λ-[Ir(ppy)₂(L-Serine)]PF₆) and Δ-[Ir(ppy)₂(L-proline)] (ΔL-proline-C9):

ΔL*proline*-C9 (23% yield)   ΛL*proline*-C9 (35% yield)
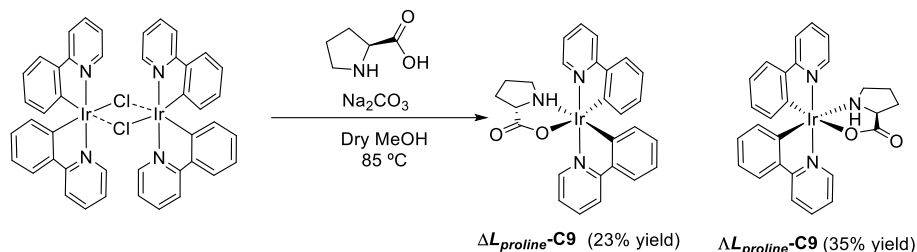
Compounds **Δ-[Ir(ppy)₂(L-Proline)]** and **Λ-[Ir(ppy)₂(L-Proline)]PF₆** was synthesized following a reported procedure[32]. Under [Ir(ppy)2Cl]2 (0.28 mmol, 0.3 g), L-Proline (1.1 mmol, 0.126 g) and K₂CO₃ (0.83 mmol, 0.114 g) were dissolved in 12 mL of dry MeOH. The yellow suspension was refluxed for 24 hours at 75 °C .The yellow suspension was centrifuged obtaining a yellow solid and a yellow solution. The yellow solid was washed with MeOH (3x10 mL) and dried under vacuum. The product **Λ-[Ir(ppy)₂(L-Proline)]PF₆** was obtained as a yellow solid. (0.118 g, 35% yield). The yellow solution was dried under vacuum and washed with CH2Cl2 (3x10 mL). The resultant suspension was filtered and the volatiles were removed, obtaining **Δ-[Ir(ppy)₂(L-Proline)]** as a yellow solid. (0.078 g, 23% yield).

¹H NMR (DMSO): δ 9.05 (d, J_{H-H} = 5.73 Hz, 1H, CH$_{ar}$), δ 8.68 (d, J_{H-H} = 6.57 Hz, 1H, CH$_{ar}$), δ 8.19 (t, J_{H-H} = 8.01 Hz, 2H, CH$_{ar}$), δ 7.97 (t, J_{H-H} = 7.41 Hz, 2H, CH$_{ar}$), δ 7.76 − 7.70 (m, 2H, CH$_{ar}$), δ 7.51 − 7.41 (m, 2H, CH$_{ar}$), δ 6.78 (t, J_{H-H} = 7.32 Hz, 2H, CH$_{ar}$), δ 6.67 − 6.58 (m, 2H, CH$_{ar}$), δ 6.31 (dd, J_{H-H} = 0.81 Hz, J_{H-H} = 7.53 Hz, 1H, CH$_{ar}$), δ 5.90 (dd, J_{H-H} = 0.93 Hz, J_{H-H} = 7.62 Hz, 1H, CH$_{ar}$), δ 3.67 − 3.59 (m, 1H, NH), δ 2.14 − 2.04 (m, 1H, CH), δ 2.00 − 1.88 (m, 2H, CH), δ 1.77 − 1.62 (m, 1H, CH), δ 1.56 − 1.41 (m, 1H, CH), δ 1.29 − 1.19 (m, 1H, CH).
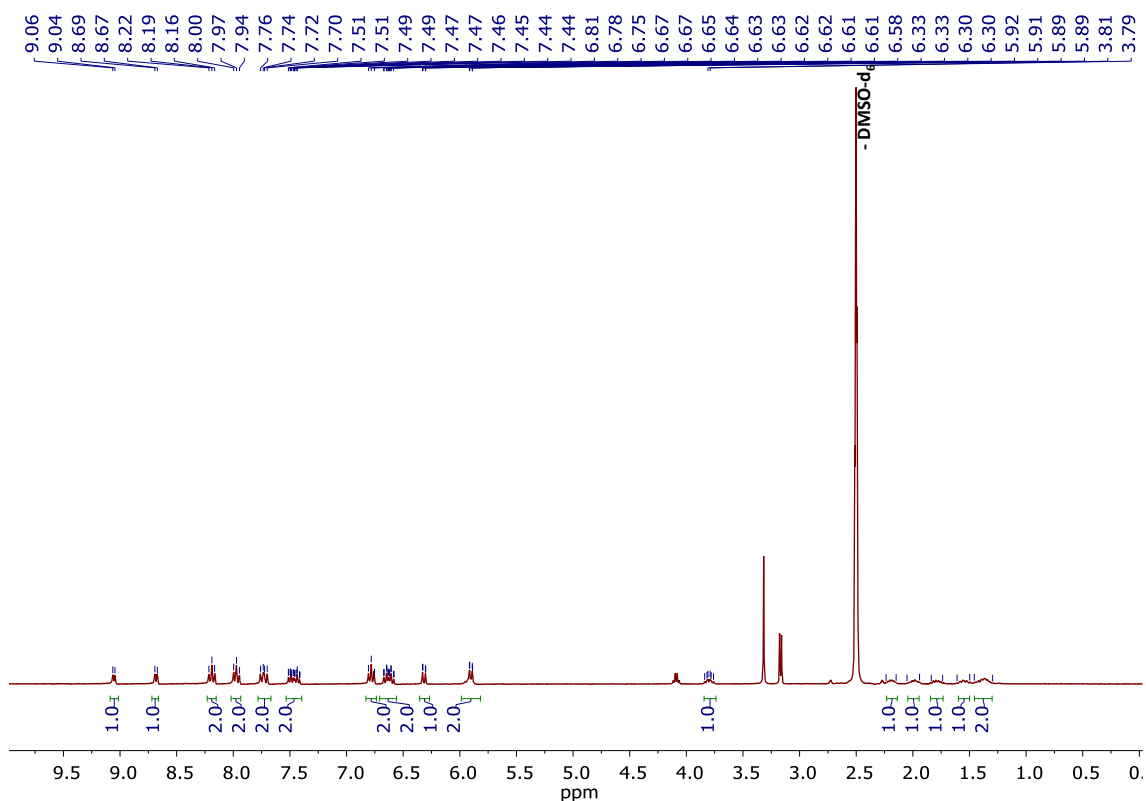
Figure S62. ^{1}H NMR of Λ-[Ir(ppy)$_2$(L-Proline)]PF$_6$ (**ΛL-proline-C9**). (DMSO, 300 MHz).

^{1}H NMR (DMSO): δ 8.69 (d, J_{H-H} = 5.94 Hz, 1H, CH$_{ar}$), δ 8.57 (d, J_{H-H} = 6.54 Hz, 1H, CH$_{ar}$), δ 8.18 (t, J_{H-H} = 8.58 Hz, 2H, CH$_{ar}$), δ 8.02– 7.95 (m, 2H, CH$_{ar}$), δ 7.72 – 7.67 (m, 2H, CH$_{ar}$), δ 7.50 – 7.44 (m, 2H, CH$_{ar}$), δ 6.76 (t, J_{H-H} = 7.29 Hz, 2H, CH$_{ar}$), δ 6.64 – 6.56 (m, 2H, CH$_{ar}$), δ 6.24 (dd, J_{H-H} = 0.87 Hz, J_{H-H} = 7.56 Hz, 1H, CH$_{ar}$), δ 5.87 (dd, J_{H-H} = 0.93 Hz, J_{H-H} = 7.68 Hz, 1H, CH$_{ar}$), δ 3.67 – 3.59 (m, 1H, NH), δ 2.14 – 2.04 (m, 1H, CH), δ 2.00 – 1.88 (m, 2H, CH), δ 1.77 – 1.62 (m, 1H, CH), δ 1.56 – 1.41 (m, 1H, CH), δ 1.29 – 1.19 (m, 1H, CH).

Figure S63. ¹H NMR of Δ-[Ir(ppy)₂(L-Proline)]PF₆ (**ΔL-proline-C9**). (DMSO, 300 MHz).

2.2.9 Complex Λ-[Ir(ppy)₂(L-serine)] (ΛL-serine-C10):

Compound **Λ-[Ir(ppy)₂(L-Serine)]PF₆** was synthesized following a reported procedure[33]. Under N₂, [Ir(ppy)₂Cl]₂ (0.093 mmol, 0.1 g), D-serine (0.37 mmol, 0.04 g), and NaOMe (0.37 mmol, 0.02 g) were dissolved in 40 mL of dry MeOH. The yellow solution was stirred for overnight at 40 °C .The yellow suspension was centrifuged and the yellow solid was washed with MeOH (3x10 mL). After removing volatiles, the resultant solid was dissolved in CH₂Cl₂ and the free L-serine traces were filtered. The product was obtained as a yellow solid. (0.08 g, 71% yield).

¹H NMR (MeOD): δ 8.91 (d, J_{H-H} = 5.73 Hz, 1H, CH$_{ar}$), δ 8.72 (dd, J_{H-H} = 0.72 Hz, J_{H-H} = 5.79 Hz, 1H, CH$_{ar}$), δ 8.05 (t, J_{H-H} = 8.61 Hz, 2H, CH$_{ar}$), δ 7.93-7.85 (m, 2H, CH$_{ar}$), δ 7.63 (t, J_{H-H} = 8.82) Hz, 1H, CH$_{ar}$), δ 7.34 – 7.29 (m, 2H, CH$_{ar}$), δ 6.79 (t, J_{H-H} = 7.35 Hz, 1H, CH$_{ar}$), δ 6.65-6.59 (m, 2H, CH$_{ar}$), δ 6.30 (dd, J_{H-H} = 0.75 Hz, J_{H-H} = 7.65 Hz, 1H, CH$_{ar}$), δ 6.10 (dd, J_{H-H} = 0.75 Hz, J_{H-H} = 7.59 Hz, 1H, CH$_{ar}$).

271

Figure S64. ^{1}H NMR of Λ-[Ir(ppy)$_2$(L-serine)] (**ΛL-serine-C10**):. (MeOD, 300 MHz).

2.2.10 Complex Δ-[Ir(ppy)$_2$(D-serine)] (ΔD-serine-C10):
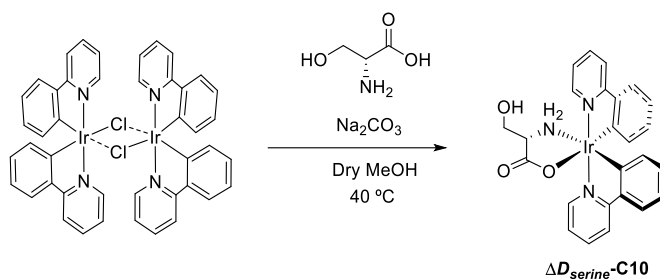
Compound **Δ-[Ir(ppy)$_2$(D-Serine)]PF$_6$** was synthesized following a reported procedure[33]. Under N$_2$, [Ir(ppy)$_2$Cl]$_2$ (0.279 mmol, 0.3 g), D-serine (1.11 mmol, 0.117 g), and NaOMe (1.11 mmol, 0.06 g) were dissolved in 40 mL of dry MeOH. The yellow solution was stirred for overnight at 40 °C .The yellow suspension was centrifuged and the yellow solid was washed with MeOH (3x10 mL). After removing volatiles, the resultant solid was dissolved in CH$_2$Cl$_2$ and the free D-serine traces were filtered. The product was obtained as a yellow solid. (0.145 g, 43% yield).

^{1}H NMR (MeOD): δ 8.91 (d, J_{H-H} = 5.73 Hz, 1H, CH$_{ar}$), δ 8.72 (dd, J_{H-H} = 0.72 Hz, J_{H-H} = 5.79 Hz, 1H, CH$_{ar}$), δ 8.05 (t, J_{H-H} = 8.61 Hz, 2H, CH$_{ar}$), δ 7.93-7.85 (m, 2H, CH$_{ar}$), δ 7.63 (t, J_{H-H} = 8.82) Hz, 1H, CH$_{ar}$), δ 7.34 − 7.29 (m, 2H, CH$_{ar}$), δ 6.79 (t, J_{H-H} = 7.35 Hz, 1H, CH$_{ar}$), δ 6.65-6.59 (m, 2H, CH$_{ar}$), δ 6.30 (dd, J_{H-H} = 0.75 Hz, J_{H-H} = 7.65 Hz, 1H, CH$_{ar}$), δ 6.10 (dd, J_{H-H} = 0.75 Hz, J_{H-H} = 7.59 Hz, 1H, CH$_{ar}$).

Figure S65. ^{1}H NMR of Δ-[Ir(ppy)$_2$(D-serine)] (**ΔD-serine-C10**). (MeOD, 300 MHz).

2.2.11 Complex Λ-[Ir(ppy)$_2$(CH$_3$CN)$_2$] (Λ-C5):

Compound **Λ-[Ir(ppy)$_2$(CH$_3$CN)$_2$]PF$_6$** was synthesized following a reported procedure[34]. Under N$_2$, Λ-[Ir(ppy)$_2$(L-Proline)] (0.17 mmol, 0.1 g) were dissolved in 10 mL of CH$_3$CN. To the yellow solution, TFA (1.02 mmol, 0.08 mL) were added. The pale yellow solution was stirred overnight. NH$_4$PF$_6$ (3.4 mmol, 0.55 g) were added and the resultant mixture was stirred for 1 hour. The residue was purified by silica gel column chromatography (CH$_2$Cl$_2$/CH$_3$CN (95:5), Rf = 0.32). The product was obtained as a yellow solid. (0.075 g, 61% yield).

^{1}H NMR (CD$_2$Cl$_2$): δ 9.02 (d, J_{H-H} = 5.76 Hz, 2H, CH$_{ar}$), δ 8.00 – 7.96 (m, 4H, CH$_{ar}$), δ 7.59 (d, J_{H-H} = 7.71 Hz, 2H, CH$_{ar}$), δ 7.45 – 7.40 (m, 2H, CH$_{ar}$), δ 6.92 (t, J_{H-H} = 7.56 Hz, 2H, CH$_{ar}$), δ 6.76 (dt, , J_{H-H} = 1.14 Hz, J_{H-H} = 7.53 Hz, 2H, CH$_{ar}$), δ 6.09 (d, J_{H-H} = 7.44 Hz, 2H, CH$_{ar}$), δ 2.31 (s, 6H, CH$_3$).

Figure S66. ^{1}H NMR of Λ-[Ir(ppy)$_2$(CH$_3$CN)$_2$]PF$_6$ (**Λ-C5**). (CD$_2$Cl$_2$, 300 MHz).

2.2.12 Complex Δ-[Ir(ppy)$_2$(CH$_3$CN)$_2$] (Δ-C5):
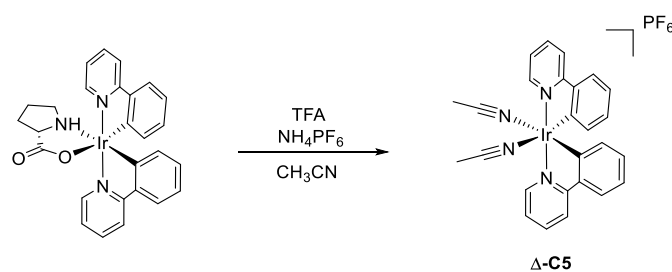
Compound **Δ-[Ir(ppy)$_2$(CH$_3$CN)$_2$]PF$_6$** was synthesized following a reported procedure[34]. Under N$_2$, Δ-[Ir(ppy)$_2$(L-Proline)] (0.33 mmol, 0.2 g) were dissolved in 20 mL of CH$_3$CN. To the yellow solution, TFA (1.96 mmol, 0.15 mL) were added. The pale yellow solution was stirred overnight. NH$_4$PF$_6$ (6.5 mmol, 1.06 g) were added and the resultant mixture was stirred for 1 hour. The residue was purified by silica gel column chromatography (CH$_2$Cl$_2$/CH$_3$CN (95:5), Rf = 0.35). The product was obtained as a yellow solid. (72 g, 30% yield).

^{1}H NMR (CD$_2$Cl$_2$): δ 9.01 (d, J$_{H-H}$ = 5.79 Hz, 2H, CH$_{ar}$), δ 8.00 − 7.94 (m, 4H, CH$_{ar}$), δ 7.59 (dd, J$_{H-H}$ = 1.14 Hz, J$_{H-H}$ = 7.83 Hz, 2H, CH$_{ar}$), δ 7.44 − 7.39 (m, 2H, CH$_{ar}$), δ 6.93 (dt, J$_{H-H}$ = 1.2 Hz, , J$_{H-H}$ = 7.35 Hz. 2H, CH$_{ar}$), δ 6.76 (dt, , J$_{H-H}$ = 1.38 Hz, J$_{H-H}$ = 7.53 Hz, 2H, CH$_{ar}$), δ 6.09 (dd, J$_{H-H}$ = 1.2 Hz, , J$_{H-H}$ = 7.65 Hz, 2H, CH$_{ar}$), δ 2.32 (s, 6H, CH$_3$).
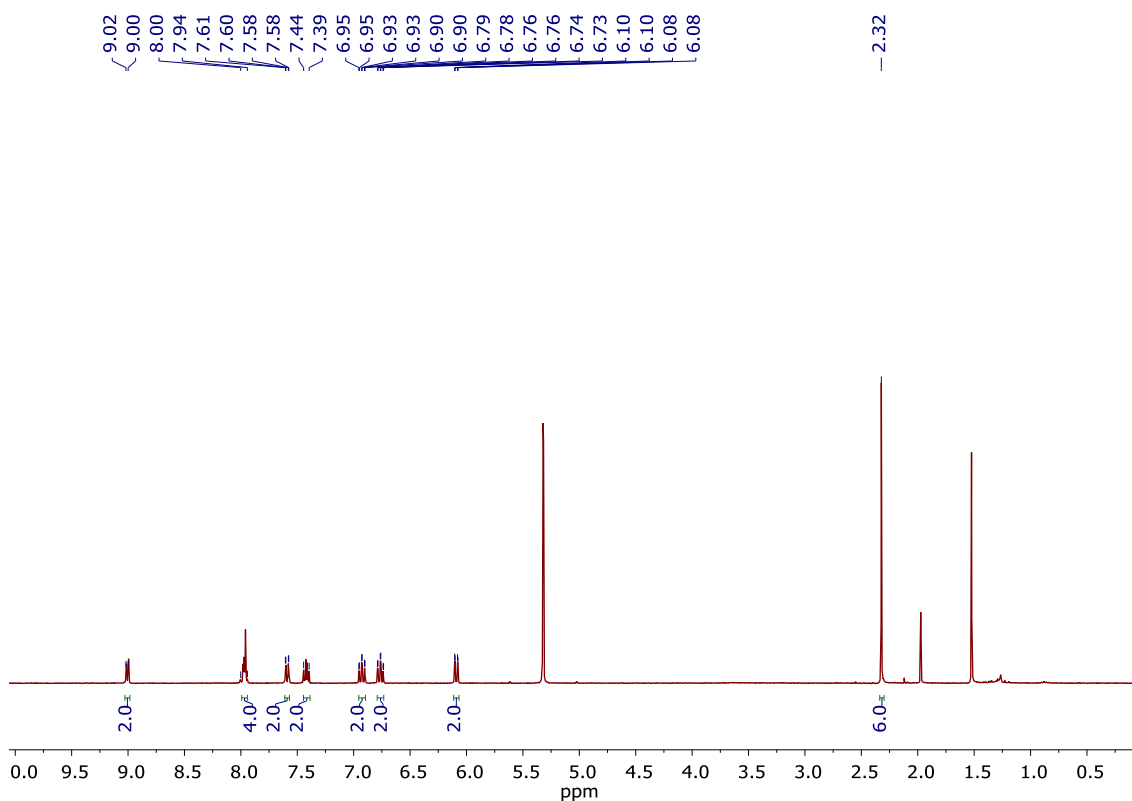
Figure S67. ^{1}H NMR of Δ-[Ir(ppy)$_2$(CH$_3$CN)$_2$]PF$_6$ (**Δ-C5**). (CD$_2$Cl$_2$, 300 MHz).

2.2.13 Complex Λ-[Ir(ppy)$_2$(CH$_3$CN)$_2$] (Λ-C5):

Λ-**C5**
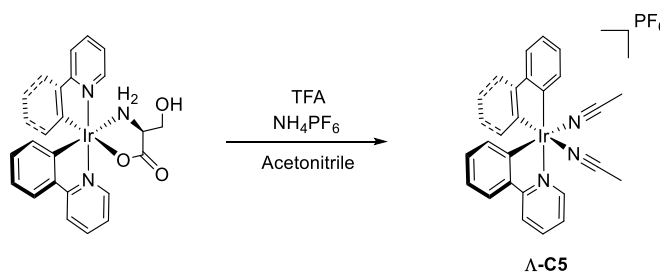
Compound **Λ-[Ir(ppy)$_2$(CH$_3$CN)$_2$]PF$_6$** was synthesized following a reported procedure[3432]. Under N$_2$, Λ-[Ir(ppy)$_2$(L-Serine)] (0.16 mmol, 0.096 g) were dissolved in 15 mL of CH$_3$CN. To the yellow solution, TFA (0.96 mmol, 0.07 mL) were added. The pale yellow solution was stirred overnight. NH$_4$PF$_6$ (3.2 mmol, 0.52 g) were added and the resultant mixture was stirred for 1 hour. The residue was purified by silica gel column chromatography (CH$_2$Cl$_2$/CH$_3$CN (95:5), Rf = 0.35). The product was obtained as a yellow solid. (0.04 g, 34% yield).

^{1}H NMR (CD$_2$Cl$_2$): δ 8.99 (d, J_{H-H} = 6.87 Hz, 2H, CH$_{ar}$), δ 7.97 – 7.95 (m, 4H, CH$_{ar}$), δ 7.58 (dd, J_{H-H} = 0.93 Hz, J_{H-H} = 7.8 Hz, 2H, CH$_{ar}$), δ 7.44 – 7.39 (m, 2H, CH$_{ar}$), δ 6.92 (dt, J_{H-H} = 1.17 Hz, , J_{H-H} = 7.44 Hz, 2H, CH$_{ar}$), δ 6.76 (dt, , J_{H-H} = 1.35 Hz, J_{H-H} = 7.53 Hz, 2H, CH$_{ar}$), δ 6.09 (dd, J_{H-H} = 7.59 Hz, 2H, CH$_{ar}$), δ 2.28 (s, 6H, CH$_3$).
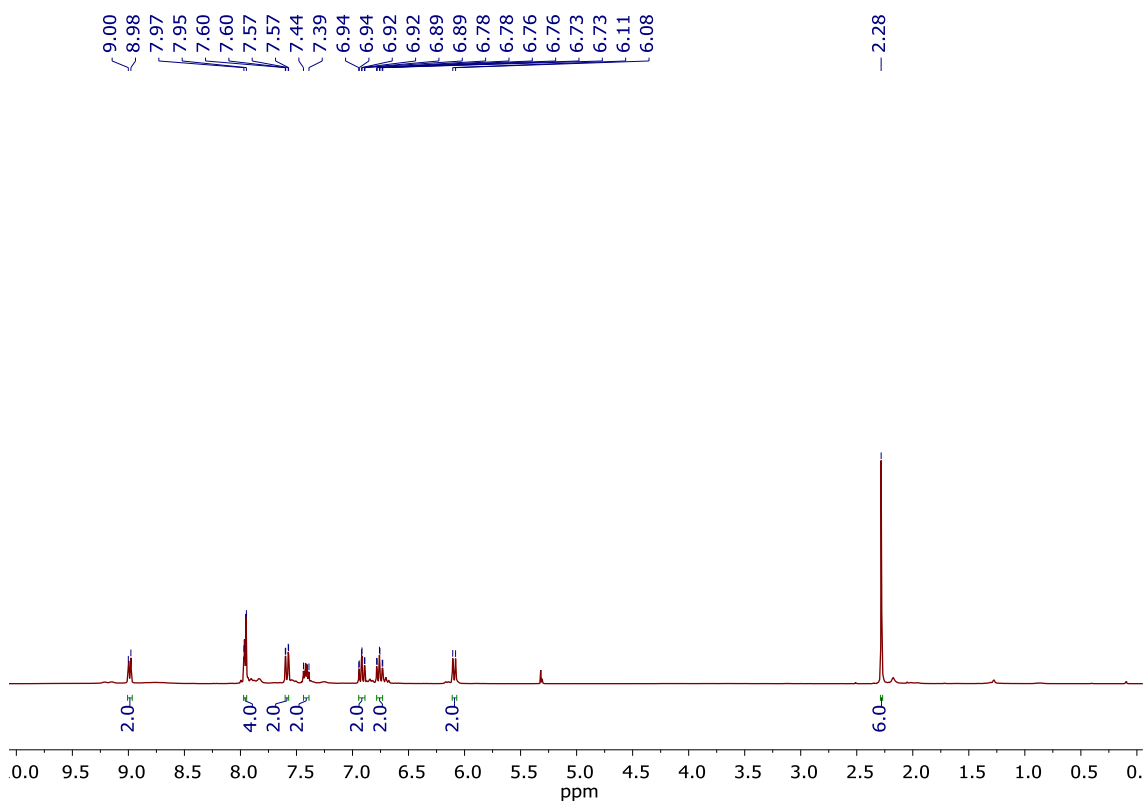
Figure S68. ^{1}H NMR of Λ-[Ir(ppy)$_2$(CH$_3$CN)$_2$]PF$_6$ (**Λ-C5**). (CD$_2$Cl$_2$, 300 MHz).

2.2.14 Complex Δ-[Ir(ppy)$_2$(CH$_3$CN)$_2$] (Δ-C5):

Δ-**C5**
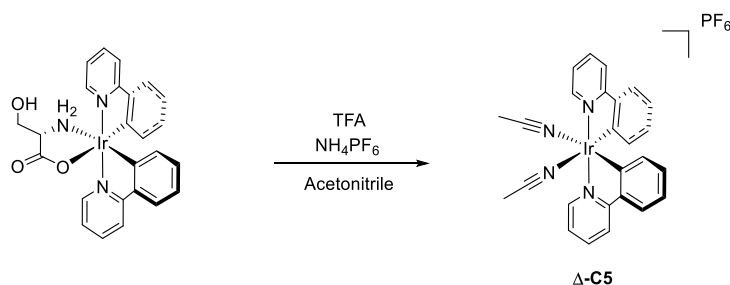
Compound **Δ-[Ir(ppy)$_2$(CH$_3$CN)$_2$]PF$_6$** was synthesized following a reported procedure[34]34. Under N$_2$, Δ-[Ir(ppy)$_2$(D-Serine)] (0.26 mmol, 0.16 g) were dissolved in 15 mL of CH$_3$CN. To the yellow solution, TFA (1.58 mmol, 0.12 mL) were added. The pale yellow solution was stirred overnight. NH$_4$PF$_6$ (5.26 mmol, 0.86 g) were added and the resultant mixture was stirred for 1 hour. The residue was purified by silica gel column chromatography (CH$_2$Cl$_2$/CH$_3$CN (95:5), Rf = 0.35). The product was obtained as a yellow solid. (0.08 g, 47% yield).

^{1}H NMR (CD$_2$Cl$_2$): δ 9.01 (d, J_{H-H} = 5.79 Hz, 2H, CH$_{ar}$), δ 8.00 − 7.94 (m, 4H, CH$_{ar}$), δ 7.59 (dd, J_{H-H} = 0.84 Hz, J_{H-H} = 7.77 Hz, 2H, CH$_{ar}$), δ 7.45 − 7.40 (m, 2H, CH$_{ar}$), δ 6.92 (dt, J_{H-H} = 1.08 Hz, , J_{H-H} = 7.62 Hz, 2H, CH$_{ar}$), δ 6.76 (dt, , J_{H-H} = 1.26 Hz, J_{H-H} = 7.53 Hz, 2H, CH$_{ar}$), δ 6.09 (dd, J_{H-H} = 0.57 Hz, J_{H-H} = 7.56 Hz, 2H, CH$_{ar}$), δ 2.31 (s, 6H, CH$_3$).
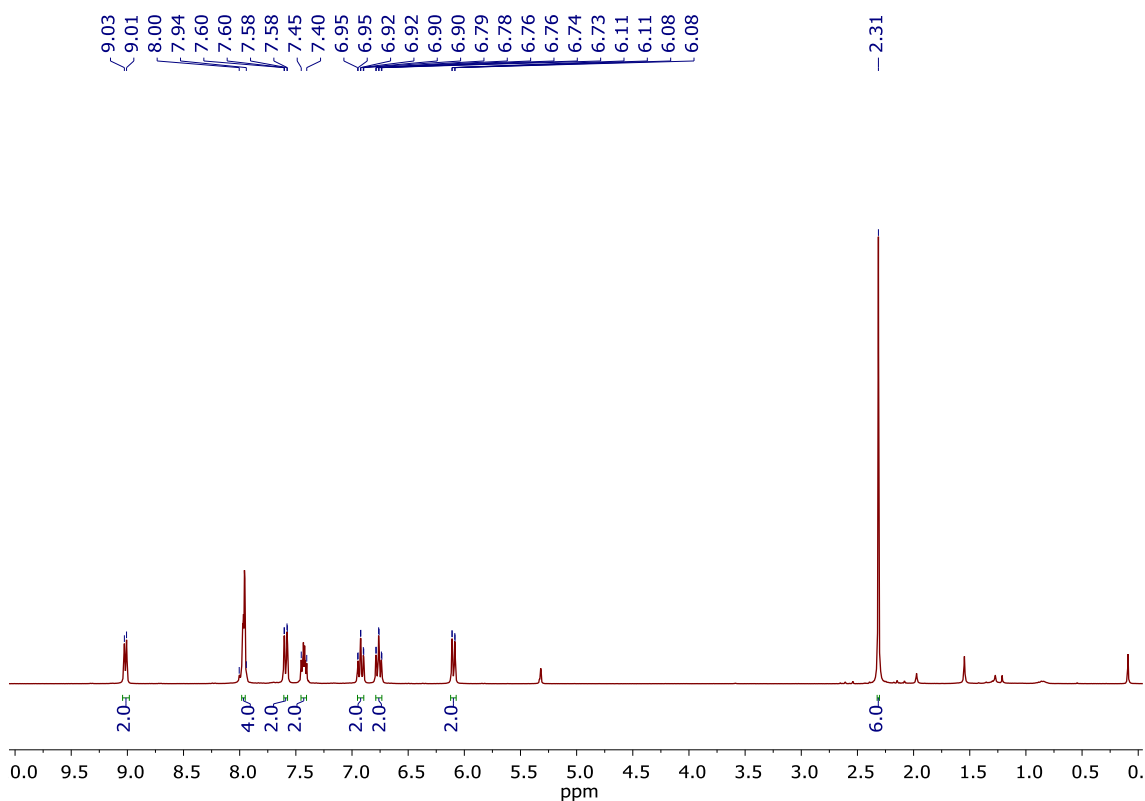
Figure S69. ^{1}H NMR of Δ-[Ir(ppy)$_2$(CH$_3$CN)$_2$]PF$_6$ (**Δ-C5**) (CD$_2$Cl$_2$, 300 MHz).

2.2.15 Complex *rac*-[Ir(ppy)$_2$(L2-A)] (*rac*-Ir-L2-A):

Ir-L2-A
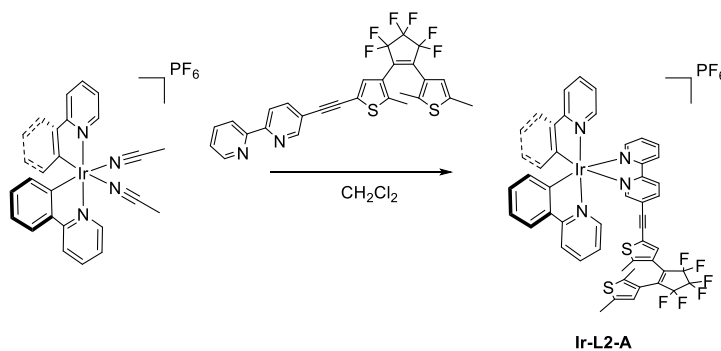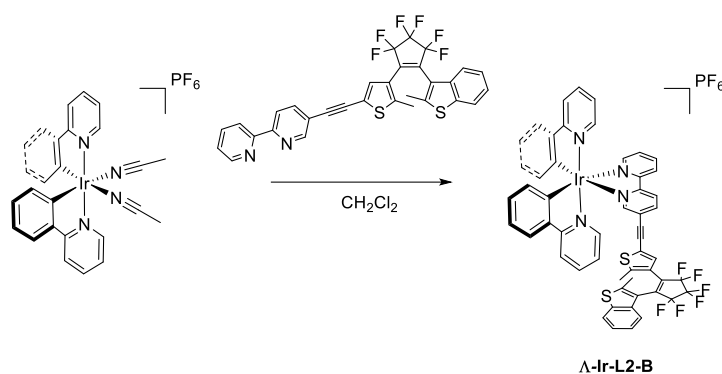
Under N$_2$, [Ir(ppy)$_2$(CH$_3$CN)$_2$]PF$_6$ (0.041 mmol, 0.03 g) and **L2-A** (0.045 mmol, 0.025 g) were dissolved in 5 mL of dry CH$_2$Cl$_2$. The dark orange solution was stirred overnight at r.t. The dark yellow solution was purified by alumine column chromatography (CH$_2$Cl$_2$/MeOH (99:1), Rf = 0.25). The product was obtained as a blue solid. (0.06 g, 69% yield).

Exact Mass: FD [C$_{50}$H$_{34}$F$_6$IrN$_4$S$_2$]: calculated: m/z = 1061.180, found: m/z = 1061.182.

^{1}H NMR (CDCl$_3$): δ 8.65 (t, J_{H-H} = 8.37 Hz, 2H, CH$_{ar}$), δ 8.17 − 8.12 (m, 2H, CH$_{ar}$), δ 7.96 − 7.91 (m, 4H, CH$_{ar}$), δ 7.78 (t, J_{H-H} =7.44 Hz, 2H, CH$_{ar}$), δ 7.69 (t, J_{H-H} = 8.25 Hz, 2H, CH$_{ar}$), δ 7.55 (d, J_{H-H} = 5.4 Hz, 1H, CH$_{ar}$), δ 7.49 (d, J_{H-H} = 5.4 Hz, 1H, CH$_{ar}$), δ 7.40 (t, J_{H-H} = 5.37 Hz, 1H, CH$_{ar}$), δ 7.28 (s, 1H, CH$_{ar}$), δ 7.07 − 6.99 (m, 5H, CH$_{ar}$), δ 6.95 − 6.88 (m, 2H, CH$_{ar}$), δ 6.68 (s, 1H, CH$_{ar}$), δ 6.31 − 6.25 (m, 2H, CH$_{ar}$), δ 2.41 (s, 3H, CH$_3$), δ 1.89 (s, 3H, CH$_3$), δ 1.82 (s, 3H, CH$_3$).

¹³C NMR (CDCl₃): δ 167.73 (C$_{quat}$), δ 167.63 (C$_{quat}$), δ 155.11 (C$_{quat}$), δ 154.54 (C$_{quat}$), δ 151.58 (CH), δ 150.30 (CH), δ 149.63 (C$_{quat}$), δ 149.55 (C$_{quat}$), δ 148.62 (CH), δ 148.59 (CH), δ 145.55 (C$_{quat}$), δ 143.46 (C$_{quat}$), δ 143.46 (C$_{quat}$), δ 141.58 (CH), δ 139.94 (C$_{quat}$), δ 139.85 (CH), δ 138.27 (CH), δ 133.59 (CH), δ 131.74 (CH), δ 131.58 (CH), δ 130.88 (CH), δ 128.26 (CH), δ 125.71 (CH), δ 124.96 (CH), δ 124.82 (CH), δ 124.40 (CH), δ 124.33 (C$_{quat}$), δ 124.06 (C$_{quat}$), δ 123.51 (CH), δ 123.46 (CH), δ 122.80 (CH), δ 119.81 (CH), δ 119.73 (CH), δ 119.28 (C$_{quat}$), δ 15.13 (CH₃), δ 14.49 (CH₃), δ 14.37 (CH₃).

Figure S70. ¹H NMR of *rac*-[Ir(ppy)₂(L2-A)]PF₆ (***rac*-Ir-L2-A**). (CDCl₃, 300 MHz).
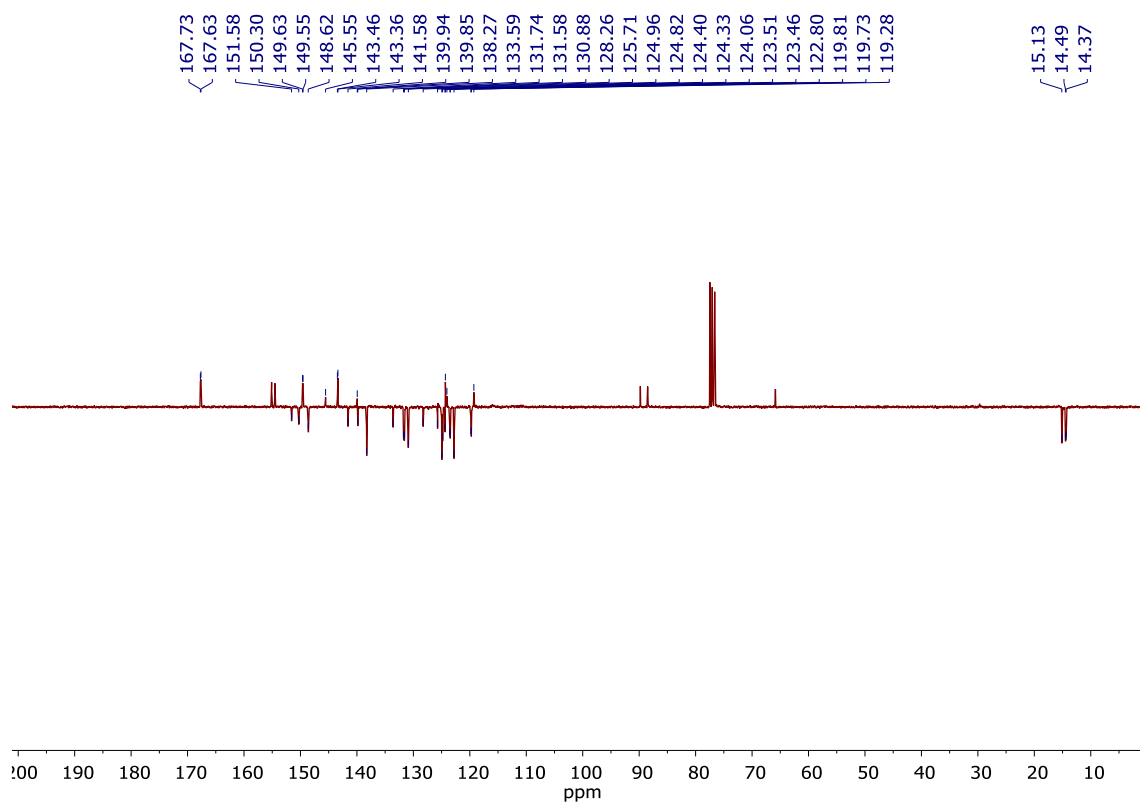
Figure S71. ^{13}C NMR of *rac*-[Ir(ppy)$_2$(L2-A)]PF$_6$ (***rac*-Ir-L2-A**). (CDCl$_3$, 300 MHz).
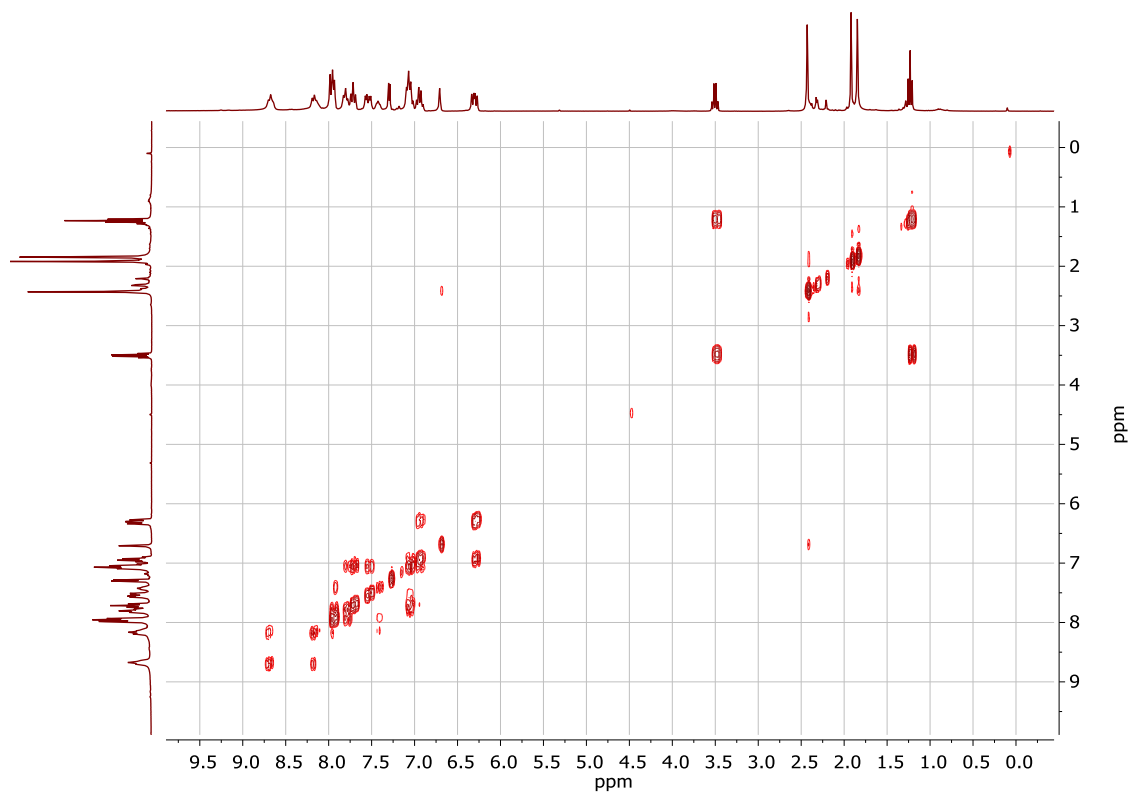
Figure S72. COSY NMR of *rac*-[Ir(ppy)$_2$(L2-A)]PF$_6$ (***rac*-Ir-L2-A**). (CDCl$_3$, 300 MHz).
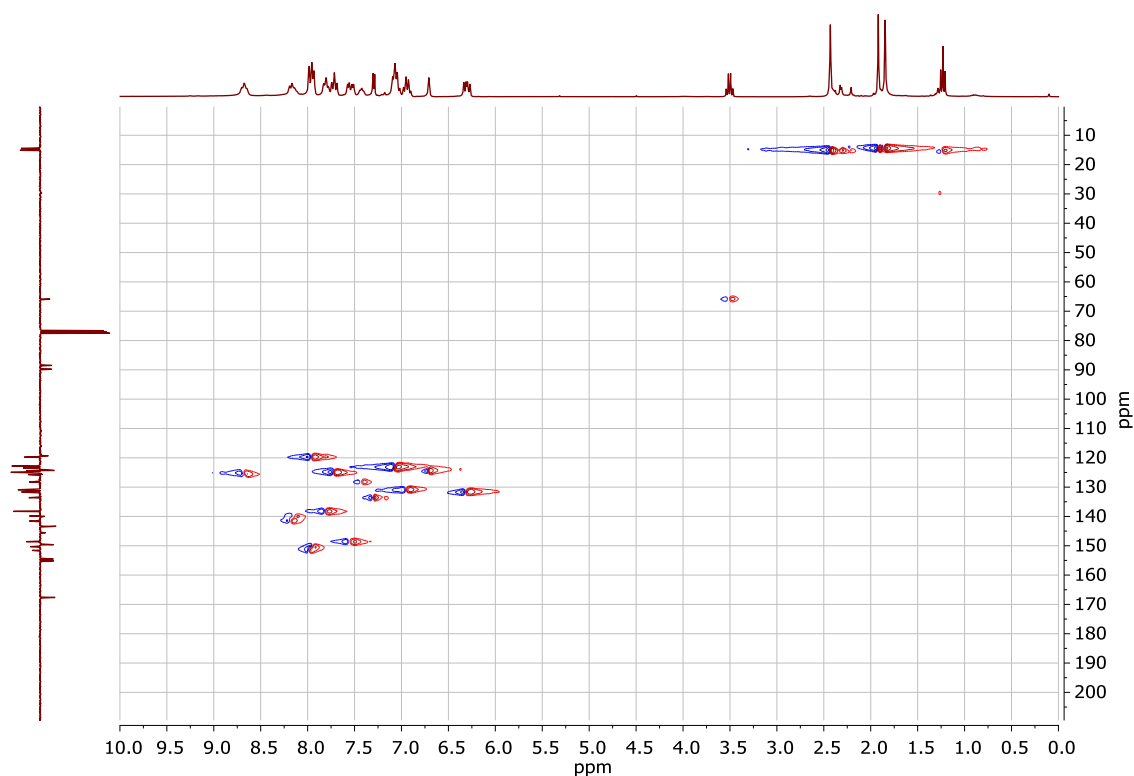
Figure S73. HSQC NMR of *rac*-[Ir(ppy)₂(L2-A)]PF₆ (***rac*-Ir-L2-A**). (CDCl₃, 300 MHz).

2.2.16 Complex Λ-[Ir(ppy)₂(L2-A)] (Λ-Ir-L2-A):
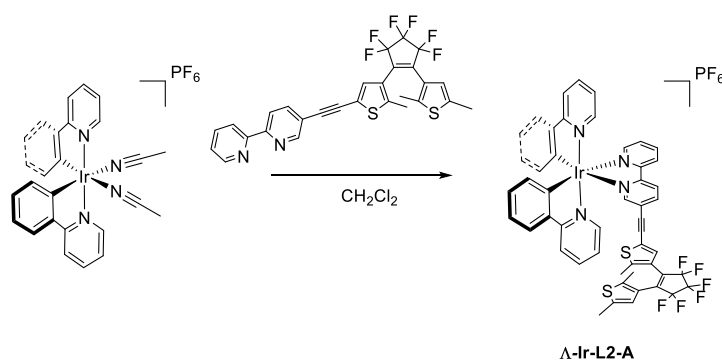
Λ-**Ir-L2-A**

Under N₂, Λ-[Ir(ppy)₂(CH₃CN)₂]PF₆ (0.041 mmol, 0.03 g) and **L2-A** (0.045 mmol, 0.025 g) were dissolved in 5 mL of dry CH₂Cl₂. The dark orange solution was stirred overnight at r.t. The blue solution was purified by alumine column chromatography (CH₂Cl₂/MeOH (99:1), Rf = 0.26). The product was obtained as a blue solid. (0.05 g, 61% yield).

¹H NMR (CDCl₃): δ 8.65 (t, J_{H-H} = 8.43 Hz, 2H, CH$_{ar}$), δ 8.17 – 8.09 (m, 2H, CH$_{ar}$), δ 7.96 – 7.91 (m, 4H, CH$_{ar}$), δ 7.78 (t, J_{H-H} =7.35 Hz, 2H, CH$_{ar}$), δ 7.6 (t, J_{H-H} = 8.46 Hz, 2H, CH$_{ar}$), δ 7.54 (d, J_{H-H} = 5.55 Hz, 1H, CH$_{ar}$), δ 7.49 (d, J_{H-H} = 5.55 Hz, 1H, CH$_{ar}$), δ 7.40 (t, J_{H-H} = 5.19 Hz, 1H, CH$_{ar}$), δ 7.27 (s, 1H, CH$_{ar}$), δ 7.07 – 7.00 (m, 5H, CH$_{ar}$), δ 6.95 – 6.88 (m, 2H, CH$_{ar}$), δ 6.68 (s, 1H, CH$_{ar}$), δ 6.30 – 6.25 (m, 2H, CH$_{ar}$), δ 2.40 (s, 3H, CH₃), δ 1.89 (s, 3H, CH₃), δ 1.82 (s, 3H, CH₃).
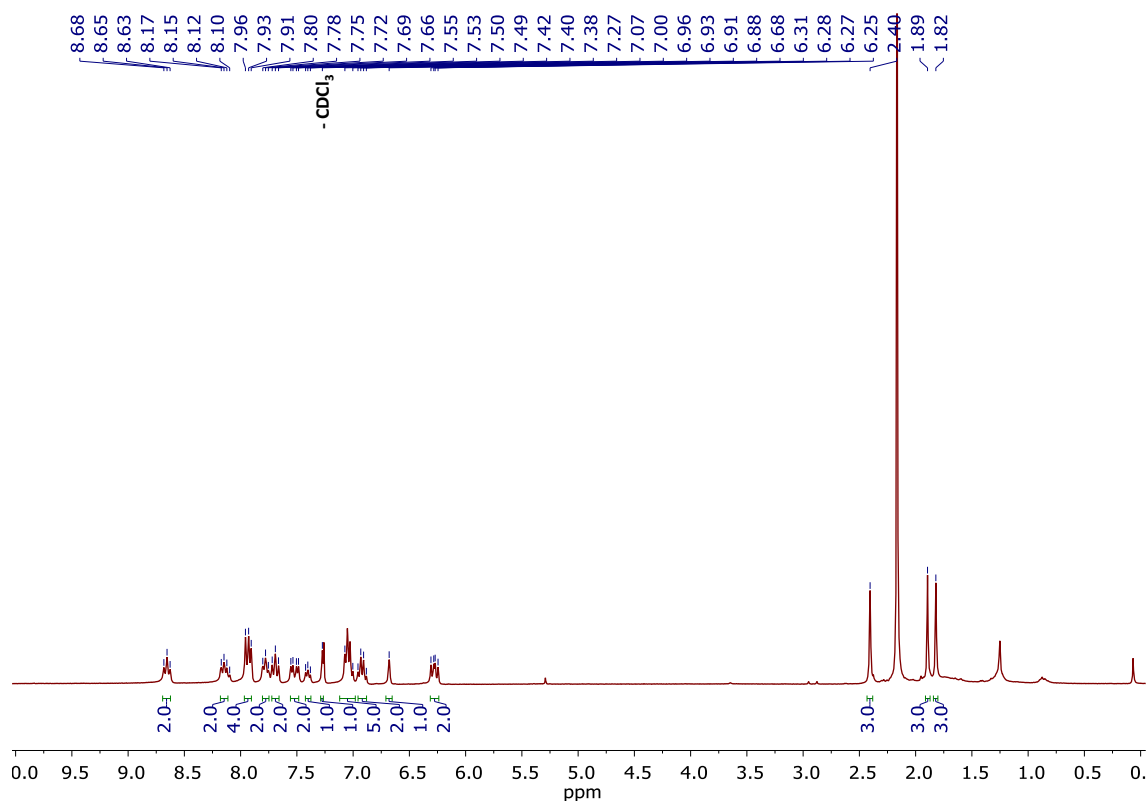
Figure S74. ^{1}H NMR of Λ-[Ir(ppy)$_2$(L2-A)]PF$_6$ (**Λ-Ir-L2-A**). (CDCl$_3$, 300 MHz).

2.2.17 Complex Δ-[Ir(ppy)$_2$(L2-A)] (Δ-Ir-L2-A):

Δ-**Ir-L2-A**
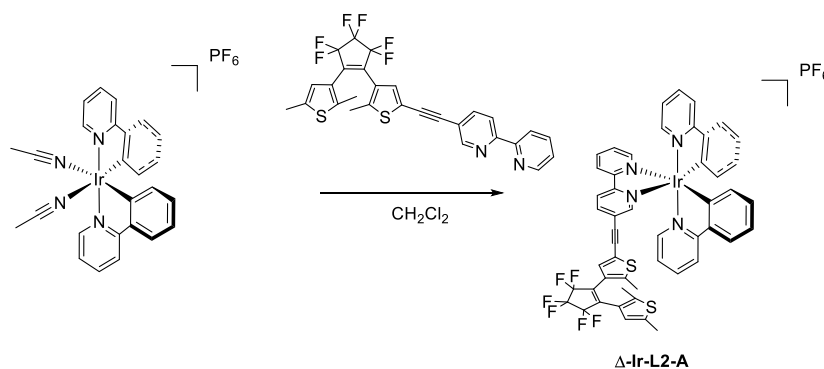
Under N$_2$, Δ-[Ir(ppy)$_2$(CH$_3$CN)$_2$] (0.068 mmol, 0.05 g) and **L2-A** (0.075 mmol, 0.04 g) were dissolved in 5 mL of dry CH$_2$Cl$_2$. The yellow solution was stirred overnight at r.t. The blue solution was purified by alumine column chromatography (CH$_2$Cl$_2$/MeOH (99.5:0.5), Rf = 0.20). The product was obtained as a blue solid. (0.03 g, 56% yield).

^{1}**H NMR (CDCl$_3$)**: δ 8.66 (t, J_{H-H} = 8.37 Hz, 2H, CH$_{ar}$),), δ 8.18 − 8.13 (m, 2H, CH$_{ar}$), δ 7.96 − 7.91 (m, 4H, CH$_{ar}$), δ 7.81 − 7.74 (m, 2H, CH$_{ar}$), δ 7.70 (t, J_{H-H} = 8.94 Hz, 2H, CH$_{ar}$), δ 7.54 (d, J_{H-H} = 5.73 Hz, 1H, CH$_{ar}$), δ 7.49 (d, J_{H-H} = 5.7 Hz, 1H, CH$_{ar}$), δ 7.40 (t, J_{H-H} = 6.39 Hz, 1H, CH$_{ar}$), δ 7.28 (s, 1H, CH$_{ar}$), δ 7.07 − 7.01 (m, 4H, CH$_{ar}$), δ 6.97 − 6.89 (m, 2H, CH$_{ar}$), δ 6.68 (s, 1H, CH$_{ar}$), δ 6.31 − 6.25 (m, 2H, CH$_{ar}$), δ 2.41 (s, 3H, CH$_3$), δ 1.90 (s, 3H, CH$_3$), δ 1.83 (s, 3H, CH$_3$).
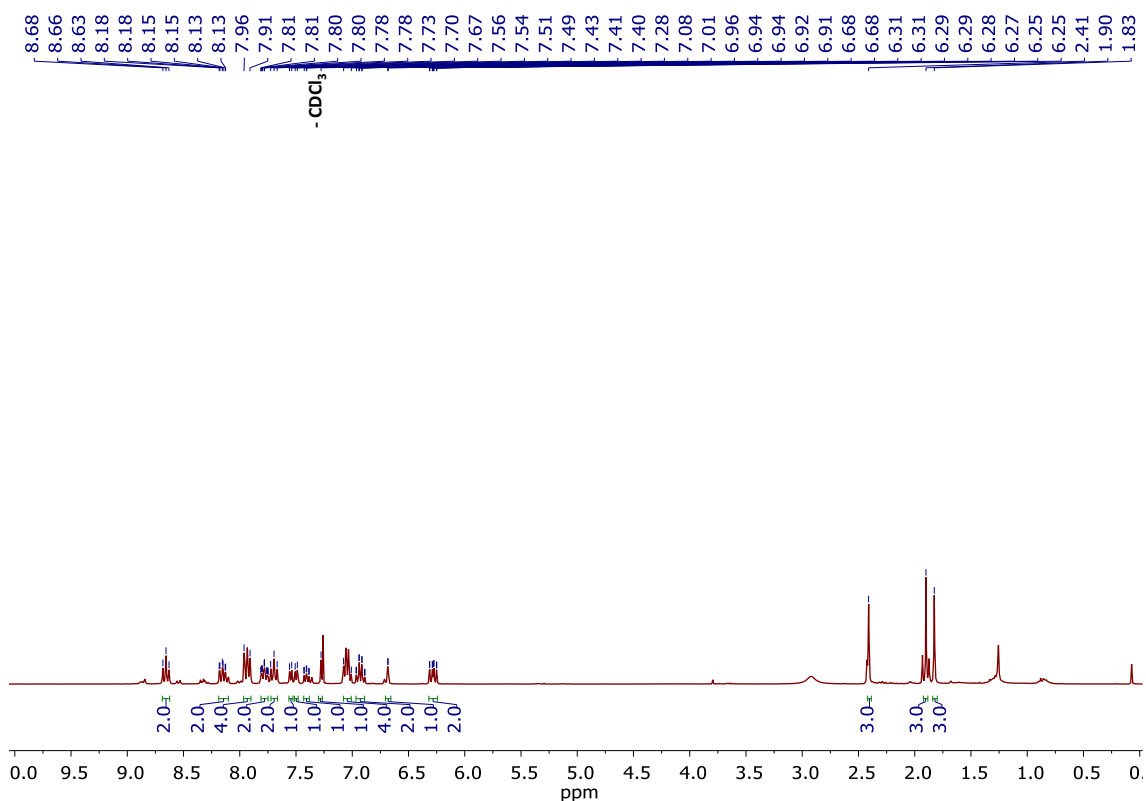
Figure S75. ^{1}H NMR of Δ-[Ir(ppy)$_2$(L2-A)]PF$_6$ (**Δ-Ir-L2-A**). (CDCl$_3$, 300 MHz).

2.2.18 Complex Λ-[Ir(ppy)$_2$(L2-B)] (Λ-Ir-L2-B):

Λ-**Ir-L2-B**

Under N$_2$, Λ-[Ir(ppy)$_2$(CH$_3$CN)$_2$]PF$_6$ (0.041 mmol, 0.03 g) and **L3-B** (0.045 mmol, 0.025 g) were dissolved in 5 mL of dry CH$_2$Cl$_2$. The dark orange solution was stirred overnight at r.t. The blue solution was purified by alumine column chromatography (CH$_2$Cl$_2$/MeOH (99.5:0.5), Rf = 0.25). The product was obtained as a blue solid. (0.030 g, 61% yield).

Exact Mass: FD [C$_{53}$H$_{34}$F$_6$IrN$_4$S$_2$]: calculated: m/z = 1095.174, found: m/z = 109.175

^{1}H NMR (CDCl$_3$): δ 8.68 (t, J$_{H-H}$ = 5.64 Hz, 2H, CH$_{ar}$), δ 8.15 − 8.11 (m, 2H, CH$_{ar}$), δ 7.95 − 7.90 (m, 4H, CH$_{ar}$), δ 7.81 − 7.67 (m, 5H, CH$_{ar}$), δ 7.55 − 7.48 (m, 3H, CH$_{ar}$), δ 7.40 (t, J$_{H-H}$ = 5.64 MHz, 1H, CH$_{ar}$), δ 7.37 − 7.29 (m, 2H, CH$_{ar}$), δ 7.22 (s, 1H, CH$_{ar}$), δ 7.11 − 7.01 (m, 4H, CH$_{ar}$), δ 6.96 − 6.89 (m, 2H, CH$_{ar}$),δ 6.28 (t, J$_{H-H}$ = 7.95 MHz, 2H, CH$_{ar}$), δ 2.28 (s, 3H, CH$_3$), δ 1.90 (s, 3H, CH$_3$).
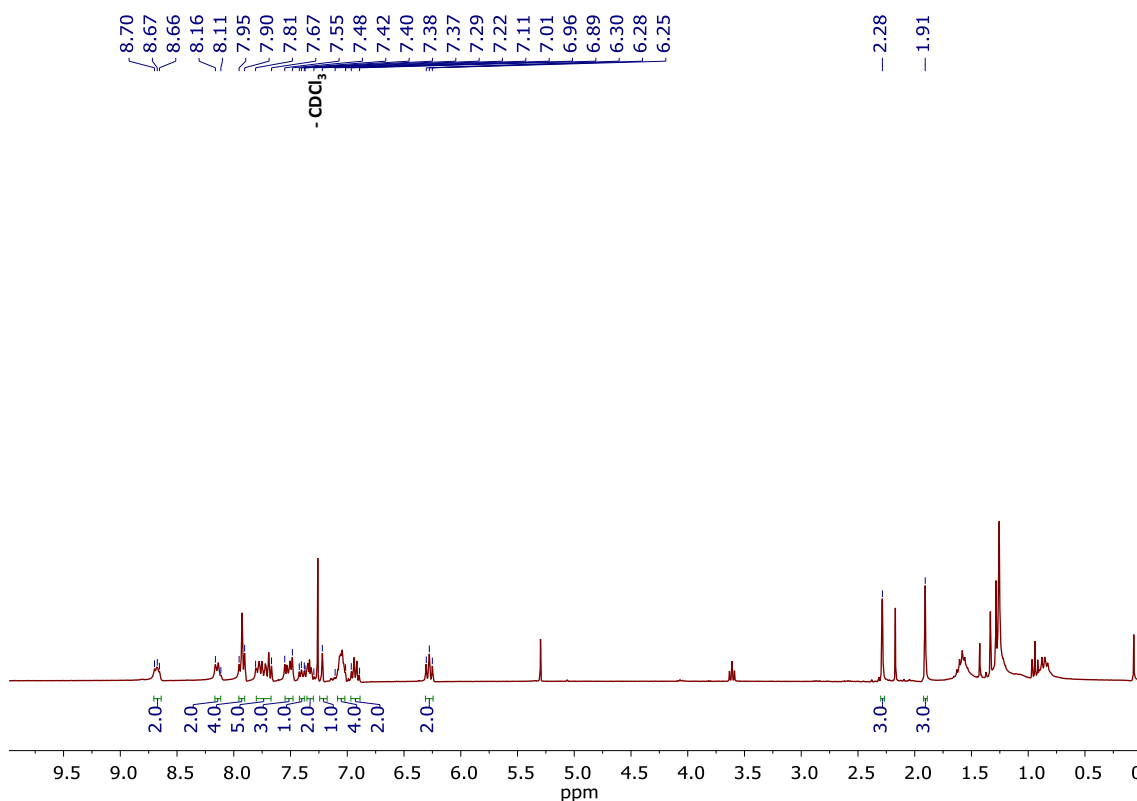
Figure S76. ^{1}H NMR of Λ-[Ir(ppy)$_2$(L2-B)]PF$_6$ (**Λ-Ir-L2-B**). (CDCl$_3$, 300 MHz).

2.2.19 Complex Δ-[Ir(ppy)$_2$(L2-B)] (Δ-Ir-L2-B):
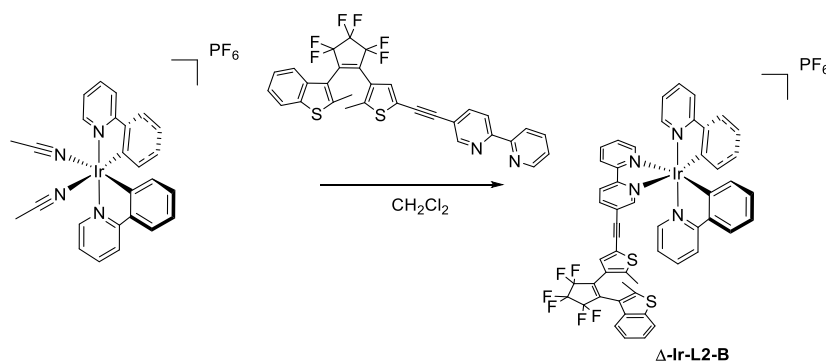
Under N$_2$, Δ-[Ir(ppy)$_2$(CH$_3$CN)$_2$]PF$_6$ (0.034 mmol, 0.025 g) and **L3-B** (0.038 mmol, 0.023 g) were dissolved in 5 mL of dry CH$_2$Cl$_2$. The orange solution was stirred overnight at r.t. The brown-orange solution was purified by alumine column chromatography (CH$_2$Cl$_2$/MeOH (99.5:0.5, Rf = 0.23). The product was obtained as a blue solid. (0.022 g, 52% yield).

^{1}H NMR (CDCl$_3$): δ 8.80 (t, J$_{H-H}$ = 8.67 Hz, 2H, CH$_{ar}$), δ 8.15 − 8.11 (m, 2H, CH$_{ar}$), δ 7.95 − 7.90 (m, 4H, CH$_{ar}$), δ 7.80 − 7.66 (m, 5H, CH$_{ar}$), δ 7.54 − 7.47 (m, 3H, CH$_{ar}$), δ 7.39 (t, J$_{H-H}$ = 6.54 MHz, 1H, CH$_{ar}$), δ 7.34 − 7.32 (m, 2H, CH$_{ar}$), δ 7.22 (s, 1H, CH$_{ar}$), δ 7.08 − 7.01 (m, 4H, CH$_{ar}$), δ 6.96 − 6.89 (m, 2H, CH$_{ar}$),δ 6.28 (d, J$_{H-H}$ = 8.46 MHz, 2H, CH$_{ar}$), δ 2.28 (s, 3H, CH$_3$), δ 1.90 (s, 3H, CH$_3$).
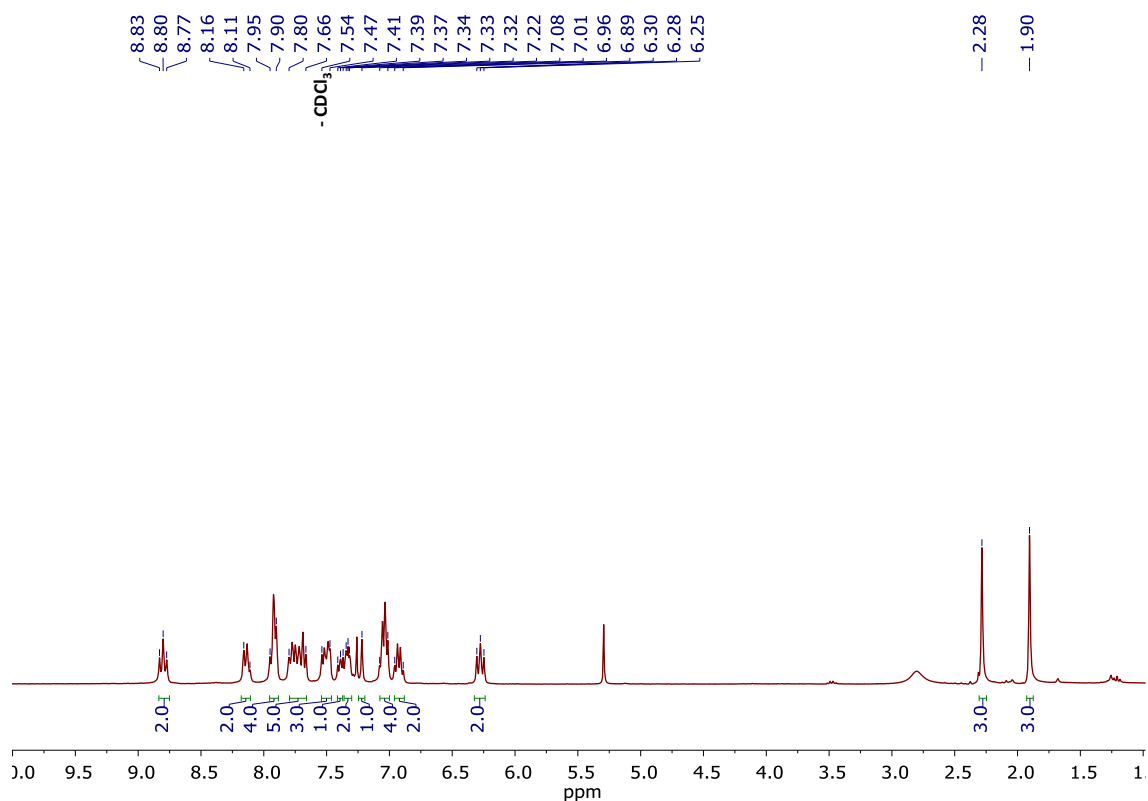
Figure S77. ¹H NMR of Δ-[Ir(ppy)₂(L2-B)]PF₆ (**Δ-Ir-L2-B**). (CDCl₃, 300 MHz).

2.2.20 Complex Λ-[Ir(ppy)₂(L3-A)] (Λ-Ir-L3-A):

Λ-**Ir-L3-A**
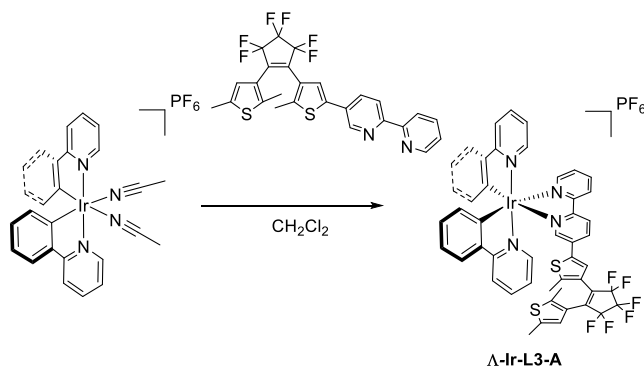
Under N₂, Λ-[Ir(ppy)₂(CH₃CN)₂]PF₆ (0.041 mmol, 0.03 g) and **L3-B** (0.045 mmol, 0.024 g) were dissolved in 5 mL of dry CH₂Cl₂. The dark purple solution was stirred overnight at r.t. The blue solution was purified by alumine column chromatography (CH₂Cl₂, Rf = 0.22). The product was obtained as a blue solid. (0.040 g, 56% yield).

Exact Mass: FD [$C_{48}H_{34}F_6IrN_4S_2$]: calculated: m/z = 1035.174, found: m/z = 1035.176.

¹H NMR (CDCl₃): δ 8.62 (d, J_{H-H} = 8.55 Hz, 2H, CH$_{ar}$), δ 8.11 (dt, J_{H-H} = 2.04 Hz, J_{H-H} = 1.77 Hz, J_{H-H} = 8.52 Hz, 2H, CH$_{ar}$), δ 7.98 − 7.91 (m, 4H, CH$_{ar}$), δ 7.77 (t, J_{H-H} = 8.46 Hz, 2H, CH$_{ar}$), δ 7.71 (d, J_{H-H} = 7.8 Hz, 2H, CH$_{ar}$), δ 7.57 (t, J_{H-H} = 4.65, 2H, CH$_{ar}$), δ 7.42 − 7.38 (m, 1H, CH$_{ar}$), δ 7.11 − 7.00 (m, 5H, CH$_{ar}$), δ 7.00 − 6.91 (m, 2H, CH$_{ar}$), δ 6.68 (s, 1H, CH$_{ar}$), δ 6.37 − 6.33 (m, 2H, CH$_{ar}$), δ 2.41 (s, 3H, CH₃), δ 1.88 (s, 3H, CH₃), δ 1.82 (s, 3H, CH₃).
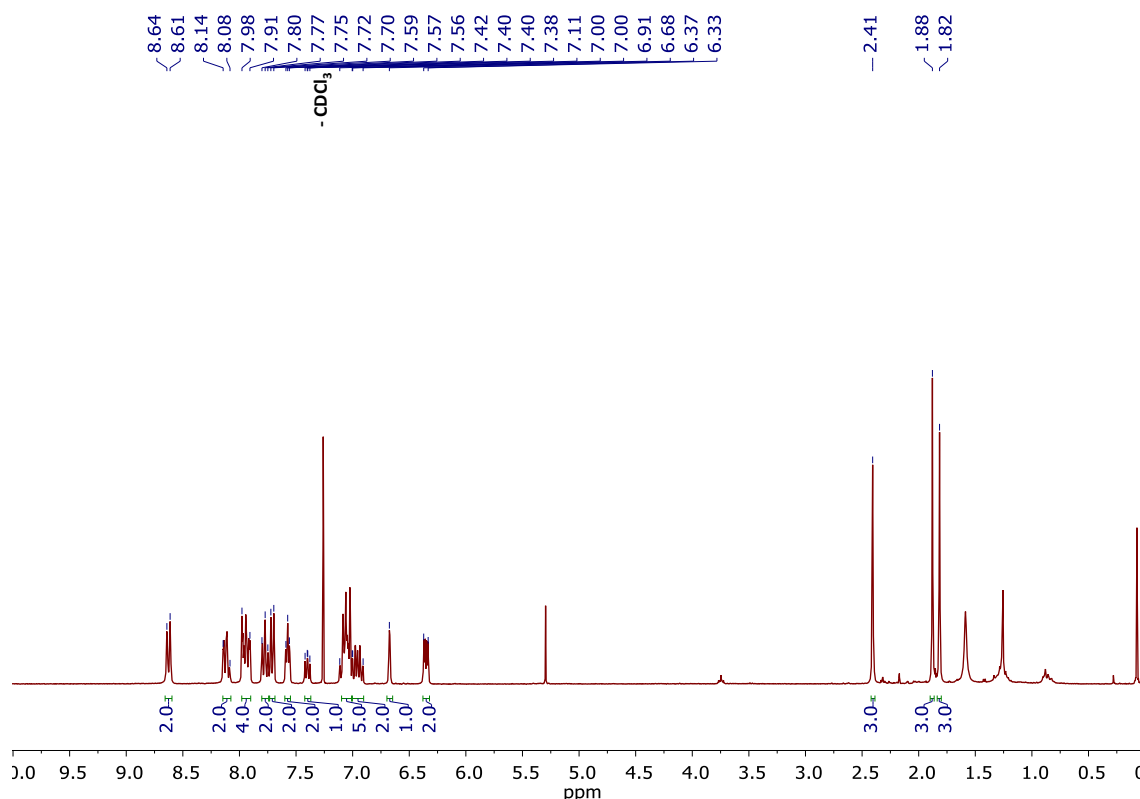
**Figure S78.** ^{1}H NMR of Λ-[Ir(ppy)$_2$(L3-A)]PF$_6$ (**Λ-Ir-L3-A**). (CDCl$_3$, 300 MHz).

2.2.21 Complex Δ-[Ir(ppy)$_2$(L3-A)] (Δ-Ir-L3-A):
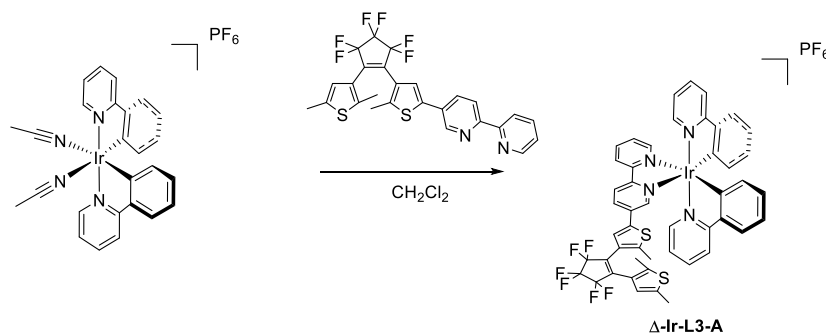
Under N$_2$, Δ-[Ir(ppy)$_2$(CH$_3$CN)$_2$]PF$_6$ (0.041 mmol, 0.030 g) and **L3-B** (0.024 mmol, 0.045 g) were dissolved in 5 mL of dry CH$_2$Cl$_2$. The dark orange solution was stirred overnight at r.t. The blue solution was purified by alumine column chromatography (CH$_2$Cl$_2$, Rf = 0.18). The product was obtained as a blue solid. (0.032 g, 66% yield).

^{1}H NMR (CDCl$_3$): δ 8.61 (d, J$_{H-H}$ = 8.49 Hz, 2H, CH$_{ar}$), δ 8.14 – 8.08 (m, 2H, CH$_{ar}$), δ 7.98 – 7.91 (m, 4H, CH$_{ar}$), δ 7.77 (t, J$_{H-H}$ = 7.32 Hz, 2H, CH$_{ar}$), δ 7.70 (d, J$_{H-H}$ = 7.71 Hz, 2H, CH$_{ar}$), δ 7.58 – 7.56 (m, 2H, CH$_{ar}$), δ 7.42 – 7.38 (m, 1H, CH$_{ar}$), δ 7.10 – 7.00 (m, 5H, CH$_{ar}$), δ 6.99 – 6.90 (m, 2H, CH$_{ar}$), δ 6.67 (s, 1H, CH$_{ar}$), δ 6.37 – 6.33 (m, 2H, CH$_{ar}$), δ 2.40 (s, 3H, CH$_3$), δ 1.87 (s, 3H, CH$_3$), δ 1.81 (s, 3H, CH$_3$).
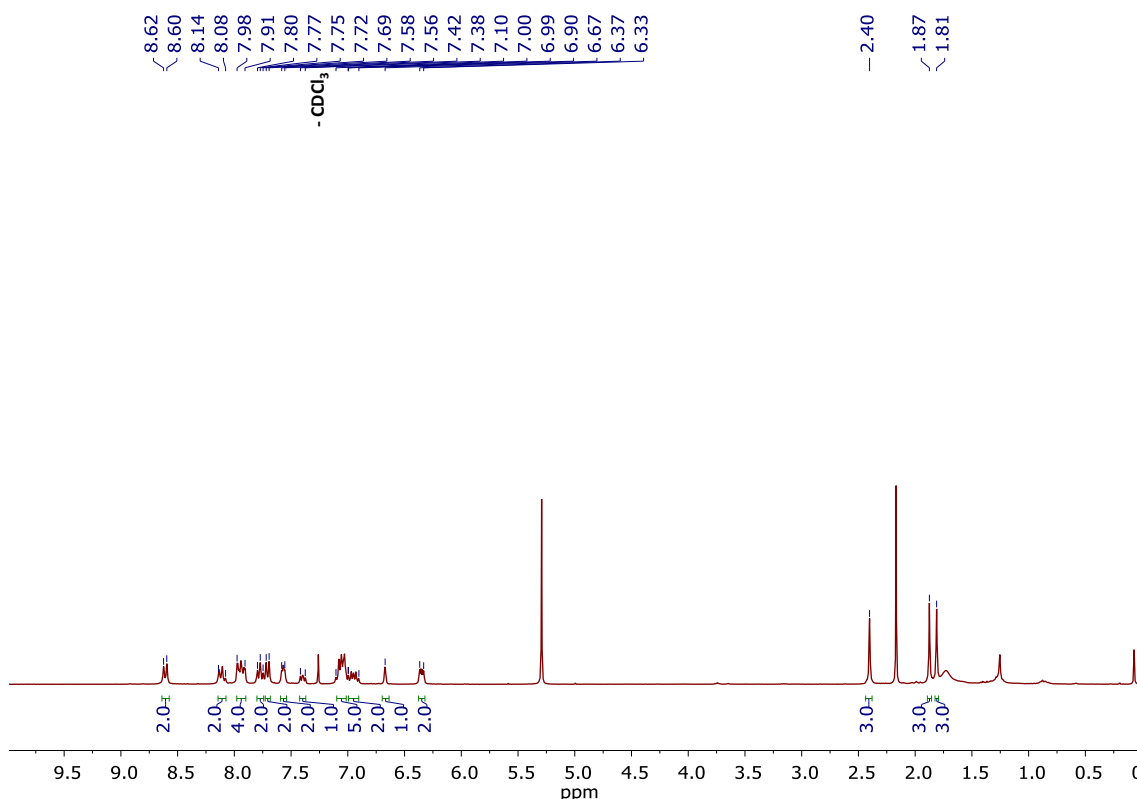
Figure S79. ^{1}H NMR of Δ-[Ir(ppy)$_2$(L3-A)]PF$_6$ (**Δ-Ir-L3-A**). (CDCl$_3$, 300 MHz).

2.2.22 Complex *rac*-[Ir(ppy)$_2$(L3-B)] (*rac*-Ir-L3-B):

C5   *rac*-Ir-L3-B
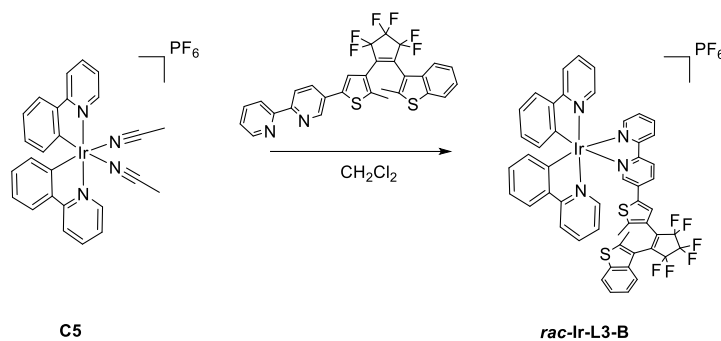
Under N$_2$, *rac*-[Ir(ppy)$_2$(CH$_3$CN)$_2$]PF$_6$ (0.096 mmol, 0.07 g) and **L3-B** (0.12 mmol, 0.07 g) were dissolved in 10 mL of dry CH$_2$Cl$_2$. The yellow solution was stirred overnight at r.t. The dark yellow solution was purified by alumine column chromatography (CH$_2$Cl$_2$, Rf = 0.2). The product was obtained as a blue solid. (0.040 g, 34% yield).

Exact Mass: FD [C$_{51}$H$_{34}$F$_6$IrN$_4$S$_2$]: calculated: m/z = 1073.180, found: m/z = 1073.182.

^{1}H NMR (CDCl$_3$): δ 8.61 (d, J$_{H-H}$ = 8.16, 2H, CH$_{ar}$), δ 8.11 (t, J$_{H-H}$ = 7.77 MHz, 1H, CH$_{ar}$), δ 8.03 (dt, J$_{H-H}$ = 1.92 Hz, J$_{H-H}$ = 8.55, 1H, CH$_{ar}$), δ 7.95 – 7.90 (m, 4H, CH$_{ar}$), δ 7.80 – 7.75 (m, 2H, CH$_{ar}$), δ 7.74 – 7.69 (m, 3H, CH$_{ar}$), δ 7.58 – 7.54 (m, 2H, CH$_{ar}$), δ 7.50 – 7.47 (m, 1H, CH$_{ar}$), δ 7.40 (t, J$_{H-H}$ = 5.82 MHz. 1H, CH$_{ar}$), δ 7.36 – 7.28 (m, 2H, CH$_{ar}$), δ 7.11 – 7.00 (m, 5H, CH$_{ar}$), δ 6.98 – 6.90 (m, 2H, CH$_{ar}$), δ 6.33 (d, J$_{H-H}$ = 7.56, 2H, CH$_{ar}$),δ 2.25 (s, 3H, CH$_3$), δ 1.88 (s, 3H, CH$_3$).
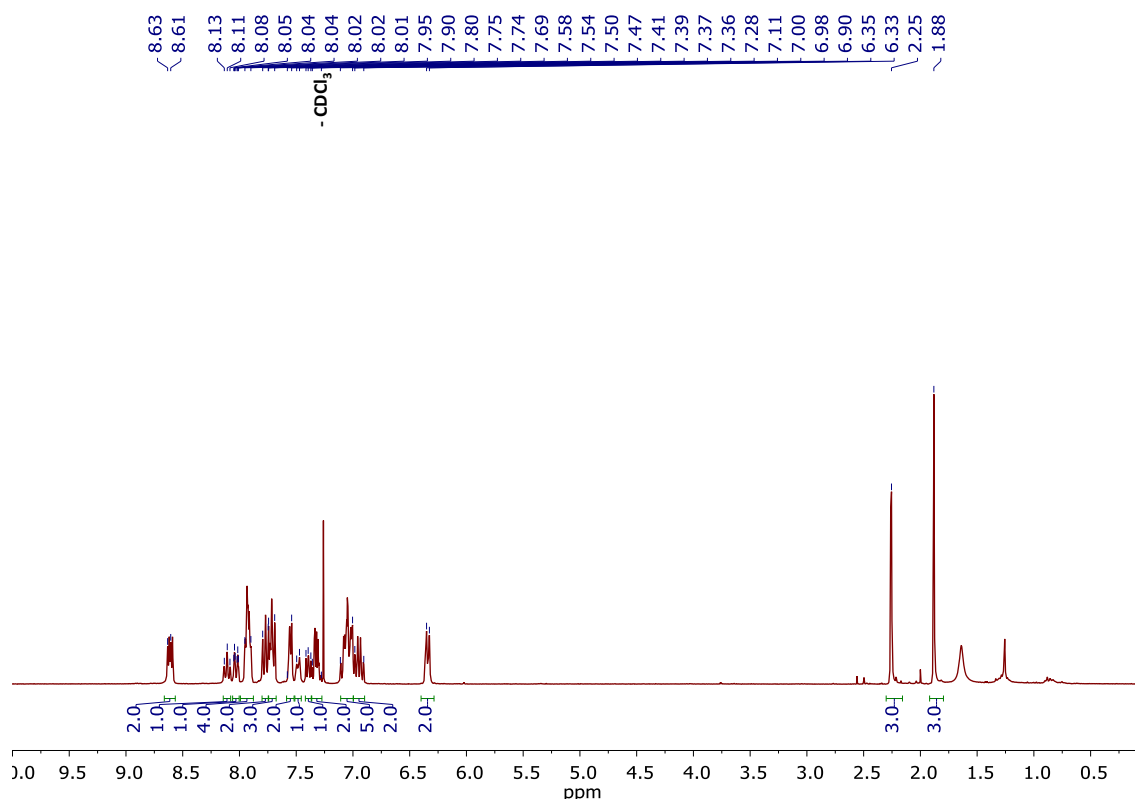
Figure S80. ¹H NMR of *rac*-[Ir(ppy)₂(L3-B)]PF₆ (*rac*-Ir-L3-B). (CDCl₃, 300 MHz).

2.2.23 Complex Λ-[Ir(ppy)₂(L3-A)] (Λ-Ir-L3-A):

Λ-**C5**

Λ-**Ir-L3-B (OF)** (61% yield) X:CH₃; Y:H
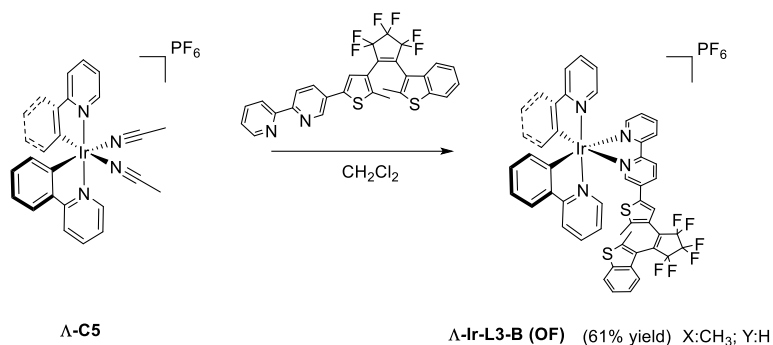
Under N₂, Λ-[Ir(ppy)₂(CH₃CN)₂]PF₆ (0.054 mmol, 0.04 g) and **L3-B** (0.059 mmol, 0.034 g) were dissolved in 5 mL of dry CH₂Cl₂. The dark orange solution was stirred overnight at r.t. The blue solution was purified by alumine column chromatography (CH₂Cl₂, Rf = 0.18). The product was obtained as a blue solid. (0.040 g, 60% yield).

¹H NMR (CDCl₃): δ 8.54 (d, J_{H-H} = 8.25, 2H, CH$_{ar}$), δ 8.06 (t, J_{H-H} = 7.77 MHz, 1H, CH$_{ar}$), δ 8.01 (dt, J_{H-H} = 2.19 Hz, J_{H-H} = 8.55, 1H, CH$_{ar}$), δ 7.95 − 7.90 (m, 4H, CH$_{ar}$), δ 7.79 − 7.77 (m, 2H, CH$_{ar}$), δ 7.74 − 7.68 (m, 3H, CH$_{ar}$), δ 7.56 − 7.47 (m, 3H, CH$_{ar}$), δ 7.37 (t, J_{H-H} = 6.33 MHz. 1H, CH$_{ar}$), δ 7.34 − 7.27 (m, 2H, CH$_{ar}$), δ 7.08 − 7.00 (m, 5H, CH$_{ar}$), δ 6.98 − 6.88 (m, 2H, CH$_{ar}$), δ 6.33 (d, J_{H-H} = 7.47, 2H, CH$_{ar}$),δ 2.25 (s, 3H, CH₃), δ 1.87 (s, 3H, CH₃).

Figure S81. ^{1}H NMR of Λ-[Ir(ppy)$_2$(L3-B)]PF$_6$ (**Λ-Ir-L3-B**). (CDCl$_3$, 300 MHz).

2.2.24 Complex Δ-[Ir(ppy)$_2$(L3-A)] (Δ-Ir-L3-A):

Δ-**Ir-L3-B**
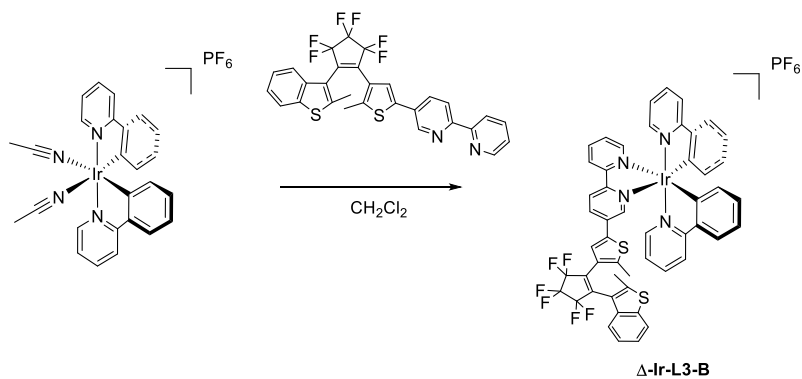
Under N$_2$, Δ-[Ir(ppy)$_2$(CH$_3$CN)$_2$]PF$_6$ (0.052 mmol, 0.038 g) and **L3-B** (0.057 mmol, 0.033 g) were dissolved in 5 mL of dry CH$_2$Cl$_2$. The dark orange solution was stirred overnight at r.t. The blue solution was purified by alumine column chromatography (CH$_2$Cl$_2$, Rf = 0.18). The product was obtained as a blue solid. (0.031 g, 49% yield).

^{1}**H NMR (CDCl$_3$)**: δ 8.57 (d, J$_{H-H}$ = 8.25, 2H, CH$_{ar}$), δ 8.07 (t, J$_{H-H}$ = 7.77 MHz, 1H, CH$_{ar}$), δ 8.02 (dt, J$_{H-H}$ = 2.07 Hz, J$_{H-H}$ = 8.55, 1H, CH$_{ar}$), δ 7.95 – 7.89 (m, 4H, CH$_{ar}$), δ 7.79 – 7.77 (m, 2H, CH$_{ar}$), δ 7.72 – 7.68 (m, 3H, CH$_{ar}$), δ 7.56 – 7.47 (m, 3H, CH$_{ar}$), δ 7.38 (t, J$_{H-H}$ = 6.24 MHz. 1H, CH$_{ar}$), δ 7.34 – 7.29 (m, 2H, CH$_{ar}$), δ 7.09 – 6.99 (m, 5H, CH$_{ar}$), δ 6.99 – 6.89 (m, 2H, CH$_{ar}$), δ 6.33 (d, J$_{H-H}$ = 8.07 MHz, 2H, CH$_{ar}$),δ 2.25 (s, 3H, CH$_3$), δ 1.87 (s, 3H, CH$_3$).
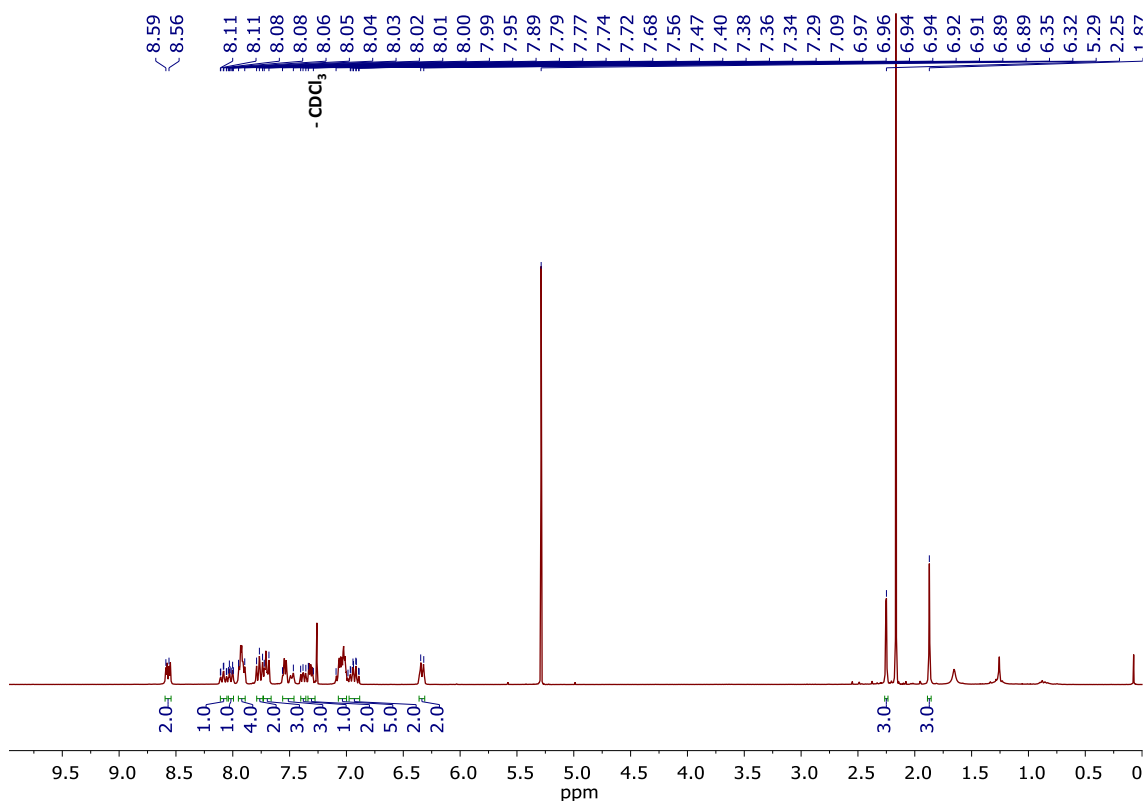
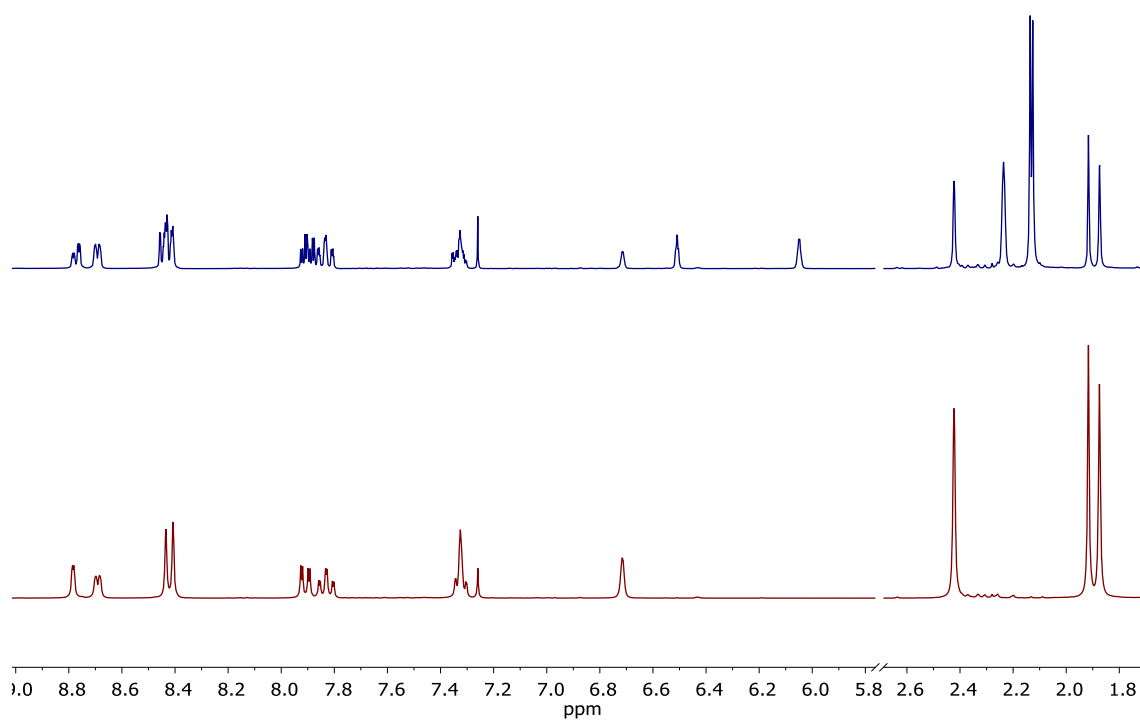**Figure S82.** ^{1}H NMR of Δ-[Ir(ppy)$_2$(L3-B)]PF$_6$ (**Δ-Ir-L3-B**). (CDCl$_3$, 300 MHz).

3. PHOTOISOMERIZATION STUDIES
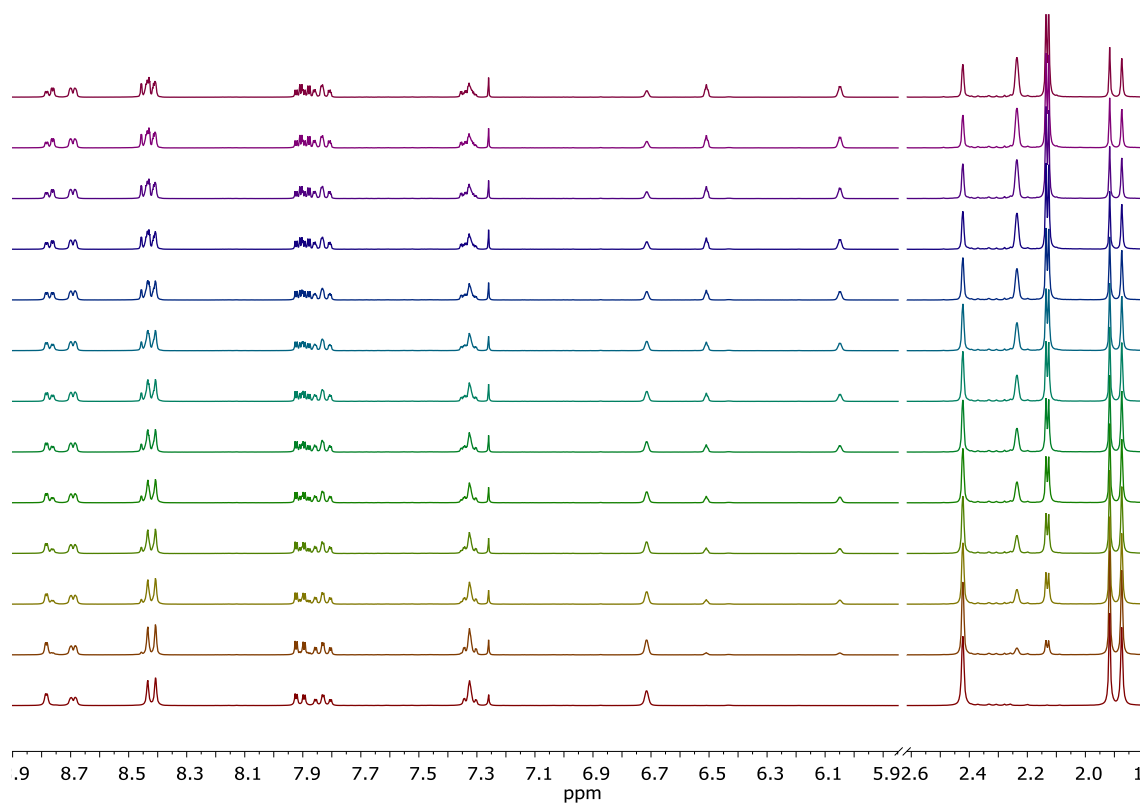
3.1 LIGANDS

3.1.1   5-((4-(2-(2,5-dimethylthiophen-3-yl)-3,3,4,4,5,5-hexafluorocyclopent-1-en-1-yl)-5-methylthiophen-2-yl)ethynyl)-2,2'-bipyridine (L2-A):
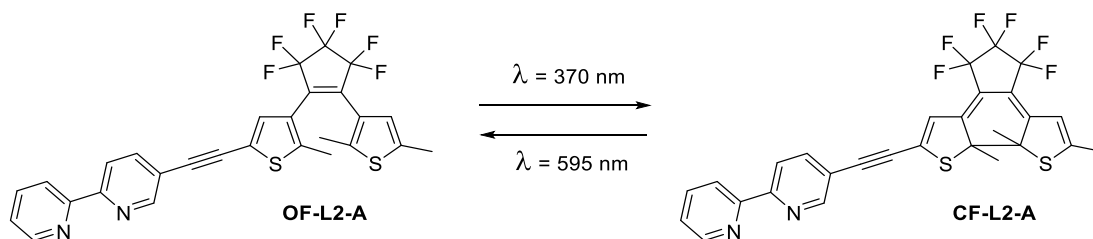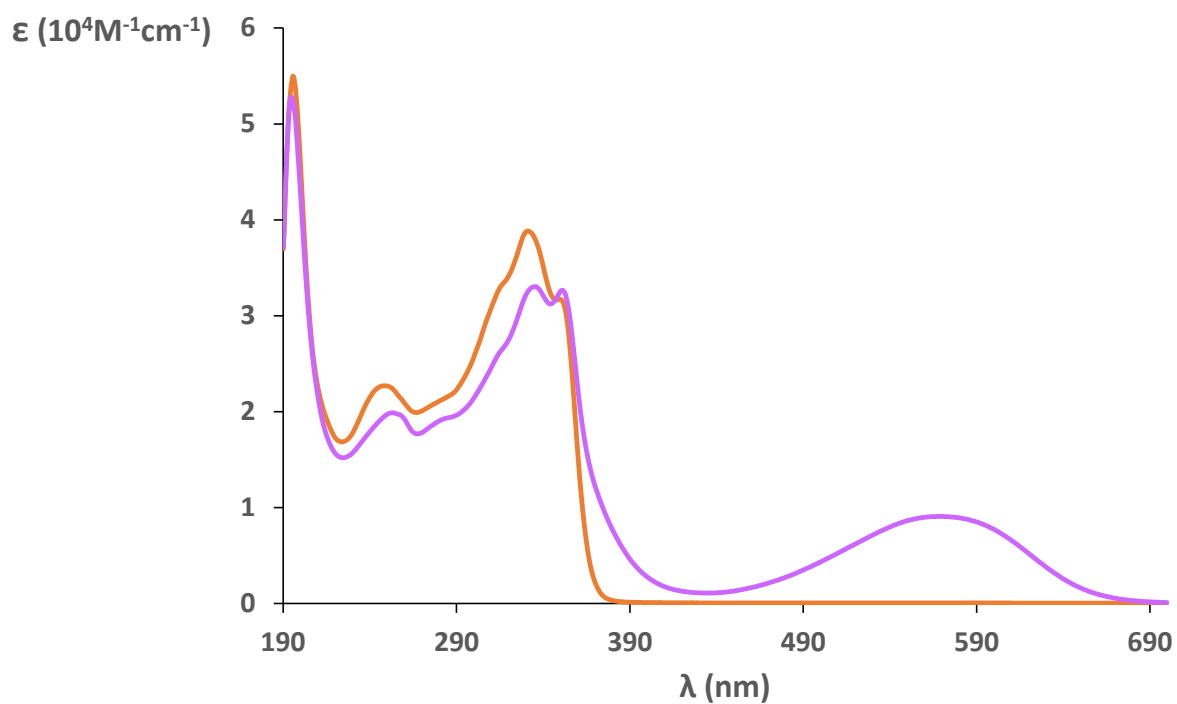

UV/Vis (CH$_3$CN), λ, nm (ε, 10^{4}M^{-1}cm^{-1}): OF: 195 (5.49) 248 (2.27) 331 (3.88) 350 (3.17). **CF:** 194 (5.27) 253 (1.98) 335 (3.30) 351 (3.26) 569 (0.91).
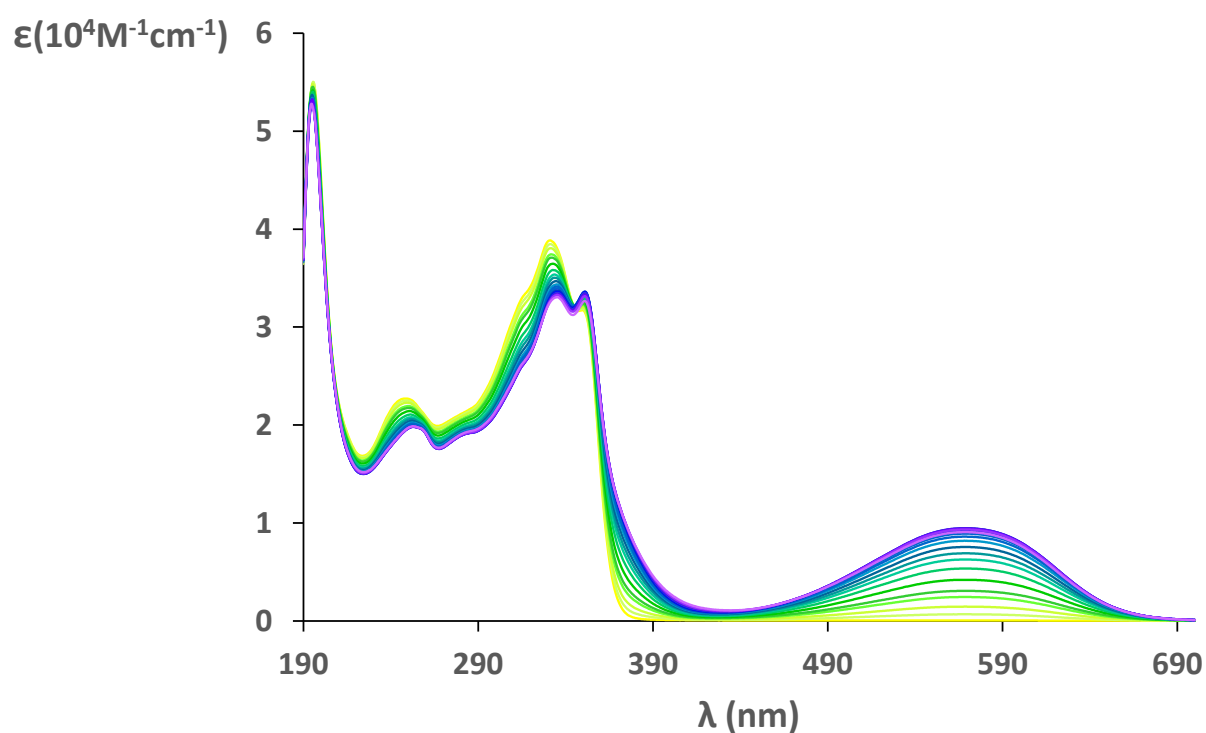
Figure S83. ^{1}H NMR spectra of **L2-A**. Before (red) and after (blue) irradiation at 370 nm. (0.053 M, CDCl$_3$, 300 MHz).

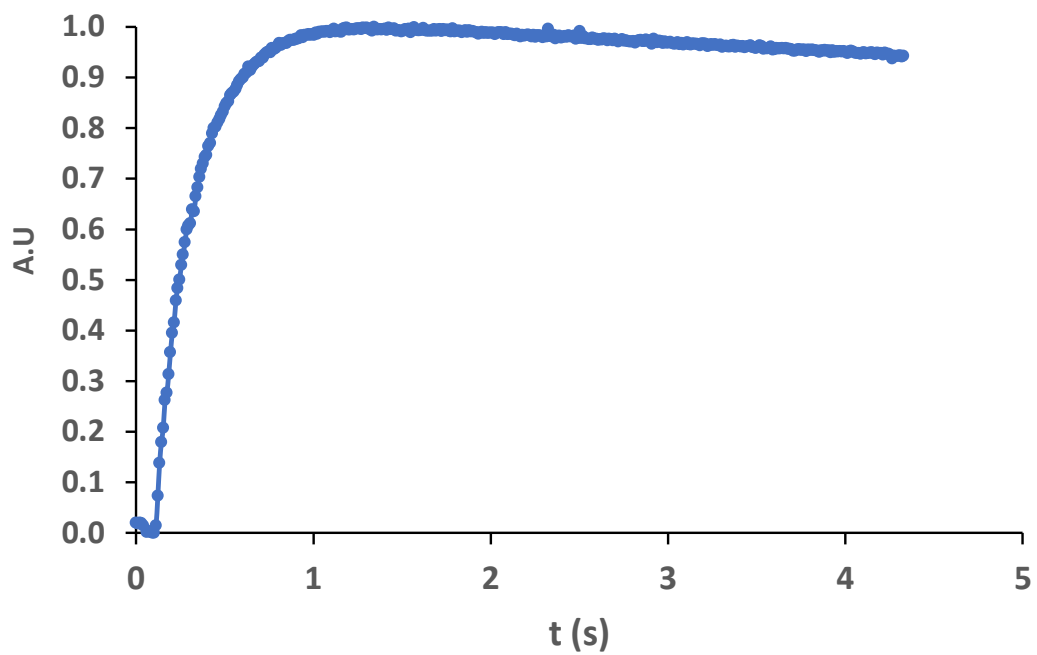**Figure S84**. ^{1}H NMR spectra of **L2-A** isomerization kinetics irradiating at 370 nm. (0.053 M, CDCl$_3$, 300 MHz).

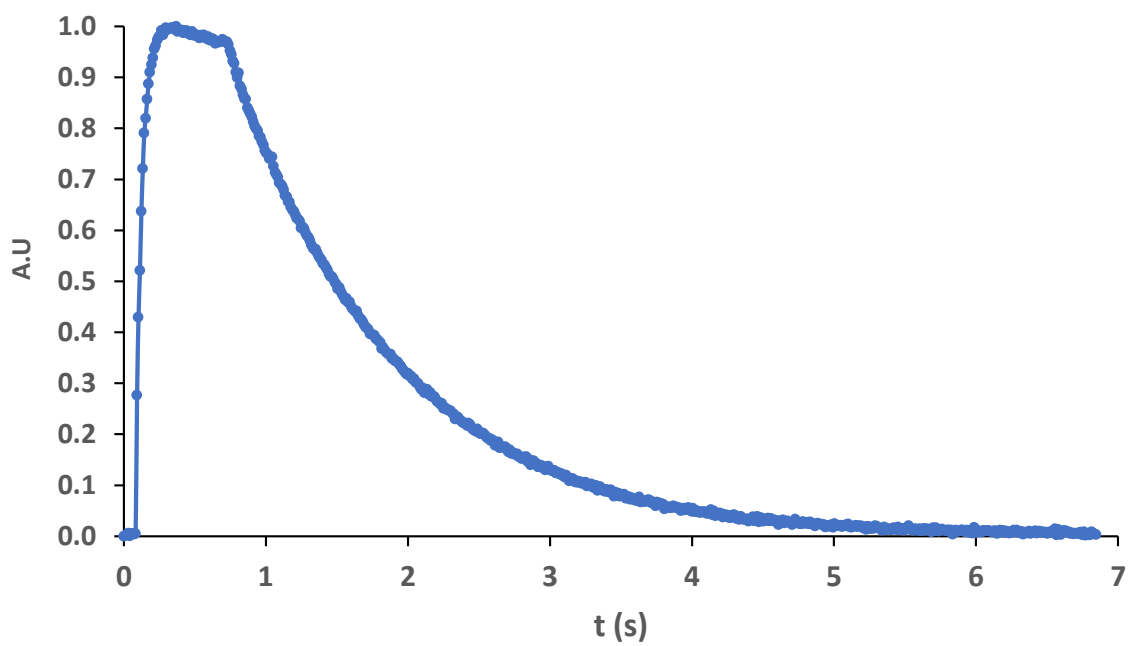**Figure S85**. UV/Vis spectra of **L2-A** in CH$_3$CN. Before (orange line) and after (purple line) irradiation at 370 nm, 5·10^{-5}M
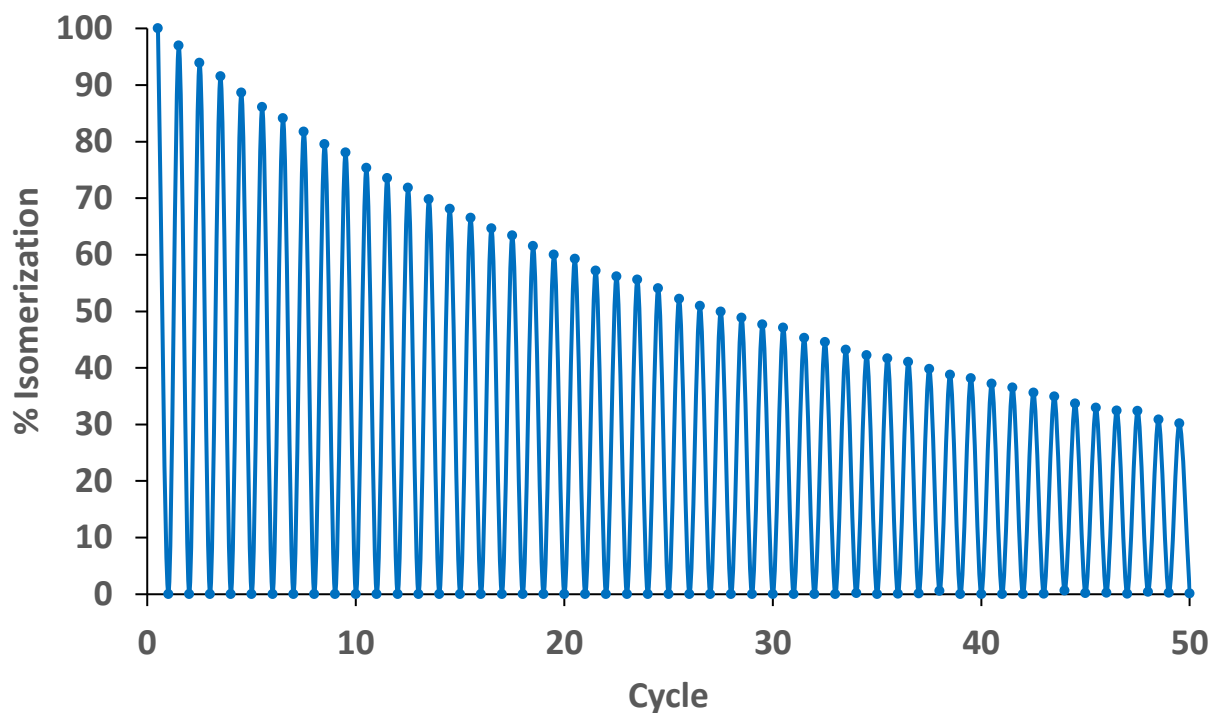

Figure S86. UV/Vis kinetic of **L2-A** in CH$_3$CN irradiating at 370 nm, 5·10^{-5}M

Figure S87. UV/Vis spectra of **L2-A** in CH₃CN. Photocyclization process by irradiation at 370 nm, $3.3 \cdot 10^{-5}$M

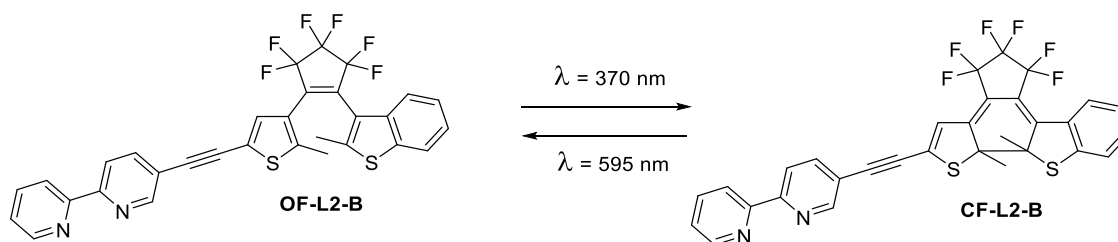

Figure S88. UV/Vis spectra of **L2-A** in CH₃CN. Photocycloreversion process by irradiation at 370 nm, $3.3 \cdot 10^{-5}$M

Figure S89. UV/Vis spectra of **L2-A** in CH₃CN. Fatigue resistance experiment by irradiation at 370 nm and 595 nm alternatively, 3.3·10⁻⁵M

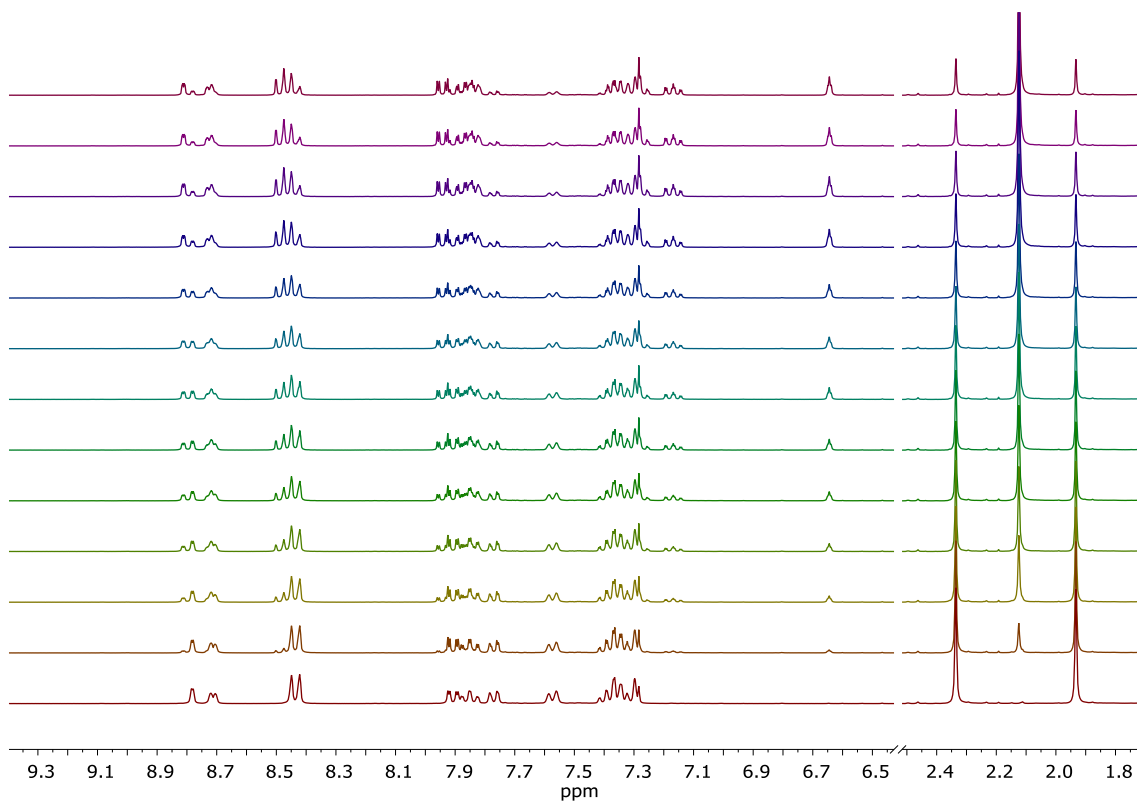### 3.1.2   5-((4-(3,3,4,4,5,5-hexafluoro-2-(2-methylbenzo[b]thiophen-3-yl)cyclopent-1-en-1-yl)-5-methylthiophen-2-yl)ethynyl)-2,2'-bipyridine (L2-B):

UV/Vis (CH₃CN), λ, nm (ε, 10⁴M⁻¹cm⁻¹): OF: 196 (5.27) 225 (2.78) 259 (2.13) 330 (3.35) 350 (2.72).
CF: 195 (4.86) 229 (1.98) 258 (1.74) 334 (2.69) 348 (2.67) 422 (0.58) 555 (1.16).
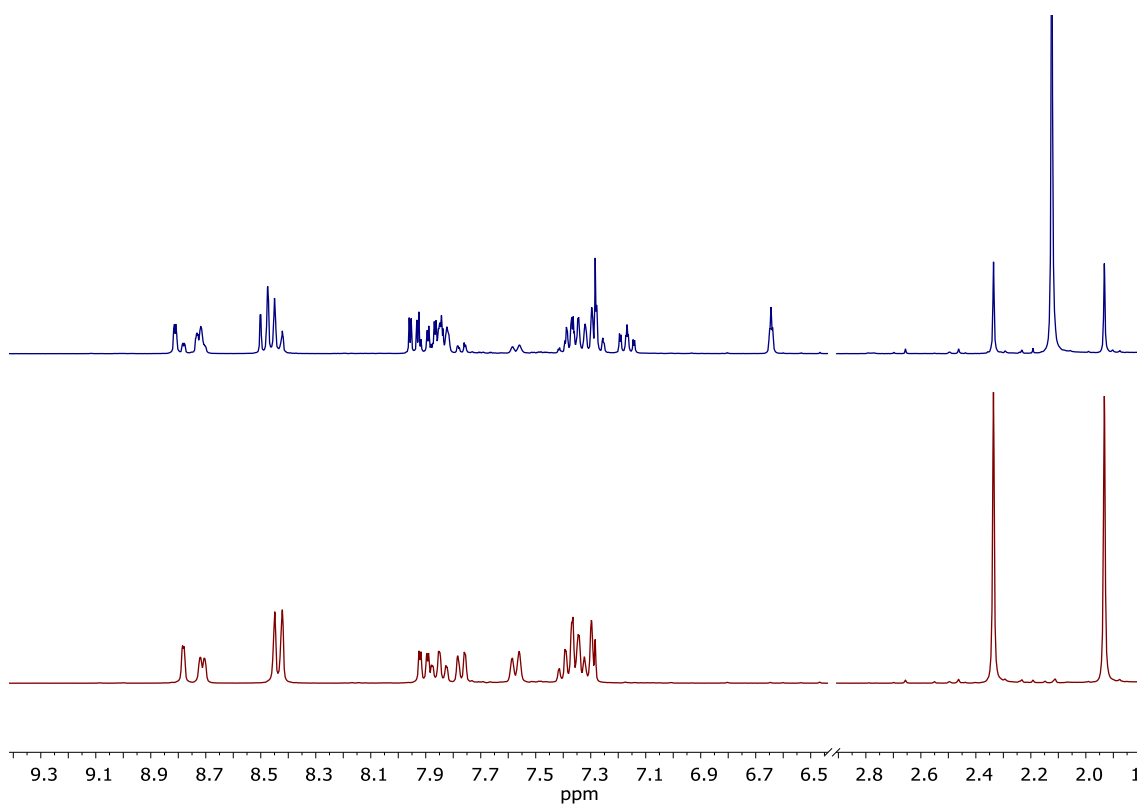
Figure S90. ^{1}H NMR spectra of **L2-A**. Before (red) and after (blue) irradiation at 370 nm. (0.050 M, CDCl$_3$, 300 MHz).

Figure S91. ^{1}H NMR spectra of **L2-B** isomerization kinetics irradiating at 370 nm. (0.050 M, CDCl$_3$, 300 MHz).
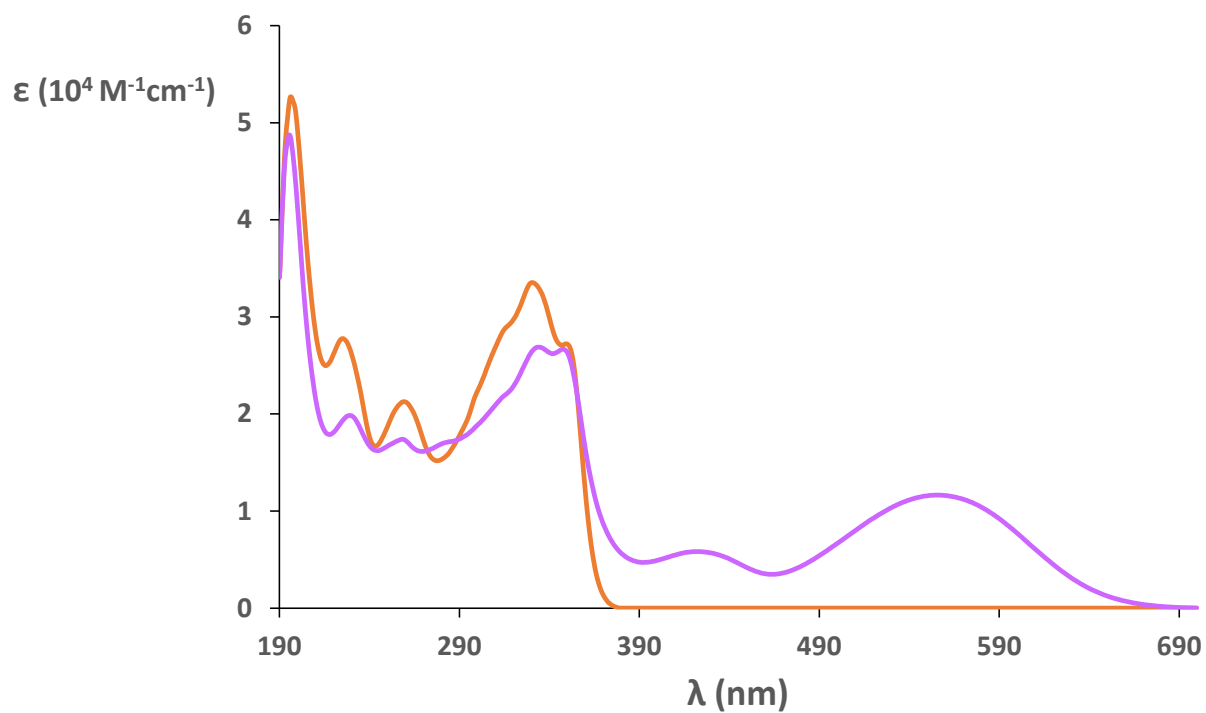
Figure S92. UV/Vis spectra of **L2-B** in CH$_3$CN. Before (orange line) and after (purple line) irradiation at 370 nm, 5·10^{-5}M
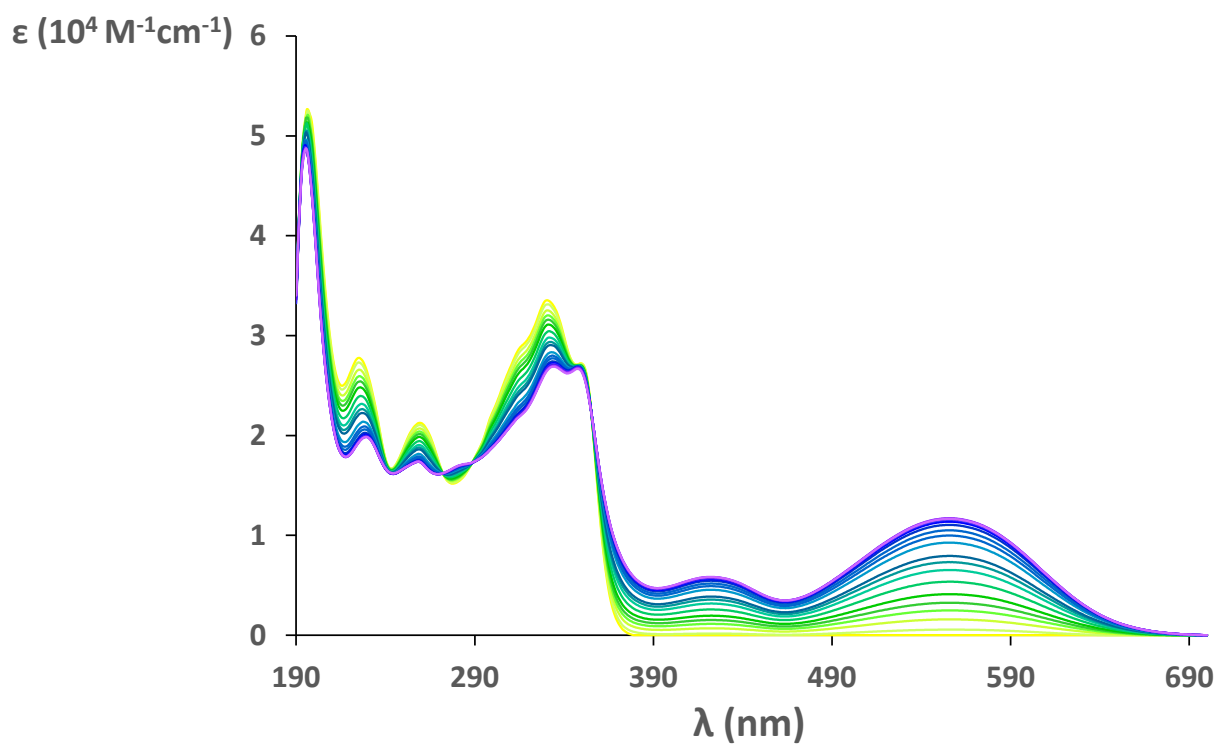
Figure S93. UV/Vis kinetic of **L2-B** in CH$_3$CN irradiating at 370 nm, 5·10^{-5}M
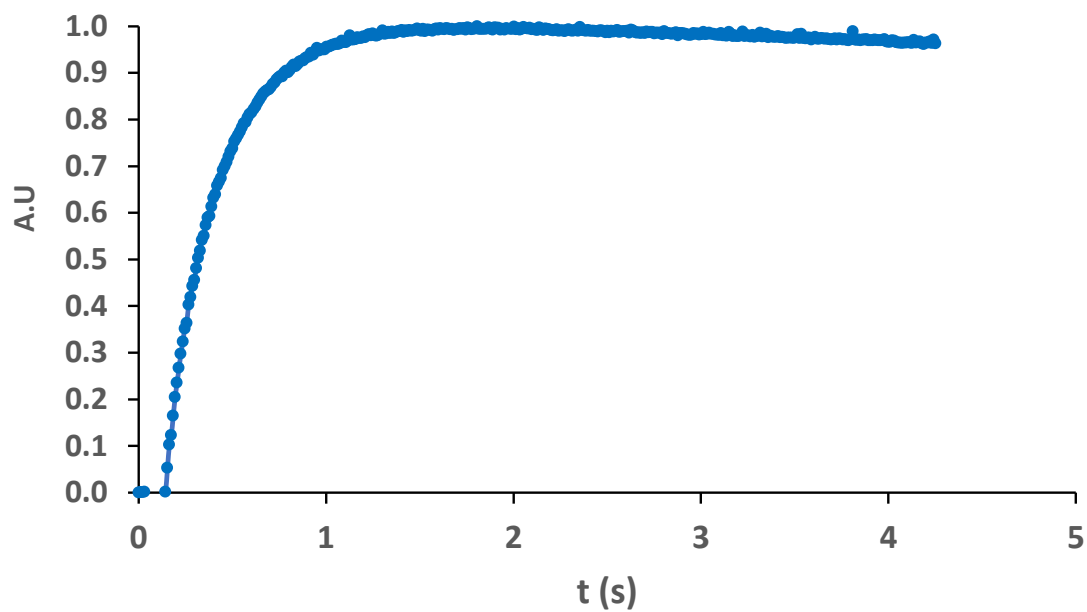
Figure S94. UV/Vis spectra of **L2-B** in CH₃CN. Photocyclization process by irradiation at 370 nm, 2.6·10⁻⁵M
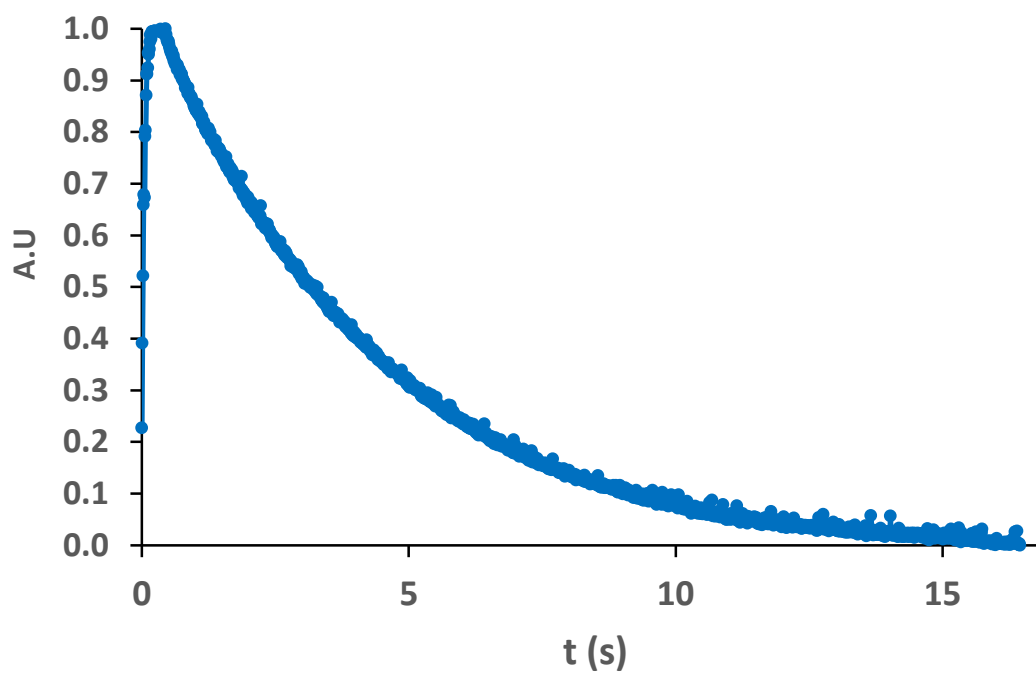
Figure S95. UV/Vis spectra of **L2-B** in CH₃CN. Photocycloreversion process by irradiation at 370 nm, 2.6·10⁻⁵M
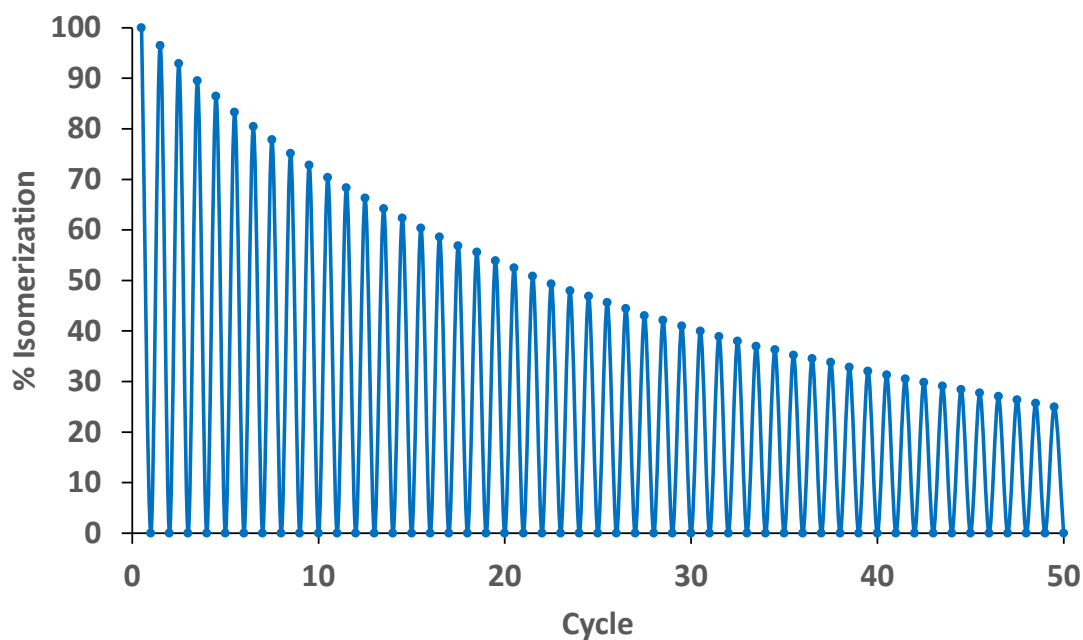
Figure S96. UV/Vis spectra of **L2-B** in CH$_3$CN. Fatigue resistance experiment by irradiation at 370 nm and 595 nm alternatively, 2.6·10^{-5}M

3.1.3   5-(4-(2-(2,5-dimethylthiophen-3-yl)-3,3,4,4,5,5-hexafluorocyclopent-1-en-1-yl)-5-methylthiophen-2-yl)-2,2'-bipyridine (L3-A):
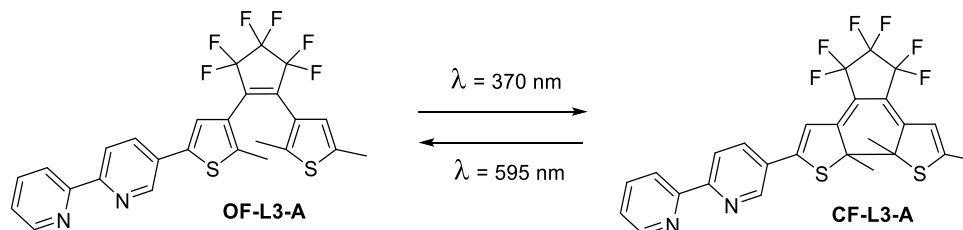
UV/Vis (CH$_3$CN), λ, nm (ε, 10^{4}M^{-1}cm^{-1}): OF: 196 (4.90) 246 (2.04) 327 (3.47) 350 (2.72). **CF:** 195 (4.68) 243 (1.86) 326 (3.07) 560 (0.58).

Figure S97. ^{1}H NMR spectra of **L3-A**. Before (red) and after (blue) irradiation at 370 nm. (0.055 M, CDCl$_3$, 300 MHz).
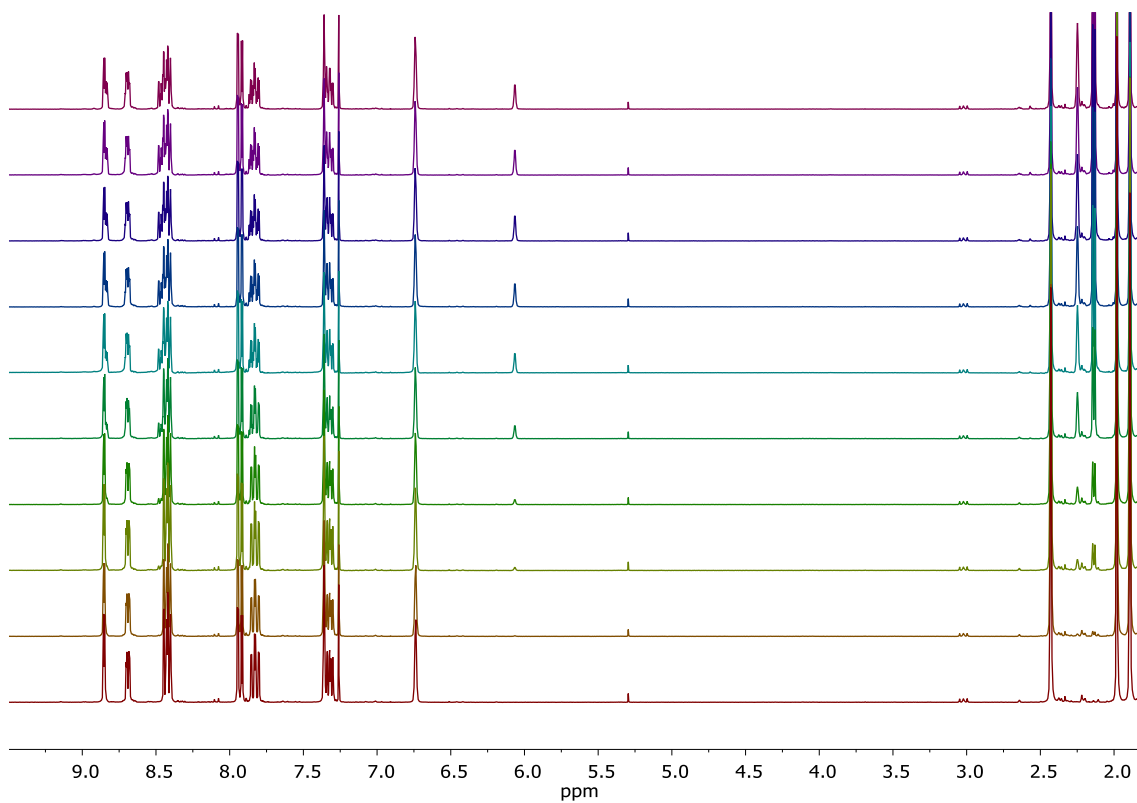

Figure S98. ^{1}H NMR spectra of **L3-A** isomerization kinetics irradiating at 370 nm. (0.055 M, CDCl$_3$, 300 MHz).
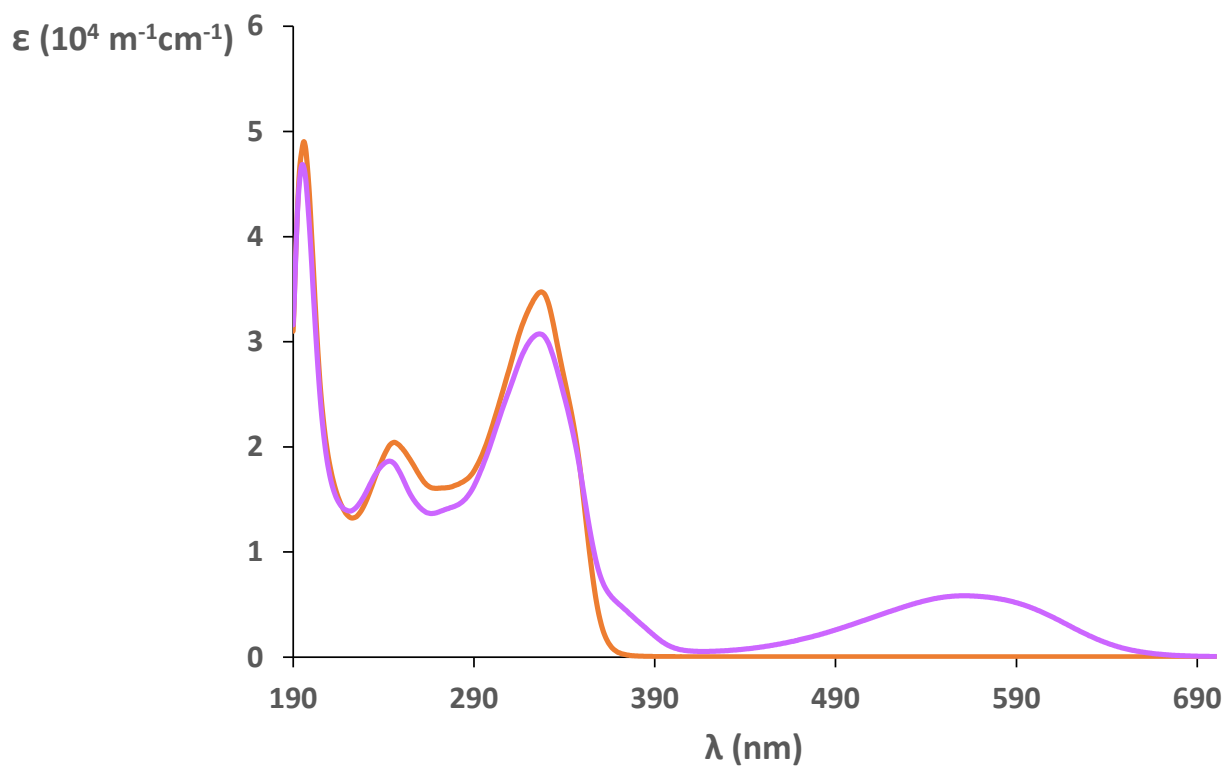
Figure S99. UV/Vis spectra of **L3-A** in CH₃CN. Before (orange line) and after (purple line) irradiation at 370 nm, 5·10⁻⁵M
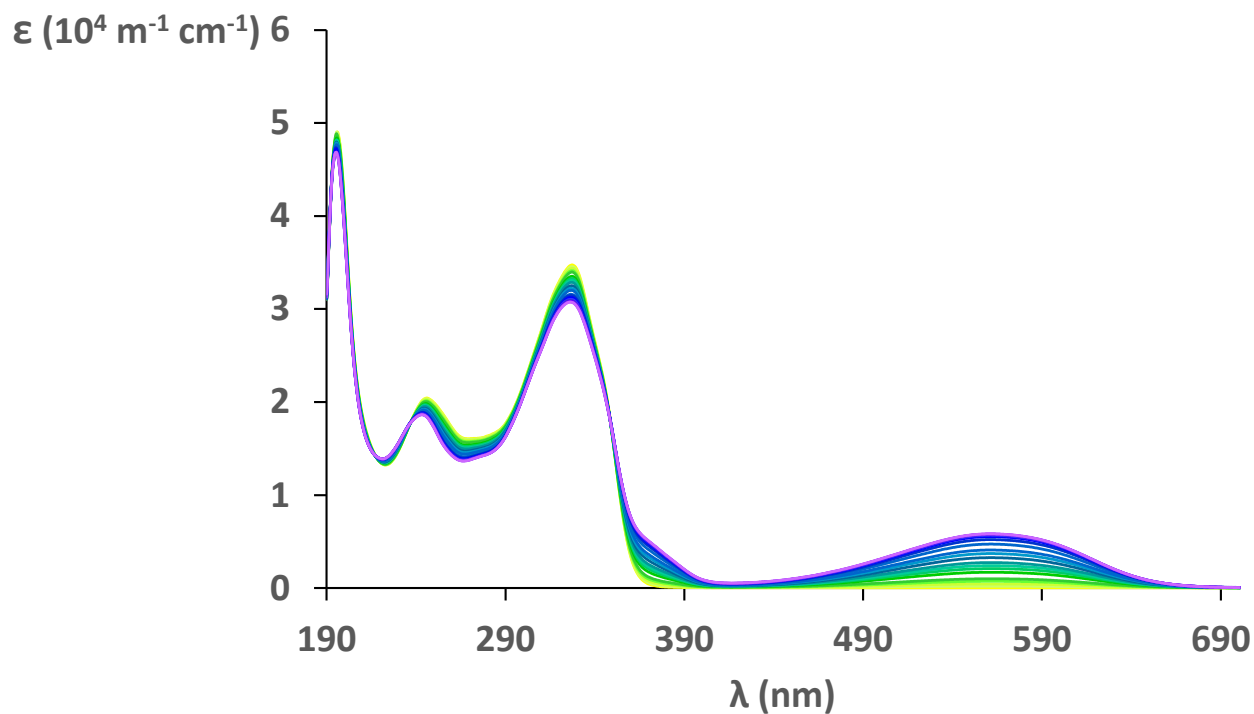
**Figure S100**. UV/Vis kinetic of **L3-A** in CH₃CN irradiating at 370 nm, 5·10⁻⁵M
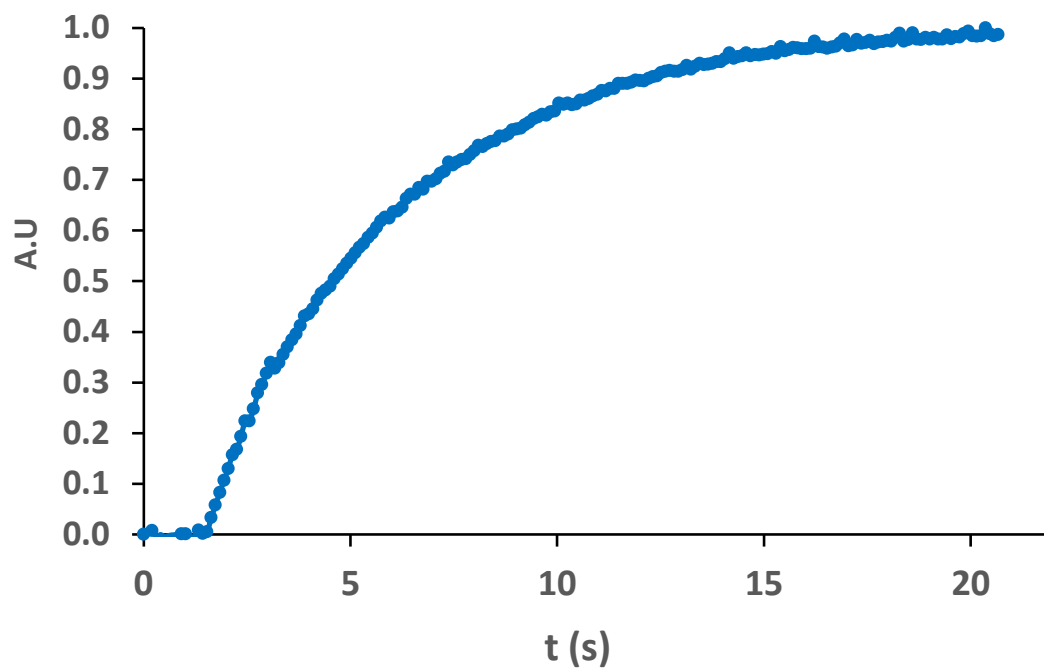
Figure S101. UV/Vis spectra of **L3-A** in CH$_3$CN. Photocyclization process by irradiation at 370 nm, 5.1·10^{-5}M
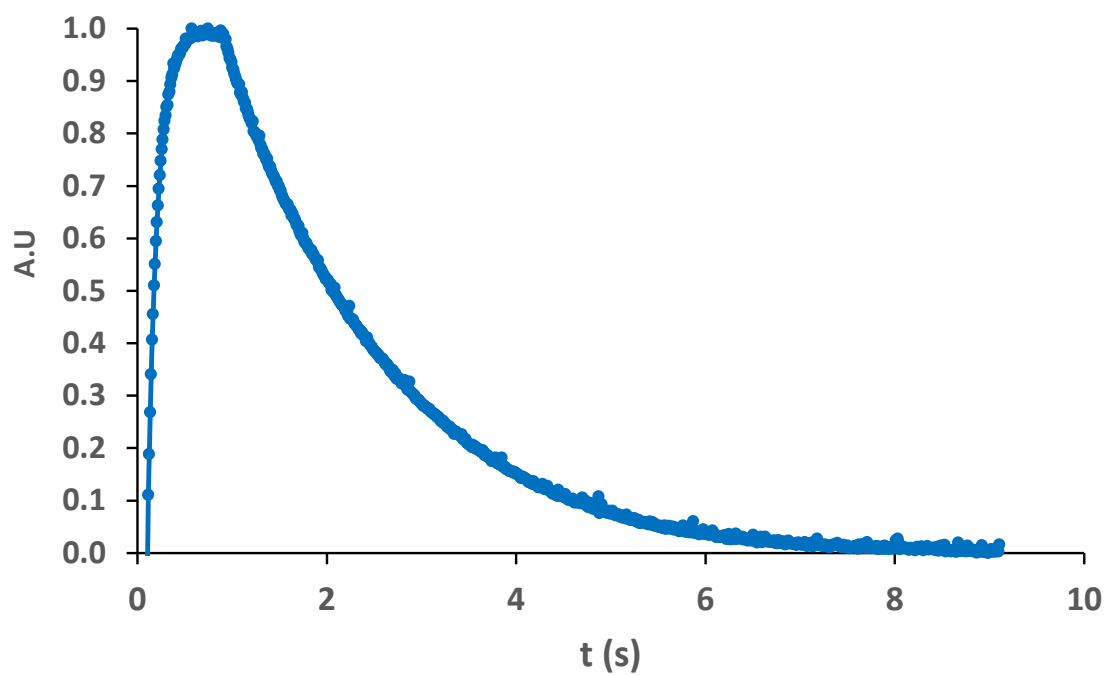


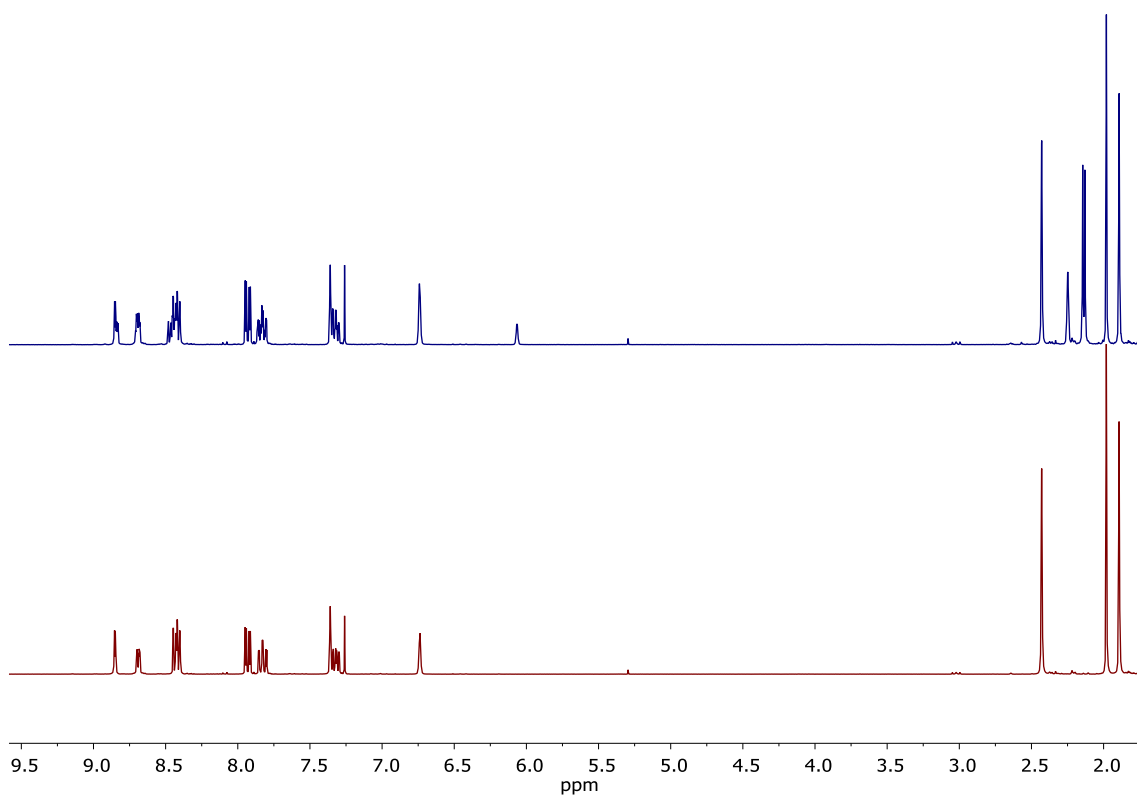**Figure S102**. UV/Vis spectra of **L3-A** in CH$_3$CN. Photocycloreversion process by irradiation at 370 nm, 5.1·10^{-5}M
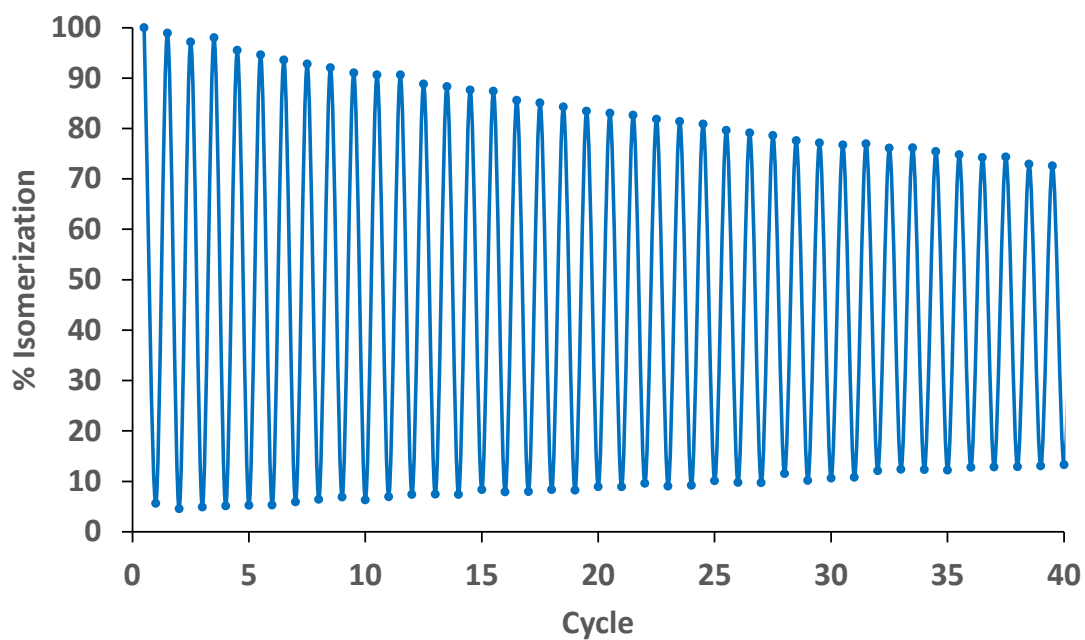
Figure S103. UV/Vis spectra of **L3-A** in CH₃CN. Fatigue resistance experiment by irradiation at 370 nm and 595 nm alternatively, 5.1·10⁻⁵M

3.1.4   3-(2-(5-bromo-2-methylthiophen-3-yl)-3,3,4,4,5,5-hexafluorocyclopent-1-en-1-yl)-2-methylbenzo[*b*]thiophene (L3-B):
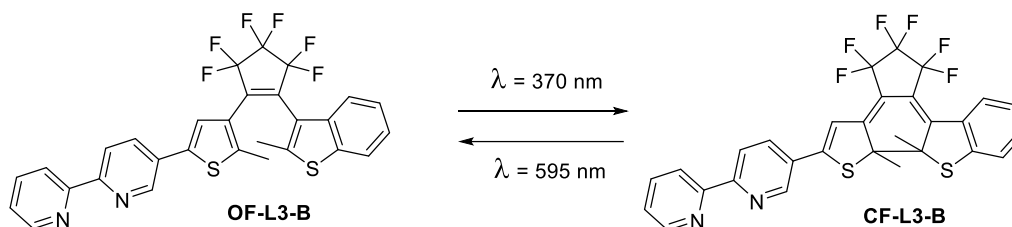
UV/Vis (CH₃CN), λ, nm (ε, 10⁴M⁻¹cm⁻¹): OF: 197 (5.48) 226 (2.90) 261 (2.14) 326 (3.39). **CF:** 195 (5.02) 220 (2.57) 327 (2.91) 418 (0.49) 552 (1.09).
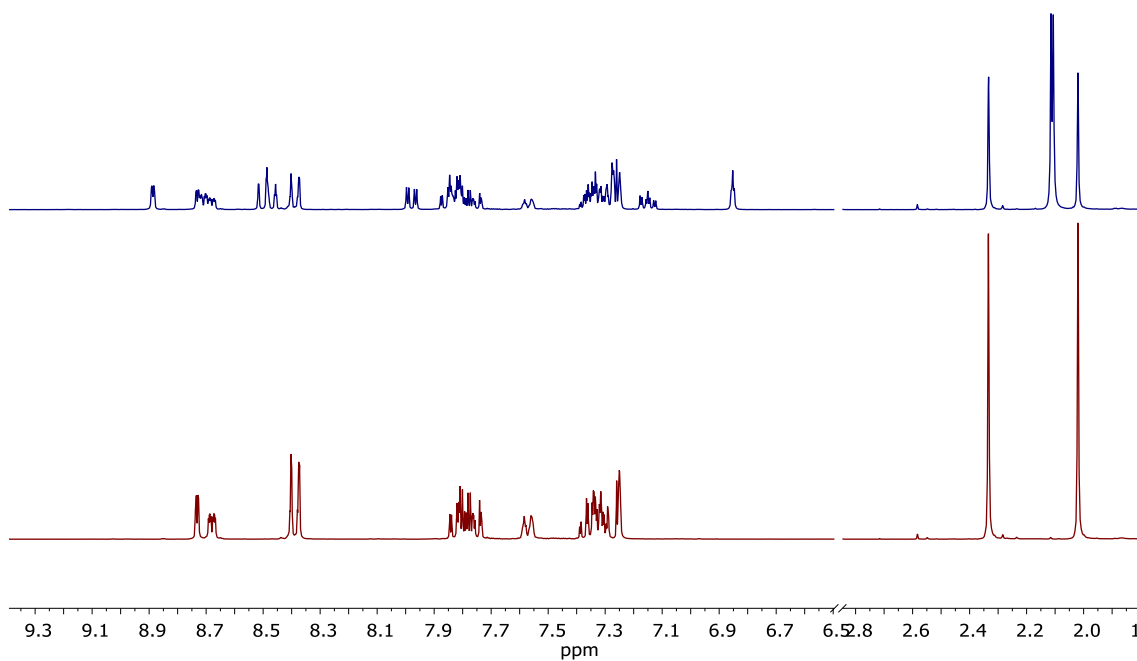
Figure S104. ^{1}H NMR spectra of **L3-B**. Before (red) and after (blue) irradiation at 370 nm. (0.052 M, CDCl$_3$, 300 MHz).
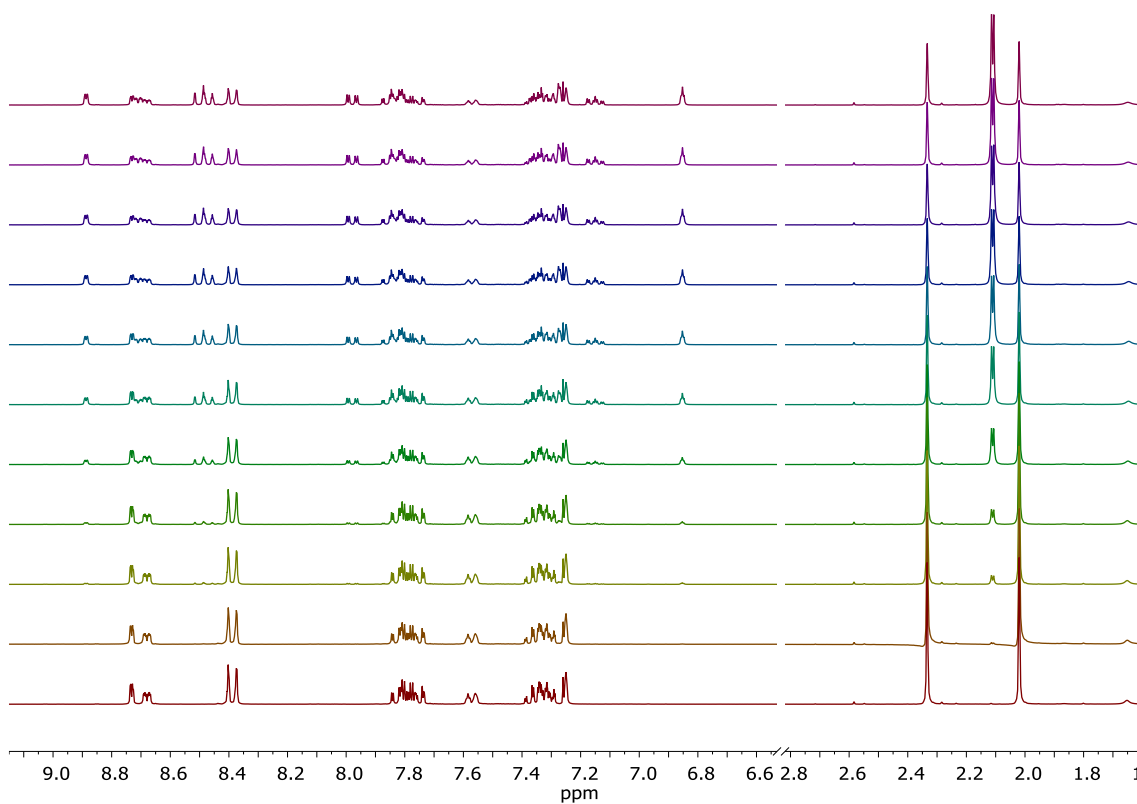
Figure S105. ^{1}H NMR spectra of **L3-B** isomerization kinetics irradiating at 370 nm. (0.052 M, CDCl$_3$, 300 MHz).
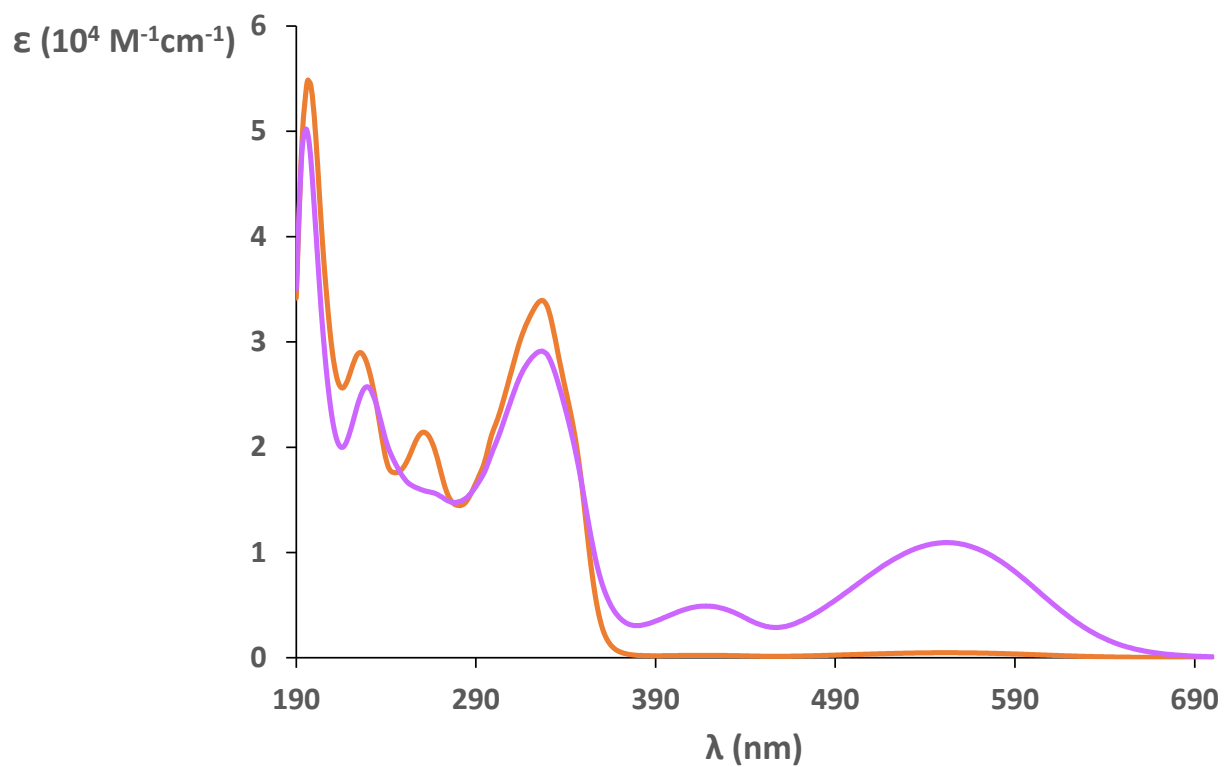
Figure S106. UV/Vis spectra of **L3-B** in CH₃CN. Before (orange line) and after (purple line) irradiation at 370 nm, 5·10⁻⁵M
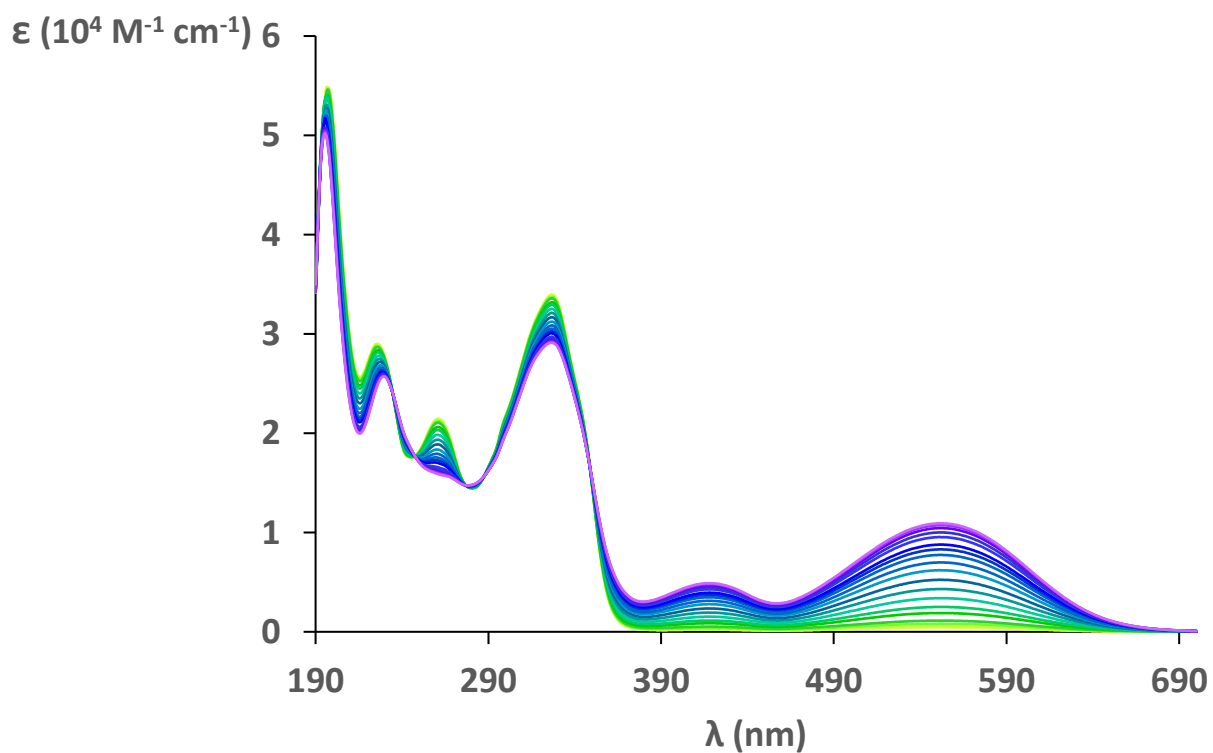
Figure S107. UV/Vis kinetic of **L3-B** in CH₃CN irradiating at 370 nm, 5·10⁻⁵M
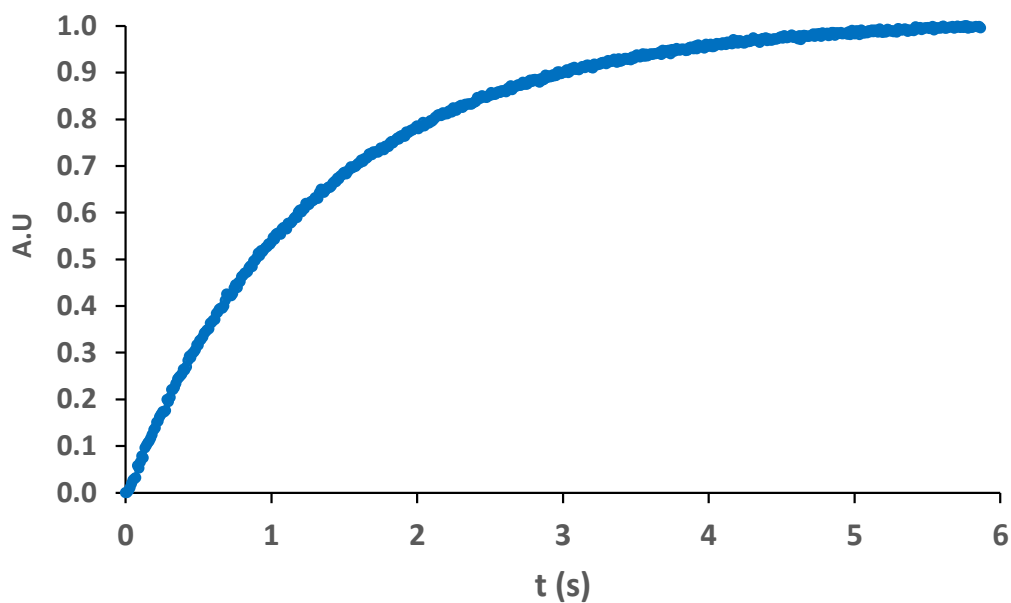
Figure S108. UV/Vis spectra of **L3-B** in CH$_3$CN. Photocyclization process by irradiation at 370 nm, 2.7·10^{-5}M
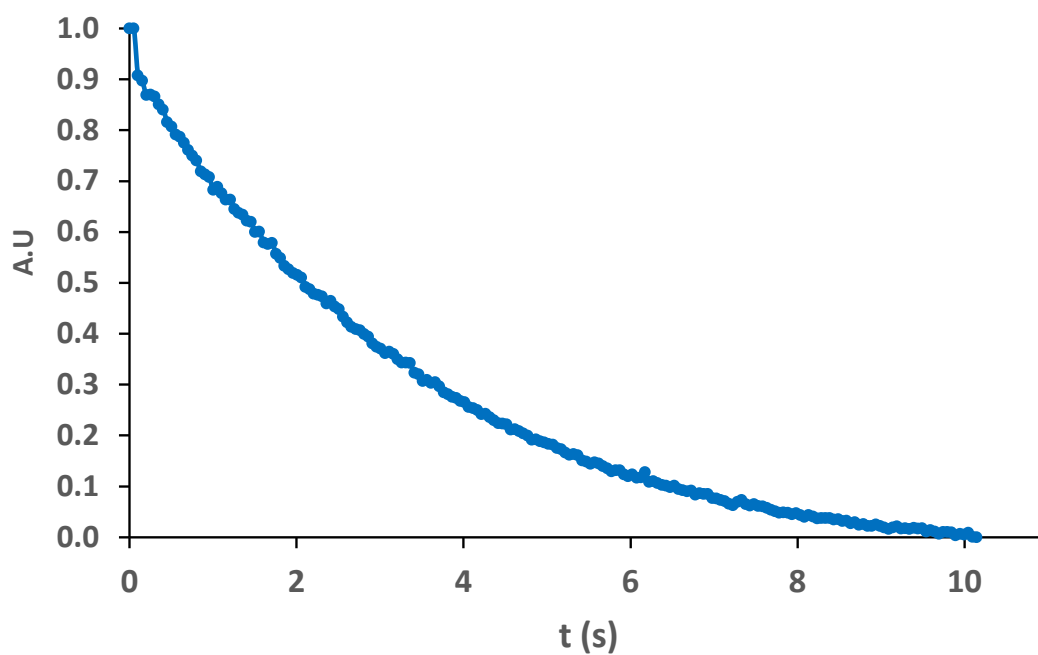
Figure S109. UV/Vis spectra of **L3-B** in CH$_3$CN. Photocycloreversion process by irradiation at 370 nm, 2.7·10^{-5}M
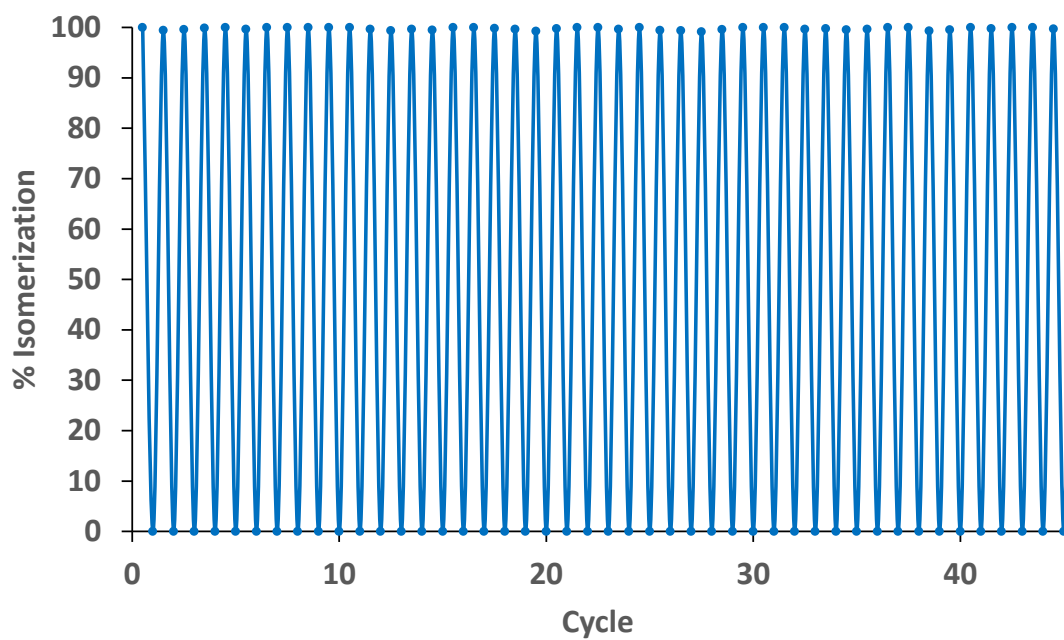
Figure S110. UV/Vis spectra of **L3-B** in CH₃CN. Fatigue resistance experiment by irradiation at 370 nm and 595 nm alternatively, $2.7·10^{-5}$M
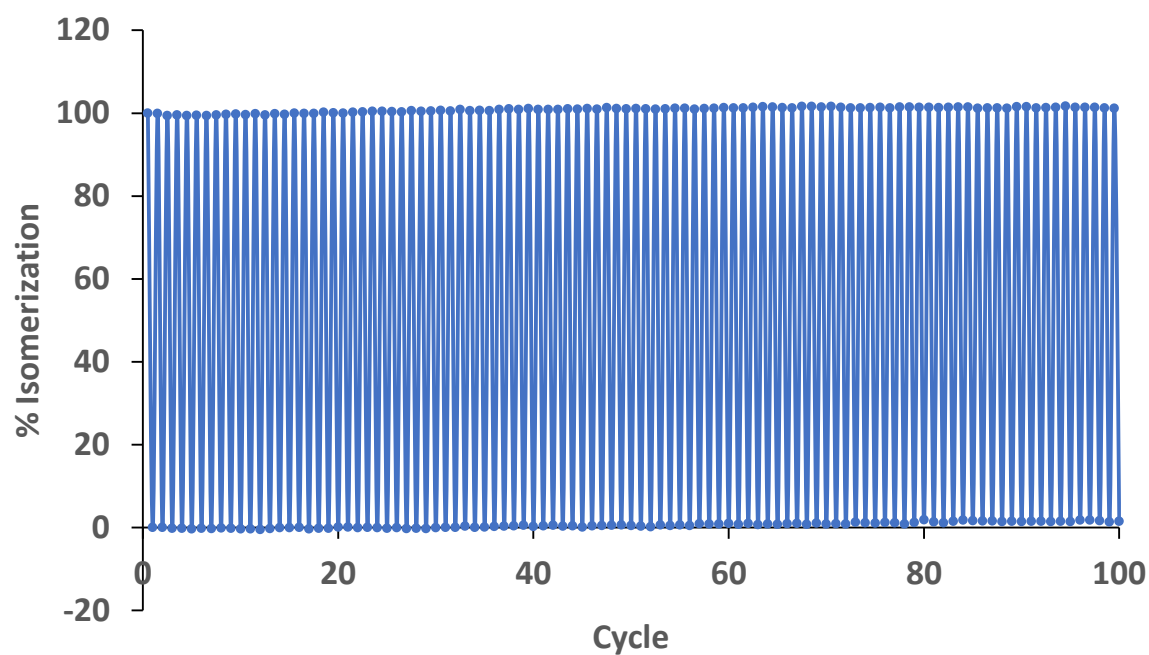
Figure S111. UV/Vis spectra of **L3-B** in CH₃CN. Fatigue resistance experiment by irradiation at 370 nm and 595 nm alternatively, $2.7·10^{-5}$M

3.2 COMPLEXES

3.2.1 [Ir(ppy)₂(L2-A)]PF6 (Ir-L2-A):
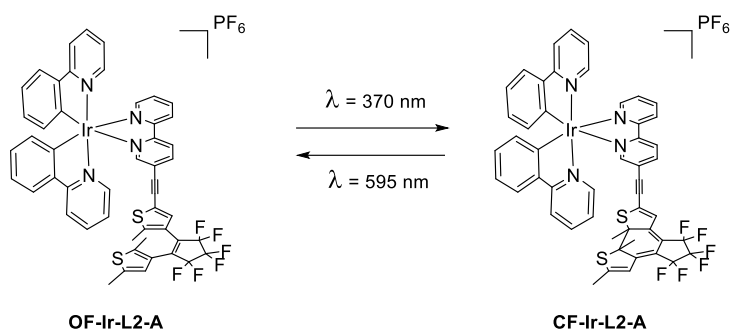
OF-Ir-L2-A   CF-Ir-L2-A

UV/Vis (CH₃CN), λ, nm (ε, 10⁴M⁻¹cm⁻¹): OF: 200 (5.85) 253 (4.88) 330 (2.71) 350. **CF:** 198 (5.58) 254 (4.38) 331 (3.48) 581 (1.31).
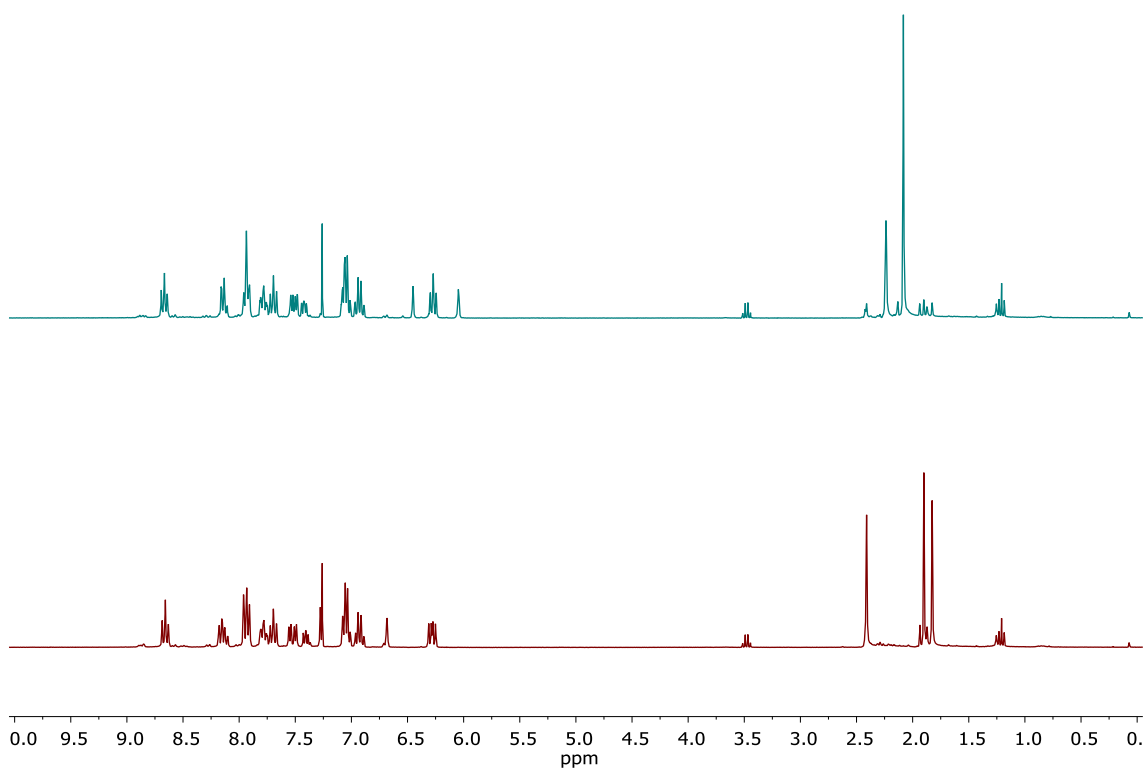
Figure S112. ¹H NMR spectra of **Ir-L2-A**. Before (red) and after (blue) irradiation at 370 nm. (0.018 M, CDCl₃, 300 MHz).
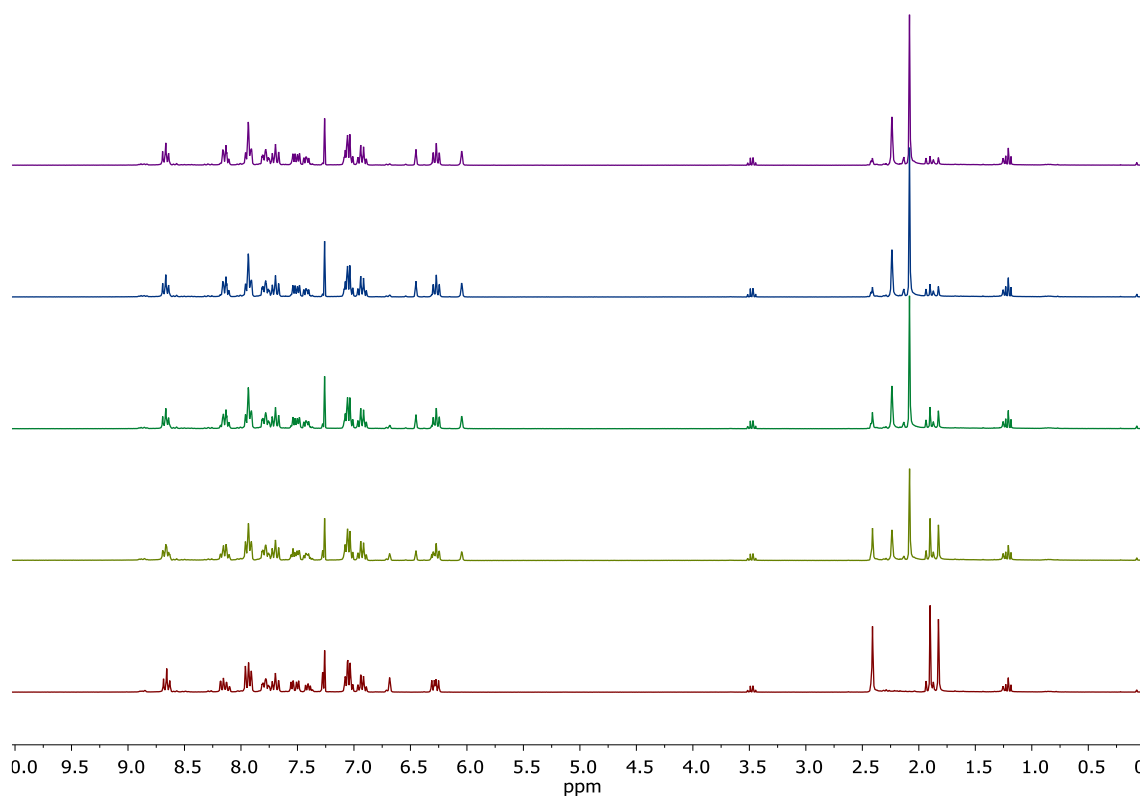
Figure S113. ^{1}H NMR spectra of **Ir-L2-A** isomerization kinetics irradiating at 370 nm. (0.018 M, CDCl$_3$, 300 MHz).
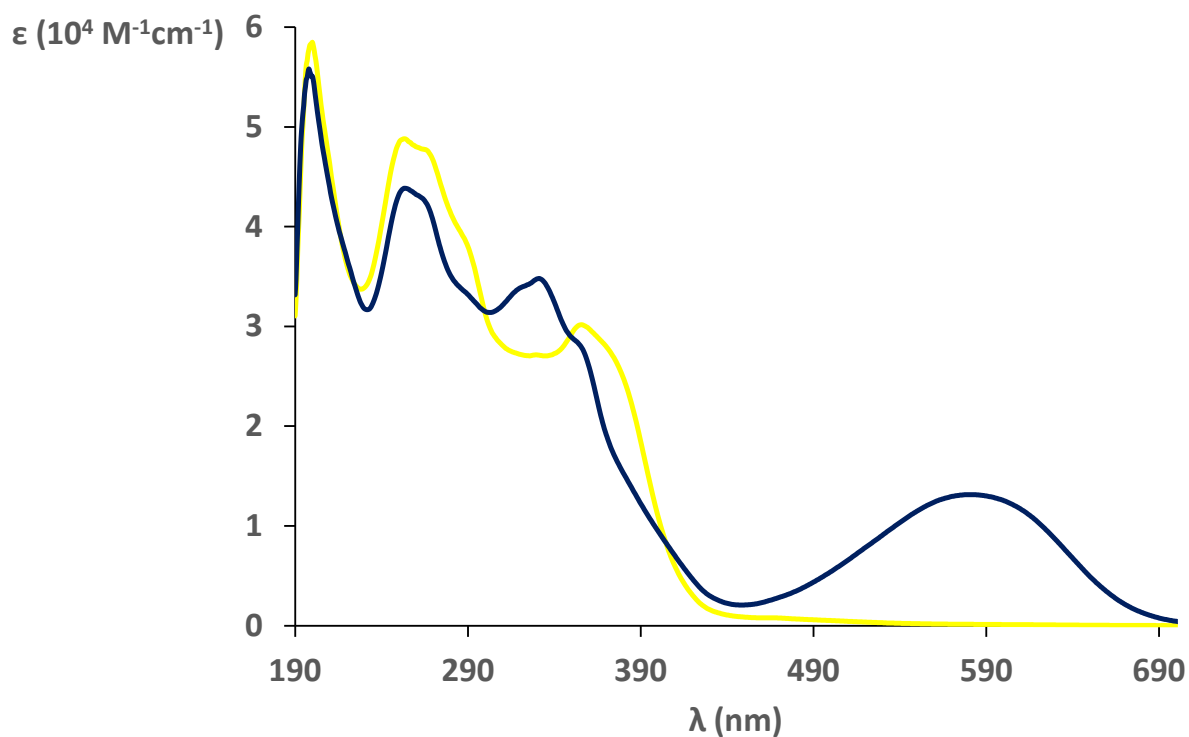

Figure S114. UV/Vis spectra of **Ir-L2-A** in CH$_3$CN. Before (yellow line) and after (blue line) irradiation at 370 nm, 5·10^{-5}M
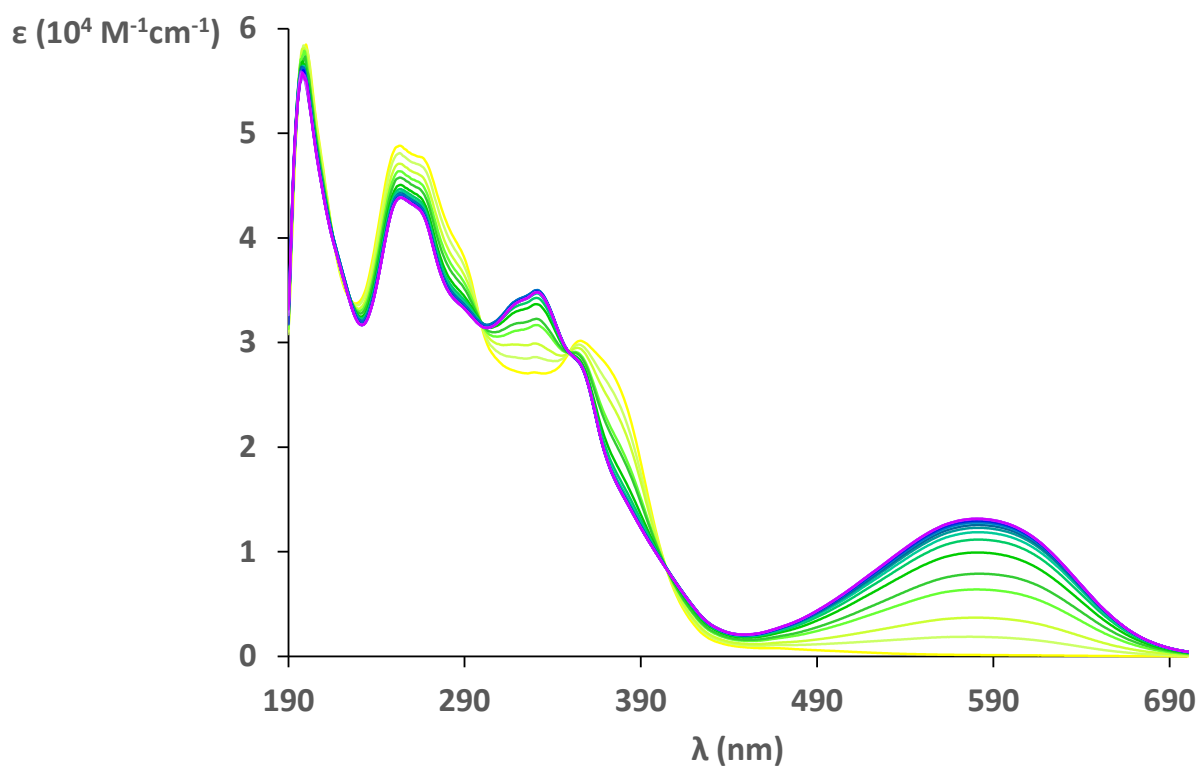
Figure S115. UV/Vis kinetic of **Ir-L2-A** in CH₃CN irradiating at 370 nm, 5·10⁻⁵M
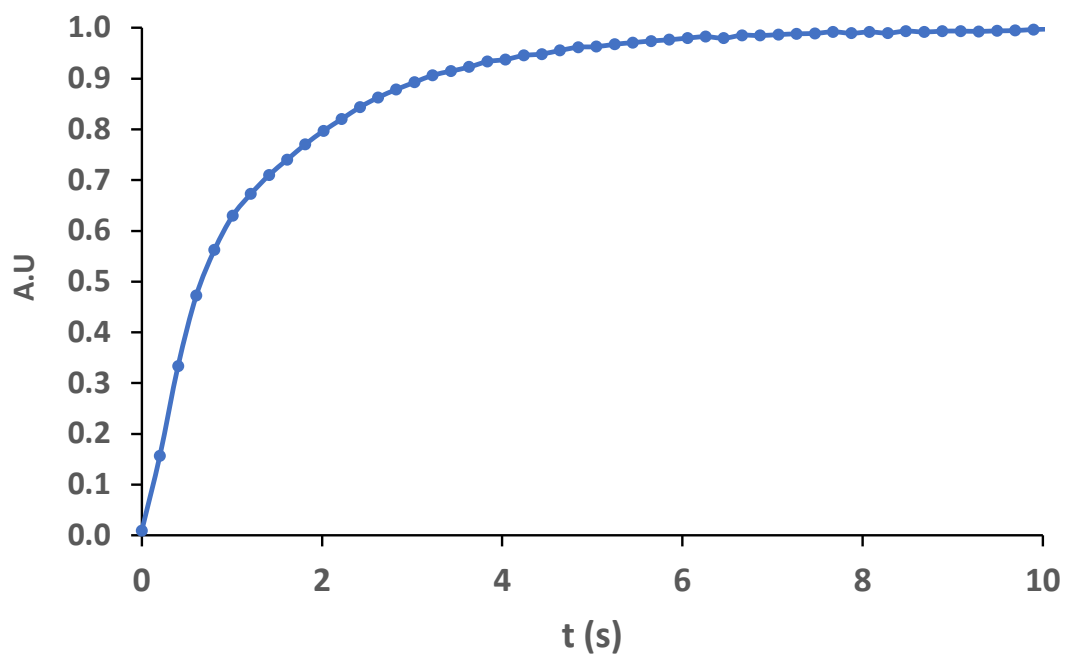
**Figure S116**. UV/Vis spectra of **Ir-L2-A** in CH₃CN. Photocyclization process by irradiation at 370 nm, 2.4·10⁻⁵M
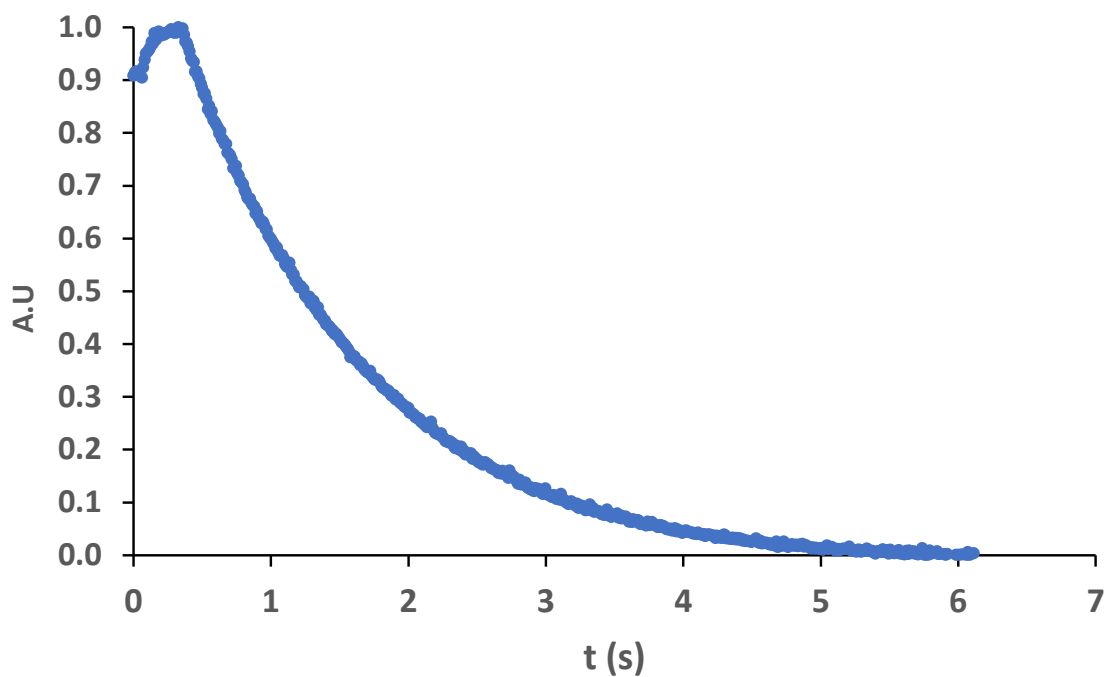
Figure S117. UV/Vis spectra of **Ir-L2-A** in CH$_3$CN. Photocycloreversion process by irradiation at 370 nm, 2.4·10^{-5}M
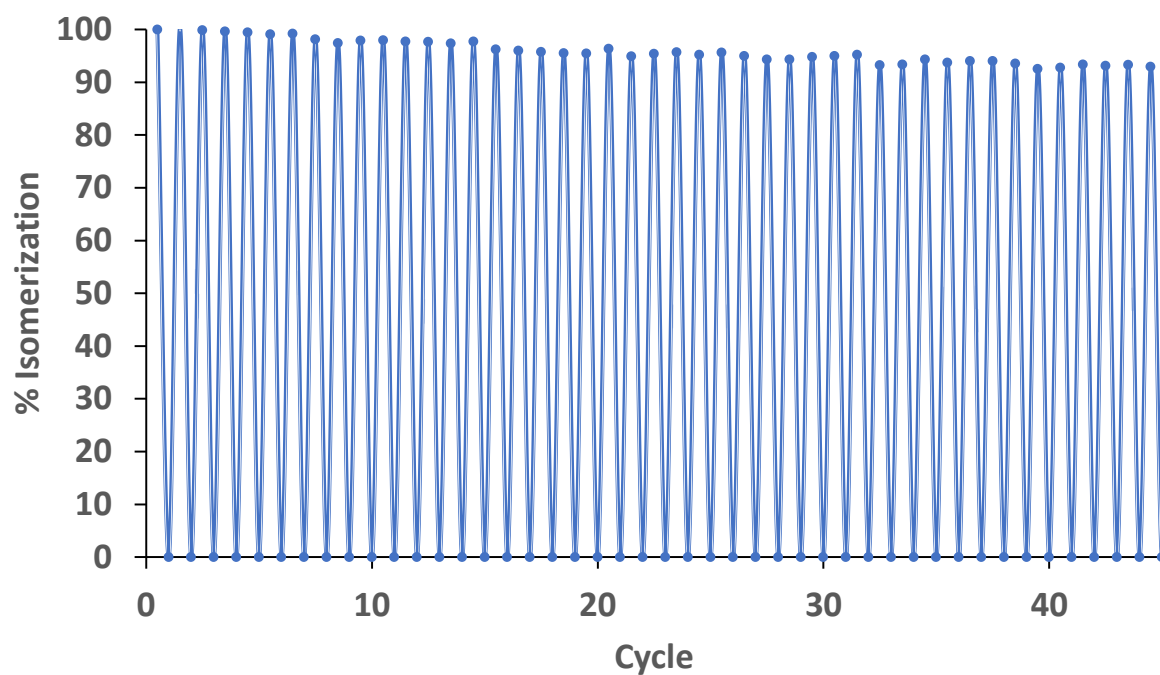
Figure S118. UV/Vis spectra of **Ir-L2-A** in CH$_3$CN. Fatigue resistance experiment by irradiation at 370 nm, 2.4·10^{-5}M

3.2.2 [Ir(ppy)₂(L2-B)]PF6 (Ir-L2-B):
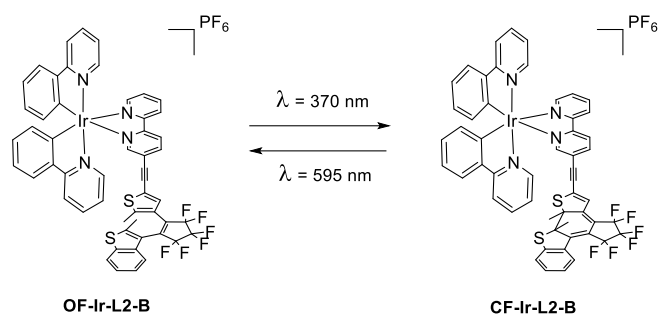
UV/Vis (CH₃CN), λ, nm (ε, 10⁴M⁻¹cm⁻¹): OF: 202 (6.84) 260 (5.24) 356 (2.93). **CF:** 197 (6.55) 254 (4.55) 330 (3.41) 408 (1.04) 562 (1.45).
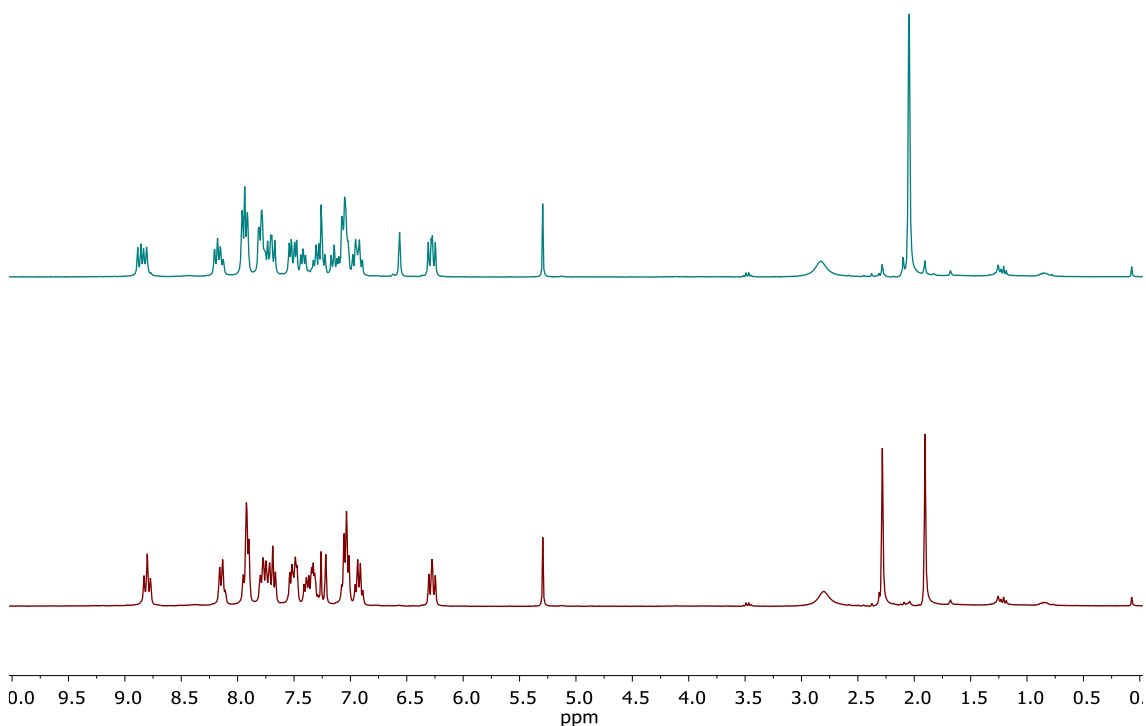
Figure S119. ¹H NMR spectra of **Ir-L2-B**. Before (red) and after (blue) irradiation at 370 nm. (0.024 M, CDCl₃, 300 MHz).
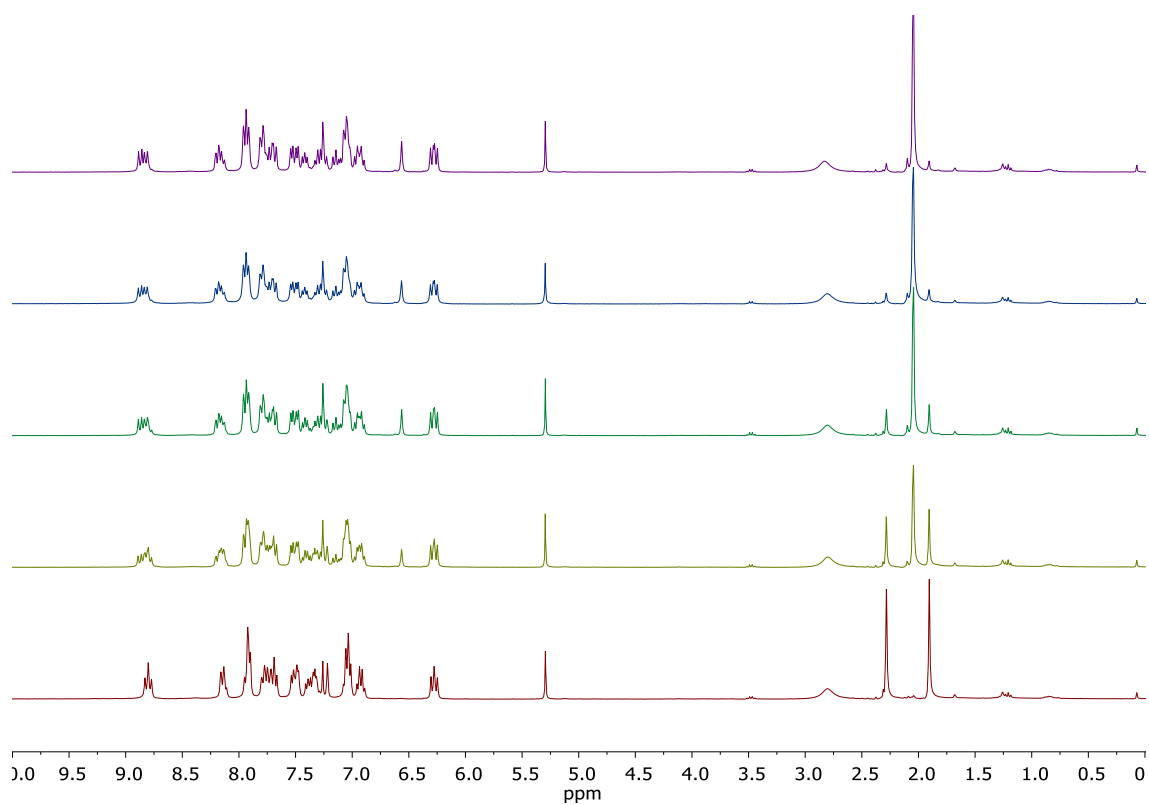
Figure S120. ^{1}H NMR spectra of **Ir-L2-B** isomerization kinetics irradiating at 370 nm. (0.024 M, CDCl$_3$, 300 MHz).
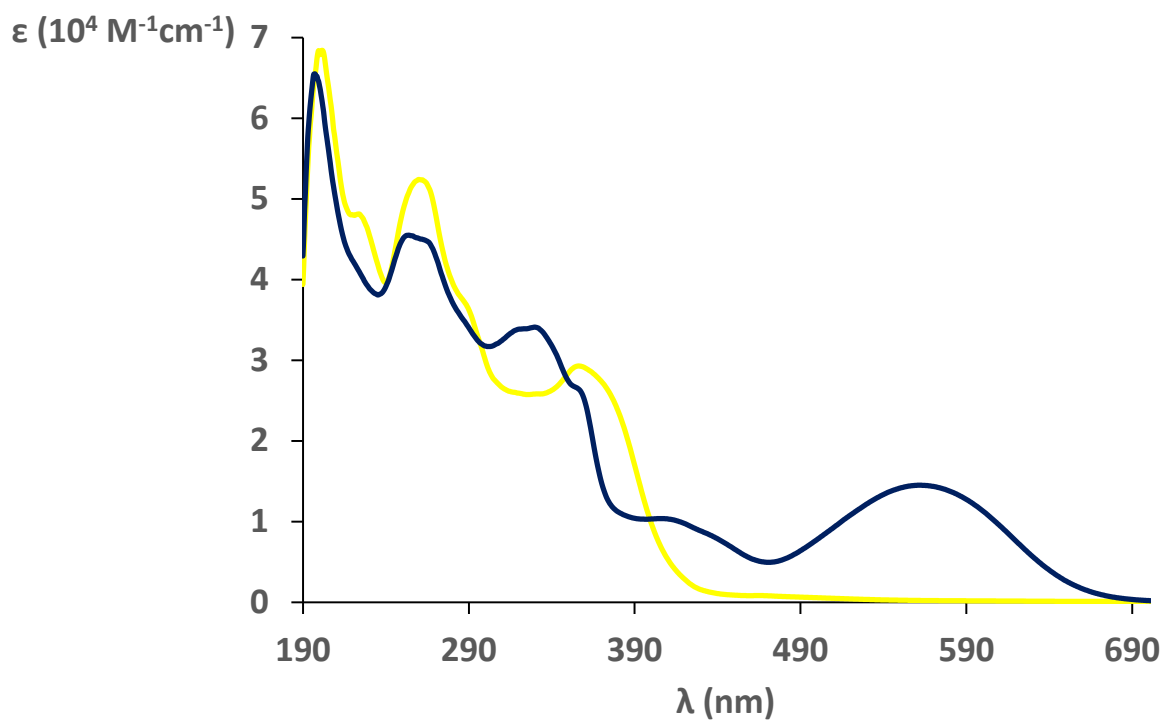
Figure S121. UV/Vis spectra of **Ir-L2-B** in CH$_3$CN. Before (yellow line) and after (blue line) irradiation at 370 nm, 5·10^{-5}M

311
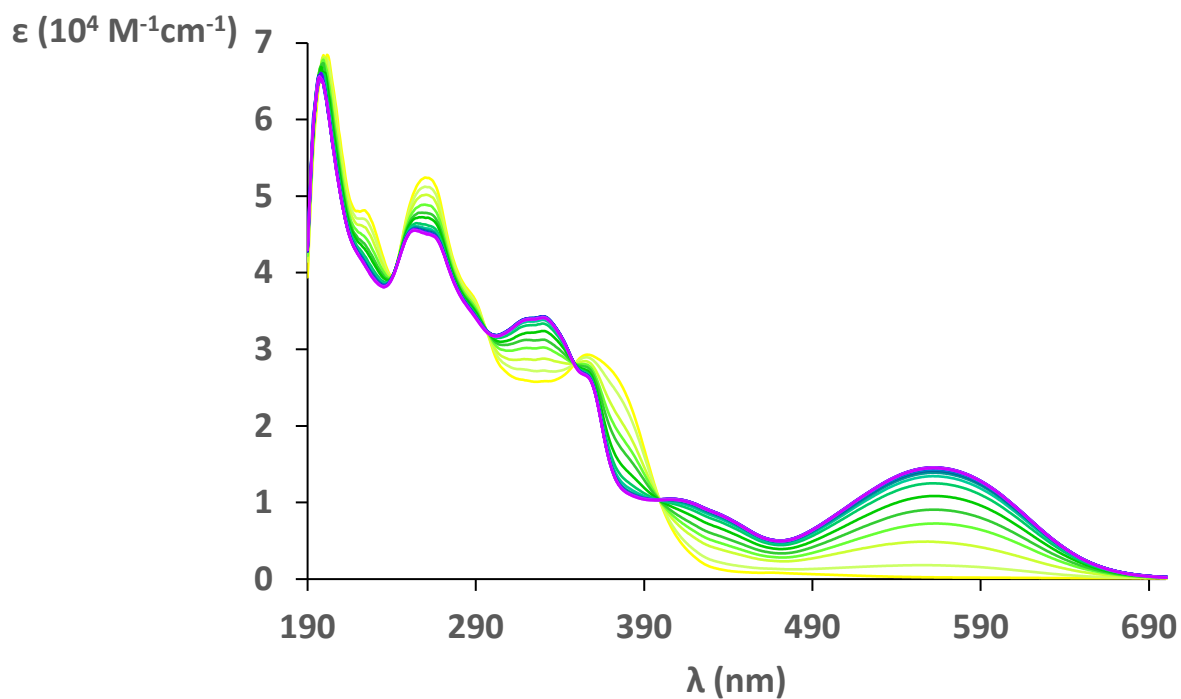
Figure S122. UV/Vis kinetic of **Ir-L2-B** in CH$_3$CN irradiating at 370 nm, 5·10^{-5}M
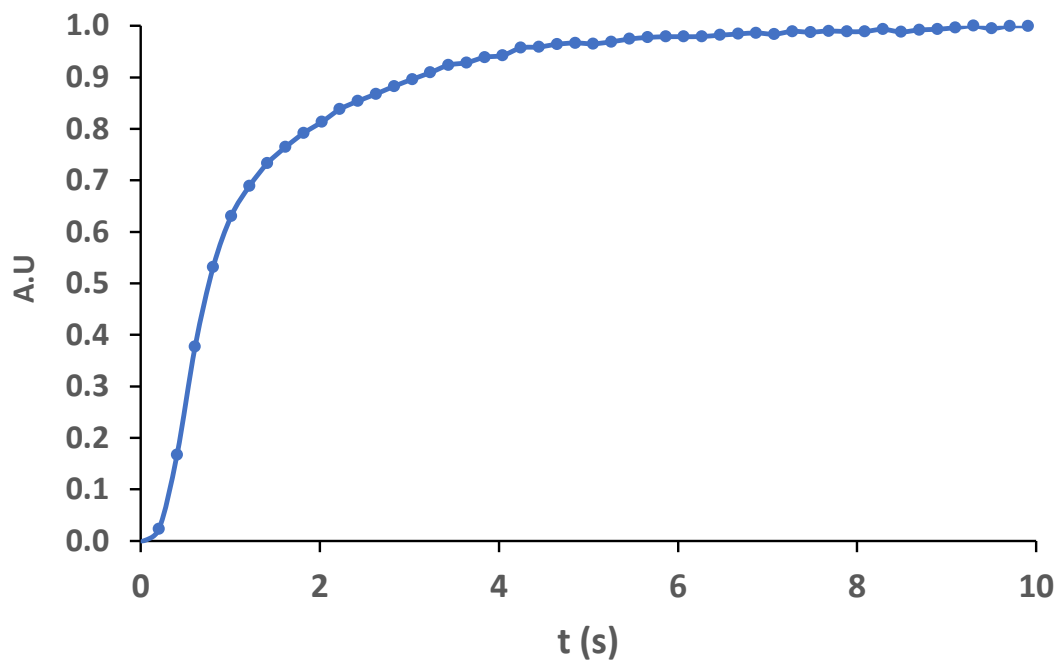
Figure S123. UV/Vis spectra of **Ir-L2-B** in CH$_3$CN. Photocyclization process by irradiation at 370 nm, 2.6·10^{-5}M
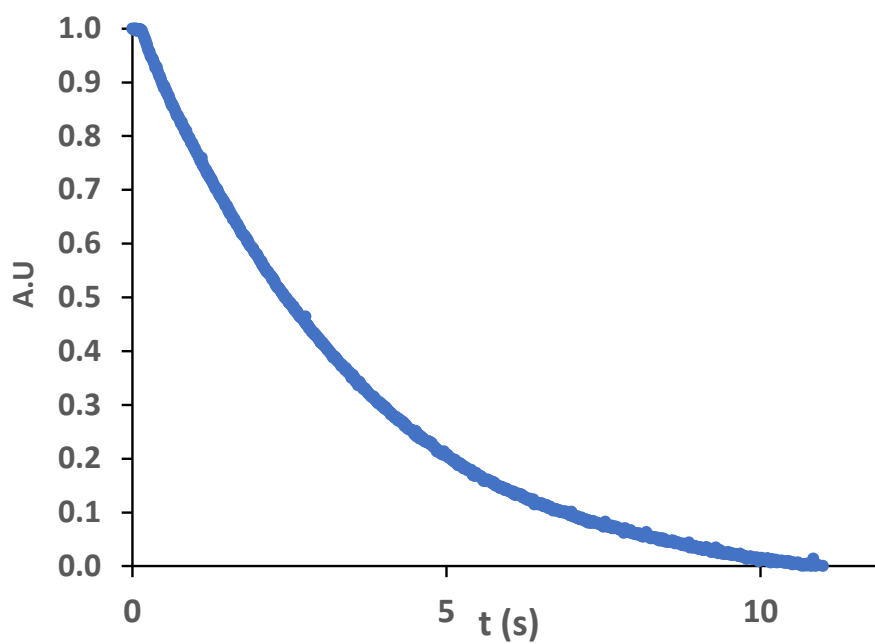
Figure S124. UV/Vis spectra of **Ir-L2-B** in CH$_3$CN. Photocycloreversion process by irradiation at 370 nm, 2.6·10^{-5}M
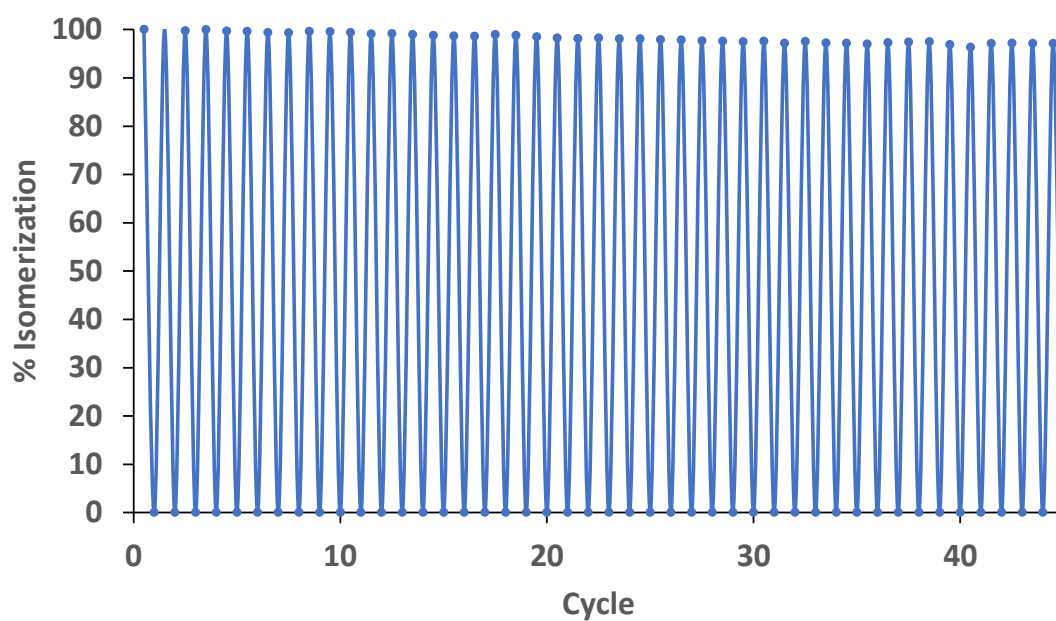
Figure S125. UV/Vis spectra of **Ir-L2-B** in CH$_3$CN. Fatigue resistance experiment by irradiation at 370 nm, 2.6·10^{-5}M

3.2.3 [Ir(ppy)₂(L3-A)]PF6 (Ir-L3-A:

OF-Ir-L3-A   **CF-Ir-L3-A**

λ = 370 nm

λ = 595 nm
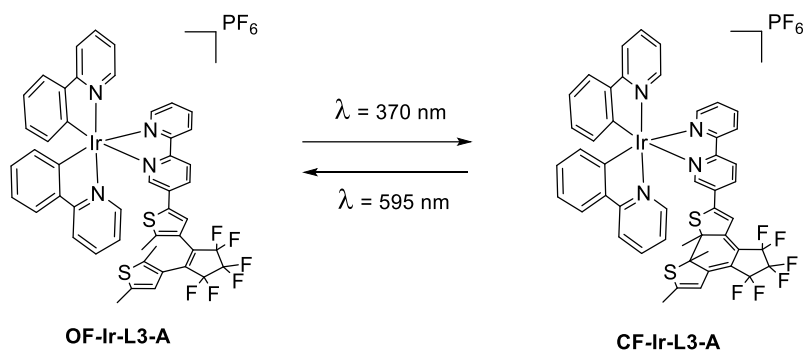
UV/Vis (CH₃CN), λ, nm (ε, 10⁴M⁻¹cm⁻¹): OF: 201 (6.20) 253 (5.29) 354 (2.81). **CF:** 200 (6.21) 252 (469) 313 (3.50) 375 (1.30) 588 (1.29).
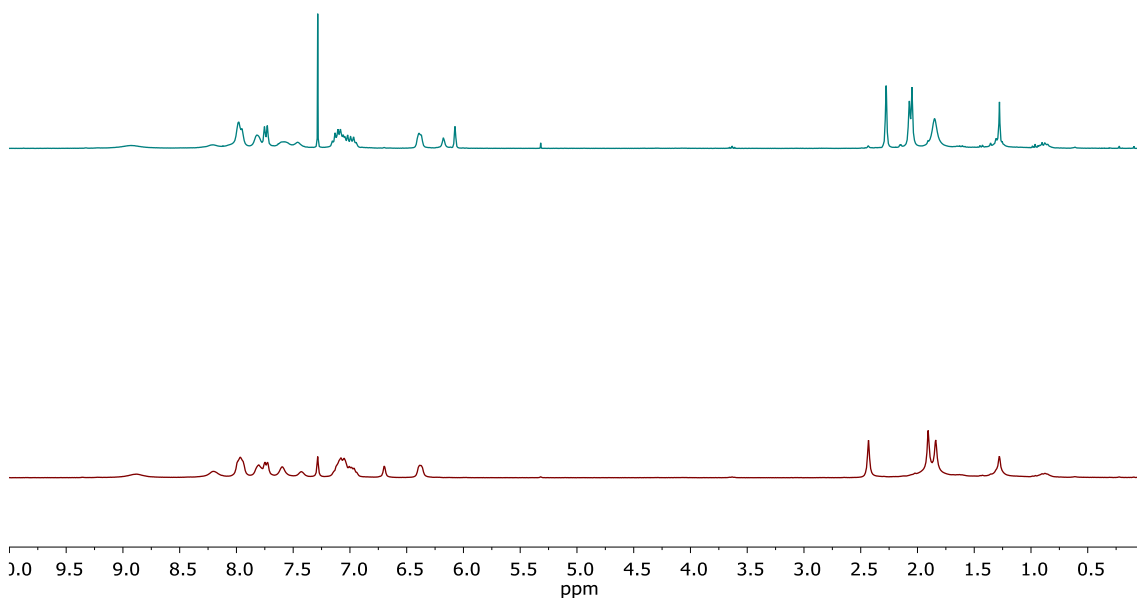
Figure S126. ¹H NMR spectra of **Ir-L3-A**. Before (red) and after (blue) irradiation at 370 nm. (0.016 M, CDCl₃, 300 MHz).
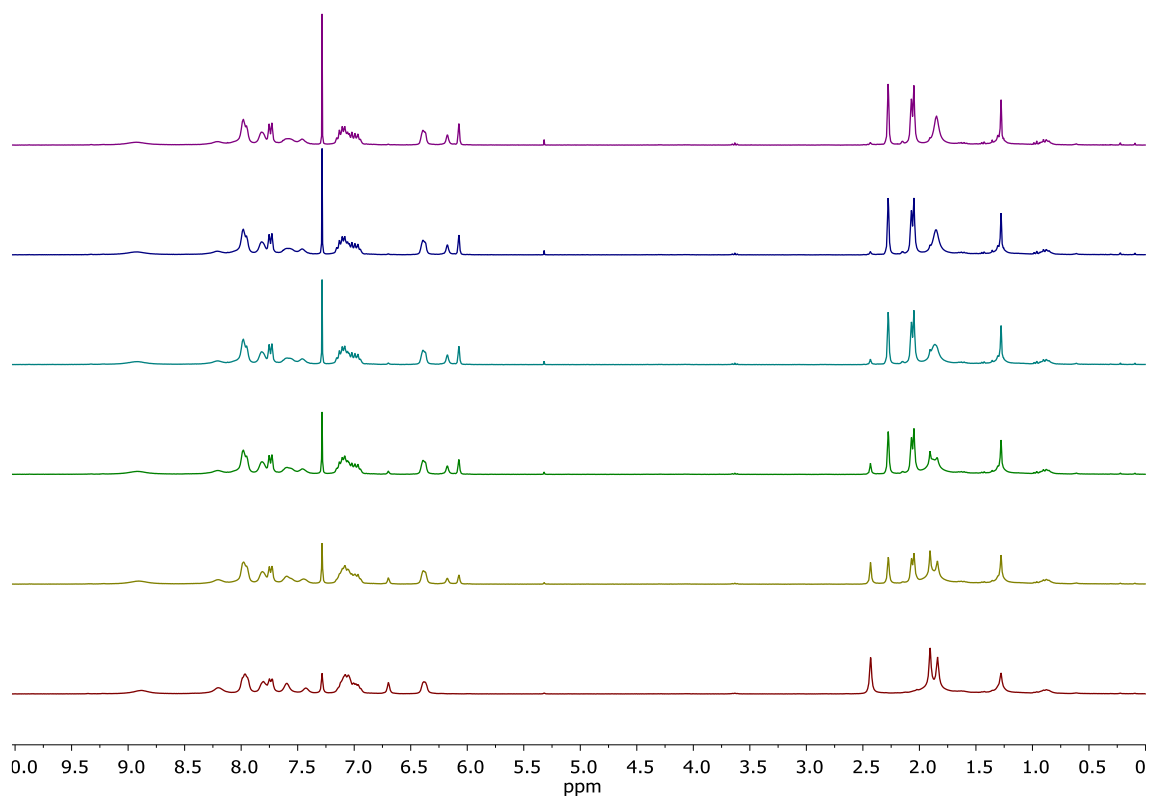
Figure S127. ^{1}H NMR spectra of **Ir-L3-A** isomerization kinetics irradiating at 370 nm. (0.016 M, CDCl$_3$, 300 MHz).
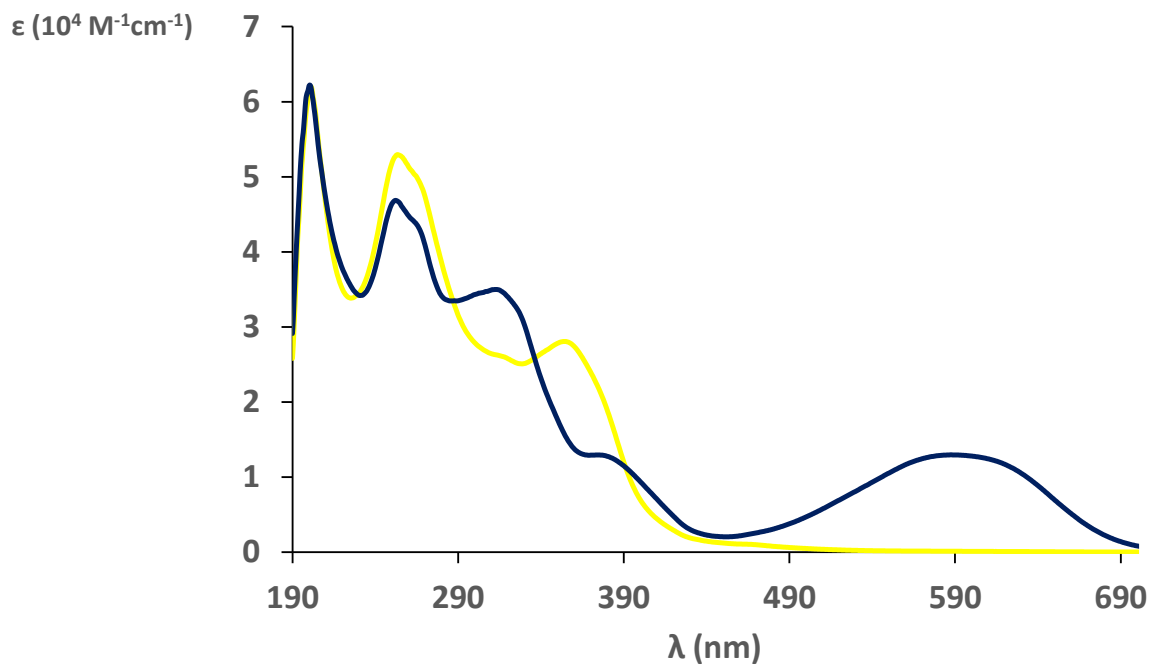
**Figure S128**. UV/Vis spectra of **Ir-L3-A** in CH$_3$CN. Before (yellow line) and after (blue line) irradiation at 370 nm, 5·10^{-5}M
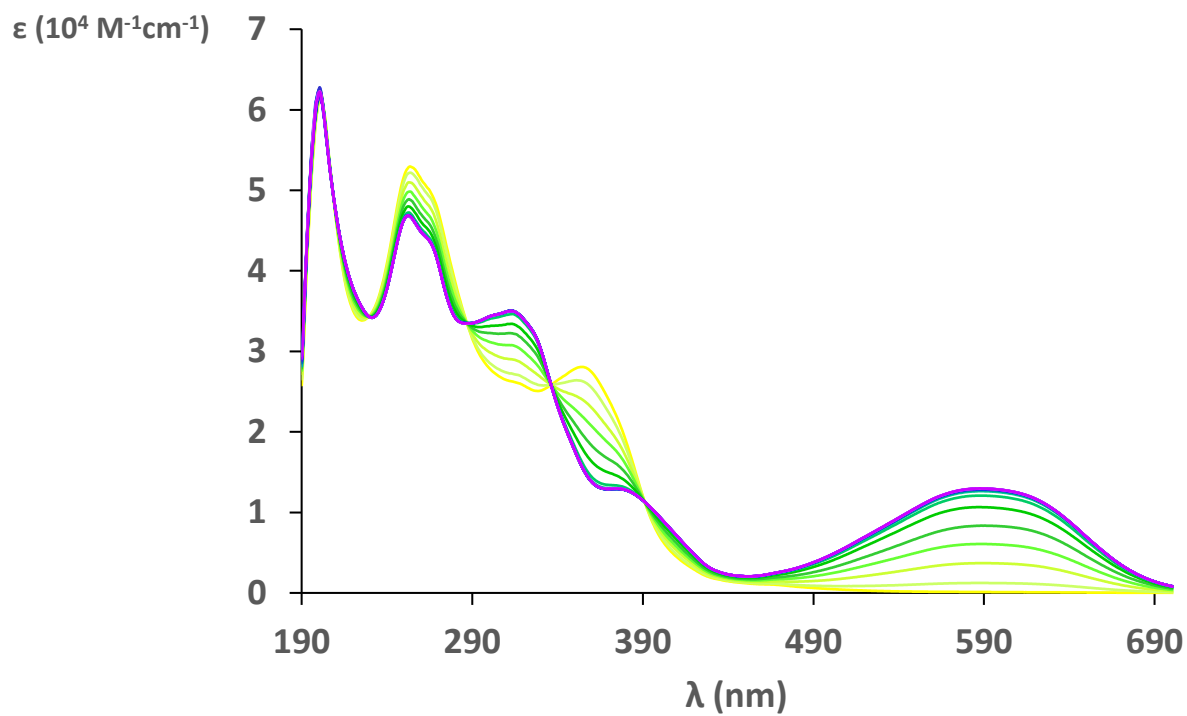
Figure S129. UV/Vis kinetic of **Ir-L2-A** in CH$_3$CN irradiating at 370 nm, 5·10^{-5}M
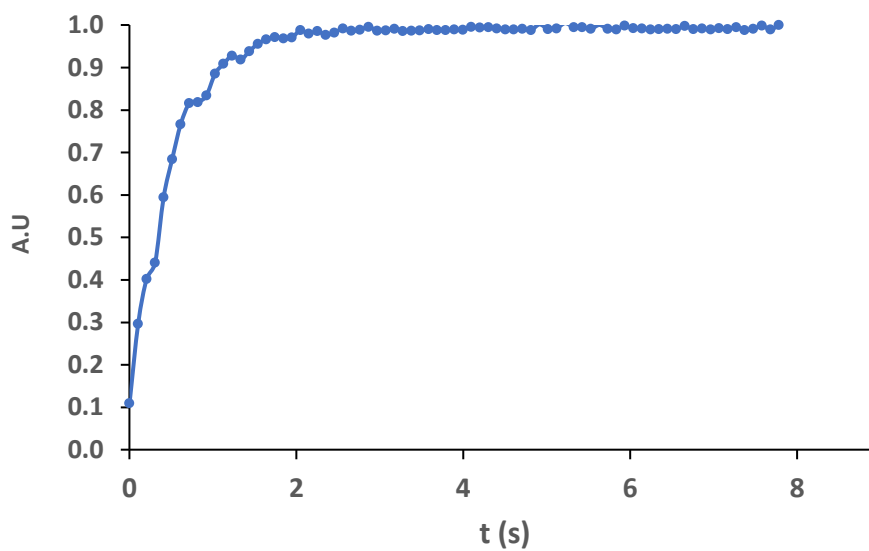
**Figure S130**. UV/Vis spectra of **Ir-L3-A** in CH$_3$CN. Photocyclization process by irradiation at 370 nm, 2.7·10^{-5}M
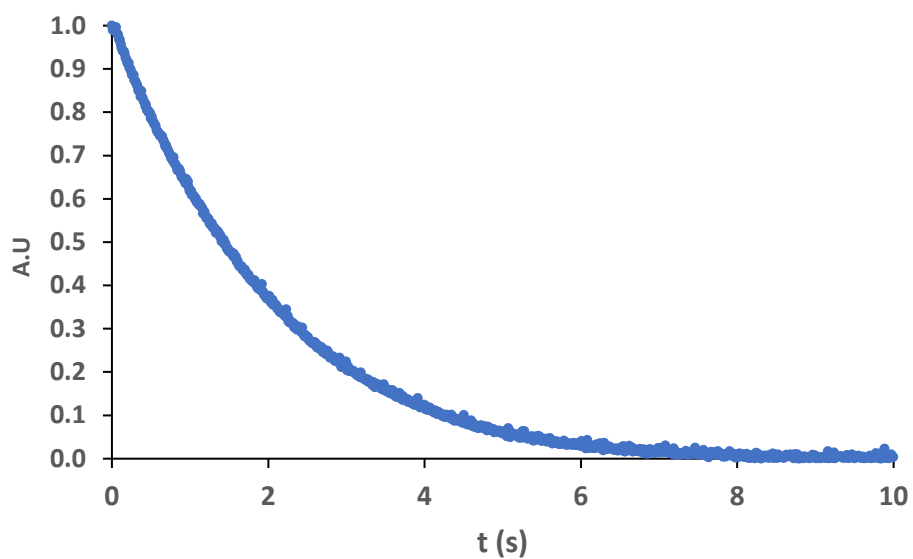
Figure S131. UV/Vis spectra of **Ir-L3-A** in CH$_3$CN. Photocycloreversion process by irradiation at 370 nm, 2.7·10^{-5}M
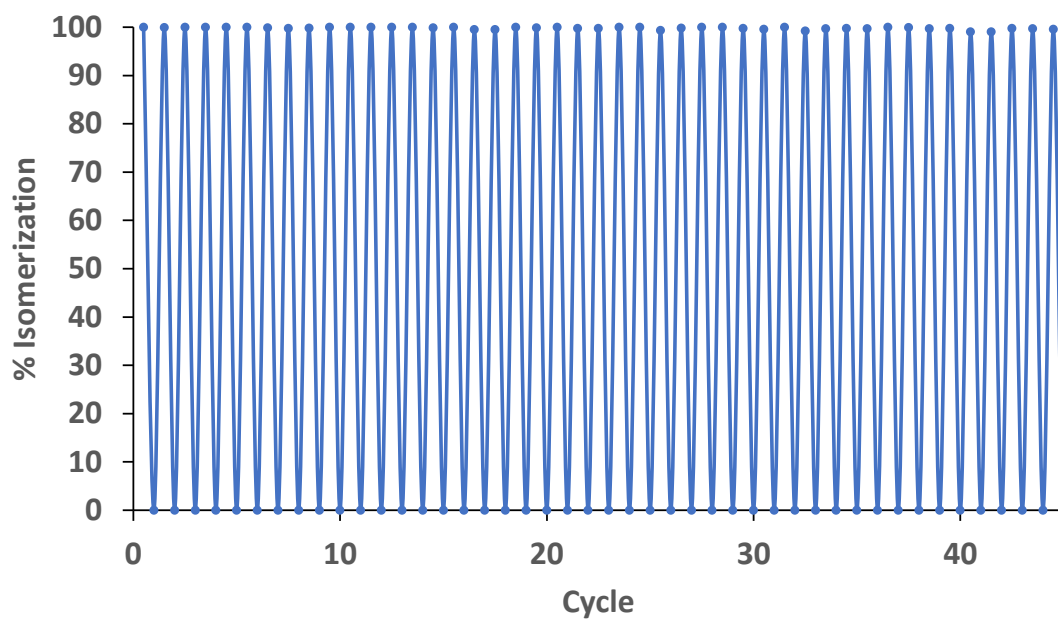
Figure S132. UV/Vis spectra of **Ir-L3-A** in CH$_3$CN. Fatigue resistance experiment by irradiation at 370 nm, 2.7·10^{-5}M

3.2.4 [Ir(ppy)₂(L3-B)]PF6 (Ir-L3-B):
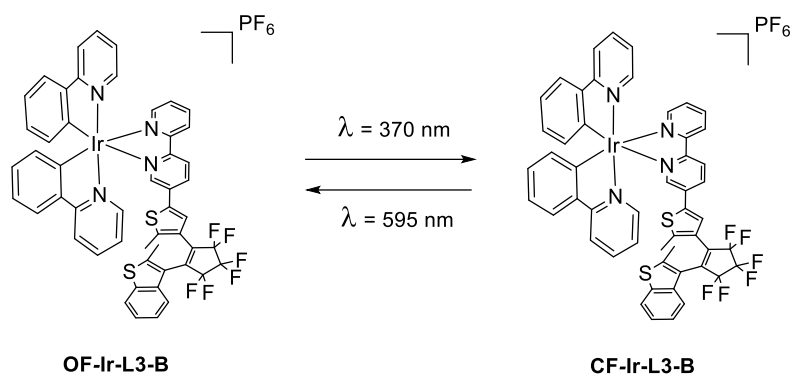
OF-Ir-L3-B $\qquad$ CF-Ir-L3-B

UV/Vis (CH₃CN), λ, nm (ε, 10⁴M⁻¹cm⁻¹): OF: 202 (6.25) 2590 (5.27) 353 (2.77). **CF:** 199 (5.95) 252 (4.53) 316 (3.37) 408 (0.91) 567 (1.44).
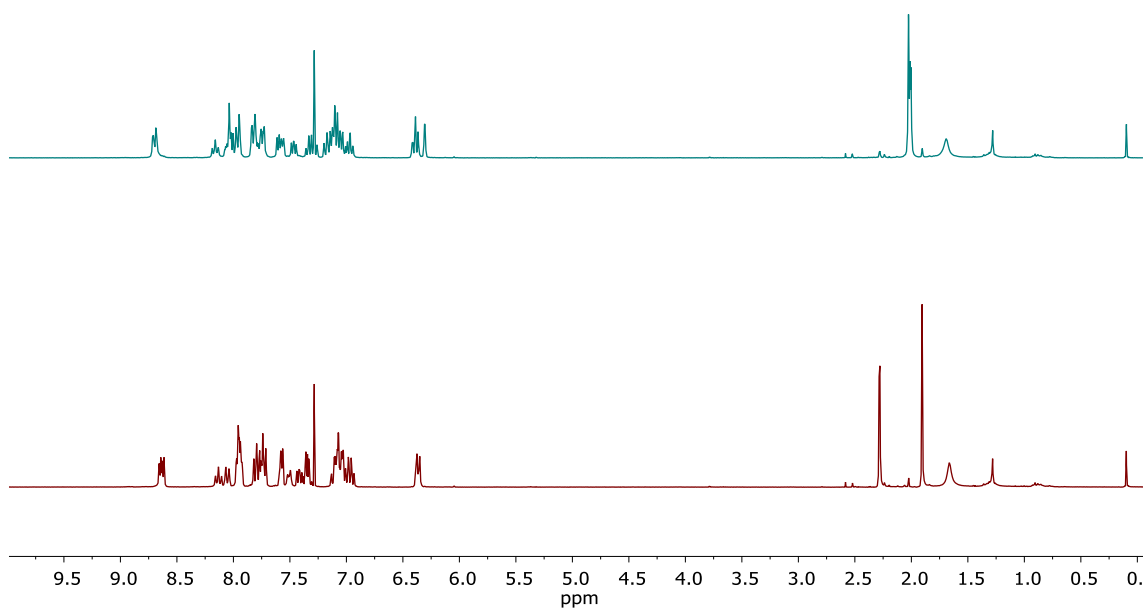
Figure S133. ¹H NMR spectra of **Ir-L3-B**. Before (red) and after (blue) irradiation at 370 nm. (0.027 M, CDCl₃, 300 MHz).
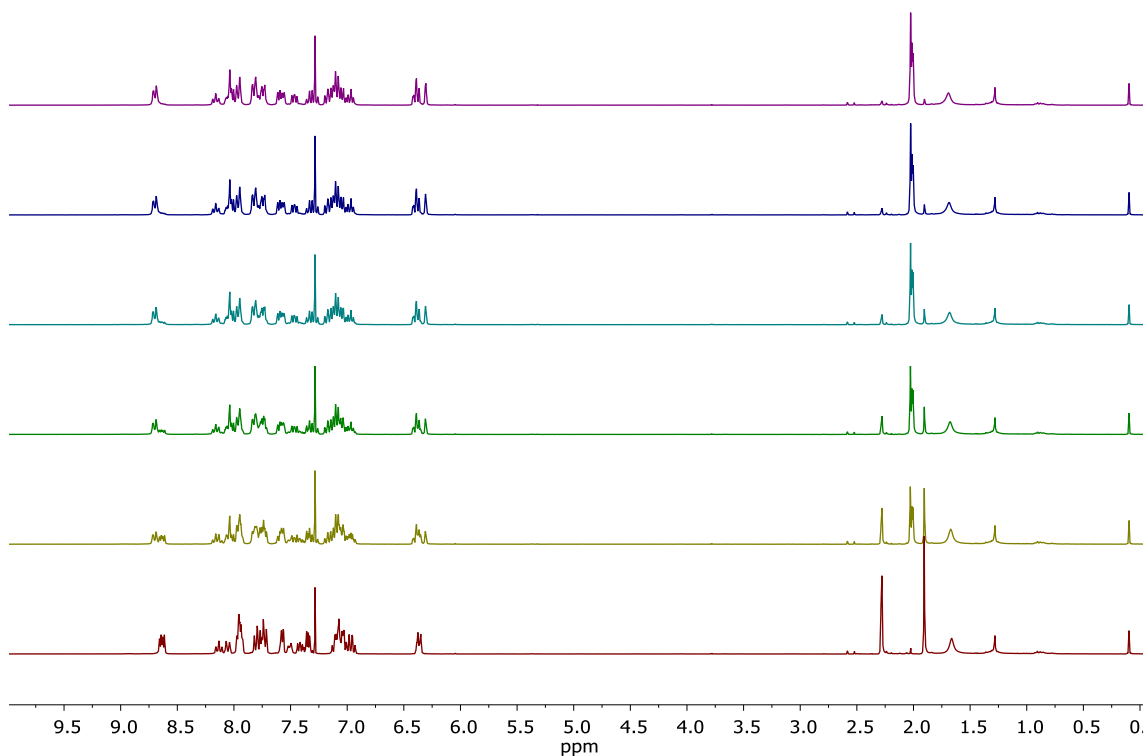
Figure S134. ^{1}H NMR spectra of **Ir-L3-B** isomerization kinetics irradiating at 370 nm. (0.027 M, CDCl$_3$, 300 MHz).
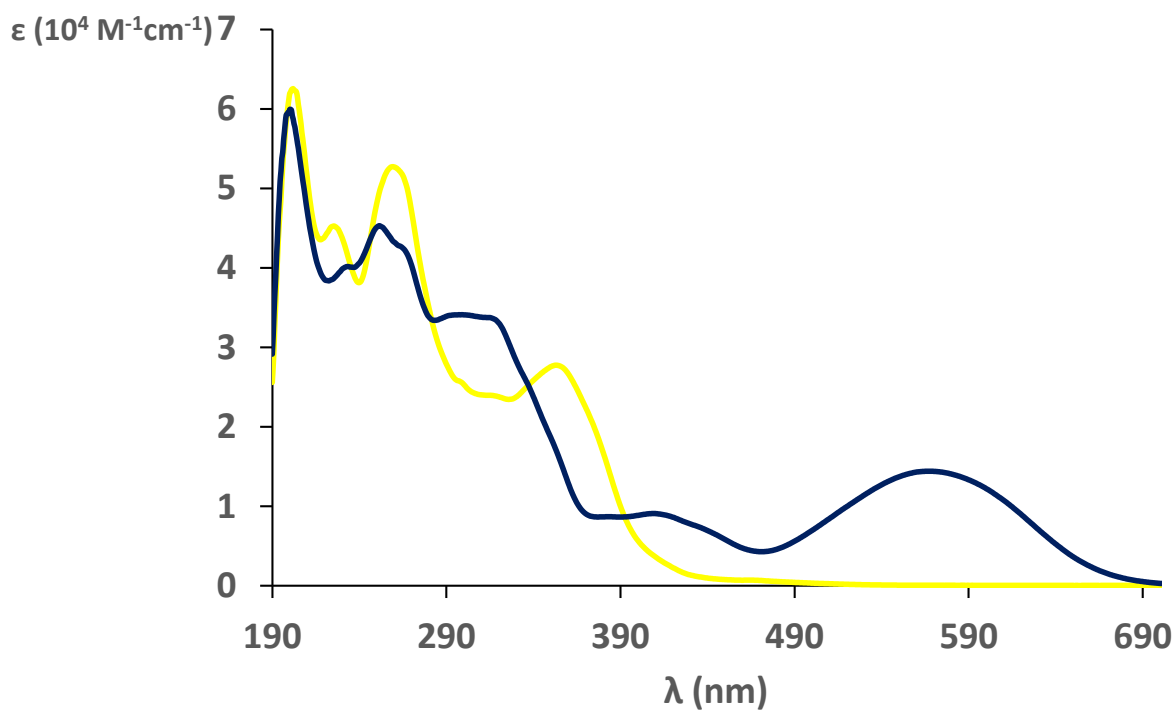
Figure S135. UV/Vis spectra of **Ir-L3-B** in CH$_3$CN. Before (yellow line) and after (blue line) irradiation at 370 nm, 5·10^{-5}M
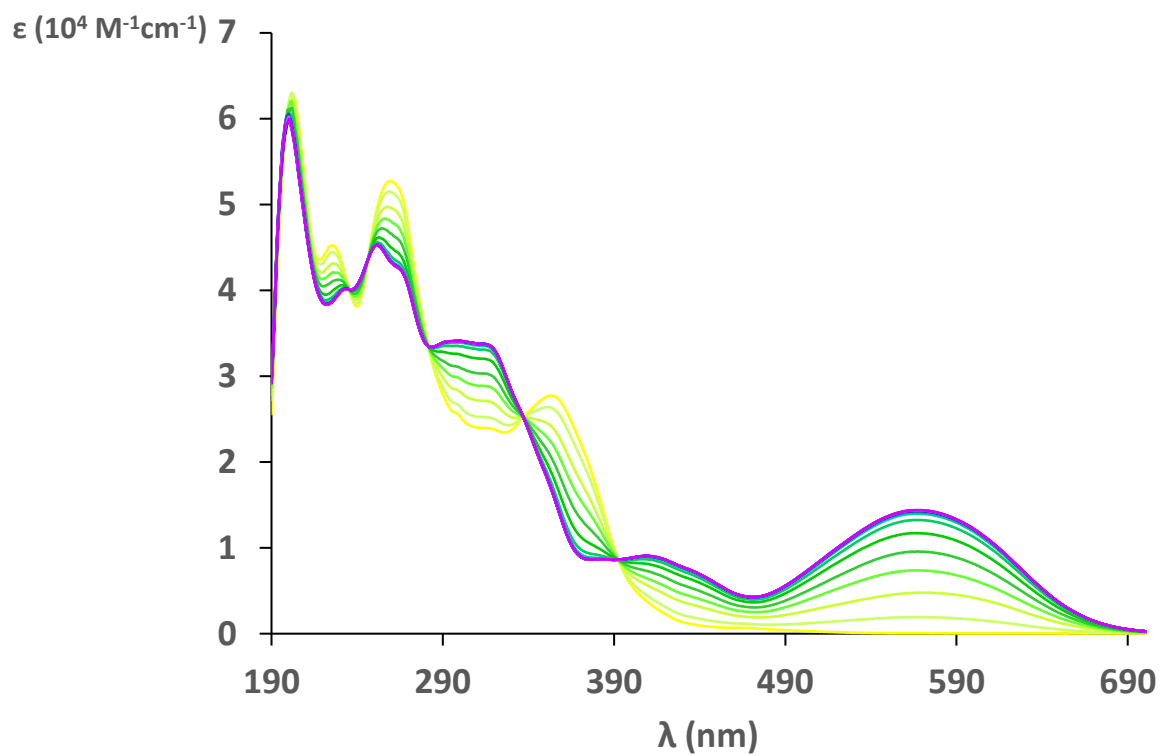
Figure S136. UV/Vis kinetic of **Ir-L3-B** in CH₃CN irradiating at 370 nm, 5·10⁻⁵M
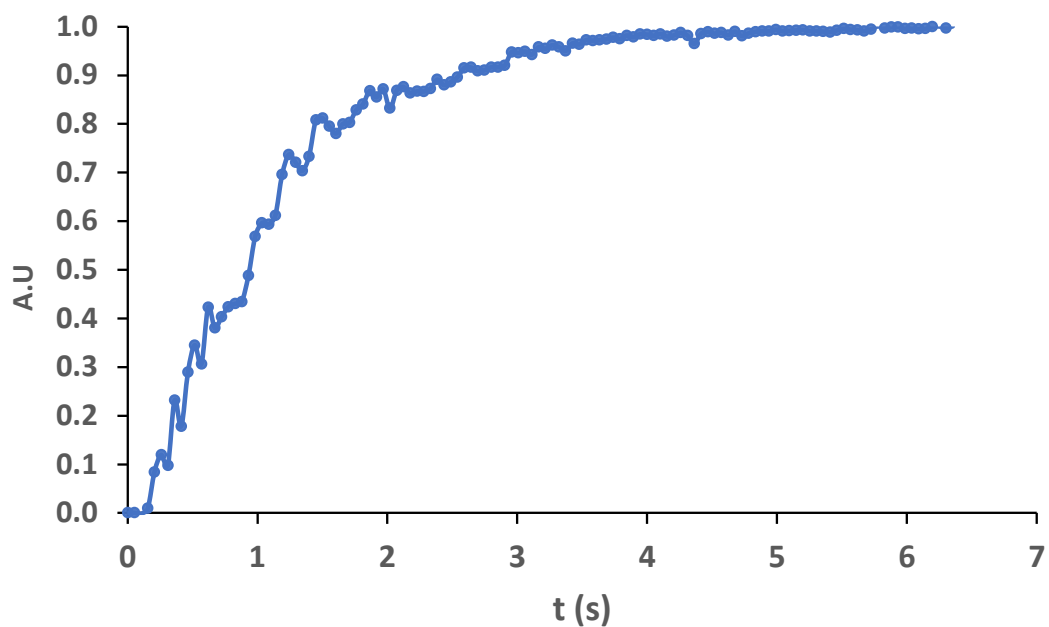
Figure S137. UV/Vis spectra of **Ir-L3-B** in CH₃CN. Photocyclization process by irradiation at 370 nm, 1.9·10⁻⁵M
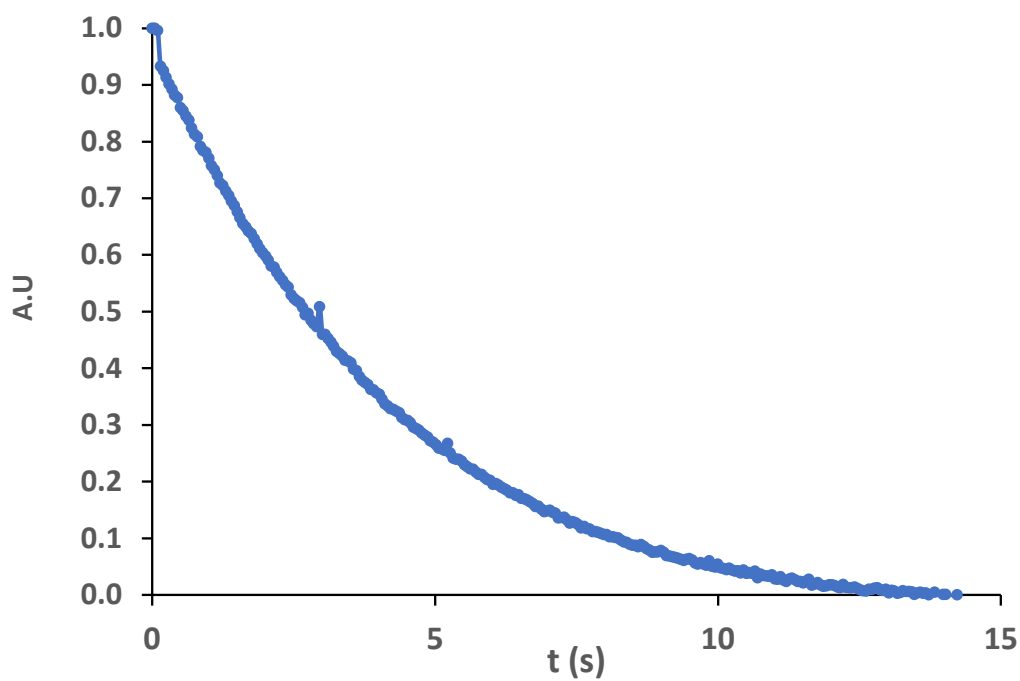
Figure S138. UV/Vis spectra of **Ir-L3-B** in CH$_3$CN. Photocycloreversion process by irradiation at 370 nm, 1.9·10^{-5}M
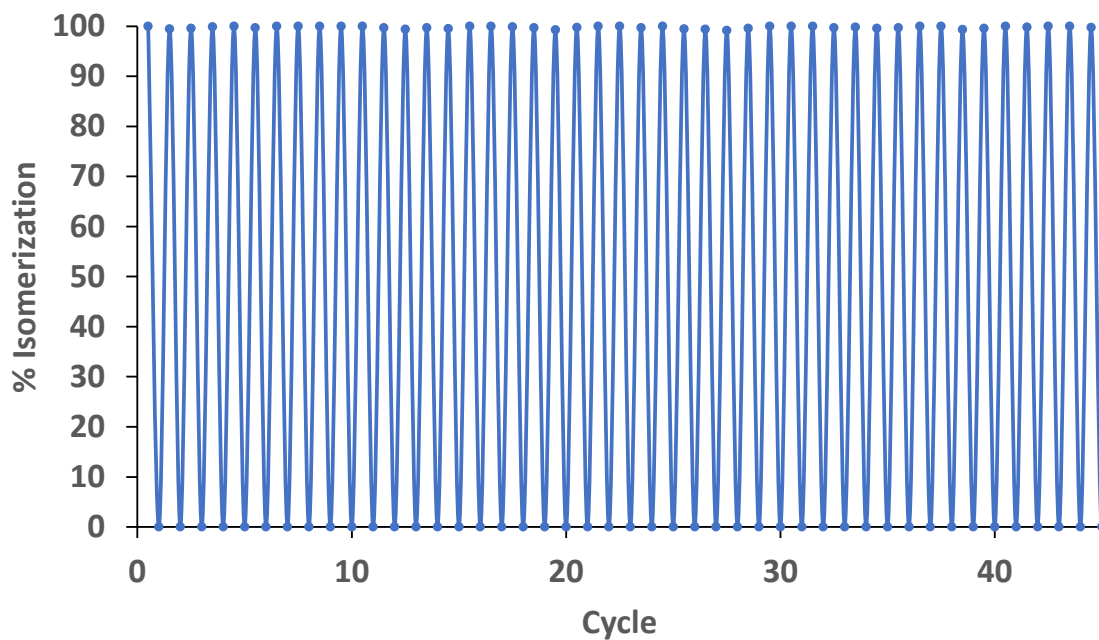
Figure S139. UV/Vis spectra of **Ir-L3-B** in CH$_3$CN. Fatigue resistance experiment by irradiation at 370 nm, 1.9·10^{-5}M

4. CRYSTALLOGRAPHIC DATA
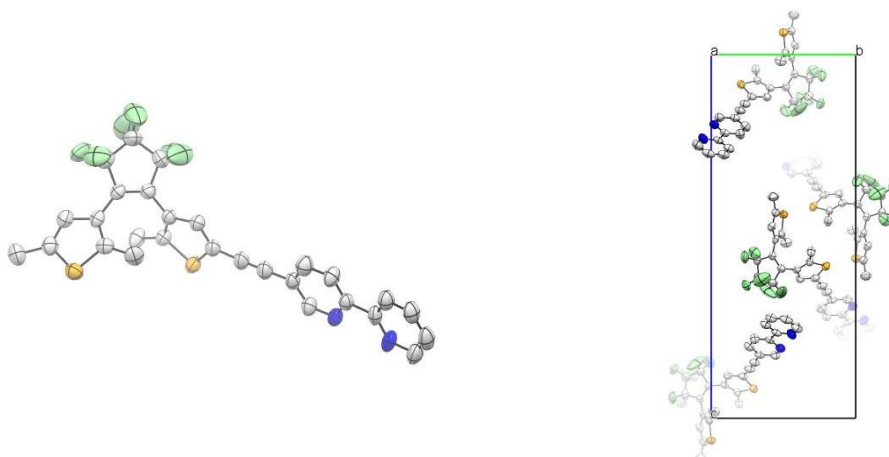
Empirical formula	$C_{14}H_9F_3NS$
Formula weight	280.28
Temperature/K	293(2)
Crystal system	orthorhombic
Space group	$P2_12_12_1$
a/Å	6.6392(4)
b/Å	12.3546(15)
c/Å	31.198(2)
α/°	90
β/°	90
γ/°	90
Volume/Å^3	2559.0(4)
Z	8
ρ_{calc}g/cm^3	1.455
μ/mm^{-1}	2.470
F(000)	1144.0
Crystal size/mm^3	$0.2 \times 0.01 \times 0.01$
Radiation	Cu Kα (λ = 1.54184)
2Θ range for data collection/°	5.666 to 145.736
Index ranges	-8 ≤ h ≤ 8, -12 ≤ k ≤ 12, -38 ≤ l ≤ 25
Reflections collected	8159
Independent reflections	4057 [R_{int} = 0.0285, R_{sigma} = 0.0493]
Data/restraints/parameters	4057/0/347
Goodness-of-fit on F^2	1.052
Final R indexes [I>=2σ (I)]	R_1 = 0.0574, wR_2 = 0.1436
Final R indexes [all data]	R_1 = 0.0721, wR_2 = 0.1532
Largest diff. peak/hole / e Å^{-3}	0.48/-0.25
Flack parameter	0.004(16)
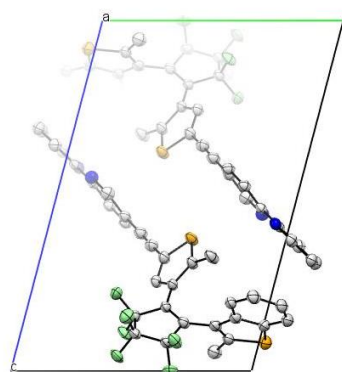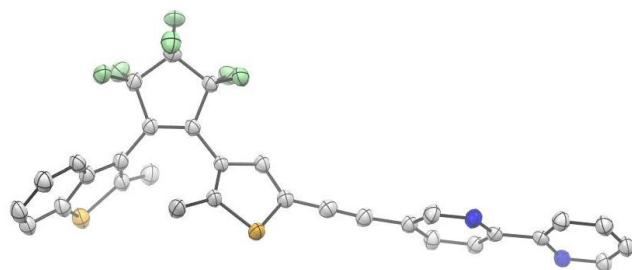
Empirical formula	$C_{31}H_{18}F_6N_2S_2$
Formula weight	596.59
Temperature/K	140
Crystal system	triclinic
Space group	P-1
a/Å	7.2595(4)
b/Å	11.6507(5)
c/Å	16.7750(9)
α/°	102.813(4)
β/°	93.776(4)
γ/°	107.243(4)
Volume/Å^3	1308.03(12)
Z	2
ρ_{calc}g/cm^3	1.515
μ/mm^{-1}	2.458
F(000)	608.0
Crystal size/mm^3	$0.1 \times 0.1 \times 0.1$
Radiation	CuKα (λ = 1.54178)
2Θ range for data collection/°	5.458 to 145.864
Index ranges	-8 ≤ h ≤ 6, -13 ≤ k ≤ 14, -19 ≤ l ≤ 20
Reflections collected	7182
Independent reflections	4149 [R_{int} = 0.0140, R_{sigma} = 0.0256]
Data/restraints/parameters	4149/0/372
Goodness-of-fit on F^2	1.059
Final R indexes [I>=2σ (I)]	R_1 = 0.0690, wR_2 = 0.1855
Final R indexes [all data]	R_1 = 0.0710, wR_2 = 0.1871
Largest diff. peak/hole / e Å^{-3}	1.62/-0.61
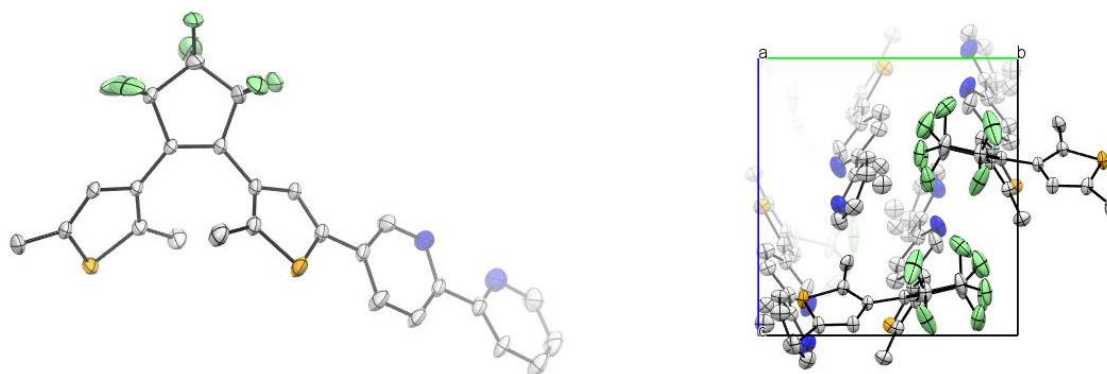
Empirical formula	$C_{26}H_{18}F_6N_2S_2$
Formula weight	536.54
Temperature/K	140
Crystal system	monoclinic
Space group	$P2_1/c$
a/Å	21.3531(2)
b/Å	10.14810(10)
c/Å	11.13760(10)
α/°	90
β/°	101.9570(10)
γ/°	90
Volume/Å^3	2361.08(4)
Z	4
ρ_{calc}g/cm^3	1.509
μ/mm^{-1}	2.647
F(000)	1096.0
Crystal size/mm^3	$0.1 \times 0.1 \times 0.1$
Radiation	CuKα (λ = 1.54178)
2Θ range for data collection/°	4.23 to 145.954
Index ranges	-26 ≤ h ≤ 26, -12 ≤ k ≤ 12, -11 ≤ l ≤ 13
Reflections collected	13182
Independent reflections	4677 [R_{int} = 0.0320, R_{sigma} = 0.0246]
Data/restraints/parameters	4677/366/383
Goodness-of-fit on F^2	1.029
Final R indexes [I>=2σ (I)]	R_1 = 0.0641, wR_2 = 0.1724
Final R indexes [all data]	R_1 = 0.0653, wR_2 = 0.1738
Largest diff. peak/hole / e Å^{-3}	0.87/-0.81
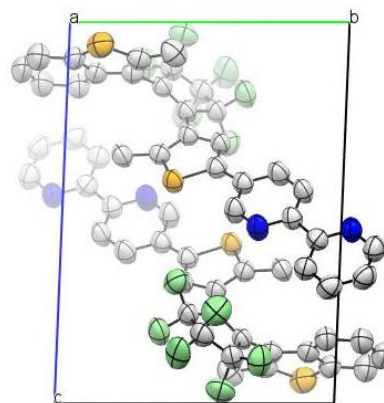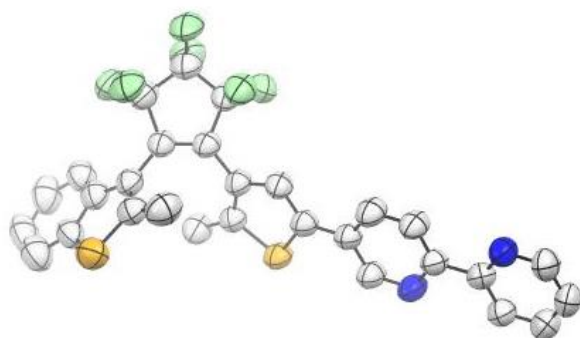
Empirical formula	$C_{29}H_{18}F_6N_2S_2$
Formula weight	572.57
Temperature/K	293
Crystal system	triclinic
Space group	P-1
a/Å	8.4952(10)
b/Å	11.0464(13)
c/Å	14.3963(14)
α/°	91.380(9)
β/°	92.824(9)
γ/°	107.706(10)
Volume/Å^3	1284.3(3)
Z	2
ρ_{calc}g/cm^3	1.481
μ/mm^{-1}	2.475
F(000)	584.0
Crystal size/mm^3	$0.1 \times 0.1 \times 0.01$
Radiation	Cu Kα (λ = 1.54184)
2Θ range for data collection/°	8.41 to 125.434
Index ranges	-8 ≤ h ≤ 9, -12 ≤ k ≤ 12, -16 ≤ l ≤ 16
Reflections collected	7948
Independent reflections	3745 [R_{int} = 0.0593, R_{sigma} = 0.0877]
Data/restraints/parameters	3745/0/355
Goodness-of-fit on F^2	0.999
Final R indexes [I>=2σ (I)]	R_1 = 0.0639, wR_2 = 0.1729
Final R indexes [all data]	R_1 = 0.1046, wR_2 = 0.2015
Largest diff. peak/hole / e Å^{-3}	0.29/-0.41

5. REFERENCES

[1] O. V. Dolomanov, L. J. Bourhis, R. J. Gildea, J. A. K. Howard, H. Puschmann, J. Appl. Cryst., 2009, 42, 339-341.

[2] G. M. Sheldrick, Acta Cryst. A, 2015, 71, 3-8.

[3] B. Oruganti, P. P. Kalapos, V. Bhargav, G. London, B. Durbeej, *J. Am. Chem. Soc.*, **2020**, *142*, 13941-13953.

[4] J. Moreno, F. Schweighöfer, J. Wachtveitl, S. Hecht, *Chem. Eur. J.*, **2016**, *22*, 1070-1075.

[5] S. M. Büllmann, A. Jäschke, *Chem. Commun.*, **2020**, *56*, 7124-7127.

[6] J. Von Irmer, F. Frieβ, D. Herold, J. Kind, C. M. Thiele, M. Gallei, *J. Mater. Chem. C.*, **2019**, *7*, 14088-14097.

[7] G. Liu, S. Pu, X. Wang, W. Liu, T. Yang, *Dyes and Pigments*, **2011**, *90*, 71-81.

[8] G. Liu, M. Liu, S. Pu, C. Fan, S. Cui, *Dyes and Pigments*, **2012**, *95*, 553-562.

[9] H. Liu, S. Pu, G. Liu, B. Chen, *Dyes and Pigments*, **2014**, *102*, 159-168.

[10] D. Becker, N. Konertz, M. Böhning, J. Schmidt, A. Thomas, *Chem. Mater.*, **2016**, *28*, 8523-8529.

[11] J. Ma, X. Cu, F. Wang, X. Wu, J. Zhao, X. Li, *J. Org. Chem.*, **2014**, *79*, 10855-10866.

[12] J. Chen, M. Kuss-Petermann, O. S. Wenger, *Chem. Eur. J.*, **2014**, *20*, 4098-4104.

[13] S. Dey, C. L. Rühl, A. Jäschke, *Chem. Eur. J.*, **2017**, *23*, 12162-12170.

[14] W. Wu, J. Sun, X. Cui, J. Zhao, *J. Mater. Chem. C.*, **2013**, *1*, 4577-4589.

[15] E. T. Luis, H. Irasnmanesh, K. S. A. Arachchige, W. A. Donald, G. Quach, E. G. Moore, J. E. Beves, *Inorg. Chem.*, **2018**, *57*, 8476-8486.

[16] M. Kamila, G. Cosquer, B. K. Breedlove, M. Yamashito, *Bull. Chem. Soc. Jpn.*, **2017**, *90*, 595-603.

[17] V. Valderrey, A. Bonasera, S. Fredrich, S. Hecht, *Angew. Chem. Int. Ed.*, **2017**, *56*, 1914-1918.

[18] Y-M. Hervault, C. M. Ndiaye, L. Norel, C. Lagrost, S. Rigaut., *Org Lett.*, **2012**, *14*, 4454-4457.

[19] H. Wang, H. Lin, W. Xu, D. Zhu, *Chem. Eur. J.*, **2013**, *19*, 3366-3373.

[20] S. Fredrich, A. Bonasera, V. Valderrey, S. Hecht, *J. Am. Chem. Soc.*, **2018**, *140*, 6432-6440.

[21] H. Zhao, E. Garoni, T. Roisnel, A. Colombo, C. Dragonetti, D. Marinotto, S. Righetto, D. Roberto, D. Jacquemin, J. Boixel, V. Guerchais, *Inorg. Chem.*, **2018**, *57*, 7051-7063.

[22] B. Li, H-M. Wen, J-Y. Wang, L-X. Shi, Z-N. Chen, *Inorg. Chem.* **2013**, *52*, 12511-12520.

[23] L. Ma, H. Xu, G. Liu, *Adv. Mat, Res.*, **2014**, *1003*, 35-38.

[24] F. Sun, S. Cui, S. Pu, *Adv. Mat. Res.*, **2014**, *952*, 79-83.

[25] S. L. Gilat, S. H. Kawai, J-M- Lehn, *Chem. Eur. J.*, **1995**, *1*, 275-284.

[26] B. Li, J-Y. Wang, H-M. Wen, L-X. Shi, Z-N. Chen, *J. Am. Chem. Soc.*, **2012**, *134*, 16059-16067.

[27] S. Cui, S. Pu, W. Liu, G. Liu, *Dyes and Pigments*, **2011**, *91*, 435-441.

[28] M. Liu, G. Liu, S. Cui, *Adv. Mat. Res.*, **2012**, *455*, 41-44.

[29] M-X. Song, Y. Li, R-P. Deng, F-Q. Bai, Z-K. Qin, *RSC Adv.*, **2016**, *6*, 68960-68963.

[30] M. Bandini, M. Bianchi, G. Valenti, F. Piccinelli, F. Paolucci, M. Monari, A. Umani-Ronchi, M. Marcaccio, *Inorg. Chem.*, **2010**, *49*, 1439-1448.

[31] K. A. McGee, K. R. Mann, *Inorg. Chem.*, **2007**, *46*, 7800-7809.

[32] M. Helms, C. Wang, B. Orth, K. Harms, E. Meggers., *Eur. J. Inorg. Chem.,* **2016**, 2896-2901.

[33] O. Chepelin, J. Ujma, X. Wu, A. M. Z. Slawin, M. B. Pitak, S. J. Coles, J. Michel, A. C. Jones, P. E. Barran, P. J. Lusby, *J. Am. Chem. Soc.*, **2012**, *134*, 19334-19337.

[34] L. Gong, S. P. Mulcahy, K. Harms, E. Meggers, *J. Am. Chem. Soc.*, **2009**, *131*, 9602-9603.

APPENDIX
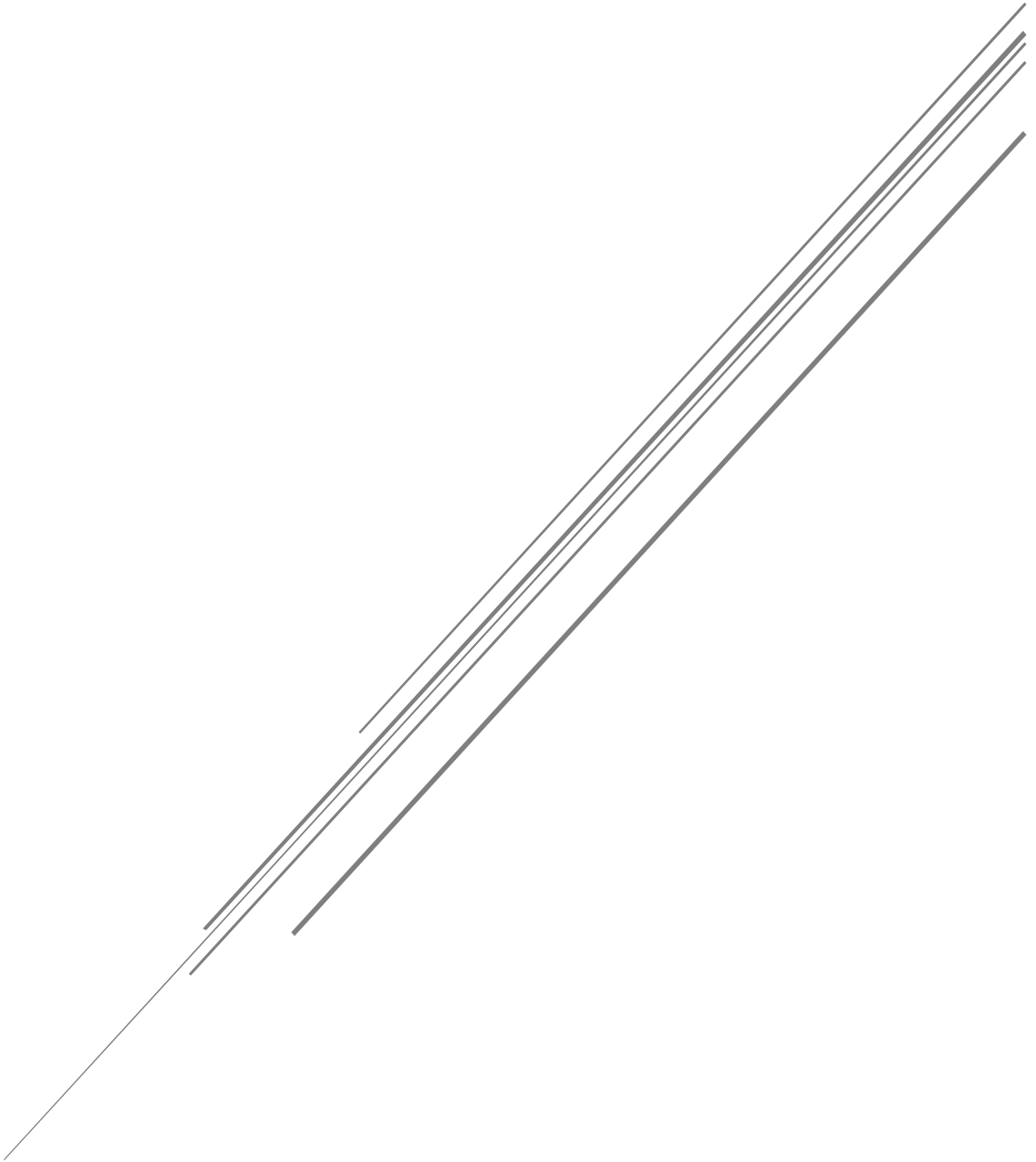
SUMMARY

For decades, the concept of chirality has represented a source of research of great interest, both for academia and for industry, mainly aimed at the generation of enantiopure compounds. The organometallic complexes (central metal combined with organic ligands) are within the different existing enantiopure compounds. The traditional methodology established for obtaining these compounds is using enantiopure chiral ligands for the subsequent construction of chiral and enantiopure organometallic complexes.

In addition to the possible chirality present in the ligand, the metal center can also "itself" be a stereogenic center, generating chiral compounds with achiral ligands. This concept is known as "chiral-at-metal only" and is a procedure that has been poorly studied in the literature due to the lack of synthetic protocols for the efficient production of the different metal enantiomers. Recently, the Fontecave and Meggers research groups focused their efforts on developing synthetic routes to obtain chiral complexes in enantiopure octahedral metals, with the complexes of Ir(III), Rh(III), and Ru(II) being the most interesting.

The strategy developed focuses on using temporary chiral agents as the key for the separation of the metal enantiomers. The procedure consists of introducing a chiral and enantiopure ligand or counterion in the racemic metallic structure, generating the appearance of diastereomers, compounds easily separable by conventional purification techniques such as purification through column chromatography or by precipitation of the product, among other techniques. Once the diastereomers have been separated, the chiral agent is removed from the complex, recycling it for future separations. As mentioned above, this type of compound can be incorporated into different applications, its use as catalysts in asymmetric catalysis or as metallodrugs, although the best-known application is the use of this type of compound in the construction of organometallic light-emitting diodes (OLEDs). For this application, a wide variety of bis- and tris-cyclometalated Ir(III) complexes have been studied as phosphorescent dopants for the construction of this type of system, as well as the construction of LEECs (electrochemical emissive cells). Despite being chiral in the metal, all of them have been used in the form of racemic compounds, containing a mixture of delta isomer (**Δ**) and lambda isomer (**Λ**). A little over a decade ago, the first enantiopure derivative was isolated from using chiral ligands, in turn demonstrating their ability to emit circularly polarized light.

In addition to organometallic systems, there are a series of organic compounds, defined as photochromic compounds, used for decades as photoswitchable systems. These compounds can alter their properties by the incidence of an external stimulus, in this specific case, light. Combining these photochromic systems and organometallic complexes has led to new photoswitchable organometallic compounds, making it possible to improve existing applications. Surprisingly, despite the many known applications for organometallic complexes, there are hardly any described examples where organometallic photochromic complexes are used, thus offering the opportunity to study an emerging and very attractive concept.

The main interest in this type of compound is the creation of intelligent chemical systems. These systems are based on the possibility of modifying their properties and their functionality through changes in the environment, more specifically irradiation. These new materials can be taken to represent the concept called molecular machines. The most straightforward strategy for obtaining photosensitive metal complexes is to incorporate photosensitive organic fragments into the structure of the ligands coordinated to the metal, transforming the compounds into dynamic entities capable of responding to external stimuli. Driven by the

importance of phenylpyridine (ppy), phosphine, and bipyridine (bpy) ligands in the synthesis of functional organometallic complexes, in recent years, our group at the University of the Basque Country (UPV-EHU) has focused on the development of photoswitchable organometallic compounds, using azobenzene groups incorporated into bipyridine, phenylpyridine and phosphine ligands. During this time, this type of compound was studied as phosphorescent dopants for OLEDs and its potential application as photocontrolled catalysts. Azobenzene was the organic fragment chosen for this function because it was easily accessible synthetically and because of the electronic change that occurs when isomerizing from its trans- to its cis- state after irradiation. Additionally, in the azobenzene isomerization process, a change in the molecule's structure is observed, transforming a flat molecule into an atropisomeric molecule (*trans-/E → cis-/Z*).

In addition to the azobenzene mentioned above, many organic fragments can act in the same way, called organic molecular switches, an example of which is dithienylethene fragments, also known as DTEs. DTE derivatives are very interesting photochromic compounds because, in the isomerization process (open-to-closed), they show excellent resistance to fatigue and thermal irreversibility. Likewise, like the azobenzene group, during the isomerization process, the DTE fragment acquires a temporary chirality, which, added to its properties already described, places it as a formidable candidate for the synthesis and subsequent application of new photosensitive organometallic complexes. Surprisingly, the temporary chirality that some photoswitch ligands obtain after the change induced by light has hardly been studied, giving rise to an interesting way of studying the concept.

The main objective of this research project is the development of new photosensitive organometallic complexes based on DTE ligands for the synthesis of chiral compounds at the ("chiral-at-metal"), showing in both cases an amplification of chirality by irradiation.

Chapter 1 consists of an introduction, divided into two sections, explaining the different concepts covered during the manuscript. The first part presents some of the most interesting photochromic compounds described and focuses on the detailed explanation of the properties of dithienylethenes and their origin and the mechanism by which the isomerization process is governed. Likewise, various examples are shown where DTE fragments are inserted into the structure of different organometallic complexes and real applications that employ DTE as a fundamental piece.

The second part of the introduction focuses on the different bis- and tris-cyclometalated Ir(III) complexes. These compounds have been widely studied due to their excellent emitting properties, which can be modified by functionalizing the C-N ligands coordinated to the metal ion. Due to their properties, Ir(III) organometallic compounds have been widely used in different applications such as OLEDs, target compounds in biological systems, or as anticancer systems. In addition, due to recent advances in the synthesis of Ir(III) octahedral complexes, obtaining these enantiopure compounds is more efficient, enhancing the possible applications already described for Ir(III) cyclometalated complexes: Emission of circularly polarized light, greater selectivity to biological centers or their possible use as catalysts in asymmetric catalysis.

Chapter 2 presents the studies carried out to obtain octahedral complexes with cyclometalated DTE ligands. The first part of the chapter is based on the synthesis and characterization of different DTE ligands. Synthesized photochromic ligands can be categorized into symmetric or non-symmetric ligands, depending on the composition of the thiophene groups in the structure.

All ligands are designed in such a way that the coordination point is through a thiophene-pyridyl group, which can vary the position in the structure of the compound.

The second part of the chapter focuses on obtaining the coordination of the previously synthesized ligands to different Ir(III) precursors. In order to obtain complexes based on cyclometalated DTE ligands, numerous reaction conditions were studied, making variations in the type of initial precursor used, in the design of the metal complex, as well as changes in solvents and reaction temperatures. Unfortunately, the different studies carried out could not confirm the cyclometallation of the synthesized DTE ligands. In order to understand the reason why the coordination was not effective, the cyclometallation of the thiophene group in its simplest structure was tested. A chloro-bridged Ir(III) dimer was first synthesized using a 2-pyridyl-4-bromo-5-methylthiophene group as the cyclometalated ligand. As a result of this reaction, an orange solid was obtained, which was identified and characterized employing NMR spectroscopy. The identification of the same was given using elemental analysis due to the insolubility of the solid in any deuterated solvent. To confirm that the cyclometallation of the thiophene fragment was effective, it was decided to introduce a third coordinating ligand to improve solubility. The product of this reaction confirmed that the cyclometallation of the two thiophene-pyridine ligands during the synthesis of the dimer was effective.

On the other hand, following the same strategy, a single thiophene-pyridine fragment was inserted into a precursor $[Ir(ppy)_2(CH_3CN)]^+$, observing that in the specific case, being introduced as a third ligand generated N-S coordination at the metal center. This type of coordination has hardly been studied, since not many publications describe it, which opens up a new and interesting research route. After obtaining these very promising results, the N-S coordination of the synthesized DTE ligands was tested, observing evidence that the coordination occurred satisfactorily. Despite this evidence, the purification of these complexes could not be carried out effectively through various classical purification methodologies such as precipitation or separation by chromatographic column. For this reason, the coordination of NS ligands to metal centers remains one of the future perspectives in our research group since the coordination of the ligands occurs at a point very close to the area of the isomerization process and may affect considerably to the cyclization process of the DTEs.

Chapter 3 presents the studies carried out to obtain octahedral complexes with non-symmetrical DTE ligands containing bipyridine groups as coordinating centers. The first section of the chapter is based on the synthesis and characterization of four previously undescribed DTE ligands. The synthesized ligands are classified into two families, **L2** and **L3**, depending on whether or not they incorporate an alkyne spacer between bipyridine and DTE. To synthesize these ligands, various synthetic routes are presented from which to obtain the desired final compounds. For an effective characterization of the organic compounds, they were studied by NMR spectroscopy (^{1}H-NMR, ^{13}C-NMR, COSY, and HSQC), mass spectrometry, and X-ray diffraction of the crystalline structures of the ligands.

The second section of *Chapter 3* is divided into two parts: the synthesis of racemic complexes and the synthesis of enantiopure complexes. In the first part, the coordination of DTE ligands to a racemic Ir(III) center will be briefly discussed. These were the preliminary tests carried out for the correct functioning of the coordination study of the synthesized ligands to enantiopure Ir(III) centers.

The second part begins with the synthesis of enantiopure precursors through chiral resolution, described by E. Meggers, a strategy that uses or employs chiral agents to generate

diasteromers. The generation of diasteromers allows the complexes' separation and subsequent purification through classical purification methodologies. For this chiral resolution, different chiral agents (*L*-proline and *L/D*-serine) were tested, obtaining good results for each of them. Once the diasteromers were purified, the chiral agent was changed using TFA, introducing two solvent molecules in the free coordinative vacancies, thus obtaining the enantiopure metal precursors Λ-[Ir(ppy)$_2$(CH$_3$CN)$_2$]$^+$ and Δ-[Ir(ppy)$_2$(CH$_3$CN)$_2$]$^+$. A circular dichroism study was carried out to confirm the enantiomeric excess of each of the precursors, demonstrating how each of the complexes presented a different Cotton effect (positive and negative), creating spectra with mirror images of each other. Next, taking the reaction conditions used for generating the enantiopure complexes, the corresponding enantiopure compounds for the four ligands were synthesized, obtaining four new pairs of Ir(III) complexes. The chapter ends with the characterization of metal complexes.

Chapter 4 collects the results obtained to study the different properties, both for the DTE ligands and the corresponding complexes. The chapter begins with the photochromic study of the different DTE ligands with a bipyridine group in their structure. The photochromic character was studied, observing how the absorption spectra varied depending on whether the ligand was in the open or closed form, identifying bands characteristic of both isomers. Similarly, using NMR spectroscopy, characteristic signals were studied and identified for each isomer. In this way, it was possible to study the evolution of the photocyclization process quantitatively, calculating the percentage of each of the species in the photostationary state. Kinetic studies were carried out, both by NMR spectroscopy and by UV-Vis spectroscopy, in order to calculate the quantum yields of the photophysical processes present in the isomerization of DTE. For this, and in collaboration with Dr. Gediminas Jonusauskas and Dr. Anh Thy Bui from the University of Bordeaux, an irradiation system was designed that measured the evolution of the process in real-time. Using a computer program developed by Dr. Anh Thy Bui, the photocyclization and photocycloreversion quantum yields for the DTE ligands were calculated from these data. To finalize the study of the ligands, the properties of resistance against fatigue and the thermal stability of the closed isomers were verified. The study of the resistance against fatigue showed that the ligand **L3-B** is the ideal candidate for its implementation in photochromic applications because it did not show decomposition during the first 100 cycles of isomerization. Similarly, in their closed form, all ligands showed high stability against the thermally activated cycloreversion process, where no thermochromic behavior was observed.

The second part of the chapter includes the repetition of the studies carried out for the Ir(III) complexes. The effect of metal coordination on the displacement of the absorption maxima of the compounds was studied, observing a shift towards the red of the different absorption bands. As for the free ligands, the speed by which the complexes reached the stationary state was studied through NMR and UV-Vis spectroscopy, observing in the photostationary state, the percentage of closed isomers was significantly higher than that obtained for the ligands. . The efficiency of the photocyclization/photocycloreversion processes (QY) was also studied. The comparison of the quantum yields between the free ligands and the Ir(III) complexes showed that the coordination to the metal center does not significantly affect the photochemical process. Following the guidelines of the DTE ligands, the fatigue resistance was studied. It was found that, once the photoswitch ligand is coordinated to the metal center, the resistance against isomerization fatigue increases very significantly for ligands **L2** and **L3-A**, while for the specific case **L3-B** it remains at Orders similar to those obtained for the free ligand. Finally, the induction of a diastereoselective isomerization of the enantiopure complexes was studied using circular dichroism spectroscopy. It was observed that for the open form of the complexes, a

positive/negative Cotton effect was obtained in the UV region, depending on the specific isomer (**Δ** or **Λ**), associated with the chirality present in the central metal. Once photocyclization is induced, it was possible to observe how, slightly, there is a positive or negative Cotton effect in the region of the spectrum characteristic of the closed-form of the complexes. This change corroborates the hypothesis proposed in the objective of this thesis of inducing the photocyclization process towards one of the two **CF-DTE** configurations, generating an excess of diastereomers.

Chapter 5 describes the general conclusions obtained throughout the thesis and the possible future perspectives that may be developed in the future within the research team.

RESUMEN

El concepto de quiralidad representa desde hace décadas una fuente de investigación de gran interés, tanto para la academia como para la industria, dirigida principalmente a la generación de compuestos enantiopuros. Dentro de los diferentes compuestos enantiopuros existentes, se encuentran los complejos organometálicos (metal central combinado con ligandos orgánicos). La metodología clásica establecida para la obtención de estos compuestos es el uso de ligandos quirales enantiopuros para la posterior construcción de los complejos organometálicos también quirales y enantiopuros.

Además de la posible quiralidad presente en el ligando, el centro metálico también puede "ser en sí mismo" un centro estereogénico, generando compuestos quirales con ligandos aquirales. Este concepto es conocido como "chiral-at-metal only" y es un procedimiento escasamente estudiado en bibliografía debido a la carencia de protocolos sintéticos para una obtención eficiente de los diferentes enantiómeros metálicos. Recientemente, los grupos de investigación de Fontecave y Meggers centraron sus esfuerzos en desarrollar rutas sintéticas para la obtención de complejos quirales en metales octaédricos enantiopuros, siendo los complejos de Ir(III), Rh(III) y Ru(II) los de mayor interés.

La estrategia desarrollada se centra en el empleo de agentes temporales quirales como clave para la separación de los enantiómeros metálicos. El procedimiento consiste en la introducción de un ligando o contraion quiral y enantiopuro en la estructura metálica racémica, generando la aparición de diastereoisomeros, compuestos fácilmente separables por técnicas de purificación convencionales como: purificación a través de columna cromatografíca o por precipitación del producto entre otras técnicas. Una vez los diastereoisomeros han sido separados se retira el agente quiral del complejo, reciclándose para futuras separaciones. Como se ha mencionado anteriormente, este tipo de compuestos pueden ser incorporados en diferentes aplicaciones su utilización como catalizadores en catálisis asimétrica o como metalofármacosaunque la aplicación más conocida es el uso de este tipo de compuesto en la construcción de diodos organometálicos emisores de luz (OLEDs). Para esta aplicación, una gran variedad de complejos bis- y tris-ciclometalados de Ir(III)han sido estudiados como dopantes fosforescentes para la construcción de este tipo de sistemas, así como la construcción de LEECs (celdas electroquímicas emisivas). Todos ellos, pese a ser quirales en el metal, han sido utilizados en forma de compuestas racémicos, conteniendo una mezcla de isómero delta (Δ) e isómero lambda (Λ). Hace poco más de una década se consiguió aislar el primer derivado enantiopuro, a partir de la utilización de ligandos quirales, demostrando a su vez la capacidad de los mismos para emitir luz circularmente polarizada.
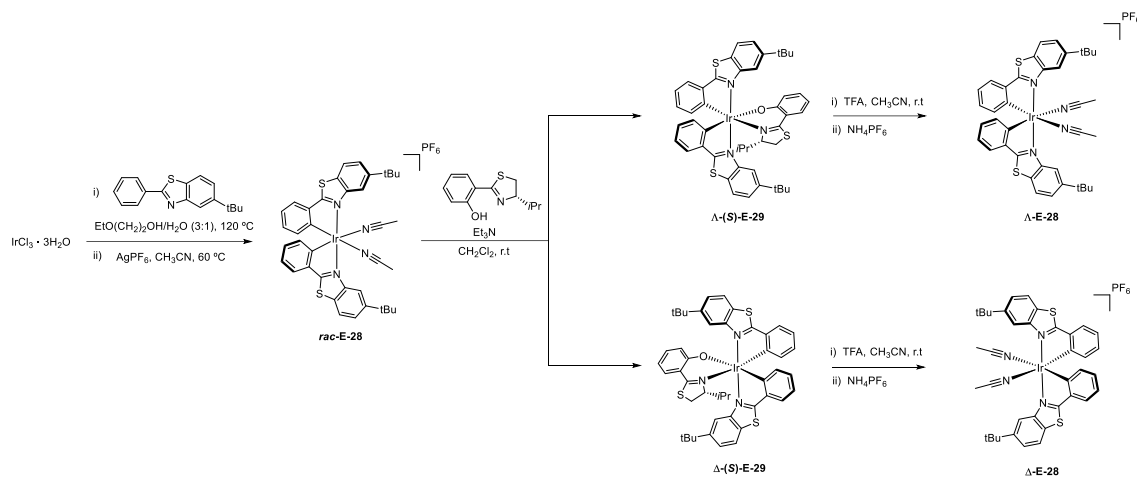
Figura R1. Resolución quiral para la obtención de complejos octaedricos de Ir(III) enantiopuros.

Además de los sistemas organometálicos, existen una serie de compuestos orgánicos, definidos como compuestos fotocrómicos, que han sido empleados desde hace décadas como sistemas fotomodulables. Estos compuestos son capaces de alterar sus propiedades por incidencia de un estímulo externo, en este caso específico, la luz. La combinación de estos sistemas fotocrómicos y los complejos organometálicos ha generado la creación de nuevos compuestos organometálicos fotomodulables, posibilitando la mejora de las aplicaciones ya existentes. Sorprendentemente, a pesar del gran número de aplicaciones conocidas para los complejos organometálicos, apenas existen ejemplos descritos en donde se usen complejos fotocrómicos organometálicos, ofreciendo de este modo la oportunidad de estudiar un concepto emergente y muy atractivo

El principal interés en este tipo de compuestos es la creación de sistemas químicos inteligentes. Estos sistemas se basan en la posibilidad de modificar sus propiedades y su funcionalidad mediante cambios del entorno, más específicamente la irradiación. Estos nuevos materiales se pueden tomar como representación del concepto denominado máquinas moleculares. La estrategia más sencilla para la obtención de complejos metálicos fotosensibles es incorporar fragmentos orgánicos fotosensibles en la estructura de los ligandos coordinados al metal, transformando a los compuestos en entidades dinámicas capaces de dar una respuesta frente a un estímulo externo. Impulsados por la importancia de los ligandos fenilpiridina (ppy), fosfinas y bipiridinas (bpy) en la síntesis de complejos organometálicos funcionales, en los últimos años, nuestro grupo en la Universidad del País Vasco (UPV-EHU) se centró en el desarrollo de compuesto organometálicos fotoisomerizables, utilizando grupos azobenceno incorporados a ligandos bipiridina, fenilpiridina y fosfina. Durante este tiempo se estudió este tipo de compuestos como dopantes fosforescentes para OLEDs, así como su potencial aplicación como catalizadores fotocontrolados. El azobenceno fue el fragmento orgánico escogido para esta función debido a que era fácilmente accesible sintéticamente, así como por el cambio electrónico, que tiene lugar al producirse la isomerización de su estado *trans*- a su estado *cis*- tras la irradiación. Adicionalmente, en el proceso de isomerización del azobenceno, se observa un cambio en la estructura de la molécula, transformando una molécula plana en una molécula atropisomérica (*trans*-/E → *cis*-/Z).

Sorprendentemente, la quiralidad temporal que obtienen algunos ligandos *photoswitch* tras el cambio inducido por la luz no ha sido apenas estudiada, dando lugar a una vía interesante de estudio del concepto. Además del ya mencionado azobenceno, existen un gran número de

fragmentos orgánicos que pueden actuar de la misma forma, denominados como interruptores moleculares orgánicos, siendo un ejemplo de ello los fragmentos ditieniletenos, también conocidos como DTEs. Los derivados de DTE son compuestos fotocrómicos muy interesantes debido a que en el proceso de isomerización (open-to-closed) muestran excelente resistencia a la fatiga e irreversibilidad térmica. Así mismo, al igual que el grupo azobenceno, durante el proceso de isomerización, el fragmento DTE adquiere una quiralidad temporal, que, sumado a sus propiedades ya descritas, lo sitúa como un formidable candidato para la síntesis y posterior aplicación de nuevos complejos organometálicos fotosensibles.

El objetivo principal de este proyecto de investigación es el desarrollo de nuevos complejos organometálicos fotosensibles basados en ligandos DTE para la síntesis de compuestos quirales en el ("*chiral-at-metal*"), mostrando en ambos casos una amplificación de la quiralidad por la irradiación.
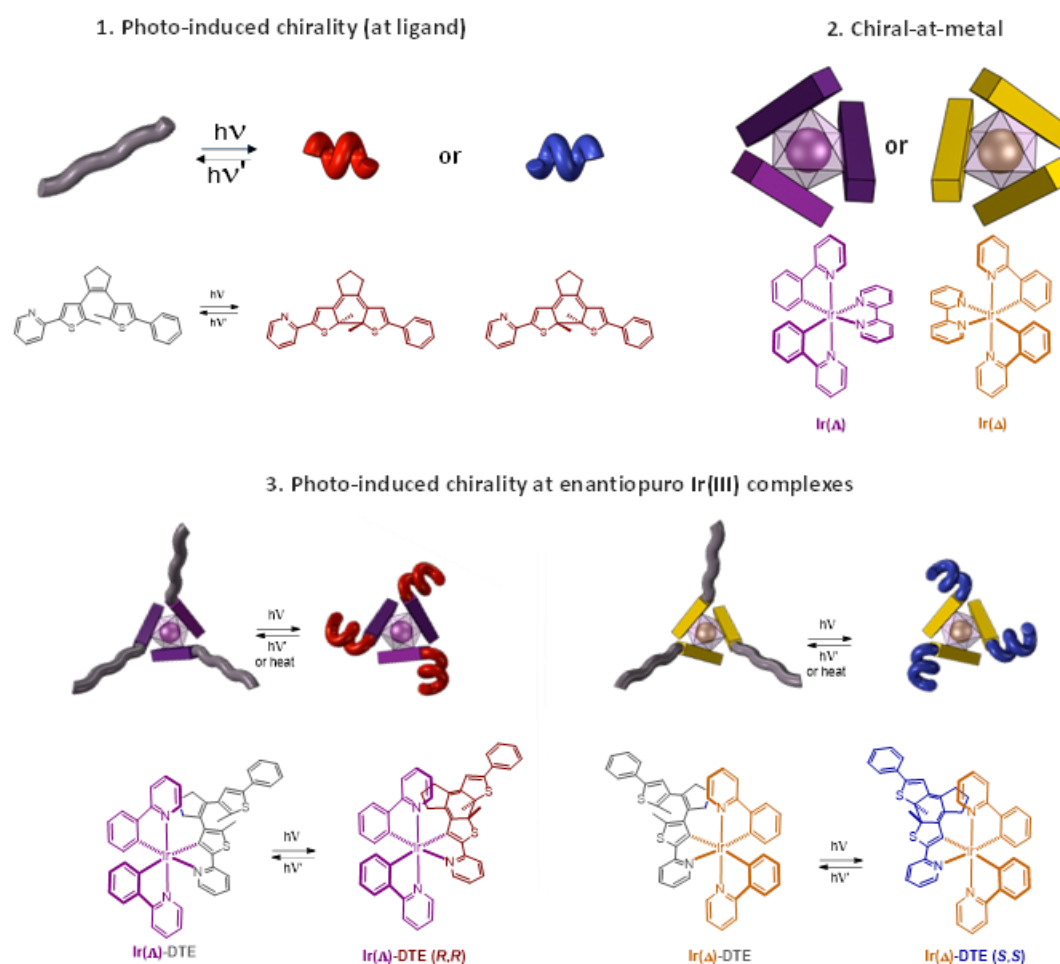
Figura R2. Representación gráfica de los objetivos generales propuestos para este trabajo.

El Capítulo 1 consta de una introducción, dividida en dos secciones, que explica los diferentes conceptos a tratar durante el manuscrito. En la primera parte se presentan algunos de los compuestos fotocrómicos descritos de mayor interesantes y se centra en la explicación detallada de las propiedades de los dithienylethenes, así como su procedencia y el mecanismo por el cual se rige el proceso de isomerización. Asimismo, se muestran diversos ejemplos en

donde se insertan fragmentos DTE en la estructura de diferentes complejos organometálicos y aplicaciones reales que emplean el uso de DTE como pieza fundamental.

La segunda parte de la introducción se centra en los diferentes complejos bis- y tris-ciclometalados de Ir(III). Estos compuestos han sido ampliamente estudiados debido a sus excelentes propiedades emisoras, las cuales pueden ser modificadas funcionalizando los ligandos C-N coordinados al ion metálico. A raíz de sus propiedades, los compuestos organometálicos de Ir(III) han sido ampliamente instaurados en diferentes aplicaciones como pueden ser OLEDs, compuestos diana en sistemas biológicos o como sistemas anticancerígenos. Además, debido a los recientes avances en la síntesis de complejos octaédricos de Ir(III), la obtención de estos compuestos enantiopuros se da de forma más eficiente, potenciando las posibles aplicaciones ya descritas para los complejos ciclometalados de Ir(III): Emisión de luz circularmente polarizada, mayor selectividad a centros biológicos o su posible empleo como catalizadores en catálisis asimétrica.

En el Capítulo 2 se presentan los estudios realizados para la obtención de complejos octaédricos con ligandos DTE ciclometalados. La primera parte del capítulo se basa en la síntesis y caracterización de diferentes ligandos DTE. Los ligandos fotocromicos sintetizados se pueden categorizar en ligandos simétricos o no simétricos, atendiendo a la composición de los grupos tiofeno en la estructura. Todos los ligandos están diseñados de tal forma que el punto de coordinación fuese a través de un grupo tiofeno-piridil, el cual puede variar la posición en la estructura del compuesto.
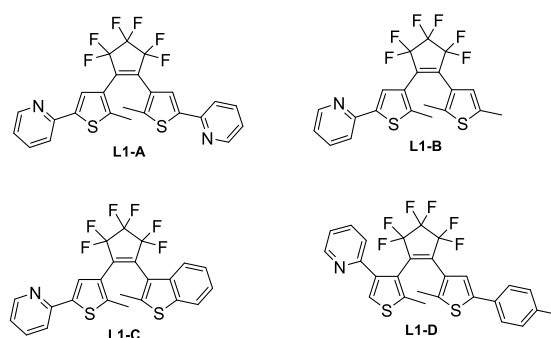
Figura R3. Ligandos DTE sintetizados propuestos para la ciclometalación a centros metálicos de Ir(III).

La segunda parte del capítulo se centra en el esfuerzo de obtener la coordinación de los ligandos previamente sintetizados a diferentes precursores de Ir(III). Con el objetivo de obtener complejos basados en ligandos DTE ciclometalados, numerosas condiciones de reacción fueron estudiadas, efectuando variaciones en el tipo de precursor inicial utilizado, en el diseño del complejo metálico, así como cambios de disolventes y temperaturas de reacción. Lamentablemente, los diferentes estudios procedidos no pudieron confirmar la ciclometalación de los ligandos DTE sintetizados. Con intención de entender la razón por la cual la coordinación no era efectiva se probó la ciclometalación del grupo tiofeno en su estructura más simple. Primero se sintetizó un dimero de Ir(III) con puentes cloro utilizando un grupo 2-pyridyl-4-bromo-5-methylthiophene como ligando ciclometalado. Como resultado de esta reacción se obtuvo un sólido naranja, el cual se procedió a identificar y caracterizar por medio de espectroscopia de RMN. La identificación del mismo se dio por medio de análisis elemental debido a la insolubilidad del sólido en cualquier disolvente deuterado. Para confirmar de forma definitiva que la ciclometalación del fragmento tiofeno era efectivo se decidió introducir un tercer ligando coordinante, con la intención de mejorar la solubilidad. El producto de esta

reacción permitió confirmar que la ciclometalación de los dos ligandos tiofeno-piridina durante la síntesis del dímero era efectiva. Por otro lado, siguiendo la misma estrategia, se insertó un único fragmento tiofeno-piridina a un precursor [Ir(ppy)(CH₃CN)]⁺, observándose que en el caso específico introducirse como tercer ligando este generaba una coordinación N-S al centro metálico. Este tipo de coordinación apenas ha sido estudiada, ya que no existen muchas publicaciones que la describan, lo que abre una nueva e interesante vía de investigación. Tras obtener estos resultados tan prometedores se probó la coordinación N-S de los ligandos DTE sintetizados, observándose evidencias de que la coordinación se dio de forma satisfactoria. A pesar de estas evidencias, la purificación de estos complejos no se pudo realizar de manera efectiva a través de diversas metodologías de purificación clásicas como precipitación o separación por columna cromatográfica. Por ello, la coordinación de ligandos N-S a centros metálicos queda como una de las perspectivas de futuro en nuestro grupo de investigación, debido a que la coordinación de los ligandos se produce en un punto muy cercano a la zona del proceso de isomerización, pudiendo afectar considerablemente al proceso de ciclación de los DTEs.

Figura R4. Coordinaciones estudiadas para los ligandos DTE sintetizados a precursores de Ir(III).
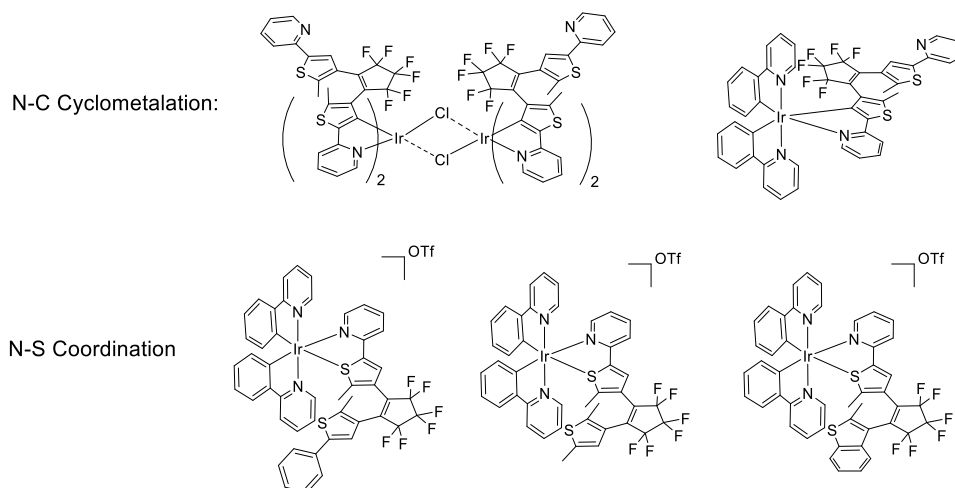
En el *Capítulo 3* se presentan los estudios realizados para la obtención de complejos octaédricos con ligandos DTE no simétricos que contienen grupos bipiridina como centros coordinantes. La primera sección del capítulo se basa en la síntesis y caracterización de cuatro ligandos DTE no descritos con anterioridad. Los ligandos sintetizados se clasifican en dos familias, **L2** y **L3**, dependiendo de si incorporan, o no, un "*spacer*" alquino entre la bipirina y el DTE. Para la síntesis de estos ligandos se presentan diversas rutas sintéticas a partir de las cuales poder obtener los compuestos finales deseados. Para una caracterización efectiva de los compuestos orgánicos se procedió a su estudio por espectroscopia de RMN (¹H-NMR, ¹³C-NMR, COSY y HSQC), espectrometría de masas, así como la difracción de rayos X de las estructuras cristalinas de los ligandos.
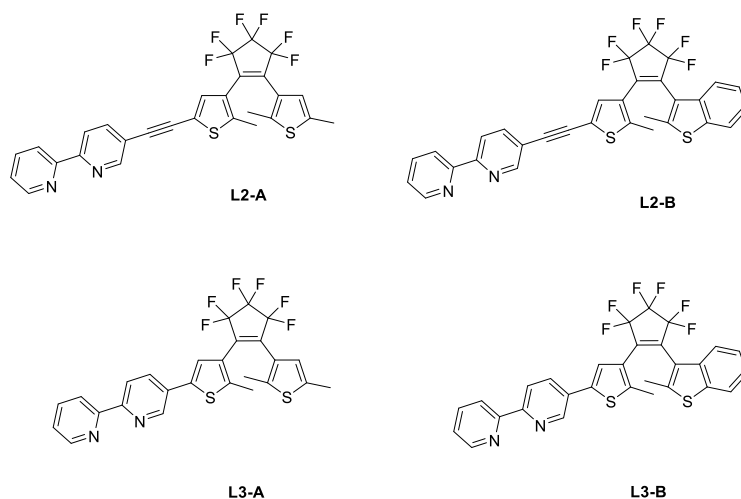
Figura R5. Ligandos DTE sintetizados basados en la inserción de grupos bipiridina como grupo coordinante.

La segunda sección del *capítulo 3* se divide a su vez en dos partes, síntesis de complejos racémicos y síntesis de complejos enantiopuros. En la primera parte se discutirá brevemente la coordinación de los ligandos DTE a un centro racémico de Ir(III). Esta fueron las pruebas preliminares realizadas para el correcto funcionamiento del estudio de coordinación de los ligandos sintetizados a centros enantipuros de Ir(III).
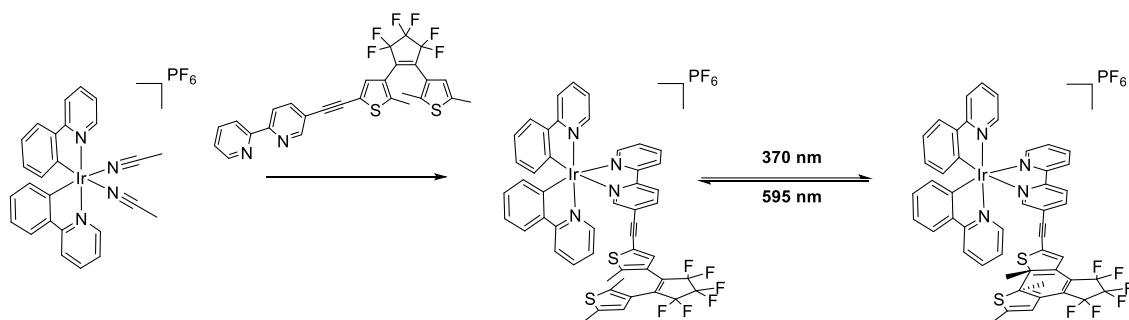
Figura R6. Síntesis de complejos catiónicos utilizando ligandos DTE como tercer ligando.

La segunda parte del *capítulo 3* comienza con la síntesis de precursores enantiopuros a través de una resolución quiral, descrita por E. Meggers, estrategia que utiliza o emplea agentes quirales para la generación de diastereoisomeros. La generación de diastereoisomeros permite una separación y posterior purificación de los complejos a través de metodologías clásicas de purificación. Para esta resolución quiral se probaron diferentes agentes quirales (*L*-prolina y *L/D*-serina), obteniéndose buenos resultados para cada uno de ellos. Una vez los diastereoisomeros fueron purificados, se cambió el agente quiral usando para ello TFA, introduciendo dos moléculas de disolvente en las vacantes coordinativas libres, obteniéndose de esta forma los precursores metálicos enantiopuros Λ-[Ir(ppy)$_2$(CH$_3$CN)$_2$]$^+$ y Δ-[Ir(ppy)$_2$(CH$_3$CN)$_2$]$^+$. Para confirmar el exceso enantiomerico de cada uno de los precursores se realizaron estudio de dicroísmo circular, demostrando como cada uno de los complejos presentaba un efecto Cotton diferente (positivo y negativo), creando espectros con imágenes especulares entre sí. A continuación, tomando las condiciones de reacción utilizadas para la generación de los complejos enantiopuros, se sintetizaron los correspondientes compuestos enantiopuros para los cuatro ligandos, obteniendo cuatro nuevas parejas de complejos de Ir(III). El capítulo finaliza con la caracterización de los complejos metálicos.
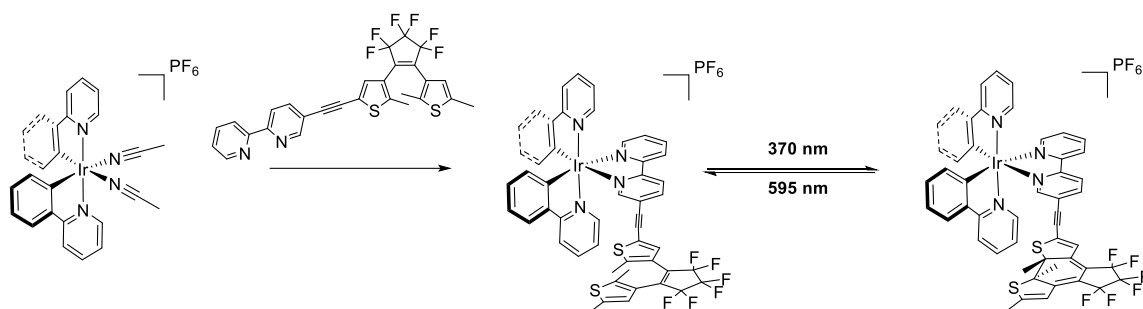
Figura R7. Síntesis de complejos catiónicos enantiopuros que incorporan fragmentos DTE en la estructura.

El *capítulo 4* recoge los resultados obtenidos para el estudio de las diferentes propiedades, tanto para los ligandos DTE como para los complejos correspondientes. El capítulo se inicia con el estudio fotocromico de los diferentes ligandos DTE con grupo bipiridina en su estructura. Se estudió carácter fotocromico, observándose como los espectros de absorción variaban en función de si el ligando se encontraba en la forma abierta o en la forma cerrada, identificando bandas características de ambos isómeros. Del mismo modo, empleando espectroscopia de RMN, se estudiaron e identificaron señales características para cada uno de los isómeros. De este modo se pudo estudiar la evolución del proceso de fotociclación de forma cuantitativa, calculando el porcentaje de cada una de las especies en el estado fotoestacionario. Se realizaron estudios cinéticos, tanto por espectroscopia de RMN como por espectroscopia de UV-Vis, con el fin de calcular los rendimientos cuánticos de los procesos fotofisicos presentes en la isomerización de los DTE. Para ello, y en colaboración con el Dr. Gediminas Jonusauskas y la Dra. Anh Thy Bui de la Universidad de Burdeos, se diseñó un sistema de irradiación el cual medía en tiempo real la evolución del proceso. A partir de estos datos y utilizando un programa informático desarrollado por la Dra. Anh Thy Bui se calcularon los rendimientos cuánticos de fotociclacion y fotocicloreversion para los ligandos DTE. Para finalizar el estudio de los ligandos, se comprobaron las propiedades de resistencia frente a la fatiga y la estabilidad térmica de los isómeros cerrados. El estudio de la resistencia frente a la fatiga mostró que el ligando **L3-B** es el candidato ideal para su implementación en aplicaciones fotocromicas debido a que no mostró descomposición durante los 100 primeros ciclos de isomerización. Del mismo modo, todos los ligandos, en su forma cerrada, mostraron una alta estabilidad frente al proceso de cicloreversion activado térmicamente, donde no se observó ningún comportamiento termocromico.
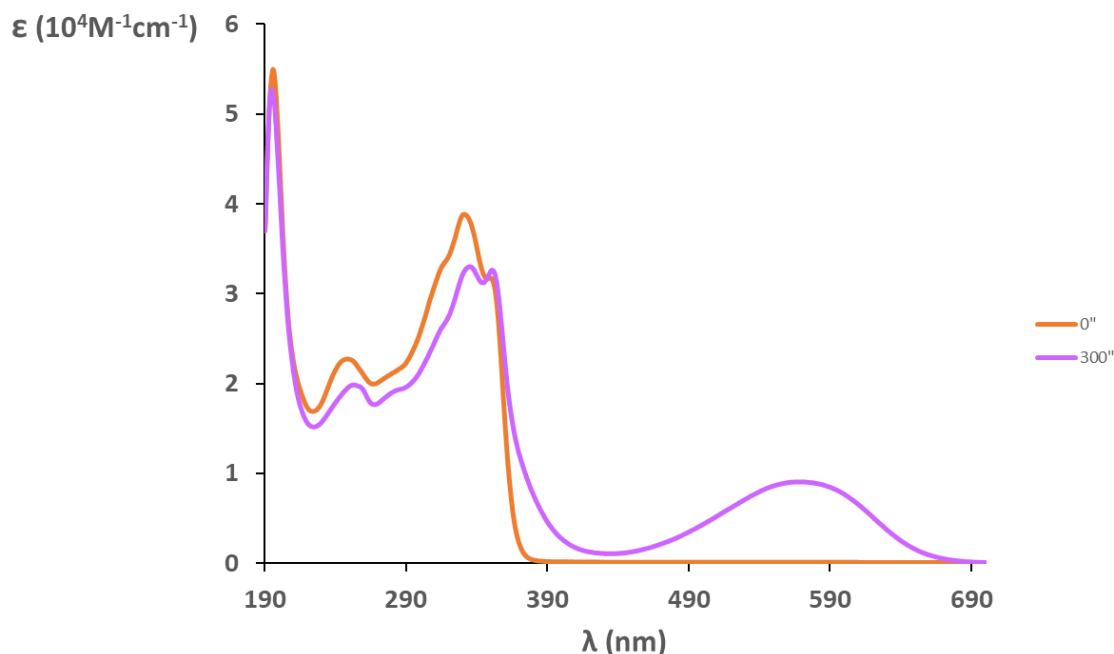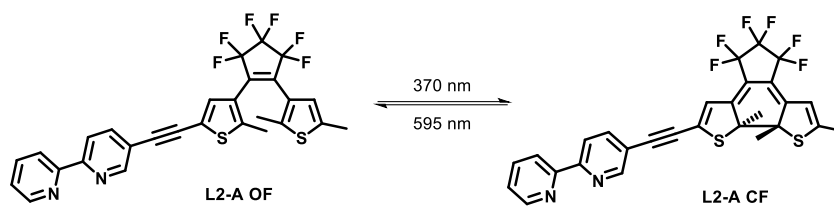
Figura R8. Comportamiento fotocromico (fotociclacion/fotocicloreversion) para los ligandos DTE sintetizados.

La segunda parte del capítulo recoge la repetición de los estudios realizados para los complejos de Ir(III). Se estudió el efecto de la coordinación del metal en el desplazamiento de los máximos de absorción de los compuestos, observando un desplazamiento hacia el rojo de las diferentes bandas de absorción. Al igual que para los ligandos libres, se estudió la velocidad por la cual los complejos alcanzaban el estado estacionario a través de espectroscopia RMN y UV-Vis, observando en el estado fotoestacionario, el porcentaje de isómeros cerrados era significativamente superior al obtenido para los ligandos. Se estudió además la eficiencia de los procesos (QY) de fotociclación/fotocicloreversion. La comparación de los rendimientos cuánticos entre los ligandos libres y los complejos de Ir(III) mostró que la coordinación al centro metálico no afecta significativamente al proceso fotoquímico. Siguiendo las directrices de los ligandos DTE se estudió la resistencia frente a la fatiga. Se pudo comprobar que, una vez el ligando photoswitch se coordina al centro metálico, la resistencia frente a la fatiga por isomerización aumenta de forma muy significativa para los ligandos **L2** y **L3-A**, mientras que para el caso específico **L3-B** se mantiene en órdenes similares a los obtenidos para el ligando libre.
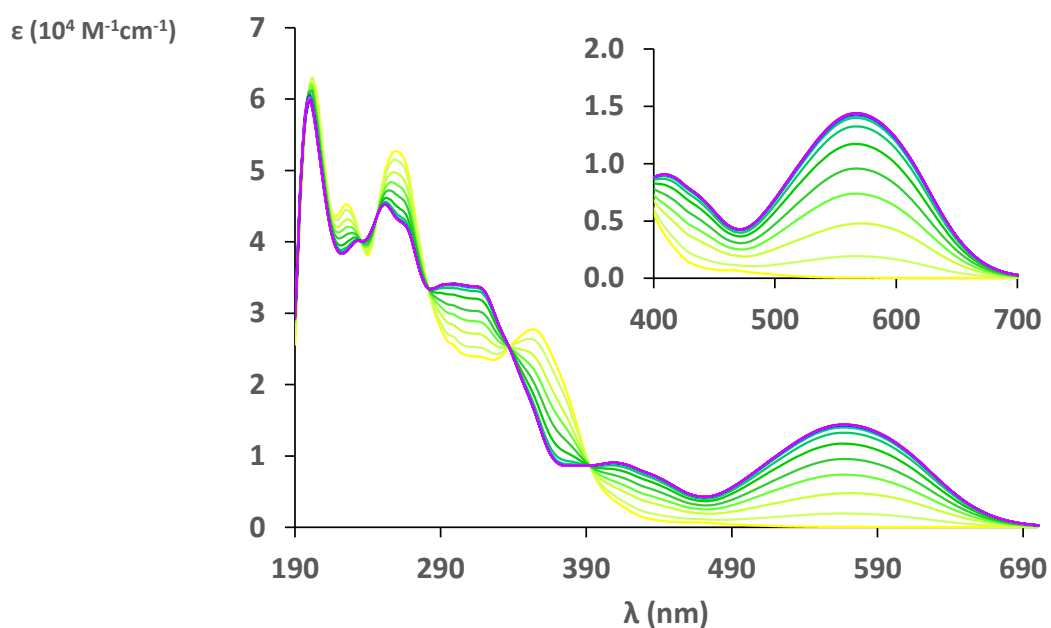
Figura R9. Estudio cinético del fotocromismo presente en los complejors Ir(III)-DTE.

Por último, se estudió la inducción de una isomerización diastereoselectiva de los complejos enantiopuros, utilizando para ello la espectroscopia de dicroísmo circular. Se pudo observar como para la forma abierta de los complejos se obtuvo un efecto Cotton positivo/negativo en la región del UV, en función del isómero específico (**Δ** o **Λ**), asociado a la quiralidad presente en el metal central. Una vez se induce la fotociclación se pudo observar cómo, levemente, existe un efecto Cotton positivo o negativo en la región del espectro característica de la forma cerrada de los complejos. Este cambio corrobora la hipótesis propuesta en el objetivo de esta tesis de inducir el proceso de fotociclación hacia una de las dos configuraciones del **CF-DTE**, generando un exceso de diastereoisomeros.
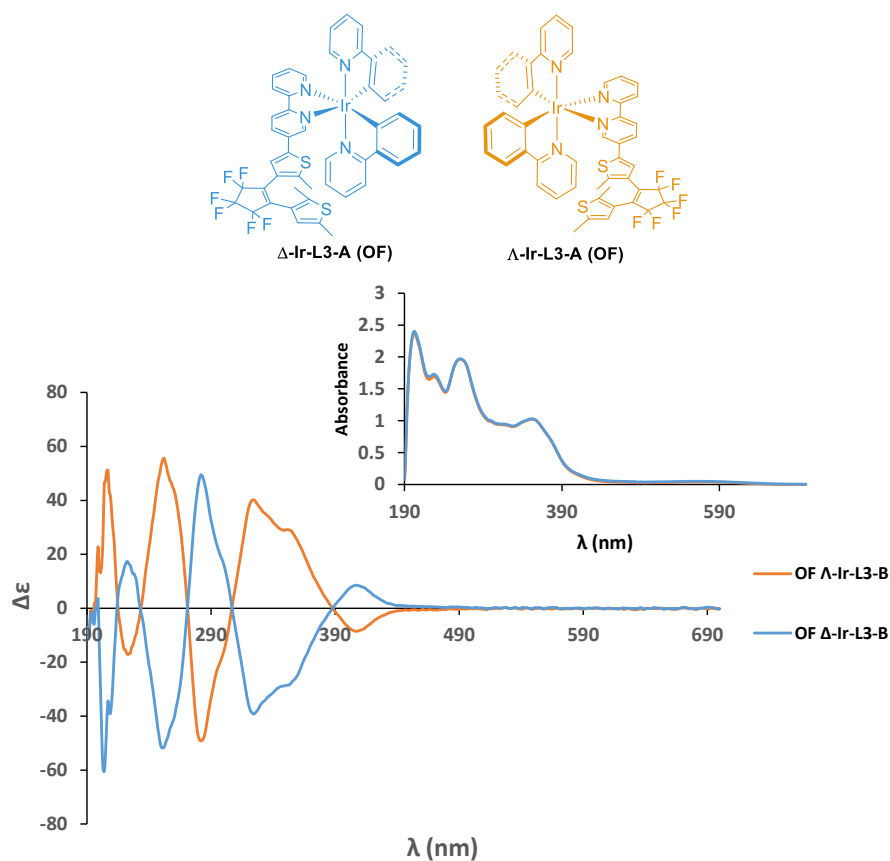
Figura R10. Espectro de dicroísmo circular para el estudio de una inducción selectiva del proceso de fotociclación para complejo de Ir(III) enantiopuros que incorporan un fragmento DTE.

En el *capítulo 5* se describen las conclusiones generales obtenidas a lo largo de la tesis y las posibles perspectivas futuras que se puedan desarrollar en el futuro dentro del equipo de investigación.

RÉSUMÉ

Depuis des décennies, le concept de chiralité est une source de recherche de grand intérêt tant pour le monde universitaire que pour l'industrie, visant principalement à la génération de composés énantiopurs. Parmi les différents composés énantiopurs existants figurent les complexes organométalliques (métal central combiné à des ligands organiques). La méthodologie classique établie pour obtenir ces composés est l'utilisation de ligands chiraux énantiopurs pour la construction ultérieure de complexes organométalliques, également chiraux et énantiopurs.

En plus de l'éventuelle chiralité présente dans le ligand, le centre métallique peut également être, lui-même, un centre stéréogène, générant des composés chiraux avec des ligands achiraux. Ce concept est connu sous le nom de complexes à "chiralité centrée sur le métal" et est une procédure rarement étudiée dans la littérature en raison du manque de protocoles synthétiques permettant d'obtenir efficacement les différents énantiomères du métal. Récemment, les groupes de recherche de Fontecave et Meggers ont concentré leurs efforts sur le développement de voies de synthèse permettant d'obtenir des complexes chiraux dans des métaux octaédriques énantiopurs, les complexes de Ir(III), Rh(III) et Ru(II) étant les plus intéressants.

La stratégie développée se concentre sur l'utilisation d'agents temporaires chiraux comme clé de la séparation des énantiomères métalliques. La procédure consiste en l'introduction d'un ligand ou d'un contre-ion chiral et énantiopur dans la structure métallique racémique, générant l'apparition de diastéréoisomères, composés facilement séparables par les techniques de purification conventionnelles telles que la purification par colonne chromatographique ou par précipitation du produit grâce à d'autres techniques. Une fois que les diastéréoisomères ont été séparés, l'agent chiral est retiré du complexe et recyclé pour de futures séparations. Comme mentionné ci-dessus, ce type de composés peut être incorporé dans différentes applications, telles que leur utilisation comme catalyseurs dans la catalyse asymétrique ou comme produits métallopharmaceutiques, bien que l'application la plus connue soit l'utilisation de ce type de composés dans la construction de diodes électroluminescentes organométalliques (OLED). Pour cette application, une grande variété de complexes bis- et tris-cyclométalates de Ir(III) ont été étudiés comme dopants phosphorescents pour la construction de ce type de systèmes, ainsi que pour la construction de LEECs (cellules électrochimiques émissives). Tous, bien qu'étant des complexes métalliques chiraux, ont été utilisés sous la forme de composés racémiques, contenant un mélange d'isomère delta (Δ) et d'isomère lambda (Λ). Il y a un peu plus de dix ans, le premier dérivé énantiopur a été isolé à l'aide de ligands chiraux, démontrant leur capacité à émettre de la lumière polarisée circulairement.
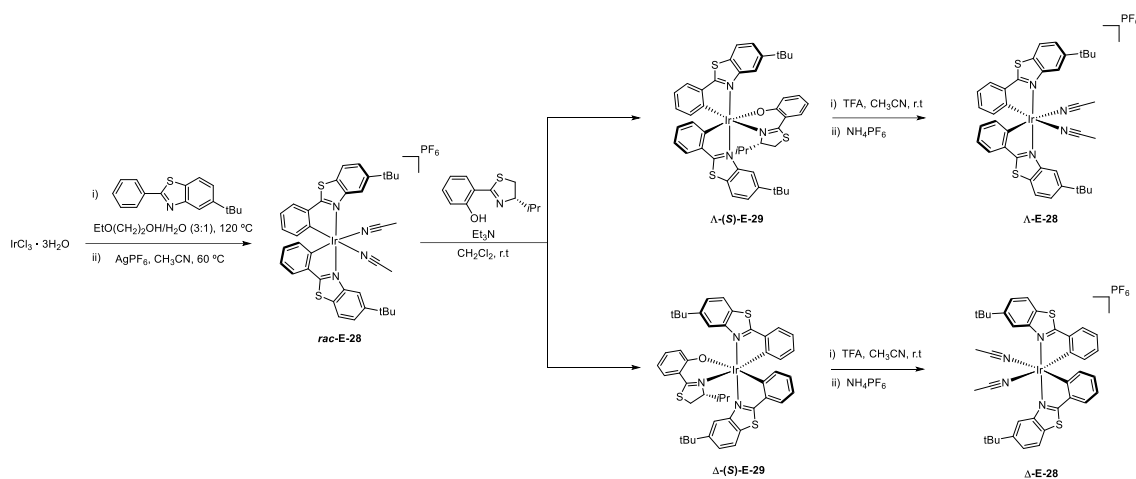
Figure R1. Résolution chirale pour obtenir des complexes octaédriques énantiopurs de Ir(III).

Outre les systèmes organométalliques, il existe un certain nombre de composés organiques, définis comme des composés photochromiques, qui sont utilisés depuis des décennies comme systèmes photomodulables. Ces composés sont capables de modifier leurs propriétés sous l'effet d'un stimulus externe, dans ce cas précis, la lumière. La combinaison de ces systèmes photochromiques et des complexes organométalliques a conduit à la création de nouveaux composés organométalliques photomodulables, permettant d'améliorer les applications existantes. De manière surprenante et malgré le grand nombre d'applications connues pour les complexes organométalliques, il n'existe pratiquement aucun exemple décrit où des complexes photochromiques organométalliques sont utilisés, offrant ainsi l'opportunité d'étudier un concept émergent très attractif.

Le principal intérêt de ce type de composés est la création de systèmes chimiques intelligents. Ces systèmes reposent sur la possibilité de modifier leurs propriétés et leur fonctionnalité par des changements de l'environnement, plus précisément par l'irradiation. Ces nouveaux matériaux peuvent être considérés comme une représentation du concept appelé "machines moléculaires". La stratégie la plus simple pour obtenir des complexes métalliques photosensibles consiste à incorporer des motifs organiques photosensibles dans la structure des ligands coordonnés au métal, transformant ainsi les composés en entités dynamiques capables de répondre à un stimulus externe. Poussé par l'importance des ligands phénylpyridine (ppy), phosphine et bipyridine (bpy) dans la synthèse de complexes organométalliques fonctionnels, notre groupe à l'Université du Pays Basque (UPV-EHU) s'est concentré ces dernières années sur le développement de composés organométalliques photoisomérisables, utilisant des groupes azobenzène incorporés dans des ligands bipyridine, phénylpyridine et phosphine. Pendant ce temps, ces composés ont été étudiés en tant que dopants phosphorescents pour les OLED, ainsi que leur application potentielle en tant que catalyseurs photocontrôlés. L'azobenzène a été la plateforme organique choisie pour cette fonction car il était facilement accessible sur le plan synthétique, ainsi qu'en raison du décalage électronique qui se produit lors de l'isomérisation de son état *trans* à son état *cis* après irradiation. De plus, dans le processus d'isomérisation de l'azobenzène, on observe une modification de la structure de la molécule, transformant une structure plane en une structure tridimensionnelle (*trans*-/E → *cis*-/Z).

De manière surprenante, la chiralité temporelle obtenue par certains ligands photocommutable après le changement induit par la lumière a à peine été étudiée, ce qui ouvre une voie intéressante pour l'étude de ce concept. Outre l'azobenzène, il existe un grand nombre

de composés organiques qui peuvent agir de la même manière, appelés interrupteurs moléculaires organiques, comme par exemple les dérivés de dithiényléthène, également connus sous le nom de DTE. Ces dérivés du DTE sont des composés photochromiques très intéressants car, dans le processus d'isomérisation (ouvert-fermé), ils présentent une excellente résistance à la fatigue et une irréversibilité thermique. En outre, comme le groupe azobenzène, au cours du processus d'isomérisation, le motif DTE acquiert une chiralité temporaire qui, ajoutée à ses propriétés déjà décrites, en fait un candidat formidable pour la synthèse et l'application ultérieure de nouveaux complexes organométalliques photosensibles.

L'objectif principal de ce projet de recherche est le développement de nouveaux complexes organométalliques photosensibles basés sur des ligands DTE pour la synthèse de composés dites "chiral-at-metal", montrant dans les deux cas une amplification de la chiralité par irradiation.
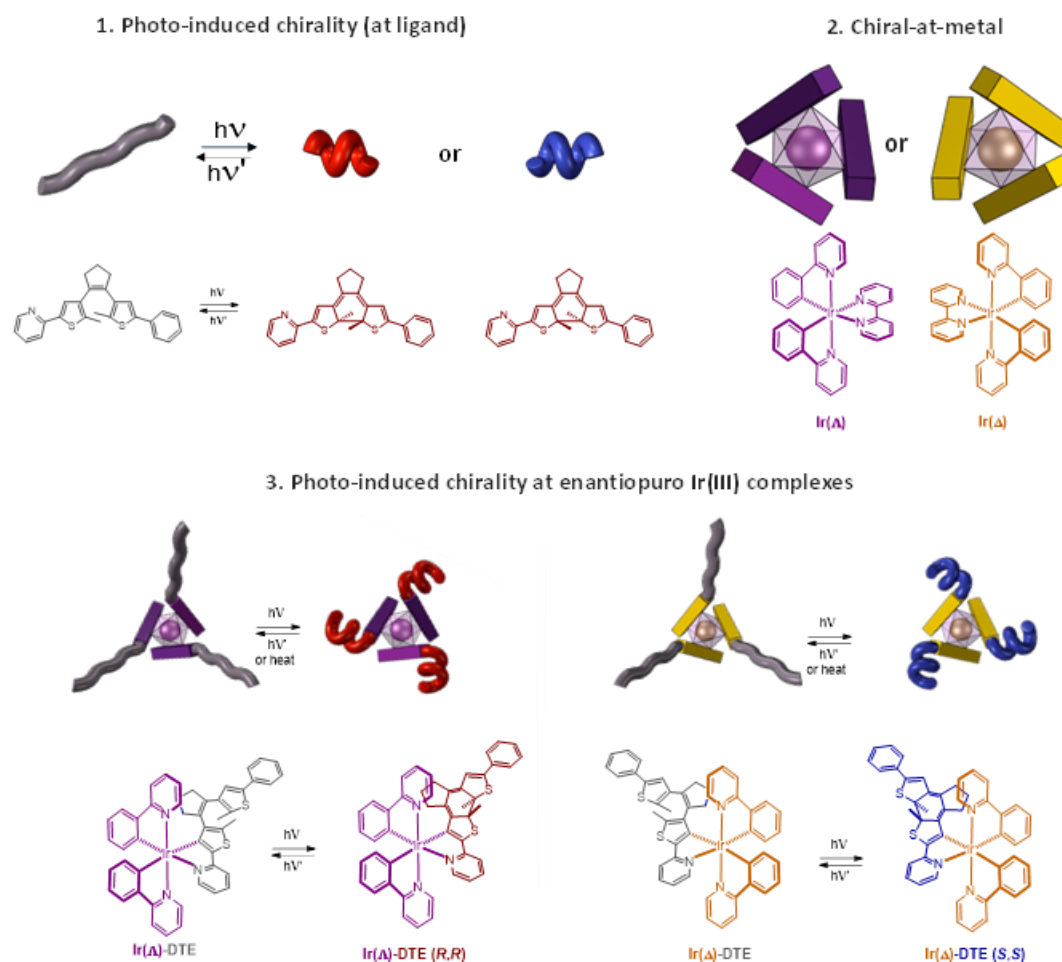
Figure R2. Représentation graphique des objectifs généraux proposés pour ce travail.

Le *chapitre 1* consiste en une introduction, divisée en deux sections, qui explique les différents concepts qui seront abordés au cours du manuscrit. La première partie présente certains des composés photochromiques les plus intéressants décrits et se concentre sur l'explication détaillée des propriétés des dithiényléthènes, ainsi que sur leur origine et le mécanisme par lequel le processus d'isomérisation est régi. Il montre également plusieurs exemples où des motifs de DTE sont insérés dans la structure de différents complexes organométalliques et des applications réelles qui utilisent le DTE comme élément de base.

La deuxième partie de l'introduction se concentre sur les différents complexes de Ir(III) bis- et tris-cyclométalés. Ces composés ont été largement étudiés en raison de leurs excellentes propriétés émissives, qui peuvent être modifiées en fonctionnalisant les ligands C-N coordonnés à l'ion métallique. En raison de leurs propriétés, les composés organométalliques Ir(III) ont été largement utilisés dans différentes applications telles que les OLED, les composés cibles dans les systèmes biologiques ou comme systèmes anticancéreux. En outre, grâce aux progrès récents dans la synthèse des complexes octaédriques de Ir(III), les composés énantiopurs peuvent être obtenus de manière plus efficace, ce qui renforce les applications possibles déjà décrites pour les complexes cyclométalés de Ir(III) : émission de lumière polarisée circulairement, plus grande sélectivité vis-à-vis des centres biologiques ou leur utilisation possible comme catalyseurs asymétriques.

Le *chapitre 2* présente les études réalisées pour obtenir des complexes octaédriques avec des ligands DTE cyclométalés. La première partie du chapitre est basée sur la synthèse et la caractérisation de différents ligands de DTE. Les ligands photochromiques synthétisés peuvent être classés en ligands symétriques ou non symétriques, en fonction de la composition des groupes thiophène dans la structure. Tous les ligands sont conçus de manière à ce que le point de coordination se fasse par le biais d'un groupe thiophène-pyridyle, ce qui permet de faire varier la position dans la structure du composé.
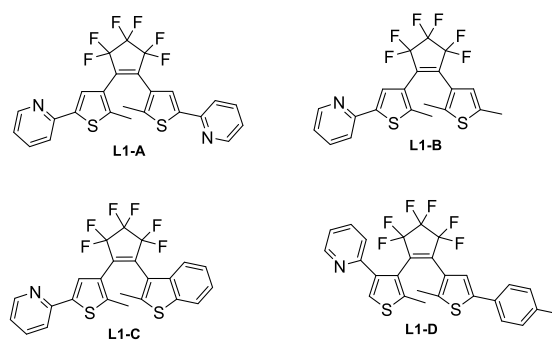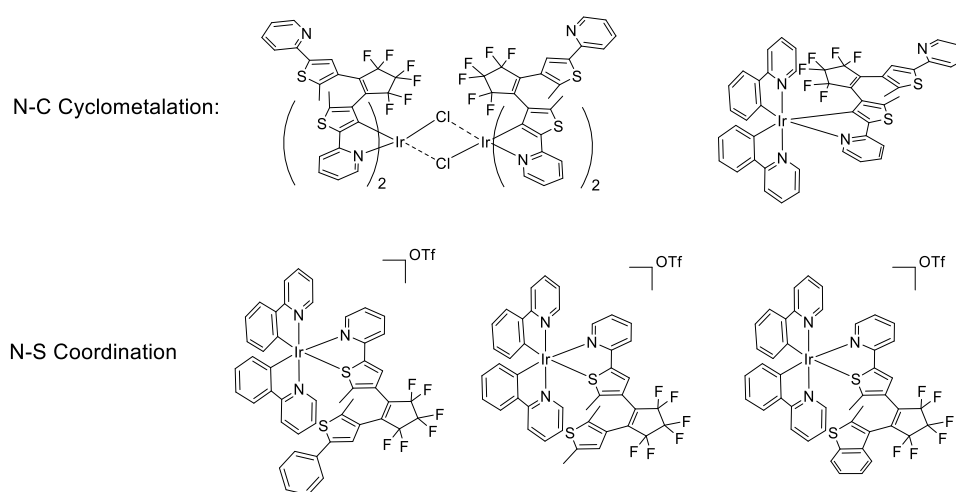

Figure R3. Ligands DTE synthétisés proposés pour la cyclométallation aux centres métalliques Ir(III).

La deuxième partie du chapitre se concentre sur l'effort pour obtenir la coordination des ligands précédemment synthétisés à différents précurseurs de Ir(III). Afin d'obtenir des complexes à base de ligands DTE cyclométalés, de nombreuses conditions réactionnelles ont été étudiées, faisant varier le type de précurseur initial utilisé, la conception du complexe métallique, ainsi que les changements du solvant et de la température de la réaction. Malheureusement, les différentes études n'ont pas permis de confirmer la cyclométallation des ligands DTE synthétisés. Afin de comprendre pourquoi la coordination n'était pas efficace, la cyclométallation du groupe thiophène dans sa structure la plus simple a été testée. Tout d'abord, un dimère Ir(III) à pont chloré a été synthétisé en utilisant un groupe 2-pyridyl-4-bromo-5-méthylthiophène comme ligand cyclométalé. Cette réaction a permis d'obtenir un solide orange, qui a été identifié et caractérisé par spectroscopie RMN. Le solide a été identifié par analyse élémentaire en raison de l'insolubilité du solide dans tout solvant deutéré. Pour confirmer définitivement que la cyclométallation du motif thiophène était efficace, il a été décidé d'introduire un troisième ligand coordinateur, dans le but d'améliorer la solubilité. Le produit de cette réaction a permis de confirmer que la cyclométallation des deux ligands thiophène-pyridine lors de la synthèse du dimère était efficace. D'autre part, en suivant la même stratégie, un fragment unique de thiophène-pyridine a été inséré dans un précurseur

[Ir(ppy)(CH₃CN)]⁺, et il a été observé que dans le cas spécifique où il a été introduit comme troisième ligand, cela a généré une coordination N-S au centre métallique. Ce type de coordination a été très peu étudié, car il n'y a pas beaucoup de publications qui le décrivent, ce qui ouvre une nouvelle et intéressante voie de recherche. Après avoir obtenu ces résultats prometteurs, la coordination N-S des ligands DTE synthétisés a été testée et il est apparu que la coordination était satisfaisante. Malgré cette évidence, la purification de ces complexes n'a pas pu être réalisée efficacement par les différentes méthodologies classiques de purification telles que la précipitation ou la séparation sur colonne chromatographique. Par conséquent, la coordination des ligands N-S aux centres métalliques reste l'une des perspectives futures de notre groupe de recherche, en raison du fait que la coordination des ligands se produit à un point très proche de la zone du processus d'isomérisation, ce qui peut considérablement affecter le processus de cyclisation des DTE.


Figure R4. Coordinations étudiées pour les ligands DTE synthétisés sur des précurseurs de Ir(III).

Le *chapitre 3* présente les études réalisées pour obtenir des complexes octaédriques avec des ligands DTE non-symétriques contenant des groupes bipyridine comme centres de coordination. La première section du chapitre est basée sur la synthèse et la caractérisation de quatre ligands de DTE non décrits auparavant. Les ligands synthétisés sont classés en deux familles, **L2** et **L3**, selon qu'ils incorporent ou non un espaceur alcyne entre la bipyridine et le DTE. Pour la synthèse de ces ligands, plusieurs voies de synthèse sont présentées à partir desquelles les composés finaux souhaités peuvent être obtenus. Pour une caractérisation efficace des composés organiques, ils ont été étudiés par spectroscopie RMN (¹H-NMR, ¹³C-NMR, COSY et HSQC), spectrométrie de masse, ainsi que par diffraction des rayons X des structures cristallines des ligands.
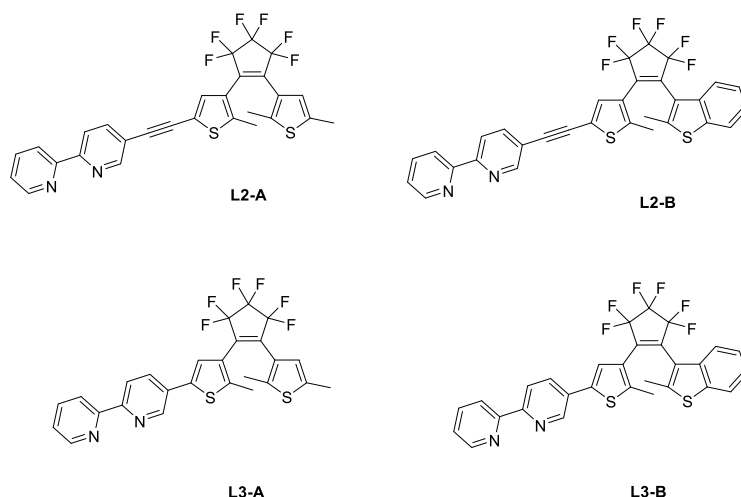
Figure R5. Synthèse de ligands DTE basés sur l'insertion de groupes bipyridine comme groupe chélatant.

La deuxième section du *chapitre 3* est divisée en deux parties, la synthèse de complexes racémiques et la synthèse de complexes énantiopurs. Dans la première partie, la coordination des ligands DTE à un centre Ir(III) racémique sera brièvement discutée. Il s'agissait des tests préliminaires réalisés pour le bon déroulement de l'étude de coordination des ligands synthétisés aux centres Ir(III) énantipurs.
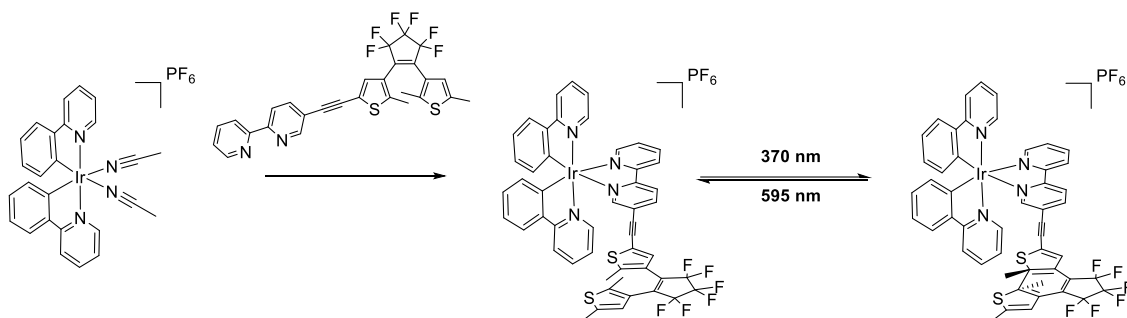

Figure R6. Synthèse de complexes cationiques utilisant des ligands DTE comme troisième ligand.

La deuxième partie du *chapitre 3* commence par la synthèse de précurseurs énantiopurs par résolution chirale, décrite par E. Meggers, une stratégie qui utilise ou emploie des agents chiraux pour la génération de diastéréoisomères. La génération de diastéréoisomères permet une séparation et une purification ultérieure des complexes par des méthodes de purification classiques. Pour cette résolution chirale, différents agents chiraux (L-proline et L/D-sérine) ont été testés, obtenant de bons résultats pour chacun d'entre eux. Une fois les diastéréoisomères purifiés, l'agent chiral a été changé en utilisant le TFA, introduisant deux molécules de solvant dans les vacuités coordinatives libres, obtenant ainsi les précurseurs métalliques énantiopurs Λ-[Ir(ppy)$_2$(CH$_3$CN)$_2$]$^+$ et Δ-[Ir(ppy)$_2$(CH$_3$CN)$_2$]$^+$. Pour confirmer l'excès énantiomérique de chacun des précurseurs, des études de dichroïsme circulaire ont été réalisées, montrant comment chacun des complexes présentait un effet Cotton différent (positif et négatif), créant des spectres avec des images miroir les uns des autres. Ensuite, en prenant les conditions de réaction utilisées pour la génération des complexes énantiopurs, les composés énantiopurs correspondants ont été synthétisés pour les quatre ligands, obtenant quatre nouvelles paires de complexes Ir(III). Le chapitre se termine par la caractérisation des complexes métalliques.
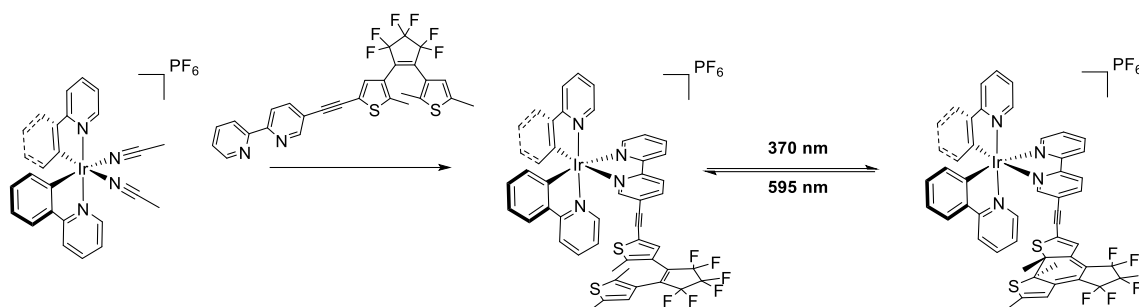
Figure R7. Synthèse de complexes cationiques énantiopurs incorporant un motif DTE dans la structure.

Le *chapitre 4* présente les résultats obtenus pour l'étude des différentes propriétés, tant pour les ligands DTE que pour les complexes correspondants. Le chapitre commence par l'étude photochromique des différents ligands DTE ayant un groupe bipyridine dans leur structure. Le caractère photochromique a été étudié, en observant comment les spectres d'absorption variaient selon que le ligand était sous forme ouverte ou fermée, en identifiant des bandes caractéristiques des deux isomères. De même, par spectroscopie RMN, des signaux caractéristiques ont été étudiés et identifiés pour chacun des isomères. De cette façon, il a été possible d'étudier quantitativement l'évolution du processus de photocyclisation, en calculant le pourcentage de chacune des espèces dans l'état photostationnaire. Des études cinétiques ont été réalisées, aussi bien par spectroscopie RMN que par spectroscopie UV-Vis, afin de calculer les rendements quantiques des processus photophysiques présents lors de l'isomérisation des DTE. Grâce à cela, une collaboration entre laboratoires LOMA & ISM de l'Université de Bordeaux a permis de concevoir un système d'irradiation pour mesurer en temps réel l'évolution du processus. À partir de ces données, les rendements quantiques de photocyclisation et de photocycloversion pour les ligands DTE ont été calculés. Pour conclure l'étude des ligands, les propriétés de résistance à la fatigue et la stabilité thermique des isomères fermés ont été testées. L'étude de résistance à la fatigue a montré que le ligand L3-B est le candidat idéal pour une mise en œuvre dans des applications photochromiques car il n'a montré aucune décomposition au cours des 100 premiers cycles d'isomérisation. De même, tous les ligands, dans leur forme fermée, ont montré une grande stabilité contre le processus de cycloréversion activé thermiquement, où aucun comportement thermochrome n'a été observé.
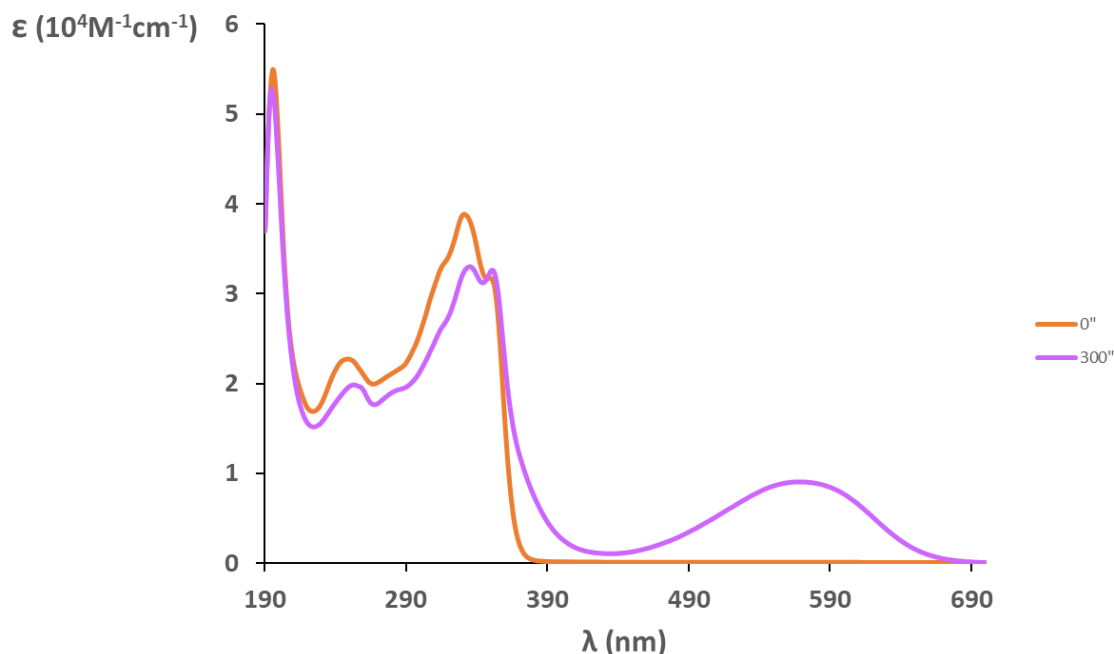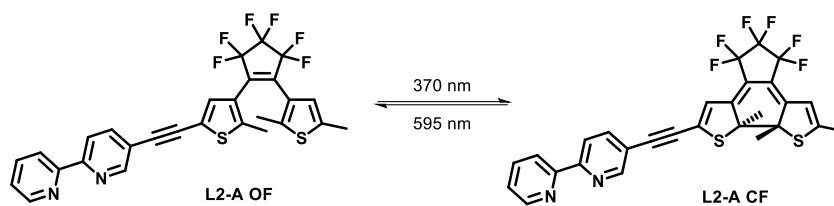
Figure R8. Comportement photochromique (photocyclisation/photocycloversion) pour les ligands DTE synthétisés.

La deuxième partie du chapitre reprend les études réalisées pour les complexes de Ir(III). L'effet de la coordination métallique sur le déplacement des maxima d'absorption des composés a été étudié, en observant un déplacement vers le rouge des différentes bandes d'absorption. Comme pour les ligands, la vitesse à laquelle les complexes ont atteint l'état d'équilibre a été étudiée par RMN et spectroscopie UV-Vis, en observant uniquement l'état photostationnaire, le pourcentage d'isomères fermés était significativement plus élevé que celui obtenu pour les ligands libres. L'efficacité des processus de photocyclisation/photocycloreversion (QY) a également été étudiée. La comparaison des rendements quantiques entre les ligands libres et les complexes de Ir(III) a montré que la coordination au centre métallique n'affecte pas de manière significative le processus photochimique. En suivant les directives des ligands DTE, la résistance à la fatigue a été étudiée. On a constaté que, une fois que le ligand photocommutable est coordonné au centre métallique, la résistance à la fatigue par isomérisation augmente très significativement pour les ligands **L2** et **L3-A**, tandis que pour le cas spécifique de L3-B, elle reste dans des ordres de grandeur similaires à ceux obtenus pour le ligand libre.
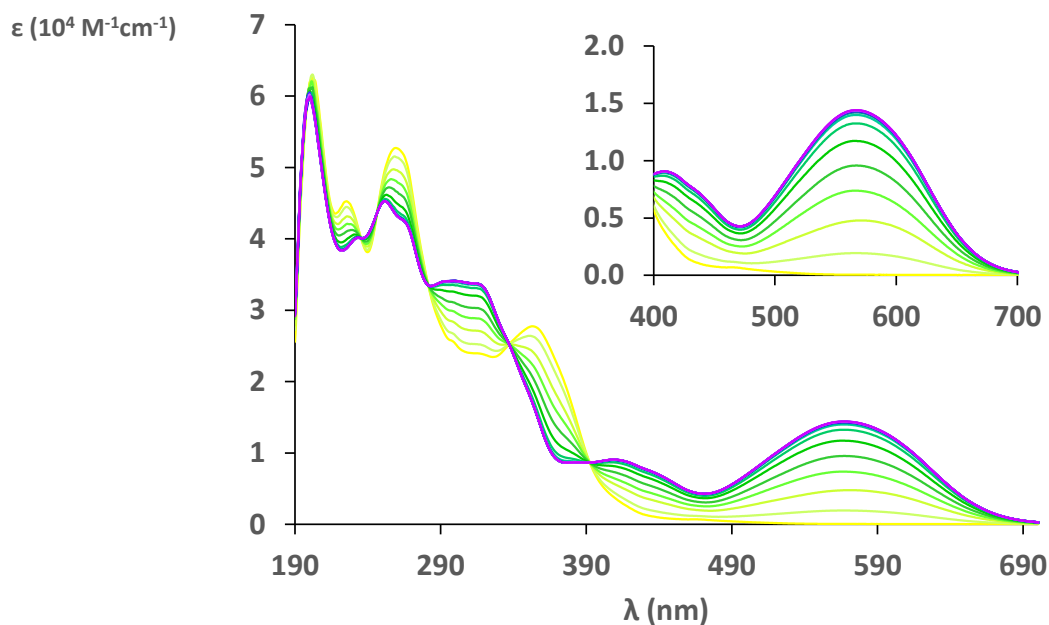
Figure R9. Changements d'absorption accompagnant la photocommutation des complexes Ir(III)-DTE.

Enfin, l'induction d'une isomérisation diastéréosélective des complexes énantiopurs a été étudiée par spectroscopie de dichroïsme circulaire. Il a été observé que pour la forme ouverte des complexes, un effet Cotton positif/négatif a été obtenu dans la région UV, selon l'isomère spécifique (Δ ou Λ), associé à la chiralité présente dans le métal central. Une fois la photocyclisation induite, un léger effet Cotton positif ou négatif a été observé dans la région du spectre caractéristique de la forme fermée des complexes. Ce changement corrobore l'hypothèse proposée dans l'objectif de cette thèse d'induire le processus de photocyclisation vers l'une des deux configurations de la **CF-DTE**, générant un excès de diastéréoisomères.
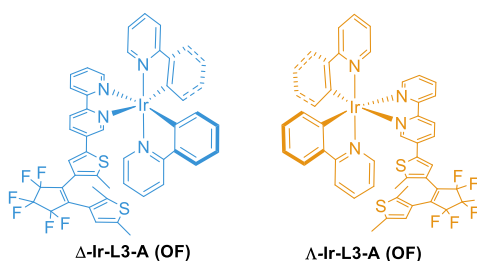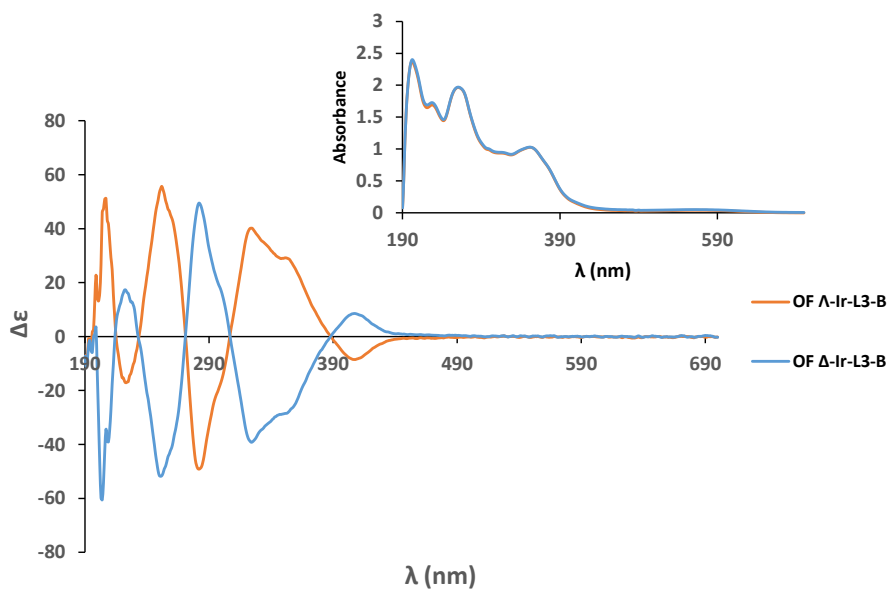
Figure R10. Spectre de dichroïsme circulaire pour l'étude d'une induction sélective du processus de photocyclisation pour les complexes énantiopurs de Ir(III) incorporant un ligand DTE.

Le *chapitre 5* décrit les conclusions générales obtenues tout au long de la thèse et les éventuelles perspectives futures qui pourront être développées à l'avenir au sein de l'équipe de recherche.